Mapping QTLs involved in trichome development in tomato and understanding their role in drought and herbivory resistance

Javier Galdon Armero

A thesis submitted to the University of East Anglia for the degree of Doctor of Philosophy

John Innes Centre

Norwich

September 2018

Abstract

The work described in this thesis aimed to identify new structural and regulatory genes involved in trichome development in tomato (*Solanum lycopersicum*). Trichomes are hairs that cover the aerial epidermis of most terrestrial plants, and they confer resistance to abiotic and biotic stresses. In species with glandular trichomes, such as tomato, trichomes can produce a vast array of specialised metabolites with diverse biological activities.

I explored the genetic variation present in the wild tomato species *Solanum pennellii*, which has high trichome density and is tolerant to biotic and abiotic stresses, to find genes involved in trichome development. I determined the trichome phenotype of the *S. pennellii* x *S. lycopersicum* cv. M82 introgression lines over two generations and identified genomic regions potentially containing genes involved in trichome development. I tested candidate gene by transient virus-induced gene silencing (VIGS) in tomato and could identify three genes with a role in trichome formation: *SlMIXTA-like, SlMX2* and *SlCycB2*.

I generated transgenic lines overexpressing *SlMIXTA-like* as well as *SlMIXTA-like* knock-out mutants using the CRISPR/Cas9 system to characterise this gene functionally. These results, combined with promoter analysis and comparisons between the MIXTA-like structure and function in *S. pennellii* and *S. lycopersicum*, showed that *SlMIXTA-like* is a negative regulator of trichome initiation and a key factor in epidermal patterning in tomato.

I used the CRISPR/Cas9 system to generate knock-out mutants of known regulators of trichome development in tomato (*SlMX1*, *Woolly*, *Hairless*, *CD2* and *DWARF*). Analyses of these knock-out mutants contributed to clarifying their precise function in trichome development and led to the establishment of a better model for trichome initiation and morphogenesis in tomato.

My research also showed a clear relationship between trichome density and tolerance to drought stress and whitefly herbivory, indicating that trichome-related traits can be targeted for agricultural improvement of tomato cultivars.

Acknowledgments

I would like to thank all the people that during these last four years have been part of my life and have contributed to some extent to make this PhD thesis possible.

I am grateful to the John Innes Centre and the Rotation Programme for providing the funding, support and facilities to develop my research and for creating a community feeling where personal and professional relationships can thrive.

I thank all the members of the Cathie Martin's group for the supportive environment we created in the last four years. I thank Cathie Martin for helping me become an independent researcher and letting me develop my own interests. I have fond memories with all present and past members of the lab: Eugenio Butelli, Vera Thole, Matt Tomlinson, Ellie Fearnley, Ingo Appelhagen, Fabio D'Orso, Dario Breitel, Noam Chayut, Aurelia Scarano, Julia Russell, Erica Hawkins, Yang Zhang, Jie Li, Vincenzo D'Amelia, Daniel Knevitt. The discussions, rants and laughter with these people were essential for finishing my thesis and am happy to be able to call them my friends. I am especially thankful to Lisette Arce, Micaela Navarro and Cara Moss for the direct contribution to this work.

This work would not have been possible without the support and training from the fantastic teams at the JIC Bioimaging facilities, especially Kim Findlay and Elaine Barclay, and the JIC insectary, especially Anna Jordan and Ian Bedford. Thanks for teaching me so much.

I also would like to use this opportunity to thank everyone at the Plant Physiology under Mediterranean conditions group at the Universitat de les Illes Balears for hosting me and becoming my second lab for 3 months. I thank all our collaborators there, especially Jeroni Galmes for helping me grow as a scientist and Mateu Fullana for being a great colleague and a better friend. *G*ràcies!

I would like to write some words about all the friends I have made throughout these years, especialmente a la familia española que hemos creado en el exilio. Gracias por hacer que casa esté un poquito menos lejos cuando estáis alrededor.

También quiero dar las gracias a mi familia, especialmente a mis padres y a mi hermano por llevar tan bien la distancia, no cuestionar mis decisiones y soportar mi mal humor. Sin su apoyo incondicional esto no habría sido posible.

Finalmente, quiero dar las gracias a Pilar, por ser mi compañera de vida y de aventuras durante muchos años y todos los que quedan por delante. Gracias por soportar mis días malos y por convertirlos en buenos. Gracias por ser mi felicidad.

Table of contents

List of figures

List of tables

Abbreviations

δ^{13C}	Leaf Carbon Isotope Composition
Ψ_{leaf}	Leaf Water Potential
2,4-D	2,4-Dichlorophenoxyacetic acid
ABA	Abscisic acid
ABI1	Abscisic acid Insensitive 1
ABI2	Abscisic acid Insensitive 2
ABI3	Abscisic acid Insensitive 3
ABI8	Abscisic acid Insensitive 8
ACR4	*Arabidopsis* Crinkly 4
AGO1	Argonaut1
AIA	After Insect Attack
ALSV	Apple Latent Spherical Virus
A_N	Net Photosynthetic Rate
AP2	Apetala 2
ARP3	ACTIN-RELATED PROTEIN 3
ARPC2A	ACTIN-RELATED PROTEIN 2/3 COMPLEX SUBUNIT 2A
ARPC3	ACTIN-RELATED PROTEIN 2/3 COMPLEX SUBUNIT 3
ARR1	Response Regulator 1
AtABF1	*Arabidopsis thaliana* ABRE BINDING FACTOR1
AtABO3	*Arabidopsis thaliana* ABA-OVERSENSITIVE 3
AtEXPA7	*Arabidopsis thaliana* α-expansin 7
AtEXPA18	*Arabidopsis thaliana* α-expansin 18
ATML1	*Arabidopsis thaliana Meristem Layer 1*
bHLH	Basic Helix-Loop-Helix
BASL	Breaking of Asymmetry in the Stomatal Lineage
BIA	Before Insect Attack
BLAST	Basic Local Alignment Search Tool
BLT	BRANCHLESS TRICHOME
BMSV	Barley Stripe Mosaic Virus
BR	Brassinosteroid
C2H2	Cysteine 2 Histidine 2
C24h	Daily Carbon Fixation Rate
CAM	Crassulacean Acid Metabolism
Cas9	CRISPR-Associated protein 9
cDNA	Complementary DNA

CDS	Coding Sequence
CRISPR	Clustered Regularly Interspaced Short Palindromic Repeats
crRNA	CRISPR RNA
Cnr	Colourless non ripening
COI1	Coronatine Insensitive 1
CTR1	CONSTITUTIVE TRIPLE RESPONSE 1
Del	Delila
dl	*dialytic*
DMSO	Dimethyl sulfoxide
DNA	Deoxyribonucleic acid
dNTPs	Deoxyribonucleoside triphosphate
dpy	*dumpy*
dsRNA	double-stranded ribonucleic acid
EGL3	Enhancer of Glabra 3
EPF1	Epidermal Patterning Factor 1
EPF2	Epidermal Patterning Factor 2
EPFL4	Epidermal Patterning Factor-like 4
ER	ERECTA
ERL1	ERECTA-like 1
ERL2	ERECTA-like 2
ETC1	ENHANCER OF TRY AND CPC 1
ETC2	ENHANCER OF TRY AND CPC 2
ETC3	ENHANCER OF TRY AND CPC 3
ETR2	ETHYLENE RECEPTOR 2
FLP	Four Lips
GA	Gibberellin
GFP	Green Fluorescent Protein
GE	Genome-edited
GIS	GLABROUS INFLORESCENCE STEMS
GIS2	GLABROUS INFLORESCENCE STEMS 2
GIS3	GLABROUS INFLORESCENCE STEMS 3
GL1	GLABROUS 1/GLABRA 1
GL2	GLABRA 2
GL3	GLABRA 3
g_m	Mesophyll conductance
GMC	Guard Mother Cell

g_s	Stomatal conductance
g_t	Total conductance
GUS	β-glucuronidase
HDG2	HOMEOBOX GLABROUS 2
HDG11	HOMEOBOX GLABROUS 11
HDG12	HOMEOBOX GLABROUS 12
HD-Zip	Homeodomain-Leucine zipper
IBA	Indole-3-butyric acid
IL	Introgression Line
IPTG	Isopropyl β-D-1-thiogalactopyranoside
JA	Jasmonate
JAZ	Jasmonate ZIM-domain
KCBP	Kinesin-like Calmodulin-Binding Protein
KO	Knock-Out
L1	Layer 1
LB	Luria-Bertani
LMA	Leaf Mass Area
LRR-RK	Leucine-rich repeat receptor kinase
LRR-RLP	Leucine-rich repeat receptor-like protein
LT	Leaf Thickness
MAPK	Mitogen-Activated Protein Kinase
MAPKK	Mitogen-Activated Protein Kinase Kinase
MAPKKK	Mitogen-Activated Protein Kinase Kinase Kinase
MBW	MYB-bHLH-WD40
MEP	Methylerythritol 4-phosphate
MMC	Meristemoid Mother Cell
MS	Murashige and Skoog
MYB	Myeloblastosis
MYBML1	MYB MIXTA-like 1
MYBML2	MYB MIXTA-like 2
MYBML3	MYB MIXTA-like 3
OE	Overexpression
PAM	Protospacer Adjacent Motif
PCR	Polymerase Chain Reaction
PDF2	Protodermal Factor 2
PVX	Potato Virus X

QTL	Quantitative Trait Loci
RAM	Root Apical Meristem
RBR1	RETINOBLASTOMA RELATED 1
RIN	Ripening Inhibitor
RISC	RNA-induced Silencing Complex
RNA	Ribonucleic acid
RNAi	Ribonucleic acid interference
RNAseq	Ribonucleic acid sequencing
Ros1	Rosea1
RPK1	Receptor-like Protein Kinase 1
RPK2	Receptor-like Protein Kinase 2
SA	Salicylic acid
SAM	Shoot Apical Meristem
SCM	SCRAMBLED
SCRM1	SCREAM 1
SCRM2	SCREAM 2
SD	Stomatal Density
SEM	Scanning Electron Microscopy
SERK	Somatic Embryogenesis Receptor Kinase
sgRNA	Small Guider RNA
sim	*siamese*
siRNA	small interference ribonucleic acid
SlABI8	*Solanum lycopersicum* ABSCISIC ACID-INSENSITIVE 8
SlbZIP17	*Solanum lycopersicum* basic leucine-zipper 17
SlARF3	*Solanum lycopersicum* AUXIN-RESPONSIVE FACTOR 3
SlCHI	*Solanum lycopersicum* chalcone isomerase
SlCycB2	*Solanum lycopersicum* type-B cyclin 2
SlDXS2	*Solanum lycopersicum* 1-deoxy-D-xylulose 5-phosphate synthase 2
SlEIN2	*Solanum lycopersicum* Ethylene Insensitive 2
SlELF1	*Solanum lycopersicum* Elongation Factor 1
SlEXP4a	*Solanum lycopersicum* α-expansin 4a
SlEXP4b	*Solanum lycopersicum* α-expansin 4b
SlEXP8	*Solanum lycopersicum* α-expansin 8
SlEXP11	*Solanum lycopersicum* α-expansin 11
SlEXP13	*Solanum lycopersicum* α-expansin 13
SlEXP15	*Solanum lycopersicum* α-expansin 15

SlG3	*Solanum lycopersicum* GLABRA 3
SLGC	Stomatal Lineage Ground Cell
SlGPS	*Solanum lycopersicum* Geranyl Diphosphate Synthase
SlLHW	*Solanum lycopersicum* Lonesome Highway
SlMX1	*Solanum lycopersicum* MIXTA 1
SlMX2	*Solanum lycopersicum* MIXTA 2
SlMX3A	*Solanum lycopersicum* MIXTA 3A
SlMX3B	*Solanum lycopersicum* MIXTA 3B
SlSHN3	*Solanum lycopersicum* SHINE 3
SOC	Super Optimal broth with Catabolite repression
SPCH	SPEECHLESS
SRA1	SPECIALLY-RAC1 ASSOCIATED
SS	Stomatal Size
START	Steroidogenic Acute Regulatory Protein-Related Lipid Transfer
STOM	STOMAGEN
T/S	Trichome-to-Stomata ratio
TCL1	TRICHOMLESS 1
TCL2	TRICHOMLESS 2
TD	Trichome Density
TMM	Too Many Mouths
TRFL10	Telomere Binding Factor 10
TRV	Tobacco Rattle Virus
TRY	TRIPTYCHON
TT8	TRANSPARENT TESTA 8
TTG1	TRANSPARENT TESTA GLABRA 1
TTG2	TRANSPARENT TESTA GLABRA 2
TY	Tryptone Yeast extract
UTR	Untranslated region
V_{cmax}	Maximum Velocity of RubisCO carboxylation
VIGS	Virus-induced gene silencing
WD	Water Deficit
WDR	WD40 repeat
WER	WEREWOLF
WOX	Wuschel-related Homeobox
WT	Wild Type
WUE	Water Use Efficiency

WUE_i	Intrinsic Water Use Efficiency
WUE_b	Plant-level Water Use Efficiency
WW	Well-Watered
X-gal	5-bromo-4-chloro-3-indolyl-β-D-galactopyranoside
YDA	YODA
ZFP5	Zinc Finger Protein 5
ZFP6	Zinc Finger Protein 6
ZFP8	Zinc Finger Protein 8
ZmOCL1	*Zea mays* Outer Cell Layer 1

Chapter 1 – Introduction

1.1.-Trichomes as part of the plant epidermis.

1.1.1.-Plant aerial epidermis and its different components.

The epidermis forms the most external tissue in plant organs. Consequently, it acts as a defensive barrier against external threats and as a first interaction point for environmental stimuli (Glover et al., 2016). The epidermis consists of a single cell layer, which develops through anticlinal division of the most external cell layer of shoot meristems (referred to as the L1 layer) expanding in two dimensions (Marcotrigiano and Bernatzky, 1995), although its growth through cell division and expansion is tightly linked to that of the immediately adjacent layer, which in leaves is the palisade mesophyll, developed by divisions of the L2 meristematic layer (Savaldi-Goldstein and Chory, 2008). This single-celled epidermal layer is, however, relatively complex and develops an array of different cellular and chemical structures. In most terrestrial plants, these structures include the cuticle, pavement cells, stomata and trichomes. Special structures such as lithocysts (Smith and Watt, 1986) or hydathodes (Fahn, 1988) can also be found in the epidermis of some plant species. Each one of these structures shows differences in their morphology, development and function.

The cuticle is a hydrophobic layer that covers the surface of aerial organs and is essential to maintain a favourable water status inside the aerial organs of land plants subjected to a desiccating environment (Yeats and Rose, 2013), and it can be found on all terrestrial plants, including bryophytes (Budke et al., 2012) and pteridophytes (Archer and Cole, 1986). Its presence is considered an important milestone in the colonisation of land by higher plants, as inferred from fossil evidence (Edwards, 1993). The cuticle consists of variable proportions of two main components, cutin and waxes. In some succulent and CAM species, a third component called cutan has been described, although little is known about its chemical structure and function (Boom et al., 2005).

Cutin is a polymer consisting of hydroxy fatty acids forming covalent ester bonds which generate an organised matrix (Yeats and Rose, 2013). The most common cutin monomer is 10,16-dihydroxyhexadecanoic acid, which can form ester bonds with other monomers using the hydroxyl group on C16 to generate linear structures or using the hydroxyl group in C10 to generate branched structures (Fig. 1.1) (Kolattukudy, 2001). Other monomers are found in cutin and their contribution to cutin biosynthesis is species-dependent. For example, the most common monomer in *Arabidopsis thaliana* is a dicarboxylic acid (Pollard et al., 2008). The cutin matrix serves as a scaffold for deposition of lipidic waxes, which can be deposited within the matrix or on its surface, forming epicuticular crystals or films that confer different properties to the surface of the organ (Jeffree, 2006). The main components of the cuticular waxes are compounds derived from very-long-chain fatty acids, including alkanes, aldehydes and ketones

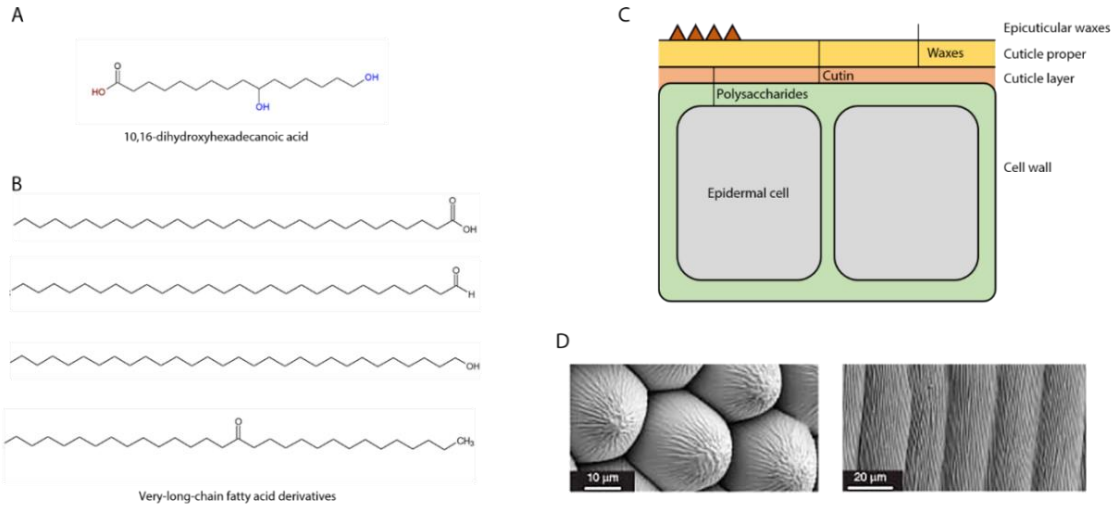

Figure 1.1.-The plant cuticle and its components. A) Chemical representation of the most common fatty acid in cutin (10,16-dihydroxyhexadecanoic acid). Chemical groups involved in esterification are shown: hydroxyl groups are highlighted in blue, and the carboxylic group is highlighted in red. B) Some of the very-long-chain fatty acid derivatives commonly found in cuticular waxes. From top to bottom: carboxylic acid, aldehyde, simple alcohol and ketone derived from a 30C fatty acid. C) Schematic representation of the cuticle structure. Cell wall is represented in green, the cuticle layer in orange, and the cuticle proper in yellow. Epicuticular waxes are represented as triangles. D) Examples of cuticular waxes deposited in organised patterns (stellar and long striations). Figure 1D has been borrowed from (Glover et al., 2016) and I have reuse permission from the copyright holder (Jon Wiley and Sons Ltd) under licence number 4421431352049.

(Fig. 1.1), although some specialised hydrophobic metabolites can also be found, such as tocopherols or flavonoids (Jetter et al., 2008). The waxes and cutin precursors are synthesised in epidermal cells and then transported to the extracellular location for esterification with the growing polymers (Kolattukudy, 2001). Two different layers of the cuticle can be distinguished at the microscopic level; the cuticular layer, with a relatively high content of polysaccharides and low content of waxes, and the cuticle proper, with a high content of waxes (Fig. 1.1) (Yeats and Rose, 2013). Finally, the pattern of cuticle secretion gives rise to different patterns of cuticle (from very organised striations to smooth surfaces, examples shown in Fig. 1.1) which are responsible for different biophysical properties of the surface and play a role in attraction of pollinators (Whitney et al., 2009b, Glover et al., 2016).

Pavement cells are the most common type of epidermal cell and they do not have specialised functions, although they are essential to maintain a correct distribution pattern of the other epidermal structures (stomata and trichomes). They also preserve the integrity of plant organs by providing mechanical support and they have different shapes in different organs, which indicates they adapt their morphology to the developmental context (Glover, 2000, Javelle et al., 2011). For example, in leaves of many plants, such as *A. thaliana* or tomato, pavement cells in leaves have an undulating outline -similar to a jigsaw piece (Fig. 1.2)- while in stems they are elongated. Whether this is a result of tension forces associated with cell division of neighbouring cell layers (Javelle et al., 2011) or whether it is an adaptation to improve the mechanical properties of the epidermis of different tissues (Jacques et al., 2014) is still unclear. A coordinated control of the cytoskeleton determining different foci for growth within a cell is required to produce the wavy shape (Mathur, 2004). The specific organisation of microtubules in bands around the lobes sinuses and the accumulation of actin filaments in lobes tips was reported as necessary for the formation of lobes in pavement cells in maize (Frank et al., 2003). Although its particular shape has been a focus of research, it now seems clear that highly undulated pavement cells are uncommon in angiosperms, and the *Arabidopsis* model might not be ideal to investigate the causes behind shape of pavement cells (Vofely et al., 2018).

Stomata are specialised structures that are found in the epidermis of aerial organs of most terrestrial plants, probably with the exception of liverworts (Chater et al., 2017). Stomata are pores on the leaf and epidermal surface surrounded by two highly specialised cells, the guard cells, which can modify their turgor to regulate the pore aperture to control carbon uptake and water loss via gas exchange (Hetherington and Woodward, 2003) (Fig. 1.2). This mechanism ensures maximal photosynthetic activity maintaining a favourable water status in the leaf organs, and also contributes to thermoregulation (Fauset et al., 2018). Therefore, they are considered as a key element of land colonisation by plants (Berry et al., 2010). Stomata are

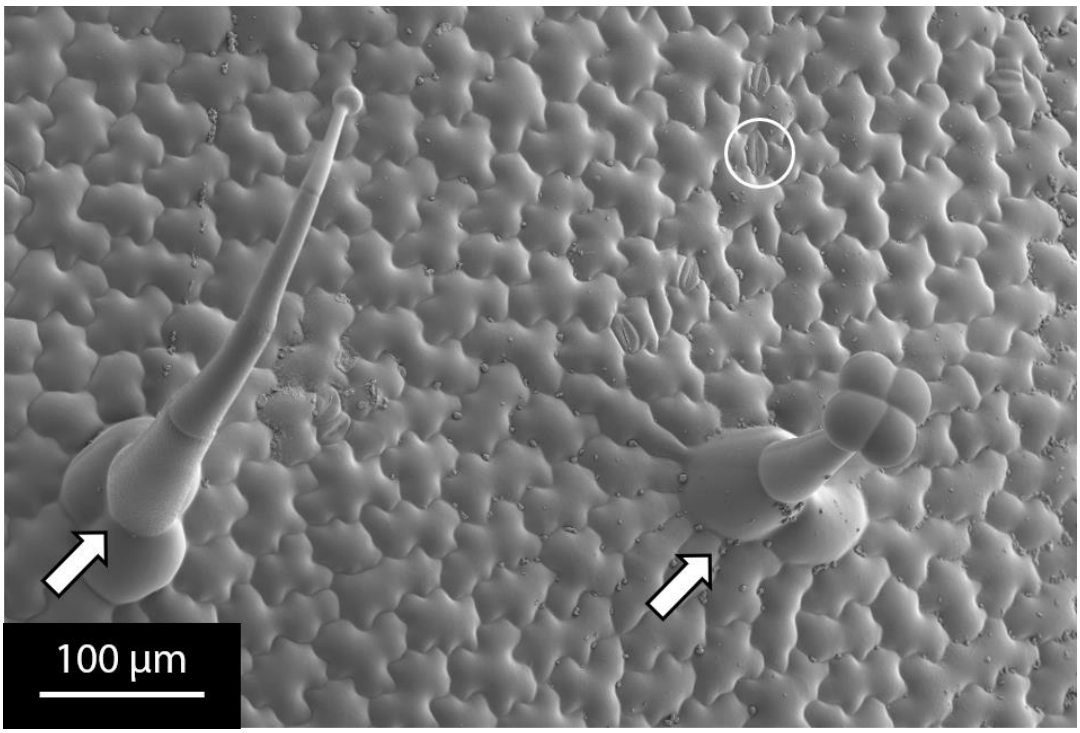

Figure 1.2.-Cryo-scanning electron micrograph of a representative section of the adaxial surface of a Solanum lycopersicum leaf. Jigsaw-piece-shaped pavement cells can be observed over the leaf surface. White circle indicates a representative stoma. White arrows indicate trichomes. Scale bar is indicated in the micrograph.

composed of two photosynthetic guard cells, which can alter their intracellular content of ions and organic compounds that generate osmotic gradients that finally determine guard cell turgor (Zeiger, 1983). Their photosynthetic function is important for this mechanism of opening and closing, probably by allowing synthesis *in situ* of organic solutes (Azoulay-Shemer et al., 2015). These changes take place very rapidly in response to environmental stimuli such as changes in humidity, soil water content, temperature or CO_2, and this response is mediated by the phytohormone abscisic acid (ABA) (Tardieu and Davies, 1992). The density of stomata tends to be higher on the abaxial surface of the leaves, which is generally more protected from radiation and is considered to be the main surface for gas exchange (Wang et al., 1998), although in many herbaceous dicots, including tomato, the numbers of stomata on both sides of the leaf are comparable (Willmer and Fricker, 1996). Due to the conserved nature of stomatal morphology and function across terrestrial plants and the key physiological roles they play, stomata have been a major focus of research on the epidermis of plants.

Trichomes are outgrowths of the epidermal surface which, contrary to the conserved nature of stomata, show great diversity in terms of morphology, distribution and function. Trichomes are highly species-specific, with even close relatives showing considerable differences in trichome types, morphology, density and distribution. Indeed, the presence or absence of hairs on stems or leaves has been a key trait for taxonomic classification since the time of Linnaeus. Several different types of trichomes may be present in a given species (Payne, 1978). This vast diversity complicates the establishment of a standardised classification of the different trichome types, but generally they can be divided in two groups, glandular and non-glandular, depending on the presence or absence of specialised metabolite-secreting cells (Werker, 2000). Further classification refers to specific morphological characteristics or composition of glandular exudates. For example, in some species, trichomes are multicellular and their development involves one or more mitotic divisions, as in the case for all trichomes of tomato (Fig. 1.2). In other species, trichomes are unicellular, although this sometimes involves endoreduplication and suppression of cytokinesis, as in the case of *Arabidopsis thaliana* (Schwab et al., 2000). All kind of shapes can be found in trichomes (stellate, hooked, t-shaped among many others) and this diversity has often been used for taxonomic classification (Werker, 2000). Glandular trichomes are present in approximately 30% of vascular plant species (Fahn, 2000), and they have been the main focus of research in trichomes in species other than the model plant *Arabidopsis*. This is due to the different specialised metabolites they can produce, ranging from drugs, such as artemisinin from *Artemisia annua* (Das, 2015), to essential oils produced in trichomes of *Mentha* species (Mucciarelli et al., 2001). They also play a protective role against environmental stresses, especially herbivory (Fürstenberg-Hägg et al., 2013). Their density and

distribution is essential for their function, and it is regulated genetically and environmentally, in an analogous way to stomata (Glover et al., 2016). Trichomes are the focus of study in this thesis, and different aspects of their development and function will be discussed in this introduction.

Other specialised structures can also be found in the epidermis of plants. Conical cells are protruding epidermal cells that are generally found in the adaxial surface of petals of most angiosperms (Whitney et al., 2011). Conical cells have a role in attracting pollinators, by deepening colour and by providing grip for pollinators (Kay et al., 1981, Kevan and Lane, 1985, Noda et al., 1994, Whitney et al., 2009a). As they are outgrowths of the epidermis, their development has been linked to that of trichomes (Glover et al., 1998, Martin et al., 2002). Hydathodes are structures evolutionary related to stomata that consist of a pore, the aperture of which cannot be regulated by changes in guard cell turgor (Pillitteri et al., 2008). These pores are typically found on leaf margins and are used by the plants to exude fluids from xylem and phloem saps to eliminate organic and inorganic compounds (including microorganisms) and this is essential for maintenance of water status (Singh, 2014). Lithocysts are specialised epidermal cells, which have large dimensions and normally invade the mesophyll, that contain crystals of calcium carbonate (Ajello, 1941). The function of these structures is not completely clear, but biomineralization has been associated to resistance to herbivory (Bauer et al., 2011).

The epidermis is a complex tissue which plays essential roles in plants and which can respond dynamically to environmental cues to ensure the maintenance of the optimum conditions for the fulfilment of the physiological functions of plants. All the cells of the aerial epidermis develop and act in an organised manner and therefore epidermal development must be regulated tightly to ensure the optimal organisation (stomatal and trichome densities, pavement cell size, cuticle thickness and composition) for any given conditions.

1.1.2.-Types of trichomes in cultivated tomato and wild relative species.

Trichomes in tomato species were systematically classified by (Luckwill, 1943), although the established trichomes types (Fig. 1.3) were revisited by (Simmons and Gurr, 2005), and (Glas et al., 2012) to some extent. Tomato has glandular and non-glandular trichomes, that can be further subdivided into seven types defined by their morphology, although some authors have claimed the existence of an eight type (Channarayappa et al., 1992). Type II, III, V and VIII are non-glandular trichomes. Type II trichomes have a long multicellular stalk (0.3-1 mm) and a multicellular base, while type III trichomes have a similar stalk but have a unicellular base. Type V are shorter (0.1-0.3 mm). Finally, type VIII is described as a consisting of a thick basal cell with a leaning cell on top. Four types of glandular trichomes have also been described. Type I trichomes are similar to type II trichomes, but they have a single-celled glandular head at the

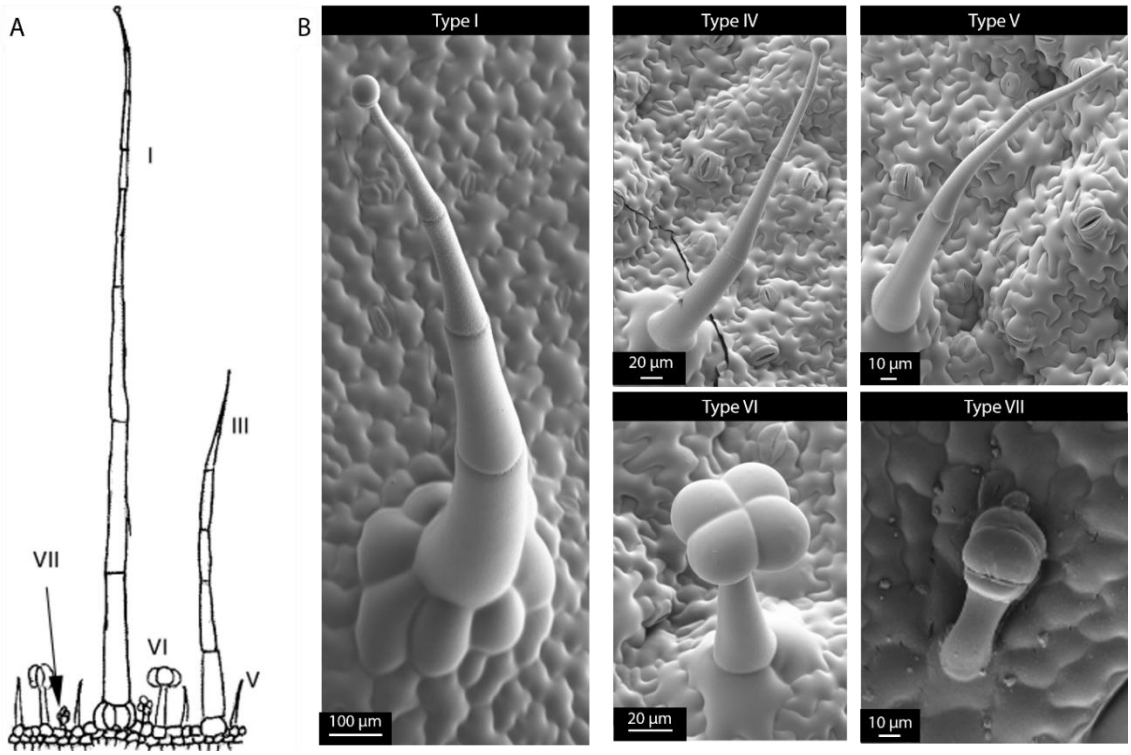

Figure 1.3.-Trichome types in *Solanum lycopersicum.* A) Schematic representation of trichome types found on cultivated tomato. This figure was borrowed from (Simmons and Gurr, 2005) and I obtained written permission for reuse from the copyright holder (Jon Wiley and Sons Ltd) under licence number 4422041317000. B) Cryo-scanning electron micrographs of the different trichome types found in tomato. Scale bars are shown for each micrograph.

top of the multicellular stalk and are slightly longer (up to 2 mm). Type IV trichomes are similar to type V, but they have a glandular head similar to that found in type I trichomes. In fact, the metabolic composition of secretions from trichome types I and IV are very similar, and some authors have considered them as the same trichome type (Kang et al., 2010a, McDowell et al., 2011). Type VI trichomes have a four-celled glandular head and are shorter than most of the other trichomes (0.1 mm). Type VII trichomes are the shortest type (<0.05 mm) and have a glandular head with multiple cells (4 to 8). For further discussion, type VIII will not be considered as no other authors considered their presence and I have never found type VIII trichomes in any tissue of *S. lycopersicum*.

In the cultivated tomato, *S. lycopersicum,* type II and IV trichomes are reported to be absent (Luckwill, 1943). However, a recent study on the differences between trichome types in juvenile and mature tissue showed that type IV trichomes are very abundant in cotyledons and young leaves (Vendemiatti et al., 2017) in *S. lycopersicum.* The morphological similarity between type IV and V (identical except for the glandular head) and the alternation in their absence/presence patterns have led to the postulation that they may be variants of the same type of trichome, and depending on leaf age or other signals, they may develop a glandular head (Vendemiatti et al., 2017). In wild tomato species, different trichome types are present and in different proportions (Table 1.1). For example, in *Solanum pennellii,* a highly stress-tolerant species (Bolger et al., 2014), type II and type V are absent, while type IV is the most common type of trichome, in contrast to cultivated tomato. *Solanum habrochaites* shows a very similar distribution of trichome types to *S. pennellii,* but with higher densities of those trichome types that are present. *S. pimpinellifolium* is considered to be the closest wild relative to cultivated tomato (Peralta, 2008) and its profile of trichome types is more similar to that of *S. lycopersicum* than to any of the wild relatives; type IV are absent and type V and IV are highly abundant. Many other tomato species have been characterised (Simmons and Gurr, 2005), although those presented in Table 1.1 are the ones most commonly used in research and breeding, especially *S. pennellii* (Barrantes et al., 2014).

Apart from the morphological differences between different glandular trichomes, each glandular trichome type produces a specific metabolic profile, which is also species-dependent (Glas et al., 2012). For example, type I and type IV trichomes are considered as centres of production of acyl sugars (McDowell et al., 2011). However, the specific structures of the acyl sugars differ between species. Acyl sugars in *S. lycopersicum* are mostly acylsucroses with 5-carbon branched acyl groups or 12-carbon linear moieties, while in *S. pennellii* they are mainly acylglucoses with 4-carbon or 8-carbon branched acyl moieties (Leckie et al., 2016, Nadakuduti et al., 2017). Type VI trichomes produce terpenes, flavonoids and methyl ketones, and the

	Trichome Type						
Species	I	II	III	IV	V	VI	VII
Solanum lycopersicum	A	-	A	-	A	A	S
Solanum pennellii	VS	-	VS	A	-	S	VS
Solanum pimpinellifolium	-	VS	-	-	A	A	-
Solanum habrochaites	A	-	S	A	-	A	S

Table 1.1.-Abundace of each trichome type in selected *Solanum species.* The letter code is as follows: A-Abundant, S-Scarce, VS-Very Scarce and the dash indicates absence of the specific trichome type. Information adapted from (Simmons and Gurr, 2005).

specific composition is also highly variable between species and accessions (Bergau et al., 2015). It is interesting to note that type VI trichomes are photosynthetic, but their high demand for carbon makes them strong sucrose sinks from the leaf (Balcke et al., 2017). The scarcity of type VII trichomes has being an obstacle to attempts to characterise the specific metabolites synthesised by these trichomes, but some evidence points towards the accumulation of alkaloids such as tomatine (McDowell et al., 2011) or production of insecticide protease inhibitors (Glas et al., 2012).

1.2.-Development of epidermal features.

Our current knowledge of epidermal differentiation in plants is based mostly on the model species *Arabidopsis thaliana*, due to the availability of genetic resources for this species (Rerie et al., 1994, Marcotrigiano and Bernatzky, 1995, Yang and Sack, 1995). However, studies on epidermal development have been performed for many other plant species, including analysis of petal development in ornamental species such as snapdragon (Noda et al., 1994) or petunia (Baumann et al., 2007) and crops as maize (Ingram et al., 1999) or tomato (Lashbrooke et al., 2015). This introduction section will aim to cover the developmental processes involved in development of aerial epidermis in embryonic and vegetative tissues, as well as the regulatory genes governing these processes.

1.2.1.-Epidermal development in embryo: from zygote to mature embryo.

After fertilisation of the egg cell by one of the pollen sperm nuclei, an asymmetric zygote is formed, with one pole of the cell containing the diploid nucleus and most of the cytoplasm, while the other pole is occupied by the vacuole. The zygote divides asymmetrically into a two-celled embryo, with the small terminal cell developing into the embryo proper, and the large basal cell developing into the suspensor (Goldberg et al., 1994). The embryo proper will continue dividing to form all the embryonic organs -cotyledons, shoot apical meristem (SAM), hypocotyl, root apical meristem (RAM) and radicle -, all of which are covered by an already differentiated epidermal layer, normally denominated as the protoderm (Javelle et al., 2011). In *Arabidopsis*, the presence of a differentiated epidermal layer occurs very early in embryo development, after four divisions of the zygote, and cells of this layer will divide only in an anticlinal fashion (Fig. 1.4) (Ingram et al., 1999). The protodermal cells are characterised by their thicker cell walls and more regular shape, traits that are accentuated after a number of divisions (Javelle et al., 2011).

The correct specification of the protodermal cell layer – and therefore of the correct development of the embryo – depends on a number of regulators that act at different levels (ten Hove et al., 2015). For example, the correct periclinal division of the early four-celled embryo proper to create the first protodermal cells is controlled by the Wuschel-related homeobox (WOX) transcription factor WOX2 (Breuninger et al., 2008). Other WOX factors are

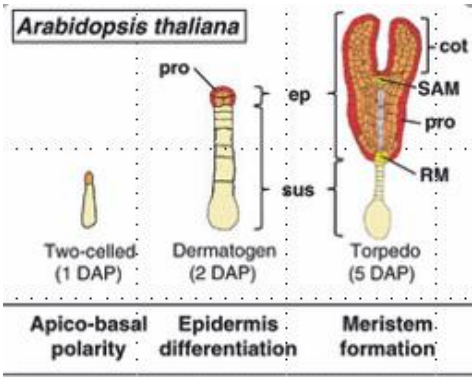

Figure 1.4.-Early stages of embryo development in *Arabidopsis thaliana*. The figure shows the three first stages of embryo development: two-celled (1 day after pollination, DAP), dermatogen (2 DAP), when the protodermal layer differentiates and torpedo (5 DAP). The orange cells correspond to the embryo proper (labelled ep), red cells correspond to the protodermal layer (labelled pro), beige cells correspond to the suspensor (labelled sus) and yellow cells correspond to the shoot apical meristem (labelled SAM) and the root apical meristem (labelled RM). This image was borrowed and adapted from (Javelle et al., 2011) with permission from the copyright holder (Jon Wiley and Sons Ltd) under licence number 4422561025470.

expressed in the embryo and coordinate the correct division of the basal and apical cells, with some overlap and complementarity in their function (Haecker et al., 2004). For example, the *wox2* mutant defect in protodermal development is enhanced in *wox2 wox8* double mutants (Breuninger et al., 2008). These WOX transcription factors regulate auxin transport to create auxin positional signals that determine the plane of division (ten Hove et al., 2015). Two closely-related HD-ZIP class IV transcription factors are also known to regulate epidermal determination in the embryo, *Arabidopsis thaliana* Meristem Layer 1 (ATML1) and protodermal factor 2 (PDF2). Double-mutants of the genes encoding those proteins failed to develop an epidermis (Abe et al., 2003), with the corresponding structural homologue in maize (ZmOCL1) performing the same function (Ingram et al., 1999), suggesting a general involvement of HD-ZIP class IV proteins in epidermal development in angiosperms. The activity of these transcription factors is regulated by receptor kinases in the embryo (Arabidopsis Crinkly 4-ACR4-) and the endosperm (GASSHO1 and GASSHO2-GSO1 and GSO2-) (San-Bento et al., 2014). Other genes, such as the leucine-rich repeat receptor-like kinases RPK1 and RPK2 are necessary for the correct patterning of divisions in the embryo (Nodine et al., 2007), although their ligands and regulatory targets are not known.

The protodermal layer of cells grows in an anticlinal way around the rest of the embryo, and it will constitute the epidermis of the cotyledons as well as most of the external layer of the shoot apical meristem (SAM), denominated L1. This L1 layer will develop into a fully differentiated epidermis in vegetative tissues, containing all the different structures discussed in the previous section.

1.2.2.-Development of stomata.

Stomatal development and patterning requires a number of successive divisions of a specific lineage of protodermal cells called meristemoid mother cells (MMC). MMCs divide asymmetrically to generate a smaller meristemoid and a bigger stomatal-lineage ground cell (SLGC). The meristemoid then divides asymmetrically up to four times, maintaining the meristemoid and generating a new SLGC in each cycle, a process termed amplifying division. The meristemoid, which has stem cell characteristics, can transition to a guard mother cell (GMC) which can divide symmetrically to generate the two final guard cells. SLGC cells can become pavement cells or divide asymmetrically again before, in a process called spacing division, generating a new meristemoid, always distal to the one originated in the first MMC division. This mechanism ensures an even distribution of stomata on the epidermal surface, with at least one pavement cell lying between any two given stomata (Geisler et al., 2000). The stomatal lineage division process (Fig. 1.5) was first described by (Zhao and Sack, 1999) and it has been used as a model for stomatal development in dicotyledonous species, while the process in monocots is known to be slightly different, as two asymmetrical divisions are required to generate the guard

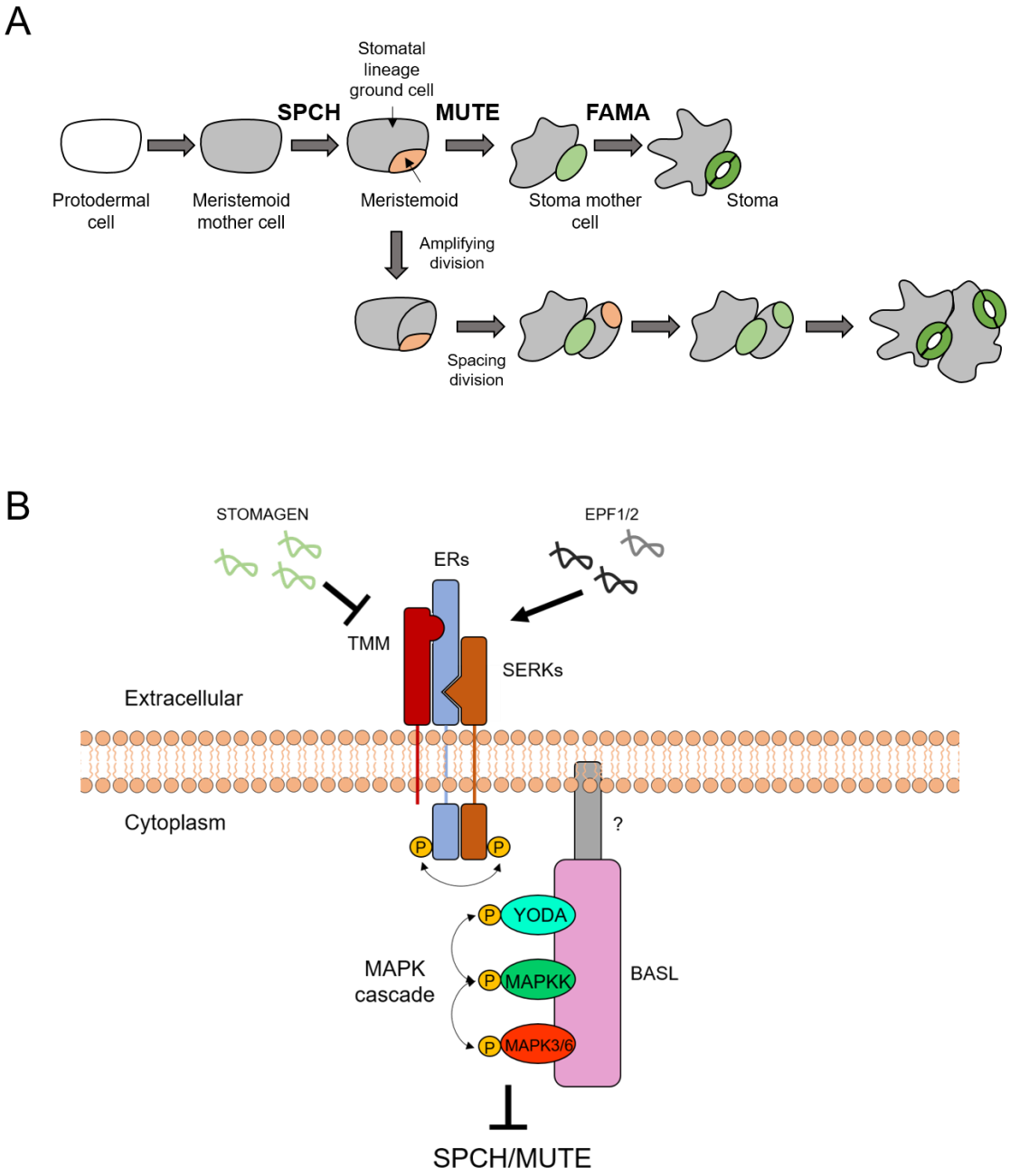

Figure 1.5.-Stomatal development in *Arabidopsis thaliana*. A) Schematic representation of the divisions of the stomatal cell lineage to generate mature stomata. The bHLH transcription factor regulating each transition are indicated in the diagram (SPCH, MUTE and FAMA). B) Schematic representation of the proteins involved in the epidermal patterning factor signalling pathway. The MAPK cascade, activated by the ER/TMM/SERK complex, ultimately inactivates the bHLH transcription factor SPCH, and possibly MUTE.

cells and a set of accompanying cells called subsidiary cells (Hepworth et al., 2018). As the focus of this thesis is on epidermal development in tomato, I will focus on the model for dicots.

The asymmetrical divisions to form the guard mother cells are regulated by a number of different genes which have been characterised over the last decade (Bergmann and Sack, 2007, Marcos et al., 2016). In *Arabidopsis,* three basic-helix-loop-helix (bHLH) transcription factors regulate the division pattern of the stomatal lineage; SPEECHLESS (SPCH), MUTE and FAMA (Torii et al., 2007). SPCH is expressed in protodermal cells and it is responsible for the first asymmetrical division leading to the formation of meristemoids and *spch* mutants have no stomata on their epidermis (MacAlister et al., 2007). MUTE regulates the transition from meristemoid to GMC, and *mute* mutants show an abnormally high number of asymmetrical divisions that led to early abortion of meristemoids. MUTE overexpressors change the identity of all epidermal cells to guard cells (Pillitteri et al., 2007). FAMA regulates the transition from GMCs to guard cells, and the *fama* mutant shows an abnormal number of symmetric divisions of GMCs, but no mature guard cells (Bergmann et al., 2004). Two other bHLH transcription factors, SCREAM1 (SCRM1) and SCREAM2 (SCRM2), are known to form heterodimers with SPCH, MUTE and FAMA to drive their functions, as shown by the *fama*-like phenotype of the *scrm1* mutant, the *spch*-like phenotype of the *scrm1 scrm2* double mutant and the *mute*-like phenotype of the *scrm2 scrm1/+* mutant (Kanaoka et al., 2008). Finally, two MYB R2R3 transcription factors, FOUR LIPS (FLP) and MYB88, have been identified as redundant regulators of the symmetrical division causing a transition from GMCs to mature guard cells, with *flp* mutants showing two stomata clustered together due to an extra symmetric division and the *flp myb88* double mutant showing clusters of abnormal stomata similar to the *fama* phenotype (Lai et al., 2005). The stages where each of these regulatory genes acts are indicated in Fig. 1.5.

The activity of these transcription factors is regulated by a peptide signalling pathway, which involves signal-transduction proteins (receptor and intracellular kinases) that ultimately regulate SPCH by phosphorylation (Zoulias et al., 2018).

Three defensin-like peptides modulate stomatal development in *Arabidopsis* leaves through this pathway, EPIDERMAL PATTERNING FACTOR1 (EPF1) (Hara et al., 2007), EPIDERMAL PATTERNING FACTOR 2 (EPF2) (Hunt and Gray, 2009) and STOMAGEN (STOM) (Sugano et al., 2010). Both EPF1 and 2 are negative regulators of stomatal development, while STOM, which competes with EPF1/2 to bind their common receptor, is a positive regulator of stomatal development (Sugano et al., 2010). EPF1 and EPF2 act at different stages of stomatal development. EPF2 is expressed by MMCs and prevents neighbouring protodermal cells from becoming MMCs by inactivating SPCH (Hara et al., 2009) while EPF1 is expressed in meristemoids and GMCs and it ensures correct spacing divisions and the transition to mature

guard cells by inactivating SPCH and MUTE (Qi et al., 2017). STOM is expressed in the mesophyll and induces stomatal formation by keeping SPCH active in protodermal cells, probably in response to the CO_2 needs of the inner leaf tissue (Sugano et al., 2010). In stem tissue, another EPF (called EPFL4 or CHALLAH) also acts as a negative regulator of stomatal development (Lin et al., 2017), indicating that stomatal development is under different regulation in different tissues. The signalling cascade is initiated by the binding of EPF peptides to leucine-rich-repeat receptor kinases (LRR-RK) genes, which are transmembrane proteins with an external domain, able to bind the signalling EPF molecules and a cytoplasmic kinase domain that can phosphorylate downstream proteins (ten Hove et al., 2011). In this case, ERECTA (ER) and ERECTA-like1 and 2 (ERL1 and ERL2) are known LRR-RKs binding EPFs. (Lee et al., 2015). The three ER genes redundantly regulate the asymmetric division of the MMCs and ERL1 and ERL2 can also regulate the transition of meristemoids to GMC (Shpak et al., 2005). These LRR-RK normally act together with leucine-rich-repeat receptor-like proteins (LRR-RLP), which contain an extracellular domain but lack the cytoplasmic kinase domain. In the context of stomatal development, the LRR-RLP is TOO MANY MOUTHS (TMM), which interacts with the ER receptors to generate binding pockets for EPFs, which otherwise cannot bind to the receptor (Lin et al., 2017). In the *tmm* mutant, there is an increased density of stomata, which appear in clusters, due to the inability of the ER family to recognise the EPF2-mediated signal (Geisler et al., 2000). TMM is necessary for recognition of EPF1, EPF2 and STOM, but it is not required for, and can even hinder, recognition of EPFL4, which might provide a mechanistic explanation for the tissue-specific regulation of stomatal development (Lin et al., 2017). Finally, another family of LRR-RKs, SOMATIC EMBRYOGENESIS RECEPTOR KINASE (SERK), interacts with the ER/TMM complex and is required for downstream signalling, probably by transphosphorylation of the cytosolic domains of ERs and SERKs (Meng et al., 2015).

The intracellular transduction of the EPF-mediated signal involves a cascade of mitogen-activated protein kinases (MAPKs) (Lampard et al., 2008). The ER/TMM/SERK complex targets a MAPK kinase kinase (MAPKKK) called YODA (YDA) (Bergmann et al., 2004). The *yda* mutant produces an excessive number of clustered stomata, which is explained by the inability of the mutant to inactivate SPCH through the EPF pathway (Bergmann et al., 2004). The phosphorylated, activated version of YDA can then phosphorylate its MAPK kinase targets, which have been identified as MAPKK4/5/7/9 (Lampard et al., 2014). These proteins, when activated, can phosphorylate MAPKs, which, in the context of stomatal development, have been identified as MAPK3/6. MAPK3 and MAPK6 have been shown to target directly SPCH for inactivation (Lampard et al., 2008), while MUTE or FAMA do not seem to be regulated by this specific pathway as no phosphorylation domains are present in these transcription factors (Qi

et al., 2017). MAPK cascades normally rely on scaffold proteins for cell-specific and effective signal transduction. In the EPF pathway, such an scaffold protein has been described and called BREAKING OF ASYMMETRY IN THE STOMATAL LINEAGE (BASL) (Dong et al., 2009). *basl* mutants show clustered stomata, and BASL is asymmetrically distributed before the MMC division, with the SLGC containing higher amount of this protein than the meristemoid (Zhang et al., 2016b). This ensures effective inactivation of SPCH in the SLGC to maintain stomatal patterning.

All the regulatory genes described in this section are graphically represented in Fig. 1.5.

1.2.3.-Development of trichomes

1.2.3.1.-Development of trichomes: structural aspects.

Trichomes are epidermal outgrowths with a very distinct morphology, which differs greatly from other epidermal cells, and their development involves a series of structural changes to reach their mature form. Most of the studies of trichome morphogenesis have been performed in *Arabidopsis,* which forms only non-glandular unicellular trichomes with three branches. Given the morphological diversity of trichomes, the available information cannot be extrapolated to all other species. For most species, trichomes are the first cells to undergo differentiation in the leaf primordia, when protodermal cells are still dividing. The final location and number of epidermal cells that lie between mature trichomes is determined later in leaf development (Larkin et al., 1996), although in some cases, such as cotton ovules, trichomes are initiated when the organ is fully developed (Larkin et al., 1997). In *Arabidopsis,* trichome development is not homogeneous, with trichomes developing earlier on the margins and distal area of the leaf (Larkin et al., 1996). New trichomes can be initiated among mature trichomes in *Arabidopsis* and tobacco (Uzelac et al., 2015), indicating trichome initiation is asynchronous. Trichome morphogenesis in *Arabidopsis* has been traditionally divided into six different stages (Szymanski et al., 1998). The first stage is defined by radial growth of the cell committed to form a trichome with respect to its surrounding cells. At this stage, endoreplication of DNA is already taking place. Once the stalk of the developing trichome is fully formed (two to three diameters larger than the surrounding cells), the second stage is reached. The third stage consists of the formation of two new growth foci, normally oriented along the basal-apical axis, that will give rise to the trichome branches. One of the branches then produces a new branch point that generates the final number of branches (generally three), which grow with blunt ends (stage four). Stage five is reached when the trichome shape is mature, with pointed ends in the branches. The sixth stage consists of the maturation of the trichome cell wall and the formation of papillae on its surface. This developmental process is similar to that of glandular trichomes, although of course not identical. In species where many types of trichomes are present, it is impossible to determine the identity of the trichome morphologically in the early stages of morphogenesis

(Fig. 1.6) (Werker, 2000). In multicellular glandular trichomes of tobacco, trichome initiation starts with commitment of a protodermal cell to radial growth to generate a protuberance, identical to the process in *Arabidopsis,* except for the lack of endoreduplication (Huchelmann et al., 2017). The nucleus of the trichome initial migrates to the tip of the protuberance, where the first cell division takes place, and an apical and a basal cell are formed. The next stage involves the asymmetrical division of the apical cell to generate a smaller glandular head and a larger stalk cell. The final trichome results from several rounds of division in the stalk cell, and sometimes divisions of the glandular head (Uzelac et al., 2015). The basal cell does not divide any further, and it forms the trichome base. It would not be surprising, however, that basal cells in trichomes with multicellular bases (as type I trichomes in tomato) undergo further division cycles. This process has been also documented in type VI in trichomes, and it takes place in the exact same way (Bergau et al., 2015). However, observations in plant species from other families have shown that trichome morphogenesis can involve the division of the apical or basal cells at different stages, and might not always be the product of a universal pattern of division (Werker, 2000).

Trichome morphogenesis depends on two main cellular processes: rapid directional growth and endoreduplication/division (depending on the type of trichome). Directional growth requires loosening of the cell wall and rearrangement of the cytoskeleton. The cell wall contains several polymers, mainly cellulose microfibrils, hemicellulose (as xyloglucans), which tether the cellulose microfibrils, and pectin, which creates a matrix for the rest of the cell wall components. Some other elements, such as cell wall proteins, are also present in the cell wall (Yokoyama et al., 2014). The increase in turgor by water uptake of the growing cell causes mechanical strain on the relatively rigid cell wall, which needs to be remodelled to allow cell expansion. The cell wall is flexible enough to allow cell expansion without requiring the tightly coordination of production of new cell wall components (Cosgrove, 2016). However, rapid polarised growth, such as that observed in the growth of pollen tubes and possibly trichomes, normally involves simultaneous deposition of different cell wall components (Rojas et al., 2011). Enzymatic lysis of the cell wall components has traditionally been considered as a main component of cell wall loosening, especially by hydrolysis of the bonds between hemicellulose and cellulose microfibrils, thought to be load-bearing points (Veytsman and Cosgrove, 1998). However, the analysis of xyloglucan-deficient mutants in *Arabidopsis* revealed a weak phenotype and little effect on cell expansion (Park and Cosgrove, 2011), which has recently led to the proposal of new models, in which cellulose microfibre contact points have major load-bearing properties (Cosgrove, 2016). This model is supported by the observation that cell wall loosening occurs mainly when cellulose and xyloglucan were hydrolysed simultaneously

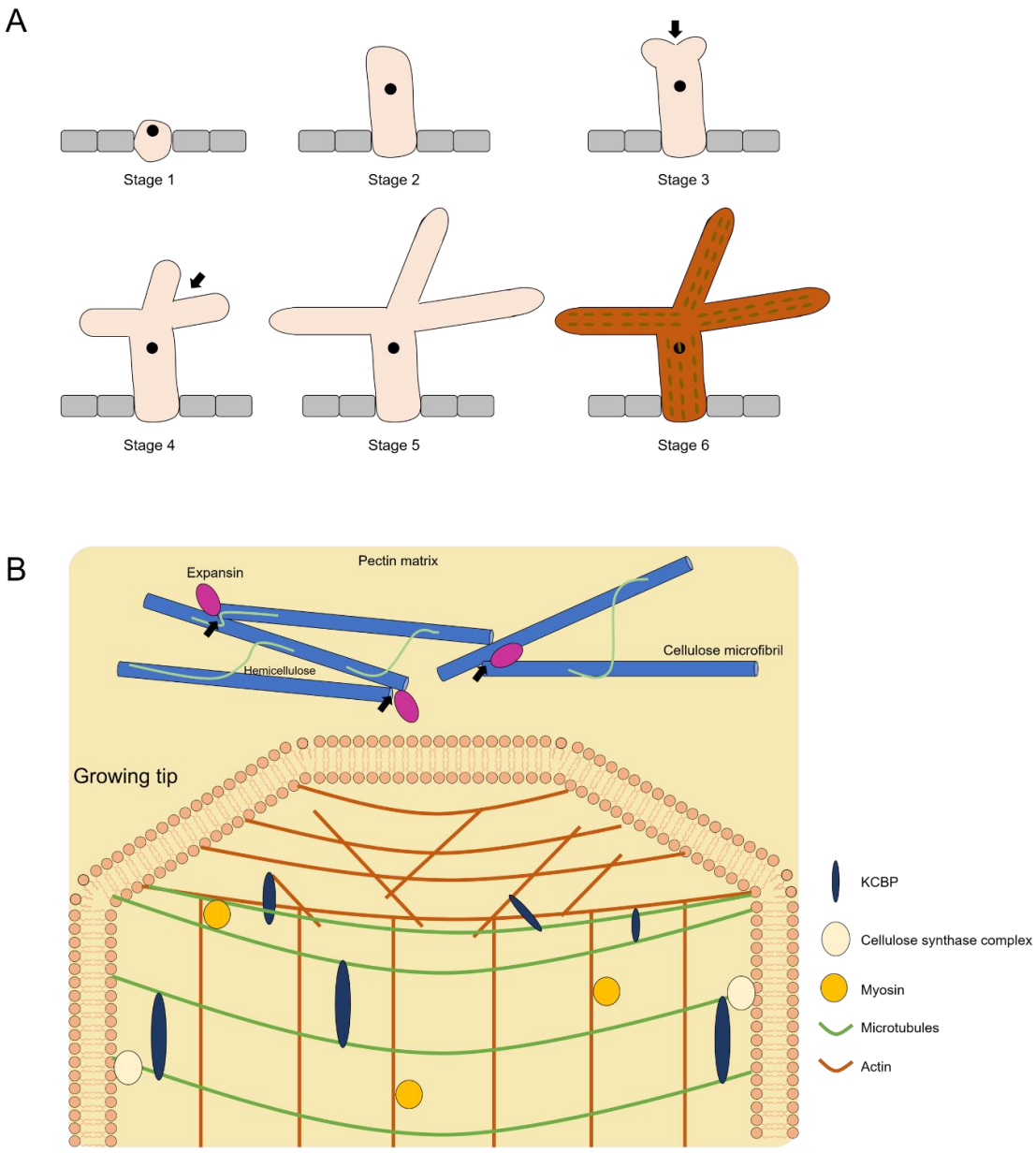

Figure 1.6.-Cellular processes in trichome development in *Arabidopsis*. A) Developmental stages of trichomes in *Arabidopsis thaliana*, as described in (Larkin et al., 1996). B) Schematic representation of cell wall and cytoskeleton processes involved in polar growth in *Arabidopsis* trichome branches. In the upper part, cellulose microfibrils are represented in blue, with hemicelullose polymers represented in green. Black arrows indicate load-bearing contact points between microfibrils, which are targeted by expansins, represented in purple. In the lower part, the cytoskeleton arrangement of the growing tip is shown, with microtubules represented in green and actin filaments represented in brown. KCBP are represented in blue, and myosin and cellulose synthase complexes are shown for representation.

(Park and Cosgrove, 2012). Currently no plant enzymes with this dual activity have been identified and the net contribution of cell wall enzymatic lysis may be probably smaller than initially thought. However, plants encode a set of small proteins called expansins which promote cell wall loosening in a non-enzymatic way (McQueen-Mason et al., 1992). Their exact mode of action is unclear, but they are known to bind cellulose (McQueen-Mason and Cosgrove, 1995) and other cell wall polymers (Nardi et al., 2013), and are believed to disrupt hydrogen bonds between cell wall components (probably between cellulose microfibrils) to induce relaxation of the cell wall (Cosgrove, 2015). The fact that expansins are key players of polarised cell growth in systems such as root hair initiation (Cho and Cosgrove, 2002), together with the fact that there are some expansins specifically expressed in trichomes (Cosgrove, 2000), indicates that expansins are likely to play a major role in the rapid polarised cell growth of trichomes (Fig. 1.6).

The cell cytoskeleton, formed by microtubules and actin filaments, is essential for cell growth. Microtubules are tightly associated with the cellulose synthase complex via cellulose-synthase interacting proteins, which determine their trajectory and expansion of the cell wall (Oda, 2015). During polar growth in trichomes, microtubules are organised transversely to the expansion axis, and the formation of a microtubule-depleted zone at the tip of the growing trichome or trichome branch is essential for correct morphogenesis (Tian et al., 2015). Actin filaments, on the other hand, are arranged longitudinal to the growth axis and also forming a fine mesh in the growing tip of the trichome (in the microtubule-depleted area) (Tian et al., 2015, Yanagisawa et al., 2015). These actin filaments direct transport of Golgi-derived vesicles via myosin transporters, and therefore likely serve to transport plasma membrane and cell wall components to the growing tip of the trichome (Smith and Oppenheimer, 2005). The importance of the correct organisation of the cytoskeleton in trichome development was confirmed by analysing the actin filaments in *Arabidopsis* mutants showing a distorted phenotype (Mathur et al., 1999). Six different mutants with the same phenotype showed aberrant organisation of actin, and the phenotype could be replicated by chemical inhibition of actin (Mathur et al., 1999). The same study showed that chemical inhibition of microtubule organisation affected trichome branching, but not elongation (Mathur et al., 1999). Subsequent studies revealed that the mutated genes either belonged to Actin-related protein2/3 (Arp2/3) complex, involved in branching of actin filaments, or the WASP family verprolin homologous protein (WAVE) complex which regulates the actin filament organisation (Szymanski, 2005). In tomato, the *hairless* mutant, which also displays a trichome-distorted phenotype, harbours a knock-out mutated version of SRA1, which encodes a member of the WAVE complex (Kang et al., 2016), and is a homolog of the PIROGI gene in *Arabidopsis,* where the *pir* gene shows a distorted-trichome phenotype (Basu et al., 2004). Recently, a kinesin-like calmodulin-binding protein (KCBP), known

to regulate trichome branching through reorganisation of the microtubule cytoskeleton (Mathur and Chua, 2000), has been shown to interact with both microtubules and actin filaments to generate the tip-located actin mesh required for polar growth (Tian et al., 2015), indicating a dynamic crosstalk between cytoskeleton components in trichome morphogenesis (Fig. 1.6).

Coordination of the cell cycle in developing trichomes is important for correct epidermal patterning and trichome morphogenesis. *Arabidopsis* trichomes are unicellular, but they undergo endoreplication cycles that increase the DNA content to up to 64 copies of the nuclear DNA, which has been associated with an increase in cell volume (Melaragno et al., 1993). In contrast, multicellular trichomes in species such as tobacco and tomato have normal DNA content and undergo a variable number of cell divisions (Werker, 2000). Trichome patterning, unlike the case for stomata, is not associated with a specific cell lineage (Larkin et al., 1996), and relies in cell-to-cell positioning signals. However, alterations to the cell cycle can result in the formation of clonally-related clustered trichomes. This is the case of the phenotype of the *sim Arabidopsis* mutant, which encodes a defective version of the cyclin-dependent kinase SIAMESE. The *sim* mutant produces multicellular trichomes often found in clusters, which have a reduced DNA content, as SIAMESE regulates endoreplication. Therefore, in *sim* mutants, trichome initials are mitotically active and can divide early in trichome morphogenesis generating a cluster of trichomes. In all other aspects, the morphology of *sim* trichomes is not affected (Walker et al., 2000). However, morphology has been shown to be affected by other cell-cycle related genes. The *BRANCHLESS TRICHOMES* (*BLT*) gene was shown to affect endoreplication, while the *blt* mutant had trichomes without branches (Kasili et al., 2011). Moreover, ectopic expression of a type-D cyclin (normally involved in initiating DNA replication) in trichomes caused mitotic divisions, accompanied by an excessive number of branches and aberrant morphologies (Schnittger et al., 2002) in *Arabidopsis*. In tomato, silencing of a type-B cyclin (controlling the transition to mitosis) led to the formation of aberrant branched trichomes (Yang et al., 2011a). This evidence indicates a tight link between the cell cycle and trichome morphogenesis in both single-celled and multicellular trichomes.

1.2.3.2.-Transcriptional regulation of trichome development in *Arabidopsis.*

The use of *Arabidopsis* trichomes as a model for cell differentiation has resulted in the identification of a large number of transcription factors involved in regulating their development, including trichome initiation, branching and their correct morphogenesis and patterning by inhibition of initiation in cells neighbouring a trichome initial.

The transcriptional regulation of trichome initiation in *Arabidopsis* has been studied extensively (Pattanaik et al., 2014). Trichome initiation is positively regulated by a complex formed by an R2R3 MYB transcription factor, a bHLH transcription factor and a WD40 repeat (WDR) protein

(MBW complex). The first MYB transcription factor identified as part of this complex was GLABROUS1 (GL1) (Oppenheimer et al., 1991, Larkin et al., 1994), from the *gl1* mutant, which lacks trichomes in its leaves. A paralog of GL1, MYB23, was shown to regulate trichome initiation in leaf edges also by forming part of the MBW complex (Kirik et al., 2005). More recently, an unrelated MYB transcription factor, MYB82, was shown to be functionally equivalent to GL1 and able to form part of the MBW complex (Liang et al., 2014). The first bHLH members of this MBW complex where GLABRA3 (GL3) (Payne et al., 2000) and ENHANCER OF GLABRA3 (EGL3) (Zhang et al., 2003), which appear to act redundantly in trichome initiation, as evidenced by analysis of single *gl3* and *egl3* mutants (both with limited phenotypic differences compared to wild type) and the double mutant *gl3 egl3,* which is completely glabrous (Zhang et al., 2003). Two other bHLH factors were later identified as members of the MBW complex. TRANSPARENT TESTA 8 (TT8) shows partial redundancy with GL3 and EGL3, regulating trichome initiation only in leaf margins (Maes et al., 2008). AtMYC1, a closely related bHLH factor, also positively regulates trichome initiation, with *atmyc1* mutants showing fewer trichomes (Zhao et al., 2012). Only one WD40 protein has been identified as a positive regulator of trichome initiation, TRANSPARENT TESTA GLABRA1 (TTG1), and it is involved in the interactions with different combinations of the previously mentioned MYB-bHLH transcription factors. The *ttg1* mutant is glabrous, and also unable to produce anthocyanins (Walker et al., 1999). Activation of the MBW complex activity initiate trichome formation by regulating the expression of target structural and regulatory genes required for trichome morphogenesis.

The genes targeted by the GL3 (and MBW partners) have been analysed (Morohashi and Grotewold, 2009). This has revealed that SIAMESE and RETINOBLASTOMA RELATED1 (RBR1) expression is induced by the MBW complex, and both genes involved in endoreplication (Walker et al., 2000, Desvoyes et al., 2006), which is the first step required for trichome initiation. Another well characterised target is *GLABRA2* (*GL2*), which encodes a class IV HD-ZIP transcription factor. The *gl2* mutant is apparently glabrous, but it produces aborted trichomes that grow parallel to the leaf surface (Szymanski et al., 1998). Interestingly, GL2 can positively induce the expression of *MYB23*, generating a positive feedback loop (Khosla et al., 2014), probably displacing GL1 from the MBW complex to activate genes that are required for trichome maturation (Morohashi and Grotewold, 2009). A functional overlap of GL2 and a closely related HD-ZIP class IV gene, *HOMEOBOX GLABROUS11* (*HDG11*) has been found, although this gene does not seem to be under the direct regulation of the MBW complex (Khosla et al., 2014). Likewise, two other HD-ZIP class IV genes, *HDG2* and *HDG12* were found to play a key role in trichome branching and cell wall maturation (Nakamura et al., 2006, Marks et al., 2009), which probably indicates that these proteins act downstream of the MBW complex. Another known

target of *GL1* is *TRANSPARENT TESTA GLABRA 2* (*TTG2*), which encodes a WRKY transcription factor (Johnson et al., 2002). *ttg2* mutants show reduced trichome branching. Finally, MYB106 is necessary for early morphogenesis of trichomes and is a negative regulator of trichome branching (Gilding and Marks, 2010).

A group of small R3 MYB transcription factors have been identified as negative regulators of trichome initiation in *Arabidopsis*. They perform this function by competing with GL1/MYB23/MYB82 in the formation of the MBW complex, inhibiting the activation of downstream genes (Pattanaik et al., 2014). The first genes identified in this group were TRIPTYCHON (TRY) (Schnittger et al., 1999) and CRAPICE (Wada et al., 1997). The *cpc* mutant shows an increase in trichome number while the *try* mutant shows clustered trichomes (Schellmann et al., 2002). ENHANCER OF TRY AND CPC1/2/3 (ETC1/2/3) were shown to act redundantly with TRY and CPC (Kirik et al., 2004a, Kirik et al., 2004b, Wester et al., 2009). The *etc1* and *etc2* mutants show an increase in trichome number, while the *etc1* mutant has no evident phenotype. However, the loss of function of ETC1 enhanced the phenotype of the single *etc1* and *etc2* mutants, indicating functional redundancy. Finally, two more R3 MYB transcription factors, TRICHOMLESS1/2 (TCL1/2) act redundantly with CPC to regulate trichome development in inflorescences. These negative regulators are key in maintaining trichome patterning. These genes are activated by the MBW complex, and given their small size, they can move from cell to cell to inhibit trichome initiation in the cells neighbouring a trichome initial (Zhao et al., 2008, Wester et al., 2009).

All these genes and their interactions in regulating trichome formation are summarised in Fig. 1.7.

1.2.3.3.-Transcriptional regulation of trichome development in tomato.

Research into the development of trichomes in species of the *Asterids* clade, which includes the model species *Nicotiana tabacum* and tomato, among other species of interest, soon revealed divergent pathways of genetic regulation of trichome development in comparison with *Arabidopsis* – and other species in the *Rosids* clade- (Serna and Martin, 2006). Overexpression of GL1, the key MYB transcription factor which activates trichome development in *Arabidopsis* (Larkin et al., 1994), did not cause any effect on trichomes in tobacco (Payne et al., 1999). Similarly, overexpression of *AmMIXTA*, encoding an unrelated MYB transcription factor from *Antirrhinum majus* which induces trichome and conical cell development ectopically in tobacco (Glover et al., 1998), did not affect trichome initiation in *Arabidopsis* and could not rescue the *gl1* mutant phenotype (Payne et al., 1999). In addition to this, expression of *SlG3*, the tomato homolog gene to GL3, in *Arabidopsis* did not have an effect on trichome phenotype (Tominaga-Wada et al., 2013). Moreover, *AmMIXTA* overexpression in tobacco affected only long

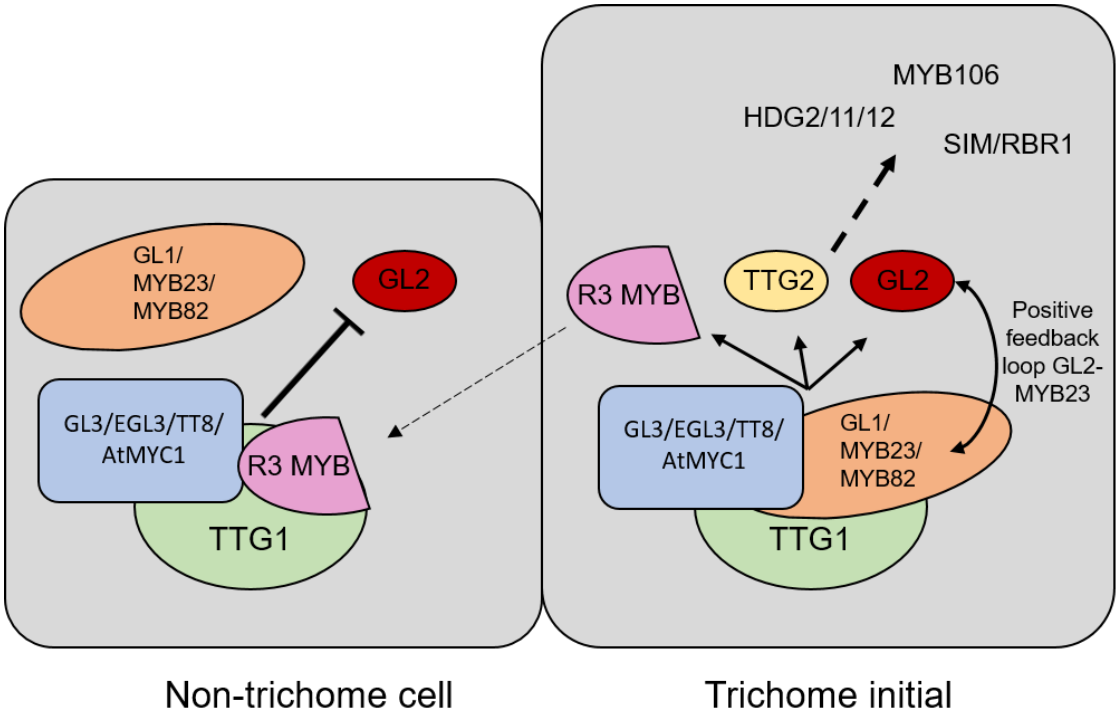

Figure 1.7.-Model for transcriptional regulation of trichome development in *Arabidopsis*. The MYB-bHLH-WD40 complex activates GL2, TG2 and downstream genes involved in trichome morphogenesis (MYB106, HDG2/11/12 and endoreplication genes), as well as small R3 MYB genes (CPC and TRY, among others discussed in the text). The latter genes can move to neighbouring cells to displace GL1 from the complex, inhibiting the activation of GL2 and downstream genes, and ensuring adequate trichome patterning. Positive interactions are indicated with an arrow line and negative interactions with a T-shaped line. Fine-dashed arrow indicates cell-to-cell movement. Wide dashed arrow indicates downstream targets.

multicellular trichomes in tobacco, while the number of short glandular trichomes (also termed hydathodes, which exude nicotine) was unaffected (Glover et al., 1998), indicating that different trichome types might be under the regulation of different regulatory factors. This is especially relevant for tomato, where many different types of glandular and non-glandular trichomes are found. Although these findings about the regulation of trichome development in *Arabidopsis* cannot be directly extrapolated to tomato, genetic advances in tomato, coupled with the analysis of trichome mutants, have led to the identification of important regulators of trichome development.

SlMX1, which is structurally closely related to AmMIXTA, was shown to control trichome development in tomato, while also regulating cuticle deposition and carotenoid content in fruit (Ewas et al., 2016). Overexpression of *SlMX1* resulted in a dramatic increase of all trichome types, as well as the formation of aberrant trichomes with multicellular branches and doubled stalks (which were also found in *AmMIXTA* overexpression lines of tobacco (Glover et al., 1998)). RNAi lines of *SlMX1* showed a reduction in trichome density and an almost complete absence of long, glandular type I trichomes (Ewas et al., 2017). These observations indicated that SlMX1 activates trichome initiation (probably by inducing anticlinal divisions, analogous to the induction of endoreduplication by the action of the GL1 MBW complex (Morohashi and Grotewold, 2009), which is evidenced by the increase in expression of the SlCycB2 gene in SlMX1 overexpression lines (Ewas et al., 2017)) and which is probably necessary for determination of the identity of type I trichomes.

Two class IV HD-ZIP genes have been identified as regulators of trichome development in tomato, which may perform a function analogous to that of GL2 and the functionally redundant HDG genes. Woolly was the first of these genes to be identified by genetic analysis of a hairy mutant (Yang et al., 2011a). Similar to GL2, which is not necessary for trichome initiation, but for downstream morphogenesis (Szymanski et al., 1998), Woolly was reported to only affect development of type I trichomes, and therefore can be considered a regulator of morphogenesis of this specific type rather than an activator of trichome initiation (Yang et al., 2011a). However, further analysis by overexpression of different Woolly alleles in tobacco seemed to induce trichome initiation (Yang et al., 2015), suggesting a dual role for this gene in both trichome initiation and morphogenesis, similar to SlMX1. In fact, recent studies in *Artemisia annua* showed the formation of a regulatory complex by interaction of a MIXTA-like protein (AaMIXTA1) and an HD-ZIP class IV gene (AaHD8) to induce trichome initiation (Yan et al., 2018). *A. annua* is an asterid, so the formation of a similar complex in tomato would not be surprising. A second gene, CUTIN DEFICIENT2 (CD2), was identified by genetic analysis of the *sticky peel* mutant, in which the fruit surface has a rubbery texture (Nadakuduti et al., 2012). Apart from

their aberrant cutin deposition, *cd2* mutants were found to have a reduced number of type VI trichomes (Nadakuduti et al., 2012). Therefore, CD2 seems to work in a similar way to Woolly, but controlling the identity of type VI trichomes instead of type I. This shows that there may be functional specialisation of HD-ZIP class IV genes in regulating trichome morphogenesis, instead of the redundancy observed in *Arabidopsis* to generate the same trichome type (Khosla et al., 2014).

The tomato homolog of TRIPTYCHON (SlTRY) was cloned and expressed in *Arabidopsis,* where it could repress trichome formation in WT and *cpc* plants (Tominaga-Wada et al., 2013). This suggested a role for R3 MYB transcription factors in trichome development in tomato. However, the native function in tomato was not tested, and the apparent lack of a MBW complex involved in trichome initiation raises new questions about the mechanism of action of SlTRY, which might be involved in regulating anthocyanin biosynthesis, which is dependent on a MBW complex in tomato.

Recently, a CH2H zinc finger transcription factor, HAIR, has been identified as a regulator of formation of type I and type VI trichomes (Chang et al., 2018). Type I trichomes are absent in the *hair* mutant, while type VI are greatly reduced. The analysis of the mutant, and subsequently generated overexpression and RNAi lines, was not undertaken quantitatively to determine whether the role of the gene was in trichome initiation or in trichome morphogenesis. Ectopic expression of SlHAIR in tobacco, as well as the pepper and tobacco genes in tomato, apparently induced trichome initiation, although proper characterisation of the number and type of trichomes was not performed, potentially masking the actual role of the HAIR protein (Chang et al., 2018). As HAIR has been shown to interact with Woolly, it is expected that their functions are shared, suggesting that HAIR plays a dual role in trichome initiation and determination of trichome identity (Chang et al., 2018). A possible scenario would involve HAIR, or other C2H2 zinc finger transcription factors, partnering with different HD-ZIP factors to determine the identity of newly initiated trichomes. A set of C2H2 genes in *Arabidopsis* are known regulators of trichome initiation, acting upstream of the MBW complex as part of the response to gibberellins (Gan et al., 2007) (which will be discussed in the next section). Whether HAIR acts in a similar way inducing initiation in response to gibberellins or whether its function is different remains to be clarified

The current model for transcriptional regulation of trichome development is shown in Fig. 1.8.

1.2.3.4.-Effect of phytohormones on trichome development.

Plant hormones are small molecules that integrate external and endogenous signals to modulate gene expression, which ultimately drives the different developmental processes in plants

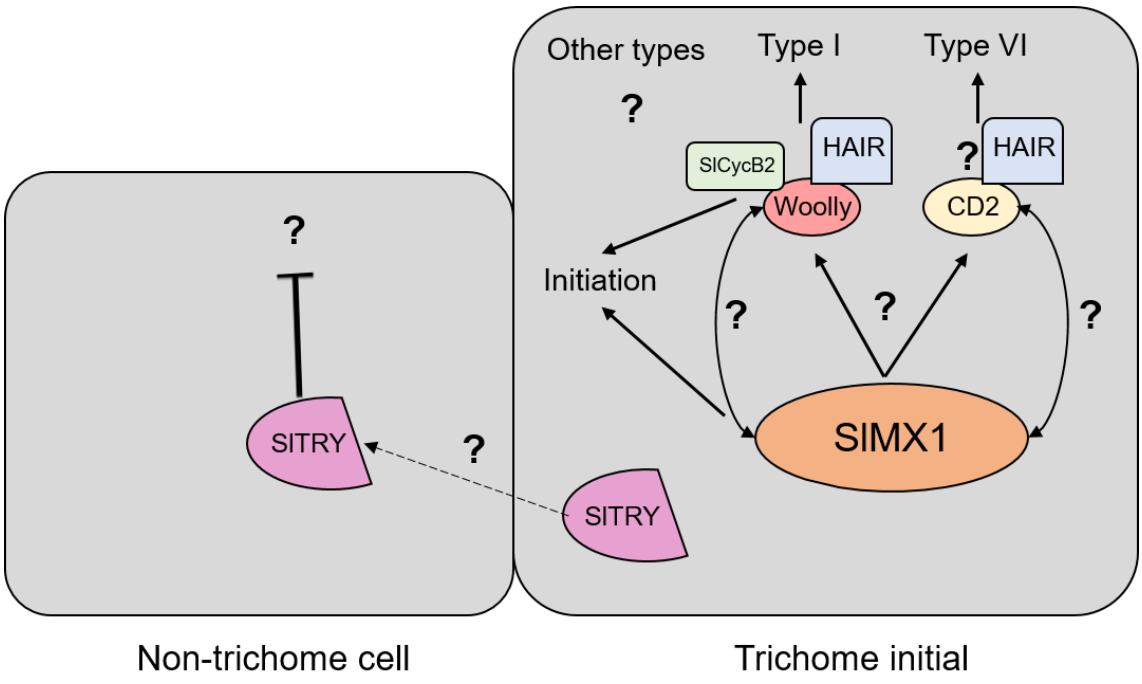

Figure 1.8.-Model for transcriptional regulation of trichome development in tomato. Initiation is activated by SlMX1 and the Woolly-HAIR-SlCycB2 complex. This complex can also regulate type I trichome morphogenesis. CD2 controls type VI trichome morphogenesis. SlTRY is a negative regulator of trichome initiation and might act in the same way as the R3 MYB genes in *Arabidopsis.* Positive interactions are indicated with an arrowed line and negative interactions with a T-shaped line. Question marks indicate possible interactions that have not been proven experimentally. Fine-dashed arrow indicate cell-to-cell movement.

(Gray, 2004). Numerous phytohormones have been identified: auxins, cytokinins, gibberellins (GAs), abscisic acid (ABA), jasmonic acid (JA), salicylic acid (SA), brassinosteroids (BR), ethylene (ET) and strigolactones (SLs) (Pozo et al., 2015). All of them, except for SLs, have been identified as regulators of trichome development in one or several species, and the signalling pathways in which they are involved in each case have been studied to different extents.

Auxin plays a major role in plant development and controls organogenesis by generating specific spatiotemporal patterns of development. Among other processes, auxin regulates polar root growth, stem elongation and leaf venation (Bar and Ori, 2014). Auxin generally functions through modulation of the activity of transcriptional regulators, which mainly include Auxin Responsive Factors (ARFs) and Aux/IAA genes, that can act as activators or repressors of downstream genes respectively (Liscum and Reed, 2002). Some of these genes have been reported to be involved in trichome development, suggesting a role for auxin in this process. For example, ARF3 was shown to regulate the juvenile-to-adult transition in *Arabidopsis*, which involves the appearance of abaxial trichomes in mature leaf tissue. Plants overexpressing ARF3 in a mutant background where siRNA-mediated silencing of ARF3 was abolished resulted in early formation of abaxial trichomes (Fahlgren et al., 2006). In tomato, RNAi-mediated silencing of SlARF3 resulted in a reduction in the density of type I, type V and type VI trichomes (Zhang et al., 2015). Similarly, silencing of SlIAA15 resulted in a reduction in trichome density and an increase in pavement cell size, while no similar phenotypes have been reported for *Arabidopsis* (Deng et al., 2012). In cotton, the transcription factor GhTCP14 regulates trichome development in an auxin-mediated manner (Wang et al., 2013). These different observations provide evidence for a role for auxin in trichome development, although this appears to be an indirect role.

GAs and cytokinins act synergistically in *Arabidopsis* to promote trichome formation (An et al., 2011). GAs can induce trichome initiation by activation of GL1 (Perazza et al., 1998), as it was also evidenced in the *spindly* mutant, which encodes a defective O-linked N-acetylglucosamine transferase that can alter protein activity in response to GAs (Qin et al., 2011), which showed an increase in trichome formation (Jacobsen and Olszewski, 1993). The induction of GL1 by GAs is mediated by a C2H2 zinc finger transcription factor, GLABROUS INFLORESCENCE STEMS (GIS). The *gis* mutant showed a decrease in trichome number, while GIS overexpression causes the opposite effect (Gan et al., 2006). More recently, other C2H2 zinc finger proteins have been identified as regulators of trichome formation as part of the GA response in *Arabidopsis*. GIS2, GIS3, ZFP5, ZFP6 and ZFP8 are all involved in this process (Gan et al., 2007, Zhou et al., 2011, Zhou et al., 2013, Sun et al., 2015). A hierarchical regulatory network has been established, in which GIS3, ZFP5 and ZFP6 act upstream of GIS, GIS2 and ZFP8 to induce trichome initiation (Sun et al., 2015). Interestingly, cytokinin, which normally acts in an antagonistic way to GA in

development (Greenboim-Wainberg et al., 2005), also can induce trichome initiation. The genes encoding C2H2 zinc finger described above are also responsible for the responses to cytokinin, and act as integrators of the GA and cytokinin signalling (Sun et al., 2015). The response to cytokinin and GAs has been studied in other plant species (Maes and Goossens, 2010). The response of two *Rosid* species, *Medicago truncatula* and *Populus tricocharpa,* which both produce multicellular trichomes, was comparable to that of *Arabidopsis.* In tomato, type I and type IV trichome development is induced by both hormones, but type VI trichomes only were induced by cytokinin. No other trichome types were affected. This indicates that the regulatory mechanisms in *Asterids* are probably different from those in *Rosids,* and that each trichome types is under different phytohormonal regulation.

ABA is considered to be a stress-related hormone, due to its role in regulating stomatal aperture under drought and pathogen stress (Lim et al., 2015). In tomato, the ABA-deficient *sitiens* mutant with deficient cuticle formation showed a reduction in trichome density (Curvers et al., 2010). No other reports of ABA inducing trichome formation exist for *Arabidopsis* or other species, which could indicate that the trichome phenotype is an indirect effect of the changes in the cuticle composition.

JA is a hormone involved in responses to wound and herbivory, as well as immunity against necrotorophic pathogens (Glauser et al., 2008), and it has been reported to often act antagonistically to SA, which is normally involved in immune responses to biotrophic pathogens (An and Mou, 2011). JA induces trichome development in *Arabidopsis* (Traw and Bergelson, 2003). Wounding of *Arabidopsis* leaves induces biosynthesis of JA (Glauser et al., 2008), and the elevated concentration of JA induces the degradation of JASMONATE ZIM-DOMAIN (JAZ) repressors by recruiting the ubiquitin ligase CORONATINE INSENSITIVE1 (COI1) (Thines et al., 2007), which then activates GL3 to induce trichome formation (Yoshida et al., 2009). In tomato, type VI trichome density increases upon treatment with JA (Boughton et al., 2005), and mutants in SlCOI1 showed a reduction in glandular trichome density (Li et al., 2004), suggesting a similar trichome induction by JA-signalling in both species. As a consequence of the negative crosstalk between JA and SA, responses to SA induce a reduction in trichome density in *Arabidopsis* (Traw and Bergelson, 2003). No reports of the effect of SA in tomato trichomes are available, but a similar effect to that of *Arabidopsis* might be expected given the effect of JA.

Ethylene is a gaseous hormone that regulates senescence, abscission, ripening and transition to the adult stage in vegetative tissues (Schaller, 2012). Ethylene affects trichome morphogenesis in several species. In *Arabidopsis,* the loss-of-function mutant of ETHYLENE RECEPTOR2 (ETR2), which senses ethylene and induces the downstream response by inactivation of the repressor CONSTITUTIVE TRIPLE RESPONSE1 (CTR1) (Grefen et al., 2008), has unbranched trichomes due

to alterations in the organisation of the microtubule cytoskeleton (Plett et al., 2009). Ethylene also stimulated trichome branching in cucumber and cotton (Kazama et al., 2004, Qin et al., 2007). No clear effects of ethylene application have been observed in tomato and responses to ethylene need to be investigated further (Tian et al., 2014).

BR is a steroid hormone with multiple roles in plant growth and development (Zhu et al., 2013). A mutant in BR-signalling in *Arabidopsis, bls1*, showed a reduced number of trichomes (Laxmi et al., 2004), while in tomato, a mutant deficient in BR biosynthesis, *dpy*, showed an increase in pubescence (Campos et al., 2009). A lack of characterisation of the molecular events underlying these observations makes it difficult to draw clear conclusions about the roles of BR in trichome development.

1.2.4.-Development of root hairs.

The work described in this thesis is based on analysis of the aerial epidermis of tomato. However, root hairs are also outgrowths of the epidermis that share some common features with trichomes, and their development may be linked to that of trichomes, and therefore it will be discussed briefly in this section.

Root hair patterning, as in the case of trichomes, is not lineage dependent but based on positional information, by which an epidermal cell becomes a root hair initial, which undergoes polar growth driven by auxins, which involves a highly organised actin cytoskeleton and remodelling of the cell wall, in a way analogous to trichome formation (Salazar-Henao et al., 2016). Interestingly, the regulation of root hair initiation in *Arabidopsis* also involves an MBW complex, in which the WD40 protein is also TTG1, and the bHLH is also GL3 or EGL3 (Zhang et al., 2003). However, the R2R3 MYB of the complex is not GL1, but WEREWOLF (WER), although WER is functionally equivalent to GL1 (Lee and Schiefelbein, 1999). When the MBW complex is active, it can induce expression of GL2, which in turn inhibits the initiation of root hairs (Lee and Schiefelbein, 1999). In the root hair initial, however, the R3 MYB factors CPC, TRY and ETC1 can compete with WER for binding the MBW complex, which inactivates the expression of GL2 and leads to the formation of a root hair (Schiefelbein et al., 2014). In this sense, regulation of cell fate determination in roots works in the opposite way to trichome initiation in the aerial epidermis. CPC, TRY and ETC1 are positively activated by the MBW complex, and they can move then to neighbouring cells to induce root hair formation. The current model also involves the movement of GL3 and EGL3 to non-hair cells (Savage et al., 2008). Regulation of cell fate in roots is modulated by a LRR-RLK, SCRAMBLED (SCM), which can inactivate WER in root hair initials (Kwak et al., 2005) upon recognition of positional signals from the underlying layer of cells, the nature of which is not clear, but which are believed to be induced by the zinc finger protein

JACKDAW (Hassan et al., 2010). A schematic representation of the regulatory network is shown in Fig. 1.9.

There are no tomato-specific reports of root hair development, but the morphological similarity and the rescue of the *cpc* phenotype by SlTRY (Tominaga-Wada et al., 2013), indicates that, unlike the case for trichomes, regulation of root hair development might be shared between the two species.

1.2.5.-Relationship between the regulation of development of epidermal structures.

The regulatory link between trichomes and root hairs has been clearly established, and an operational model exists for *Arabidopsis*. The relationship between epidermal structures in the aerial epidermal (stomata and trichomes) remains a subject of discussion. First, the fact that these epidermal structures emerge from the same pool of protodermal cells suggests a possible limitation to the number of each type of structure that can develop on the same epidermal surface, as the cells committed to a specific cell fate become unavailable, indicating a mutually exclusive relationship. This idea is reflected in observations on *AmMIXTA*-overexpression tobacco plants, where an increase in trichome density resulted in a decrease in stomatal density (Glover et al., 1998). However, the importance of this relationship might be restricted by the degree of plasticity of the protodermis (which could undergo a variable number of divisions to accommodate the demands of the growing organ) or by the non-limiting nature of the protodermal pool (native proteins expressed at native levels might be unable to exhaust the protodermal cells available for differentiation). Second, trichomes are the first cells to undergo differentiation in leaf primordia (Larkin et al., 1996), and therefore are the main determinants of the mutually exclusive relationship. A higher number of trichomes might limit the number of potential stomatal meristemoids, reducing the final number of stomata; an increase in the number of stomata might not reduce the number of trichomes as these would have already developed before the asymmetrical division of the stomatal lineage. In this scenario, it seems plausible that common regulators of stomata-trichome communication exist to coordinate epidermal patterning. Finally, hormonal regulation affects both trichome and stomatal densities, sometimes in the same direction, with increases in density of both structures in response to cytokinins (Farber et al., 2016) or gibberellins (Saibo et al., 2003), for example, and sometimes in opposite directions, as the case of jasmonate (Han et al., 2018). These developmental responses cannot be the result of a mutually exclusive relationship by itself, but necessarily involve the presence of upstream regulators of both processes which ultimately would be a common regulator.

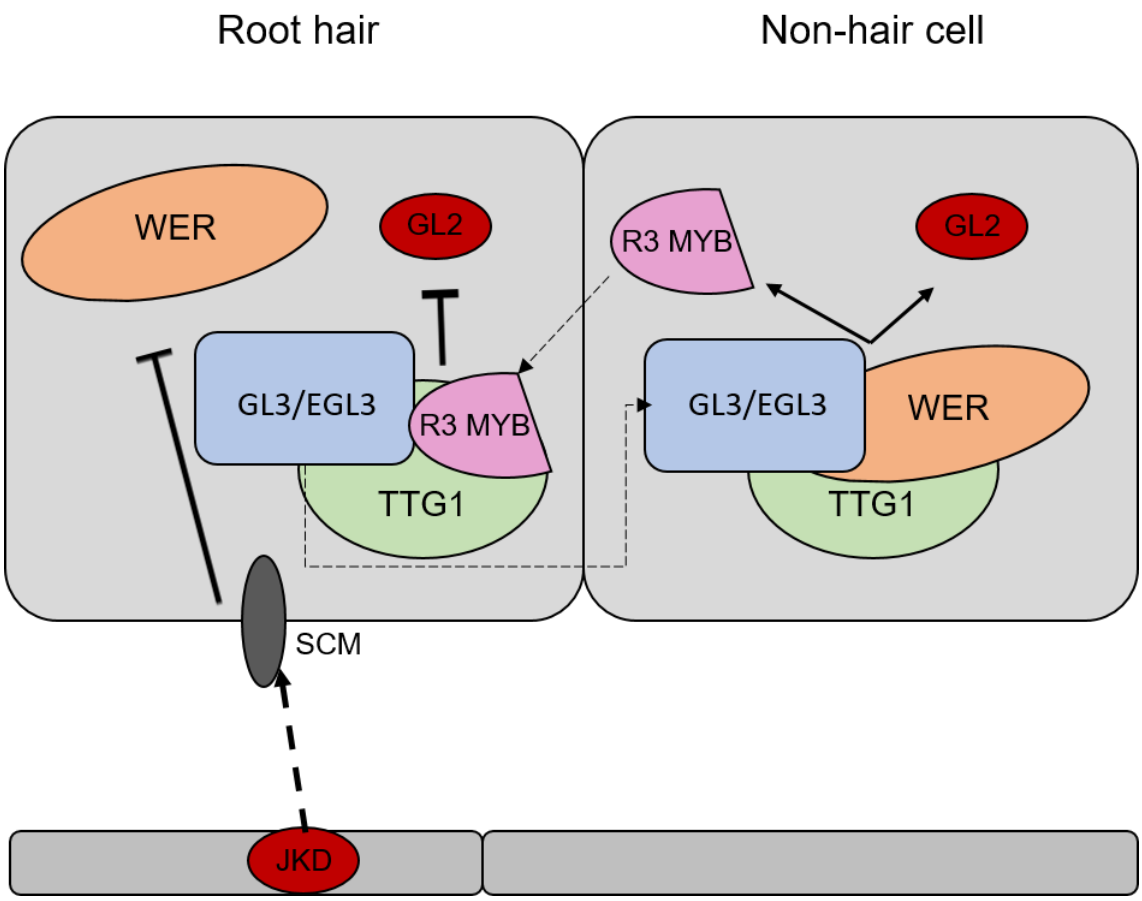

Figure 1.9.-Model for transcriptional regulation of root hair development in *Arabidopsis*. The MYB-bHLH-WD40 complex activates GL2, inhibiting root hair formation, as well as small R3 MYB genes (CPC and TRY, among others discussed in the text). The later genes can move to neighbouring cells to displace WER from the complex, inhibiting the activation of GL2 and downstream genes, and ensuring root hair initiation. Positive interactions are indicated with an arrow line and negative interactions with a T-shaped line. Fine-dashed arrow indicate cell-to-cell movement. Wide dashed arrow indicates downstream targets.

1.3.-Physiological roles of trichomes.

The production of trichomes has a fitness cost for the plant, since the allocation of resources for trichome development would limit their availability for other processes, such as flower development and fruit set, as observed for *Arabidopsis* species (Mauricio, 1998, Sletvold et al., 2010) and tomato (Wilkens et al., 1996). Therefore, if the allocation of resources to trichome production can compromise other fitness-related processes, trichomes are likely to perform important physiological roles under specific circumstances, such as biotic or abiotic stress.

1.3.1.-Role of trichomes in resistance to herbivory.

One of the most studied roles of trichomes is their ability to provide resistance against herbivory by arthropods (and in some cases, bigger animals, such as mammals) (Levin, 1973). Non-glandular trichomes act as structural defences, affecting insect feeding by blocking the access to leaf tissue and negatively affecting oviposition and larval development by hindering attachment to the leaf and access to nutritious tissues (Levin, 1973, Hanley et al., 2007, War et al., 2012). In some cases, it has been reported that hooked non-glandular trichomes can impale small herbivores, causing direct damage to the insects (QulRing et al., 1992). This type of structural defence has been reported for a number of plant species, including crops such as wheat, soybean, cotton or tomato (Levin, 1973)as well as wild species, such as *Arabidopsis thaliana* and *Datura stramonium* (Valverde et al., 2001, Handley et al., 2005).

In species where glandular trichomes are present, the specialised metabolites in trichome exudates have been often associated with repellent, deterrent or toxic effects on insects (Levin, 1973). The compounds present in glandular trichome exudates include acyl sugars, terpenoids, flavonoids and methyl ketones among others (Glas et al., 2012). The diversity of glandular trichomes present in tomato, as well as the diverse profiles of insect resistance in tomato wild species, have led to extensive research into the role of tomato trichome exudates in resistance to herbivory (McDowell et al., 2011, Glas et al., 2012). For example, type VI trichomes are the site of biosynthesis of terpenoids and methyl ketones (Bergau et al., 2015). A sesquiterpene produced in type VI trichomes in *Solanum habrochaites,* 7-epizingeberene, provided resistance against several tomato pests (Bleeker et al., 2012), and it can be recognised as a repellent by whiteflies (Bleeker et al., 2012). A methyl ketone, 2-tridecanone, which is present in *S. lycopersicum* but is much more abundant in *S. habrochaites,* had lethal effects on aphids and *Lepidoptera* larvae (Williams et al., 1980). Type I and type IV trichomes produce acyl sugars, which constitute a sticky secretion that can trap insects and affect their feeding and reproductive behaviour (Glas et al., 2012). The structure of acyl sugars in the wild relative *Solanum pennellii* has a greater impact in oviposition of several pests, including aphids and thrips (Leckie et al., 2016), and the high content of acyl sucroses in *Solanum galapagense* was

associated to a higher resistance to herbivory (Vosman et al., 2018). Finally, some alkaloids as tomatine, probably produced in type VII trichomes (McDowell et al., 2011) can have repellent effects on insects (Levinson, 1976), and they might have toxic effects, as observed for nicotine in *Nicotiana* species (Levinson, 1976). Research on the huge variety of compounds produced in glandular trichomes is likely to identify new compounds that act as defence metabolites against herbivory. Glandular trichomes in some species, such as nettle (*Urtica*), contain urticant compounds that can deter mammalian herbivores from feeding (Otles and Yalcin, 2012).

Finally, the important role of trichomes in herbivore resistance is evidenced by the increase in trichome density in new developing leaves in plants under herbivory stress (Dalin et al., 2008). This has been observed in *Arabidopsis* (Traw and Bergelson, 2003) and tomato (Peiffer et al., 2009), among many other species (Dalin et al., 2008). This adaptation takes place through the jasmonate-signalling pathway. Herbivory activates JA-response genes (Nabity et al., 2013), which can activate downstream genes to elicit trichome formation, as discussed in section 1.2.3.4 of this chapter. By this mechanism, the plant diverts resources towards defence mechanisms, including trichome formation, which limit the degree of damage caused by further herbivory.

1.3.2.-Role of trichomes in resistance to other biotic stresses.

It has been suggested that trichomes may play a negative role in providing resistance to fungal pathogens. In apple, leaves with a greater number of hairs accumulated more fungal spores, probably increasing the frequency of infection (Roda et al., 2003). In *Arabidopsis,* the glabrous mutant, *gl1,* showed an increases resistance to the fungal pathogen *Botrytis cynerea* compared to the WT as well as the highly pubescent *try* mutant (Calo et al., 2006). The presence of the defence compounds glucosinolates in *Arabidopsis* trichomes, which have antifungal and antibacterial properties, seems to indicate that they might play a positive role in defence against pathogens (Frerigmann et al., 2012). However, the amount of glucosinolates in trichomes is far lower than in other epidermal cells, suggesting that their contribution to pathogen resistance is probably small (Frerigmann et al., 2012). This evidence suggests a negative contribution of trichomes to defence against pathogen infection. In addition to this, the systemic response to pathogen infection is normally mediated by the hormone salicylic acid (SA) (An and Mou, 2011). SA is known to antagonise JA-mediated responses, and application of SA to *Arabidopsis* plants reduces trichome density (Traw and Bergelson, 2003), highlighting further the potential negative contribution of trichomes -at least non-glandular ones- to plant immunity. However, some of the diverse specialised metabolites produced in glandular trichomes have been associated with antifungal or antibiotic activities. For example, gossypol and its derivatives, produced in the glandular trichomes of cotton, have a broad antifungal activity (Mellon et al., 2012). The

essential oils of a number of aromatic plants, produced in exudates of glandular trichomes, show antibacterial activity (Burt, 2004). Therefore, any generalised conclusion about the contribution of all types of trichomes to plant defences against pathogens is difficult.

1.3.3.-Role of trichomes in resistance to drought.

Trichomes are essential drivers of the water relations of plants, and they contribute to minimising the effects of drought on the physiology of the plant (Bickford, 2016). Trichome traits such as density, morphology and length determine many physical properties of the leaf and influence the responses to water scarcity. For example, highly pubescent leaves can reflect radiation and reduce leaf temperature in arid climates (Ehleringer, 1988), which reduces the needs of the plant for water to regulate their temperature by transpiration through stomata. The optical properties of trichomes can also contribute to reducing UV-damage to photosystem II (Galmés et al., 2007b), which has been linked to the flavonoid content of trichomes (Skaltsa et al., 1994). In fact, exposure of *Arabidopsis* plants to UV-B radiation induced the formation of trichomes in new leaves, suggesting an important role in energy dissipation (Yan et al., 2012). Trichomes are also known to influence leaf wettability, defined as the ability of leaves to accumulate water on their surface. High wettability can cause stomatal occlusion and affect gas exchange (Bickford, 2016), and it has been shown for several species that low trichome density increases wettability (Fernandez et al., 2011, Fernández et al., 2014), probably due to the hydrophobic cuticle of trichomes repelling surface water (Bickford, 2016). Trichomes also affect the resistance of the leaf-air boundary layer, which can reduce water loss through stomata, but also potentially limit CO_2 intake (Nobel, 2009), although the net contributions of trichomes to stomatal conductance are thought to be relatively small (Bickford, 2016). In general, these properties of trichomes can affect the water use efficiency of the plant, as both photosynthetic activity and water loss are impacted by energy dissipation, leaf wettability and boundary layer resistance (Ehleringer and Mooney, 1978), and specific trichome phenotypes might be advantageous under drought stress. In fact, many drought-resistant varieties show a higher trichome density in species such as watermelon (Mo et al., 2016), *A. lyrata* (Sletvold and Ågren, 2012) and tomato (Ewas et al., 2016). Trichome production is also induced upon drought stress in several species, including barley and aubergine (Fu et al., 2013, Liu and Liu, 2016), indicating that increases trichome formation might protect the plant from drought stress.

Another example of the role of trichomes in water relations is in the case of *Bromeliads*, which are epiphytic plants that grow on other plants for support, but do not parasite them and obtain their nutrients and water from the environment (Adams and Martin, 1986). Some *Bromeliads* have been reported to uptake water directly through their trichomes (Ohrui et al., 2007), especially those lacking any other water-retentive structures (Martin, 1994).

1.3.4.-Role of trichomes in resistance to other abiotic stresses.

Trichomes have been associated with responses to other abiotic stresses, as high salinity or heavy metal content in the soil. High soil salinity impairs normal growth by imposing high osmotic and ionic stress on the plant. Many species accumulate excessive sodium ions on their roots, while some others transport them to their aerial tissues where they can be excreted through glandular trichomes (Tester and Davenport, 2003). Some of these glandular hairs seem to be specialised for saline secretion and their glandular heads are called salt glands (San and Ke_Fu, 2003). These structures have been found in several species, including cotton (Peng et al., 2016), rice (Flowers et al., 1990) and maize (Ramadan and Flowers, 2004). Trichomes are also associated with the secretion of heavy metal contaminants, normally though chelation of the metal ions in sulphur-containing structures (Wagner et al., 2004). A heavy metal hyperaccumulator, *Arabidopsis halleri,* has been shown to accumulate Cd and Zn in its trichomes (Kupper et al., 2000). Tobacco plants have been shown to excrete Cd and Zn-containing crystals through their trichomes (Choi et al., 2001, Sarret et al., 2006). In addition to this, exposure to zinc increases trichome density in tobacco, indicating an important role for trichomes in detoxification of heavy metals (Sarret et al., 2006).

1.3.5.-Trichomes beyond stress: other suggested roles.

The main roles of trichomes seem to be associated with stress responses, evidenced by the increases in trichome density that occur under most biotic and abiotic stresses and the improved performance of pubescent plants under stress conditions (although there may be cost trade-offs with other plant functions). However, there are observations -sometimes anecdotical- of other functions for trichomes, not necessarily linked to stress responses. This is the case of pollinator attraction in some species. In *Theobroma* species, specialised trichomes in the sepals are believed to attract pollinators via production of volatile compounds (Young et al., 1984). Trichomes in floral organs also have been shown to perform a structural function. For example, trichomes in cotton stick petals together to form a floral architecture protecting anthers and stigma (Tan et al., 2016b). In tomato, the anther cone is held together by a mesh of trichomes which hold the anthers together and ensure pollination of the stigma held within the anther cone (Glover et al., 2004). In citrus, the juice sacs in the fruit are considered to be modified trichomes arising from epidermal layers of the pericarp (Simpson, 2010).

These reports indicate that the machinery controlling trichome development is often exploited by plants to develop advantageous structures at the organ level.

1.4.-Biotechnological opportunities in relation to trichomes.

The physiological functions discussed above highlight potential agricultural applications for the results of research on trichomes. Selection of lines with higher trichome density, more secreting glandular trichomes or with an ability to produce more trichomes upon stress without compromising yield under non-stress conditions might have positive impacts in agriculture, especially in terms of resistance to drought and herbivory. Identification of key genes involved in trichome development in crops, especially those *Asterids* which are relatively uncharacterised, will generate opportunities to shape the trichome-related developmental responses in major crops.

Glandular trichomes also are sources of important metabolites that can have clinical or commercial applications (Schilmiller et al., 2008). The list of compounds produced in plant trichomes is practically endless and grows with the analysis of new species and cultivars. One of the most studied examples is the anti-malarial drug artemisinin, produced in glandular trichomes of *Artemisia annua*. Artemisinin supplies dependent on the harvesting of *A. annua* fluctuate depending on the growing season, but the elucidation of the enzymatic pathway leading to its production resulted in the option of semi-synthetic production of the compound, by the combination of the expression of biosynthetic genes in yeast and some synthetic chemical steps (Kung et al., 2018). This has led to more stable supplies and prices for the anti-malarial drug, although microbial production looks unlikely to completely replace the production from *A. annua*. Because the production of trichome-specific compounds takes place in the context of the glandular cells, several attempts to characterise the metabolic and transcriptional profiles of these cells have been carried out (Huchelmann et al., 2017). Engineering specific biosynthetic pathways in plants might result in cheaper and more sustainable solutions to the use of microbial species for drug production. However, our current understanding of glandular trichome development and chemistry is probably insufficient to use trichomes in model species, such as tobacco, as a routine bio factory (Huchelmann et al., 2017).

In conclusion, advances in trichome research, especially in *Asterids* bearing glandular trichomes, are likely to have a substantial impact in agriculture and in biotechnological applications.

1.5.-Aims of the work described in this thesis.

In this thesis, I aimed to gain a better understanding of the process of trichome and epidermal development in tomato and the physiological roles performed by epidermal structures. Specifically, the objectives driving this work are:

1.-Quantifying the natural variation in trichome and stomatal formation present in the *Solanum lycopersicum* cv. M82 x *Solanum pennellii* introgression lines (ILs) using scanning electron microscopy.

2.-Testing candidate genes found in promising genomic regions by transient assays (virus-induced gene silencing) as well as stable assays (overexpression and CRISPR/Cas9 gene editing), with especial emphasis on *SlMIXTA-like.*

3.-Generating a collection of knock-out mutants for known regulators of trichome development in the same genetic background using CRISPR/Cas9.

4.-Testing the effect of the differences on trichome development observed in the ILs and the mutants generated on tolerance to drought and whitefly infestation.

Chapter 2 – General methods

2.1.-Plant material.

The *S. pennellii* x *S. lycopersicum* cv. M82 were used for this thesis (Eshed and Zamir, 1995), and were grown always alongside the cultivated *S. lycopersicum* parent, M82.

The cultivar MoneyMaker, acquired commercially, was used for stable transformations given the existence of a well-established transformation protocol.

The tomato MicroTom line (semi-dwarf) transformed with proSlPNH:AmRosea1/35S:Delila insertion, referred to as *Valencia* plants hereafter (Martin et al., 2012), were used for silencing assays, using the loss of purple coloration in leaves and stems as a visual marker for silencing.

The *ttg1* and *ttg2* mutans of *Arabidopsis thaliana* were obtained from Ingo Appelhagen (Appelhagen et al., 2014).

The specific tomato or *Arabidopsis thaliana* lines used for each chapter are detailed in their corresponding method sections, as well as their specific growth conditions.

2.2.-DNA extraction.

DNA extraction from leaves was carried out using the Plant DNeasy kit (QIAGEN, USA). Briefly, <100 mg of leaf tissue was collected, flash-frozen in liquid nitrogen and ground using a TissueLyser LT (QIAGEN, USA) in the presence of carbide beads. To break the cells, the AP1 lysis buffer was added as well as RNAse A, to digest RNA present in the sample. After lysis, the proteins and polysaccharides were removed by salt precipitation by addition of the buffer P3. The debris was removed by filtration using a QIAshredder spin column. The DNA in the sample bound to the membrane in the DNeasy Mini spin column, and remaining contaminants were removed by successive washing steps with the washing buffer AW2. Finally, the DNA was eluted using water and its concentration and purity were measured using a NanoDrop before any downstream application. The specific compositions of the buffers are not publicly available. The buffer volumes and reaction times of each step were as indicated by the supplier.

2.3.-RNA extraction.

RNA extraction from leaves was carried out using the Plant RNeasy kit (QIAGEN, USA). Leaf samples were collected and disrupted as indicated for DNA extraction in section 2.2. The lysis buffer in this case, RLT, contained the denaturing agent guanidine thiocyanate as well as β-mercaptoethanol to inactivate RNses upon lysis and ensure integrity of the RNA. Polysaccharides and proteins were eliminated by filtration using a QIAshredder spin column, and ethanol was added to the sample to induce binding to the membrane of the RNeasy Mini spin column. Contaminants were removed by successive washing of the membrane with buffers RW1 and

RPE. The RNA was eluted in water and its concentration and purity were measured using a NanoDrop before proceeding with cDNA synthesis. The specific compositions of the buffers are not publicly available. The buffer volumes and reaction times of each step were as indicated by the supplier. RNA was stored at -80 °C until required.

2.4.-cDNA synthesis.

cDNA was synthesised using RNA extracted from leaf samples of interest. First, contaminant genomic DNA was eliminated by treating the samples with Amplification Grade DNase I (Merck, USA). The reaction was carried out in 10 µL with 1x DNase I buffer and 1 unit of DNase I, both supplied in the commercial kit. The digestion of genomic DNA was performed at room temperature (approximately 25 °C) for 15 min. The DNase I was inactivated by addition of the STOP solution (50 mM EDTA) to a final concentration of approximately 5 mM EDTA and heating at 70 °C for 10 min. The cDNA was then synthesised using the High-Capacity cDNA Reverse Transcription kit (Applied Biosystems, USA). Reactions were carried out in volume of 20 µL using up to 2 µg of RNA as a template for retro transcription (RT) to single-stranded DNA. The reaction mix consisted of 1x RT buffer, 4 mM dNTPs, 1x Random Primers, 1 unit MultiScribe™ Reverse Transcriptase and 1 unit RNase inhibitor, all provided by the supplier (Applied Biosystems, USA). The reaction consisted of three steps, a 10-min step at 25 °C, a 120-min step at 37 °C and a 5-min step at 85 °C to inactivate the reverse transcriptase. cDNA was then stored at -20 °C until required.

2.5.-Quantitative Polymerase Chain Reaction (qPCR).

qPCR was used to determine the abundance of specific transcripts in the cDNA made from RNA samples collected for different purposes. The qPCR reactions were carried out using the SYBR® Green JumpStart™ ready kit in volumes of 25 µL including 1x SYBR ® buffer (1.25 unit Taq polymerase, 10 mM Tris-HCl, 50 mM KCl, 3.5 mM $MgCl_2$ and 0.2 mM dNTPs final concentrations), 1 mM of each primer (see *Appendix 1* for more information about the primers) and 5 µL of template cDNA, diluted 1:10 from the final volume after cDNA synthesis. At least three technical replicates were done for each reaction. The qPCR reaction programme consisted of an initial denaturation step at 94 °C for 2 min followed by 40 cycles with an initial denaturation step at 94 °C for 15 s followed by an annealing and extension step at 61.2 °C for 1 min. After each cycle, the fluorescence of the SYBR® dye bound to the dsDNA was measured and plotted. After the 40 cycles, the samples were subjected to a multi-step temperature gradient coupled with fluorescence readings to build a melting curve and ensure specificity of the primers. The thermocycler used was a CFX96 Touch™ (Bio-Rad, USA), and the background value and C_t values were automatically calculated by its software. Primer efficiency was calculated for each pair of primers (indicated in *Appendix 1*) by calculating the slope of the regression line of the plotted

values of C_t vs log(DNA dilution) of five serial dilutions of the same cDNA sample (normally 1:2, 1:4, 1:8, 1:16 and 1:32) and comparing it to an ideal exponential amplification. I used the qPCR efficiency calculator tool in the ThermoFisher Scientific website (www.thermofisher.com). Two reference genes were used to estimate expression levels, SlActin and SlGAPDH, retrieved from (Exposito-Rodriguez et al., 2008), and the geometric mean of their C_t value was used as the reference C_t of the sample. Expression level was estimated as $2^{-\Delta Ct}$, where ΔC_t was calculated as the difference between the C_t value of the target gene in the sample and the reference C_t value for the sample. At least three biological replicates were used for each line of interest.

2.6.-Polymerase Chain Reaction (PCR) protocols.

For all protocols, the PCR product was run in 1% agarose gels containing 0.5 µg/mL ethidium bromide for at least 20 min, together with a DNA molecular marker (O'generuler express, ThermoFisher Scientific). The gels were imaged using a Gel Doc™ transilluminator (Bio-Rad, USA) equipped with an UV lamp that makes the ethidium bromide bound to the DNA fluoresce.

2.6.1.-Phusion® polymerase.

Phusion® (New England Biolabs, USA) is a high-fidelity polymerase, which I used to clone coding sequences (CDS) of genes of interest and promoters from genomic DNA. Reactions were carried out in a volume of 20 µL containing 0.2 µM dNTPs, 0.5 µM of each primer (see *Appendix 1* for primer information), 1x HF buffer (supplied with Phusion® kit), 3% DMSO and 0.4 units of Phusion® polymerase. As template, less than 250 ng of DNA (either cDNA or genomic DNA) were added to the reaction. The PCR programme included an initial denaturation step at 98 °C for 2 min, followed by 40 cycles consisting of an initial denaturation step at 98 °C for 10 s, followed by an annealing step at variable temperature for 20 s and an extension step at 72 °C of variable duration. After the cycles, a final extension step at 72 °C for 5 min was added. The annealing temperature was equal to the lower melting temperature of the primer pair if these were shorter than 20 nucleotides, and, if longer, 3 °C above the lower melting temperature of the pair. The extension step required 20 s per kb of DNA fragment to amplify.

2.6.2.-Phire Plant Direct PCR Master Mix.

The Phire Master Mix (ThermoFisher Scientific, USA) allows direct amplification of plant samples without the need to extract DNA. This allowed quick genotyping of a large numbers of plants, including overexpression and CRISPR/Cas9 edited lines. The template for Phire reactions consisted of a tip of an emerging leaf submerged in the 20 µL of dilution buffer (supplied in the kit) and gently disrupted with a pipette tip. This DNA-containing solution was diluted 1:10 before adding it to the PCR reaction. The reaction was carried out in a volume of 20 µL, containing 1x Phire Master Mix, 0.5 µM of each primer (see *Appendix 1* for primer information) and 0.5 µL of the template. The protocol consisted of an initial denaturation step at 98 °C for 5 min, followed

by 40 cycles with a denaturation step at 98°C for 5 s, followed by an annealing step at a variable temperature for 15 s and an extension step at 72°C for a variable duration. After the cycles, a final extension step at 72°C for 1 min was added. The annealing temperature was equal to the lower melting temperature of the primer pair. The extension step required 20 s per kb of DNA fragment to amplify.

2.7.-Purification of PCR products.

The products of PCR reactions were purified for downstream use, either sequencing or cloning into vectors of interest. PCR products run on a gel were excised using a razor blade and purified using the QIAquick Gel Extraction Kit (QIAGEN, USA), which includes the QG gel, which can solubilise the agarose and provide the salt concentration and pH necessary to induce DNA binding to the silica membrane of the QIAquick spin columns. The contaminants were removed by centrifugation and successive washes with PE buffer, and the purified DNA was eluted with water. If the PCR product was not run on a gel and directly purified from the PCR reaction, the QIAquick PCR Purification Kit (QIAGEN, USA), was used instead. It relies on the binding of DNA to the same silica membranes but does not involved the agarose solubilisation step. The binding buffer, PB, was used instead and provided the right conditions for DNA binding to the membrane. Removal of contaminants, washes and elution were identical to the gel extraction procedure.

2.8.-Cloning systems.

Several cloning systems were used depending on the intended use of the cloned DNA fragment. For virus-induced gene silencing (VIGS) and overexpression vectors, Gateway™ technology was used. For CRISPR/Cas9 vectors, Golden Gate cloning was used. Finally, for sequencing of multiple alleles in CRISPR/Cas9 edited plants, the TOPO™ cloning system was used for cloning of the PCR products.

2.8.1.-Gateway™ recombination cloning.

The Gateway™ system (ThermoFisher Scientific, USA) is based on the use of the recombination sites (called *attachment -att-* sites) found in the bacteriophage lambda, which are used for integration into the bacterial chromosome by means of a recombinase protein (called Clonase™ in the commercial kit). In the interaction between the bacteriophage lambda and *Escherichia coli*, the recombination takes place between the *attB* sites on the *E. coli* chromosome and the *attP* sites on the lambda chromosome. Upon recombination, new *att* sites are generated (*attL* and *attR*) (Landy, 1989). The addition of *attB* sites flanking the DNA fragment of interest by PCR (see primers used in *Appendix 1*) allows specific insertion into a donor vector carrying *attP* sites. In this case, the donor vector I used was pDONR207 (see *Appendix 2*), which contains a gentamycin resistance selection marker and *attP* sites flanking a Gateway™ cassette, which

contains a chloramphenicol resistance selection marker and a cytotoxic gene, CcdB, to ensure specific growth of the clones of interest. Recombination between the DNA fragment and the pDONR207 vector was mediated by the BP clonase™ and the reactions were carried out in volumes of 5 µL using equimolar concentrations of the DNA insert and the pDONR207 vector and 1 µL of the BP Clonase™ enzyme mix with an overnight incubation at room temperature, followed by an inactivation of the BP Clonase™ in presence of proteinase K (37°C for 10 min). The entry vector containing the DNA fragment flanked by the newly generated *attL* sites was recovered after transformation into *E. coli* DH5α (see section 2.9 for more details). The final expression vectors were obtained by recombination of the *attL* sites into the entry vector and the *attR* sites in the destination vector. In each case, the destination vector was different (see *Appendix 2*), but they all contained a Gateway™ cassette (chloramphenicol resistance and CcdB cytotoxic gene) flanked by *attR* sites. The recombination between the entry and destination vectors was performed in a volume of 5 µL with 300 ng of each vector and 1 µL of LR Clonase™ incubating at room temperature overnight. The LR Clonase™ was inactivated at 37°C for 10 min with proteinase K and the expression vector was recovered after transformation in *E. coli* DH5α (see section 2.9). The identity of entry vectors and expression vectors was confirmed by Sanger sequencing, using primers indicated in *Appendix 1*. The list of constructs built using this system is included in *Appendix 2*.

2.8.2.-Golden Gate cloning.

The Golden Gate system relies on the use of type IIS restriction enzymes, which cleave dsDNA in a different region to their recognition site. Therefore, the overhang created by digestion with these restriction enzymes will not depend on its recognition site and can be designed to be any overhang of choice. The ability to design multiple specific overhangs with a single restriction site allows the ordered assembly of a given number of DNA fragments (normally called parts), and upon ligation, the restriction sites in the final plasmid are not regenerated and digestion and ligation can be coupled (in a process called dig-lig) to increase the efficiency of cloning. All documentation and plasmids were retrieved from the TSL SynBio database (synbio.tsl.ac.uk). I used Golden Gate to clone the sgRNAs for the CRISPR/Cas9-mediated gene editing and I decided to use pICSL002218A, a vector already containing the necessary elements for gene editing (Cas9, kanamycin resistance as the selectable marker for transformed plants and sgRNA backbones) which required only the specific addition of the 20-nucleotide sequence specific to the target gene for editing, which could be purchased directly as oligonucleotides including the overhang necessary for ligation in the right position (Merck, USA). pICSL002218A accepts two different sgRNAs with different target sequences. To introduce the first one, a LacZ marker (for blue/white selection) located in front of the sgRNA backbone is surrounded by BsaI (a type IIS enzyme) sites, which releases the LacZ gene and allows ligation of the 20-nucleotide sequence via specific

overhangs. The second target sequences can be introduced in an analogous way, but in this case the selection marker is dsRed (red/white selection) and it is surrounded by BbsI (a different type IIS enzyme) sites. By successive dig-lig reactions, both target sequences can be introduced into the plasmid. The dig-lig reactions were performed in volumes of 10 µL, including 500 ng of the plasmid, 0.5 unit of T4 ligase, 0.5 units of the corresponding restriction enzyme and 2 µM of each oligonucleotide (see *Appendix 1*). The reaction programme included an initial step at 37 °C for 20 s, followed by 15 cycles with a digestion step at 37 °C for 3 min followed by a ligation step at 16 °C for 4 min. A final ligation step at 16 °C for 30 min was included after the cycles, followed by inactivation steps at 50 °C for 5 min and 80°C for 15 min. The resulting vector was then transformed into *E. coli* DH5α for selection of the plasmid bearing both inserts in presence of kanamycin. The identity of the plasmid was checked by Sanger sequencing using a right-border reverse primer (see *Appendix 1*).

2.8.3.- Zero Blunt™ TOPO™ cloning.

The Zero Blunt™ TOPO™ system (ThermoFisher Scientific, USA) uses the ability of DNA-bound topoisomerases to join dsDNA fragmnets. In this system, the plasmid is provided in a linearized form with toposiomerases from Vaccinia virus bound to their blunt ends. These topoisomerases can be released in presence of blunt end DNA fragments (such as the ones produced by Phusion® or PhireTM polymerases) which are inserted in the vector which becomes circularised. The reaction was carried out in volumes of 5 µL including 10 ng of the linearized vector, salt solution (200 mM NaCl and 10 mM MgCl2 final concentration) and the PCR product to be inserted. Reactions were carried out at room temperature for 5 to 30 min and then the plasmid was transformed into *E. coli* DH5α (see section 2.9) and selected using the CcdB cytotoxic selection marker and kanamycin resistance as selection for positive transformants. Inserts were checked by Sanger sequencing using the primers provided in the commercial kit (see *Appendix 1*).

2.9.-*Escherichia coli* transformation.

E. coli was transformed with vectors of interest for propagation and storage. Two different strains were used: DH5α and *ccdB* survival. The DH5α strain is used for general plasmid propagation as it bears the *recA* mutation that ensures stability of the insert as homologous recombination is impaired and the *endA* mutation that prevents digestion of the plasmid by endonucleases and increases the yield of plasmid. It can also be used for blue/white selection as it has a mutated version of the LacZ gene. The *ccdB* survival strain was used for propagation of plasmids including a Gateway™ cassette. This strain bears similar mutations to ensure yield and stability of the plasmid, but also has resistance to the cytotoxic activity of the CcdB gene. In both cases, approximately 100 ng of the plasmid of interest were incubated with 50 µL of commercial cells (ThermoFisher Scientific, USA) for 30 min on ice. The plasmid was then

transformed by heat shock (42 °C for 45 s) and kept on ice for 2 min. The cells were then incubated for at least an hour at 37 °C in 950 mL of SOC medium before spreading on LB media plates with the appropriate selection (see *Appendix 3* for media recipes and antibiotic concentrations). Plates were incubated at 37 °C for at least 8 h and single colonies were selected and grown in liquid LB with antibiotic for 8 h. The liquid cultures were preserved in 20% glycerol at -80 °C and plasmids were purified by miniprep (see section 2.10).

2.10.-Plasmid extraction and purification.

E. coli liquid cultures were centrifuged for 10 min at 2900xg and the bacterial pellet was used for plasmid extraction and purification using the QIAprep Spin Miniprep Kit (QIAGEN, USA). The bacterial pellet was resuspended in buffer P1. Cell alkaline lysis was induced by addition of the lysis buffer P2, and the process was stopped by addition of the neutralisation buffer N3, with a salt concentration that promotes plasmid DNA binding to the silica membrane of the QIAprep columns. The lysate was cleared by centrifugation (10 min at ~18000xg) and the DNA was bound to the silica membrane. The membrane was washed twice with PE buffer to remove contaminants and the plasmid was finally eluted in water. The concentration and purity of the DNA was checked using a NanoDrop.

2.11.-Sanger sequencing.

Plasmids and PCR products were sequenced using the Mix2Seq overnight service (EuroFins, Belgium), where 1-1.5 µg of plasmid DNA or 50-100 ng of PCR product were sent with a specific sequencing oligonucleotide to prime the Sanger reaction.

2.12.-*Agrobacterium* transformation.

Two *Agrobacterium* species were used for the work described in this thesis. *Agrobacterium tumefaciens* strain AGL1 was used as a delivery species for plant transformation (both transient and stable). This *A. tumefaciens* strain carries rifampicin and ampicillin resistance genes. *Agrobacterium rhizogenes* strain ATCC15834 was used for hairy root induction and transient transformation of hairy root tissue. This strain does not carry any resistance gene. The strains used for both species were electrocompetent. Electroporation was carried out by incubating 50 µL of the *Agrobacterium* strain with 50-100 ng of the plasmid of interest on ice for 10 min. The cells with the plasmid were transferred to a prechilled 2 mm cuvette and subjected to a 2.5 kV electric pulse. Cells were incubated at 28 °C for at least 3 hours after addition of 450 µL of SOC medium (see *Appendix 3*) and spread on plates containing TY medium (see *Appendix 3*) and selection antibiotics.

2.13.-Transient *Agrobacterium* infiltration in tomato seedlings.

Transient infiltration was carried out on Valencia plants to test the effect of gene silencing by VIGS. *A. tumefaciens* AGL1 carrying the plasmid of interest was grown in liquid TY with selection

antibiotics at 28°C to an OD_{600} 0.5-0.8. Bacteria were then pelleted and resuspended in 10mM MgCl2, 10mM MES pH 5.6, 200μM acetosyringone buffer to an OD_{600} 0.1. For VIGS assays, the pTRV1 and pTRV2 plasmids (see *chapter 4* for details) were mixed in a 2:1 ratio to a final OD_{600} 0.1. Valencia seedlings that were 10 days old were submerged in the *A. tumefaciens* solution and leaves and cotyledons were vacuum-infiltrated using chemical duty pump (Merck, USA) and a vaccuum dissecator for 10 minutes.

2.13.-Transient *Agrobacterium* infiltration in *Nicotiana benthamiana* leaves

Transient expression was performed by manually injecting *Agrobacterium tumefaciens* strain AGL1 transformed with the construct of interest into mature leaves of 4-week-old *N. benthamiana* plants grown at 20–22 °C under greenhouse conditions. Transformed *A. tumefaciens* were grown in TY medium with selection antibiotics to an OD_{600} 0.5-0.8. Cells were pelleted and resuspended in 10mM MgCl2, 10mM MES pH 5.6 buffer with 200 μM of acetosyringone to a final OD_{600}=0.1.

2.14.-Stable tomato transformation.

Stable transformation of expression vectors and CRISPR/Cas9 constructs was performed in MoneyMaker tomato plants. Approximately 100 MoneyMaker seeds per transformation were sterilised in 10% domestic bleach for three hours and plated in sterile boxes containing Germination Media (see *Appendix 3*) and subjected to cold treatment for 3 weeks at 4°C in darkness to promote synchronous germination in the growth chamber (16 h photoperiod, 20°C in average). After 7-10 days, cotyledons from the MoneyMaker seedlings were used as explants (two square explants per cotyledon, adding up to approximately 400 explants per transformation) and they were submerged in a solution (OD_{600} 0.4-0.5) of *A. tumefaciens* AGL1 carrying the construct of interest in MS 3% sucrose for approximately one hour. The explants were dried on sterile filter paper and transferred to plates containing Cell Suspension Media (see *Appendix 3*) and a layer of tobacco cells to feed explants for two days of co-cultivation. Explants were then transferred after 48 h to Regeneration Media plates (see *Appendix 3*), which induce callus formation and shoot regeneration. Explants were transferred every other week to plates (or boxes) with new Regeneration Media. When shoots were mature, they were excised from callus and transferred to Rooting Media (see *Appendix 3*), where roots developed in two to four weeks. When the root system was fully developed, T0 plantlets were transferred to boxes with sterile soil and water and grown in vitro for two weeks to help with acclimation to greenhouse conditions. Finally, plants were transferred to soil and genotyped to test for the presence of the transgene or the CRISPR/Cas9-mediated mutations.

2.15.-Scanning Electron Microscopy (SEM).

Trichome phenotypes were always assessed using SEM. Two different ways of sample fixation were used to preserve the structure of trichomes and other epidermal structures. In both cases, the samples were imaged either using a Zeiss Supra 55 VP SEM (Zeiss, Germany) or a FEI Nova NanoSEM450 (FEI, USA). Specific characteristics of samples or imaging patterns are indicated in each chapter.

2.15.1.-Cryo-SEM.

The cryo-SEM imaging approach relies on freezing the sample and imaging at very low temperature to avoid the damage to the sample due to water evaporation under vacuum conditions inside the electron microscope. For cryo-fixation, plant samples are glued to a cryo-stage and then submerged in liquid nitrogen in a vacuum-generating environment to reduce frosting of water vapour. The samples are then introduced in the microscope preparation chamber, where any frost is removed by sublimation at -95 °C for 3.5 min. The samples are then sputter coated with platinum for 150 s and they are transferred to the main microscope chamber, at -125 °C. The imaging took place in the main chamber, where the electron beam was active, and the secondary and back-scattered electrons could be perceived by the detectors. This fixation protocol is destructive, and samples cannot be stored for further imaging.

2.15.2.-Chemical fixation and Critical Point Drying.

Chemical fixation of the samples was achieved by vacuum infiltrating them with a glutaraldehyde 2.5% cacodylate solution and dehydrated through an ethanol series. Samples were dried in a Leica CPD300 critical-point dryer (Leica Microsystems, Germany), where water was replaced by liquid CO_2 and then evaporated at the critical point for CO_2, removing all the liquid without damaging the structures of the sample. Dried samples were glued to a SEM stub and gold-coated before imaging in the main chamber of the microscope, at high vacuum and room temperature conditions.

Chapter 3 – Screening the *S. lycopersicum x S. pennellii* IL population to determine natural variation in trichome development in tomato.

3.1.-Abstract

In this chapter, I described the characterisation by scanning electron microscopy (SEM) of the adaxial epidermis of two generations of the *Solanum lycopersicum* cv. M82 x *Solanum pennellii* introgression lines (ILs). The quantification of the trichome and stomatal densities in the ILs revealed 18 genomic regions with a low trichome density and 4 ILs with a high stomatal density. I also found ILs with abnormal proportions of different trichome types and aberrant trichome morphologies. This characterisation has generated a very powerful dataset for the study of epidermal development in tomato.

3.2.-Introduction

3.2.1.-Introgression lines as a source of exotic genetic material in tomato.

Wild relatives of important crops have been used extensively in modern breeding to introduce beneficial traits in commercial cultivars (Prescott-Allen and Prescott-Allen, 1986, Hajjar and Hodgkin, 2007), including tomato. Most of the traits introduced from wild relatives involve resistance to biotic or abiotic stress, which have been lost during domestication and breeding of commercial crops (Tanksley and McCouch, 1997). In the case of tomato, most of the disease resistance genes have been introduced from wild species such as *Solanum peruvianum, Solanum chesmanii* or *Solanum pennellii* (Rick and Chetelat, 1995, Hajjar and Hodgkin, 2007). *Solanum chilense* and *S. pennellii* have been used as a genetic source for tolerance to drought and salinity (Rick and Chetelat, 1995). The natural diversity present in the germplasm of wild relatives can also be exploited to gain a better understanding of physiological, developmental and metabolic processes in tomato and other crops. The potential of exotic germplasm in tomato is especially important given the narrow genetic diversity of the self-pollinated cultivated tomato (Eshed and Zamir, 1995).

An introgression line (IL) population is a set of near-isogenic lines generated by successive backcrossing of the offspring of a cross between a crop wild relative and a cultivated line to the cultivated parent (Eshed and Zamir, 1995). The phenotypic variation observed in this population can be attributed to a relatively small and well-defined genomic region derived from the wild relative donor, making them very useful tools for mapping of quantitative trait loci (QTLs) associated with traits of interest (Fig 3.1). IL populations have been used successfully to map genes of interest in many species, including barley (Schmalenbach et al., 2011), rice (Mei et al., 2006), wheat (Liu et al., 2006) and maize (Szalma et al., 2007), as well as horticultural crops such as aubergine (Gramazio et al., 2017), melon (Perpina et al., 2016) and tomato (Eshed and Zamir, 1995, Canady et al., 2005, Finkers et al., 2007, Barrantes et al., 2014). The numbers of IL populations available, many of which have been generated fairly recently, and the numbers of

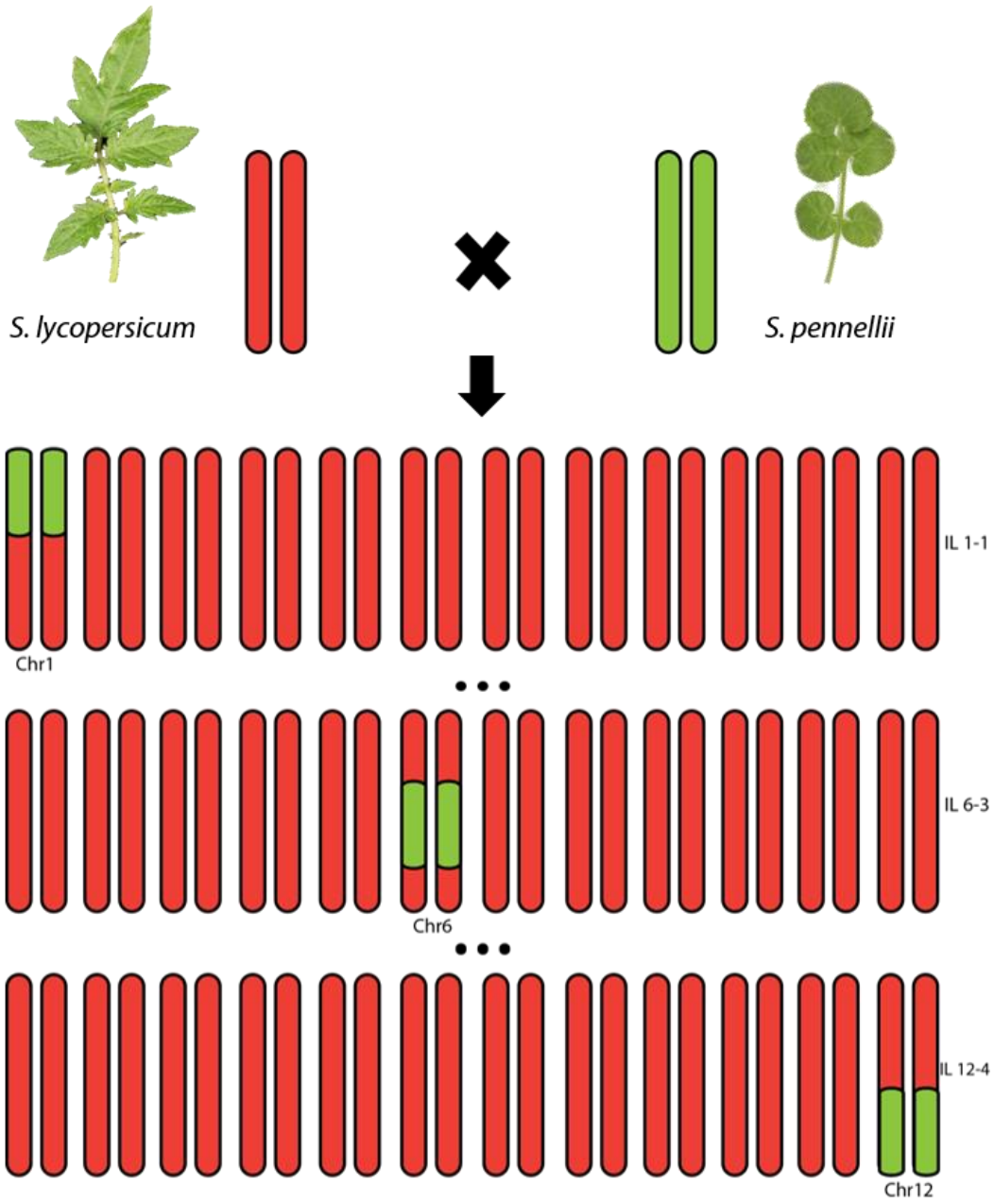

Figure 3.1.-Schematic representation of the introgression lines (IL) population. The IL population was generated by crossing the cultivated tomato (*S. lycopersicum* cv. M82) and the wild relative *S. pennellii* and successively backcrossing the offspring to the cultivated parental lines. The resulting population consists of 76 lines, each one with a well-defined genomic region from the wild parent in the genetic background of M82, covering the complete tomato genome.

studies in which they have been employed, highlights the potential of these resources as a research tool and as breeding material.

In the case of tomato, several different IL populations have been developed using different wild relative parents (Fernie et al., 2006). The *S. pennellii* x *S. lycopersicum* cv. M82 population was developed in the late 20th century (Eshed and Zamir, 1995), and has been extensively curated and genotyped precisely (for example, (Chitwood et al., 2013)) becoming a very reliable platform for the study of different physiological and developmental processes. In fact, complementary populations have been developed to improve the mapping resolution in the *S. pennellii* IL population, including sub-ILs (Alseekh et al., 2013), which were formed by further backcrossing with the cultivated parent to reduce the size of the introgressed region, or the backcross inbred lines (BILs) (Ofner et al., 2016), which consist of lines including small, scattered *S. pennellii* genomic regions. Moreover, other tomato IL populations are currently available to the scientific community, including populations with *Solanum lycopersicoides* (Canady et al., 2005), *Solanum habrochaites* (Finkers et al., 2007), *Solanum pimpinelifollium* (Barrantes et al., 2014) and some other wild *Solanum* species (Fernie et al., 2006) as wild genetic donors. All of these populations have been used to different extents to introduce new genes or map specific QTLs in tomato. However, the size of resources available for the *S. pennellii* population, its widespread use and the physiological characteristics of the wild species (Rick, 1973, Peralta, 2008) make it the most powerful and convenient population for research purposes.

The number of traits explored using the *S. pennellii* ILs is vast. For example, they have been used to map loci involved in resistance to bacterial spot caused by *Xanthomonas perforans* (Sharlach et al., 2013) or to late blight caused by *Phytophtora infestans* (Smart et al., 2007). Tolerance to abiotic stresses has been also investigated in this population. For instance, drought and salinity tolerance were studied in this population (Frary et al., 2010, Rigano et al., 2014), leading to selection of promising genotypes. On top of their use in research for stress tolerance, the IL population has been used to dissect physiological, metabolic and developmental processes in tomato. A comprehensive study of the photosynthetic activity and gas exchange of the ILs (Magnum et al., 2018) has recently helped identify regulators of primary metabolism in tomato. Efforts have been made to improve yield (Eshed and Zamir, 1995) and fruit quality (Calafiore et al., 2016, Yang et al., 2016) using *S. pennellii* ILs. Analysis of the ILs has led to the discovery of regulators of developmental processes, such as leaf shape determination (Chitwood et al., 2013) and root morphology (Ron et al., 2013), although there has not been a comprehensive characterisation of the aerial epidermis of the different genotypes in the population. With respect to trichomes, an extensive work on characterising trichome secretion in the ILs has been

carried out, revealing new QTLs involved in synthesis of acyl sugars and terpenoids (Schilmiller et al., 2010), but we lack understanding of the variability in trichome development in the ILs.

3.2.2.-The IL population as a tool to investigate epidermal development in tomato.

Trichomes are species-specific, and even closely related species show a relatively high degree of variability in terms of density, morphology and metabolic profiles of the trichomes in their aerial organs. This is also the case for *Solanum* species related to tomato, where differences in the distribution and morphology of trichomes had been characterised and reported (Luckwill, 1943, Simmons and Gurr, 2005, McDowell et al., 2011). Although the differences observed within the genus are high and introgressions of any wild donor could be of interest, *S. pennellii* is particularly interesting. First, non-glandular trichomes, which are very abundant in *S. lycopersicum* (Simmons and Gurr, 2005, Vendemiatti et al., 2017) are virtually non-existent in *S. pennellii*. The abundant type VI trichome in cultivated tomato is very scarce in *S. pennellii* (Simmons and Gurr, 2005). Also, the total density of trichomes is higher in *S. pennellii* (McDowell et al., 2011). These differences reinforce the idea of using the IL as a platform for the study of trichome development in tomato.

The epidermis is a dynamic tissue where communication between different cell types (stomata, trichomes and pavement cells) is essential for the determination of cell fate and epidermal patterning (Larkin et al., 1997, Glover, 2000, Larkin et al., 2003). It is likely that changes in the features of one specific cell type lead to alterations of the other types, as observed in *Arabidopsis* (Bean et al., 2002), tobacco (Glover et al., 1998) and *Solanum* species (Glover and Martin, 2000, Chitwood et al., 2013, Fu et al., 2013). Therefore, differences in stomata and pavement cells between *S. pennellii* and *S. lycopersicum* need to be investigated. A comprehensive analysis of the stomatal and pavement cell characteristics in the IL population was carried out (Chitwood et al., 2013), and several QTLs were identified for their size, density and shape. Previous reports also indicated a lower stomatal density in *S. pennellii* (Heichel and Anagnostakis, 1978). However, none of these studies considered trichomes, and they were carried out either in cotyledons or in plants grown in the field, and therefore observations might be biased due to the effects of the age of the tissue (Ceulemans et al., 1995) or the environmental conditions (Beerling and Chaloner, 1993). In any case, the existence of a natural variation in other epidermal features in the IL population can be exploited to understand better the relationship between trichomes and their surrounding epidermal cells.

3.2.3.-Scanning electron microscopy (SEM) as a phenotyping tool for tomato leaf epidermis

Trichomes are relatively big structures that can be seen with the naked eye. However, a more detailed analysis of their structure and other epidermal structures requires the use of microscopy techniques. Traditionally, studies aimed at understanding epidermal development

have relied heavily on light microscopy as an imaging tool (for example, (Snyder and Hyatt, 1984, Gurr and McGrath, 2001). Stomatal density has been traditionally assessed using leaf impressions (Ceulemans et al., 1995, Xu and Zhou, 2008) rather than on live tissue, with potential implications in terms of distortion of stomatal and pavement cell morphology. Although these approaches have led to important discoveries, they have some shortcomings. First, light microscopy techniques used to assess trichome density do not reach the magnification required to determine stomatal and trichome densities simultaneously. Trichomes are much bigger structures, and they are normally observed under low magnification and without mounting slides to determine the trichome types. Second, leaf impressions used to assess stomatal density or size do not allow observation of trichomes, as they are normally removed to allow a clear impression, or their morphology cannot be determined easily from the impressions.

A solution to this problem is the use of Scanning Electron Microscopy (SEM), which allows a direct observation of the surface of the sample and a simultaneous assessment of the different epidermal features. SEM imaging is carried out under high vacuum conditions, which leads to distortion of highly hydrated samples as it is the case of leaves (Holloway and Baker, 1974). Therefore, a fixation step is required, and this can be done either chemically or by cryopreservation (Pathan et al., 2008). Chemical fixation allows conservation of the sample, while cryofixation is destructive and samples can be only assessed once. However, the latter approach allows observation of live structures without any distortion or artefact (Read and Jeffree, 1991), which makes it the preferred approach to assess trichome morphology. In fact, it has been used widely to characterise trichome mutants, as it is the case for the *hairless* (Kang et al., 2010a)*, Woolly* (Yang et al., 2011a) or *odourless2* (Kang et al., 2010b) mutants. Cryo-SEM has also been used successfully before in assessing quantitative traits of epidermal tissue, such as trichome and stomatal density in tobacco (Glover et al., 1998) or conical cell density in petals of petunia (Baumann et al., 2007). However, the impossibility of preserving samples for later imaging is a bottleneck in medium-to-high throughput phenotyping platforms. Where trichome morphology might be of secondary interest, chemical fixation can contribute to a more consistent and robust phenotyping of the sampled leaves because samples can be collected at the same time point and imaged later (Pathan et al., 2008). A powerful data set would combine information obtained by means of an array of different imaging techniques. For the work presented in this chapter, I combined chemical and cryo fixation to improve the quality and usefulness of the data collected.

3.3.-Experimental procedures

3.3.1.-Plant material

I grew two generations of the *S. lycopersicum* cv. M82 x *S. pennellii* ac. LA716 introgression lines (ILs) (Eshed and Zamir, 1995) to assess the adaxial leaf epidermis. The first generation consisted of 67 ILs, which were grown under greenhouse condition at the John Innes Centre, with an average temperature of 20-22 °C. These lines were grown successively from October 2015 to February 2016, with approximately 6 ILs phenotyped per week. The second generation consisted of 74 ILs grown under the same conditions, but all seeds were sown simultaneously in October 2016. For both generations, plants were grown for 4-weeks, until the first true leaf was fully expanded. The terminal leaflet of the first true leaf was excised and leaf sections of approximately 0.5x0.5 cm were used as SEM samples. For each line, 3-4 plants in each generation were phenotyped. *S. pennellii,* M82, IL 2-5 and IL 2-6 plants were kept for 3 months to image stem tissues and leaves that developed later in the life of the plant.

The *Arabidopsis thaliana* Col-0 and the *ttg1* and *ttg2* (Appelhagen et al., 2014) mutants were grown under greenhouse conditions at the John Innes Centre under natural light, and with an average temperature of 20-22 °C. Plants were sown in March 2017 and grown for 7 weeks. The first true leaf was used for imaging. The whole leaf area was used as sample.

3.3.2.-Qualitative and quantitative analysis of epidermal features.

For each leaf sample, 8-15 micrographs of 0.3 mm^2 were generated. I used cryofixation for the first generation of the ILs, and chemical fixation for the second generation (please see *Chapter 2. General methods* for more information) to prepare the samples before imaging. In every case, the same leaf (first fully expanded leaf) and the same part of the leaf (intervein space close to the central vein) was used for assessment of stomatal, trichome and pavement cell numbers. These three cell types were manually quantified in micrographs at a relatively low magnification (x600) using ImageJ v. 1.49 (National Institutes of Health, USA). Trichome and stomatal densities were calculated as percentage of total epidermal cells and expressed as fold change of each line with respect to the M82 values obtained in the corresponding generation. Trichomes were classified in different groups according to (Luckwill, 1943), although type I and type IV trichomes were grouped together under type I (McDowell et al., 2011) and all non-glandular trichomes were classified as type V. For trichome density values, all trichomes were considered together. Aberrant trichome morphologies were recorded and SEM pictures were taken at the most appropriate magnification settings. For ILs 2-5 and 2-6, younger leaves were also imaged to assess aberrant patterning of trichomes.

3.3.3.-Statistical analysis

To assess differences in trichome and stomatal density in the IL population, I performed a t-test to compare the value of each individual line to the value of M82 for the corresponding generation. For the first generation, where values were more extreme and variable, I used a p-value cut-off of 0.005. For the second generation, where values were more consistent, I used a p-value cut-off of 0.05. For the type distribution, low numbers of some types of trichomes and differences in trichome density led to artefactual statistical results, so I decided to make a qualitative observation without determining significance. For comparisons between *Arabidopsis* lines, each mutant was compared to Col-0 using a t-test. The relation between trichome density and stomatal density in M82 was determined by correlation coefficient (R^2). The analyses were performed using R software (ver. 3.2.2; R Core Team, Vienna, Austria).

3.4.-Results

3.4.1.-Characterisation of trichomes in parental lines M82 and *S. pennellii.*

I analysed the surface of leaves and stems of the parental lines of the IL population, *S. lycopersicum* cv. M82 and *S. pennellii*, and characterised the features of their trichomes (Fig 3.2). On stems, I observed a high presence of type I, IV, V and VI trichomes in *S. lycopersicum* (Fig. 3.2A) while I observed a predominance of type IV trichomes in *S. pennellii* (Fig 3.2B). Type IV trichome in *S. pennellii* showed a slightly different morphology,with longer stems and bigger glandular heads. I measured trichome density on the adaxial surface of leaves in both species, and I observed a three-fold higher trichome density in *S. pennellii* compared to M82 (Fig. 3.2C).

3.4.2.-Identification of genomic regions involved in determination of trichome density.

I measured the trichome density on the adaxial surface of leaves of two generations of the ILs (Fig. 3.3 and 3.4). In both generations, I observed a high variability of the values of trichome density between lines and within each line. In general, most lines had a lower trichome density than the cultivated parent M82, the trichome density of which ranks amongst the highest lines in the population. I identified 37 lines with a significantly lower trichome density than M82 in the first generation of the population (Fig. 3.3) and none of the lines showed a significantly higher trichome density than M82. In the second generation, I identified 34 lines with a significantly lower trichome density than the cultivated parent (Fig. 3.4) and one line had a significantly higher trichome density.

I selected those lines that showed a consistent phenotype in both generations, and I could therefore identify 18 ILs with a low trichome density. These are: ILs 2-1-1, 2-2 and 2-3 in chromosome 2; IL 4-1 in chromosome 4; ILs 5-3 and 5-4 in chromosome 5, IL 7-2 in chromosome 7; ILs 8-1, 8-1-1 and 8-2-1 in chromosome 8; ILs 9-1-3, 9-3-1 and 9-3-2 in chromosome 9; ILs 10-

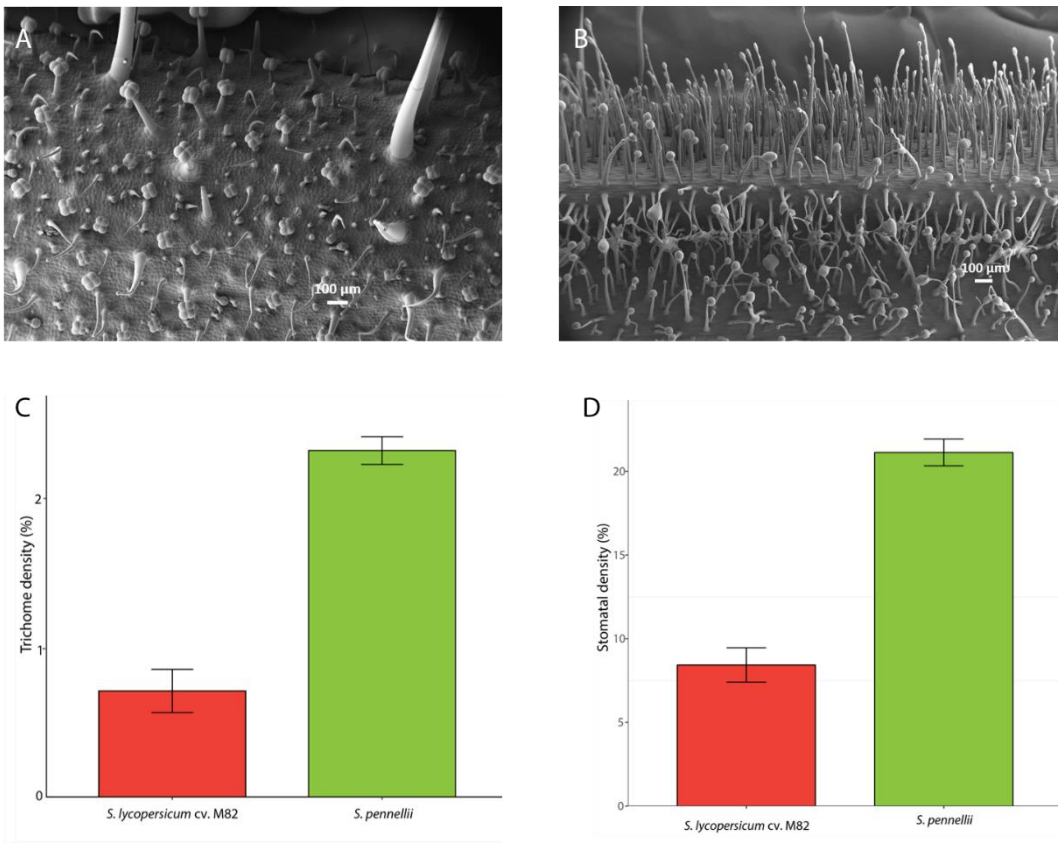

Figure 3.2.- Differences in trichome features in M82 and *S. pennellii*. Micrographs of the surface of the third internode of a stem of A) M82 and B) S. pennellii reveal differences in types and morphology of trichomes. C) Trichome density on the adaxial surface of the first true leaf of M82 and *S. pennellii.* D) Stomatal density on the adaxial surface of the first true leaf of M82 and *S. pennellii.* The values for C) and D) are mean±SEM (n=3). *S. pennellii* showed a significantly higher trichome and stomatal density compared to M82 (p-value<0.01).

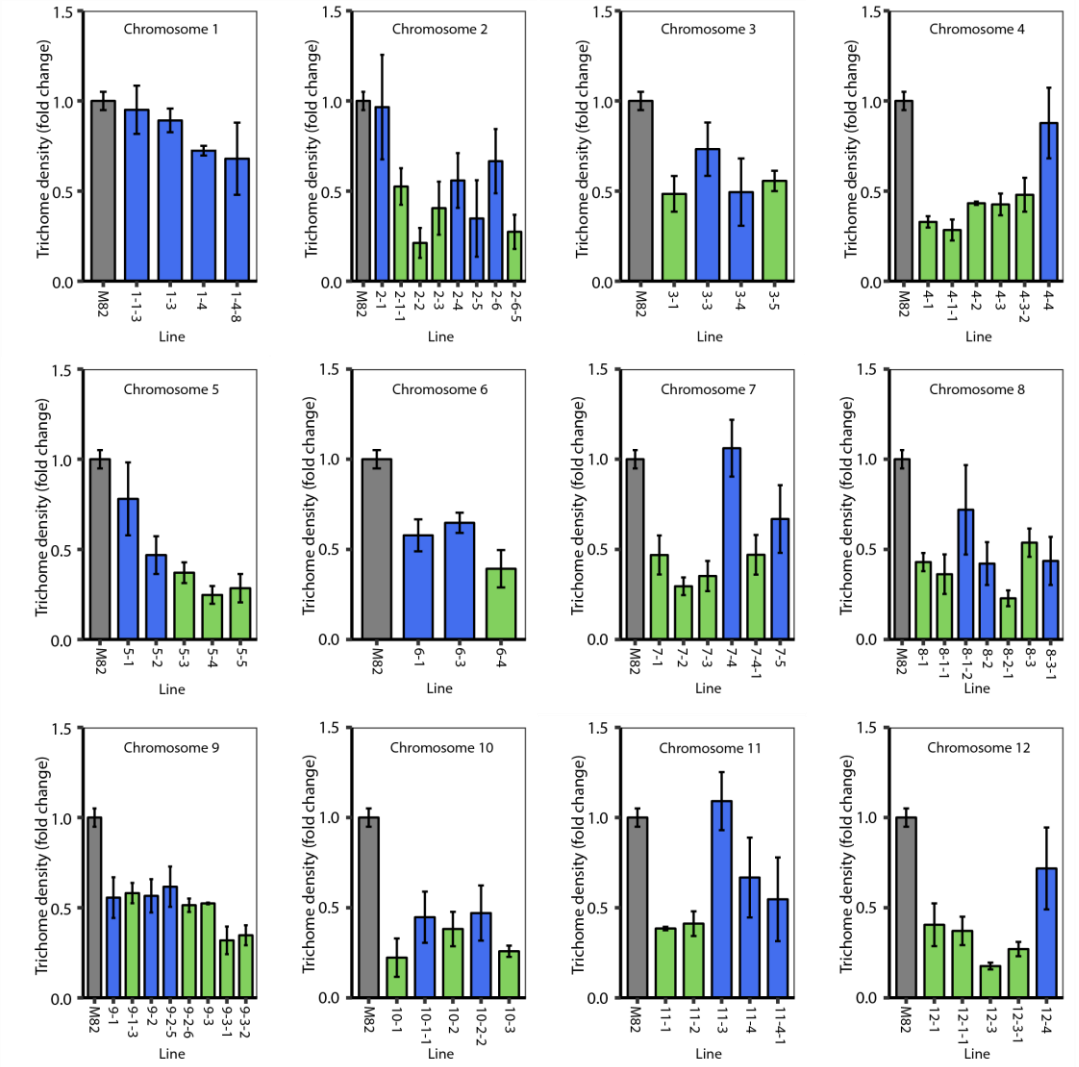

Figure 3.3.- Trichome density of the first generation of the IL population. Trichome density is expressed as fold-change of the ratio of trichomes to total epidermal cells compared to M82. Lines are classified according to the chromosomal region introgressed from *S. pennellii* and each bar represents an IL. Green bars represent lines showing a significant (p-value<0.005) decrease in trichome density when compared to M82. The gray bars represent the value for M82, used for comparison. For each line, the adaxial surface of the first fully-expanded true leaf from three plants was sampled.

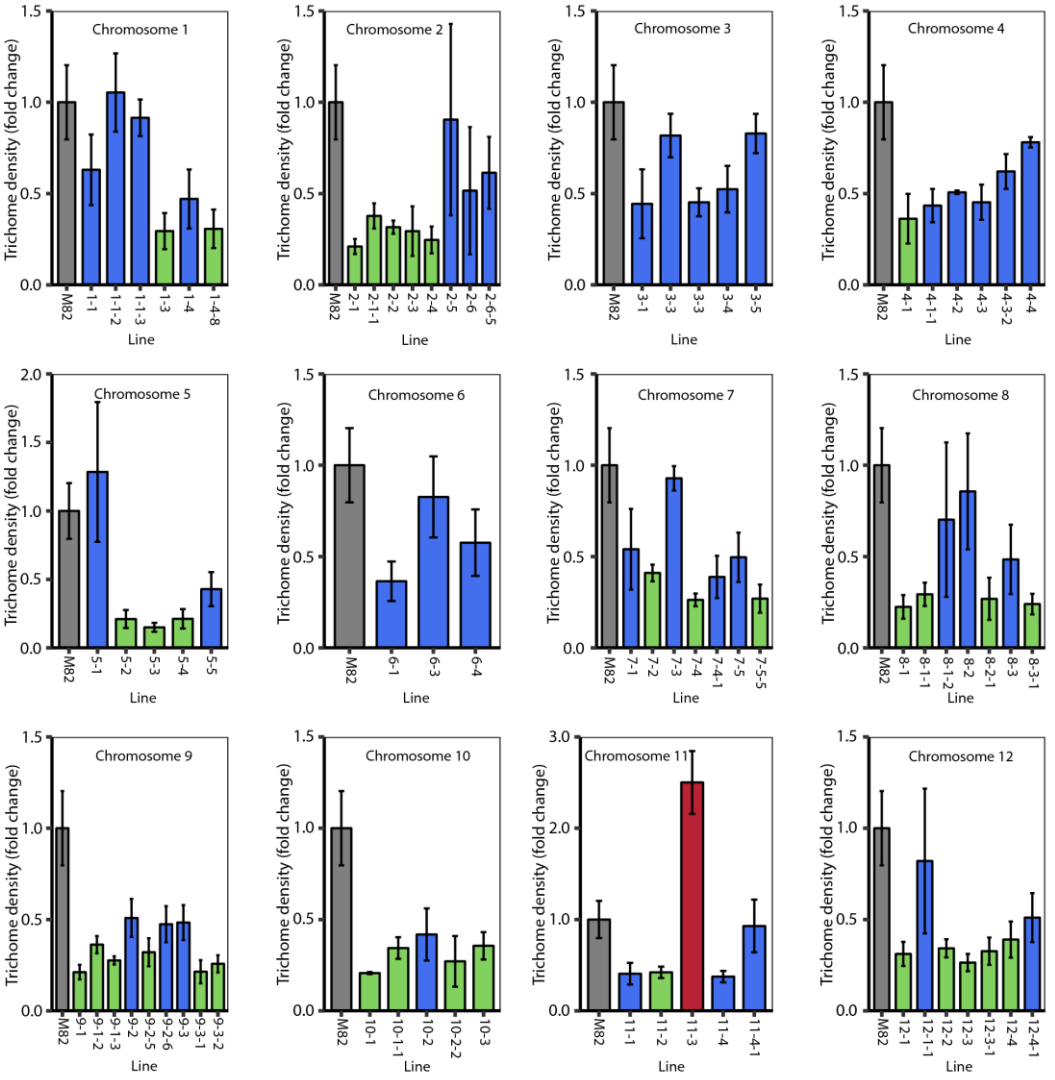

Figure 3.4.- Trichome density of the second generation of the IL population. Trichome density is expressed as fold-change of the ratio of trichomes to total epidermal cells compared to M82. Lines are classified according to the chromosomal region introgressed from *S. pennellii* and each bar represents an IL. Green bars represent lines showing a significant (p-value<0.05) decrease in trichome density and red bars represent lines showing a significant increase in trichome density (p-value<0.05) when compared to M82. The grey bars represent the value for M82, used for comparison. For each line, the adaxial surface of the first fully-expanded true leaf from three plants was sampled.

1 and 10-3 in chromosome 10 and ILs 12-1, 12-3 and 12-3-1 in chromosome 12. IL 11-3 had a significantly higher trichome density only in the second generation, but in the first generation, although not significantly different from M82, it averaged the highest value for trichome density.

3.4.3.-Identification of genomic regions involved in determination of trichome identity.

I classified the trichomes observed in the adaxial surface of leaves for two generations of the IL population in different types (Fig. 3.5 and 3.6). In the first generation, in M82, the main trichome type is type I, accounting for 63% of the total. The rest of the types of trichomes found in *S. lycopersicum* were observed in smaller percentages (5-10%). I used this distribution as standard for comparison with the rest of the ILs.

For most lines, type I trichomes were the most abundant, although ILs 2-1, 3-3, 4-3-2 and 8-1-1 showed a substantial reduction of this type of trichome. This reduction in type I trichomes was compensated by an increase in non-glandular type V trichomes in ILs 2-1 and 3-3. I also observed increased type V trichome density in ILs 1-3 and 11-4. For 21 of the ILs, I could not observe any type V trichomes in the assessed tissue. Type VI trichomes were generally found in low proportions, but it was the most common type in IL 8-1-1, 8-2-1 and 8-3-1. A total of 7 ILs showed no type VI trichomes in the assessed tissue. Type VII trichomes were the scarcest and absent in 32 of the ILs. Importantly, absence of any type of trichome in the assessed tissue does not mean complete absence in other tissues.

In the second generation, most trichomes were damaged because of the chemical fixation used for sample preparation (Fig. 3.6). Therefore, I could not extract any conclusions from the trichome classification.

It is important to note that there was not any line with a complete absence of type I trichomes in either of the two generations.

3.4.4.-Identification of genomic regions involved in determination of trichome morphology.

For each line under study, trichomes showing an aberrant morphology were recorded (Fig. 3.7). The most common type of aberrant trichome found in the population consisted of two swollen cells emerging from a type I-like multicellular base. This type of trichome was observed in ILs 1-1-2, 4-3-2, 5-3, 6-4, 7-4/7-4-1/7-5, 8-1-2 and 11-3 (Fig. 3.7A-F and H). In IL 10-2, I observed another type of aberrant trichome, consisting of a branched, multicellular, non-glandular trichomes (Fig. 3.7G). In every IL with aberrant trichomes, the aberrant forms always appeared alongside wild type-like trichomes in both generations (Fig. 3.5 and 3.6).

3.4.5.-Identification of genomic regions involved in determination of trichome patterning.

I observed unusual clusters of trichomes on the adaxial surface of leaves in ILs 2-5 and 2-6 (Fig 8). In young leaves, trichomes in M82 are equally distributed on the leaf surface and they are oriented in the same direction (Fig. 3.8A). However, in IL 2-5 trichomes were clustered in groups of up to 4 trichomes and they were randomly oriented (Fig. 3.8B). In mature, fully expanded

leaves, I could still observe clusters of two trichomes in ILs 2-5 and 2-6, and these observations

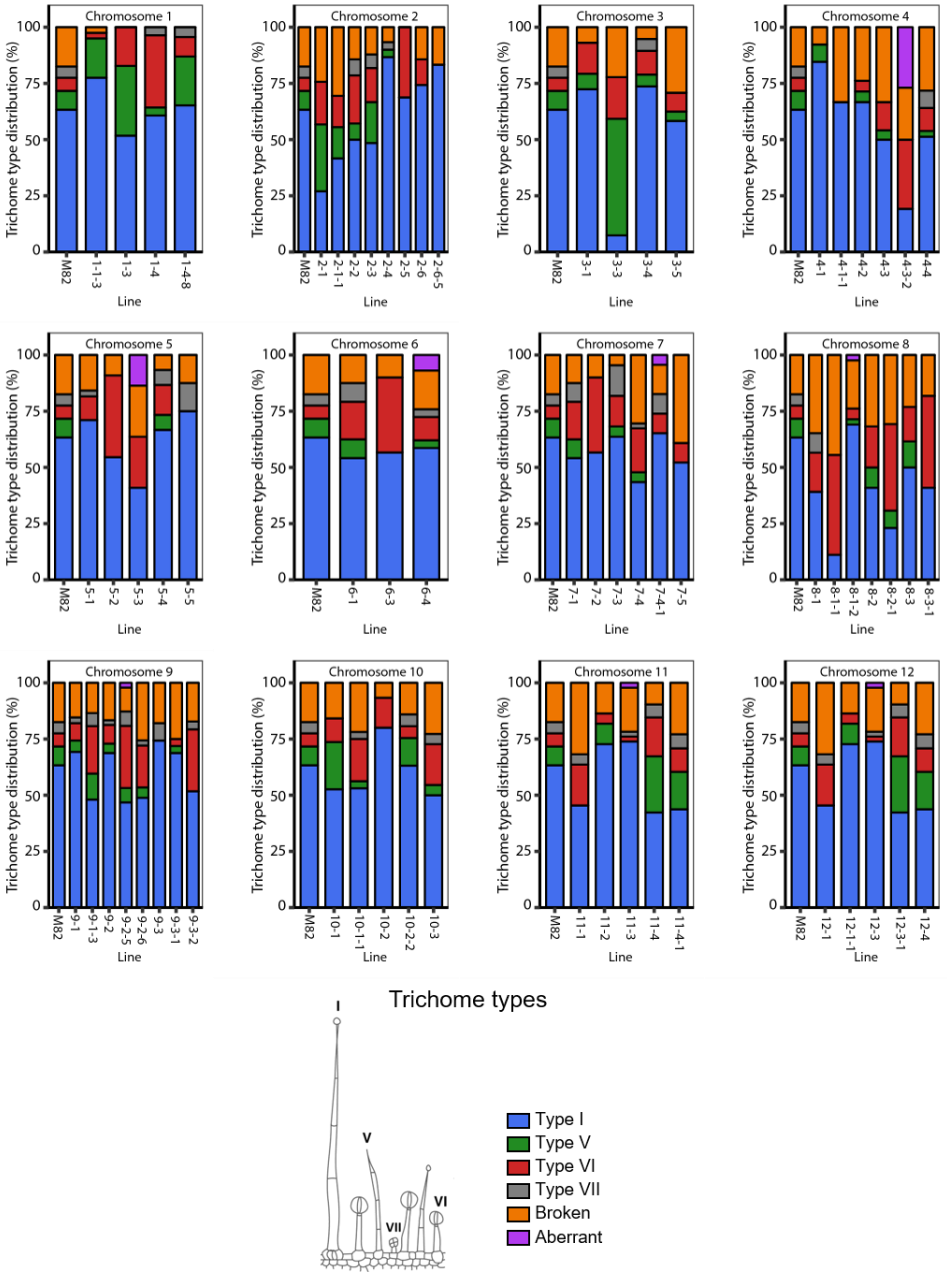

Figure 3.5.-Trichome type distribution in the first generation of the IL population. Lines are classified according to the chromosomal region introgressed from *S. pennellii* and each bar represents an IL, and the height of each colour section represents the proportion in percentage of each type of trichome. Blue represents type I trichomes; green represents type V trichomes; red represents type VI trichomes; grey represents type VII trichomes, orange represents damaged trichomes and purple represents aberrant trichomes. A schematic representation of each type of trichome is displayed in the legend. Trichomes are classified in different types according to (Luckwill, 1943).

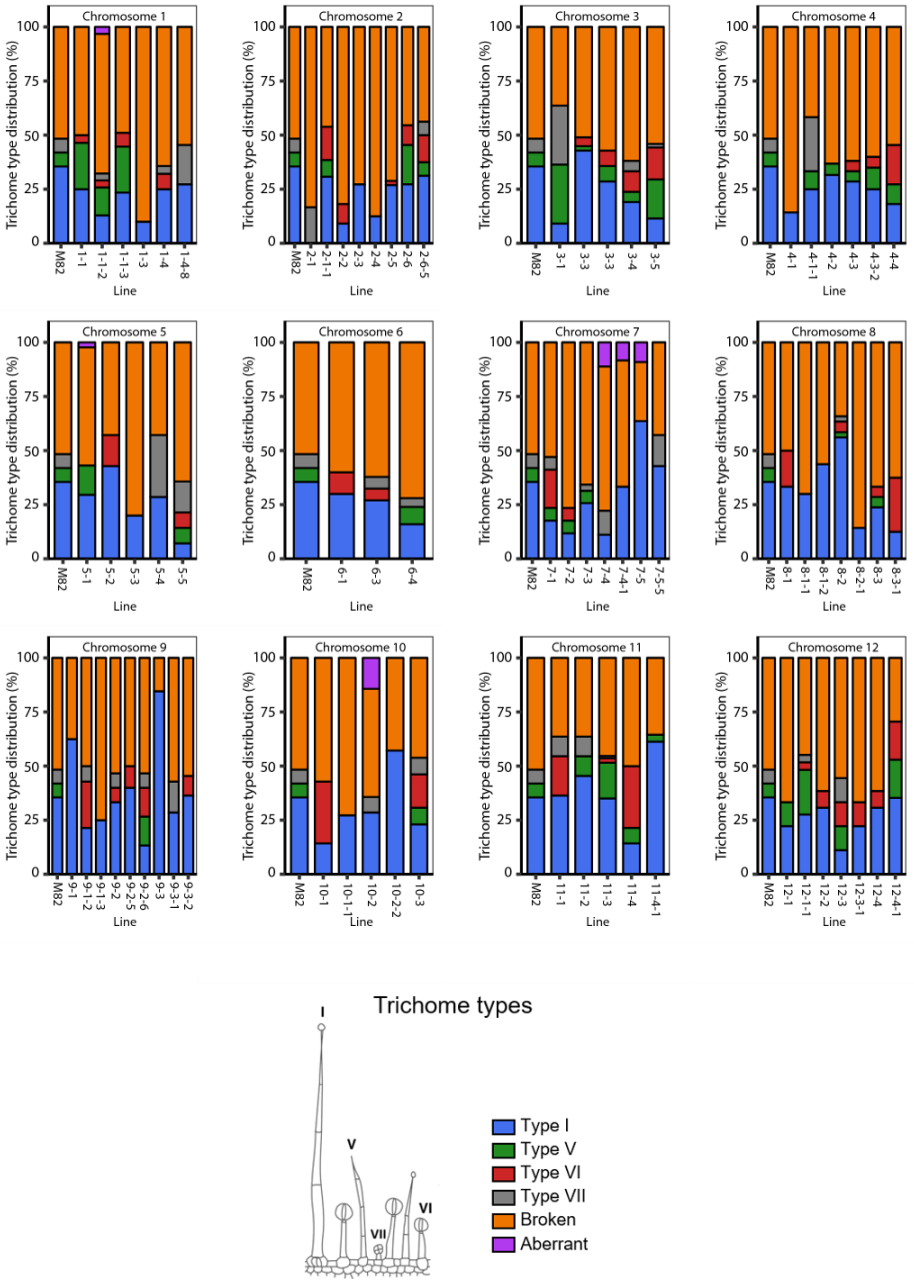

Figure 3.6.- Trichome type distribution in the second generation of the IL population. Lines are classified according to the chromosomal region introgressed from *S. pennellii* and each bar represents an IL, and the height of each colour section represents the proportion in percentage of each type of trichome. Blue represents type I trichomes; green represents type V trichomes; red represents type VI trichomes; grey represents type VII trichomes, orange represents damaged trichomes and purple represents aberrant trichomes. A schematic representation of each type of trichome is displayed in the legend. Trichomes are classified in different types according to (Luckwill, 1943).

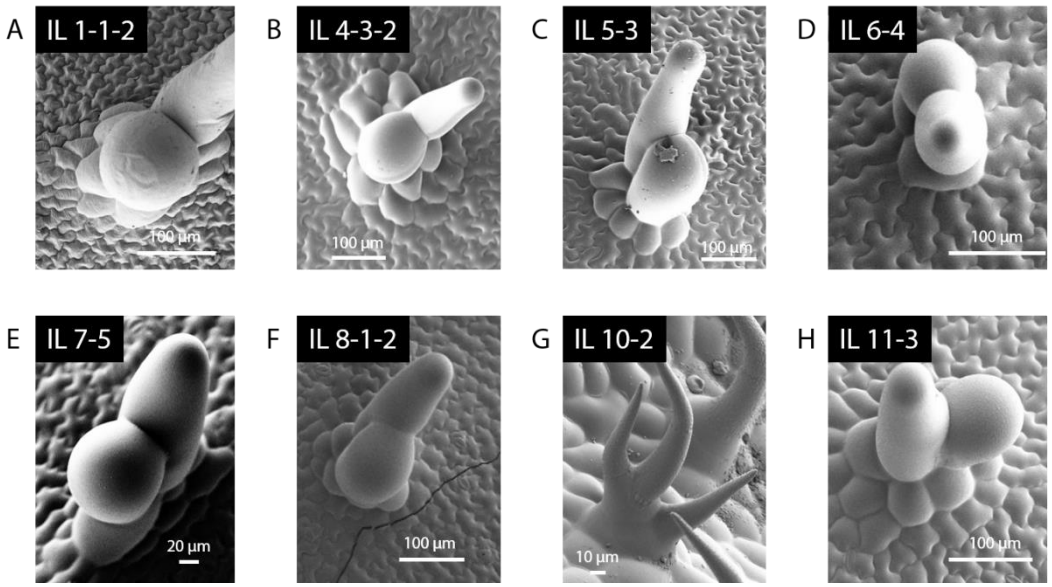

Figure 3.7.-Aberrant trichome morphologies in the IL population. Micrographs of representative aberrant trichomes are shown for ILs A) 1-1-2, B) 4-3-2, C) 5-3, D) 6-4, E) 7-5, F) 8-1-2, G) 10-2 and H) 11-3. The most common type of aberrant trichome is a type I-like swollen structure (A, B, C, D, E, F and H). Non-glandular branched trichomes were also observed (G). Scale is indicated in each micrograph.

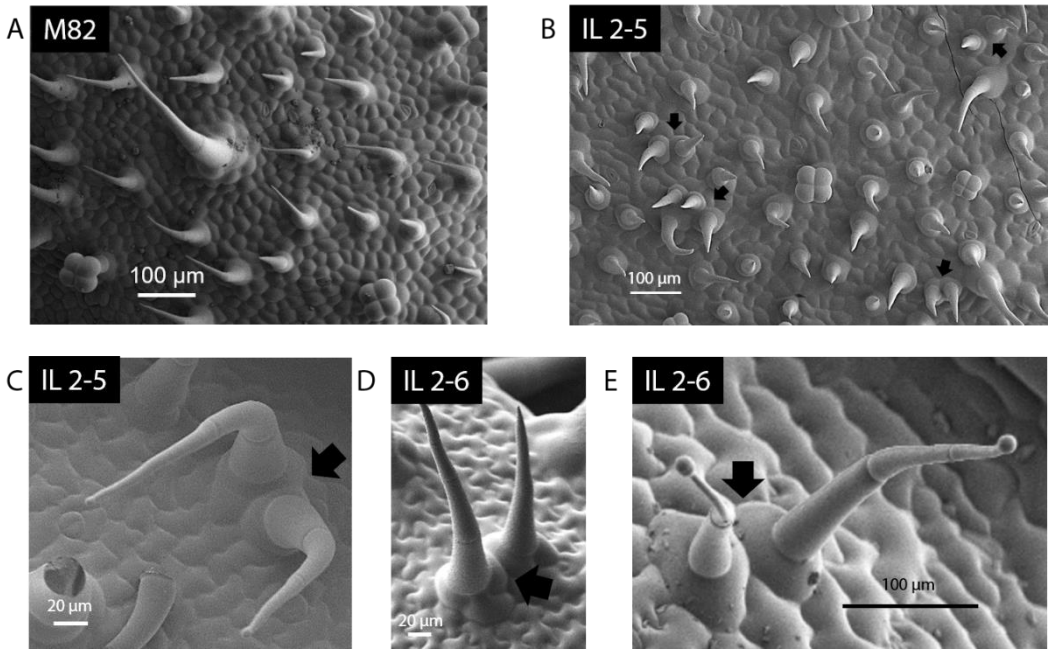

Figure 3.8.- Abnormal trichome clusters in the IL population. Micrographs of the adaxial surface of A) a young leaf of IL 2-5, B) a mature leaf of IL 2-5 and C), D) and E) mature leaves of IL 2-6 reveals abnormal patterning of type I and type V trichomes leading to clusters of up to four trichomes. Black arrows point to trichome clusters. Scale is indicated in each micrograph.

were made for glandular and non-glandular trichomes (Fig. 3.8C-E). Trichomes in these clusters were found oriented in all possible directions respectively to each other.

3.4.6.-Identification of genomic regions involved in the determination of stomatal density.

I measured the stomatal density on the adaxial surface of leaves of the two generations of the IL population (Fig. 3.9 and 3.10). As observed for trichomes, I found a high degree of variability in the population between and within lines. In contrast to the observation for trichome density, most ILs had a higher stomatal density than the parental line M82, which had one of the lowest values for stomatal density in the population. In the first generation, I identified 23 ILs with a significantly higher stomatal density compared to M82 (Fig. 3.9) and none of the lines showed a significantly lower stomatal density than M82. In the second generation, I found 10 lines with a significantly higher stomatal density compared to M82 and three lines with a lower stomatal density (Fig. 3.10).

I selected those lines that had a consistent stomatal phenotype in both generations, and this led to the identification of four ILs with a high stomatal density. These were: IL 5-1 in chromosome 5; ILs 7-2 and 7-5 in chromosome 7 and IL 8-3-1 in chromosome 8. It is interesting to note that only IL 7-2 appeared in both the lists of selected lines for trichome density and stomatal density. Interestingly, IL 11-3 behaved in opposite ways in the two generations, having a higher stomatal density compared to M82 in the first generation and a lower stomatal density in the second generation.

3.4.7.-Characterisation of the relationship between trichome and stomatal densities.

I observed a generally lower trichome density for most ILs (Fig. 3.3 and 3.4) and a generally higher stomatal density for most ILs (Fig. 3.9 and 3.10) compared to M82. I calculated the average trichome and stomatal densities for the whole population and compared these to the value for M82. For trichome density, in both generations, the average of the population was approximately half of the value recorded for M82 (Fig. 3.11A). Regarding stomatal density, the average for the population was approximately double the value for M82 in the first generation and slightly higher in the second generation (Fig. 3.11B). These observations indicated a potential correlation between both variables, as I also observed for the M82 values (Fig. 3.11C, R^2=0.60, p-value=0.04). However, no correlation was observed at the population level between trichome density and stomatal density.

To understand whether the observations made for the cultivated tomato (Fig. 3.11C) occurred in other species outside the *Asterids* clade, I measured trichome and stomatal density in *A. thaliana* Col-0 plants, as well as the trichome mutants *ttg1* and *ttg2* (Fig 3.12). As expected, *ttg1* mutant had no trichomes, and *ttg2* had aberrant trichomes but did not have lower or higher

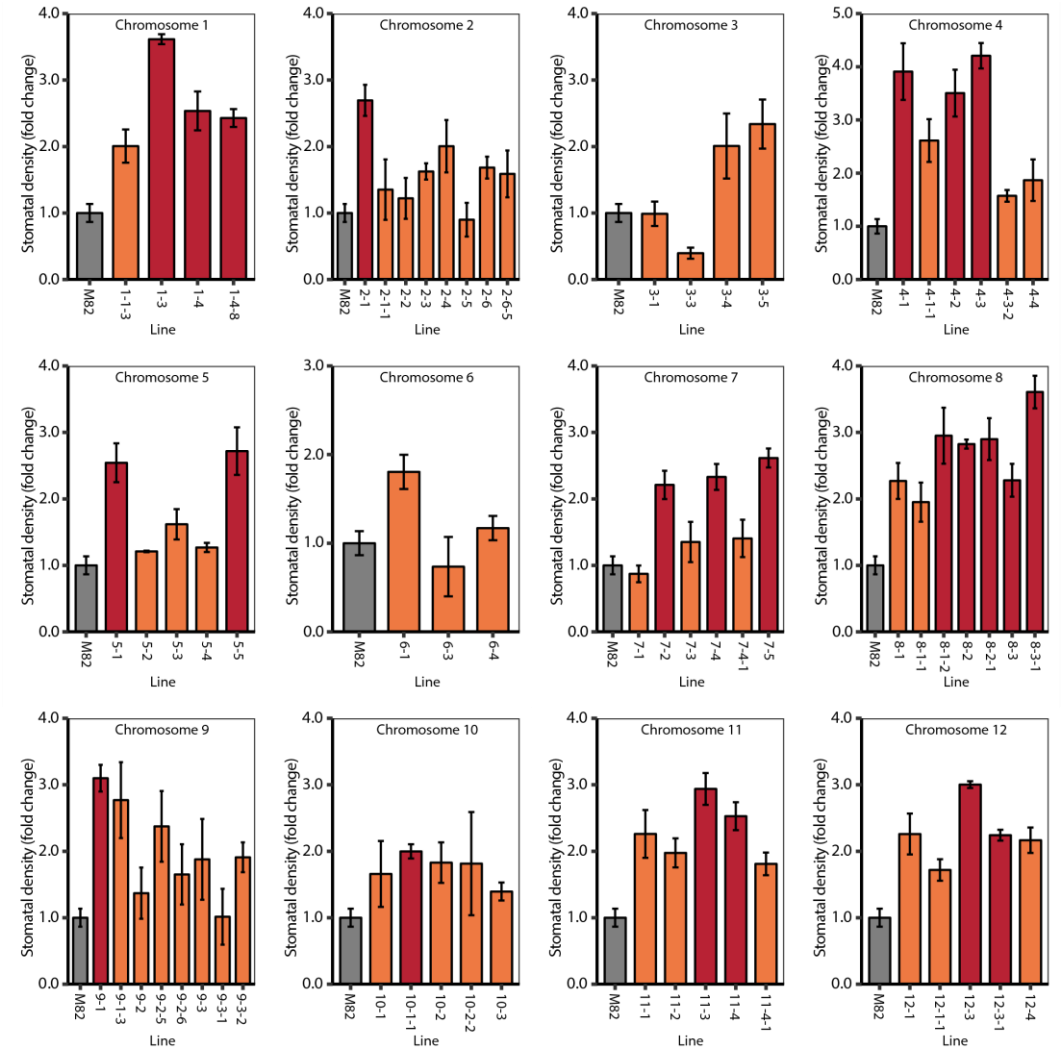

Figure 3.9.-Stomatal density of the first generation of the IL population. Stomatal density is expressed as fold-change of the ratio of stomata to total epidermal cells compared to M82. Lines are classified according to the chromosomal region introgressed from *S. pennellii* and each bar represents an IL. red bars represent lines showing a significant increase in stomatal density (p-value<0.005) when compared to M82. The grey bars represent the value for M82, used for comparison. For each line, the adaxial surface of the first fully-expanded true leaf from three plants was sampled.

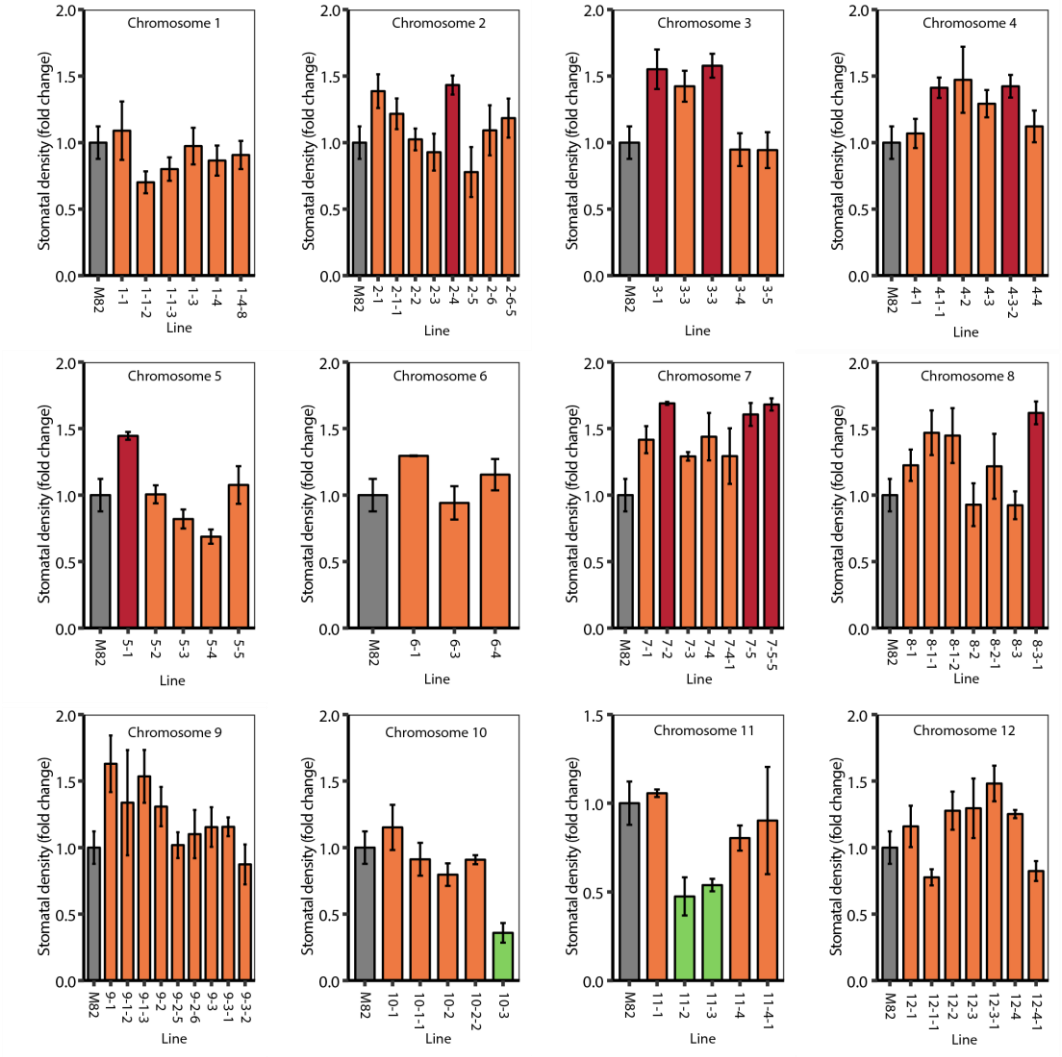

Figure 3.10.- Stomatal density of the second generation of the IL population. Stomatal density is expressed as fold-change of the ratio of stomata to total epidermal cells compared to M82. Lines are classified according to the chromosomal region introgressed from *S. pennellii* and each bar represents an IL. Green bars represent lines showing a significant (p-value<0.05) decrease in stomatal density and red bars represent lines showing a significant increase in stomatal density (p-value<0.05) when compared to M82. The grey bars represent the value for M82, used for comparison. For each line, the adaxial surface of the first fully-expanded true leaf from three plants was sampled.

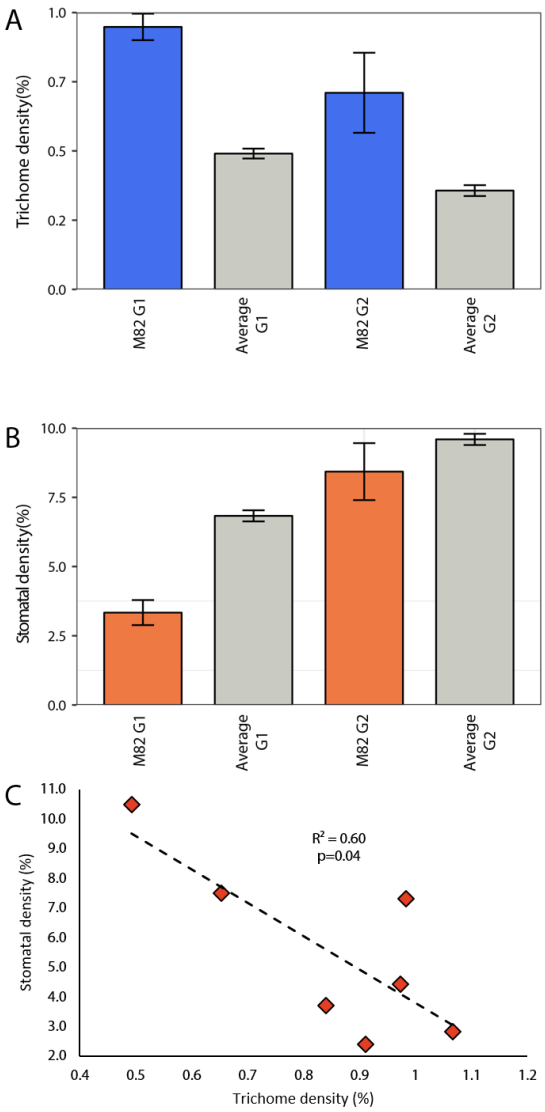

Figure 3.11.-Relationship between trichome and stomatal density in M82 and its comparison to the ILs. A) Trichome density in percentage of total epidermal cells of M82 in the first (G1) and second (G2) generations of the ILs compared to the average trichome density of the population. Blue bars represent M82 values and grey bars represent average values. B) Stomatal density in percentage of total epidermal cells of M82 in the first (G1) and second (G2) generations of the ILs compared to the average stomatal density of the population. Orange bars represent M82 values and grey bars represent average values. For A) and B), values are mean ± SEM (N=4 in M82 G1, N=3 in M82 G2, N=67 for Average G1 and N=74 for Average G2). C) Negative association between trichome density and stomatal density for M82 values combined for both generations. Correlation index and p-value are shown in the graph. Each point corresponds to an individual plant (N=7, N=4 in first generation and N=3 in second generation).

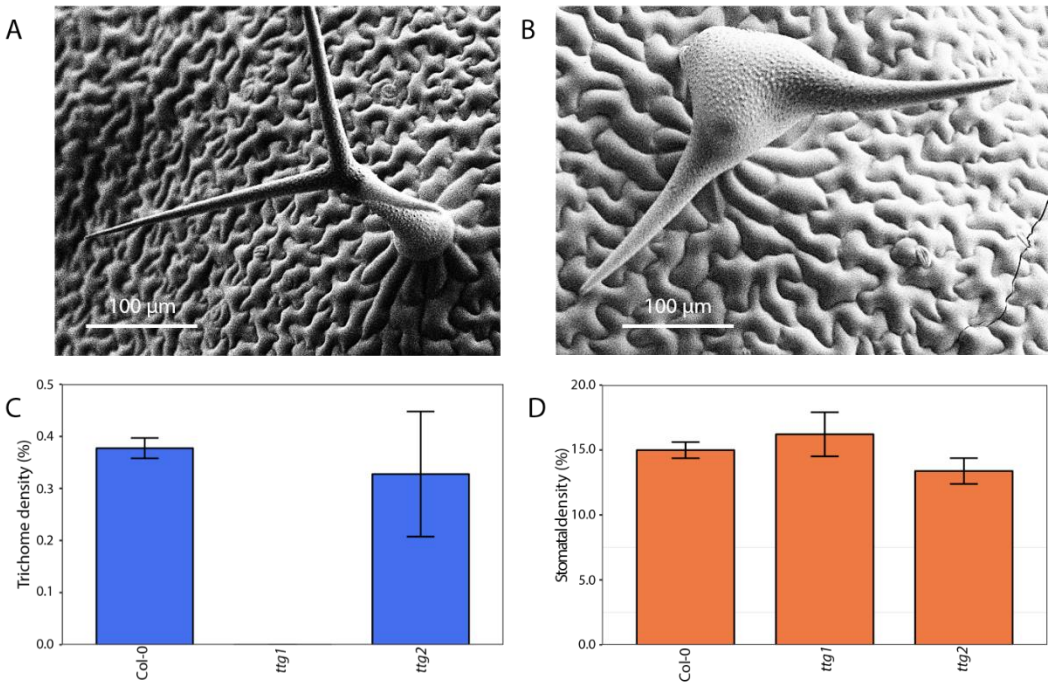

Figure 3.12.-Trichome and stomatal density in *A. thaliana* Col-0 and trichome mutants *ttg1* and *ttg2*. A) Unicellular, branched trichome in Col-0 *A. thaliana.* B) Aberrant trichome in *ttg2* mutant. C) Trichome density in percentage of total epidermal cells of Col-0, *ttg1* and *ttg2*. D) Stomatal density in percentage of total epidermal cells of Col-0, *ttg1* and *ttg2*. For C) and D) values are mean ± SEM (N=3). No significant differences were found between Col-0 and the mutant lines.

trichome density than Col-0 (Fig. 3.12A). For the three lines, no differences were observed in stomatal density (Fig. 3.12B). No correlation was observed between either variable for any of the lines individually or considering all of them together.

3.5.-Discussion

3.5.1.-Natural variation from the wild relative *Solanum pennellii* reveals new QTLs for trichome density in tomato

Trichome density is tightly associated with the physiological functions fulfilled by trichomes. Higher trichome density has been linked to improved tolerance to abiotic and biotic stresses, including tolerance to drought (Hauser, 2014, Mo et al., 2016) and insect attack (Bleeker et al., 2012, Tian et al., 2012). Therefore, understanding how trichome density is determined in tomato can have important agronomic impacts.

Wild relative species have been used for genetic improvement of commercially important crops, as they tend to preserve traits lost during domestication. In the case of *Solanum pennellii*, the IL population has been extensively used to identify QTLs involved in many different developmental, metabolic and physiological processes, including leaf development (Chitwood et al., 2013), fruit quality (Fernandez-Moreno et al., 2017) and photosynthetic activity (Magnum et al., 2018). These success stories supported the use of the natural variation present in the IL population to explore trichome development in tomato.

I measured the trichome density of *S. pennellii* and *S. lycopersicum* cv. M82 on the adaxial surface of leaves and found it was three-fold higher in *S. pennellii* compared to *S. lycopersicum* cv. M82 (Fig. 3.2C). This is in agreement to previous reports about trichomes in *Solanum* species (Simmons and Gurr, 2005). This difference supported the use of *S. pennellii* as a donor species to study trichome density determination in *Solanum.*

I observed a high variability in trichome density in both generations of the IL population, between lines and even between plants of the same line (Fig. 3.3 and 3.4). Trichome density is affected by several external stimuli, and changes in environmental conditions (water availability, temperature, light) can lead to increases or decreases in the number of trichomes (Gianfagna et al., 1992, Fu et al., 2013). Therefore, although the plants were grown in greenhouse under relatively stable conditions, changes in environmental and microenvironmental conditions (position effects, shadowing) may have been responsible for the observed variation. This is especially true for the first IL generation, where lines were grown successively over a period of six months. In any case, I could identify 18 ILs that showed a consistent phenotype over two generations, pointing towards a stable genetic component regulating trichome density in these lines.

Interestingly, most of the ILs analysed for this work showed a lower trichome density than M82, and these differences were consistent in both generations of the population (Fig. 3.3 and 3.4), with the average value of trichome density of the population being two-fold lower than M82 (Fig. 3.11A). This was unexpected given the values observed for the parents (Fig. 3.2C). Trichome development in tomato is a complex process which involves expansion of the cell wall, cell division and differentiation of glandular cells (Glover, 2000), and each one of these processes is under the control of positive and negative regulators (Tian et al., 2017). In addition to this, there is evidence that the development of different types of trichomes is regulated by different pathways. For example, the *Woolly* mutant in tomato showed an increase in type I trichomes but no other types were affected (Yang et al., 2011a). Small alterations in any of these steps, due to a different activity or expression level of the *S. pennellii* alleles of the genes controlling them, may explain the low trichome density observed in these lines.

The introgressed genomic regions from *S. pennellii* have been mapped precisely to the tomato genome and there is a high degree of certainty about their borders and the genes that are present in each IL (Fig. 3.13). Some of the ILs we identified by their low trichome density, harbour overlapping *S. pennellii* genomic regions, indicating that probably the genomic feature responsible for the phenotype is in the shared region. This is the case of ILs 2-2 and 2-3, 5-3 and 5-4, 9-3-1 and 9-3-2, and 12-3-1 and 12-3. This may help to narrow down the candidate genes responsible for the observed phenotypes. Interestingly, some of the selected genomic regions are completely contained within bigger regions corresponding to ILs which did not show a low trichome density in both generations. For example, this is the case of IL 2-1-1 the genomic region of which is fully contained in the region of IL 2-1 or IL 8-2-1 and IL 8-2. It is difficult to explain the reasons behind this observation. Perhaps ILs 2-1 and 8-2 might have missed the p-value cut-off due to the high variability of the population or as a result of type II error in the statistical analysis. This might be the case for the QTL in chromosome 2, as IL 2-1 also showed low trichome density in the second generation (Fig. 3.4). Another explanation involves the possible existence of a compensatory mechanism in the bigger genomic region. Finally, IL 8-1 and 8-1-1 harbour exactly the same region (Smeda et al., 2016).

I searched the genomic regions of interest for genes known to be involved in trichome development in tomato or related species. An aquaporin-like gene (Solyc08g066840) has been proposed as a candidate gene for the *dialytic* (*dl*) mutant phenotype (Chang et al., 2016), which maps to the IL 8-2-1 region. However, this mutant was not compromised in trichome initiation but rather in trichome development, displaying aberrant, forked trichomes on its leaf surface. The auxin-responsive factor 3 (SlARF3) plays an important role in the development of epidermis in tomato, and when knocked-down, trichome density was reduced (Zhang et al., 2015). SlARF3

maps to the region covered by IL 2-3. The HD-Zip transcription factor responsible for the *Woolly* (Solyc02g080260) mutant phenotype, with increased trichome density (Yang et al., 2011a), also maps to this region of chromosome 2. These genes might be potential candidates for the phenotype observed in this line (Fig. 4.3 and 4.4). The Woolly transcription factor interacts with a type-B cyclin (SlCycB2, Solyc10g083140), essential for division of multicellular trichomes, which causes a dramatic reduction in trichome density when silenced in RNAi lines (Gao et al., 2017). This gene maps to the region covered by IL 10-3, and might also be responsible for the low trichome density in this line. Finally, MIXTA-like1 is a known regulator of trichome development in *A. thaliana* (Oshima et al., 2013) and *Antirrhinum majus* (Perez-Rodriguez et al., 2005), although it remains uncharacterised in tomato. The tomato *MIXTA-like1* gene (*SlMX2*, Solyc04g005600) maps to the region corresponding to IL 4-1 and it is a good candidate for further analysis of its role in trichome development.

In conclusion, the natural genetic variation present in the IL population, coupled with our phenotyping screen, revealed new genomic areas of interest containing genes with potential roles in determination of epidermal development. This IL screen will aid any future research on trichome development in *Solanum* species.

3.5.2.-Cryo-SEM allows precise classification of trichome identity and morphology in the IL population.

I classified trichomes on the adaxial surface of the first true leaf of two generations of the ILs, using cryo-scanning electron microscopy (SEM) for the first generation (Fig. 3.5) and using chemical fixation coupled with room temperature SEM for the second generation (Fig. 3.6). Trichomes are fragile structures and their function as factories of secondary metabolites make them prone to abscission of the glandular heads that are used for trichome classification (Bergau et al., 2015). They are also hydrated structures which tend to collapse under high-vacuum conditions, required for traditional SEM. The use of the cryo-fixation allowed me to determine the trichome types with a low percentage of broken trichomes (Fig. 3.5). However, the use of chemical-fixation was highly damaging and most trichomes were found broken on the assessed surfaces (Fig. 3.6). Therefore, although chemical fixation might be a better tool for analysis of trichome density (Fig. 3.4), cryo-fixation should be used preferentially for assessing trichome identity (Fig. 3.5) or aberrant morphologies or patterning (Fig. 3.7 and 3.8).

I classified trichomes according to (Luckwill, 1943), although I grouped type I and type IV under the same group (Type I in Fig. 3.5 and 3.6). Type I and IV share the same morphology and metabolic profiles, and their differences are based mostly on their length, so some authors consider type I and type IV as a single type (McDowell et al., 2011). In a similar fashion, non-

glandular trichomes are traditionally classified as type II, III or V depending on their length, but for comparative purposes they were all labelled as type V (Fig. 3.5 and 3.6).

The most abundant trichome type in M82 and most ILs was type I (Fig. 3.5), in contradiction to previous reports, that ranked type VI as the most common glandular trichomes (Bergau et al., 2015). This observation may have been due to a difference between M82 and the cultivars used in other studies. Importantly, the density of type I trichomes was reported to be a juvenility trait, being very high in the first leaf – the one we assessed for every plant- and going down in leaves formed afterwards, and this happens as a trade-off with type V trichomes, which are less abundant in early leaves and become much more abundant in late ones (Vendemiatti et al., 2017). This report agrees with our results and therefore indicates a potential bias in our observations but reinforces the necessity for consistency in sampled tissues for meaningful comparisons. This also explains why we observed 21 ILs with no type V trichomes. I observed four lines with a low proportion of type I trichomes. In the case of ILs 2-1 and 3-3, this was compensated by an increase in the percentage of type V trichomes, with an inverted trend to the observations in (Vendemiatti et al., 2017), making them good lines for further research on the control of juvenile phase development. In the case of ILs 8-1-1 and 8-2-1, the observed reduction in type I trichomes was accompanied by a reduction in trichome density (Fig. 3.3 and 3.4). This suggests that the pathway controlling the formation of type I trichomes may be compromised in these lines, while other types might not be affected. Both lines also showed an increased proportion of type VI trichomes. This could indicate that different types of trichomes are controlled by different regulatory mechanisms and that these mechanisms might be interlinked to compensate for alterations in the type distributions. This is in agreement with previous reports in tomato (Li et al., 2004, Yang et al., 2011a) and tobacco (Payne et al., 1999).

Type VI trichomes were relatively unabundant in the sampled leaves, but absent only in 7 ILs of the population. IL 4-1 had no type VI trichomes, and this line also had low trichome density (Fig. 3.3 and 3.4). As inferred before for ILs on chromosome 8, this low trichome density could be due to a specific reduction in this type of trichome. It is important to note that, even though I could not find type VI trichomes in the assessed tissues, they were found on stems and major veins (not shown), suggesting a tissue specific regulation of epidermal development, which is not uncommon in other species such as *A. thaliana* (Schnittger et al., 1998) or *A. majus* (Glover et al., 1998). Type VII trichomes were very scarce in the interveinal leaf tissue in all lines, and this led to finding none in half of the lines (Fig. 3.5). This type of trichome was however commonly found on major and minor veins (data not shown), indicating that their number is higher in these stem-like tissues.

While phenotyping the IL population, I found several aberrant morphologies (Fig. 3.7) and unusual epidermal patterning (Fig. 3.8). The most common aberrant morphology consisted of a multicellular base similar to the one found in type I trichomes, with two swollen cells emerging from this base (Fig. 3.7 A-F and H). These structures are reminiscent of the aberrant type I trichomes in the *odourless-2* mutant (Kang et al., 2010b), still uncharacterised, and the *dialytic* mutant (Chang et al., 2016). In some ways, the swollen appearance of these trichomes is similar to that observed in the *hairless* mutant (Kang et al., 2010a, Kang et al., 2016b), which presents a truncated version of the *SPECIALLY-RAC1 ASSOCIATED* (*SRA1*) gene and is therefore compromised in the actin cytoskeleton organisation in trichomes, or the *inquieta* mutant, which harbours an altered copy of the *ACTIN-RELATED PROTEIN 2/3 COMPLEX SUBUNIT 2A* (*ARPC2A*) (Jeong et al., 2017). It is possible that the observed phenotype might be to alterations in the process of cell elongation or cytoskeleton development. In fact, the *ARPC2A* gene maps to the IL 11-3 region (Fig 7H). The *ACTIN-RELATED PROTEIN 3* (*ARP3*) and *ACTIN-RELATED PROTEIN 2/3 COMPLEX SUBUNIT 3* (*ARPC3*) genes encode proteins that are part of the complex required for actin filament formation (Goley and Welch, 2006), and map to the IL 4-3-2 and IL 7-4/7-4-1/7-5 regions respectively (Fig. 3.7B and E). All these lines need further analysis to understand whether the phenotype is caused by impairment of the same pathway or whether they are the structures resulting from alterations in different pathways. The fact that all of these appear amid wild-type looking trichomes (Fig. 3.5) points towards a phenotype caused by small changes in expression or functionality of *S. pennellii* versions of the genes rather than gain- or loss-of-function mutations. I also observed a branched, multicellular, non-glandular type of trichome in ILs 10-2 and 10-3, which lacks a multicellular base (Fig. 3.7G). This structure resembles the type V-like trichomes observed in SlCycB2 or Woolly RNAi lines (Yang et al., 2011a), and actually, SlCycB2 maps to the region delimited by these two ILs, indicating that the *S. pennellii* version of the gene might have reduced activity compared to that of M82.

Finally, I observed an unusual clustering of trichomes in ILs 2-5 and 2-6 (Fig. 3.8). These clusters were much more evident in young leaves (Fig. 3.8B) but were usually found in mature leaves as well (Fig. 3.8C-E). Trichomes are evenly distributed over the leaf surface in tomato (Fig. 3.8A), although the mechanisms by which this patterning is determined are unclear. In *A. thaliana*, trichome patterning is mediated by small MYB transcription factors that inhibit trichome initiation in cells adjacent to newly formed trichomes (Hauser, 2014), but the mechanism in tomato and related species is not understood yet (Tominaga-Wada et al., 2013). These lines provide useful tools to gain new insights into cell fate determination in the epidermis of leaf.

3.5.3.-Screening the IL population reveals new QTLs for stomatal density and a link between trichome and stomatal development.

I also measured the stomatal density for each line in both generations of the ILs (Fig. 3.9 and 3.10). Stomatal density is a key trait in tolerance to abiotic stresses as stomata have a direct role in gas exchange and maintenance of water status (Masle et al., 2005, Wentworth et al., 2006), and a low stomatal density has been associated with an improved response to drought conditions (Zhao et al., 2017). Similar to the observations made for trichomes, variability in stomatal density in the population and within lines was very high, and this may be a response to small alterations of environmental conditions, since stomatal density is affected by light, CO_2 concentration and temperature (Beerling and Chaloner, 1993, Rogiers et al., 2011), and this again may be especially true for the first generation of the ILs (Fig. 3.9). Overall, I identified 4 ILs with a consistently high stomatal density in both generations, and these were selected as candidate lines.

Interestingly, most of the lines had a higher stomatal density than the parental line M82 (Fig. 3.9 and 3.10), with the average value for the population being two-fold higher in the first generation and slightly higher in the second (Fig. 3.11B). This was unexpected as previous studies had reported a lower stomatal density in *S. pennellii* (Heichel and Anagnostakis, 1978, Chitwood et al., 2013), bur my own measurements showed a stomatal density significantly higher in *S. pennellii* than in the cultivated parent (Fig. 3.2D). This behaviour was the opposite to my observations for trichomes, where most lines had a lower trichome density than M82 (Fig. 3.3, 3.4 and 3.11A). These observations suggested a potential link between trichome and stomatal development, as has been reported before for tomato and tobacco (Glover et al., 1998, Glover and Martin, 2000). I did observe a significant correlation between trichome density and stomatal density in M82 plants (Fig. 3.11C), but this was not observed at the population level, where we found no correlation between the two variables. The former observations suggest a possible developmental link between both epidermal structures, probably involving an early commitment of cell fate to trichome formation that prevents stomatal formation thereafter as described for tobacco (Glover et al., 1998). I also have evidence that this negative association between trichomes and stomatal densities might take place preferentially under stress conditions (discussed in *chapters 7* and *8*).

Epidermal development is a complex process that involves many regulators. Some of them might act in determining both stomatal and trichome development, such as MIXTA (Glover et al., 1998) or GL1 and TRY in *Arabidopsis* (Bean et al., 2002), which determine stomatal and trichome patterning in cotyledons. Other genes, however, might affect different steps of trichome or stomatal development without affecting the formation of other epidermal structures. This is the

case of the TRANSPARENT TESTA GLABRA 1 (TTG1) (Walker et al., 1999) and 2 (TTG2) (Pesch et al., 2014) in *Arabidopsis*, both known regulators of trichome development, which were analysed to understand whether the correlation observed for tomato (Fig. 3.11C) was observed in other distant species. Trichomes were completely absent in the *ttg1* mutant, while their density in *ttg2* mutants was not substantially lower (Fig. 3.12C), despite the fact that they presented aberrant branching (Fig. 3.12B). The lack of trichomes in the *ttg1* mutant did not result in an increase in stomatal density (Fig. 3.12D), and no changes in stomatal density were observed either for the *ttg2* mutant (Fig. 3.12D). Therefore, I concluded that neither of these genes had a role in stomatal development in *Arabidopsis*. It is plausible that other genes in tomato might act in similar ways, affecting one of the two structures, and this might be the case for ILs where changes in trichome density were not accompanied by changes in stomatal density (Fig. 3.3-3.6). In general, my results suggested that a link between stomatal and trichome development exist, but this might be restricted to certain conditions or regulatory mechanisms, and its universality is unlikely.

I analysed the genomic regions covered by the 4 ILs with consistent high stomatal density to determine if any known regulators of stomatal development (Pillitteri and Dong, 2013) mapped to them. I could not find any of the genes in the introgressed regions, and this suggested that new genes involved in determination of stomatal density might be responsible for the phenotype.

In summary, I found new interesting QTLs in the IL population controlling stomatal density. I observed a link between stomatal and trichome development, but its extent and the mechanisms regulating this crosstalk require further investigation. It is important to note that all these analyses were done on the adaxial surface of the leaves, which has fewer stomata than the abaxial surface, and a detailed analysis of both sides of the leaves would be beneficial for a better understanding of epidermal development.

3.6.-Conclusion

In this chapter, I present a comprehensive analysis of the epidermal structures in the adaxial surface of leaves of the *S. pennellii* x *S. lycopersicum* cv. M82 IL population. By combining two fixation methods, chemical fixation and cryofixation, and two generations of the ILs, I produced a very powerful data set to study variation of trichome and stomatal density, trichome identity and trichome formation.

This analysis allowed me to identify 18 ILs with a low trichome density and 4 ILs with high stomatal density. Most of the genomic regions corresponding to these ILs do not map to any known regulatory gene of either trichome or stomatal development, so I have identified new

loci that need to be researched further. In a similar way, we found important differences in the proportion of trichome types in the ILs and also trichomes with aberrant shapes. Further analysis of the introgressed regions harboured by these lines will shed light on regulation and structural development of trichomes.

Finally, I have produced further evidence that trichome and stomatal development is negatively associated in tomato, although I observed some limitations to the universality of the phenomenon. First, the negative association between stomatal and trichome density was not observed in the whole IL population, but only in the parental cultivated line. Second, this relationship was not observed at all in *A. thaliana* trichome mutants.

In conclusion, I believe that the data generated for this chapter will contribute to the phenotypic data available to the tomato scientific community and will make an important contribution to future research projects.

Acknowledgement to contributors

This chapter benefitted of the contribution of the visiting student Magda Lisette Arce-Rodríguez, from Centro de Investigación y de Estudios Avanzados del Instituto Politécnico Nacional-Unidad Irapuato in Guanajuato, Mexico, who worked under my supervision three months in winter 2016-2017. She helped in the generation of SEM micrographs of the second generation of the IL population, as detailed in the main text.

Chapter 4 – Virus-Induced Gene Silencing of candidate genes potentially involved in trichome development.

4.1.-Abstract

In this chapter I describe the functional characterisation of candidate genes selected from the phenotypic screen of the ILs performed in *chapter 3* for their potential involvement in trichome development, by means of virus-induced gene silencing (VIGS). I discuss the advantages and limitations of this transient assay. The work in this chapter led to the identification of two *MIXTA* genes (*SlMIXTA-like* and *SlMX2*) with a role in trichome patterning and trichome initiation respectively. I could also validate the function of *SlCycB2* in regulating trichome morphogenesis.

4.2.-Introduction

4.2.1.-Tools available for QTL mapping using the IL population.

The DNA sequence of the tomato genome has been available for several years (The Tomato Genome, 2012), and since its publication, the volume of work devoted to understanding its main features has been vast (Aoki et al., 2013, Causse et al., 2013, Karlova et al., 2013, Kim et al., 2014, Lin et al., 2014, Jung et al., 2016). The Sol Genomics Network (Fernandez-Pozo et al., 2015a) is an online database containing all the available genomic information for tomato, as well as other *Solanaceae* species. This platform includes information about wild crop relatives -where available-, gene annotation for known loci and provides tools for molecular studies (molecular markers, BLAST, genetic maps). The database is updated periodically to reflect the latest discoveries in tomato genomics.

The introgression line populations have proven to be useful for breeding and research (see *chapter 3*). The widespread use of wild crop relatives in tomato has benefitted from the sequencing of some of their genomes, including *Solanum pimpinellifolium* (The Tomato Genome, 2012)*, Solanum lycopersicoides* (The Solanum lycopersicoides Genome Consortium, unpublished but available) and *Solanum pennellii* (Bolger et al., 2014), the parent of the IL population used for this thesis. The genomic information available for both the cultivated and the wild parents of the populations has been extremely useful to find differences and potential candidates for trichome development. In addition to this, there has been an effort to map precisely the genomic regions introgressed in each one of the ILs (Chitwood et al., 2013, Fernandez-Pozo et al., 2015a), allowing fast trait mapping to a relatively small region containing a manageable number of candidate genes.

The accessibility and affordability of sequencing approaches have led to the generation of a huge number of RNAseq datasets for tomato, for different organs, developmental stages, physiological processes and stress conditions. Specifically, RNAseq data for *S. lycopersicum* cv. M82 and *S. pennellii* (as well as other wild relatives) is publicly available (Koenig et al., 2013, Dai et al., 2017) and it can be browsed easily through the eFP browser (Winter et al., 2007). Apart

from transcriptomic profiling of the parental lines of the IL population, several attempts have been made to characterise the whole set of ILs. For example, the Tomato Functional Genomics database provides information about gene expression in tomato fruit, combined with information about metabolite content and small RNAs, for the whole *S. pennellii* IL population (Fei et al., 2011), alongside many other useful datasets. The transcriptomic data has been used successfully to identify candidate genes involved in lycopene and ascorbic acid accumulation in fruit (Calafiore et al., 2016). In a similar way, RNA from leaves of all the ILs was sequenced and the dataset was made available (Chitwood et al., 2013). This information has aided in understanding several leaf developmental and hormonal processes (Bucksch et al., 2017, Coneva et al., 2017, Wang et al., 2018). Finally, we have access to different cell type-specific RNAseq data, including the Tomato Expression Atlas (Shinozaki et al., 2018) that provides stage-specific transcriptomic data for each cell type in the tomato fruit, or trichome-specific transcriptomics (Spyropoulou et al., 2014).

All the available resources, together with the characterisation of the different phenotypes of the IL population for hundreds of traits (see *chapter 3*), have facilitated functional genetics approaches in tomato and have been essential for the work described in this thesis.

4.2.2.-Virus-induced gene silencing (VIGS) as a tool for molecular characterisation

Virus-induced gene silencing (VIGS) is a system for transient silencing of target genes *in planta* using a viral vector which is targeted by the silencing machinery of the cell (Sahu et al., 2012). The dsRNA generated during viral replication are targeted by DICER, which cleaves them into short interference RNAs (siRNA), that are recruited by the RNA-induced Silencing Complex (RISC). This complex can recognise transcripts complementary to the siRNA generated by DICER, and cause the degradation of the complementary transcript and, consequently, the silencing of the target gene (Baulcombe, 2004, Becker and Lange, 2010). This mechanism is used by plants to stop viral infection by silencing the viral genome (Waterhouse and Fusaro, 2006), but modification of the viral sequence to include a sequence complementary to the target host gene can be used for functional studies. It is a rapid system that does not require stable transformation of the crop or plant under study and can be performed transiently (Sahu et al., 2012), and it also leads to a systemic silencing of the gene, with tissues generated after infiltration showing also a reduction in the expression of the target gene (Kriton et al., 2008).

Despite its usefulness for characterisation of gene functions, VIGS has some limitations. First, the sequence similarity between different genes can cause off-target silencing, leading to inaccurate conclusions being drawn from the phenotypes observed (Sahu et al., 2012). This can be overcome by selecting a highly-specific gene fragment, and computing tools are available for tomato genes to determine the best VIGS fragment embedded in the Sol Genomics Network

website (Fernandez-Pozo et al., 2015a). Second, the silencing does not take place homogenously in infiltrated plants, but rather in a patchy fashion (Senthil-Kumar et al., 2007), which limits the applicability of this technique when phenotypes cannot be visually inspected or need quantitative assessment (for example, trichome density on leaves). This problem has been partially overcome in tomato using co-silencing of visual markers such as GFP (Quadrana et al., 2011) or Delila/Rosea1 (Orzaez et al., 2009) together with the gene of interest. With this reporter gene approach, it is relatively straightforward to delimit the regions where silencing is taking place.

VIGS has been extensively used for functional characterisation of genes in many different species, including model species and crops (Senthil-Kumar and Mysore, 2011). In fact, a huge number of viral vectors have been developed to infect a wide range of hosts, including *Barley stripe mosaic virus* (BSMV) as the preferred choice for monocotyledonous species (Steve et al., 2002, Yuan et al., 2011) and *Tobacco Rattle Virus* (TRV) as the most widely used vector for dicotyledonous species, including pepper (Arce-Rodríguez and Ochoa-Alejo, 2017), cotton (Gao et al., 2011), *Nicotiana* (George et al., 2010) and tomato (Liu et al., 2002) among many examples (Senthil-Kumar and Mysore, 2011). In the case of tomato, other vectors have been developed for VIGS assays, including *Apple Latent Spherical Virus* (ALSV) (Igarashi et al., 2009) or Potato Virus X (PVX) (Lacomme and Chapman, 2008), but their use is essentially anecdotical compared to examples using TRV-based vectors. The TRV-based system involves co-infiltration with two different constructs, pTRV1 and pTRV2. pTRV1 contains the RNA-dependent RNA polymerase required for the replication of the virus (and the formation of dsRNA necessary for silencing), as well as the movement protein required for the systemic spread of the viral infection. pTRV2 includes the viral coat protein as well as the recombinant DNA fragment complementary to the target gene for silencing. This system is versatile and different cloning methods can be used for the construction of the recombinant pTRV2, including Gateway (Liu et al., 2002) or ligation-independent cloning (Dong et al., 2007).

VIGS has been an essential tool for characterisation of genes in tomato and the number of reports of its use is very extensive (Sahu et al., 2012). Some interesting examples include the characterisation of SlMYB12 as a regulator of flavonoid biosynthesis that, when silenced, produces a pink-coloured rather than a scarlet-coloured fruit (Ballester et al., 2010). VIGS was also used to characterise some fruit ripening regulators, such as the *SQUAMOSA promoter binding protein-like* gene in the Colourless non ripening (Cnr) locus (Manning et al., 2006) or *Ethylene Insensitive 2* (*SlEIN2*) (Fu et al., 2005). The silencing of both of these genes caused an inhibition of fruit ripening. The VIGS approach has also been used to study the development of vegetative organs in *Solanum.* For example, silencing of the *Geranyl Diphosphate Synthase* gene

(SlGPS) caused a dramatic dwarf phenotype (Van Schie et al., 2007), and helped characterise the role of this gene in the gibberellin biosynthetic pathway. More recently, VIGS-mediated silencing of *Argonaut1* (*AGO1*) – a member of the RISC complex required for small RNA silencing- showed the important role of this gene in the development of compound leaves and determination of trichome density (Wang et al., 2015a). It is inferred from transcriptomic studies in AGO1-silenced tissue that this role might be mediated by deregulation of auxin signalling-related genes, and specifically for trichomes, the *SlIAA15* gene, which is known to affect trichome density (Deng et al., 2012). However, this is probably the only study in tomato where transient silencing though VIGS has been used to test the role of candidate genes in trichome development, and its use as a mid-to-high throughput testing tool can be exploited to understand this and other developmental processes.

In this chapter, I will describe the selection of candidate genes affecting trichome formation in tomato, based on the results described in *Chapter 3*, using the available genomic and transcriptomic tools and the phenotypes observed when these were silenced using VIGS in young tomato plants.

4.3.-Methods

4.3.1.-Candidate gene selection.

I selected interesting genomic regions based on the screen of the ILs phenotypes described in *chapter 3*. I analysed the selected IL intervals for candidate genes with a potential involvement in the observed trichome phenotypes. I used the bin map developed by (Chitwood et al., 2013) to narrow down the number of genes using information from adjacent ILs, although in most cases I included neighbouring bins, due to the diffuse nature of the borders between introgressed regions and the potential for epistatic effects of other genes or genomic features contained in the target and adjacent ILs. The genes corresponding to the selected bins were filtered based on their annotation (The Tomato Genome, 2012, Fernandez-Pozo et al., 2015a), and I picked those genes with annotation terms with a potential relation to trichome development, including hormone-signalling (especially auxin), structural genes necessary for cell expansion (expansins, cytoskeleton-related genes) and transcription factors. These genes were further filtered using the available transcriptomic information. Therefore, I determined whether each gene was expressed or not in trichomes (Spyropoulou et al., 2014) and whether its expression was downregulated or upregulated in the target IL (Chitwood et al., 2013). Downregulation and upregulation were called by comparing the expression values for the target gene in the selected IL compared to the average of the population. A gene was considered downregulated when the expression level was less than 80% of the average value for the population. A gene was considered upregulated when the expression level was more than 120%

of the average value of the population. The significance of changes could not be assigned as I lacked data for the parental line M82 or replicate values, and was thus used as a supporting tool. The final candidates for molecular characterisation were selected depending on all the previous criteria. Finally, the *S. pennellii* version of each gene (Bolger et al., 2014) was analysed to check for significant changes in sequence that could lead to lack or gain of functionality as well as to determine whether the gene was *S. lycopersicum*-specific using the BLAST tool in the Sol Genomics Website (Fernandez-Pozo et al., 2015a).

4.3.2.-Plant material for VIGS assays.

Virus-induced gene silencing assays were performed on transgenic *S. lycopersicum* cv. Microtom plants carrying a proSlPNH:AmRosea1/35S:Delila insertion, referred to as *Valencia* plants hereafter (Martin et al., 2012). The promoter of the *AmRosea1* gene corresponds the *PNH* gene, of unknown function, initially described as fruit-specific (Estornell et al., 2009). However, when the described construct was stably transformed in tomato (work done by Dr Eugenio Butelli in Cathie Martin's lab), its expression was generalised in all tissues, including leaves, roots, anthers and fruits (Fig. 4.1 A and B), where both genes combined drove the expression of anthocyanin biosynthetic genes and produced a strong purple colouration. No differences in trichome phenotype were observed between MicroTom and *Valencia* leaves (Fig. 4.1 C and D).

4.3.3.-Generation of VIGS constructs.

For VIGS assays, 300 bp fragments of the target gene coding sequence were selected for amplification and insertion into a pTRV2-Del/Ros1-GW plasmid (Orzaez et al., 2009). This pTRV2 version is a modification of the original one described by (Liu et al., 2002), and it includes a recombinant fragment targeting *Delila* and *Rosea1,* followed by a Gateway cassette to allow efficient cloning of DNA fragments targeting the gene of interest in each case. This allows silencing of the candidate gene together with silencing of the *Del/Ros1* genes overexpressed in Valencia plants, which leads to formation of green tissue (compared to purple, unsilenced tissue) that can be used as a visual marker for silenced sectors.

For each one of the ten candidate genes, a 300 bp fragment was chosen using the VIGS tool in the Sol Genomics Network website (Fernandez-Pozo et al., 2015b). This tool indicated the best gene fragment to reduce off-target silencing. The fragment was amplified from *S. lycopersicum* cv. MoneyMaker and cloned using the Gateway system (see *chapter 2*). The primers for each one of the fragments are shown in Appendix 1. The presence of the insert in the final construct was verified by sequencing using pTRV2-specific primers.

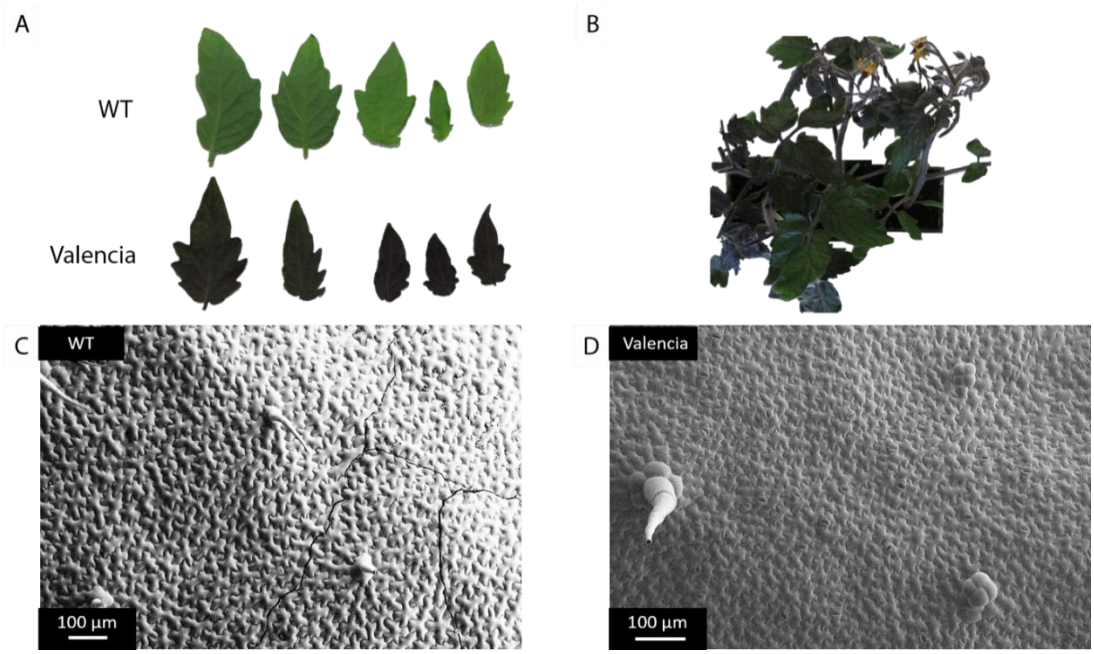

Figure 4.1.-Phenotype of *Valencia* (proSlPNH:AmRosea1/35S:Delila) plants. A) Close-up view of WT *S. lycopersicum* cv. Microtom leaves and Valencia leaves are shown. B) Overview of Valencia plants, where the purple colouration can be observed in stems, leaves and anthers. Strong anthocyanin pigmentation is responsible for the purple colour. C) Scanning electron micrograph of the adaxial surface of a WT microtom leaf. D) Scanning electron micrograph of the adaxial surface of a Valencia leaf. No differences were observed between the trichome phenotype for both lines.

4.3.4.-Agroinfiltration and assessment of silenced phenotype.

Seeds from Valencia plants were grown under greenhouse conditions for 7-10 days before agroinfiltration. *Agrobacterium tumefaciens* strain AGL1 were transformed by electroporation with the pTRV1 plasmid and the pTRV2-Del/Ros1-Target and grown in selective media containing kanamycin (50 µg/mL), ampicillin (100 µg/mL) and rifampicin (50 µg/mL). Liquid cultures were grown to an OD_{600}=0.5-0.8, and the cells were pelleted and resuspended in 10mM $MgCl_2$, 10mM MES pH 5.6 buffer with 200 µM of acetosyringone to a final OD_{600}=0.1. The pTRV1 and pTRV2 solutions were mixed in a 2:1 ratio, and Valencia plantlets were vacuum-infiltrated using a chemical duty pump (Merck, USA) and a vaccuum dissecator for 10 minutes. pTRV1 and pTRV2-Del/Ros1-GW empty vectors were also infiltrated as a positive control for silencing. After infiltration, plants were grown for 3 weeks, and fully-expanded leaves where the silencing was obvious due to presence of purple and green sectors (Fig. 4.2) were sampled for trichome phenotyping.Green (silenced) and purple (unsilenced) sectors of the same leaf were imaged using a cryo-SEM (see *chapter 2*). When trichome density was assessed, at least 8 micrographs of approximately 0.3 mm^2 per sample were used for manual quantification of trichomes, stomata and pavement cells. This was done with the aid of ImageJ v. 1.49 (National Institutes of Health, USA). Trichomes were also scored according to the current classification (Luckwill, 1943, Simmons and Gurr, 2005). When trichome morphology was assessed, I made records of the aberrant shapes or patterns found in silenced plants.

When I observed differences between silenced and unsilenced tissue, the effective silencing of the gene was assessed by quantitative PCR (qPCR, see *chapter 2*). Primers used and efficiencies are shown in Appendix 1. This was not done for SlCycB2, as the gene function had been described previously.

4.3.5.-Statistical analysis.

To compare trichome density between silenced and unsilenced tissue, I performed t-tests using R software (ver. 3.2.2; R Core Team, Vienna, Austria). The p-value cut-off for significance was set at 0.05.

4.3.6.- Transcriptomic data retrieval.

The expression profile of SlMX2 in the leaves of *S. pennellii* ILs was retrieved from the RNAseq data for leaves obtained from (Chitwood et al., 2013). The colour-coded display of gene expression used in this chapter was generated using the Tomato eFP Browser.

Figure 4.2.-*Valencia* (proSlPNH:AmRosea1/35S:Delila) leaves after VIGS-mediated silencing of Del/Ros1 and gene of interest. Purple sectors of the leaf correspond to regions where silencing did not take place, while green sectors correspond to areas where the genes were co-silenced.

4.4.-Results

4.4.1.-Silencing of candidate genes in the genomic region covered by ILs 2-5/2-6.

I screened the candidate genes contained in the genomic region in chromosome 2 covered by ILs 2-5 and 2-6 (Fig. 4.3). The most likely bin to contain a gene responsible for the phenotype is bin 2-L, which corresponds to the overlapping region between both ILs displaying an aberrant phenotype. I included also bin 2-K, as the borders of the regions are sometimes not very well defined. I selected two genes, *SlMIXTA-like* and *SlEXP15* (Table 4.1). SlMIXTA-like was expressed in trichomes and its expression was downregulated in IL 2-6 compared to other ILs. *SlMIXTA-like* is a homolog of the *MIXTA-like2* gene in *Antirrhinum majus* (Perez-Rodriguez et al., 2005, Baumann et al., 2007). *SlEXP15* was expressed in trichomes and its expression did not change in the ILs under study. SlEXP15 has a role in loosening of cell walls for cell expansion.

Silencing of *SlMIXTA-like* by VIGS resulted in the development of trichome clusters on the adaxial (Fig. 4.4B and C) and abaxial (Fig. 4.4D) surfaces of silenced tissue, similar to those observed in ILs 2-5 and 2-6 (See *Chapter 3*). Analysis of the abundance of SlMIXTA-like transcripts in silenced and unsilenced tissue indicated an effective reduction of the expression level of *SlMIXTA-like* (Fig. 4.5). Silencing of *SlEXP15* by VIGS did not have any effect on the trichome phenotype of silenced tissue (Fig. 4.6).

4.4.2.-Silencing of candidate genes in the genomic region covered by IL 4-1.

I screened the candidate genes contained in the genomic region in chromosome 4 covered by the IL 4-1 (Fig. 4.7). The most likely bin to contain a gene responsible for the phenotype is bin 4-B, which corresponds to the region covered only by IL 4-1. However, I included also bin 4-A, which corresponds to the overlapping region between IL 4-1-1 and 4-1, because of the inexact borders and because IL 4-1-1 showed a similar phenotype (low trichome density in first generation of the ILs, and absence of type VI trichomes, see *Chapter 3*). I selected one gene, *SlMX2* (Table 4.2). *SlMX2* was not expressed in trichomes, but its expression in leaves was greatly reduced in IL 4-1-1 and completely knocked down in IL 4-1. It is also a homolog of the MIXTA-like1 gene in *Antirrhinum majus* (Perez-Rodriguez et al., 2005), and the *S. pennellii* version of the gene lacks a DNA-binding domain (Fig. 4.8).

Silencing of *SlMX2* by VIGS resulted in a significant reduction in the total trichome density (Fig. 4.9B and C). This observation was in agreement with the low trichome density observed in IL 4-1 (see *chapter 3*) Upon classification of trichome types, the number of type VI trichomes did not change significantly between silenced and unsilenced tissue, while the number of non-glandular type V trichomes was reduced substantially (Fig. 4.9D). Analysis of the abundance of SlMX2

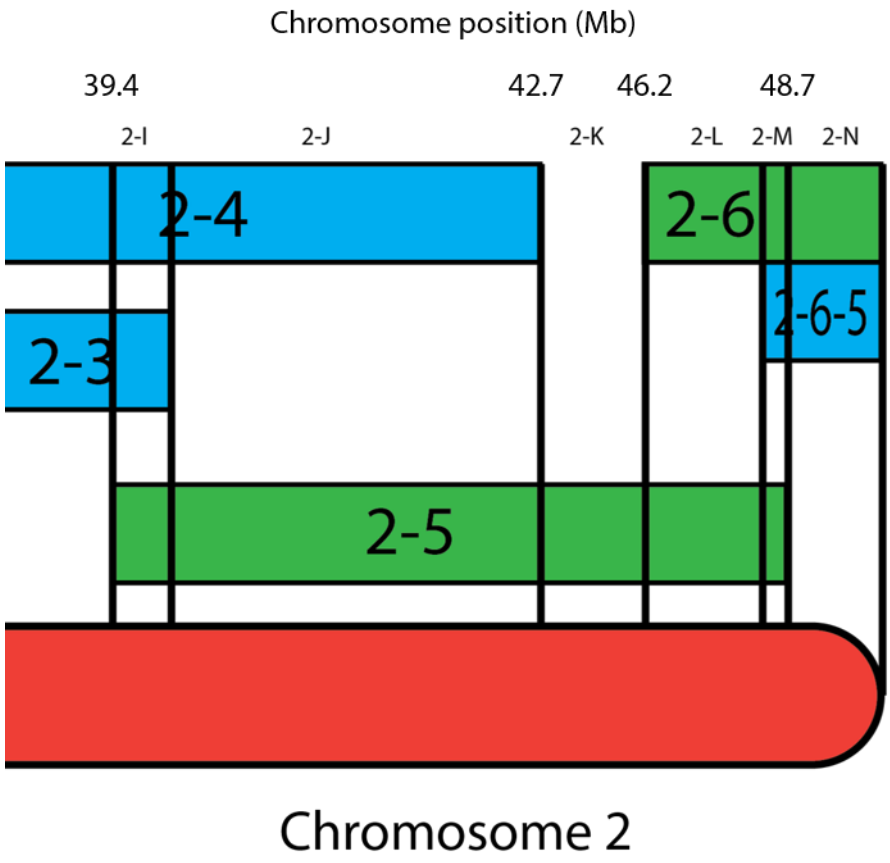

Figure 4.3.-Bin map of the regions covered by ILs 2-5 and 2-6. The code 2-I to 2-N refers to the genomic bin delimited by the overlapping regions corresponding to each IL and the chromosome position of the bin boundaries is indicated in the map. Bins were mapped by (Chitwood et al., 2013). Each rectangle represents a specific IL, and the green rectangles represent the ILs 2-5 and 2-6 where we observed the phenotype of interest (See *chapter 3*).

Gene	ID	Bin	Expressed in trichomes	Expression change in IL	Extra information
SlMIXTA-like	Solyc02g088190	2-K	Yes	Downregulated in IL 2-6	Homolog of AmMIXTA-like 2
SlEXP15	Solyc02g088100	2-K	Yes	Unchanged	-

Table 4.1.- Candidate genes in region covered by ILs 2-5 and 2-6. The genes were selected by their functional annotation, their expression level in trichomes (Spyropoulou et al., 2014) and their expression level in leaves of the target ILs (Chitwood et al., 2013). Genomic bins were mapped in (Chitwood et al., 2013).

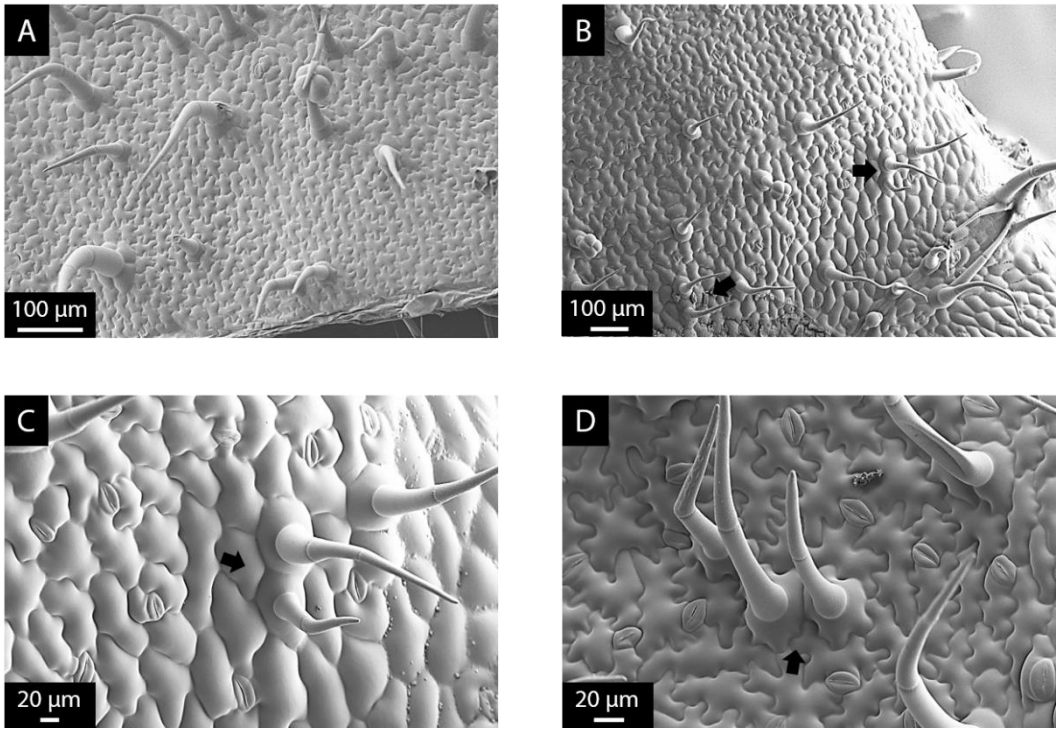

Figure 4.426.-Silencing of SlMIXTA-like on tomato leaves. A) Adaxial leaf surface of unsilenced tissue. B, C) Adaxial leaf surface of tissue where SlMIXTA-like was silenced. D) Abaxial leaf surface of tissue where SlMIXTA-like was silenced. Trichome clusters were found on both leaf surfaces. Black arrows indicate trichome clusters. Scale bars are shown for each micrograph.

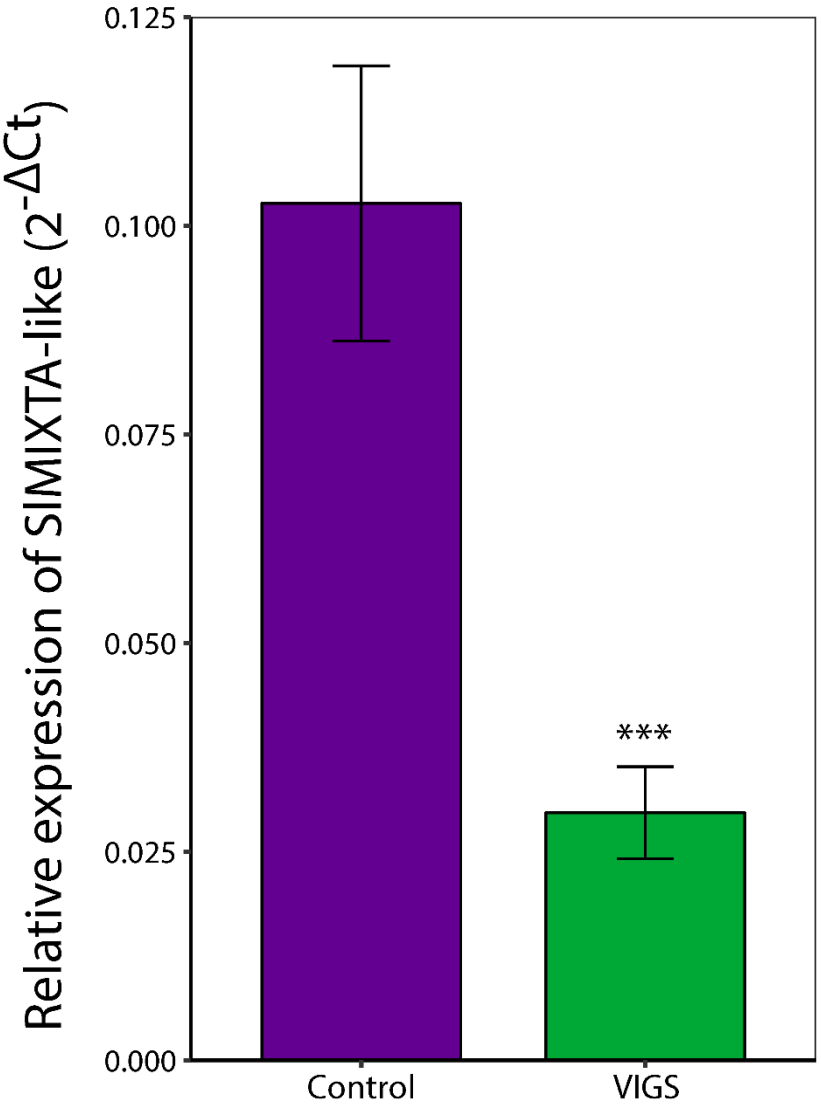

Figure 4.5.-Expression level of SlMIXTA-like in unsilenced and silenced tissue. The purple bar represents the expression level of SlMIXTA-like in unsilenced control tissue, and the green bar represents the expression level in tissue where SlMIXTA-like was silenced by VIGS. Expression level was significantly lower in the silenced tissue, as indicated by the two stars (p-value<0.05).

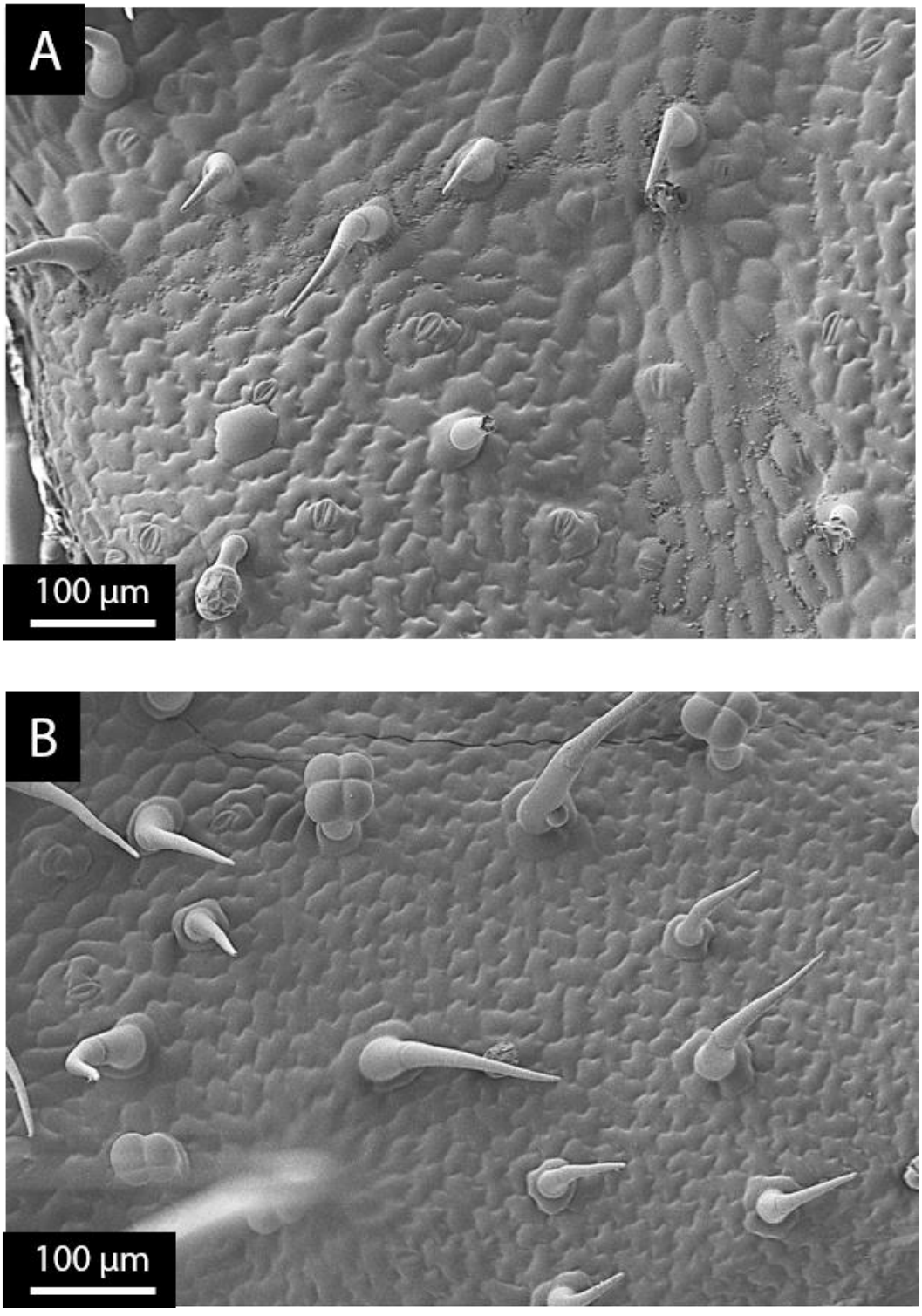

Figure 4.6.-Silencing of SlEXP15 on tomato leaves. A) Leaf surface of unsilenced tissue. B) Leaf surface of tissue where SlEXP15 was silenced. No differences in trichome patterning were observed. Scale bars are shown for each micrograph.

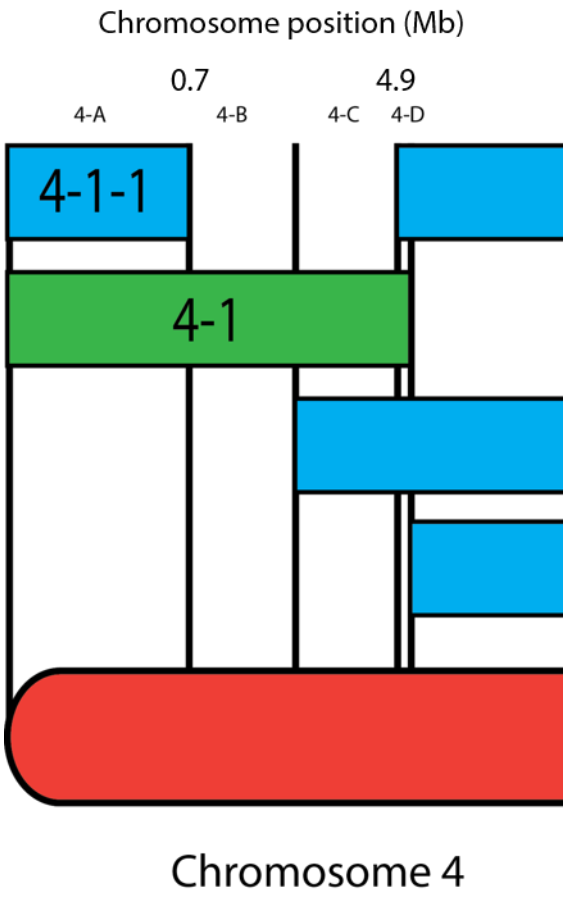

Figure 4.7.-Bin map of the regions covered by IL 4-1. The code 4-A to 4-D refers to the genomic bin delimited by the overlapping regions corresponding to each IL and the chromosome position of the bin boundaries is indicated in the map. Bins were mapped by (Chitwood et al., 2013). Each rectangle represents a specific IL, and the green rectangle represents the IL 4-1 where we observed the phenotype of interest (See *chapter 3*).

Gene	ID	Bin	Expressed in trichomes	Expression change in IL	Extra info
SlMX2	Solyc04g005600	4-A	No	Extremely downregulated	Homolog of AmMIXTA-like 1 DNA-binding domain absent in SpMX2

Table 4.2.-Candidate genes in region covered by IL 4-1. The gene was selected for their functional annotation, their expression level in trichomes (Spyropoulou et al., 2014) and their expression level in leaves of the target ILs (Chitwood et al., 2013). Genomic bins were mapped in (Chitwood et al., 2013).

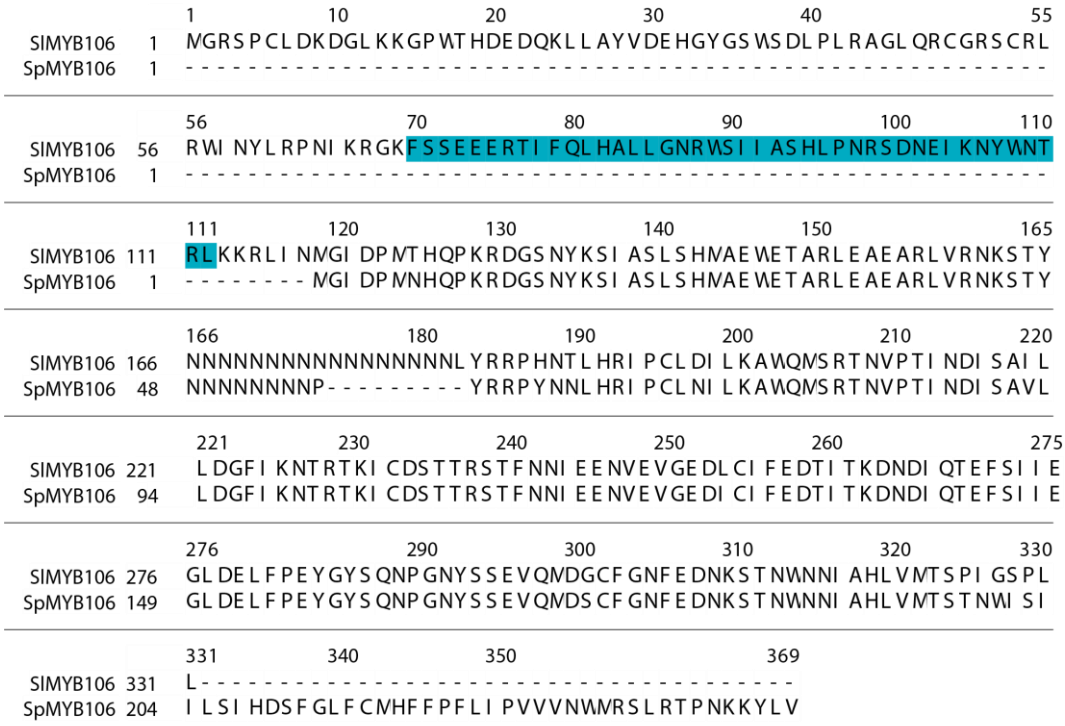

Figure 4.8.-Alignment of SlMX2 and SpMX2 amino acid sequences. The highlighted blue sequence corresponds to the MYB DNA-binding domain, which is absent in the *S. pennellii* version of the protein.

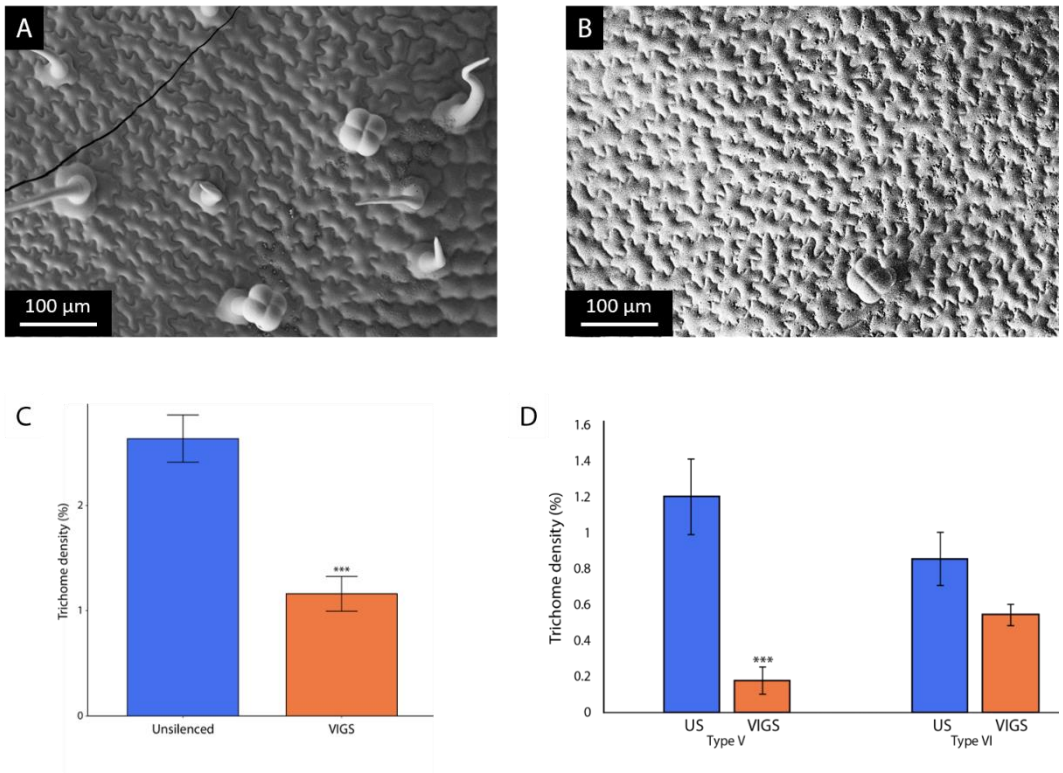

Figure 4.9.- Silencing of SlMX2 on tomato leaves. A) Adaxial leaf surface of unsilenced tissue. B) Adaxial leaf surface of tissue where SlMIXTA-like was silenced. C) Total trichome density in unsilenced and silenced tissue. D) Trichome density of type V and type VI trichomes in unsilenced (US) and silenced (VIGS) tissue. For A and B, scale bars are shown for each micrograph. For C and D, blue bars represent unsilenced tissue and orange bars represent tissue where SlMX2 was silenced. The triple star indicates statistical significance (p-value<0.01) according to t-test.

transcripts in silenced and unsilenced tissue indicated an effective reduction of the expression level of *SlMX2* (Fig. 4.10).

4.4.3.-Silencing of candidate genes in the genomic region covered by IL 10-2.

I analysed the candidate genes contained in the genomic region in chromosome 10 corresponding the IL 10-2 (Fig. 4.11). The most likely bin to contain a gene responsible for the phenotype is 10-D, although I expanded this region a bit as I did for the previous examples. IL 10-2 showed aberrant branched trichomes (see *Chapter 3*), shared with IL 10-3 (Fig. 4.12), and also had a very distinctive *hairless*-like phenotype (Fig 4.13), and I tried to test whether my candidate genes play a role in causing either phenotype.

I finally selected five candidate genes for further testing (Table 4.3). *sMYB10-2* (Solyc10g08030) encodes a small MYB transcription factor with just a DNA-binding domain, and its expression is reduced in IL 10-2, although it is not expressed in trichomes. *SlbZIP17* (Solyc10g078290) was not expressed in trichomes and showed no changes in expression level in the target IL, but it was chosen as the *A. thaliana* homolog has a role in root development during stress. *SlABI8* (Solyc10g079210) showed no expression in trichomes, but it was downregulated in IL 10-2. *SlCycB2* (Solyc10g083140) is a small cyclin interacting with the Woolly transcription factor, known for its role in trichome development. It is not expressed in trichomes and its expression is unchanged in IL 10-2. Finally, *MYB10-2* is expressed in trichomes and upregulated in IL 10-2.

I silenced the candidate genes by VIGS. Silencing of *sMYB10-2* did not lead to any clear phenotype, with no aberrant trichomes such as those observed in IL 10-2 (Fig. 4.14). Moreover, trichome density was not affected by silencing of *sMYB10-2* (Fig. 4.14C). Silencing of *SlbZIP17* did not affect trichome morphology (Fig. 4.15), and I did not observe any clear phenotype in tissue where *SlABI8* was silenced (Fig. 4.16). Silencing of *SlCycB2* did influence trichome morphology, as silenced tissue contained branched multicellular trichomes similar to the ones observed in IL 10-2 (Fig. 4.17). However, silenced leaves and stems did not show a *hairless*-like phenotype equivalent to the phenotype of IL 10-2 (Fig. 4.18). I did not observe any differences between control unsilenced tissue and tissue where *MYB10-2* was silenced (Fig. 4.19). Consequently, my candidate gene screen did not lead to the discovery of the gene responsible for the *hairless*-like phenotype.

4.4.4.-Silencing of candidate genes in other genomic regions.

I selected other candidate genes for functional characterisation in regions outside the ones described above (Table 4.4).

In particular, I selected a basic helix-loop-helix (bHLH) transcription factor (SlLHW, Solyc11g06890) contained in the region covered by IL 11-3, which consistently showed the

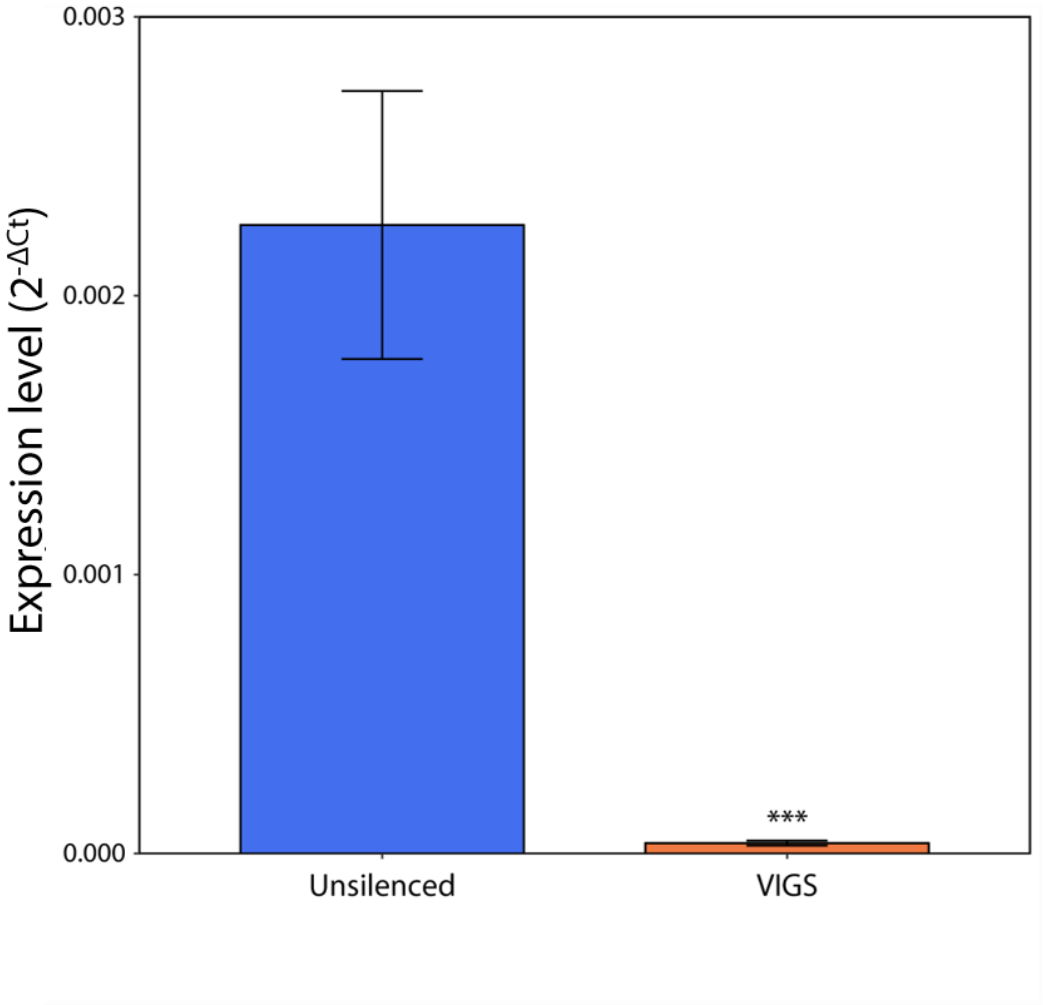

Figure 4.10.- Expression level of SlMX2 in unsilenced and silenced tissue. The blue bar represents the expression level of SlMX2 in unsilenced control tissue, and the orange bar represents the expression level in tissue where SlMX2 was silenced by VIGS. Expression level was significantly lower in the silenced tissue, as indicated by the three stars (p-value<0.01).

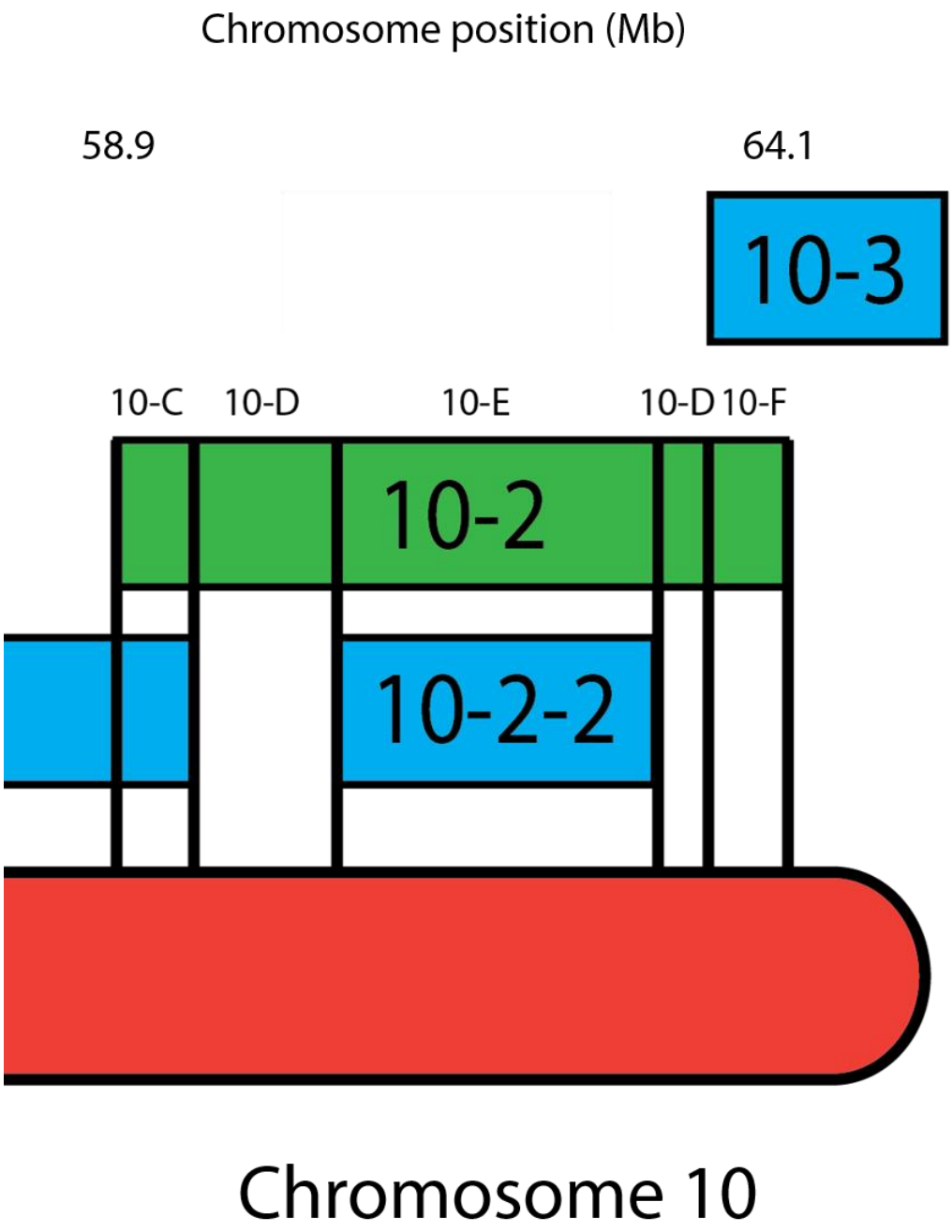

Figure 4.11.-Bin map of the regions covered by IL 10-2. The code 10-C to 10-F refers to the genomic bin delimited by the overlapping regions corresponding to each IL and the chromosome position of the bin boundaries is indicated in the map. Bins were mapped by (Chitwood et al., 2013). Each rectangle represents a specific IL, and the green rectangle represents the IL 10-2 where we observed the phenotype of interest (See *chapter 3*).

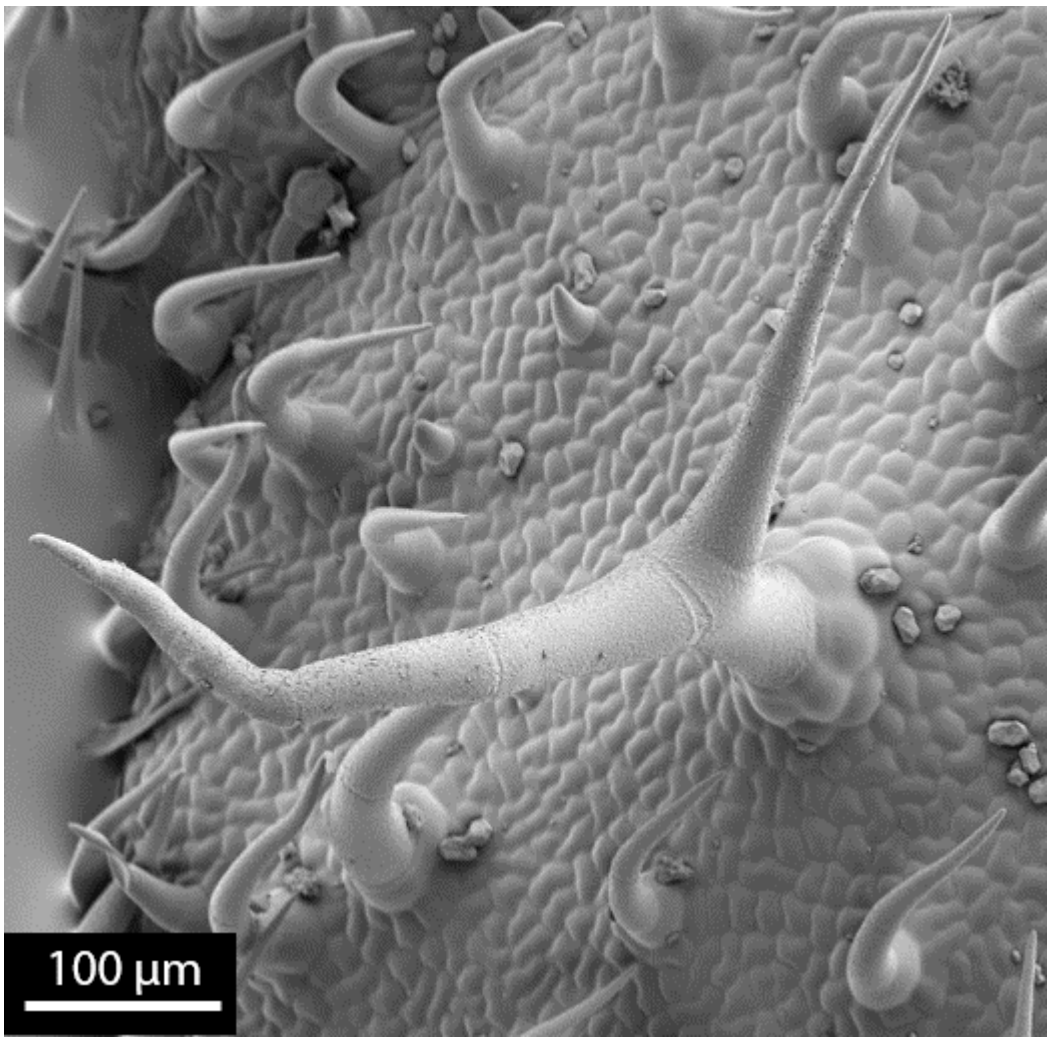

Figure 4.12.-Aberrant trichome on the adaxial surface of IL 10-3. Micrograph of the leaf surface of IL 10-3, where a branched, aberrant trichome is shown. Scale bars are shown in each micrograph.

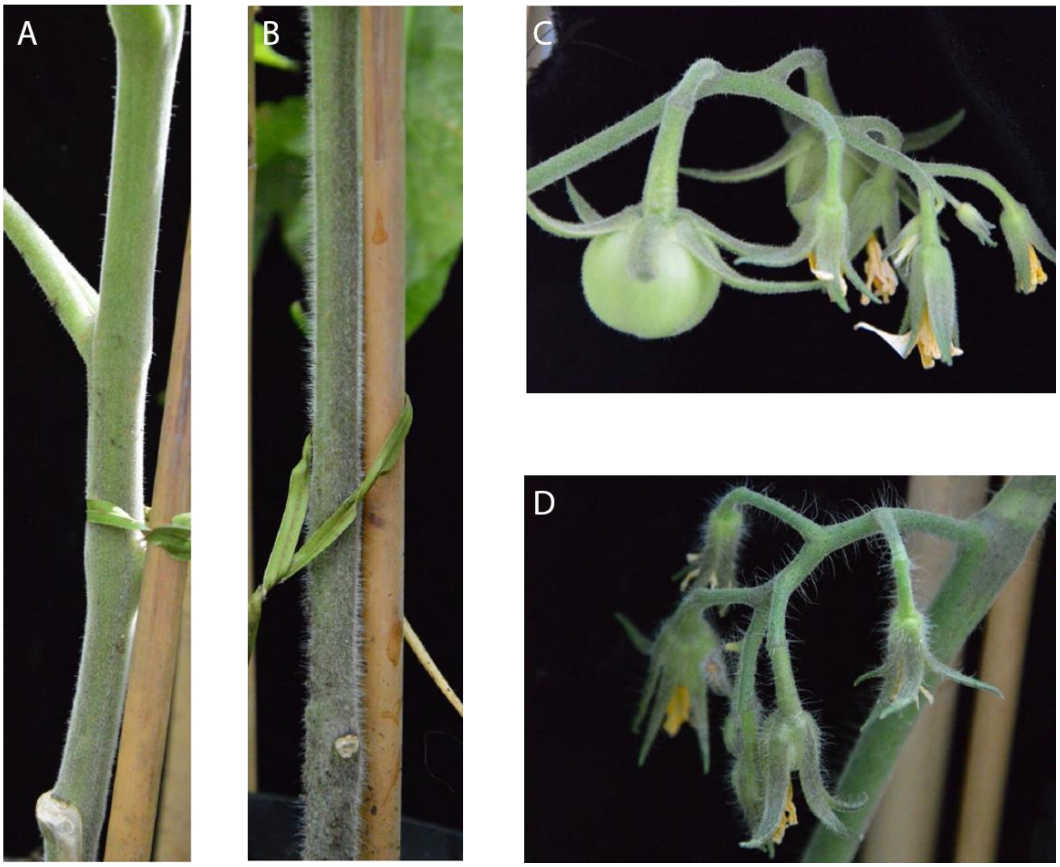

Figure 4.13.- *Hairless*-like phenotype in IL 10-2. A) Close up view of the stem of IL 10-2. B) Close up view of the stem of M82. C) Close up view of flower buds of IL 10-2. D) Close up view of flower buds in M82. The *hairless-like* phenotype is due to a reduction in the number of long trichomes, rather than a change in trichome density (see *chapter 3*).

Gene	ID	BIN	Expressed in trichomes	Expression change in IL	Extra info
sMYB 10-2	Solyc10g080300	10-E	No	Downregulated	-
SlBZIP17	Solyc10g078290	10-C	No	Unchanged	-
SlABI8	Solyc10g079210	10-D	No	Downregulated	-
SlCycB2	Solyc10g083140	10-F	No	Unchanged	Interacts with Woolly
MYB 10-2	Solyc10g078310	10-C	Yes	Upregulated	-

Table 4.3.-Candidate genes in region covered by IL 10-2. The genes were selected for their functional annotation, their expression level in trichomes (Spyropoulou et al., 2014) and their expression level in leaves of the target ILs (Chitwood et al., 2013). Genomic bins were mapped in (Chitwood et al., 2013).

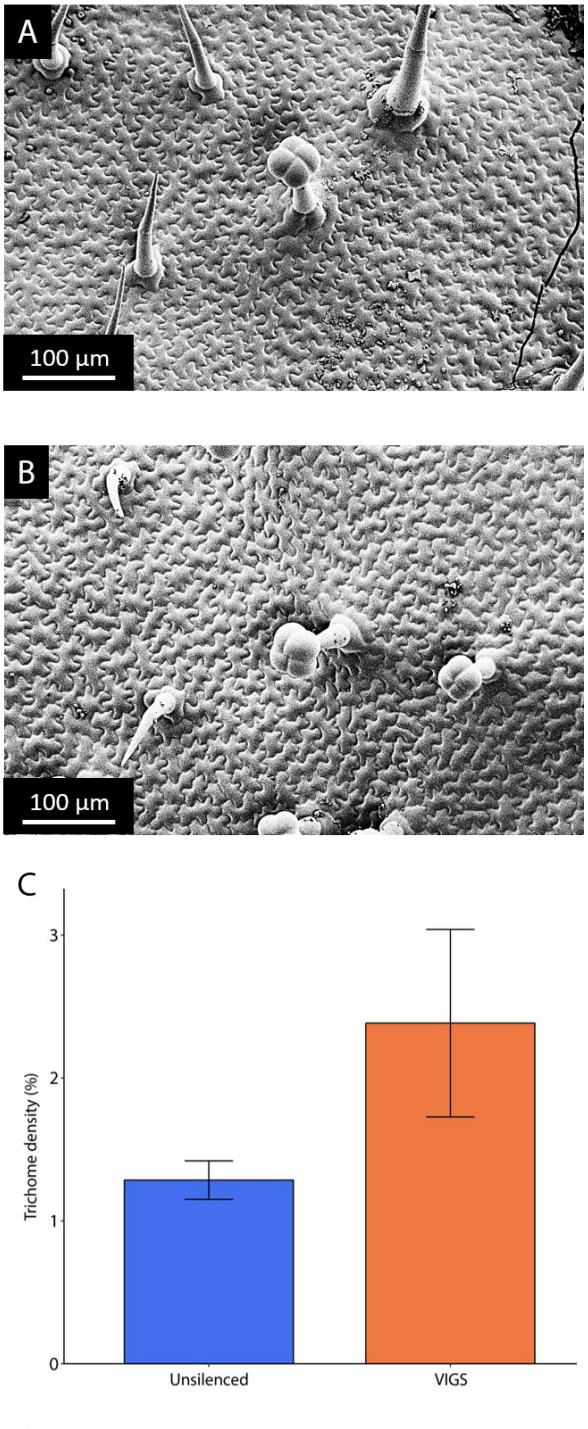

Figure 4.14.-**Silencing of sMYB10-2 on tomato leaves.** A) Micrograph of the adaxial leaf surface of unsilenced tissue. B) Micrograph of the leaf surface of tissue where sMYB10-2 was silenced. C) Trichome density in unsilenced and silenced (VIGS) tissue. No significant differences were observed (p-value>0.05). For A) and B), scale bars are shown in each micrograh. For C), the blue bar represents unsilenced tissue and the orange bar represents silenced tissue.

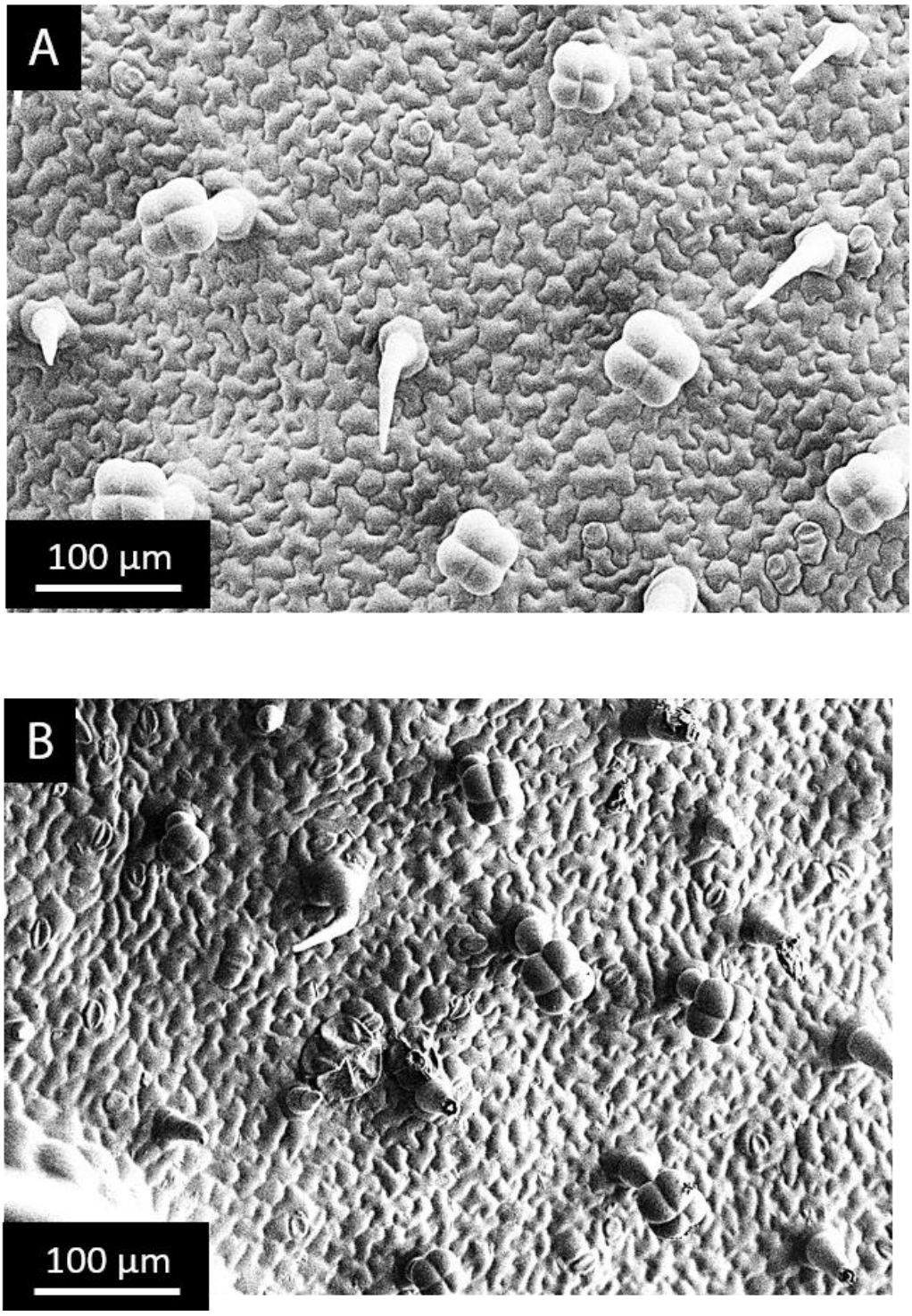

Figure 4.15.-Silencing of SlbZIP17 on tomato leaves. A) Micrograph of the adaxial leaf surface of unsilenced tissue. B) Micrograph of the leaf surface of tissue where SlbZIP17 was silenced. No differences were observed. Scale bars are shown in each micrograph.

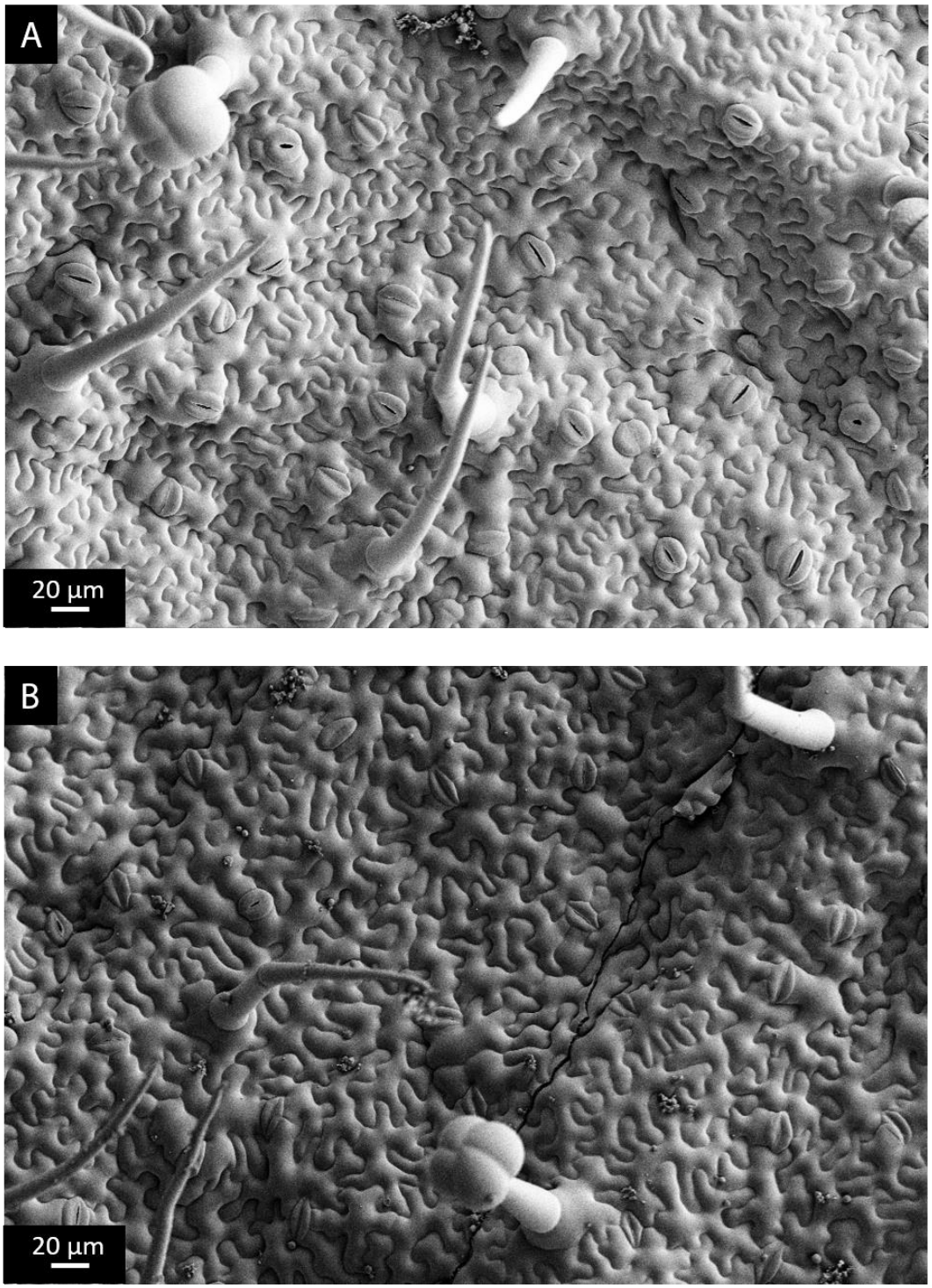

Figure 4.16.-Silencing of SlABI8 on tomato leaves. A) Micrograph of the abaxial leaf surface of unsilenced tissue. B) Micrograph of the leaf surface of tissue where SlABI8 was silenced. No differences were observed. Scale bars are shown in each micrograph.

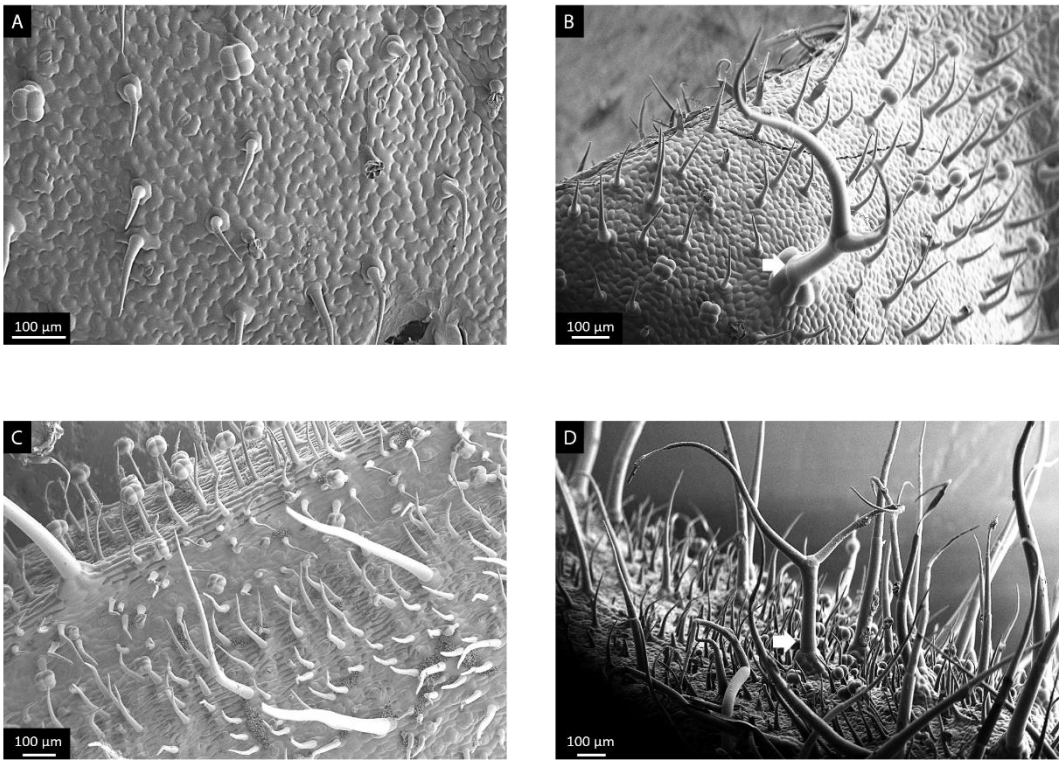

Figure 4.17.-Silencing of SlCycB2 on tomato leaves. A) Micrograph of the abaxial leaf surface of unsilenced tissue. B) Micrograph of the adaxial leaf surface of tissue where SlCycB2 was silenced. C) Micrograph of the stem surface of unsilenced tissue. D) Micrograph of the stem surface of tissue where SlCycB2 was silenced. White arrows indicate branched aberrant trichomes in B) and D). Scale bars are shown in each micrograph.

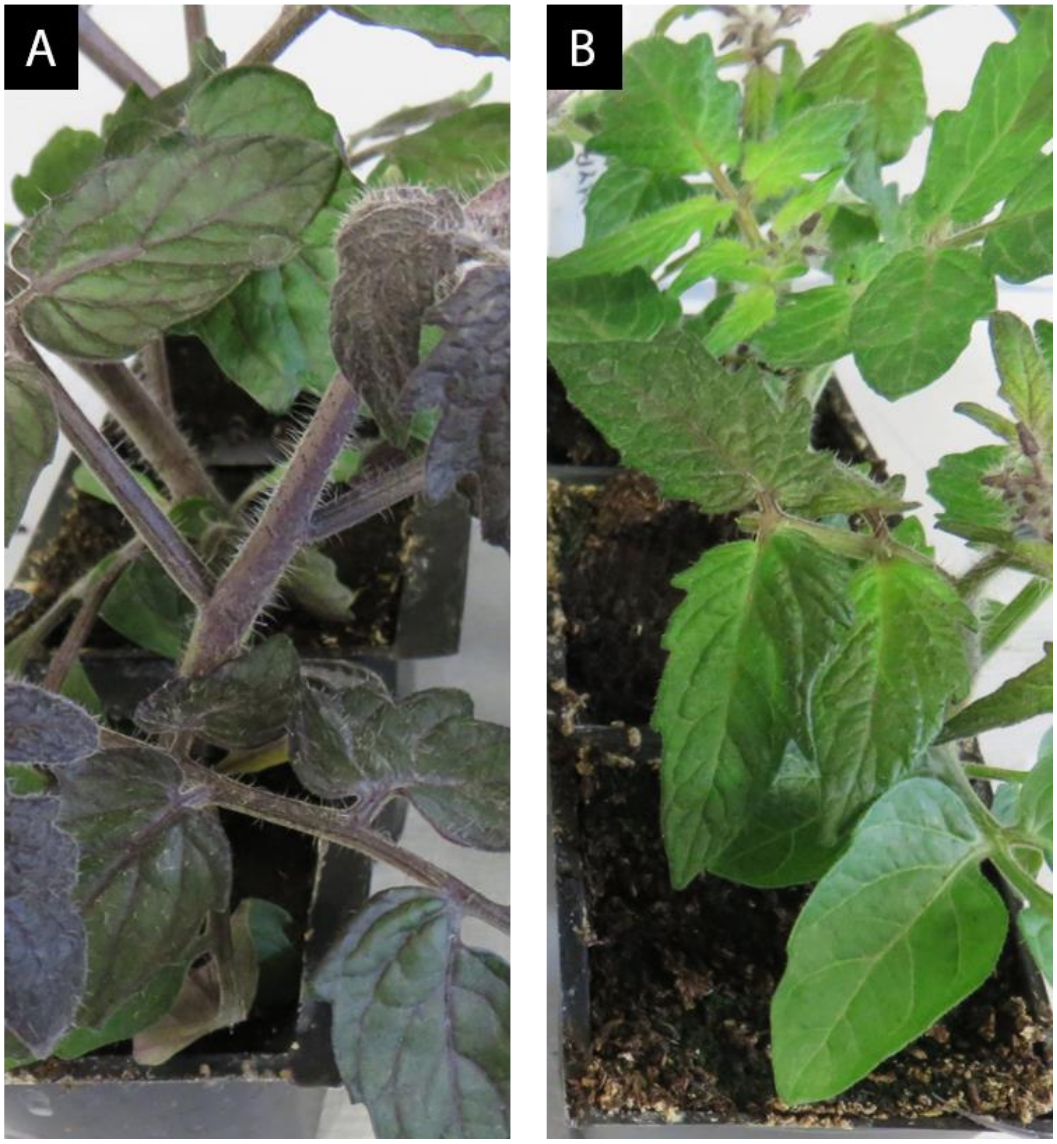

Figure 4.18.-Silencing of SlCycB2 on tomato plants. A) Close up view of an unsilenced proSlPNH:AmRos1/35S:Del tomato plant. B) Close up view of a proSlPNH:AmRos1/35S:Del tomato plant where SlCycB2 was silenced. Both plants display the same visual trichome phenotype, distinct from the *hairless*-like phenotype observed in IL 10-2.

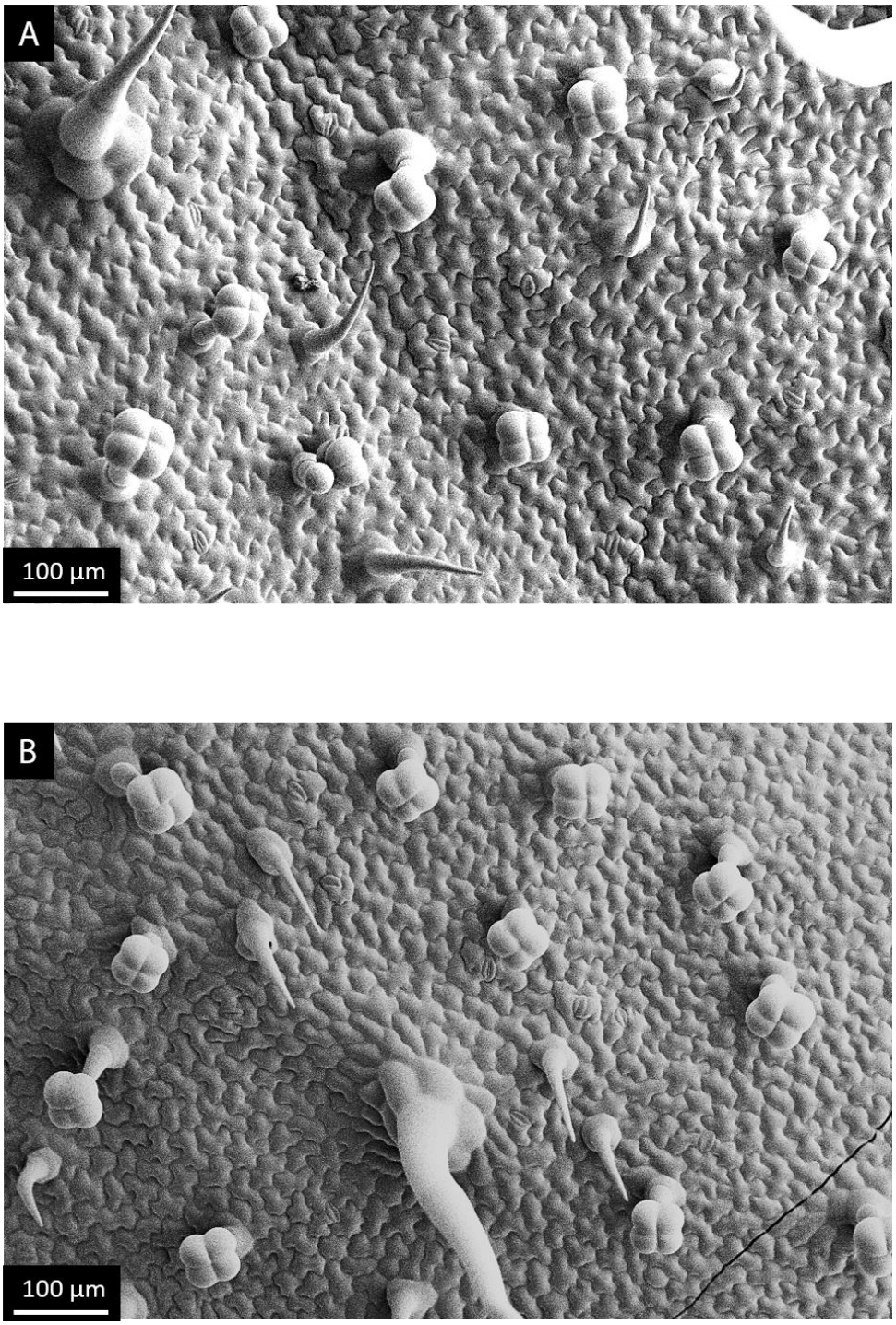

Figure 4.19.-Silencing of MYB10-2 on tomato leaves. A) Micrograph of the abaxial leaf surface of unsilenced tissue. B) Micrograph of the leaf surface of tissue where MYB10-2 was silenced. No differences were observed. Scale bars are shown in each micrograph.

Gene	ID	Bin	Expressed in trichomes	Expression change in IL	Extra info
SlLHW	Solyc11g06890	11-E	Yes	Upregulated	Downregulated in MIXTA-like-RNAi lines.
SlEIF1	Solyc07g016150	7-C	Yes	Unchanged	Absent in *Solanum pennellii* (SGN)

Table 4.4.-Candidate genes in regions covered by other ILs. The genes were selected for their functional annotation, their expression level in trichomes (Spyropoulou et al., 2014) and their expression level in leaves of the target ILs (Chitwood et al., 2013). Genomic bins were mapped in (Chitwood et al., 2013).

highest trichome density among all the ILs (see *Chapter 3*) (Fig. 4.20). This gene was in bin 11-E, exclusive to IL 11-3, and was expressed in trichomes and upregulated in IL 11-3. Moreover, it was downregulated in *SlMIXTA-like*-RNAi lines. Silencing of *SlLHW* did not have any effect on trichomes on the leaf surface and did not result in any effects on morphology, patterning or density (Fig. 4.21). I also selected a gene in the region covered by IL 7-4-1 (Fig. 4.22), which showed a swollen type of aberrant trichomes (see *Chapter 3*). *Elongation factor 1* (*SlElF1*, Solyc07g016150) was expressed in trichomes and its expression remained unchanged compared to other ILs. The gene seemed to be *S. lycopersicum*-specific according to the annotation in the Sol Genomics Network, although it was present in the NCBI database. It mapped to the bin 7-C, which correspond to the region shared by IL 7-4-1 and 7-4, both of which showed aberrant trichomes. Silencing of *SlElF1* did not affect trichome morphology, and no differences were observed between unsilenced tissue and tissue where *SlElF1* was silenced (Fig. 4.23). Consequently, I could not find a gene responsible for the phenotypes observed in IL 11-3 and 7-4-1 by this candidate gene approach.

4.5.-Discussion

4.5.1.-SlMIXTA-like plays an important role in trichome patterning in tomato.

The altered trichome patterning in ILs 2-5 and 2-6 involved clustering of trichomes with two or more trichomes grouped together. Trichome patterning in *Arabidopsis* and related species is mediated by small R3 MYB transcription factors, which lack an activation domain and compete with positive regulators of trichome initiation (Ishida et al., 2008). In fact, *Arabidopsis* mutants of TRIPTYCHON (TRY) and CAPRICE (CPC), both R3 MYB factors, have trichome clusters (Schellmann et al., 2002, Kirik et al., 2004a), similar to the ones observed for these ILs (see *Chapter 3*). The homologs of these genes have been identified and their role has been partially characterised by ectopic expression in *Arabidopsis* (Tominaga-Wada et al., 2013, Wada et al., 2014), but their function in tomato is still unclear. Little is known about how trichome patterning is regulated in *Solanum* and related species.

I screened the genes contained in the genomic region covered by ILs 2-5 and 2-6 (Fig. 4.3) and I picked two genes for further characterisation (Table 4.1) among the 774 genes contained in the analysed region. I focused on bins 2-K (IL 2-5-specific, containing 479 genes) and 2-L (overlapping region between ILs 2-5 and 2-6, containing 295 genes). The final candidates were in bin 2-K, which corresponds only to IL 2-5. However, their functional annotation and transcriptional behaviour pointed towards a potential role in trichome development.

SlEXP15 is a member of the α-expansin family, a family of proteins which are involved in the process of cell wall loosening to allow cell expansion (Cosgrove, 1998) and are known to be

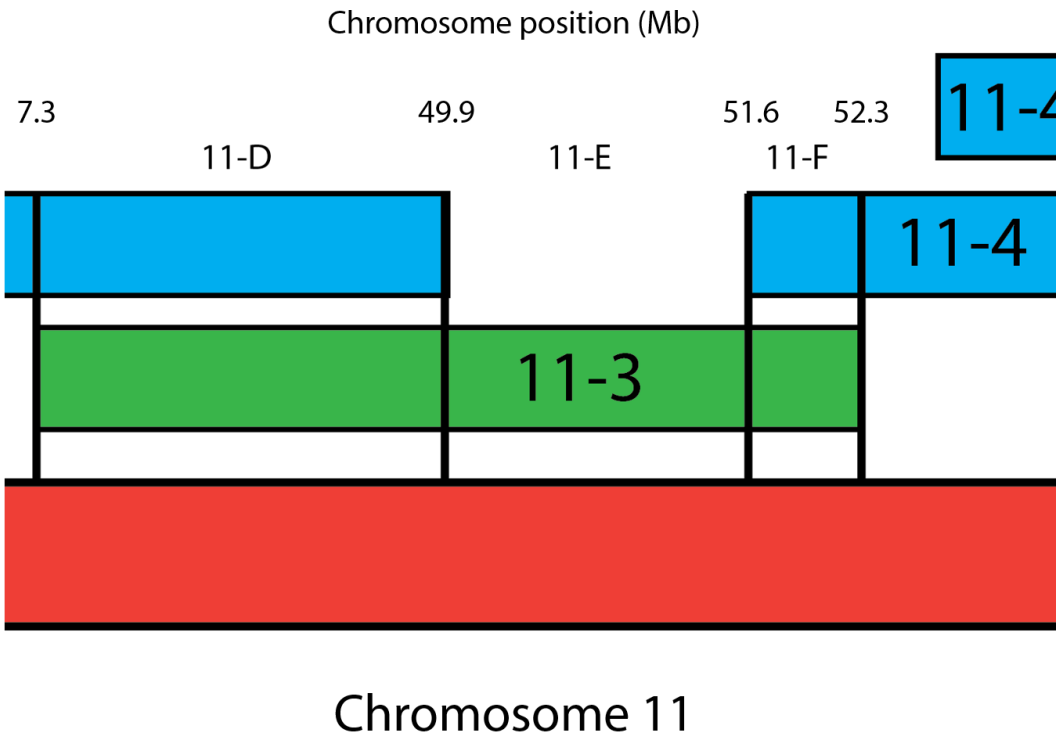

Figure 4.20.-Bin map of the region covered by IL 11-3. The code 11-D to 11-F refers to the genomic bin delimited by the overlapping regions corresponding to each IL. Bins were mapped by (Chitwood et al., 2013). Each rectangle represents a specific IL, and the green rectangle represents the IL 11-3 where we observed the phenotype of interest (See *chapter 3*).

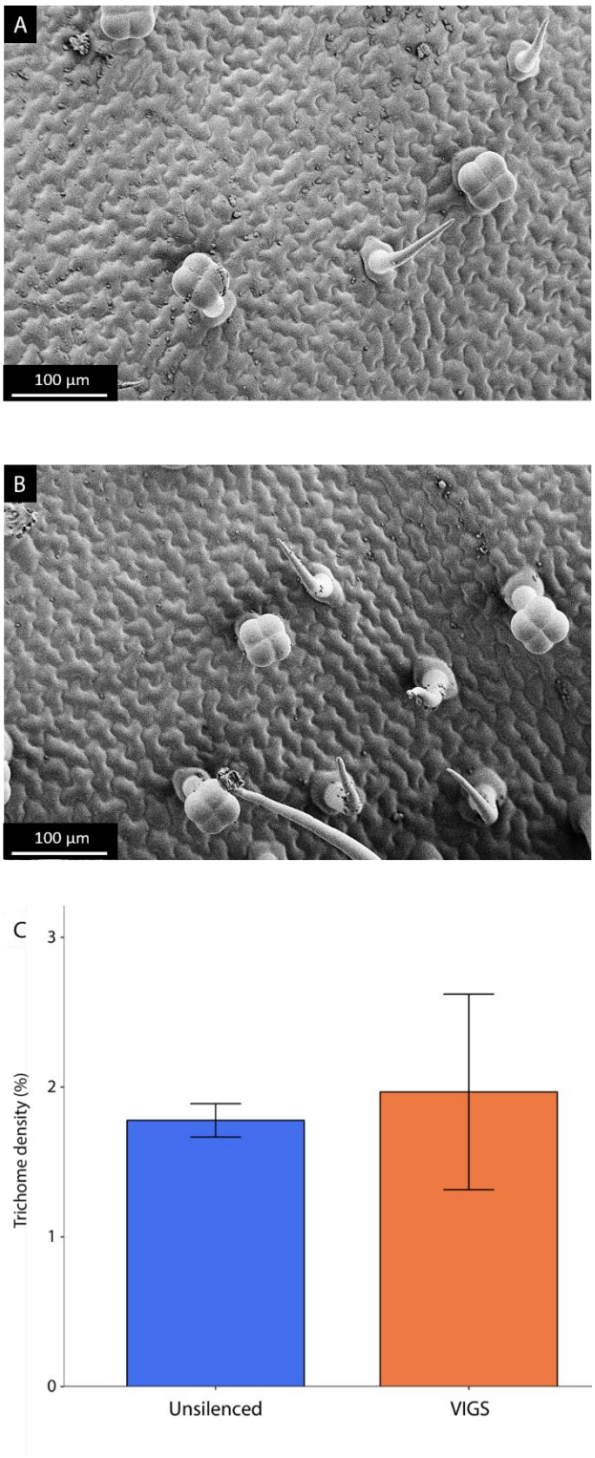

Figure 4.21.-Silencing of SlLHW on tomato leaves. A) Micrograph of the adaxial leaf surface of unsilenced tissue. B) Micrograph of the leaf surface of tissue where SlLHW was silenced. C) Trichome density in unsilenced and silenced (VIGS) tissue. No significant differences were observed (n=3, p-value>0.05). For A) and B), scale bars are shown in each micrograh. For C), the blue bar represents unsilenced tissue and the orange bar represents silenced tissue.

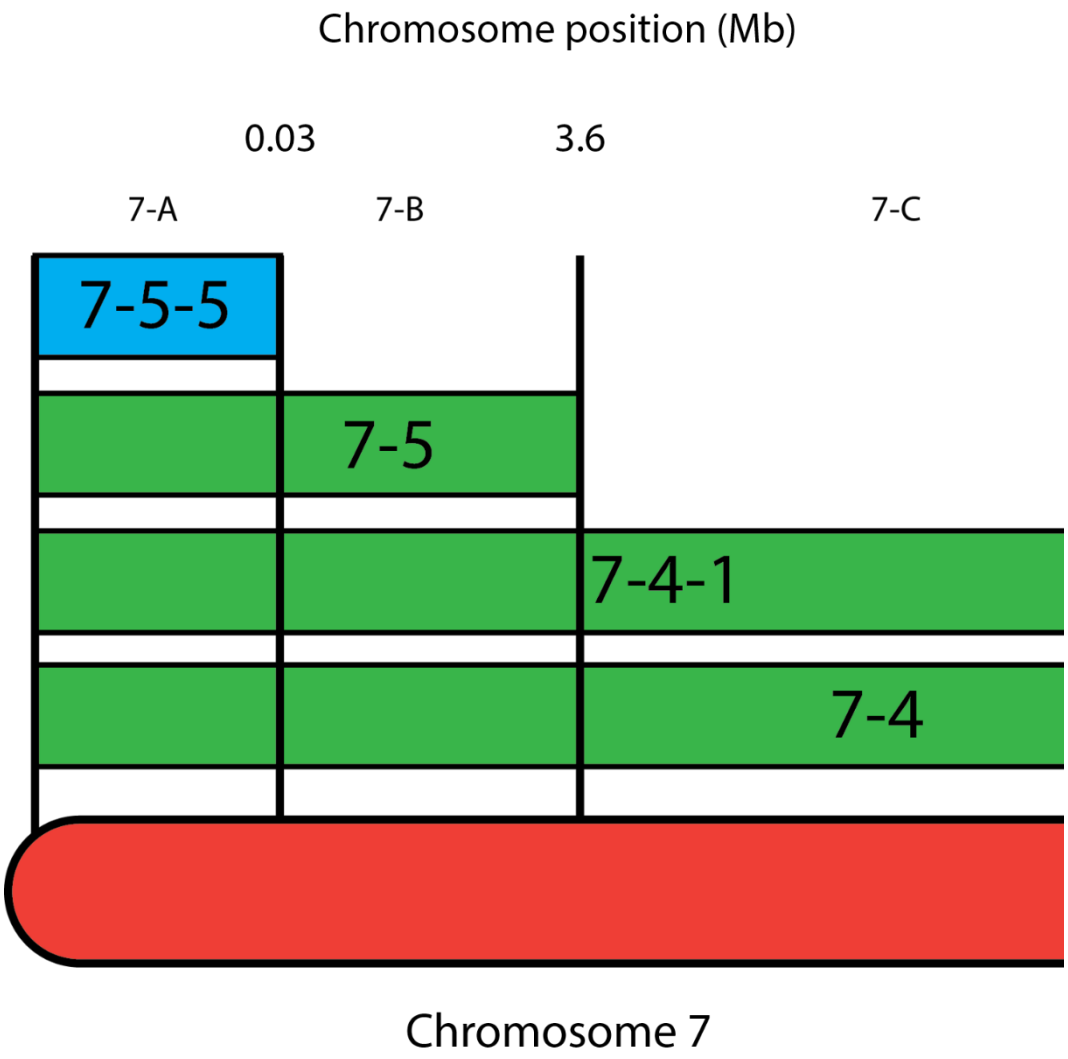

Figure 4.22.-Bin map of the region covered by IL 7-4-1. The code 7-A to 7-C refers to the genomic bin delimited by the overlapping regions corresponding to each IL. Bins were mapped by (Chitwood et al., 2013). Each rectangle represents a specific IL, and the green rectangle represents the ILs where we observed the phenotype of interest (See *chapter 3*).

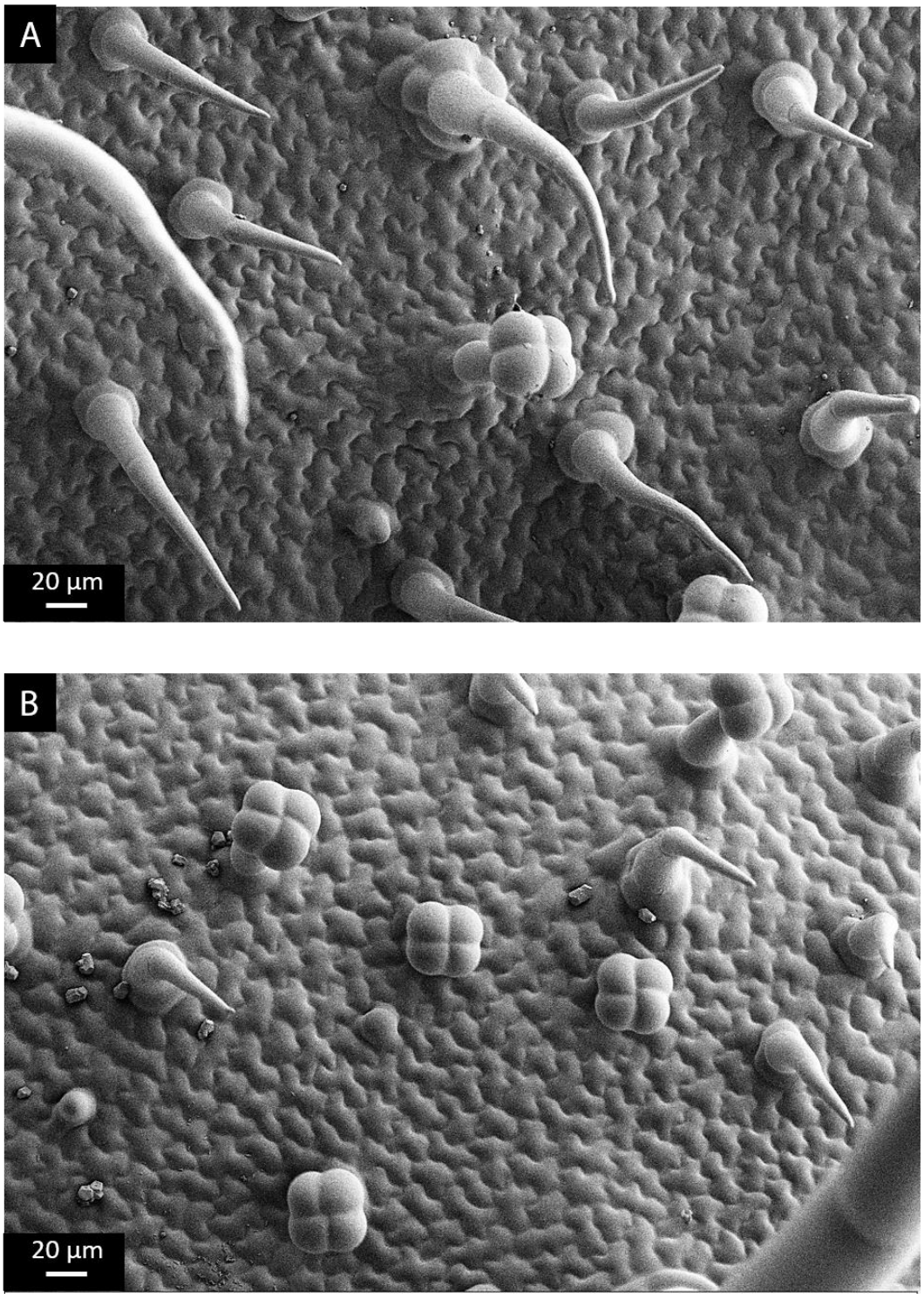

Figure 4.23.-Silencing of SlElF1 on tomato leaves. A) Micrograph of the adaxial leaf surface of unsilenced tissue. B) Micrograph of the leaf surface of tissue where SlElF1 was silenced. No differences in trichome morphology were observed. Scale bars are shown in each micrograph.

involved in fibre (trichome) formation in cotton (Arpat et al., 2004, Wu et al., 2006). The *Arabidopsis* α-expansins AtEXPA7 and AtEXPA18 are involved in hair root (Rose et al., 2000, Kaur et al., 2010) and leaf (Fleming et al., 1997) development but no reports of their function in trichome development are publicly available. Silencing of SlEXP15 did not affect trichome formation in tomato plants (Fig. 4.7), and I could not observe any alteration of trichome patterning or morphology. This indicated that SlEXP15 is unlikely to be responsible for the phenotype observed in ILs 2-5 and 2-6, however its expression in trichomes (Spyropoulou et al., 2014) points towards a potential role in cell wall expansion during trichome formation in tomato. The reason why silencing of *SlEXP15* did not cause any phenotype might be an ineffective downregulation of the target gene using the VIGS system. The use of Del/Ros1 as a visual marker allowed me to analyse leaf tissue expressing the VIGS fragment, but I did not analyse SlEXP15 expression and it maybe was not effective. A more likely reason might be a functional redundancy of α-expansins in trichome development, as at least five other members of this family are expressed in trichomes (SlEXP4a, SlEXP4b, SlEXP8, SlEXP11 and SlEXP13) (Spyropoulou et al., 2014). These might perhaps compensate functionally for any reduction in expression level of the SlEXP15 gene in silenced tissue. In fact, SlEXP11 (Solyc04g081870) was the gene family member with the highest expression (5-fold higher than the target gene SlEXP15), which indicates it is likely to be the main driver of cell wall loosening for expansion in tomato trichomes. Further analysis of these genes is required to generate a clearer picture of the role of expansins in trichome development.

SlMIXTA-like is a homolog of MIXTA-like2 in *A. majus* (Fig 4.24). This gene mapped to the bin 2-K, corresponding to the region specific to IL 2-5 (Fig. 4.3). However, its expression was relatively low in IL 2-6 compared to other ILs (Chitwood et al., 2013), and its location was close to the border between bins 2-K and 2-L. *MIXTA/MIXTA-like* genes are known regulators of epidermal development in several species (Brockington et al., 2013). SlMIXTA-like is very closely related to PhMYB1 in *Petunia hybrida* and MIXTA-like2 in *A. majus* (Lashbrooke et al., 2015). These two genes, together with the *A. thaliana* MYB16, are known positive regulators of conical cell formation (Baumann et al., 2007). SlMIXTA-like has also been characterised in tomato for its role in regulating conical cell formation in fruits, but not petals (Lashbrooke et al., 2015). AtMYB16 also regulates trichome branching (Oshima et al., 2013), but the role of this gene in trichome development has not been investigated for any of the aforementioned species. Silencing of SlMIXTA-like in tomato leaves led to the formation of trichome clusters (Fig. 4.4) similar to the ones observed in the ILs 2-5 and 2-6 (see *Chapter 3*).

The fact that an effective reduction of the expression of *SlMIXTA-like* (Fig. 4.5) resulted in an abnormal trichome patterning indicates that this gene plays an important role in trichome

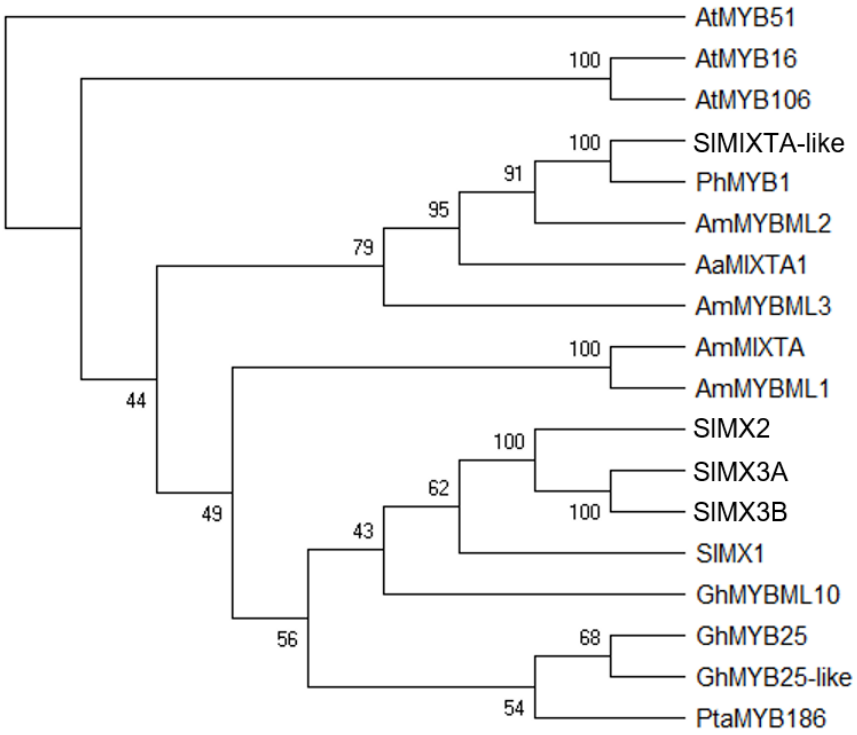

Figure 4.24.-Evolutionary relationship between functionally characterised members of the MIXTA/MIXTA-like family. The phylogenetic tree was built using the Neighbour-Joining method. The bootstrap consensus tree was inferred from 10000 replicates, with the percentage of replicate trees in which branches were clustered together is shown next to each branch. The evolutionary distance was calculated using the Jones-Taylor-Thorton substitution method. 18 MIXTA/MIXTA-like amino acid sequences were included. AtMYB51, a distantly related MYB protein, was used to root the tree.

distribution over the epidermal surface and that it might act as a negative regulator of trichome initiation in leaves, since its expression is necessary to prevent the formation of one trichome next to a previously formed one. A close homolog of SlMIXTA-like in *Mimulus guttatus* (MgMIXTA-like 8) was identified as a potential negative regulator of trichome initiation (Scoville et al., 2011), which would confirm my observations. The fact that these clusters appeared alongside non-clustered trichomes indicate that it might be part of a more complex regulatory network or that other genes might have redundant functions in tomato. *SlMIXTA-like* is expressed in trichomes (Spyropoulou et al., 2014), which seems to contradict its potential function as a negative regulator of trichome initiation. In *A. thaliana,* there is a similar situation, as R3 MYB transcription factors, such as TRY or CPC (Schellmann et al., 2002), act as negative regulators of trichome initiation but are actually expressed in trichomes and then move to the neighbouring cell to repress trichome initiation (Wang and Chen, 2014). However, this mechanism is unlikely to work in a similar fashion in tomato. SlMIXTA-like is not a small R3 MYB gene, and it lacks the S1 and S2 amino acid motifs required for cell-to-cell movement (Tominaga-Wada and Wada, 2018). Understanding how trichome patterning is controlled in tomato requires further analysis of the function of SlMIXTA-like.

It is interesting to note that although the expression level of SlMIXTA-like in IL 2-6 was slightly lower than the average of the IL population (Chitwood et al., 2013), and that change of SlMIXTA-like expression pattern might be the cause for the observed phenotype, its expression level is not reduced in IL 2-5. This seems to indicate that the *S. pennellii* MIXTA-like protein is likely to be less active or effective than the *S. lycopersicum* version, even when its expression is unaltered. The functional and structural differences between both protein versions must be investigated further to fully understand the nature of their molecular role (see *chapter 5* for further discussion).

4.5.2.-*SlMX2* silencing caused a reduction in trichome density in tomato.

I selected the region covered by IL 4-1 due to its consistent low trichome density in both generations of the ILs (see *chapter 3*). Moreover, this line seemed to lack type VI trichomes in the assessed tissue, indicating a reduction of this type of trichome specifically rather than a reduction of the total trichome density. The most likely genetic bin to contain the gene responsible for the phenotype is 4-B, which contains 130 genes (Fig. 4.7). I also included in my analysis the genes included in bin 4-A (containing 98 genes) because of the unclear borders between bins and because IL 4-1-1 showed a very similar phenotype, with a low trichome density in the first generation grown of the ILs and absence of type VI trichomes in the assessed tissue. In the second generation, this IL was not significantly different from M82 in terms of

trichome density, but its trichome density was low and not very dissimilar from the value recorded for IL 4-1 (see *chapter 3*).

I selected one gene, *SlMX2*, as a potential candidate for the trichome phenotype. *SlMX2* is clustered together with other tomato *MIXTA* genes (*SlMX1* and *SlMX3A/B*) in the evolutionary tree of proteins encoded by *MIXTA/MIXTA-like* genes, in a distant clade from SlMIXTA-like and relatively close to AmMIXTA and AmMIXTA-like 1 (Fig. 4.24). The *MIXTA/MIXTA-like* family are known regulators of epidermal development (Martin et al., 2002, Brockington et al., 2013). This gene is generally expressed at low levels in tomato (Fig. 4.10), and its potential involvement in regulation of epidermal development had been ruled out before as it was believed not to be expressed at all (Lashbrooke et al., 2015). However, it is now known to be expressed in most aerial tissues (Winter et al., 2007, Koenig et al., 2013) in tomato, and actually its expression is extremely downregulated in ILs 4-1 and 4-1-1 (Chitwood et al., 2013). It is interesting to note that the *S. pennellii* version of this protein seems to be lacking its DNA-binding domain according to its annotation in the Sol Genomics Network website (Fig. 4.8). This seems to indicate that the protein is not functional in *S. pennellii* and therefore it is a very strong candidate for the trichome phenotype observed in the ILs. Whether the annotation is right or not will need to be addressed by studying the actual sequence of the SpMX2 coding sequence *in vivo*. However, its null expression in *S. pennellii* (Koenig et al., 2013) made it impossible to clone a coding sequence for this gene, which indicated that this automatic annotation is not a reflection of the situation *in vivo*, where *SpMX2* is not expressed and can be considered a pseudogene.

Silencing of *SlMX2* in tomato leaves resulted in a reduction in trichome density, compared to the unsilenced tissue (Fig. 4.9). Interestingly, only non-glandular type V trichomes were affected by the silencing of *SlMX2*, while type VI trichome density was not significantly lower between silenced and unsilenced tissue (Fig. 4.9D). This contrasted with what was expected from the IL phenotyping, as IL 4-1 had no type VI trichome on the assessed tissue (see *chapter 3*), and in the silencing experiment, this type of trichome was not affected by the effective knock-down of the gene (Fig. 4.9 and 4.10). The closely-related gene *AmMIXTA-like 1* is a known positive regulator of trichome initiation (Perez-Rodriguez et al., 2005). The *AtMYB106* gene, which is the closest *Arabidopsis* gene to *SlMX2*, performs a dual function, acting as both negative and positive regulator of trichome development, depending on the time of expression (Gilding and Marks, 2010). SlMX2 is also closely related structurally to SlMIX1 (Fig. 4.24), a positive regulator of trichome initiation in tomato (Ewas et al., 2016b). All the evidence from different species support the role of SlMX2 as a regulator of trichome formation. Regarding the fact that only non-glandular trichomes are affected, it has been suggested that determination of trichome identity takes place after initiation, and that initiation and determination are independent

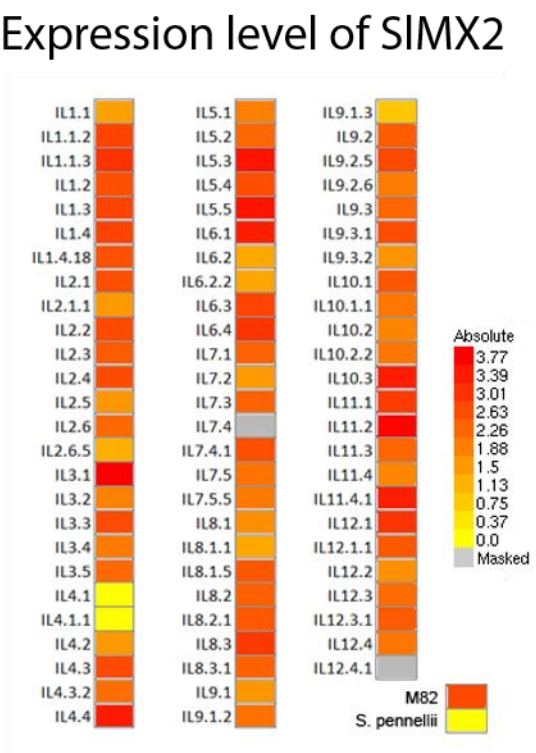

Figure 4.25.-Expression level of SlMX2 in the *S. pennellii* ILs. Absolute expression level of SlMX2 in leaves of the *S. pennellii* ILs, from the RNAseq data generated by (Chitwood et al., 2013). The image was generated using the eFP expression browser (Winter et al., 2007). Note the null expression in *S. pennellii* and the ILs 4-1 and 4-1-1. The expression level in IL 9-1-3 was 30% of the value recorded for M82.

processes (Bergau et al., 2015). In fact, most known regulators in tomato tend to affect all trichome types simultaneously (Deng et al., 2012, Ewas et al., 2016). Therefore, SlMX2 likely regulates both trichome initiation, affecting the total trichome number, and non-glandular trichome determination.

In conclusion, my data suggest that SlMX2 is a possible regulator of trichome initiation and determination in tomato. Its low expression in ILs 4-1 and 4-1-1 is enough to cause a reduction in trichome density, comparable to VIGS-mediated gene silencing (Fig. 4.9). It is interesting to note that IL 9-1-3, another low trichome density line (see *Chapter 3*) also shows a very low expression of this gene, around 30% of the expression value observed for M82 (Fig 4.25) (Chitwood et al., 2013), pointing towards a possible upstream regulator in that genomic region. Also, the non-functional *SpMX2*, according to the available annotation, is likely to be unable to

fulfil the functions of the SlMX2 gene in the ILs 4-1 and 4-1-1. Apart from being non-functional, its expression is consistently null in all tissues in *S. pennellii* (Koenig et al., 2013). This, together with the fact that only non-glandular trichomes seem to be affected by silencing, would explain the absence of type V and type II non-glandular trichomes in *S. pennellii* (Simmons and Gurr, 2005).

4.5.3.-The *hairless-like* phenotype was not caused by any of the selected candidate genes.

I chose to investigate the genomic region covered by IL 10-2. IL 10-2 has a very distinctive *hairless*-like phenotype (Fig. 4.13), and it also has aberrant, branched trichomes (see *chapter 3*). Given that the neighbouring ILs did not show the same phenotype, the region containing the best candidate genes corresponded to bin 10-D, which contains 55 genes and is specific to IL 10-2 (Fig. 4.11). However, as for other ILs, I widened my search to the whole region covered by IL 10-2, containing 693 genes, to avoid missing genes that might not have been mapped correctly. Therefore, I picked genes contained in several different bins (Table 4.3).

I selected *sMYB10-2* because its expression was low in IL 10-2 (Chitwood et al., 2013). Moreover, it was an interesting gene to test, as it contains a MYB-like DNA binding domain, but it has no homologs in *Arabidopsis,* and even where homologs exist in closely related species (*Capsicum* or *Nicotiana*), its function has not been described. Given that *Arabidopsis* lacks multicellular glandular trichomes, this small MYB gene was apparently a good candidate. It was not expressed in trichomes (Spyropoulou et al., 2014), but it might be expressed in other epidermal cells or even expressed at the initial stage of trichome development. Silencing though VIGS of *sMYB10-2* did not have any clear effect on trichome morphology or density (Fig. 4.14) and did not lead to a *hairless*-like phenotype. Although no *Arabidopsis* proteins were very closely related to

sMYB10-2, its DNA-binding domain shared a relatively high degree of similarity with Telomere Repeat Binding Factors (45% identity with TRFL10). TRFL10 is unable to bind DNA *in vitro* (Fulcher and Riha, 2015), although it is expressed in most tissues and developmental stages, indicating it must fulfil an important role *in planta* (Klepikova et al., 2016). In any case, the silencing of this gene did not have an effect on trichomes, which suggested it does not play a role in epidermal development. It is also possible that gene silencing was not effective or homogenous throughout the assessed tissue.

SlbZIP17 was selected even though it was not expressed in trichomes and its expression did not change in IL 10-2 (Table 4.3) (Chitwood et al., 2013, Spyropoulou et al., 2014). The main reason why I decided to analyse this gene further is the fact that in *A. thaliana* it is a known regulator of plant development, affecting mostly primary root elongation, but also over-developed trichomes have been observed in *bzip17* mutants (Kim et al., 2018a). In tomato, other bZIP transcription factors are involved in response to drought and salt stress (Zhu et al., 2018c), and changes in trichome density are associated to stress responses (Fu et al., 2013, Liu and Liu, 2016). Moreover, in fibre mutants in cotton, *bZIP17* is highly upregulated (Wan et al., 2014), suggesting a role in fibre -trichome- development. However, silencing of *SlbZIP17* did not result in altered trichome phenotypes (Fig. 4.15). This indicates that this gene is probably not involved in trichome development, although the lack of phenotypic effects might be due to an ineffective silencing of the gene when using VIGS.

SlABI8 was located in bin 10-D, and although not expressed in trichomes, was downregulated in IL 10-2 (Table 4.3). The a*bscisic acid (ABA) insensitive* (*ABI*) genes were initially described in *A. thaliana* based on the ability of mutants of these genes to germinate when ABA was exogenously applied (Koornneef et al., 1982), and they are a set of different genes with different functions, including transcription factors (ABI3) (Bedi et al., 2016) or phosphatases involved in signal transduction (ABI1 and ABI2) (Merlot et al., 2001). ABI8 is a glycosyltransferase-like protein with a role in cellulose biosynthesis and cell elongation (Brocard-Gifford et al., 2004, Wang et al., 2015b). Moreover, mutations of this gene led to the formation of stomatal clusters in *A. thaliana*, due to an impairment of the plasmodesmatal transport of transcription factors with a role in cell fate determination (Kong et al., 2012). When *SlABI8* was silenced in tomato plants, I observed no effect on trichomes or on any other epidermal cell type (Fig. 4.16). This indicated that, although *AtABI8* has a role in epidermal development, the silencing of the *S. lycopersicum* version is not enough to cause a change in epidermal development, and therefore this gene is likely not responsible for the trichome phenotypes observed in IL 10-2.

I decided to silence *SlCycB2*, a small cyclin reported as not expressed in trichomes and with no changes in expression in IL 10-2 (Table 4.3). However, it is expressed in trichomes as shown by

GUS expression under the control of the *SlCycB2* promoter (Gao et al., 2017). Cyclins control cell cycle and cell division by binding to cyclin-dependent kinases (Hirt, 1996). Different types of cyclins control different transitions in the cell cycle, and type B cyclins (as SlCycB2) control the transition from the G_2 phase to mitotic activity (Dewitte and Murray, 2003). In plants, however, there are many different cyclins and cyclin-dependent kinases and the differences and overlaps in function are unclear (Van Leene et al., 2010). This specific cyclin, however, has been characterised as an interacting partner for Woolly, a HD-ZIP transcription factor which positively regulates trichome initiation (Yang et al., 2011a). Silencing of this gene by RNAi led to the formation of branched trichomes similar to those observed in the IL 10-2 (Yang et al., 2011a), and this phenotype agreed with the observations I made on leaves and stems where *SlCycB2* was silenced by VIGS (Fig. 4.17). Silencing of *SlCycB2* has been reported to induce an increase in trichome density (Gao et al., 2017), however, I did not observe a clear effect in my VIGS experiment (Fig. 4.18). Therefore, my data suggest that SlCycB2 is likely responsible for the aberrant trichome formation observed in IL 10-2, in agreement with previous reports (Yang et al., 2011a, Gao et al., 2017), but it is unlikely to be responsible for the *hairless*-like phenotype. This was confirmed as *SlCycB2* maps to the bin 10-F, which is shared by IL 10-2 and 10-3, which does not show the *hairless*-like phenotype but does have aberrant trichomes (Fig. 4.12).

The final candidate I selected for further testing was another MYB gene, *MYB10-2*, which is expressed in trichomes and upregulated in IL 10-2 (Table 4.3). The function of this MYB transcription factor has not been studied yet, and, although it has no clear homologs in *Arabidopsis*, it shares some sequence homology at the protein level with the response regulator 1 (ARR1) in *Capsicum,* a transcription factor involved in plant development through cytokinin signalling (Oka et al., 2002). Silencing of this gene under my experimental conditions did not cause any clear phenotype in trichome or epidermal cell development (Fig. 4.19). I concluded that this gene is probably not involved in trichome formation in tomato.

In conclusion, I confirmed that the branched, aberrant trichomes observed in IL 10-2 were caused by variation in activity of SlCycB2. The fact that its expression was unchanged in IL 10-2 (Chitwood et al., 2013), indicates that probably the *S. pennellii* version of the gene is sufficient to cause this type of aberrant trichome. This is in fact supported by the presence of branched trichomes in IL 10-3 (Fig. 4.12). However, I failed to find a gene responsible for the *hairless*-like phenotype among the pool of candidate genes I tested through VIGS. Other approaches to narrow down the potential candidate genes, such as the use of backcrossed inbred lines (BILs) or sub-ILs (Alseekh et al., 2013, Ofner et al., 2016) might have been useful to identify the causative gene. In fact, recently, a C2H2 zinc finger transcription factor, denominated HAIR, has been identified as the gene responsible for the *hairless*-like phenotype of IL 10-2 (Chang et al.,

2018) by genome-wide association study of 180 tomato varieties followed by a map-based cloning approach in a F2 segregating population of a cross between IL 10-2 and the *S. lycopersicum* cultivar Ailsa Craig. The function of HAIR was further characterised by overexpression and silencing. This gene was never considered as a candidate in my screen, as its expression is shown as null for every line (including M82) in the IL RNAseq data I used (Chitwood et al., 2013). This highlights the limitations of an expression-based candidate gene approach.

4.5.4.-Analysis of candidate genes outside the main target genomic regions.

I decided to test some other genes by VIGS that were not contained in the main genomic regions on which I focused for the data included in this chapter.

The first candidate I selected was *SlLHW*, which is a bHLH transcription factor expressed in trichomes which was highly expressed in IL 11-3 (Table 4.4). IL 11-3 showed a consistently high trichome density, with a significantly higher trichome density compared to M82 in the second generation of the ILs (see *chapter 3*), and therefore genes in this region are likely to play roles in trichome development (Fig. 4.20). Moreover, this gene was found to be downregulated in *SlMIXTA-like*-RNAi lines (Lashbrooke et al., 2015), indicating that it is possibly under the control of this potential regulator of trichome formation (see *section 4.4.1*). The *A. thaliana* homolog of this gene, *Lonesome Highway* (*LHW*), regulates the formation of vascular tissue in roots and mutants of this gene showed changes in root symmetry and lateral root development (Ohashi-Ito and Bergmann, 2007). In plants, leaf and root development share common regulators (Kwak et al., 2014), in some cases including regulators of trichome and root hair development such as CPC or TRY (Schellmann et al., 2002). These shared regulatory pathways, together with the fact that *SlLHW* is expressed in trichomes (Spyropoulou et al., 2014), made LHW a good candidate for further analysis. Silencing of *SlLHW* in tomato caused no changes in trichome morphology or density (Fig. 4.21). These results suggest that *SlLHW* does not play a role in trichome formation, although possibly it plays roles in other processes controlled by SlMIXTA-like.

I also analysed the genomic region corresponding to IL 7-4-1, as this line, as well as the neighbouring ILs 7-4 and 7-5, had aberrant, swollen trichomes (see *chapter 3*). The region most likely to contain genes responsible for the phenotype is bin 7-B (containing 33 genes), which corresponds to the overlapping region between the three ILs (Fig. 4.21). However, I decided to look in a wider region, including bin 7-C (containing 1072 genes). In this region I found *SlElF1*, which is a translation elongation factor expressed in trichomes and with no changes in expression in IL 7-4-1 (Table 4.4). According to the annotation in the Sol Genomics Network website, this gene is absent in *S. pennellii*, indicating that the introgressed genomic region must lack this gene, making it a good candidate for the observed phenotype. Moreover, ElF1 in *A. thaliana* is involved in cell wall formation, which is essential for cell expansion during outgrowth

formation (Hossain et al., 2012). However, when this gene was silenced by VIGS in tomato, I observed no effect on trichome morphology, and no aberrant trichomes were spotted in silenced tissue (Fig. 4.22). Therefore, this gene is unlikely to play any role in trichome formation.

In conclusion, neither *SlLHW* nor *SlEIF1* silencing had any effects on trichome development in tomato.

4.6.-Conclusion.

In this chapter, I present the results from the functional characterisation of candidate genes selected for their potential role in trichome development from my initial screen of the natural variation in the IL population. This work demonstrates the usefulness of the combination of the phenotypic data from the chapter 3, access to the available genomic and transcriptomic resources and transient gene-silencing approaches for the discovery of new genes and new gene functions.

The VIGS assay has proven to be a rapid method for molecular characterisation and has helped identify two MIXTA/MIXTA-like transcription factors possibly involved in trichome development at different stages in tomato. *SlMIXTA-like*, described for its role in cutin deposition and conical cell formation in fruit, functions as a regulator of trichome patterning of tomato leaves. *SlMX2*, not described previously in tomato, plays a role in determination of trichome density and non-glandular trichome formation. Moreover, we have been able to validate the loss of function of *SlCycB2* in the formation of aberrant branched trichomes, as described previously (Yang et al., 2011a, Gao et al., 2017). I failed to identify the gene responsible for the *hairless*-like phenotype in IL 10-2, the most prominent trichome-related phenotype observed in the ILs screen, which was not included in my candidate gene pool due to the lack of expression in the RNAseq data which I used (Chitwood et al., 2013). In summary, I managed to identify three genes underpinning the natural variation in trichome formation between *S. lycopersicum* and *S. pennellii*, which demonstrates the usefulness of the ILs in identifying and characterising natural variation.

This chapter also reveals some of the limitations of VIGS for functional characterisation. A definite answer regarding the actual function of the candidate genes in tomato would require further analysis, including stable overexpression and knock-out through genome editing techniques. Nevertheless, the work described provides new insights in the regulation of trichome development in *Solanum* species.

Chapter 5 – Functional characterisation of the role of *SlMIXTA-like* in trichome formation in tomato.

5.1.-Abstract

In this chapter I describe a thorough characterisation of the function of *SlMIXTA-like* in epidermal development by using a range of complementary approaches. The analysis of stable overexpressing lines and CRISPR/Cas9 knock-outs, together with the transient silencing described in *Chapter 4*, revealed that SlMIXTA-like acts as a negative regulator of trichome initiation in leaves, and it is responsible for trichome patterning. I also validated its function as a positive regulator of the elongation of conical cells in the epidermis of fruits and petals. Analyses of the SlMIXTA-like promoter activity using GUS staining revealed new potential functions in the development of lateral roots.

5.2.-Introduction

5.2.1.-The role of *MIXTA/MIXTA-like* genes in epidermal development.

Genes in the *MIXTA/MIXTA-like* family are R2R3 MYB transcription factors belonging to subgroup 9, according to the first classification of MYB genes in *Arabidopsis thaliana* based on alignments of the amino acid sequence of the DNA binding domains as well as the conserved amino acid motifs outside the MYB DNA-binding domain (Kranz et al., 1998) In *Arabidopsis*, subgroup 9 includes MYB16, MYB106 and MYB17, although only MYB16 and MYB106 are considered to belong to the *MIXTA* family as a result of comparison with genes described in many other species (Brockington et al., 2013). The first gene functionally characterised in the *MIXTA/MIXTA-like* family was the *MIXTA* gene in snapdragon (*Antirrhinum majus*), which encodes a regulator of conical cell formation in petals (Noda et al., 1994). The overexpression of this gene in a heterologous system, *Nicotiana tabacum*, led to ectopic formation of trichomes and conical cells in carpels and leaves (Glover et al., 1998), and when constitutively expressed in *Antirrhinum*, also showed ectopic trichome formation on leaves (Martin et al., 2002). Analysis of the time of expression of *MIXTA* relative to the cell cycle indicated that early expression of *MIXTA* in cells where cell division is still possible leads to the formation of multicellular trichomes, while later expression, at a time when cell division is no longer possible, leads to the formation of conical epidermal cells (Glover et al., 1998). Other related genes were later described in *Antirrhinum* and named *MIXTA-like 1*, *2* and *3* (*MYBML1*, *MYBML2* and *MYBML3*). Each one of these genes fulfils distinct functions which are generally related to epidermal development. The function of *MYBML1* was also investigated by ectopic expression in *N. tabacum*, where it can drive both the formation of trichomes and conical cells (Perez-Rodriguez et al., 2005). Analysis of its expression pattern seemed to indicate that *MYBML1* plays a role in the formation of trichomes in the ventral petal of the *A. majus* corolla, although it also regulates conical cell formation in the ventral petal and cell expansion in the mesophyll cells of the ventral petal (Perez-Rodriguez et al., 2005). *MYBML2* was characterised in a similar way as a positive

regulator of conical cell formation, although its function was distinct from that of MIXTA as conical cells were more conical in tobacco petals overexpressing *MYBML2* (Baumann et al., 2007). This function was confirmed by analysis of a mutant of the functional homologue of *MYBML2* in petunia (*PhMYB1*) (Baumann et al., 2007). Finally, *MYBML3* is a truncated protein with a shorter C-terminus that retains some ability to positively regulate epidermal outgrowths (Jaffé et al., 2007). The research on these genes has been essential to establish a framework in which to study epidermal development in plants, but the use of heterologous systems limits our ability to draw general conclusions from these studies.

More *MIXTA/MIXTA-like* genes have been described in other species, which suggests further specialisation in their function (Brockington et al., 2013), which is normally described in comparison to the genes from *Antirrhinum*. In the model species *Arabidopsis thaliana*, only two members of the *MIXTA* family are present, *MYB16* and *MYB106*. The proteins encoded by both these genes are clustered in their own clade, separated from the other MIXTA proteins (Fig. 5.1), and the closest degree of similarity with genes from *Antirrhinum* is found for AmMYBML2 (Baumann et al., 2007), and no orthologues of AmMIXTA are found in the *Arabidopsis* genome (Baumann et al., 2007). *MYB16* can also promote conical cell formation when overexpressed in tobacco, performing an equivalent function to *AmMYBML2* (Baumann et al., 2007). *MYB106* acts a positive and negative regulator of trichome formation, both inducing epidermal outgrowth to form trichomes but limiting trichome branching (Gilding and Marks, 2010). Both genes are also involved in cuticle biosynthesis and deposition (Oshima et al., 2013), which indicates functional diversity in different species. The *Arabidopsis* gene *MYB17*, although belonging to the MYB subgroup 9, is not considered a *MIXTA* or *MIXTA-like* gene and it functions as a regulator of transition from vegetative to reproductive growth (Pastore et al., 2011).

In non-model species, *MIXTA/MIXTA-like* genes have also been described, indicating a generally conserved function of these genes in terms of epidermal development. For example, in *Artemisia annua,* AaMIXTA1 is closely related structurally to AmMYBML2/3 (Fig. 5.1) and regulates the formation of glandular trichomes as well as cuticle deposition (Pu et al., 2018), and does this through interaction with HD-ZIP transcription factors (Yan et al., 2018), which are known regulators of trichome development in other species (Yang et al., 2011a, Nadakuduti et al., 2012). In cotton, three genes in this family have been described, including *GhMYBML10*, a regulator of trichome development on petals (Tan et al., 2016), and *GhMYB25* and *GhMYB25-like*, both of which regulate early cotton fibre and trichome development (Machado et al., 2009, Walford et al., 2011). In petunia, *PhMYB1* has the same function as *AmMYBML2* or *AtMYB16* in terms of development of conical cells (Baumann et al., 2007). *MIXTA/MIXTA-like* genes also seem to play a similar role in woody species, as poplar *MYB186* controls trichome formation in

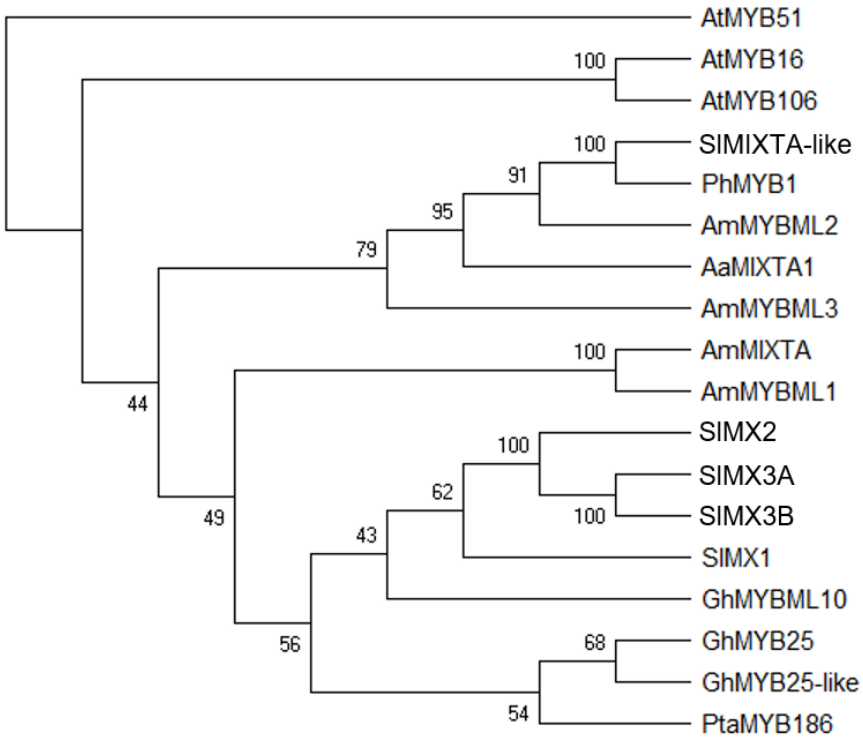

Figure 5.1.- Evolutionary relationship between functionally characterised members of the MIXTA/MIXTA-like family. The phylogenetic tree was built using the Neighbour-Joining method. The bootstrap consensus tree was inferred from 10000 replicates, with the percentage of replicate trees in which branches were clustered together is shown next to each branch. The evolutionary distance was calculated using the Jones-Taylor-Thorton substitution method. 18 MIXTA/MIXTA-like amino acid sequences were included. AtMYB51, a distantly related MYB protein, was used to root the tree. This figure is already shown as figure 4.24 in *chapter 4.*

this species (Plett et al., 2010). In *Thalictrum,* an herbaceous species outside the core eudicots, the homologue of *AmMYBML2*, *TtMYBML2*, was shown to control conical cell formation when overexpressed in tobacco (Di Stilio et al., 2009). Interestingly, some of genes in this family also can act as negative regulators of epidermal outgrowths. This is the case of *MYB6* in cucumber, which is a negative regulator of spine development in fruits (Yang et al., 2018) or *MIXTA-like 8* in *Mimulus guttatus,* the expression of which is known to be negatively associated with trichome formation (Scoville et al., 2011). In general, the MIXTA/MIXTA-like family of MYB transcription factors are present in many different plant families and play distinct, although related, roles in development of epidermal tissue in different organs.

5.2.2.-*MIXTA/MIXTA-like* genes in tomato.

In tomato, seven genes have been identified as members of the subgroup 9 of R2R3 MYB transcription factors (The Tomato Genome, 2012, Lashbrooke et al., 2015). Among these, two of them are more closely related to AtMYB17, and therefore are not considered to be MIXTA/MIXTA-like regulatory factors. The other five show different degrees of sequence divergence from AmMIXTA and other members of the family described in the previous section (Fig. 5.1) (Lashbrooke et al., 2015), with only SlMIXTA-like being closely related to these, although all of them share the attributes of members of subgroup 9. Only two of these have been functionally characterised, *SlMX1* (Ewas et al., 2016b, Ewas et al., 2017) and *SlMIXTA-like* (Lashbrooke et al., 2015).

SlMX1 (Solyc01g010910) is evolutionary related to the *AmMIXTA* and *AmMYBML1* genes (Fig. 5.1), and it has an extended number of functions in tomato. First, *SlMX1* is a regulator of trichome development. Overexpression of this gene in tomato plants caused a substantial increase in trichome density, although it caused the appearance of branched, aberrant trichomes. Consequently, silencing via RNAi caused a reduction in the trichome density. There was a reduction in all type of glandular and non-glandular trichomes. Other effects on development were observed in the fruit cuticle, which was thicker in *SlMX1* overexpression plants and thinner in RNAi lines, and in the leaf thickness, which was also thinner in RNAi lines and thicker in overexpression lines. Finally, *SlMX1* also controlled carotenoid content in fruit by regulation of the main enzymes in the biosynthetic pathways (Ewas et al., 2016, Ewas et al., 2017). *SlMX1* appears to be a good example of conservation of core MIXTA functions while gaining new functions in specialised tissues.

SlMIXTA-like (Solyc02g088190) is closely related to *AmMYBML2* (Fig. 5.1) and its function has been described in RNAi tomato lines (Lashbrooke et al., 2015). Silencing of *SlMIXTA-like* had two main effects: flattening of conical cells in the epidermis of the fruit and reduction of the cuticle thickness in fruit. Silencing also had some pleiotropic effect in vegetative growth, including

delayed growth and curling and wrinkling of leaves. No effect was observed on conical cells in petals or in trichomes, which suggested that *SlMIXTA-like* has a highly specialised function. Both cuticle deposition and conical cell formation are processes traditionally controlled by *MIXTA/MIXTA-like* genes. These findings are reported by (Lashbrooke et al., 2015). The lack of description of overexpression lines limited the full characterisation of the activity of this gene in tomato.

SlMX2 (Solyc04g005600), although not described in the literature, is a potential regulator of trichome development, as suggested by my VIGS assays results described in *chapter 4* and is a close homolog of *AmMIXTA* and *AmMYBML1* (Fig. 5.1).

The function of both *SlMX1* and *SlMIXTA-like* has been studied through silencing approaches. RNAi, although very useful for gaining a better understanding of physiological and developmental processes, has limitations. These include off-target silencing as well as silencing not reaching a low enough expression level of the gene to develop a scorable phenotype (Boutros and Ahringer, 2008). The use of knock-out mutants, either by screening of populations or generated by CRISPR-mediated genome editing facilitate understanding of how these genes function in tomato, especially in terms of trichome development.

5.3.-Methods

5.3.1.-Plant material.

All transformations were done in *Solanum lycopersicum* cv. MoneyMaker, following the procedure described in *chapter 2*. Transient expression assays were performed in *Nicotiana benthamiana*. For overexpression of *SlMIXTA-like* and *SpMIXTA-like* – the equivalent gene from *Solanum pennellii*, the full-length gene was amplified from cDNA of *S. lycopersicum* cv. MoneyMaker and *S. pennellii* respectively, using primers with overhang sequences including the *attB* sites required for cloning into pDONR207 using the Gateway® recombination system (Thermo Fisher Scientific, USA) to generate entry vectors. Gene fragments were introduced into a pBIN19-based expression vector, driven by a 35S promoter, generating the final expression vectors 35S:*SlMIXTA-like* and 35S:*SpMIXTA-like*. Primers and plasmids used for generation of these constructs can be found in *Appendices 1 and 2*. For generation of CRISPR knock-outs, two highly specific guides were selected from the genomic sequence of *SlMIXTA-like*, using NGG as PAM sequence, using the online tool CRISPR direct (Naito et al., 2015). The guide sequences were introduced into the pICSL002218A plasmid (TSLSynBio, Norwich, UK) using a Golden Gate digestion-ligation procedure. Primers and plasmids used are listed in Appendices 1 and 2. For generation of a construct for reporting promoter activity, a 1000 bp region upstream of the translation start of *SlMIXTA-like* was cloned into pDONR207 and then transferred to the

destination vector pKGWFS7 (Karimi et al., 2002), where the insert was positioned upstream of a GFP:GUS fusion protein, generating a proMIXTA-like:GFP:GUS construct. All primers and plasmids for these assays are included in Appendices 1 and 2. In each case, all the assays were done on T1 plants, except for *SpMIXTA-like* OE lines, were seeds of the T1 were not available.

Positive transformants were identified by PCR using the Phire kit (see *chapter 2*). For overexpression lines, the transcript abundance of *SlMIXTA-like* and *SpMIXTA-like* was determined by qPCR, using the primers shown in appendix 1. None of the SpMIXTA-like-specific primers performed well in qPCR assays, so, in the case of *SpMIXTA-like*-OE plants, the transcript abundance of both *SpMIXTA-like* and *SlMIXTA-like* was measured together using a common primer. Details of the qPCR protocol can be found in *chapter 2*.

5.3.2.-Evaluation of trichome phenotype.

For evaluation of the trichome phenotypes in each of the generated lines, the line of interest (OE or KO) was grown alongside MoneyMaker plants in seed trays under greenhouse conditions for 4 weeks until the first true leaf was fully expanded (with an average temperature of 20-22 °C). The terminal leaflet of the first fully expanded leaf of five plants per line for *SlMIXTA-like* KO characterisation and three plants per line for *SlMIXTA-like* OE (except for OE #1, where only two plants were available) were excised and leaf sections of 0.5 x 0.5 cm were used for cryo-SEM imaging of their adaxial surface (see details in *chapter 2*). For trichome, stomata and pavement cell quantification, 8-15 micrographs of approximately 0.3 mm^2 were manually counted, and trichomes were also sorted according to the established classification (Simmons and Gurr, 2005). Trichome and stomatal density were expressed as percentage of total epidermal cell number. Trichome-to-stomata ratio was calculated as the ratio relating trichome density to stomatal density. Aberrant morphologies and patterning of trichomes were recorded.

For SpMIXTA-like OE lines, mature fully expanded leaves were analysed in the T0 generation and compared visually to equivalent MoneyMaker plants of similar age. No detailedquantifications were done for this line.

5.3.3.-Evaluation of phenotype in flowers, fruits and roots.

Flowers of the SlMIXTA-like KO line from the T1 generation, as well as MoneyMaker flowers, were collected and the adaxial side was imaged using cryo-SEM (see *chapter 2* for details). Mature green fruits from MoneyMaker and SlMIXTA-like KO lines were harvested and sectioned for cryo-SEM imaging of their epidermis. Differences in conical cell shape were recorded.

For root phenotyping, seeds from MoneyMaker and SlMIXTA-like KO lines were germinated in MS + 3% sucrose in square plates and grown vertically *in vitro*. Roots were assayed in 10-days-

old seedlings, and their architecture was recorded visually. Root hairs were imaged using a Leica 205F stereomicroscope (Leica, Germany).

5.3.4.-Generation of hairy roots through *Agrobacterium rhizogenes* transformation in tomato.

The proMIXTA-like:GFP:GUS construct was transformed into electrocompetent *Agrobacterium rhizogenes* strain ATCC15834, and bacteria were grown under antibiotic selection for 3-5 days. Liquid cultures were generated from positive colonies and they were grown for 3 days. Tomato (cv. MoneyMaker) cotyledons and hypocotyls were used as explants, and were co-cultivated for 3 days in MS+3% sucrose plates, and then were transferred to MS+3% sucrose plates with 200 µg/L cefotaxime and 100 µg/L kanamycin for selection of positively transformed roots. Hairy (adventitious) roots emerged approximately 2-3 weeks after transformation. Explants were subcultured every two weeks, and, when roots were over 5 cm longs, they were excised from the explant and cultured on their own. This protocol was adapted from (Ron et al., 2014).

5.3.5.-Transient expression in *N. benthamiana.*

Transient expression of pro*MIXTA-like*:GFP:GUS was performed by manually injecting *Agrobacterium tumefaciens* strain agl1 transformed with the construct into mature leaves of 4-week-old *N. benthamiana* plants grown at 20–22 °C under greenhouse conditions. Transformed *A. tumefaciens* were grown in TY cultures with streptomycin (100 µg/mL), ampicillin (100 µg/mL) and rifampicin (50 µg/mL) as selection antibiotics to an OD_{600} 0.5-0.8. Cells were pelleted and resuspended in 10mM MgCl2, 10mM MES pH 5.6 buffer with 200 µM of acetosyringone to a final OD_{600}=0.1. Injected leaves were harvested 5 days post infection and used for GUS staining assays.

5.3.6.-GUS staining.

Tomato hairy roots, *N. benthamiana* leaves or tissue from stably transformed tomato plants (petals, leaves, seedlings and roots) were stained using X-Glucose, which is metabolised into a blue pigment by the β-glucuronidase (GUS) enzyme, the expression of which is driven by the SlMIXTA-like promoter in these transformed tissues. The procedure consisted of fully submerging the tissue to be assayed in a 50 mM phosphate buffer, pH 7.0 with 0.5 mg/mL of X-Glc and incubating overnight at 37 °C in darkness. After staining, green tissues were submerged in 70% ethanol for two hours and 100% ethanol for up to 24 hours to remove chlorophyll. The samples were then imaged using a Leica 205F stereomicroscope (Leica, Germany). All transformed samples were assayed alongside untransformed controls.

5.3.7.-Statistical analysis.

Comparisons of trichome and stomatal density, trichome-to-stomata ratio and trichome type densities and percentages were assessed using a t-test between the control line and each OE or KO line. Significant differences were considered when p-value<0.05. The relationship between trichome density and stomatal density was assessed by correlation coefficient (R^2), and significance by Pearson correlation test (p-value<0.05 used as cut-off for significance). The analyses were performed using R software (ver. 3.2.2; R Core Team, Vienna, Austria).

5.3.8.-Transcriptomic data retrieval.

The tissue-specific expression profiles of *SlMIXTA-like* in *S. lycopersicum* cv. M82 and the expression level in the leaves of *S. pennellii* ILs was retrieved. The tissue-specific transcriptome were obtained from (Koenig et al., 2013) and the RNAseq data for leaves were obtained from (Chitwood et al., 2013). The colour-coded display of gene expression used in this chapter was generated using the Tomato eFP Browser.

5.4.-Results

5.4.1.-Analysis of the leaf epidermis in *SlMIXTA-like* overexpression lines.

I generated seven independent *SlMIXTA-like* overexpression (OE) lines, which were transformed with a 35S:*SlMIXTA-like* construct. I used the T1 generation of these lines for the work described. I determined the abundance of the *SlMIXTA-like* transcript in four of these OE lines by qPCR, and analysed three lines (OE #1-3) with significantly higher expression levels of *SlMIXTA-like* (Fig. 5.2). I selected these lines for further analysis.

I observed a low trichome number in the adaxial surface of *SlMIXTA-like* OE lines (Fig. 5.3). When quantified, the three OE lines had a significantly lower trichome density compared to the MoneyMaker control line (Fig. 5.4A). Together with the change in trichome density, I observed an increase in stomatal density in all three OE lines, although it was significant only for lines OE #2 and #3 (Fig. 5.4B). The OE lines had a lower trichome-to-stomata ratio when they were compared to MoneyMaker (Fig. 5.4C). I observed a negative association between trichome and stomatal density when all the data points were considered (Fig. 5.4D). I classified the trichomes in different groups according to the established categories (Luckwill, 1943, Simmons and Gurr, 2005) to determine whether the observed changes in trichome density affected specific trichome types. No differences in the density of type I or VII between were observed control and OE lines. However, the density of type V trichomes was lower in OE #2 and OE #3 compared to the control. Similarly, the density of type VI trichomes was lower in OE #1 and OE #3 compared to the control (Fig. 5.5A). When I compared the percentages of each type of trichome in respect to the total trichome number in each line, I observed no differences between MoneyMaker and OE lines (Fig. 5.5B). In OE #2 and OE #3, which had the highest expression of *SlMIXTA-like*, I

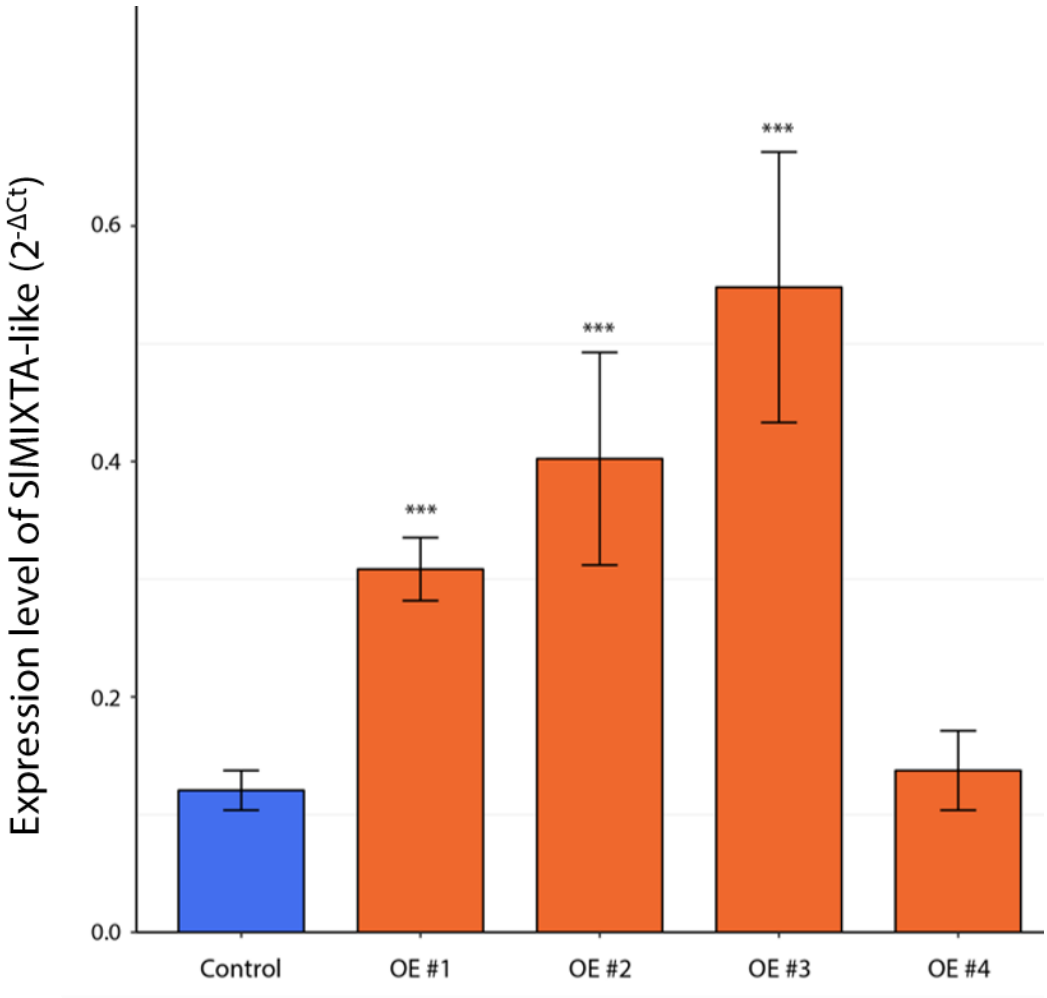

Figure 5.2.-Expression level of *SlMIXTA-like* in leaves from control untransformed tomato plants and four independent *SlMIXTA-like* overexpression (35S:*SlMIXTA-like*) lines. The blue bar corresponds to the values for control leaves. The orange bars correspond to each overexpression line (OE #1-4). Values are mean±SEM of n=3-7 for each line. Three stars indicate a significant difference between the corresponding line and the control lines (p-value<0.01) according to a t-test.

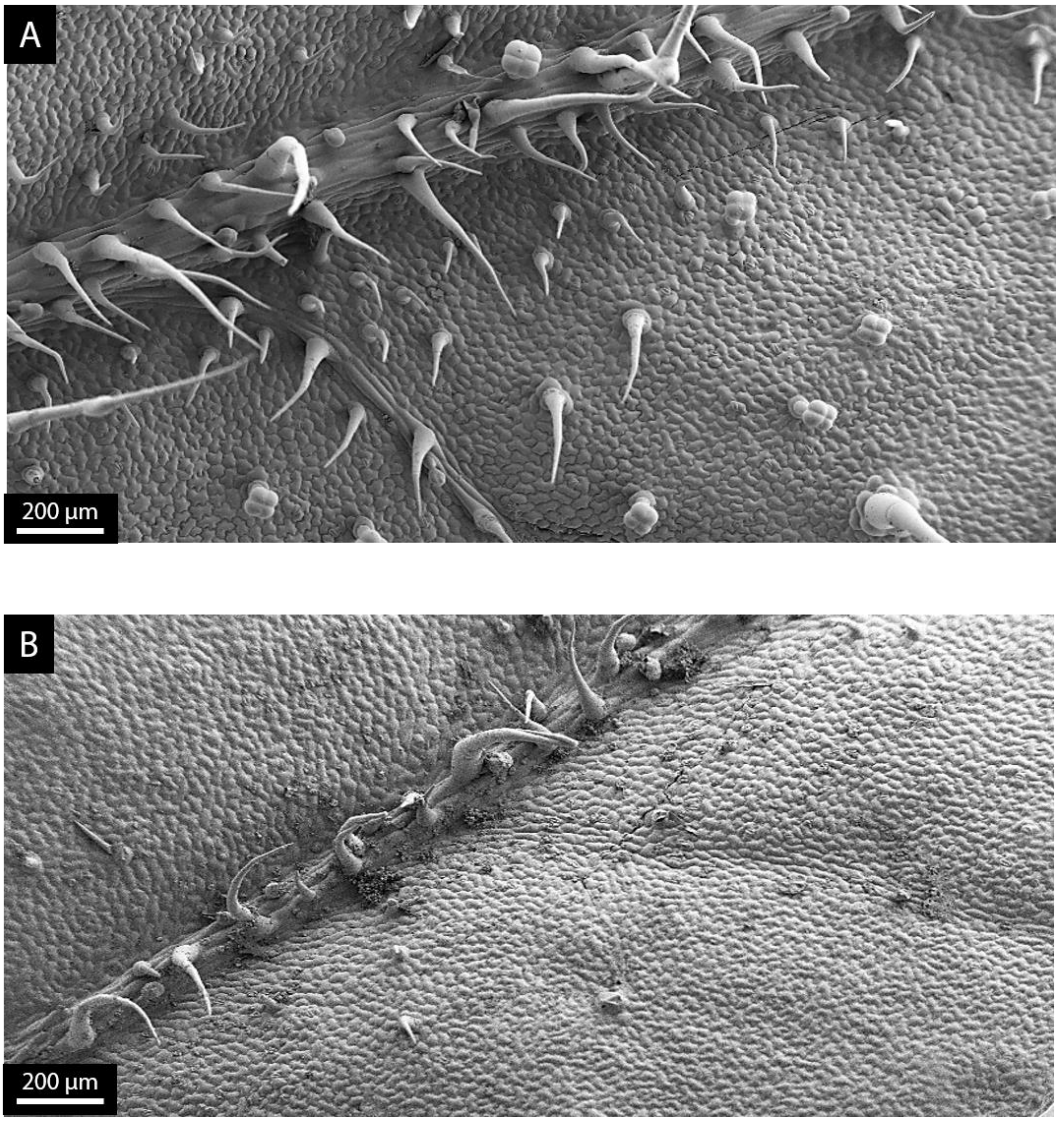

Figure 5.3.- Adaxial leaf surface of control *S. lycopersicum* and *SlMIXTA-like* overexpression lines. A) Micrograph of the surface of a control, untransformed leaf. B) Micrograph of the surface of a *SlMIXTA-like* overexpression (35S:*SlMIXTA-like*) line (OE #1). Scale bars are shown in each micrograph.

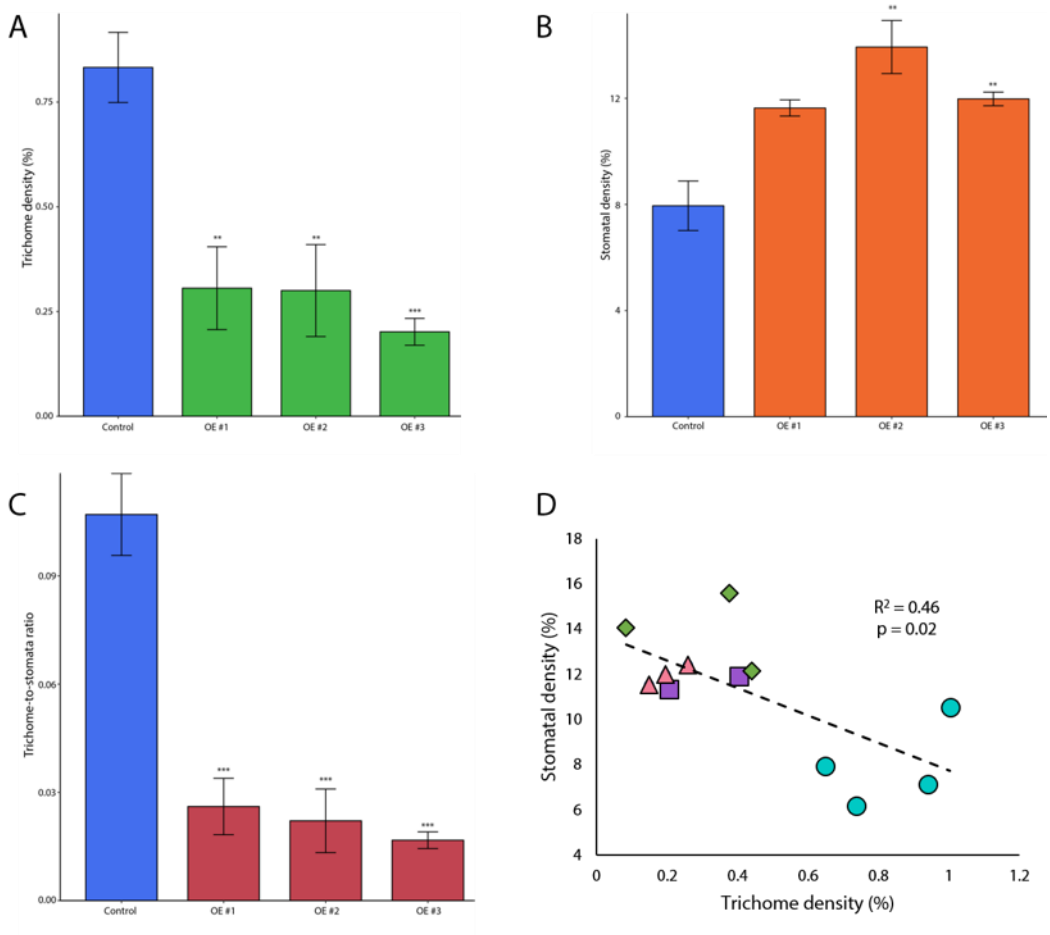

Figure 5.4.-Quantification of epidermal structures in *SlMIXTA-like* overexpression leaves and control tomato leaves. A) Trichome density, expressed as percentage of total epidermal cells, in control leaves (blue bar) and leaves from three independent overexpression lines (green bars). B) Stomatal density, expressed as percentage of total epidermal cells, in control leaves (blue bar) and leaves from three independent overexpression lines (orange bars). C) Trichome-to-stomata ratio of control tomato leaves (blue bar) and three independent overexpression lines (pink bars). D) Correlation between trichome and stomatal density in the assessed leaves. Turquoise circles correspond to values from control leaves, purple squares correspond to OE #1 values, green diamonds correspond to values from to OE #2 values and pink triangles correspond to OE #3 values. Correlation index and p-value are shown in the graph. For A, B and C, values are expressed as mean±SEM of n=4 for control leaves, n=2 for OE #1 and n=3 for OE #2 and #3. Two starts indicate a p-value<0.05 and three stars indicate a p-value<0.01 according to a t-test between the corresponding OE line and the control value.

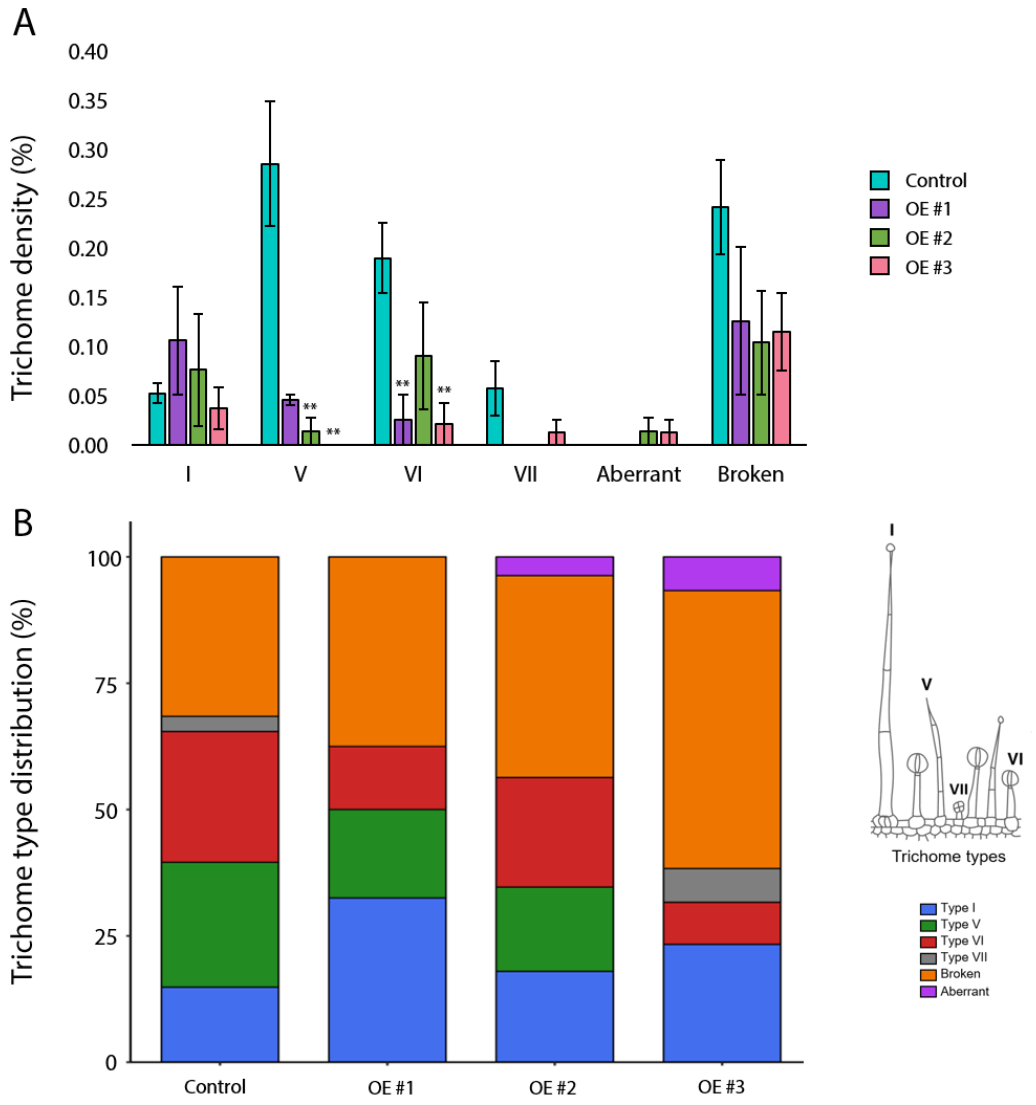

Figure 5.5.-Differences in trichome types in control, untransformed tomato leaves and three independent *SlMIXTA-like* overexpression (35S:*SlMIXTA-like*) lines. A) Trichome density of each trichome type is expressed as percentage of total epidermal cells. Turquoise bars correspond to control values, and purple, green and pink bars correspond to overexpression lines 1, 2 and 3 (OE #1-3) respectively. Two stars indicate significant difference between control values and values for a given overexpression line (p-value<0.05) according to a t-test. Values are mean±SEM of n=4 for control leaves, n=2 for OE #1 and n=3 for OE #2 and #3. B) Percentage of each trichome type of the total number of trichomes for each line. No significant differences were observed in this comparison.

observed swollen aberrant trichomes (Fig. 5.6). In every case, a large percentage of the trichomes were broken (Fig. 5.5).

5.4.2.-Analysis of the leaf epidermis in *SlMIXTA-like* knock-out lines.

I generated four independent *SlMIXTA-like* knock-out lines by CRISPR/Cas9 (named KO #1-4). I targeted two different gene sequences, one in the 5' untranslated region and the other in the coding sequence of the first exon, using two different sgRNAs (Fig. 5.7A). Both sgRNAs were effective and I observed deletions in both regions (Fig. 5.8). I selected line KO #1 for further analysis as the 2 bp deletion in the coding sequence caused a translation frameshift and an early stop codon and led to the production of a truncated 34 amino acid protein (Fig. 5.7B and C). I used T1 homozygous plants for the analysis described in this section.

I observed a higher abundance of trichomes in the adaxial surface of the leaves of the KO line leaves (Fig. 5.9). There were also clusters of two trichomes involving type I (Fig. 5.9B and C), type VII (Fig. 5.9D) and type VI (Fig. 5.9E) trichomes. In some cases, I observed outgrowths of the basal cells of type I trichomes (Fig. 5.9F), which resembled conical cells. I also observed some clusters of stomata (Fig. 5.10).

When trichome and stomatal densities were quantified, the KO line showed a significantly higher trichome density compared to the control MoneyMaker leaves (Fig. 5.11A). Stomatal density was also significantly higher in the KO line (Fig. 5.11B), and consequently, the trichome-to-stomata ratio was not statistically significant different between WT and KO lines (Fig. 5.11C). Interestingly, the previously observed correlation between trichome and stomatal density was maintained when the data points for the control MoneyMaker leaves were used, while this correlation was not observed when the KO data points were considered and when all data points for both lines were taken together (Fig. 5.11D).

As for OE lines, I classified the different trichomes into types according to (Luckwill, 1943, Simmons and Gurr, 2005). Type I trichome density was significantly higher in the KO line compared to the control MoneyMaker leaves (Fig. 5.12A), but the densities of other types were not affected. When the percentages of each trichome type were compared, the percentage of type I trichomes was still significantly different between the KO and control lines (Fig. 5.12B). I did not observe any aberrant trichomes in the KO lines.

5.4.3.-Analysis of the leaf epidermis in *SpMIXTA-like* OE lines.

I cloned the *S. pennellii* version of MIXTA-like. The amino acid sequence is almost identical to the *S. lycopersicum* one, and the MYB DNA-binding region is very conserved in the two species, with the exception of an amino acid change (Fig. 5.13). I generated eight independent *SpMIXTA-like* overexpression lines, which were transformed with a 35S*:SpMIXTA-like* construct. These

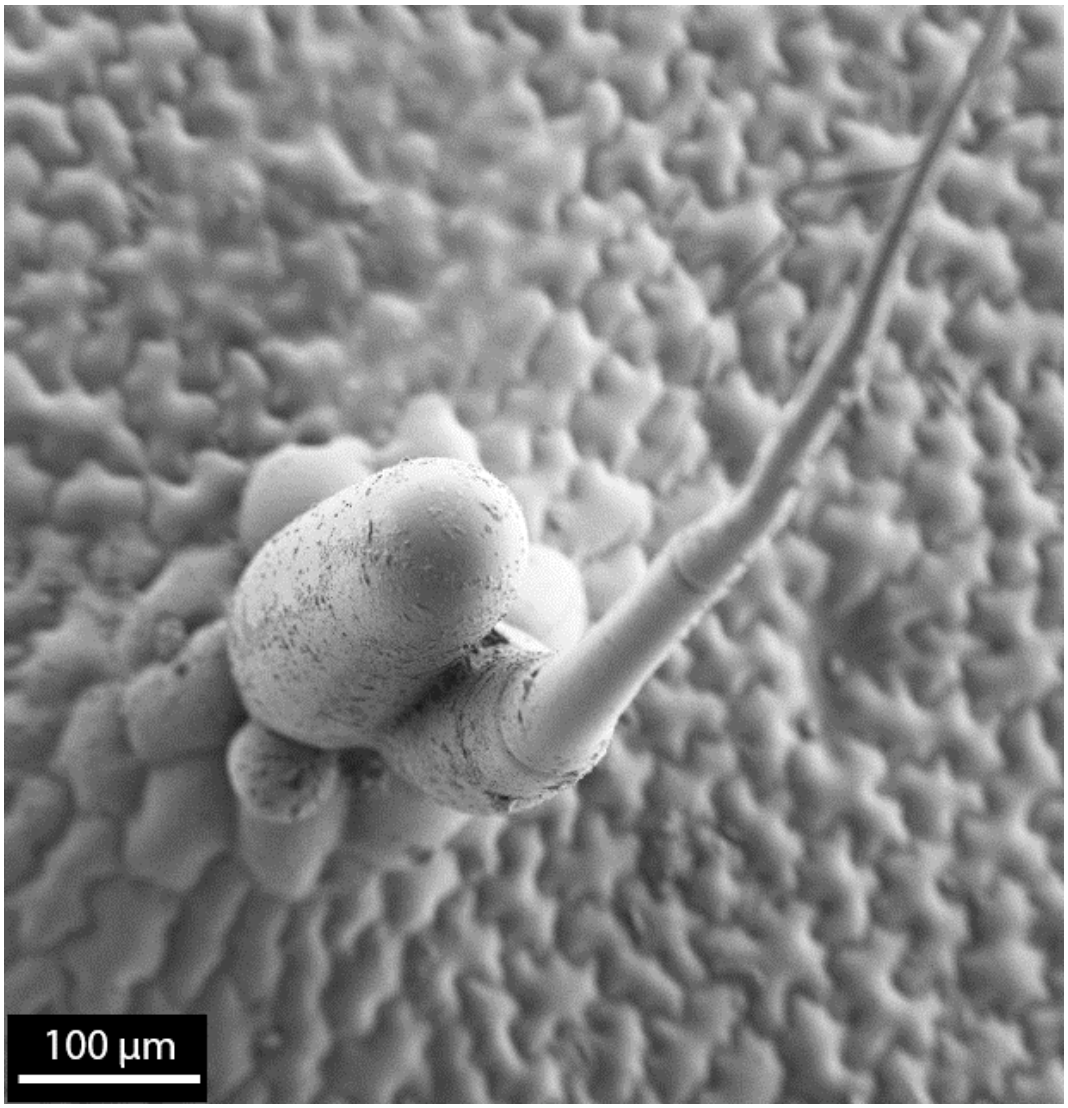

Figure 5.6.-Micrograph of aberrant trichome found on *SlMIXTA-like* overexpression line OE #2.

Scale bar is indicated in the picture.

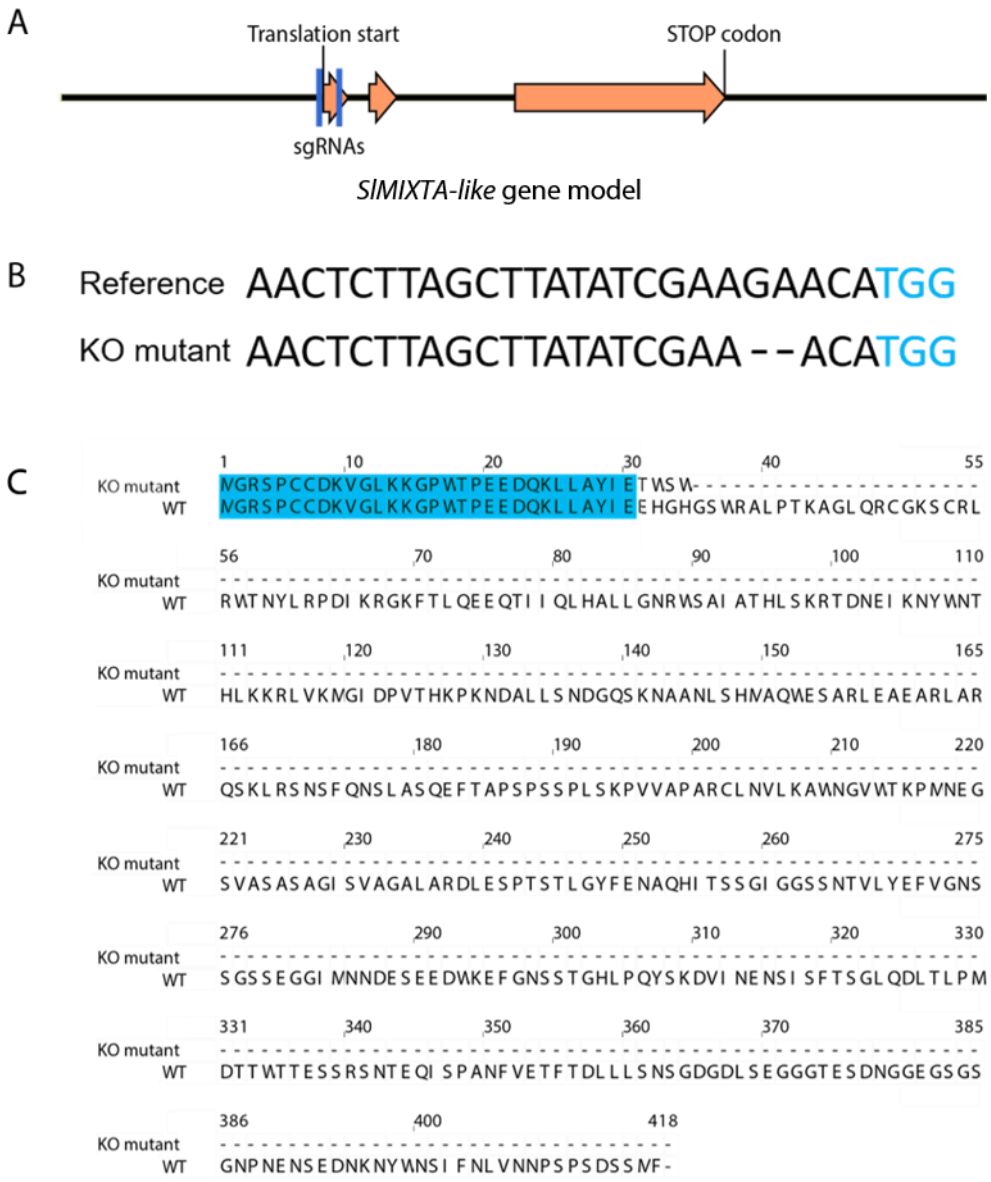

Figure 5.7.-Description of *SlMIXTA-like* KO mutant generated by CRISPR/Cas9. A) Gene model of *SlMIXTA-like*. The orange arrows represent the gene coding sequence split into three exons. The blue vertical lines represent the chosen sgRNAs for gene edition, located right before the translation start and in the beginning of the coding sequence. The translation start and STOP codon are shown in the model. The black line represents non-coding sequences (promoter, UTRs and introns). B) Sequence of the genomic region edited in the KO mutant and the reference sequence from the non-mutated gene. The blue letters correspond to the PAM sequence of the sgRNA 2. C) Sequence of the mutated protein in the KO line (34 aa, with an early stop codon caused by the frameshift) and the SlMIXTA-like WT version (417 aa).

Figure 5.8.-Deletions observed in the *SlMIXTA-like* genomic sequence of CRISPR-edited plants. Four independent lines with deletions in their genomic sequence were generated. The figure shows the alignment between the MoneyMaker sequence (MM) and the sequence in each one of the knock-out lines (KO #1-4). The translation start is underlined in blue. The PAM sequences selected for targeted genomic edition are underlined in orange. Lines KO #1 and KO #3 had the same 2 bp deletion that cause a frameshift and early stop codon. Lines KO #2 and #4 had the same 1 bp deletion in the coding sequence and different deletions in the 5' UTR. In both cases, there was a frameshift and early stop codon.

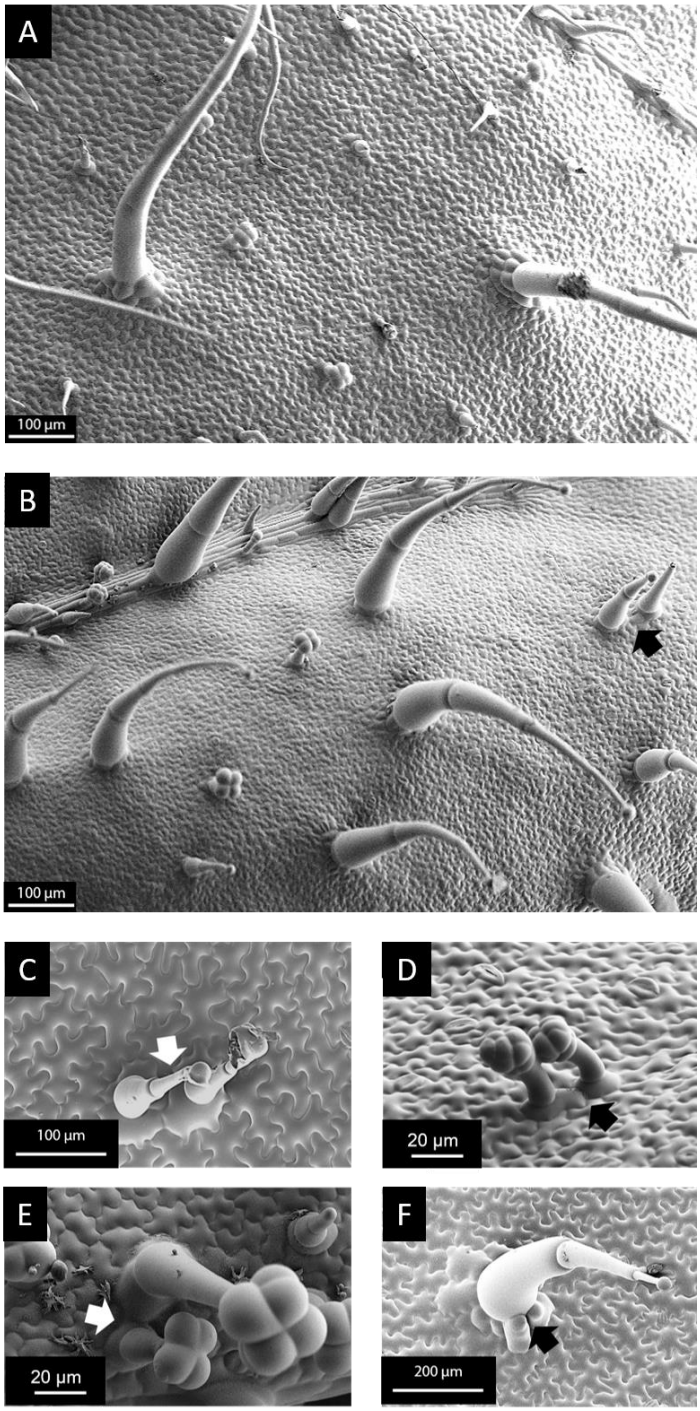

Figure 5.9.-Scanning electron micrographs of the adaxial surface of *SlMIXTA-like* CRISPR knock-out plants. A) Overview of the adaxial surface of a MoneyMaker control leaf. B) Overview of the adaxial surface of the *SlMIXTA-like* KO leaves. B) Detail of a cluster of two type IV trichomes. C) Detail of a cluster of two type VII trichomes. D) detail of a cluster of two type VI trichomes. E) Detail of outgrowths on the basal cells of a type I trichome. The scale bar is indicated for each micrograph. In B-E, arrows point trichome clusters. In F, the arrow indicates aberrant trichome basal cells.

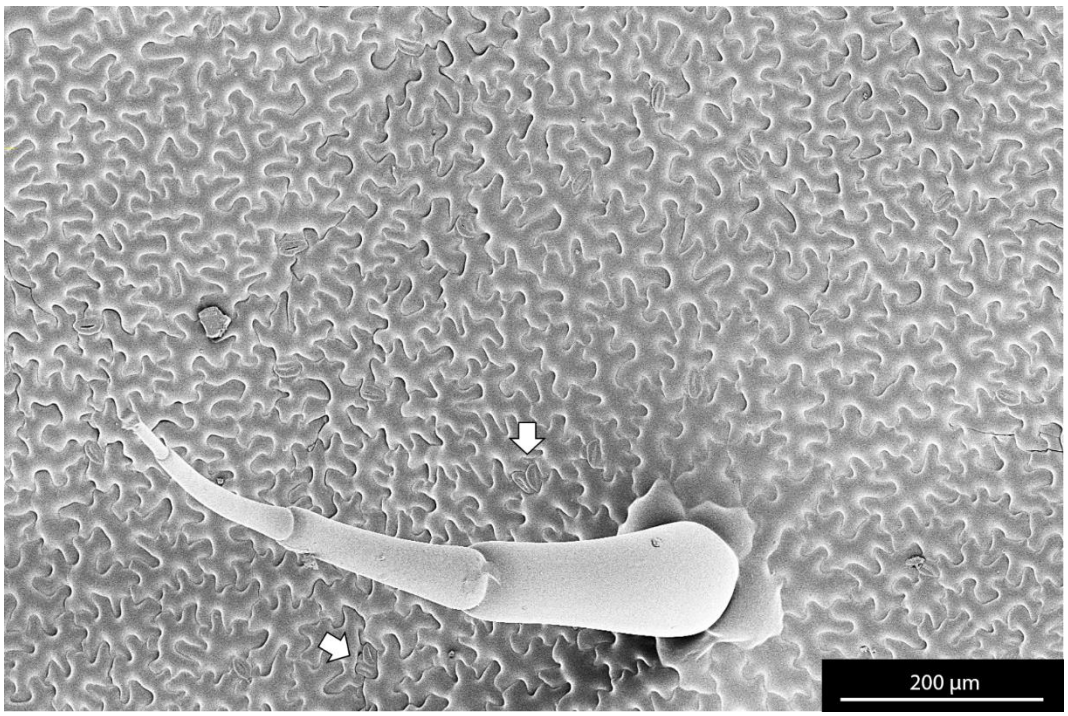

Figure 5.10.-Stomatal clusters on the adaxial surface of *SlMIXTA-like* KO leaves. The scale bar is indicated in the micrograph. The white arrows point towards stomata clusters.

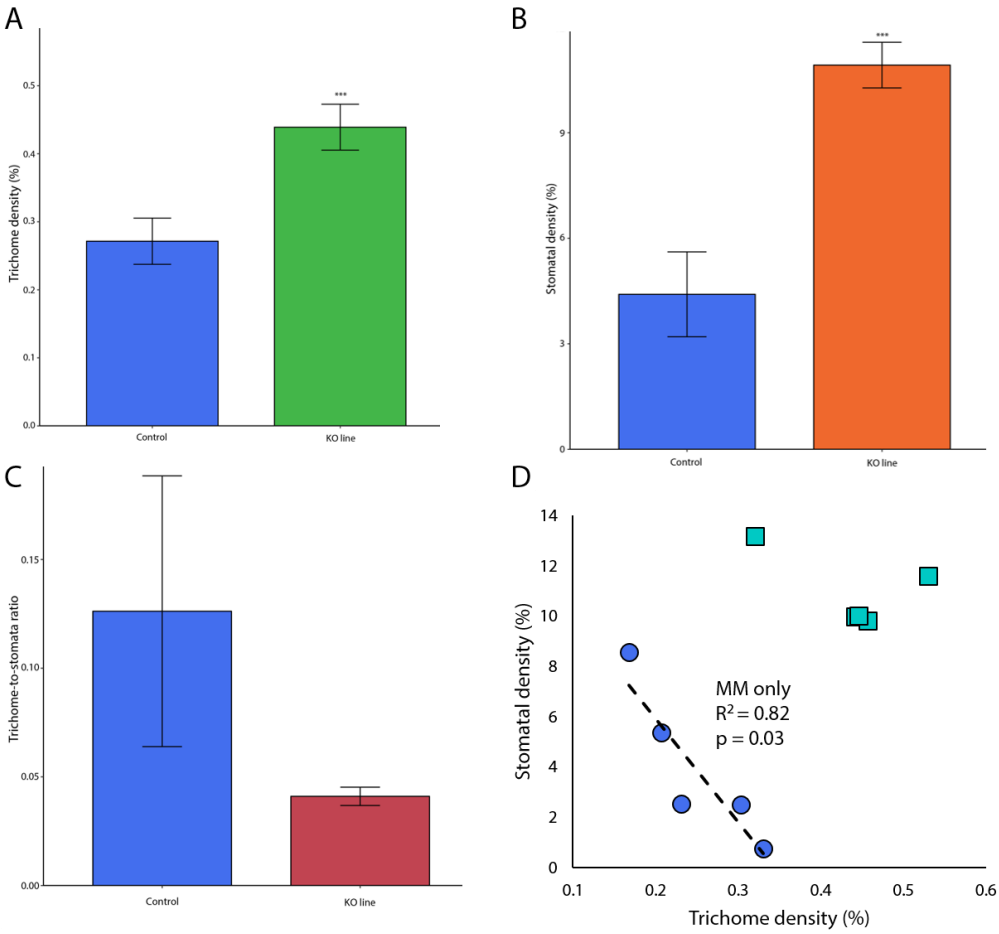

Figure 5.11.-Quantification of epidermal structures in *SlMIXTA-like* knock-out leaves and control tomato leaves. A) Trichome density, expressed as percentage of total epidermal cells, in control leaves (blue bar) and leaves from the described KO mutant (green bar). B) Stomatal density, expressed as percentage of total epidermal cells, in control leaves (blue bar) and leaves from the KO mutant (orange bar). C) Trichome-to-stomata ratio of control tomato leaves (blue bar) and the KO mutant (pink bar). D) Correlation between trichome and stomatal density in the assessed leaves. Blue circles correspond to values from control leaves, turquoise squares correspond to the described KO mutant. A significant correlation was seen only in control leaves. Correlation index and p-value are shown in the graph. For A, B and C, n=5 per line. Three stars indicate a p-value<0.01 according to a t-test between both lines' values.

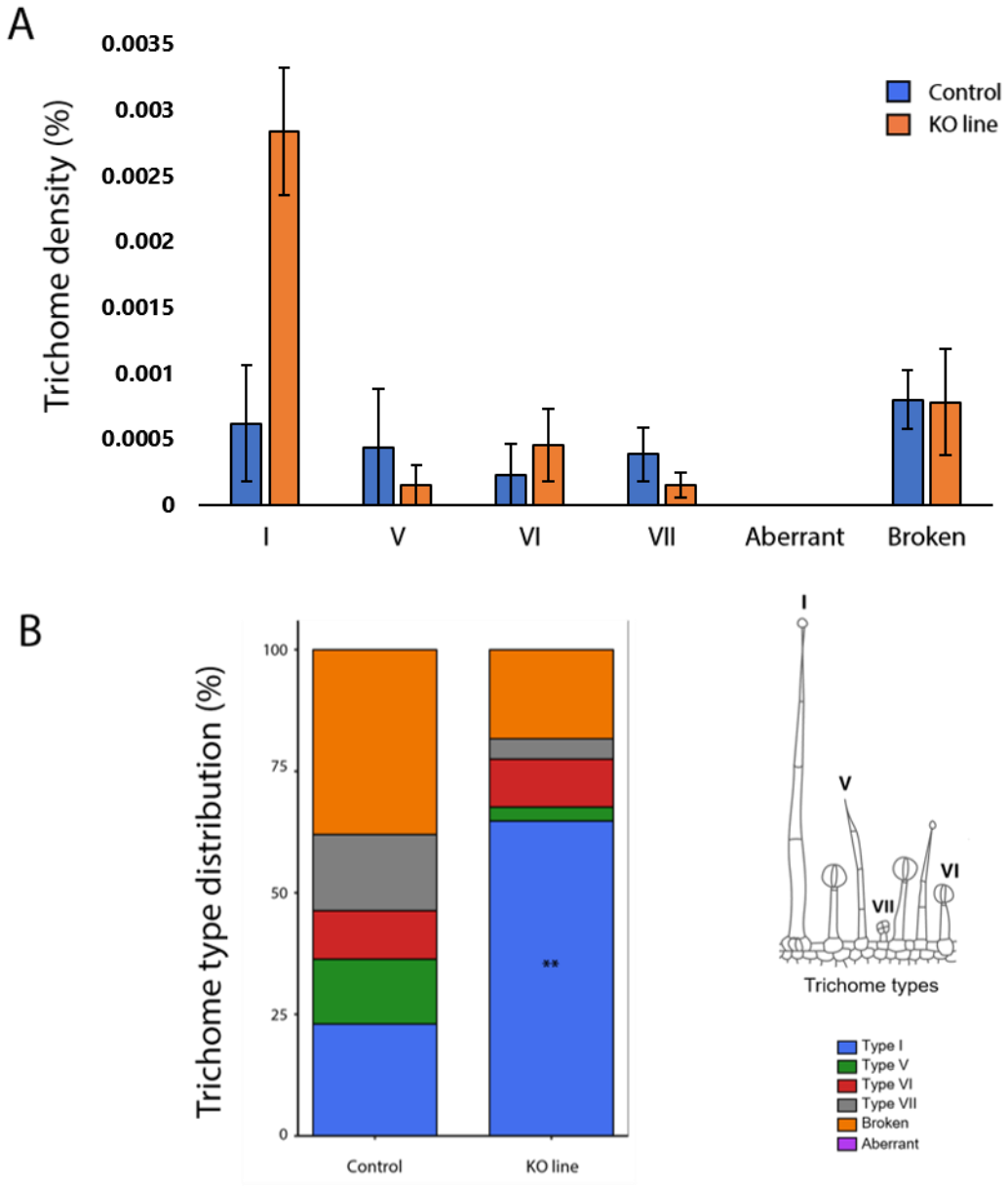

Figure 5.12.-Differences in trichome types in control tomato leaves and *SlMIXTA-like* KO leaves. A) Trichome density of each trichome type is expressed as percentage of total epidermal cells. Blue bars correspond to control values, and orange bars correspond to SlMYB16 KO values. Three stars indicate significant difference between control and KO values (p-value<0.01) according to a t-test. Values are mean±SEM of n=5 for each line. B) Percentage of each trichome type of the total number of trichomes for each line. Two stars indicate significant differences between control and KO percentages (p-value<0.05) according to a t-test.

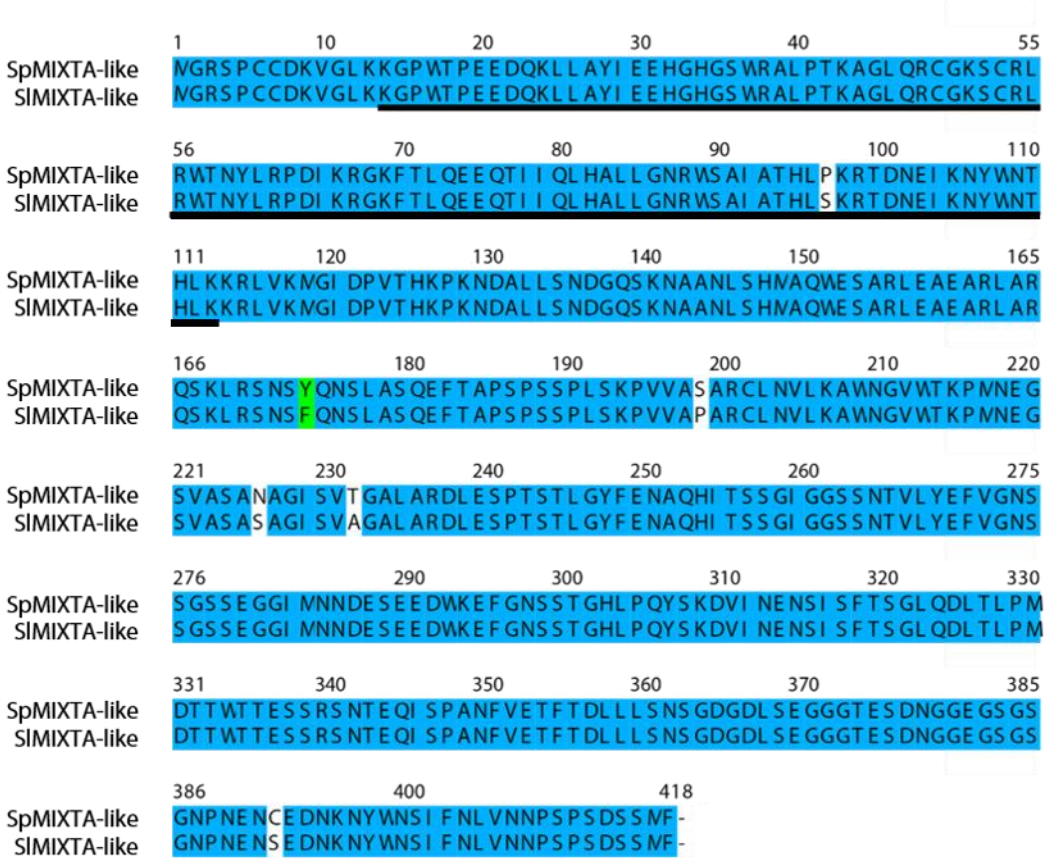

Figure 5.13.-Alignment of the amino acid sequences of SpMIXTA-like and SlMIXTA-like. The blue colour indicates amino acids that are conserved between both sequences. The green colour indicates amino acid changes within the same chemical group. The white colour indicates amino acid changes outside the same chemical group. The DNA-binding domain is underlined.

plants had some problems in the development of reproductive structures and were slow to produce fruit. Therefore, the analysis of the T1 generation could not be performed due to time constrains. I measured the MIXTA-like transcript abundance in the OE lines by qPCR, using three of the independent OE lines (Fig. 5.14). The expression level was significantly higher in the OE lines. It is important to note that the primers used for qPCR were common to the *S. lycopersicum* and *S. pennellii* versions of the gene, and therefore the expression of both genes contributed to the observed transcript abundance. The lack of T1 plants did not allow for proper comparison between lines. Similar leaves from MoneyMaker control plants and one of the OE lines (SpOE #1) were analysed under the microscope for outstanding differences. I did not observe a clear phenotype in SpOE #1 (Fig. 5.15), although it is possible that trichome density was lower, similar to the observations in *SlMIXTA-like* OE lines. Phenotyping of the T1 generation will shed light on any possible functional differences between both gene versions.

5.4.4.-Analysis of *SlMIXTA-like* promoter activity in aerial and underground tissues.

I cloned the promoter region of *SlMIXTA-like* corresponding to the 1000 bp upstream of the start codon (proMIXTA-like) to build a proMIXTA-like:GFP:GUS construct. The promoter activity was generally low, and the GFP expression was hard to evaluate in tissues other than roots. Therefore, I based my results on the observation of GUS-stained tissue. I transformed the construct in *Agrobacterium rhizogenes* and analysed tomato hairy roots expressing the construct (Fig. 5.16A and B). The promoter activity was high in the epidermal tissue, the pericycle and especially the lateral root primordia. Expression of GUS was not observed in root hairs (Fig. 5.16A and B). No background staining was observed in control hairy roots transformed with the empty vector.

I also generated three independent tomato lines stably transformed with the reporter construct. I analysed the petals and leaves from the T0 plants, as well as seedlings from the T1 generation. Comparisons were made to control, untransformed MoneyMaker plants. I observed promoter activity in petals, especially in the marginal areas and in the veins, where trichomes are usually present in petals (Fig. 5.16C and D). Analysis of the promoter activity in leaves revealed that *SlMIXTA-like* expression takes place in most of the epidermal tissue, especially in marginal areas, but it is not expressed in trichome cells, only in basal cells of type I trichomes (Fig. 5.16E and F). No background expression was observed in control leaves (Fig. 5.16G). Finally, the expression of the reporter gene in cotyledons was equivalent to the observations in leaves, with staining of the epidermal cells (Fig. 5.16H and I). In roots of stably transformed plants, I observed staining in lateral root primordia and in the meristematic and distal elongation zones of the root (Fig. 5.17).

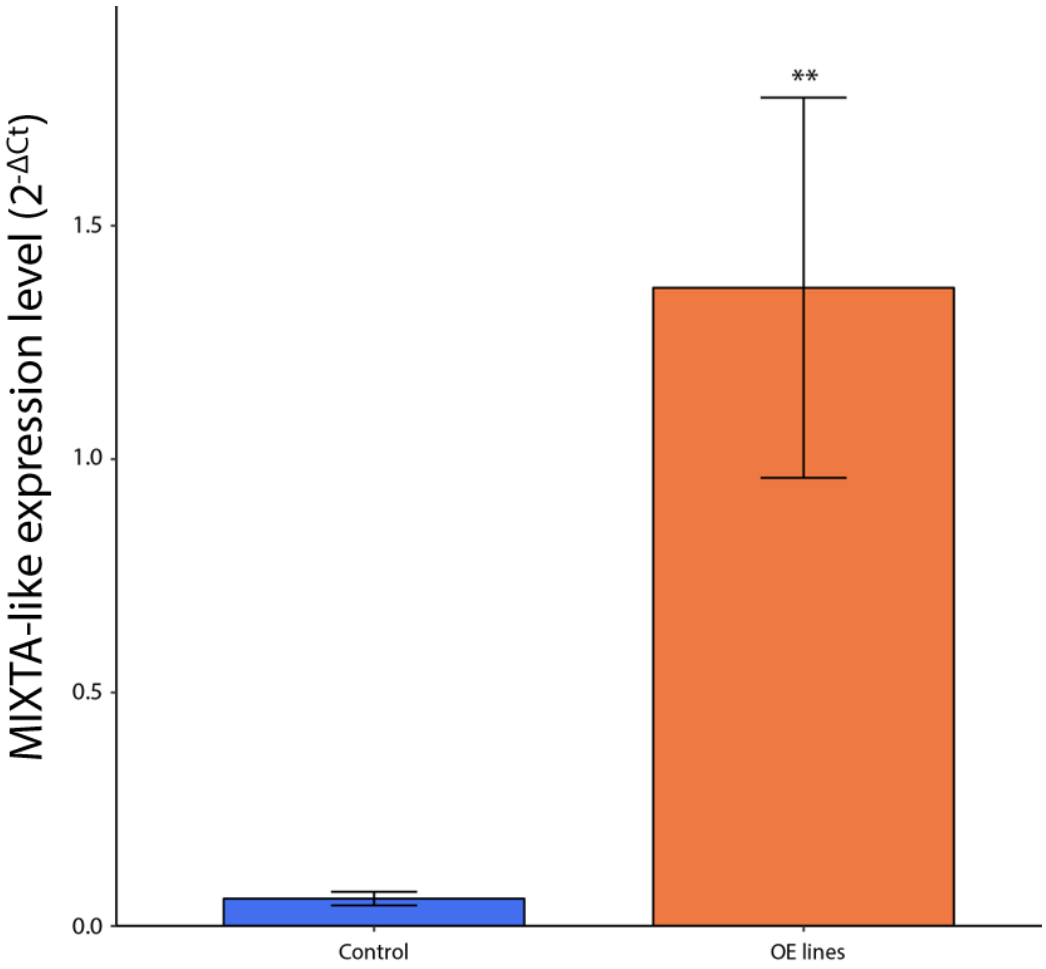

Figure 5.14.-Expression level of *MIXTA-like* in leaves from control untransformed tomato plants and T0 *SpMIXTA-like* overexpression (35S:*SpMIXTA-like*) lines. The blue bar corresponds to the values for control leaves. The orange bar corresponds to the expression values of MIXTA-like of three independent T0 OE lines. Values are mean±SEM of n=4 for control values and n=3 for OE values. Two stars indicate a significant difference between the corresponding line and the control lines (p-value<0.05) according to a t-test.

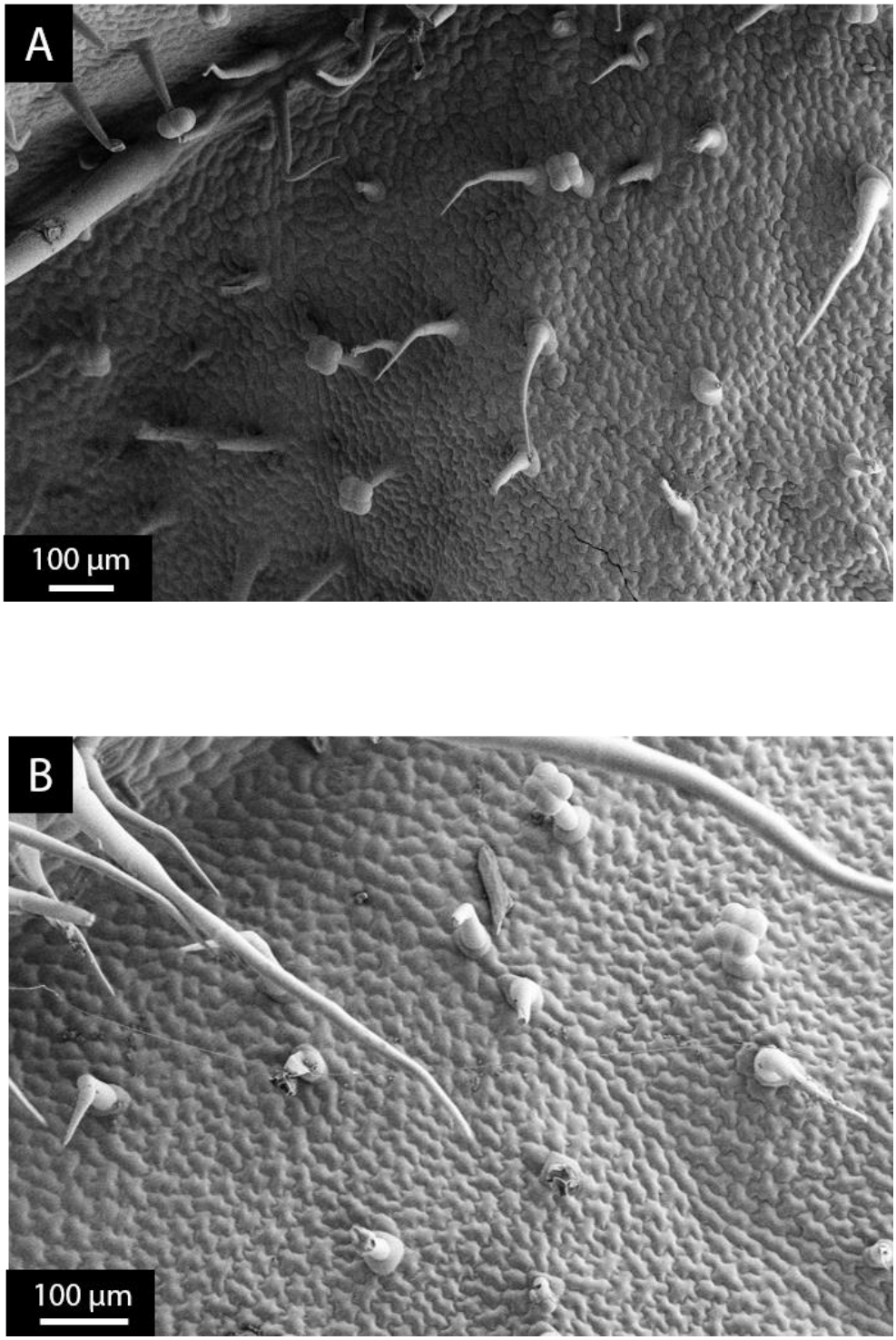

Figure 5.15.-Adaxial leaf surface of control *S. lycopersicum* and *SpMIXTA-like* overexpression lines. A) Micrograph of the surface of a control, untransformed leaf. B) Micrograph of the surface of a *SpMIXTA-like* overexpression (35S:*SpMIXTA-like*) line. Scale bars are shown in each micrograph.

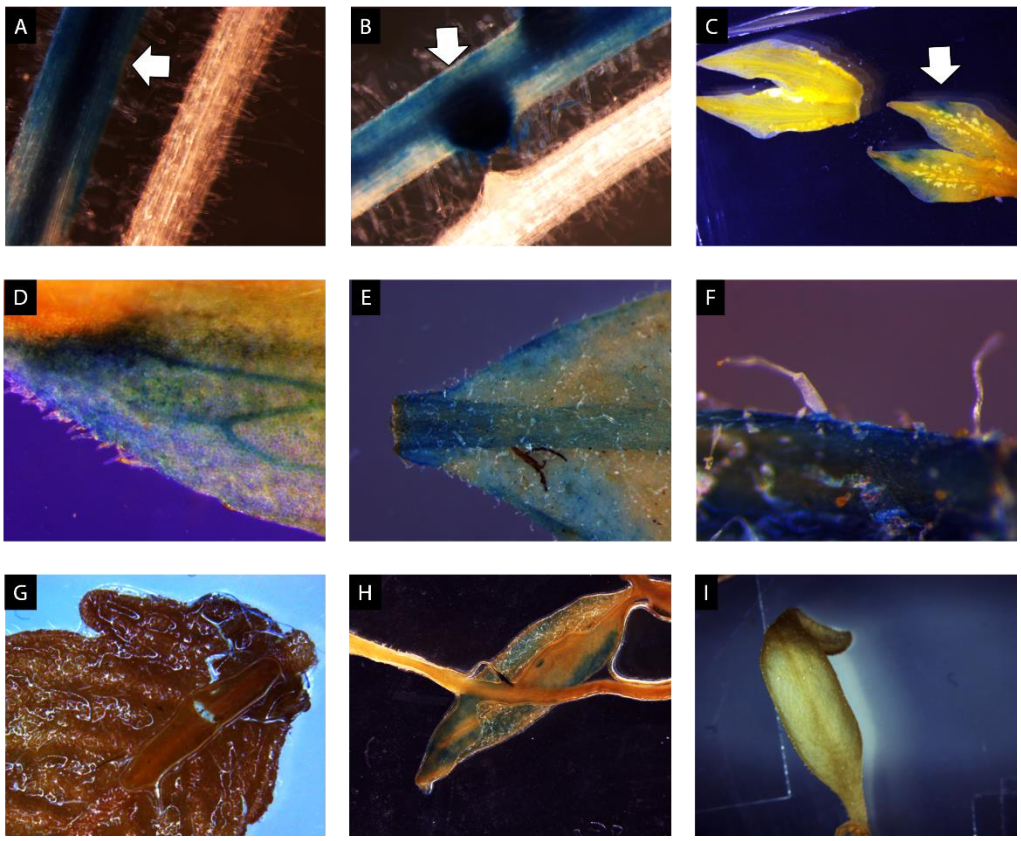

Figure 5.16. GUS staining of different tissues expressing proMIXTA-like:GFP:GUS. A and B) GUS staining of transformed and control (empty vector) hairy roots. C) GUS staining of petals of transformed and control *S. lycopersicum* cv. MoneyMaker plants. D) Detail of GUS-stained petal of transformed plant. E and F) GUS staining of leaves of transformed tomato plants. G) GUS staining of a leaf from a control, untransformed tomato plant. H) GUS staining in cotyledons of a transformed plant. I) GUS staining of cotyledons of a control, untransformed plant. In A, B and C, the white arrows indicate the transformed tissue.

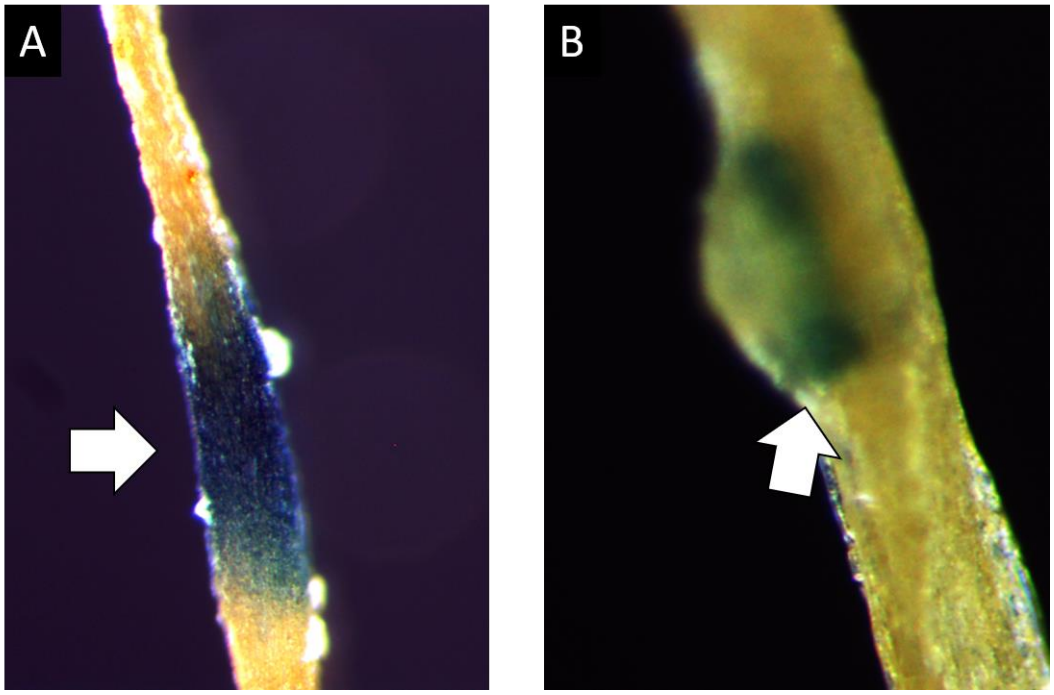

Figure 5.17.-GUS staining of roots of stably transformed lines expressing *proMIXTA-like*:GFP:GUS. A) GUS staining in the meristematic and distal elongation zone of lateral roots. B) GUS staining in lateral root primordia. White arrows point the described region in each picture.

This indicates that *SlMIXTA-like* is expressed in more tissues and in a very spatially determined fashion. I transiently expressed the *proMIXTA-like*:GFP:GUS construct in *Nicotiana benthamiana* leaves. I observed an intense promoter activity in epidermal cells, but similar to the case of tomato leaves, trichome cells did not show expression of the reporter gene (Fig. 5.18).

5.4.5.-Analysis of flowers, fruit and roots of *SlMIXTA-like* knock-out lines.

I analysed the surface of petals in of one of the *SpMIXTA-like* OE line, *SlMIXTA-like* KO #1 line and MoneyMaker control plants. No flowers from the *SlMIXTA-like* OE lines were available at the time of the assay. Conical cells in petals were flattened in the KO line, compared to the control petals (Fig. 5.19), although upon close inspection they did not look completely flat. The conical cells in *SpMIXTA-like* OE lines were slightly more elongated (Fig. 5.19C). A similar situation was observed on the fruit surface. Conical cells were flatter in the KO line (Fig. 5.20), as shown by (Lashbrooke et al., 2015). Interestingly, KO fruits had protuberances all over their surface, some of them with trichomes on. (Fig. 5.20). This produced a very rough feeling to the tomato skin when touched with bare hands. No *SlMIXTA-like* or *SpMIXTA-like* OE fruits were available for the assay.

When roots of seedlings were analysed, I observed a reduced number of lateral roots in *SlMIXTA-like* KO plants, and their lateral roots were shorter than those found in MoneyMaker plants. Moreover, the lateral root patterning in *SlMIXTA-like* lines was aberrant, with lateral roots primordia initiating next to each other (Fig. 5.21). Root hairs were, however, not different either in length or density between the lines (Fig. 5.22).

5.5.-Discussion

5.5.1.-*SlMIXTA-like* is a positive regulator of the development of conical cells.

I observed *SlMIXTA-like* promoter activity in petals (Fig. 5.16C and D). I observed that petals of the *SlMIXTA-like* KO line had much flatter conical cells compared to MoneyMaker petals, while *SpMIXTA-like* OE petals had more elongated conical cells (Fig. 5.19), and this is in agreement with reports of homologs of *SlMIXTA-like*, including *MYB1* in petunia, MYB16 in *Arabidopsis* and *MIXTA-like 2* in snapdragon (Baumann et al., 2007). As described for these genes, the appearance of the conical cells was not completely flat, suggesting that other factors are necessary for initiation of conical cells in tomato petals, in a similar way to the distinct functions of MIXTA and MIXTA-like 2 in *Antirrhinum* (Baumann et al., 2007). This function of SlMIXTA-like was not identified in a previous study with RNAi silencing of *SlMIXTA-like* tomato, where no effect of silencing was observed in petals (Lashbrooke et al., 2015). This indicates that even low levels of expression may be sufficient to fulfil this function of SlMIXTA-like or maybe that silencing mediated by stable expression of RNAi might not be very effective in petals. This

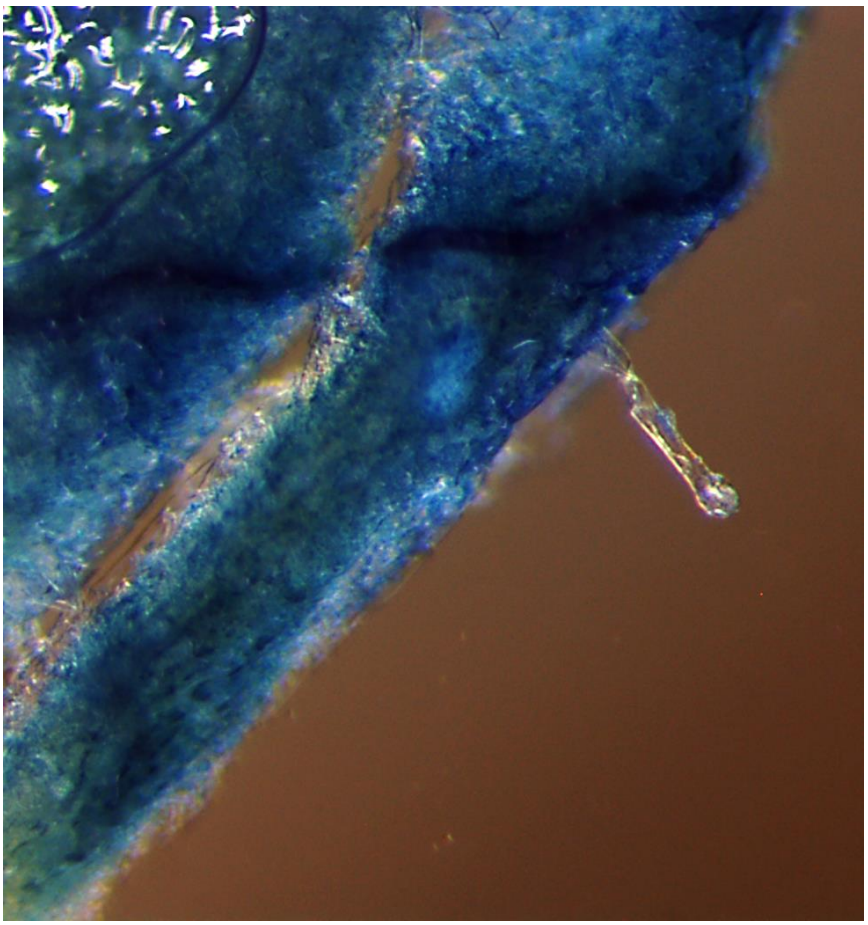

Figure 5.18.-**GUS staining of *Nicotiana benthamiana* leaves transiently expressing *proMIXTA-like:*GFP:GUS.** GUS activity was detected in the leaf epidermis, but not in trichomes.

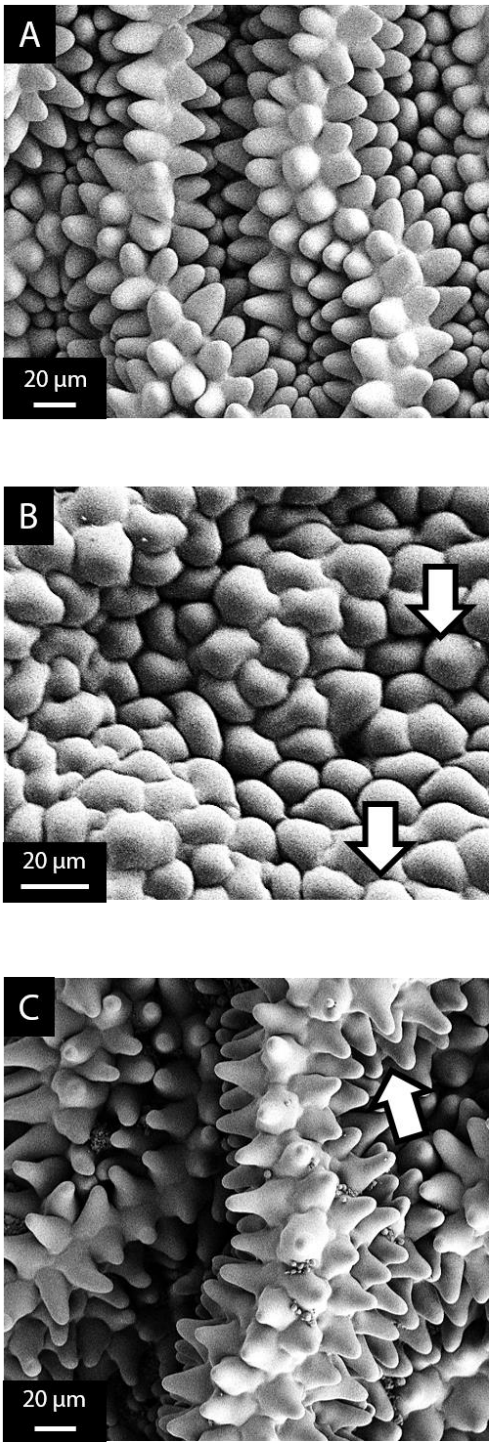

Figure 5.19.-Conical cells in petal surfaces in control and *SlMIXTA-like* KO lines. A) Adaxial surface of a petal in control plants. B) Adaxial surface of *SlMIXTA-like* KO petals. White arrows point to cells were the pseudoconical shape of the cells can be distinguished. C) Adaxial surface of *SpMIXTA-like* OE petals. The white arrows point to cells were the more elongated conical shape can be observed.

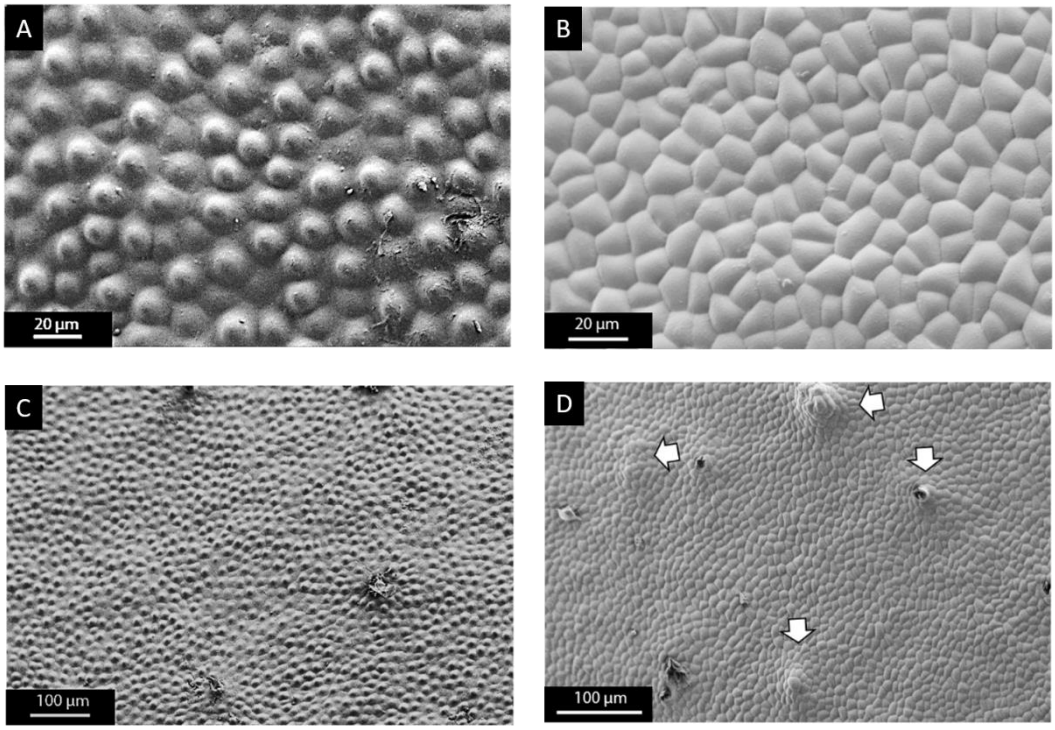

Figure 5.20.-Conical cells in the fruit surface in control and *SlMIXTA-like* KO lines. A) Micrograph of the conical cells on the surface of a control green tomato. B) Micrograph of the conical cells on the surface of a *SlMIXTA-like* KO green tomato. C) Micrograph of the surface of a control green tomato. D) Micrograph of the surface of a *SlMIXTA-like* KO green tomato. The white arrows indicate protuberances in the fruit surface. The scale bars are indicated in every image.

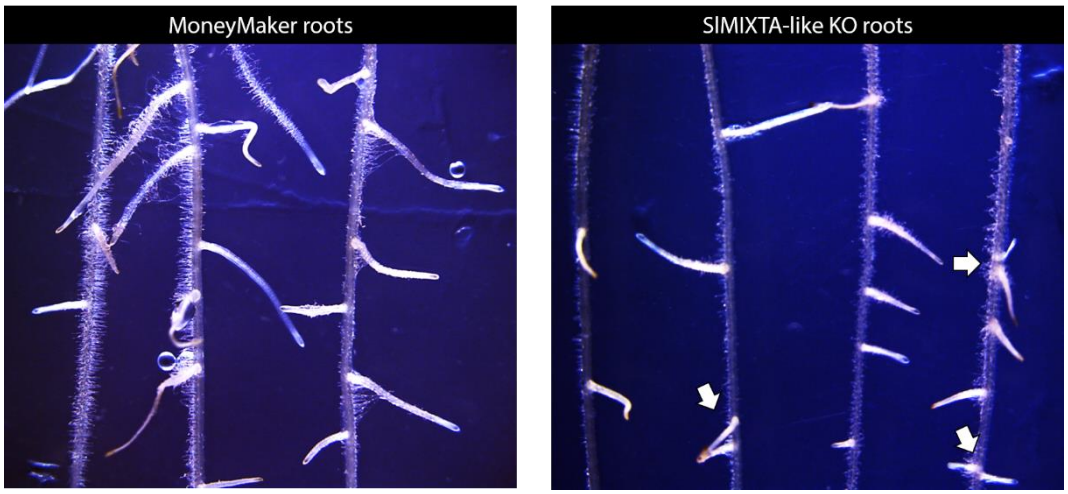

Figure 5.21.-Roots of control and *SlMIXTA-like* KO lines. On the left, roots of 2-week-old MoneyMaker control seedlings. On the right, roots of 2-week-old *SlMIXTA-like* KO seedlings, which have shorter and less abundant lateral roots. White arrows indicate aberrant patterning of lateral roots. Both pictures are taken at the same magnification and correspond to the equivalent distal regions of the root.

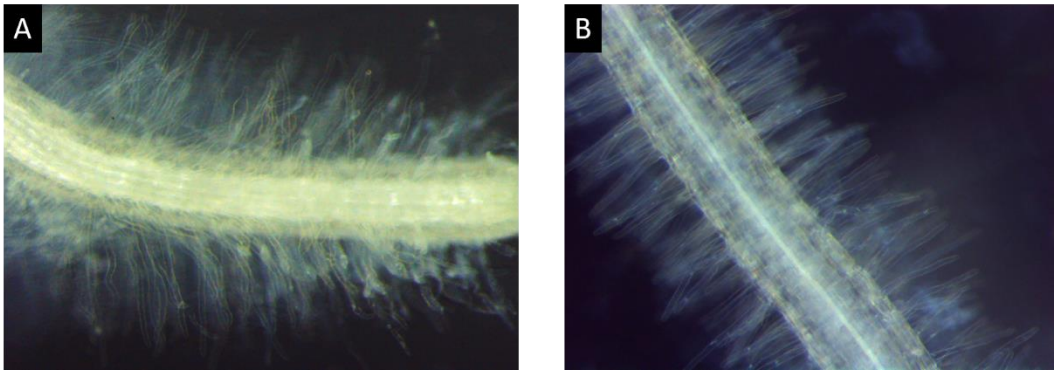

Figure 5.22.-Root hairs of control MoneyMaker plants and *SlMIXTA-like* KO line. A) Apical region of the root of a MoneyMaker plant. B) Apical region of a root of a *SlMIXTA-like* KO plant. No clear differences were observed between both lines.

supports the use of KO mutants in combination with silencing approaches (see *chapter 4*) to obtain a better understanding of the function of a gene. I observed a similar effect on conical cells in the fruit epidermis (Fig. 5.20), which were also much flatter in the KO line compared to MoneyMaker fruits. These finding agreed with the previous report on the function of SlMIXTA-like in conical cell development in fruit (Lashbrooke et al., 2015).

The tomato skin of the *SlMIXTA-like* KO line was very rough to the touch, even though the cells on the surface were flatter. This rough feeling of the fruit was observed in all the different KO mutants generated for this chapter (see line KO #1-4, Fig. 5.8), and in all different stages of fruit development and ripening. This effect could be due to defects in the cuticle formation given the role of SlMIXTA-like in controlling cutin synthesis and deposition (Lashbrooke et al., 2015), although after examining the tomato surface of the KO line under the SEM, I observed protrusions in the epidermis (Fig. 20C and D), which were not present on the surface of the MoneyMaker fruits. Some of these protrusions had trichome on top might also impact the texture of the fruit. The cause of the formation of these multicellular outgrowths is unclear at this stage, and it is unclear whether those are caused directly by the absence of SlMIXTA-like activity or whether they are a mechanical consequence of the altered fruit surface. Further research on this aspect of the function of *SlMIXTA-like* will help understand the mechanics of epidermal development.

5.5.2.-*SlMIXTA-like* is a negative regulator of trichome initiation.

SlMIXTA-like is an R2R3 MYB transcription factor in tomato, which belongs to the MIXTA-like family (Fig. 5.1).

When *SlMIXTA-like* was overexpressed in tomato, I observed a reduction in trichome density of about three-fold in the three independent lines that were analysed (Fig. 5.4A). Moreover, in the knock-out line, trichome density was increased compared to the control MoneyMaker plants (Fig. 11A). Therefore, SlMIXTA-like must function as a negative regulator of trichome initiation in tomato leaves. This function contrasts with the previously described function for different MIXTA and MIXTA-like proteins. In tomato, SlMX1 (belonging to a separate phylogenetic clade, Fig. 5.1) is a positive regulator of trichome density (Ewas et al., 2016) and SlMIXTA-like (ortholog of the AmMIXTA-like 2 and PhMYB1 proteins) has been reported to positively regulate conical cell development in fruit (Lashbrooke et al., 2015) and petals (Fig. 5.19). In other species, most *MIXTA-like* genes have been characterised as positive regulators of conical cell formation or trichome formation (Brockington et al., 2013). For example, *MYB1* in *Petunia hybrida*, *MIXTA-like 2* in *A. majus* or *MYB16* in *A. thaliana* are close homologs that positively regulate conical cell

development in their respective species (Baumann et al., 2007). Indeed, *PhMYB1* is the likely orthologue of *SlMIXTA-like* in tomato (Fig. 5.1). Moreover, MYB16 regulates branching of trichomes and wax deposition on vegetative tissues in *A. thaliana* (Oshima et al., 2013) pointing to a dual function in vegetative and reproductive organs.

In terms of trichome regulation, most described MIXTA-like proteins are also positive regulators. This is the case of *Populus* MYB186 (Plett et al., 2010), MIXTA1 in *Artemisia annua* (Pu et al., 2018), MYB25 in cotton (Machado et al., 2009) and MYBML3 in *Medicago truncatula* (Gilding and Marks, 2010). However, some genes in this family are also negative regulators of trichome development. In *Mimulus guttatus,* the expression of MYBML8 correlated negatively with trichome density. In *A. thaliana,* MYB106 acts as both a positive and negative regulator of trichome development, affecting branching of trichomes (Gilding and Marks, 2010). Recently, a MIXTA-like protein in cucumber (*Cucumis sativus*), CsMYB6, was described as a negative regulator of trichome development on the fruit surface (Yang et al., 2018), acting in a very similar way to our observations for *SlMIXTA-like* in tomato. This evidences the pleiotropic effects of MIXTA/MIXTA-like proteins in plants, and supports the role of SlMIXTA-like as a negative regulator of trichome initiation. Moreover, our initial observations of *SpMIXTA-like* OE lines suggest that its function is conserved with that of *SlMIXTA-like* (Fig. 5.15). It is important to note that the overexpression lines were not completely glabrous (Fig. 5.3 and 4A) and the knock-out was not extremely pubescent, showing an increase of about 2-fold compared to the control leaves (Fig 5.11A). This suggests that the function of this gene on its own is not sufficient to inhibit completely trichome formation, and it is probably part of a much more complex network that involves other known regulators of trichome development in tomato, as SlMX1 (Ewas et al., 2016b) or Woolly (Yang et al., 2011a).

SlMIXTA-like also plays an important role in epidermal patterning and spatial distribution of trichomes. SlMIXTA-like was identified in the screen of the IL population I carried out due to the presence of clusters of two or three misoriented trichomes in ILs 2-5 and 2-6 (see *chapter 3*). The downregulated expression of SlMIXTA-like in leaves of the ILs (Chitwood et al., 2013), especially in IL 2-6 (Fig. 5.23B), suggested a potential involvement of this gene in the trichome phenotype observed. Moreover, an amino acid change in the DNA-domain was observed between SlMIXTA-like and SpMIXTA-like (Fig. 5.13). This proline to serine substitution could explain a different activity of both proteins, as this residue is conserved in the *Antirrhinum* MIXTA proteins (Perez-Rodriguez et al., 2005). The analysis of the *SpMIXTA-like*-OE plants will help understand the significance of the differences in amino acid sequences between both species. Its role in preventing trichome clustering was confirmed by transient silencing in tomato, which gave rise to clustered trichomes (see *chapter 4*). I analysed the surface of

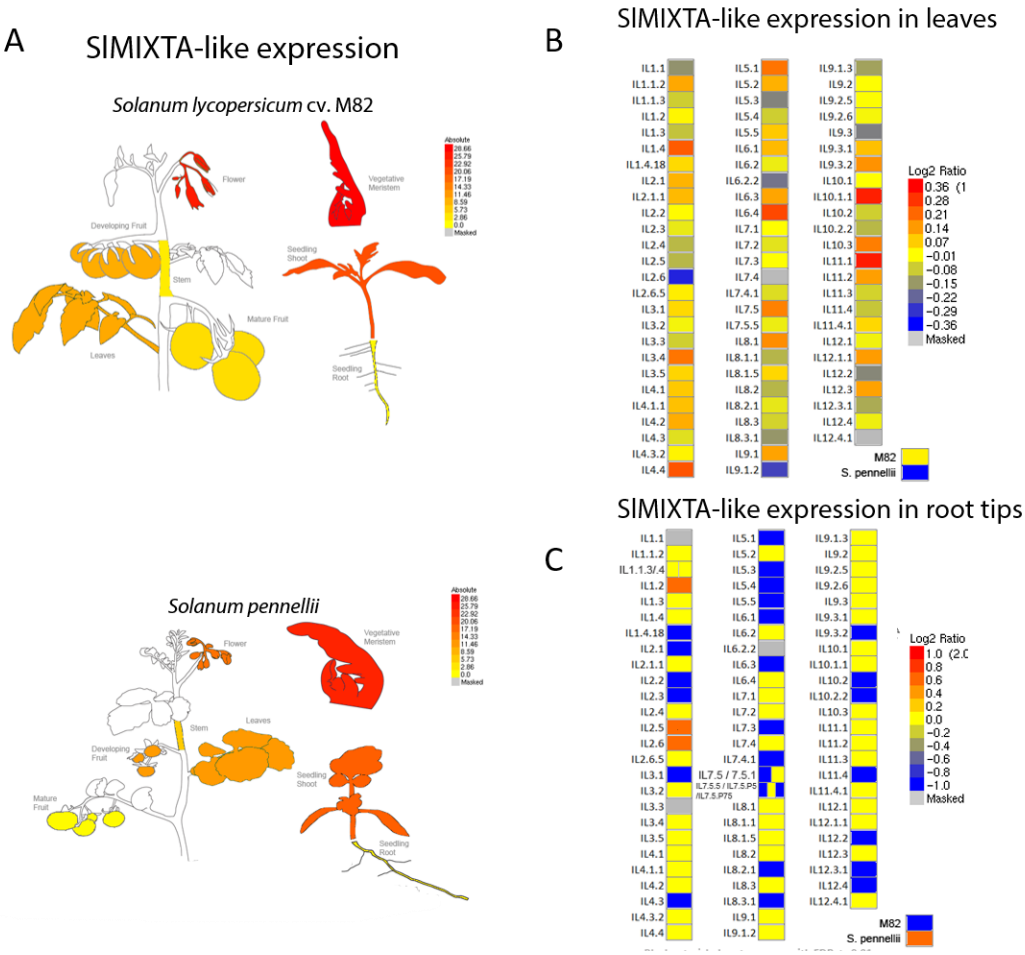

Figure 5.23.-Expression level of SlMIXTA-like in different tissues and *S. pennellii* ILs. A) Absolute expression level of SlMIXTA-like in *S. lycopersicum* cv. M82 and *S. pennellii* based on RNAseq data generated by (Koenig et al., 2013). B) Relative expression level of SlMIXTA-like in leaves of the *S. pennellii* ILs, from the RNAseq data generated by (Chitwood et al., 2013). C) Relative expression level of SlMIXTA-like in root tips of the *S. pennellii* ILs, from the RNAseq data generated by (Ron et al., 2013). The images were generated using the eFP expression browser (Winter et al., 2007).

SlMIXTA-like OE and KO lines and scored for the absence or presence of trichome clusters. OE lines did not have any clusters. KO lines had trichome clusters that affected all trichome types (Fig. 5.9). Although these groups of trichomes were found all over the leaf surface, they were more frequently found on the marginal ends of the leaf. This is in agreement with the spatial pattern of expression of *SlMIXTA-like*, as I observed stronger GUS activity in the leaf margins of plants transformed with a proMIXTA-like:GFP:GUS construct (Fig. 5.16E and H). I also observed aberrant outgrowths in basal cells of type I trichomes in KO lines (Fig. 5.9F). This could be explained by a lack of repression of further outgrowths by MIXTA-like, especially in a set of cells where intense GUS staining was observed (Fig. 5.16F). A mechanism for determination of epidermal patterning involving a MIXTA-related protein is substantially different from the regulation of trichome patterning in *A. thaliana*, where the small R3 MYBs Trypricon (TRY) and Caprice (CPC) prevent trichome initiation in cells adjacent to a newly initiated trichome (Wada et al., 1997, Schnittger et al., 1999, Ishida et al., 2008). Remarkably, although trichome clusters were commonly found in leaves of SlMIXTA-like KO lines, they were found alongside individual trichomes (Fig. 5.9B). This indicates a possible involvement of other regulatory genes in the determination of trichome clustering, similar to the case of trichome clustering mutants in *Arabidopsis*, where *try cpc* double mutants have a much higher clustering frequency than the single mutants (Schellmann et al., 2002). The presence of four more *MIXTA* genes in tomato (*SlMX1*, *SlMX2* and *SlMX3A/B*) suggests that they might act redundantly. However, these four genes are evolutionary distant from *SlMIXTA-like* and clustered together in a different clade (Fig. 5.1), which could indicate functional divergence. Moreover, SlMX1 was reported as a positive regulator of trichome initiation (Ewas et al., 2016) and silencing of *SlMX2* led to a reduction of trichome density (see *chapter 4*), indicating that they fulfil different functions in the leaf epidermis. The function of SlMX3A/B has not been studied to this date.

I tried to determine if the effect of *SlMIXTA-like* overexpression or knock-out was specific for some trichome types (Fig. 5.5, 5.9 and 5.12). My observations for SlMIXTA-like OE lines suggested that type I trichome density was unaffected, while type V and VI density was specifically reduced (Fig. 5.5A). However, when the percentage of each type was compared between OE and control lines, I could not observe significant differences (Fig. 5.5B). The observed densities in type V and VI trichomes were probably the result of the lower numbers of trichomes in OE lines and the high frequency of broken trichomes may have masked the effect of *SlMIXTA-like* on type V and type VI trichomes. In the *SlMIXTA-like* KO mutant, I observed that cluster formation was type-independent (Fig. 5.9B, C and D), suggesting that patterning and spatial distribution of trichomes are determined before type specification takes place, as it has been suggested in studies of type VI trichome development in tomato species (Bergau et al.,

2015). However, analysing the effect of the mutation on trichome density, I observed that the increase in the *SlMIXTA-like* KO line was predominantly in type I trichomes, and that the differences persisted even when values were expressed as a percentage of total trichomes (Fig. 5.12). The greater number of trichomes in these lines supports the significance of the differences observed. However, if trichome initiation is likely to take place before the final trichome type identity has been determined (Bergau et al., 2015) and SlMIXTA-like controls trichome initiation, this difference could be the result of an independent mechanism of trichome type determination. Type I trichomes are the most common type of trichome on the adaxial surface of the first true leaf (see *chapter* 3) and it is predictable that an increase in trichome initiation would lead to an increase in type I trichome density, even if the regulator does not play a direct role in trichome type determination. This view is supported by the lack of expression of *SlMIXTA-like* in type I glandular trichomes (Fig. 5.16F), indicating it does not determine specific features of this type of trichome. In light of my results, the function of SlMIXTA-like in controlling trichome initiation is most likely trichome-type independent.

5.5.3.-SlMIXTA-like plays a role in stomatal patterning in tomato leaves.

I also observed some stomatal clusters in *SlMIXTA-like* KO lines (Fig. 5.10). Stomatal clusters occur when asymmetrical division of the stomatal cell-lineage is impaired (Dow et al., 2014), and many genes involved in stomatal development have been characterised in *A. thaliana* (Fig. 5.24). For example, TOO MANY MOUTHS (TMM) is a leucine-rich repeat receptor-like protein which, when mutated, leads to the development of stomatal clusters (Yang and Sack, 1995, Shpak et al., 2005) similar to those observed in *SlMIXTA-like* KO lines. The ERECTA family consists of transmembrane receptors which determine the fate of protodermal cells, and mutants of these genes also lead to clustering of trichomes (Lee et al., 2012). Other signalling proteins, as the serine protease STOMATAL DENSITY AND DISTRIBUTION (SDD1) (von Groll et al., 2002) also trigger the differentiation of stomatal meristemoids, and *sdd1* mutants show stomatal clusters and increase stomatal density. Finally, BREAKING OF ASYMMETRY IN THE STOMATAL LINEAGE (BASL) is a polarity molecule essential for correct asymmetric division, and in *basl* mutants stomatal clusters are commonplace (Dong et al., 2009). In tomato, stomatal development has not been studied in any depth at the molecular level, but there is some evidence that similar regulators to those in *Arabidopsis* might be involved. Overexpression of a truncated version of *AtERECTA* in tomato affected stomatal density in tomato (Villagarcia et al., 2012) and overexpression of the *Solanum chilense SDD1-like* gene caused a reduction in stomatal density in both *Arabidopsis* and tomato (Morales-Navarro et al., 2018), suggesting that stomatal development and patterning are similarly regulated in both species. Therefore, my results indicate that SlMIXTA-like either controls directly these or other similar genes or that the role of

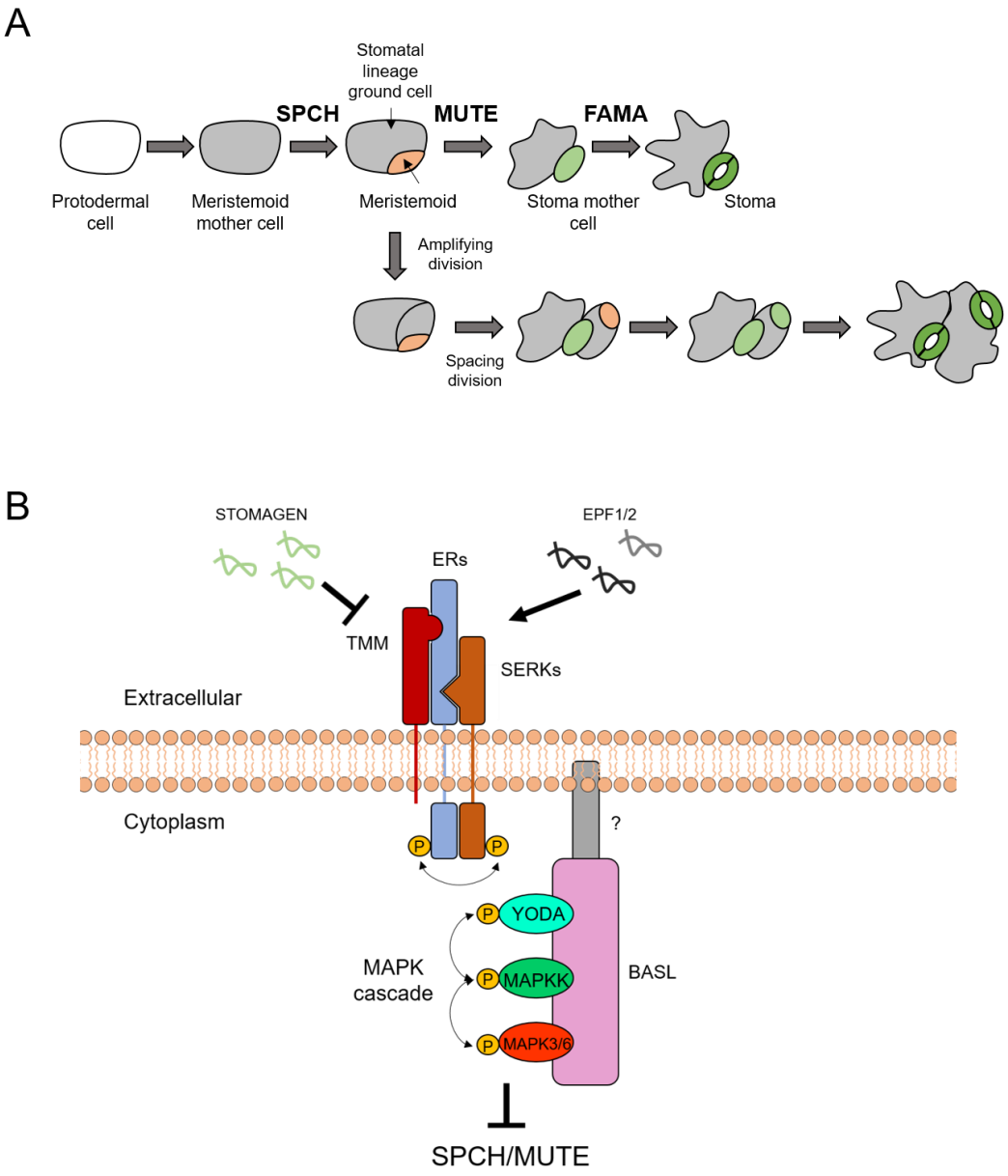

Figure 5.24.-Stomatal development in *Arabidopsis thaliana.* A) Schematic representation of the divisions of the stomatal cell lineage to generate mature stomata. The bHLH transcription factor regulating each transition are indicated in the diagram (SPCH, MUTE and FAMA). B) Schematic representation of the proteins involved in the Epidermal patterning factor signalling pathway. The MAPK cascade, activated by the ER/TMM/SERK complex, ultimately inactivates the bHLH transcription factor SPCH, and possibly MUTE. This figure appeared in *chapter 1* as Fig. 1.5. Further information of each gene can be found in *chapter 1*.

SlMIXTA-like in trichome development indirectly affects stomatal development by means of independent regulatory mechanisms. In *A. thaliana, try* and *gl1* mutants show effects on stomatal patterning, and the genes mutated in these lines are known regulators of trichome formation (Bean et al., 2002). This suggests that a dual role of regulators in trichome and stomatal development is not uncommon. Determining the targets of SlMIXTA-like will be extremely useful to characterise its function in more detail.

5.5.4.-SlMIXTA-like is essential for maintenance of the negative association between trichome and stomatal development.

In *SlMIXTA-like* OE lines, the decrease in trichome density (Fig. 5.4A) was accompanied by an increase in stomatal density (Fig. 5.4B). In fact, this change caused a significant decrease in the trichome-to-stomata ratio (Fig. 5.4C), which has been suggested to be an important physiological parameter in tomato (see *chapter 7*). A significant negative correlation between trichome density and stomatal density was observed when all data points were considered together (Fig. 5.4D). This kind of relationship has been observed before in tobacco and tomato (Glover et al., 1998, Glover, 2000) although this relationship may be limited to certain varieties and species (see *chapter 3*) or may be heavily dependent on environmental conditions, such as water availability (Galdon-Armero et al., 2018). In the *SlMIXTA-like* KO mutant, the increase in trichome density was accompanied by an increase in stomatal density (Fig. 5.11A and B), contrary to expectations from the OE data. Moreover, the trichome-to-stomata ratio was unaffected (as the density of both structures grew in similar ways) (Fig. 5.11C). More importantly, the correlation between trichome and stomatal densities was not observed for the *SlMIXTA-like* KO line (Fig. 5.11D), while it was for the MoneyMaker controls. The observations made of *SlMIXTA-like* OE and KO lines suggest that *SlMIXTA-like* plays a pivotal role in development of stomata as well as trichomes and pavement cells, and it plays an essential role in the mechanism controlling the negative association between trichome and stomatal densities. *SlMIXTA-like* is therefore central for the dynamics of cell specialisation in the leaf epidermis and physiological leaf functions, especially under stress, are likely dependent on the correct functioning and modulation of this regulatory gene.

It is also possible that *SlMIXTA-like* is involved in stress responses. Drought stress, for instance, can lead to changes in trichome and stomatal density (Fu et al., 2013) and in tomato drought tends to lead to increases in trichome density and decreases in stomatal density (see *chapter 7*) as also observed in *SlMIXTA-like* OE lines (Fig. 5.4). Stress perception and response are very complicated processes that involve stress sensing, signal transduction and cell and tissue reprogramming to respond to the initial stimulus (Zhu, 2016). Many MYB transcription factors in different species have been identified as regulators of different stress responses (Li et al.,

2015), and SlMIXTA-like may fulfil similar functions in tomato. SlMIXTA-like is a known regulator of cutin biosynthesis for the cuticular epidermal layer (Lashbrooke et al., 2015), and its *Arabidopsis thaliana* homolog also regulates cuticle deposition (Oshima et al., 2013). The cuticle is the main barrier for the plant to prevent water loss (Xue et al., 2017) and protect it from pathogens and UV damage (Krauss et al., 1997, Bargel et al., 2006, Leveau Johan, 2006). In addition to this, cuticle content changes upon stress, such as UV exposure (Steinmuller and Tevini, 1985) and water scarcity (Seo et al., 2011, Lee and Suh, 2015) and these changes may be mediated by MYB transcription factors (Cominelli et al., 2008, Seo et al., 2011). Another process associated with the stress responses and regulated by MYB genes is expansin-mediated cell wall expansion (Schmidt et al., 2013), which is essential for trichome development. Therefore, SlMIXTA-like might act in stress responses, and it may function in changing the trichome-to-stomata ratio under stress conditions. The *SlMIXTA-like* KO mutation could lead to a stress insensitive phenotype, unable to adapt to environmental cues by changing trichome and stomatal densities. However, the analysis of the *SlMIXTA-like* native promoter activity indicates that this gene plays a function in most tissues independently of the environment (Fig. 5.16) and *SlMIXTA-like* expression is recorded in all tissues in the absence of stress (Fig. 5.24). Studies of response to stresses such as drought, pathogen attack or herbivory using the *SlMIXTA-like* OE and KO lines could provide more evidence to understand the function of this gene. Moreover, transcriptomic analysis of the KO and OE lines could be useful to understand its potential involvement in stress responses.

5.5.5.-The spatial expression pattern of *SlMIXTA-like* provides insights into its function.

The results presented in this chapter focus on the role of SlMIXTA-like in trichome development, and its relationship to determination of other epidermal cell types. However, the observed expression pattern of *SlMIXTA-like* in different tissues (Fig. 5.16) drew my attention to other functions of this transcription factor.

I observed intense activity of the *SlMIXTA-like* promoter in hairy roots, especially in the pericycle tissue (Fig. 5.16A) and in meristems of lateral roots (Fig. 5.16B). The expression of *SlMIXTA-like* in root tips of the *S. pennellii* ILs showed a high level of expression in *S. pennellii* compared to *S. lycopersicum*, and this high level of expression was observed in the ILs 2-5 and 2-6, which had the aberrant trichome patterning phenotype (Fig. 5.24). This contrasts with the expression in leaves, which shows the opposite trend. Therefore, SlMIXTA-like seems to have an active function in growing root tips. Lateral root primordia are formed through division of cells in pericycle tissue (Péret et al., 2009), and the continuity of expression in both tissues suggested a potential role of SlMIXTA-like in controlling root architecture through orchestration of pericycle division and primordia initiation. GUS staining of roots of mature plantlets expressing the

reporter construct showed expression in lateral root primordia and the meristematic and distal elongation zones of the lateral roots (Fig. 5.17). Analysis of root architecture in the *SlMIXTA-like* KO showed a reduced number of lateral roots (Fig. 5.21), suggesting a role of this gene in formation of lateral roots. Some transcription factors have been identified as regulators of lateral root development, such as the PLETHORA family (Du and Scheres, 2017), the LBD complexes (Kim et al., 2017) and MYB genes. This is the case for MYB77 in *A. thaliana*, which regulates lateral root development through the modulation of expression of auxin response genes (Shin et al., 2007). The expression profile of MYB77 is similar to that of the GUS staining for proMIXTA-like, indicating that it might be modulating similar auxin-related genes, which might relate to auxin involvement in the development of conical cells (Varaud et al., 2011) and trichomes (Deng et al., 2012, Zhang et al., 2015). MYB93, in contrast, is a negative regulator of lateral root development (Gibbs et al., 2014), but its expression pattern is very specific and distinct from the expression of *SlMIXTA-like*, indicating that these genes are unlikely to be involved in the same pathways. Expression analysis of another known trichome regulator, Woolly, showed high promoter activity in lateral root primordia (Yang et al., 2011a), indicating a potential role for these genes in this process. Analysis of roots in the *SlMIXTA-like* KO line suggests an important function of SlMIXTA-like in root development, particularly in lateral root primordia formation. This would be the first report of a function for *MIXTA/MIXTA-like* genes in root development. It is interesting to note that in *SlMIXTA-like*-RNAi lines, the expression of the *Lonesome Highway* (*SlLHW*) gene was reduced (Lashbrooke et al., 2015). In *A. thaliana, lhw* mutants show defects in the development of vascular tissue in roots as well as the number of stele cells (Ohashi-Ito and Bergmann, 2007). Interestingly, this mutant produces lateral roots only on one side of the primary root. The role of SlMIXTA-like in root development of tomato requires considerable further research.

Some GUS staining was observed on the root epidermis in hairy roots (Fig. 5.16A and B), but root hairs did not seem to express *proMIXTA-like*-driven GUS. In roots from stably transformed plants, there was no clear expression in root epidermal cells, and the staining was restricted to the lateral root primordia and meristematic and distal elongation zones of the root (Fig. 5.17). I did not observe any differences in root hair density between MoneyMaker roots and *SlMIXTA-like* KO roots (Fig. 5.23). These findings suggest that SlMIXTA-like is not involved in the development of root hairs, even though these are often considered as epidermal outgrowths comparable to trichomes. In *Arabidopsis,* the molecular mechanisms governing trichome and root hair formation are very similar and involve the same players, including TTG1, GL2, GL3, TRY and CPC, although the functionally equivalent MYB factors GL1 and WER regulate trichome initiation and root hair formation respectively (Ishida et al., 2008). However, whether this is the

case in tomato and other related species is still unclear. SlTRY has been reported to participate in regulation of both trichomes and root hairs (Tominaga-Wada et al., 2013), but evidence about this is limited to complementation assays in *Arabidopsis,* which are not very informative in the context of tomato development. For most known trichome mutants in tomato, the mutations either do not affect root hairs (Kang et al., 2010a) or their effect on root hairs has not been reported (Kang et al., 2010b, Nadakuduti et al., 2012, Chang et al., 2016), probably indicating there were no clear phenotypes. These observations seem to point towards a distinct regulation of both trichome and root hair development in tomato, and a probable lack of a role for SlMIXTA-like in the formation of root hairs.

Further conclusions about the function of SlMIXTA-like could be drawn based on the expression data. The lack of *SlMIXTA-like* promoter activity in trichomes (except for basal cells) (Fig. 5.16F) suggested that the loss of expression of MIXTA-like is required for their development. This would explain why aberrant trichomes (similar to those observed in the dialytic mutant (Chang et al., 2016)) were observed in OE lines (Fig. 5.6). It is interesting to note that transient expression of the proMIXTA-like reporter construct in *N. benthamiana* resulted in the same observation, with high promoter activity in the epidermis and basal cells, but a lack of expression on the trichomes themselves (Fig. 5.18). This suggests a similar function for MIXTA-like in *Nicotiana* (and probably other *Asterids*) to the role of SlMIXTA-like in tomato. A comparison of the promoter of *SlMIXTA-like* with those regions of *MIXTA-like* genes in *N. benthamiana* (Fig. 5.25) revealed a very conserved promoter region upstream of NbMIXTA-like 8 (the closest homolog to SlMIXTA-like in this species), to which MYC2 can bind *in silico* (Chen et al., 2012) and *in vivo* (Du et al., 2017). MYC2 is a bHLH transcription factor that functions as a regulator of the jasmonate-mediated immunity in tomato and *Arabidopsis* (Dombrecht et al., 2007) in response to pathogens and wounding (Du et al., 2017). In *Arabidopsis,* MYC2 is known to regulate stomatal development (Han et al., 2018) and lateral root growth (Gangappa et al., 2010) in response to jasmonate. This reinforces the idea of an *Asterid*-wide role for SlMIXTA-like in response to stress and raises new questions about its regulation by upstream factors such as SlMYC2 in determination of trichome and stomatal density. I observed that GUS staining, although present over the whole leaf surface, was most intense in marginal areas of leaves and cotyledons (Fig. 5.16E and H). This suggested that the function of SlMIXTA-like might be more important in marginal areas of the leaf. A differential regulation of the development of marginal and lamina trichomes has been reported in *Arabidopsis,* where TRANSPARENT TESTA 8 (TT8), a bHLH interacting with GLABRA1, is responsible for the development of marginal trichomes, while GLABRA3 is responsible for the development of lamina trichomes (Baudry et al., 2006, Maes et al., 2008). The existence of

Figure 5.25.-Comparison of the DNA sequences of the *NbMIXTA-like 8* and *SlMIXTA-like* gene promoters. A fragment of 1000 bp upstream of the start codon of the gene was used for alignment. The only detected conserved region is found between the positions 750-820. A MYC2 binding motif was found in this region using the AtPAN software (Chen et al., 2012).

similar developmental specialisations in tomato cannot be ruled out, and SlMIXTA-like may play a role in this.

5.6.-Conclusion

In this chapter, I offer a detailed functional characterisation of SlMIXTA-like using overexpression lines and CRISPR/Cas9-mediated knock-out mutants, as well as promoter activity analysis using GUS as a reporter gene. The results described in this chapter show that SlMIXTA-like is a negative regulator of trichome initiation on leaves and plays a key role in trichome patterning on tomato leaves. My data also indicate that SlMIXTA-like is necessary for conical cell elongation in petal epidermis and fruit epidermis, and suggest that SlMIXTA-like also plays a role in development of lateral roots.

In silico promoter analysis and the effect of the SlMIXTA-like KO mutation on the ratio of trichome to stomata in leaves suggest a possible involvement of SlMIXTA-like in responses to stresses, raising new biological questions regarding the function of *MIXTA/MIXTA-like* genes in plants.

In conclusion, the work described in this chapter, complemented with the silencing assays described in *chapter 4*, provides new information about the function of SlMIXTA-like in tomato, and opens new research lines.

Acknowledgement to contributors

This chapter benefitted from the contribution of the visiting student Micaela Navarro Correa from Centro Nacional de Biotecnología in Madrid, Spain, who worked under my supervision four months in 2018. She helped in the assessment of root phenotypes.

Chapter 6 – Analysis of CRISPR/Cas9 tomato mutants affecting regulators of trichome development

6.1.-Abstract

In this chapter I describe the generation of a collection of mutants by CRISPR/Cas9 of known genes involved in trichome formation in the same genetic background, the cultivar MoneyMaker. I selected ten target genes from the literature affecting trichome development at different levels (structural, regulatory and hormone-related genes) and I managed to generate mutant for five of these genes (*Woolly, CD2, SlMX1, Hairless* and *DWARF*). I revisited the phenotypes observed in these lines and added new observations to the current model for trichome development in tomato.

6.2.-Introduction.

6.2.1.-Trichome development in tomato: key players at different levels.

Trichomes in tomato are multicellular and have different morphologies and metabolic activities (Simmons and Gurr, 2005). Their development is a complex process that involves many different players working at different levels including regulation of trichome initiation, cell expansion and division, identity determination and the integration of trichome formation and function in complex signalling networks in response to environmental and developmental stimuli.

Initiation is the first step in trichome development, in which a protodermal cell is selected to undergo differentiation into a trichome (Hülskamp, 2004). This involves modulations in the transcriptome of the cell that lead to the next steps of trichome development, with cell expansion in the plane perpendicular to the epidermal surface and subsequent cell division, in the case of multicellular trichomes. The processes of trichome initiation and development need to occur in harmony with the development of other cell types in the aerial epidermis to ensure the adequate patterning of stomata, pavement cells and trichomes (Glover, 2000). It is not clear at which stage different trichome types are determined, but anatomical studies of the ultrastructure of type VI trichomes indicate that, in the initial steps of cell initiation, all trichome types are indistinguishable in tomato (Bergau et al., 2015). The similar structures of type IV -glandular- and type V -non-glandular- trichomes (and probably type I and type II, which are bigger versions of these, respectively) suggests that their identities are determined after several cell division cycles and that these trichome types likely share a common ontogenesis (Vendemiatti et al., 2017), while type VI and VII are recognisable after the first asymmetrical division (Bergau et al., 2015). Finally, all the steps of trichome development are influenced by external and internal stimuli, including biotic and abiotic stresses and plant age and organ, which normally elicit responses integrated through hormonal signalling cascades. For example, jasmonate, cytokinins, gibberellins and brassinosteroids increase trichome density in tomato, affecting different trichome types in different ways (Campos et al., 2009, Maes and Goossens, 2010).

In tomato, genes involved in most of the stages of trichome development have been identified and characterised to different extents. For example, *SlMX1*, a MIXTA transcription factor, and *Woolly,* a class IV HD-ZIP transcription factor, are considered to be regulators of trichome initiation which therefore control the determination of trichome density in aerial tissues (Yang et al., 2011a, Ewas et al., 2016, Ewas et al., 2017). *SlTRY*, the homolog of *TRYPTICON* in *Arabidopsis,* which controls trichome and root hair patterning, is functionally equivalent to *AtTRY* when expressed in Arabidopsis (Tominaga-Wada et al., 2013). In the work described in this thesis, I have characterised two members of the MIXTA-like MYB transcription factor family as regulators of trichome initiation in leaves (*SlMIXTA-like* and *SlMX2*, see *chapter 4 and 5*), although they have distinct functions and SlMIXTA-like also controls conical cell formation in tomato.

These regulatory genes therefore control the expression of structural genes involved in cell expansion, which probably include unidentified expansins and cell-wall related enzymes (Marowa et al., 2016), as well as regulators of cytoskeleton dynamics, as it is the case of the gene responsible for the *hairless* mutation (Kang et al., 2010a). *Hairless* encodes a member of the WAVE complex, SRA1, which establishes branching points in the actin filaments and is essential for maintaining the erect structure of trichomes (Kang et al., 2016). An aquaporin-like gene has been identified as the locus affected in the *dialytic* mutant, which has aberrant forked trichomes (Chang et al., 2016), and this aquaporin-like protein is probably involved in cell expansion. Trichome development also involves cell division in tomato, and this seems to be regulated by a cyclin, SlCycB2 (Yang et al., 2011a, Gao et al., 2017).

Regulation of trichome type determination is unclear. For example, *Woolly*, *SlMX1* and *HAIR* (encoding a C2H2 zinc finger transcription factor) have been reported to regulate mainly type I trichome density (Yang et al., 2011a, Ewas et al., 2017, Chang et al., 2018), and *CD2*, another HD-ZIP IV gene, showed a decrease in type VI trichomes when mutated (Nadakuduti et al., 2012). Finally, many genes involved in hormone signalling have been studied in relation to their impact on trichome development. This is the case of *SlIAA15*, a repressor of auxin-signalling genes, which affects total trichome density (Deng et al., 2012) or *Auxin Response Factor 3* (*SlARF3*) which can also regulate total trichome density (Zhang et al., 2015), indicating a major role for auxin in trichome development.

The complicated network which regulates trichome development in tomato is starting to be unravelled. The current understanding of regulation of trichome development is summarises in Fig. 6.1. Some regulators are involved in several of the stages (SlMX1 and Woolly control both trichome initiation and identity) and some others are probably restricted to specific organs or environmental conditions. A full characterisation of all these genes using mutants generated by

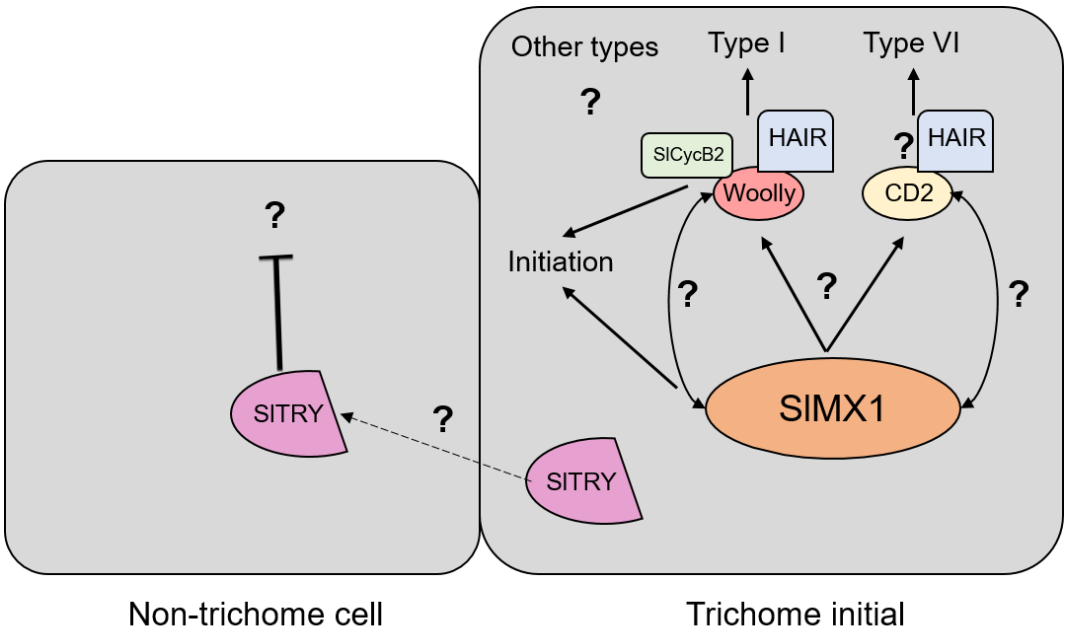

Figure 6.1.-Model for transcriptional regulation of trichome development in tomato. Initiation is activated by SlMX1 and the Woolly-HAIR-SlCycB2 complex. This complex can also regulate type I trichome morphogenesis. CD2 controls type VI trichome morphogenesis. SlTRY is a negative regulator of trichome initiation and might act as the R3 MYB genes in *Arabidopsis.* Positive interactions are indicated with an arrow line and negative interactions with a T-shaped line. Question marks indicate possible interactions that have not been proved experimentally. Fine-dashed arrow indicate cell-to-cell movement. This figure appeared in *chapter 1* as Figure 1.8.

genome editing in the same background will provide new insights into trichome development in tomato.

6.2.2.-CRISPR/Cas9 as a tool for genome editing.

The CRISPR/Cas9 system was developed in 2013 as a tool for genome editing and it has been used for editing in many eukaryotic species (Rath et al., 2015). The CRISPR (Clustered Regularly Interspaced Short Palindromic Repeats) locus was initially identified in bacteria (Ishino et al., 1987, Mojica et al., 2005) as a number of repeated sequences with spacing sequences with a high homology to exogenous DNA, mostly from viruses (Bolotin et al., 2005). This locus can be transcribed into a CRISPR RNA (crRNA) molecule, which is used by the CRISPR-associated proteins (Cas) to degrade target nucleic acids from the virus (Rath et al., 2015). The system is present in most Archaea and in a big proportion of bacteria (Grissa et al., 2007), which use it as a defence system.

For genome editing, synthetic small guide RNAs (sgRNAs) containing 20 nt of the target sequence to edit are generated, which can acquire the secondary structure required for recognition by the Cas9 protein, a specific Cas protein which produces a single doubled-stranded break in the target nucleotide sequence (Jinek et al., 2012). Mutations resulting from the activity of the Cas9 depend on the mechanisms of repair of the double-stranded breaks in DNA, and two pathways exist: nonhomologous end-joining (NHEJ), which binds the ends of the broken strands, generally creating small deletions, or homologous recombination (HR), which uses a homologous sequence as a template for DNA synthesis (Chapman et al., 2012). This latter mechanism can be exploited to introduce any exogenous DNA using homologous sequences, although the low frequency of this reparation system in plants limits its applicability (Liu et al., 2017). The ability to generate small deletions via NHEJ repair in the coding sequence of genes of interest can be used to obtain knock-out genome-edited (GE) mutants for genes of interest at high frequency in tomato. Due to its high specificity, CRISPR/Cas9 genome editing provides an excellent tool to generate targeted mutants. However, there is an accompanying risk of generating off-target mutations which can mask or confuse the phenotype of interest.

The CRISPR/Cas9 system has been used successfully to obtain edited plants in many species (Liu et al., 2017), including tomato. Some examples include editing of *SlIAA9* to produce parthenocarpic tomatoes (Ueta et al., 2017) and mutation of the *RIN* locus of tomato, which regulates ripening (Ito et al., 2015). In this chapter, I describe the generation of CRISPR/Cas9 edited mutants of genes known to be involved in trichome development in tomato in the same MoneyMaker genetic background. My aim was to get a collection of mutants which can be compared directly for their roles in trichome development and used for interaction assays by

generation of multiply mutant lines by crossing different mutants of interest. In this way, I was able to revisit the functional characterisation of these genes.

6.3.-Methods.

6.3.1.-Selection of target genes for edition.

Regulatory, structural and signalling genes known for their roles in trichome development in tomato were selected from the literature (Table 6.1). *DWARF* has not been described as having a direct effect on trichomes, but the end product of the reaction catalysed by the enzyme encoded by *DWARF*, brassinolide, is an active brassinosteroid, and brassinosteroids have been associated to modulation of trichome density (Campos et al., 2009). Genomic sequences for each gene were retrieved from the SolGenomics Network website (Fernandez-Pozo et al., 2015a) and gene models were built using Vector NTI (Thermo Fisher Scientific, USA).

6.3.2.-Generation of CRISPR/Cas9 GE plants.

For each gene selected for genome editing (Table 6.1), I selected two specific sgRNAs using the CRISPRdirect website (Naito et al., 2015) with NGG as the PAM sequence. The 20 nt-long guide sequences were incorporated in the pICSL002218A plasmid (TSLSynBio, Norwich, UK) using the Golden Gate digestion-ligation procedure described in *chapter 2*. Primers and plasmids generated are shown in appendices 1 and 2 respectively. The constructs were transformed in *Agrobacterium tumefaciens* strain AGL1 and transformed into tomato cv. MoneyMaker following the procedure described in *chapter 2*. T0 plants for each transformation were genotyped by PCR using the primers shown in appendix 1 and the Phire Kit (see *chapter 2*). PCR products were sequenced to determine the incidence of mutations in the target sequence. PCR products of heterozygous and biallelic lines were cloned into the TOPO Zero Blunt plasmid (Thermo Fisher Scientific, USA) and each allele was sequenced separately. Sequences were analysed using Geneious 9.0.5 (www.geneious.com) Homozygous T1 plants were used for analysis unless otherwise stated.

6.3.3.-Evaluation of epidermal phenotypes.

For quantitative analysis of *Woolly* and *SlMX1* edited lines, plants were grown alongside MoneyMaker controls for 4 weeks at an average temperature of 20-22 °C. The terminal leaflet of the first fully expanded leaf of three or four plants per line were excised and leaf sections of 0.5 x 0.5 cm were used for cryo-SEM imaging of their adaxial surface (see details in *chapter 2*). For trichome, stomata and pavement cell quantification, 8-15 micrographs of approximately 0.3 mm^2 were counted manually. For analysis of trichome types, 2.6 mm^2 of 3 young leaves per plant were assessed, with trichomes being scored according to the established classification (Simmons and Gurr, 2005). Trichome and stomatal density were expressed as percentage of total

Gene	ID	Reference
SlTIP4	Solyc08g066840	(Chang et al., 2016)
SlARF3	Solyc02g077560	(Zhang et al., 2015)
DWARF	Solyc02g089160	(Li et al., 2016b)
SlTRY	Solyc01g095640	(Tominaga-Wada et al., 2013)
CD2	Solyc01g091630	(Nadakuduti et al., 2012)
SlIAA15	Solyc03g120390	(Deng et al., 2012)
Hairless	Solyc11g013280	(Kang et al., 2016)
	Solyc11g013290	(Kang et al., 2016)
Woolly	Solyc02g080260	(Yang et al., 2011a)
SlMX1	Solyc01g010910	(Ewas et al., 2016)
SlMYB106	Solyc04g005600	See *chapter 4*
SlCycB2	Solyc10g083140	(Gao et al., 2017)
HAIR	Solyc10g078970	(Chang et al., 2018)

Table 6.1.-Genes described as structural or regulatory genes in trichome development. For each gene, the gene ID and source is indicated. These genes have been characterised to different extents and were selected as candidates for the generation of CRISPR/Cas9 genome-edited mutants.

epidermal cell number. Trichome-to-stomata ratio was calculated as the division of trichome density and stomatal density. For quantification of pavement cell size in the *DWARF* edited line, 60 cells per line were measured using Fiji (ImageJ distribution) (Schindelin et al., 2012).

6.3.4.-Evaluation of root phenotypes.

For each line under study, seeds were sterilised for 3 hours in 10% domestic bleach and plated in MS + 3% sucrose. Plates were grown vertically for 2 weeks and plantlets were harvested for analysis of root hairs and architecture. Root hairs were imaged using a Leica 205F stereomicroscope (Leica, Germany).

6.3.5.-Generation of phylogenetic tree.

A phylogenetic tree was built for members of the class IV HD-ZIP transcription factor family. The amino acid sequence of the 16 *Arabidopsis thaliana* genes, 15 *Solanum lycopersicum* genes, two *Artemisia annua* genes, one *Gossypium hirsutum* gene, one *Cucumis sativus* gene and one *Cucumis melo* gene were used for the analysis of evolutionary distance. Sequences were retrieved from The Arabidopsis Information Resource (TAIR, www.arabidopsis.org) for *A. thaliana*, the SolGenomics Network (SGN) (Fernandez-Pozo et al., 2015a) for *S. lycopersicum,* and from the National Center for Biotechnology Information (NCBI, USA) for the remaining species. Amino acid sequences were aligned using ClustalW and a phylogeny was built using the neighbour-joining approach, based on the evolutionary distance computed by the JTT matrix-based method. Bootstrap values were calculated based on 1000 bootstrap replicates.

6.3.6.-Statistical analysis.

Comparisons for trichome and stomatal density, trichome-to-stomata ratio and trichomes type count were performed using a t-test between the control MoneyMaker values and the edited line under study. Significant differences were considered when the p-value was <0.05. The analyses were performed using R software (ver. 3.2.2; R Core Team, Vienna, Austria).

6.3.7.-Transcriptomic data retrieval.

The tissue-specific expression profiles of specific genes in *S. lycopersicum* cv. M82 and the expression level in the leaves of *S. pennellii* ILs were retrieved for *Woolly, CD2, SlHDZIP-IV 7, SlMX1, SlMX3A* and *SlMX3B*. The tissue-specific transcriptome were obtained from (Koenig et al., 2013) and the RNAseq data for leaves were obtained from (Chitwood et al., 2013). The colour-coded display of gene expression used in this chapter was generated using the Tomato eFP Browser.

6.4.-Results

6.4.1.-Selection of genes with a known role in trichome development in tomato.

I selected a set of genes that had been previously described as structural or regulatory genes involved in trichome development in tomato (Table 6.1). For all of them, there is evidence to support their role, although the depth of the functional characterisation varies, ranging from limited functional knowledge (marker-assisted mapping and differential expression) to very detailed characterisation (overexpression and silencing, coupled with identification of interacting partners). I decided to generate genome-edited (GE) mutants for these genes using CRISPR/Cas9, to gain better insights into their functions. I managed to generate mutants for *Woolly, SlMX1, Hairless, DWARF* and *CD2* in the time available during my PhD.

6.4.2.-Analysis of Woolly genome-edited mutants.

Woolly is a Homeodomain leucine-zipper (HD-ZIP) IV transcription factor, containing a HD DNA-binding domain and a START domain. The *Woolly* coding sequence is relatively long, 2532 bp split between 11 exons (Fig. 6.2A). I chose 2 sgRNAs for genome editing which targeted sequences in the fourth exon, which encodes the DNA-binding domain of the transcription factor (Fig. 6.2A). I generated six mutant alleles, with variable deletion sizes (4 bp, 7 bp, 8 bp, 9 bp, 10 bp and 14 bp) (Fig. 6.2B). Interestingly, all deletions were caused by the activity of the second sgRNA, and no mutations around the expected target region of the first sgRNA were observed (Fig. 6.2B). I selected three independent lines homozygous for three mutated alleles (GE #2, #3 and #5, respectively) for further analysis. The product of the mutated alleles consisted of truncated proteins, as the deletions caused frameshifts in protein translation leading to early stop codons. In all the truncated versions, the DNA-binding domain was still present (Fig. 6.3). The peptide length ranged from 226 to 231 aa in the mutated proteins compared to the 752 aa long Woolly WT protein.

The GE plants harbouring deleterious alleles each had a *hairless*-like appearance, with an almost complete absence of long type I trichomes in stems or leaves (Fig. 6.4). On top of this effect on trichome length, the *Woolly* GE lines had fewer trichomes on leaves, with the first true leaf showing almost no trichomes compared to MoneyMaker WT plants (Fig. 6.5). I analysed quantitatively the epidermis of two GE lines (#2 and #3), and in both, trichome density was significantly lower than in MoneyMaker (Fig. 6.6A). Stomatal density showed no difference between *Woolly* GE lines and MoneyMaker (Fig. 6.6b). Finally, the trichome-to-stomata ratio was lower in the GE lines compared to MoneyMaker (Fig 6.6c). No correlation was observed between trichome and stomatal density for any of the lines.

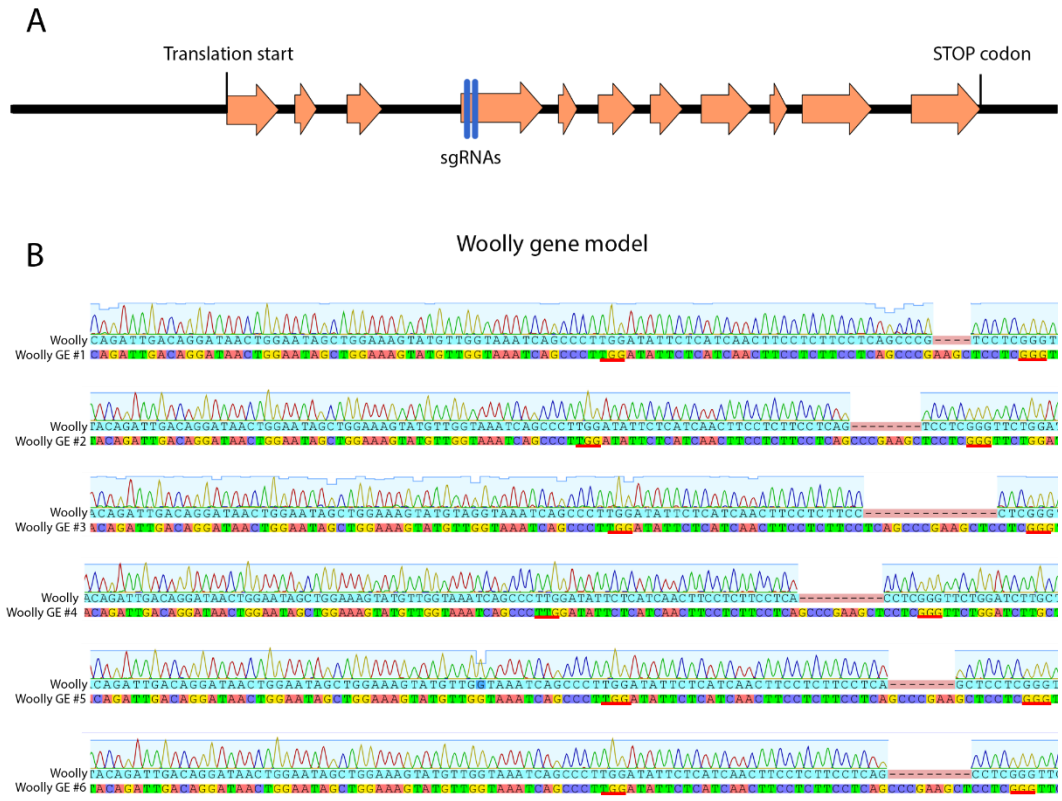

Figure 6.2.-Description of *Woolly* GE mutants generated by CRISPR/Cas9. A) Gene model of Woolly. The orange arrows represent the gene coding sequence split between 11 different exons. The blue vertical lines represent the sgRNAs chosen for gene editing, located in the fourth exon. The translation start and STOP codon are shown in the model. The black line represents non-coding sequences (promoter, UTRs and introns). B) Sequence of the genomic region edited in the GE mutants and the reference sequence from the non-mutated gene. The PAM sequences are underlined in red. Six different alleles were found in the mutated population.

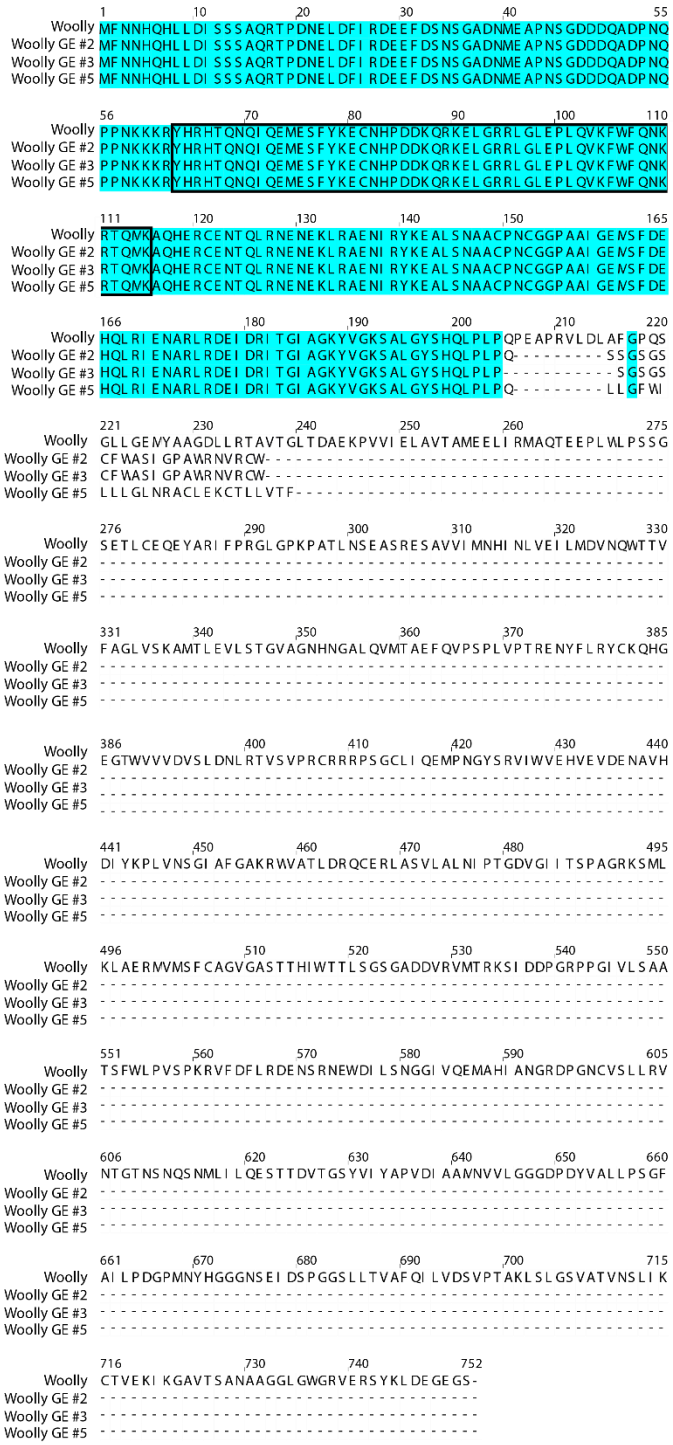

Figure 6.3.- Alignment of the peptide sequences of Woolly and three GE lines (#2, #3 and #5). The Woolly WT protein is 752 aa long, and the protein in the GE lines #2, #3 and #5 are 228, 226 and 231 aa long respectively. The homeobox DNA-binding domain is shown in the black box. The START domain is absent in the GE lines.

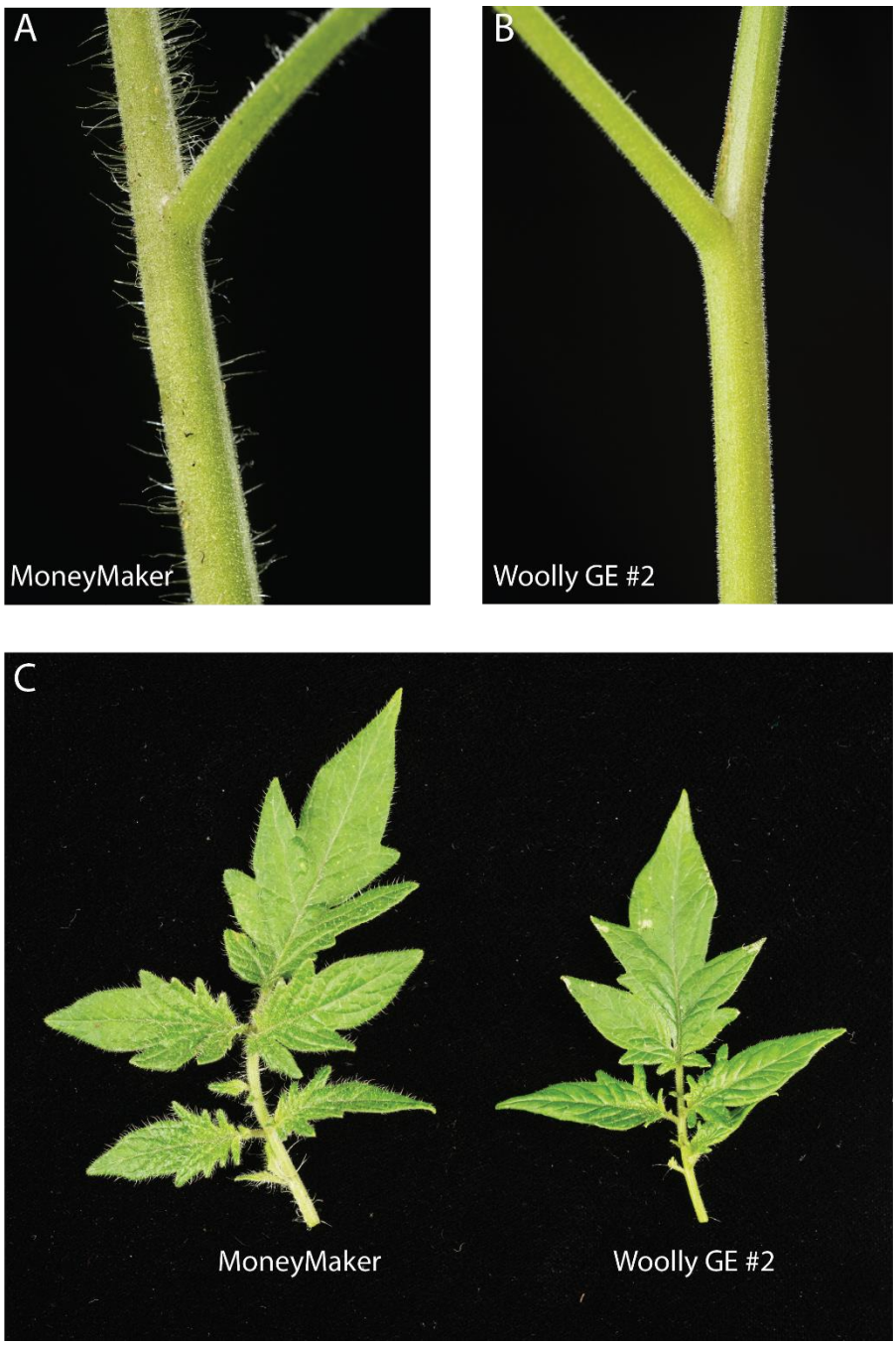

Figure 6.4.- Stem and leaves from *S. lycopersicum* cv. Moneymaker and *Woolly* genome-edited line #2. A) Close up view of a control MoneyMaker stem. B) Close up view of a *Woolly* GE #2 stem. C) Close up view from a control MoneyMaker leaf (left) and a *Woolly* GE #2 leaf (right). Long type I trichomes were almost completely absent in *Woolly* GE #2.

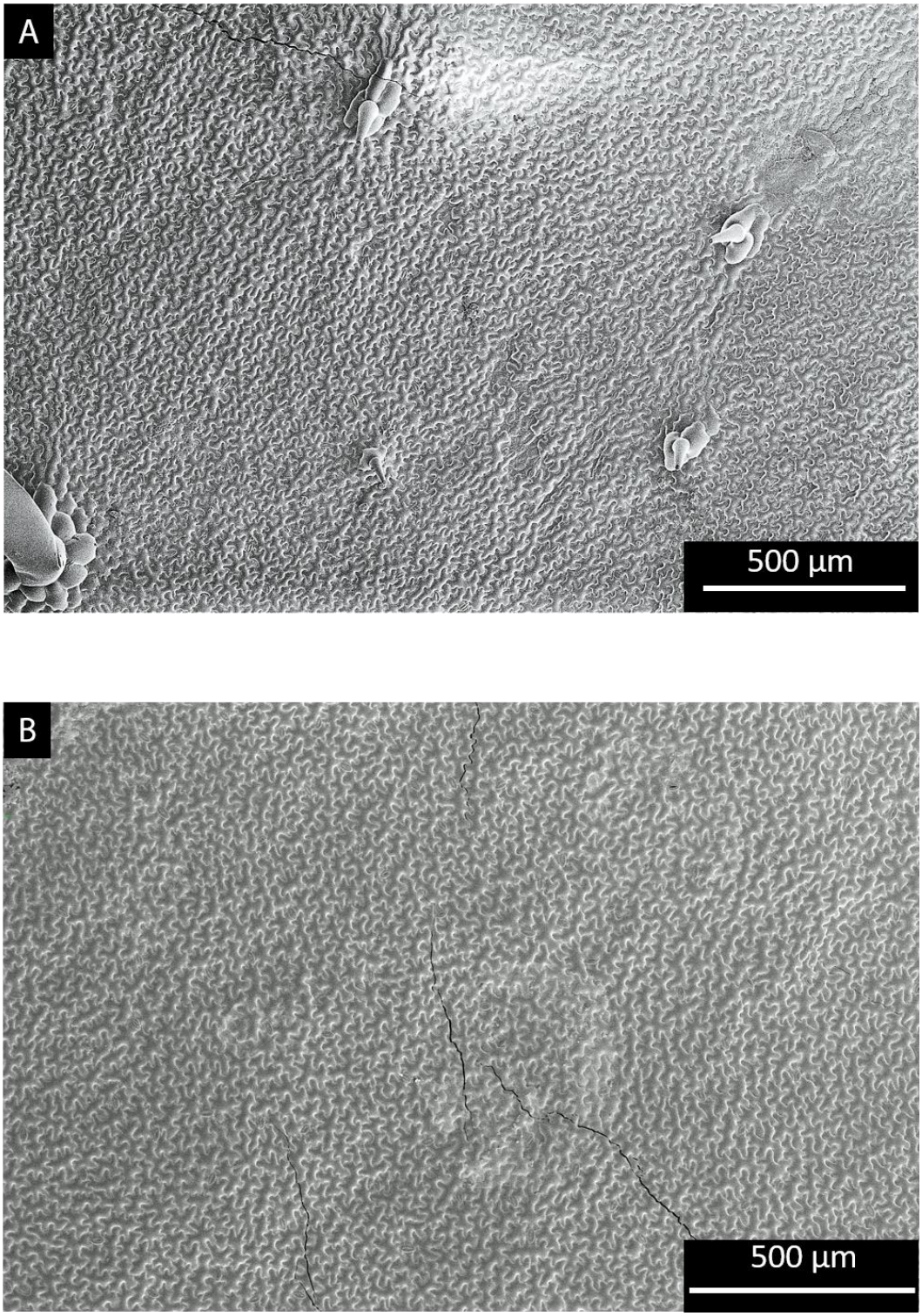

Figure 6.5.- Adaxial leaf surface of control *S. lycopersicum* cv. Moneymaker and *Woolly* genome-edited line #2. A) Micrograph of the surface of a control MoneyMaker leaf. B) Micrograph of the surface of *Woolly* GE #2 line. Trichome density was dramatically reduced in line GE #2. Scale bars are shown in each micrograph.

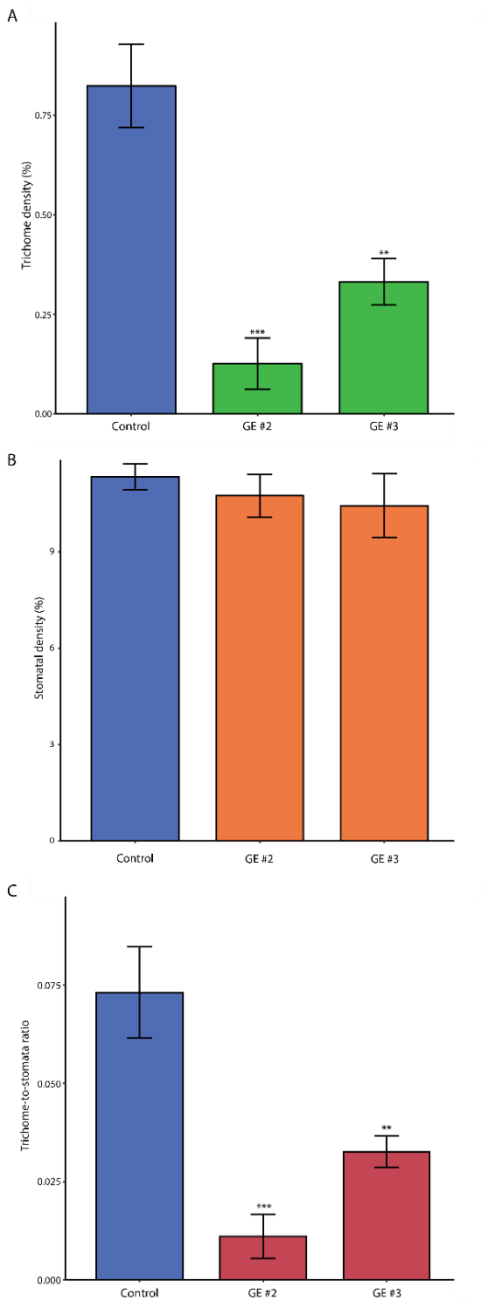

Figure 6.6.-Quantification of epidermal structures in *Woolly* GE leaves and control tomato leaves. A) Trichome density, expressed as percentage of total epidermal cells, in control leaves (blue bar) and leaves from two independent GE lines (green bars). B) Stomatal density, expressed as percentage of total epidermal cells, in control leaves (blue bar) and leaves from two independent GE lines (orange bars). C) Trichome-to-stomata ratio of control tomato leaves (blue bar) and two independent GE lines. Values are expressed as mean±SEM of n=3. Two starts indicate a p-value<0.05 and three stars indicate a p-value<0.01 according to a t-test between the corresponding GE line and the control value.

I also observed a dramatic reduction of root hair density and length in *Woolly* GE lines #2 and #3 compared to MoneyMaker roots (Fig. 6.7).

6.4.3.-Analysis of *Hairless* genome-edited mutants.

Hairless is the tomato homolog of the conserved Specifically Rac1-Associated protein (SRA1), a member of the WAVE regulatory complex (WRC) that orchestrates the formation of the actin cytoskeleton. The *Hairless* gene maps to two annotated genes in the tomato genome (Table 6.1), one corresponding to the N-terminus (Solyc11g013280, Fig. 6.8A) and C-terminus (Solyc11g013290) of SRA1. The combined genomic region of the two loci is over 46 kb long and has 30 exons. I focused on generating mutants targeting the first locus, which consists of 19 exons. I selected sgRNAs located in the second exon of Solyc11g013280 to generate a complete knock-out mutant (Fig. 6.8A). I generated only one *Hairless* GE plant, which was biallelic, harbouring two different alleles: the allele GE #1 had two small deletions (6 bp and 2 bp), and the allele GE #2 had two similar deletions (6 bp and 5 bp) (Fig. 6.8B). In this case, the activity of both sgRNAs caused deletions (Fig. 6.8B). Each mutated allele caused a two-amino acid deletion (first 6bp deletion) in the SRA1 protein and a translation frameshift. In both alleles, the translation frameshift gave rise to early stop codons (Fig. 6.9). Therefore, the proteins encoded by the edited *Hairless* alleles were 62-63 aa long in the GE line compared to the 915 aa-long WT protein, leading to a complete knock-out of *Hairless* (*SRA1*) in this plant.

The *Hairless* GE plant showed a clear phenotype in terms of trichomes, with an apparent absence of long type I trichomes, similar to the visual phenotype observed for the *Woolly* GE lines (Fig. 6.10). The *Hairless* mutation also caused sterility, with an inability to produce fruit. Therefore, this plant is currently only propagated vegetatively.

I analysed the epidermis of *Hairless* GE leaves and observed swollen, deformed trichomes (Fig. 6.11). All trichome types were present, including distorted type I trichomes, and all the types were affected in the same way and were unable to stay erect perpendicular to the leaf surface. The lack of T1 seeds prevented further quantitative characterisation of the *Hairless* mutant, but my preliminary assessment does not indicate that there are differences in terms of trichome density between the GE line and MoneyMaker (Fig. 6.11). Consequently, *Hairless* is required for the establishment of trichome morphology and edited plants are not, in fact, hairless. Therefore, *Hairless* is unlikely to be involved in trichome initiation.

6.4.4.-Analysis of *DWARF* genome-edited mutants.

The *DWARF* locus encodes the tomato brassinosteroid-6-oxidase 2, which catalyses the last reaction in the biosynthesis of brassinolide. The coding sequence of *DWARF* is 1659 bp long

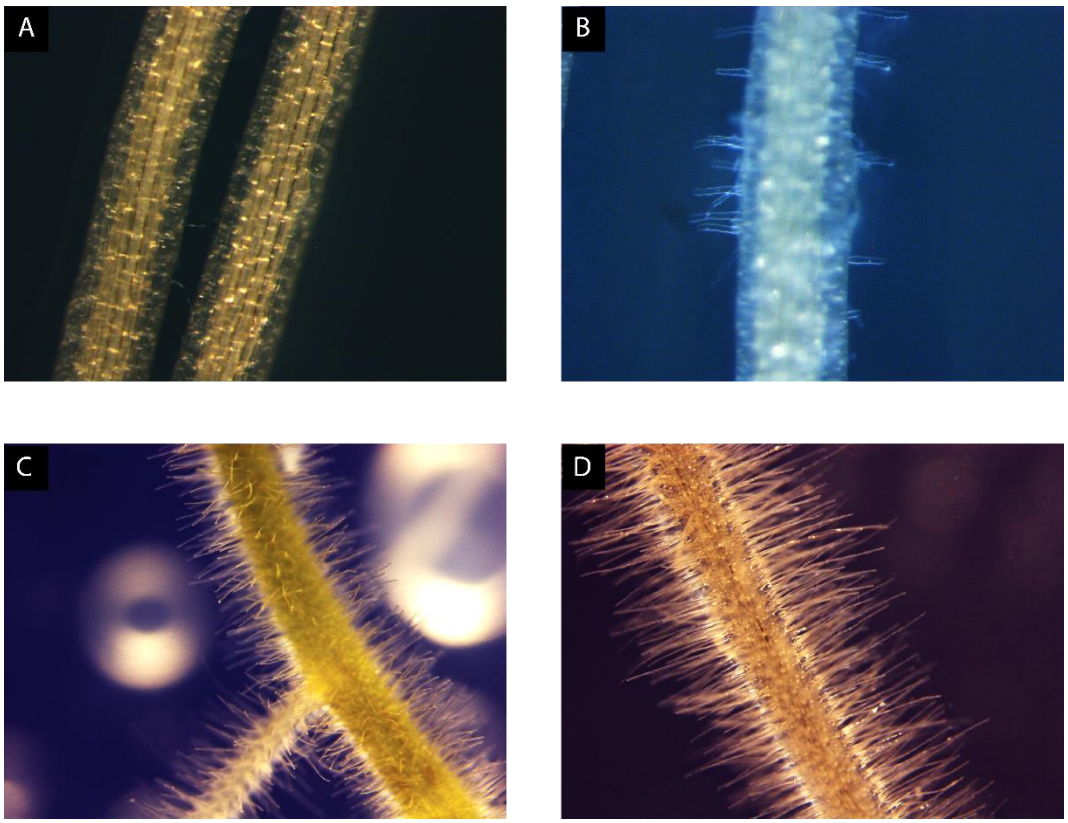

Figure 6.7.- Root phenotype of *Woolly* GE lines and MoneyMaker control plants. A and B) Roots of *Woolly* GE plants. C and D) Roots of MoneyMaker plants. The *Woolly* GE lines showed a huge reduction in root hair density, and root hair length seemed to be compromised in those root hairs that could be found

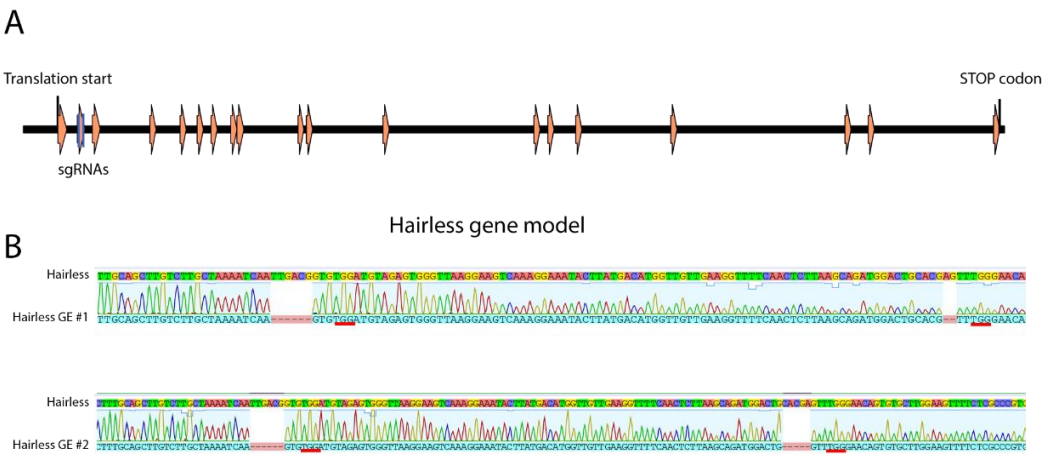

Figure 6.8.-Description of *Hairless* GE mutant generated by CRISPR/Cas9. A) Gene model of *Hairless* (Solyc11g013280). The orange arrows represent the gene coding sequence split in 19 different exons. The blue vertical lines represent the chosen sgRNAs for gene edition, located in the second exon. The translation start and STOP codon are shown in the model. The black line represents non-coding sequences (promoter, UTRs and introns). B) Sequence of the genomic region edited in the GE mutant and the reference sequence from the non-mutated gene. The PAM sequences are underlined in red. Two different edited alleles were found in the mutant plant.

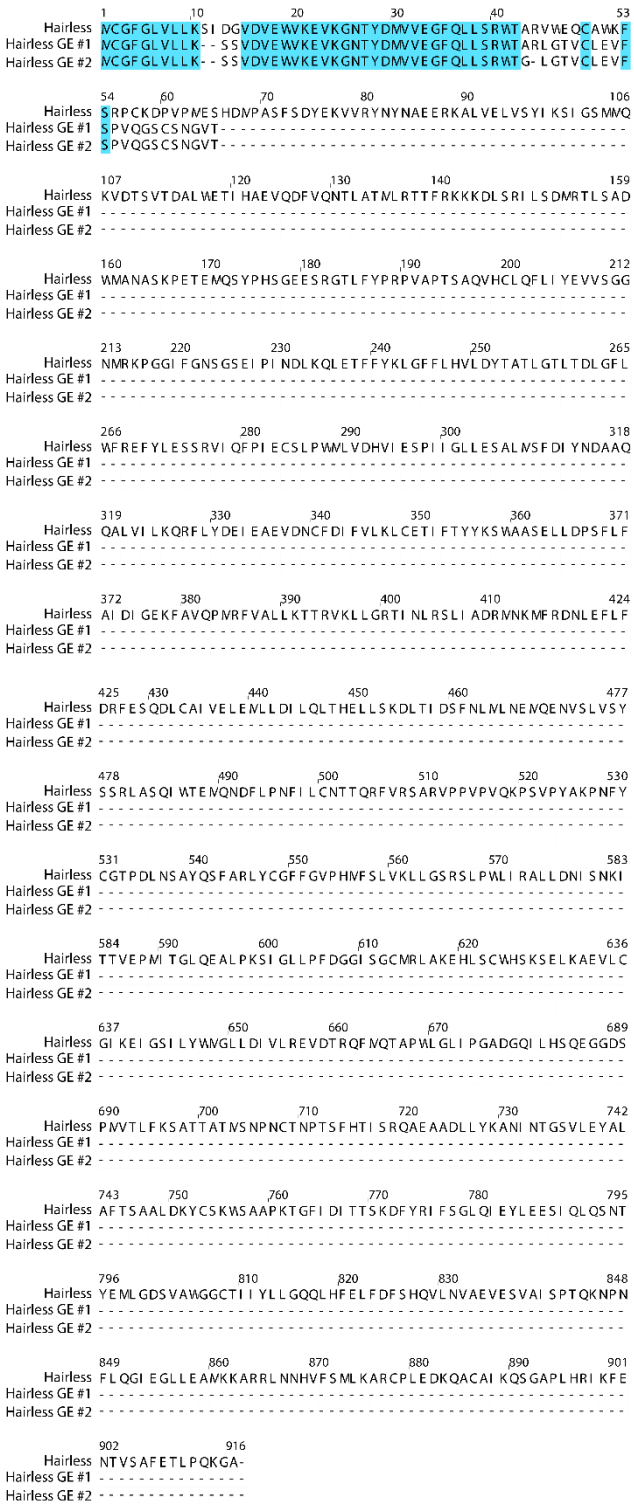

Figure 6.9.-Alignment of the peptide sequences of Hairless and the product of two GE alleles (#1 and #2). The Hairless (Solyc11g013280) WT protein is 915 aa long, and the product of the GE alleles #1 and #2 are 63 and 62 aa long respectively.

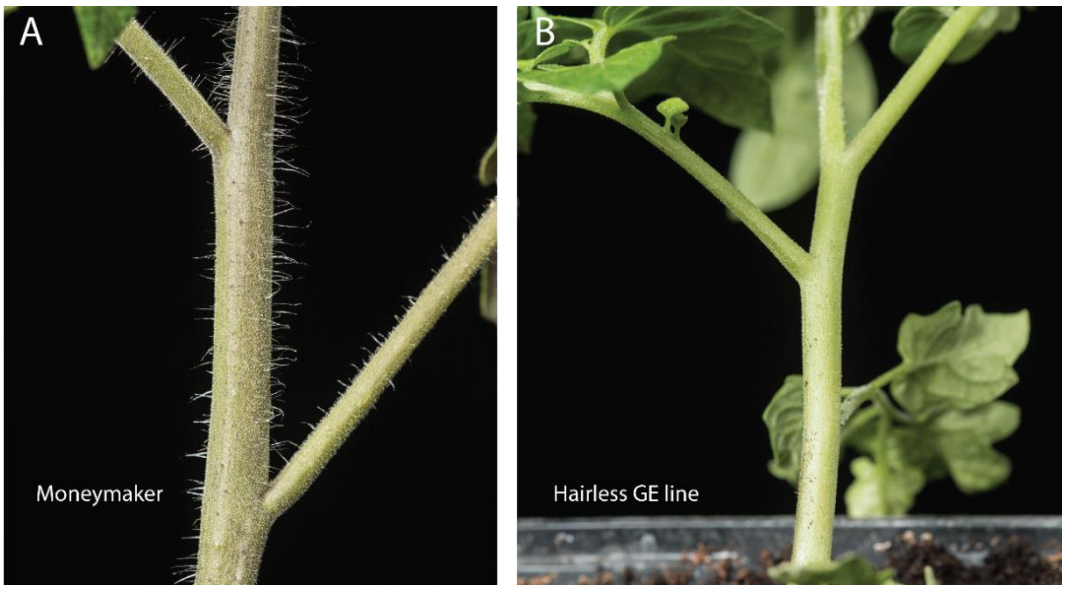

Figure 6.10.-Stem from *S. lycopersicum* cv. Moneymaker and *Hairless* genome-edited line. A) Close up view of a control MoneyMaker stem. B) Close up view of *Hairless* GE stem. The appearance of the traditional *hairless* mutant was observed in this GE line.

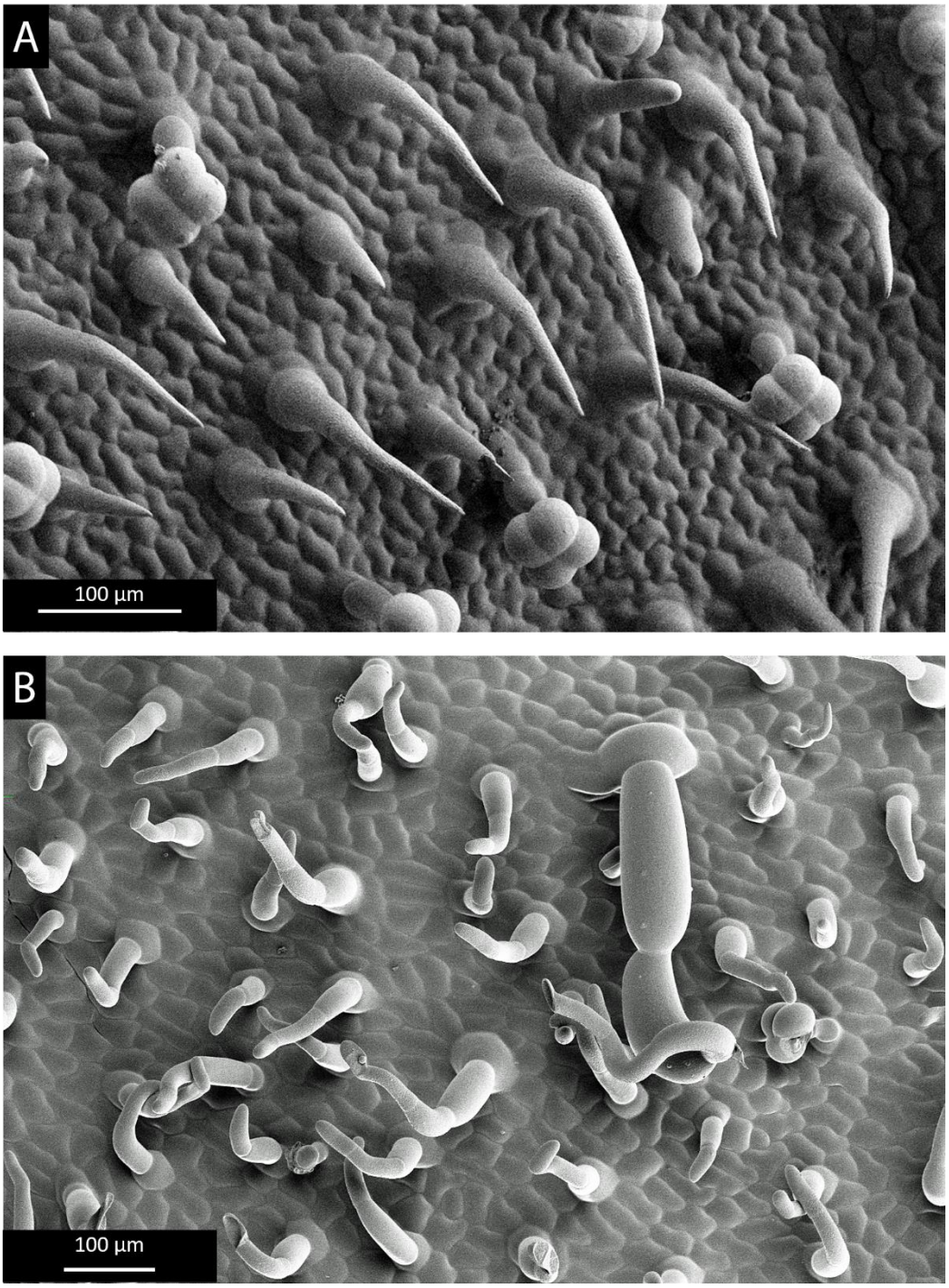

Figure 6.11.-Adaxial leaf surface of control *S. lycopersicum* cv. Moneymaker and *Hairless* genome-edited line. A) Micrograph of the surface of a control MoneyMaker leaf. B) Micrograph of the surface of *Hairless* GE line. In the GE line, trichomes have aberrant morphologies with swollen cells and inability to stay erect. This phenotype is similar to that observed in the traditional *hairless* mutant (Kang et al., 2010a). Scale bars are shown in each micrograph. The distortions affect all trichome types.

which is split between nine exons (Fig. 6.12A). I chose two sgRNAs that targeted DNA in the second exon to generate mutations at the beginning of the coding sequence. I obtained one GE line with one mutated allele with a 5 bp deletion caused by the activity of the first sgRNA (Fig. 6.12B). No deletions were observed as a consequence of the activity of the second sgRNA. The deletion caused a translation frameshift which led to an early STOP codon. The mutant protein was 110 aa long compared to the DWARF WT protein, which is 464 aa long (Fig. 6.12C). Heterozygous plants had a WT-like phenotype, but homozygous T1 plants showed a severe DWARF phenotype (Fig 12). This consisted of a reduction in height and vegetative organ size, accompanied by leaf curling and wider stems (Fig. 6.13). A general delay in growth and fruit ripening was observed. Flowers also showed signs of dwarfism (Fig. 6.14), but fruits had a size similar to MoneyMaker fruits (Fig. 6.15). The *DWARF* GE plants preserved the indeterminate growth trait observed in MoneyMaker plants (Fig. 6.16).

I analysed the leaf epidermis to determine the effect of the mutation in *DWARF* GE plants on trichome development. I observed a similar trichome density in the first true fully expanded leaf to that of MoneyMaker controls (Fig. 6.17A and B). The extreme curling of the leaf in *DWARF* GE leaves complicated the quantitative assessment of trichome and stomatal density, so I could not perform a clear characterisation. However, my visual inspection of the leaf epidermis indicated that the mutation did not have a substantial effect on trichome density or on individual trichome types, as all types of trichomes were observed in the *DWARF* GE plants (Fig. 6.17C and D). As cell size is affected in brassinosteroid mutants, I measured the pavement cell size in *DWARF* GE and MoneyMaker leaves. I observed a significantly lower pavement cell size in the GE line (Fig. 6.18).

6.4.5.-Analysis of *SlMX1* genome-edited mutants.

SlMX1 is a MYB transcription factor belonging to the *MIXTA/MIXTA-like* family. The *SlMX1* coding sequence is 1005 bp long, and it is split into three exons (Fig. 6.19A). I selected two sgRNAs targeting the beginning of the gene, with the first sgRNA lying in the first exon and the second one just at the beginning of the first intron (Fig. 6.19A). I obtained two *SlMX1* GE lines. *SlMX1* GE #1 had a 30 bp deletion caused by the activity of both sgRNAs and a complete deletion of the region delimited by them. *SlMX1* GE #2 had two small deletions around the first and second sgRNAs, of 4 bp and 1 bp respectively (Fig. 6.19B). The mutated allele in *SlMX1* GE #1, encoded a protein lacking 10 aa around the N-terminus, where the MYB DNA-binding domain is located, with the rest of the protein remaining unaffected. This allele was denominated *slmx1Δ10*. The mutation in *SlMX1* GE #2 caused a translational frameshift and an early STOP codon generating a truncated protein of 33 aa of length compared to the 334-aa long SlMX1 WT protein. This allele was denominated *slmx1* (Fig. 6.19C). In the T1 generation, I found homozygous plants carrying the *slmx1Δ10* allele (*slmx1Δ10/slmx1Δ10),* which were selected for further analysis. However,

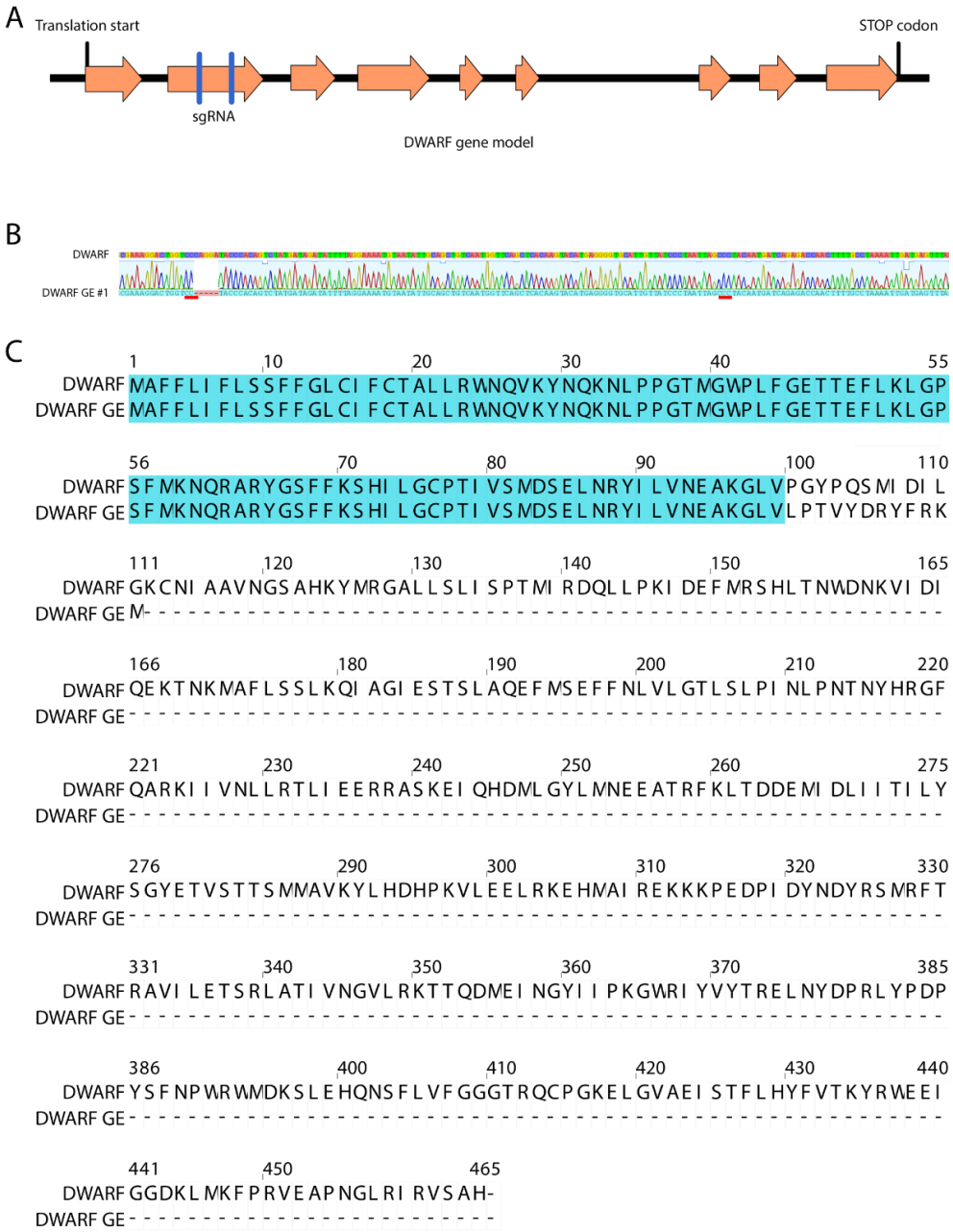

Figure 6.12.-Description of the *DWARF* GE mutant generated by CRISPR/Cas9. A) Gene model of *DWARF*. The orange arrows represent the gene coding sequence split between nine exons. The blue vertical lines represent the sgRNAs chosen for gene editing, located in the second exon. The translation start and STOP codons are shown in the model. The black line represents non-coding sequences (promoter, UTRs and introns). B) Sequence of the genomic region edited in the GE mutant and the reference sequence from the non-mutated gene. The PAM sequences are underlined in red. C) Predicted sequence of the mutated protein in the GE line (111 aa) and the DWARF WT version (464 aa).

Figure 6.13.-Phenotype of a *DWARF* genome-edited plant (left) and a *S. lycopersicum* cv. MoneyMaker control plant. Plants were 6 weeks old when the picture was taken. The *DWARF* GE plant exhibited acute dwarfism, with reduced height, reduced organ size and leaf curling.

Figure 6.14.- Flowers in *DWARF* GE plants. Flowers in the *DWARF* GE plants showed a dwarf phenotype, with a reduction in the size of the floral whorls. The dwarf phenotype did not cause sterility and plants were fertile.

Figure 6.15.-Fruits in *DWARF* GE plants. A) Green and ripening fruits on a *DWARF* GE plant. B) *DWARF* GE and MoneyMaker fruits. Fruit size was not affected by the severe dwarfism of the GE plants, with mature fruits being of a similar size to the ones produced by MoneyMaker WT plants.

Figure 6.16.- Mature *DWARF* GE plant. *DWARF* GE plants conserved the indeterminate growth style observed in the cultivar MoneyMaker. Therefore, absence of brassinosteroids did not affect the indeterminacy of growth.

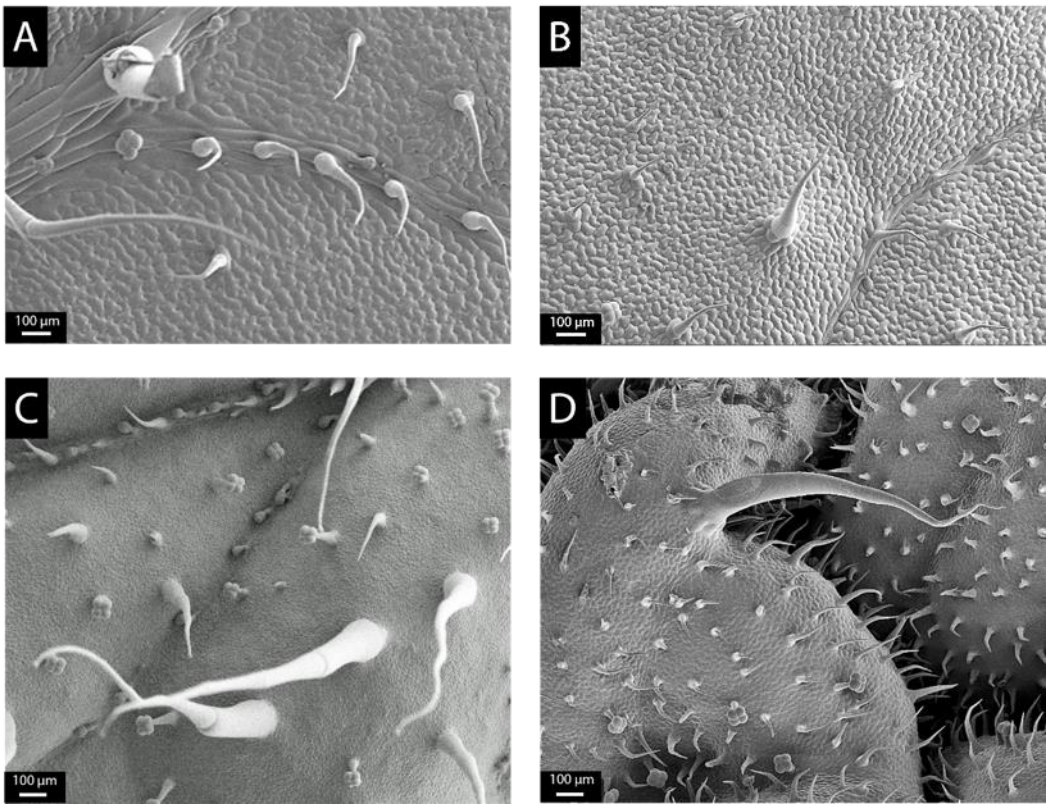

Figure 6.17.-Adaxial leaf surface of control *S. lycopersicum* cv. Moneymaker and *DWARF* genome-edited line. A) Micrograph of the adaxial surface of the first fully-expanded true leaf of a control MoneyMaker plant. B) Micrograph of the adaxial surface of the first fully-expanded true leaf of a *DWARF* GE plant. C) Micrograph of the adaxial surface of a young MoneyMaker leaf. D) Micrograph of the adaxial surface of a young *DWARF* GE leaf. Scale bars are shown in each micrograph, with A and B, and C and D taken at the same magnification.

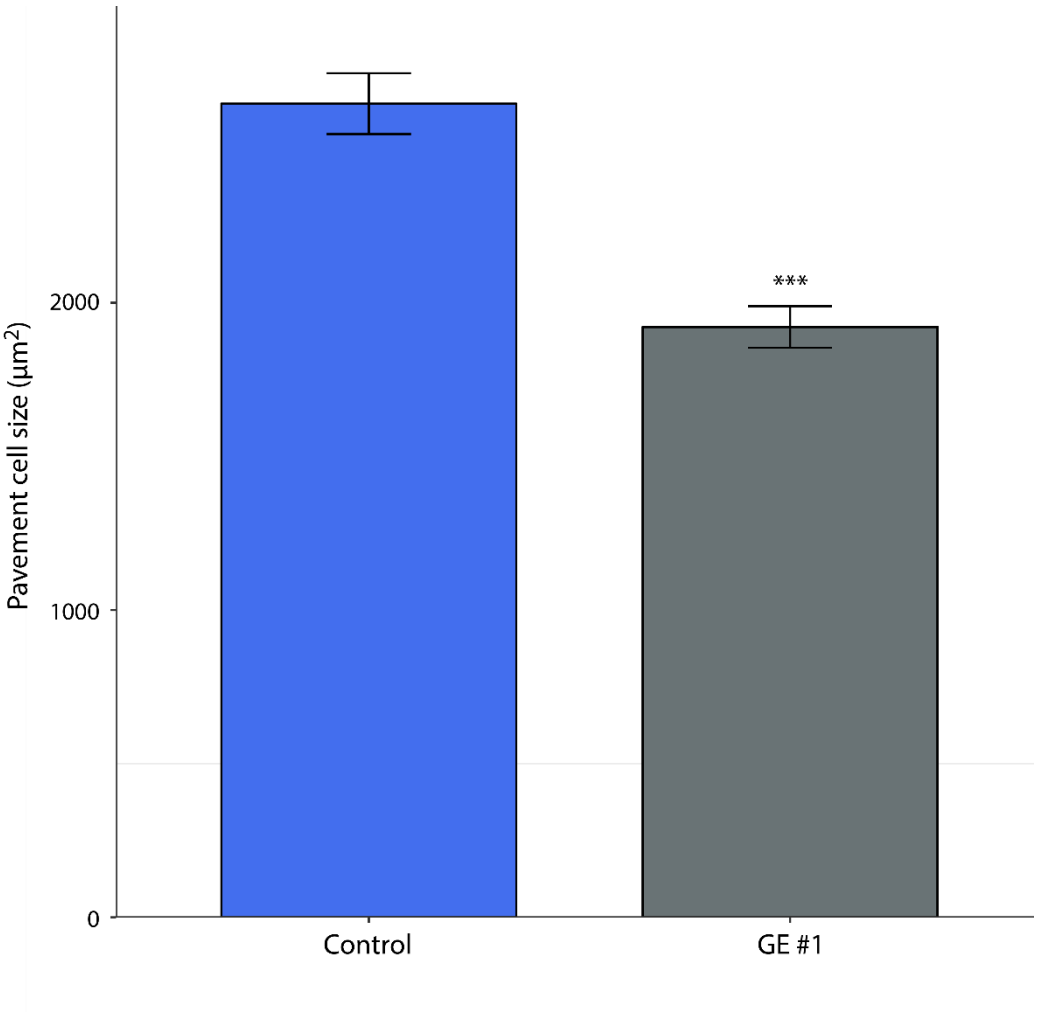

Figure 6.18.-Pavement cell size in *DWARF* GE and MoneyMaker leaves. Cell size was measured as the surface of the pavement cells in the first true fully expanded leaf of three plants per line. Values are mean±SEM of n=60 per line (n=20 per plant). Three stars indicate a significant difference between the control and *DWARF* GE values (p-value<0.01).

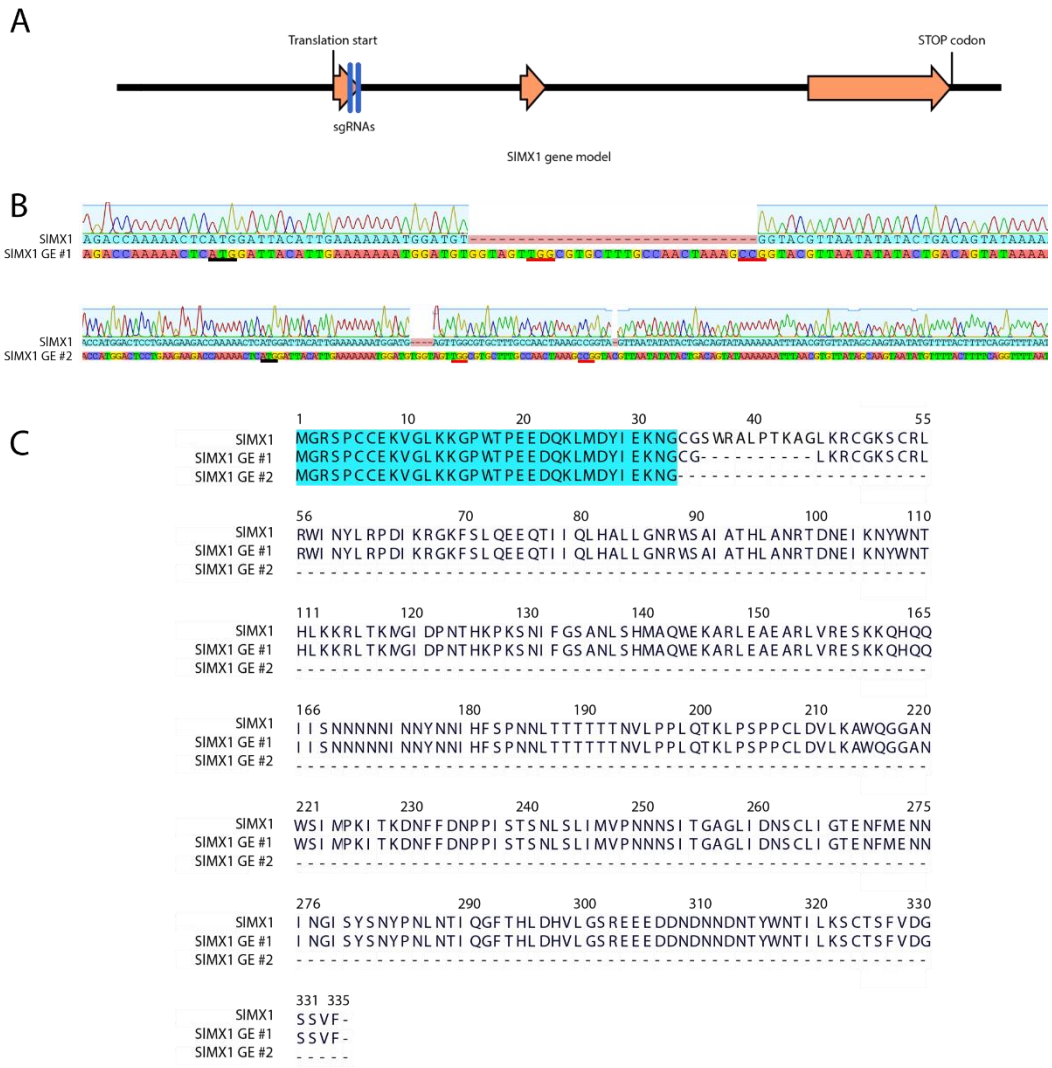

Figure 6.19.-Description of *SlMX1* GE mutants generated by CRISPR/Cas9. A) Gene model of *SlMX1*. The orange arrows represent the gene coding sequence split between three exons. The blue vertical lines represent the sgRNAs chosen for gene editing, located in the first exon and the beginning of the first intron. The translation start and STOP codons are shown in the model. The black line represents non-coding sequences (promoter, UTRs and introns). B) Sequence of the genomic region edited in the GE mutants and the reference sequence from the non-mutated gene. The start codon is underlined in black. The PAM sequences are underlined in red. C) Predicted sequence of the mutated proteins in the GE lines (325 and 34 aa, respectively) and the SlMX1 WT version (335 aa).

no homozygous plants carrying the allele *slmx1* were found in the T1 generation. Therefore, heterozygous plants (*SlMX1/slmx1*) were selected for further analysis.

I observed a remarkable reduction in trichome density in SlMX1 GE #2 lines (*SlMX1/slmx1*), even though they were heterozygous with a WT allele, noticeable in stems and leaves (Fig. 6.20). GE lines showed a slight dwarfism, with delayed growth, reduced height and leaf curling (Fig. 6.20C and 6.21). Leaf shape was also affected, with rounder leaflet edges (Fig. 6.20C). Interestingly, hypocotyls were much hairier than vegetative stems (Fig. 6.21). The same phenotype was observed for the *SlMX1* GE #1 line (*slmx1Δ10/slmx1Δ10*) (not shown). I compared the epidermal phenotype of *SlMX1* GE and MoneyMaker leaves. An overview of the leaf surface showed an apparent decrease in trichome density, especially remarkable in veins for both GE lines (Fig. 6.22). I found all trichome types in the *SlMX1* GE lines. I quantified trichome density in MoneyMaker and *SlMX1* GE #1 (*slmx1Δ10/slmx1Δ10*) plants and observed a significant reduction in trichome density in the mutant line (Fig. 6.23A). Stomatal density was not significantly higher, although we observed a trend to higher stomatal density values in the GE #1 (*slmx1Δ10/slmx1Δ10)* line (p-value=0.09) (Fig. 6.23B). I observed a significant reduction in the trichome-to-stomata ratio in the GE #1 (*slmx1Δ10/slmx1Δ10)* line (Fig. 6.23C). I did not observe correlation between TD and SD for this data set. Similar results were observed for the *SlMX1* GE #2 line (*SlMX1/slmx1* genotype), with a significant reduction in trichome density (Fig. 6.24). Interestingly, the reduction in trichome density in the two *SlMX1* GE lines was mainly due to a reduction in the number of non-glandular type V trichomes (Fig. 6.25).

6.4.6.-Analysis of *CD2* genome-edited mutants.

The *CD2* locus in tomato encodes a homeodomain leucine zipper (HD-ZIP) IV transcription factor with a HD DNA-binding domain and a START domain, similar to the structure of *Woolly*. The coding sequence of *CD2* is 3 kb long and it is split between nine exons. I selected two sgRNAs targeting the DNA-binding domain located in the fourth exon (Fig. 6.26A). I could generate only one *CD2* GE line, which had a 1bp insertion in the region targeted by the second sgRNA. The first sgRNA did not cause any mutations (Fig. 6.26B). This 1 bp insertion caused a translation frameshift that led to an early STOP codon and a truncated protein as a result of the mutation. The truncated protein is 225 aa long compared to the 821 aa-long CD2 WT protein (Fig. 6.26C). The truncated CD2 GE protein preserved the DNA-binding domain. The GE allele was found in heterozygosity in the T0, and no T1 seeds were obtained in the time available for my thesis to perform detailed analyses of the epidermis in homozygous GE plants. Leaves of the GE plant (CD2/cd2 genotype) showed a glossy phenotype due to defects in cuticle formation (Fig. 6.27). Preliminary investigation by SEM of the leaf surface showed that the density of type VI trichomes

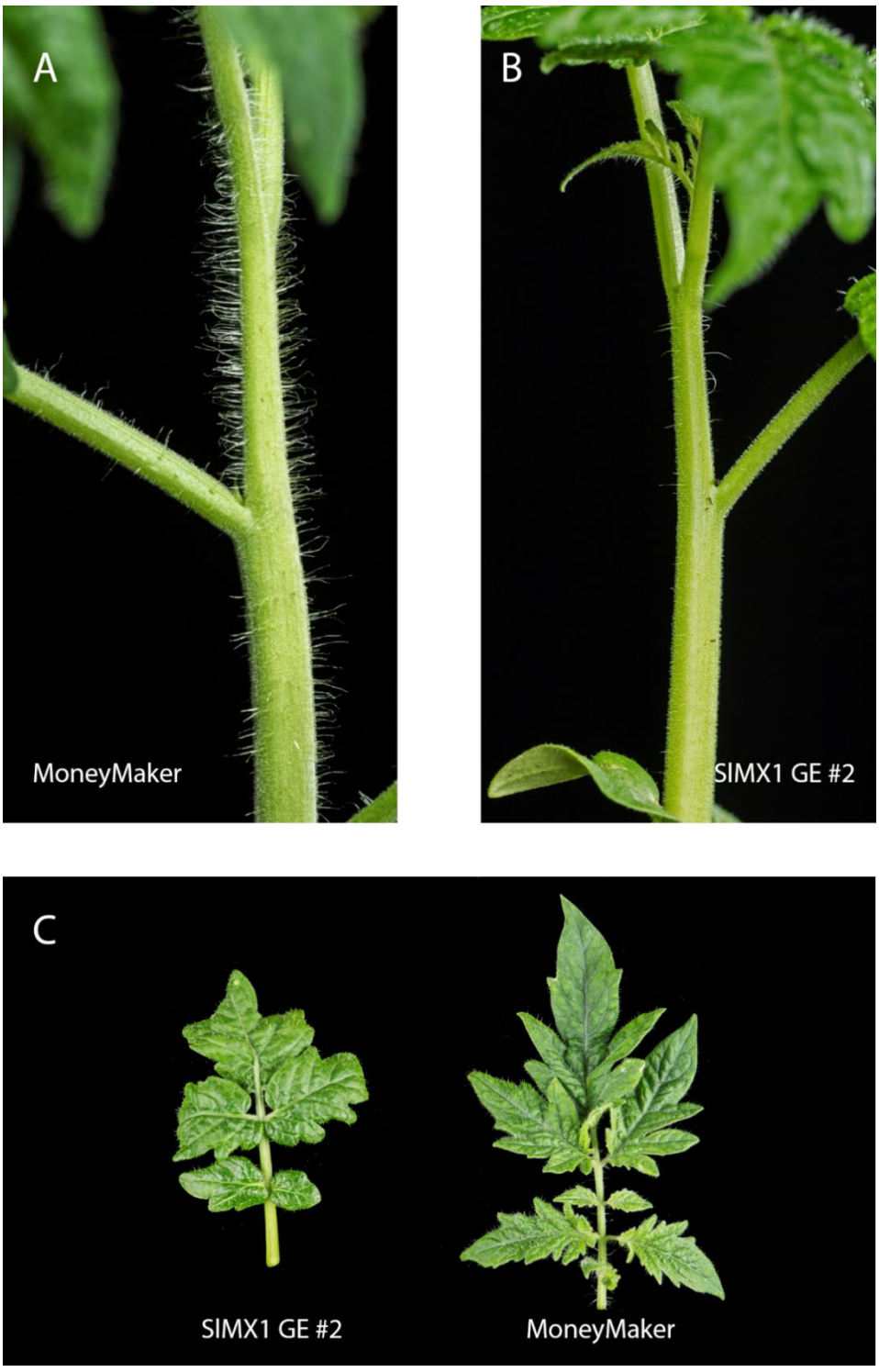

Figure 6.20.-Stem and leaves from *S. lycopersicum* cv. Moneymaker and *SlMX1* genome-edited line #2 (*SlMX1/slmx1*). A) Close up view of a control MoneyMaker stem. B) Close up view of a *SlMX1* GE #2 stem. C) Close up view from a control MoneyMaker leaf (right) and a *SlMX1* GE #2 leaf (left). Trichome density of type I trichomes was noticeably lower in the GE heterozygous line.

Figure 6.21.-Phenotype of a *S. lycopersicum* cv. Moneymaker control plant (left) and a *SlMX1* GE #2 plant (right). Plants were 5-week-old when the picture was taken. The *SlMX1* GE #2 plants exhibited signs of dwarfism (delayed growth, reduced height, leaf curling). Hypocotyls (marked with a white line) had a hairy, wild type-like phenotype.

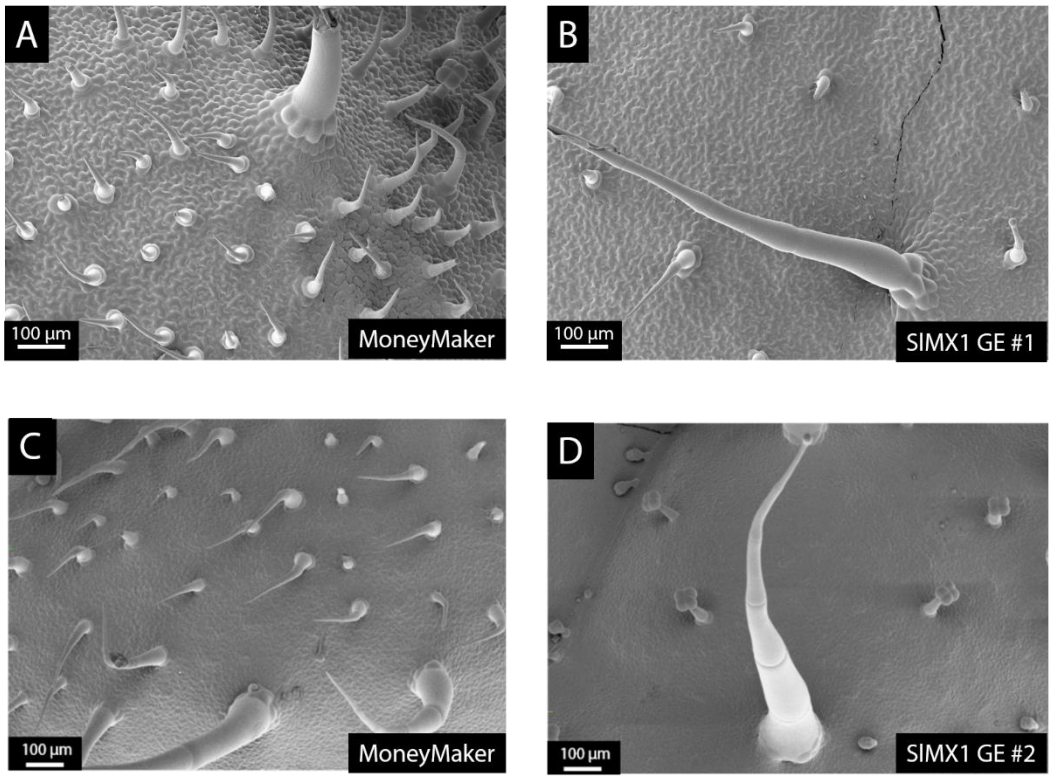

Figure 6.22.-Leaf surface of control *S. lycopersicum* cv. Moneymaker and *SlMX1* genome-edited lines #1 (*slmx1Δ10/slmx1Δ10*) #2 (*SlMX1/slmx1*). A) and C) Micrographs of the adaxial surface of control MoneyMaker leaves, grown alongside *SlMX1* GE #1 and #2 respectively. B) Micrograph of the adaxial surface of *SlMX1* GE #1 line. D) Micrograph of the adaxial surface of *SlMX1* GE #2 line. Imaged leaves were collected from 5-week-old plants. Scale bars are shown in each micrograph, both taken at the same magnification. A clear reduction in trichome density is observed in leaves and stems in the *SlMX1* GE #1 and #2 lines.

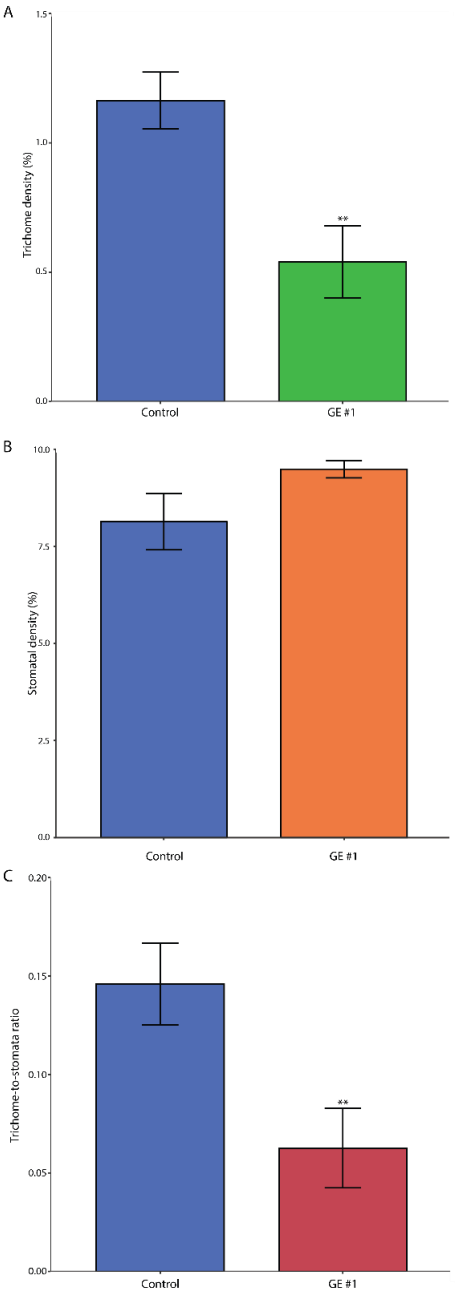

Figure 6.23.-Quantification of epidermal structures in *SlMX1* GE #1 (*slmx1Δ10/slmx1Δ10)* leaves and control tomato leaves. A) Trichome density, expressed as percentage of total epidermal cells, in control leaves (blue bar) and leaves from line *SlMX1* GE #1 (green bar). B) Stomatal density, expressed as percentage of total epidermal cells, in control leaves (blue bar) and from line *SlMX1* GE #1 (orange bar). C) Trichome-to-stomata ratio of control tomato leaves (blue bar) and line *SlMX1* GE #1 (pink bar). Values are expressed as mean±SEM of n=3-4. Two starts indicate a p-value<0.05 according to a t-test between the GE line and the control value.

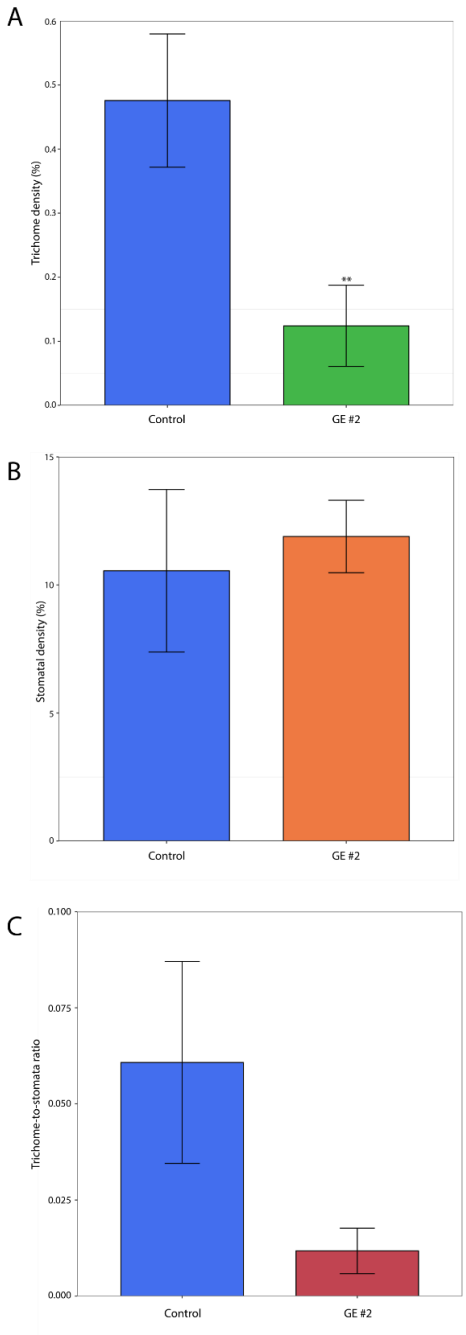

Figure 6.24.- Quantification of epidermal structures in *SlMX1* GE #2 (*SlMX1/slmx1*) leaves and control tomato leaves. A) Trichome density, expressed as percentage of total epidermal cells, in control leaves (blue bar) and leaves from line *SlMX1* GE #2 (green bar). B) Stomatal density, expressed as percentage of total epidermal cells, in control leaves (blue bar) and from line *SlMX1* GE #2 (orange bar). C) Trichome-to-stomata ratio of control tomato leaves (blue bar) and line *SlMX1* GE #2 (pink bar). Values are expressed as mean±SEM of n=3. Two starts indicate a p-value<0.05 according to a t-test between the GE line and the control value.

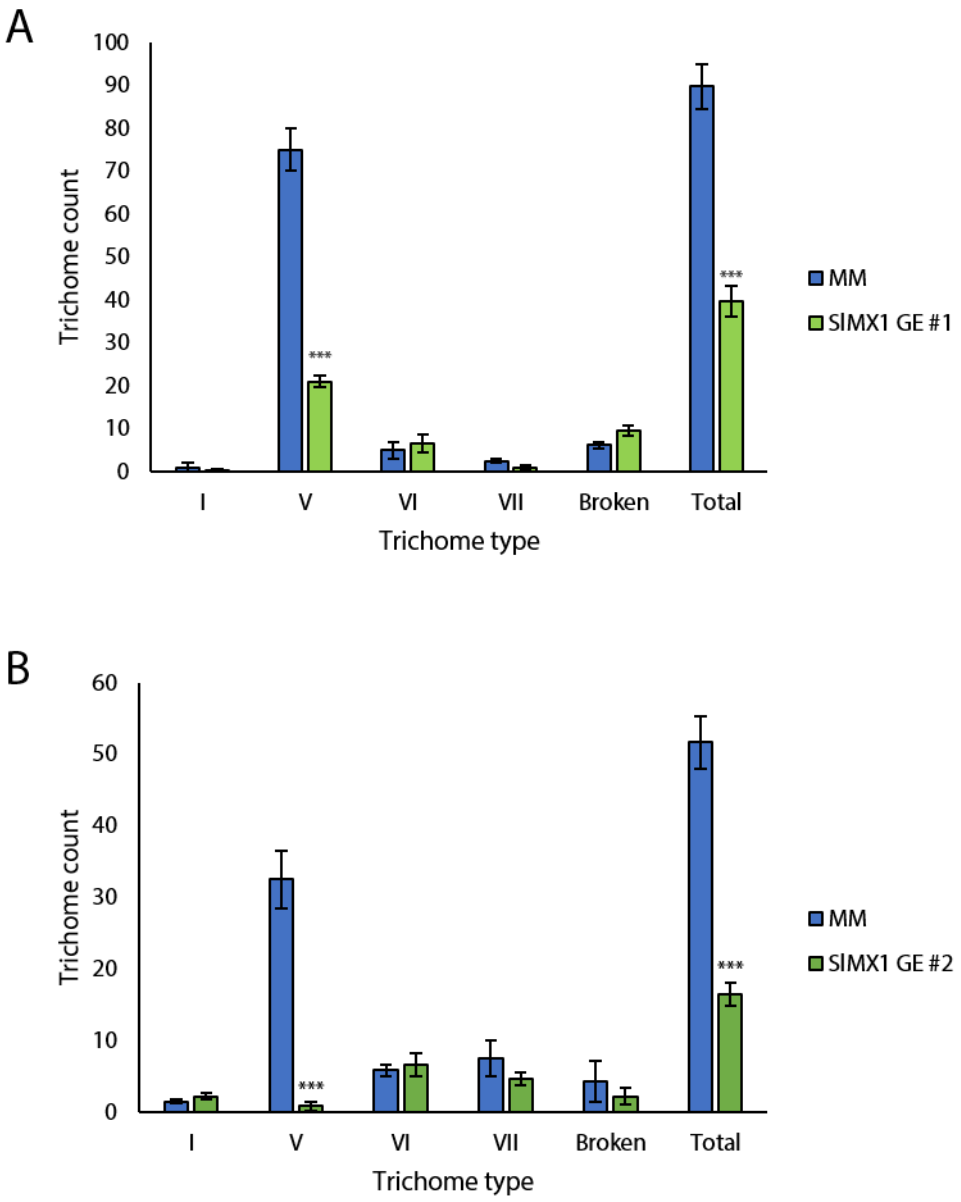

Figure 6.25.-Trichome count of different trichome types in young leaves from MoneyMaker and *SlMX1* GE #1 (*slmx1Δ10/slmx1Δ10*) and #2 (*SlMX1/slmx1)* plants. The blue bars represent MM values and the green bars represent *SlMX1* GE #2 values. Trichome count was calculates as the number of trichomes in an area of approximately 2.6 mm^2 of the adaxial surface of either MM o *SlMX1* GE #2 leaves (n=3 per line). Three stars indicate a significant difference (p-value<0.01) between lines, according to a t-test. Type V density was the only individual type significantly affected by the *SlMX1* mutation, which also affected the total count. Trichomes were grouped according to the classification in Luckwill, 1943.

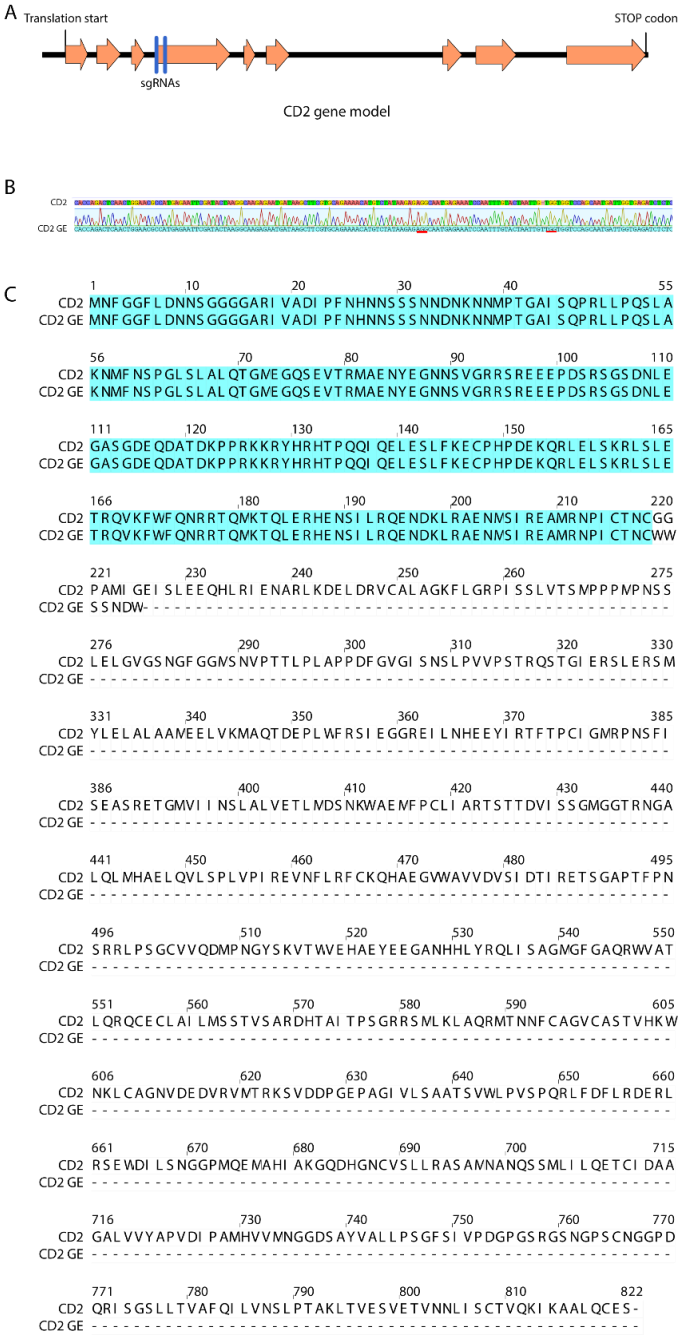

Figure 6.26.-Description of the *CD2* GE mutant generated by CRISPR/Cas9. A) Gene model of *CD2*. The orange arrows represent the gene coding sequence split between nine different exons. The blue vertical lines represent the sgRNAs chosen for gene editing, located in the fourth exon. The translation start and STOP codon are shown in the model. The black line represents non-coding sequences (promoter, UTRs and introns). B) Sequence of the genomic region edited in the GE mutant and the reference sequence from the non-mutated gene. The PAM sequences are underlined in red. C) Predicted sequence of the mutated protein in the GE line (225 aa) and the CD2 WT version (821 aa).

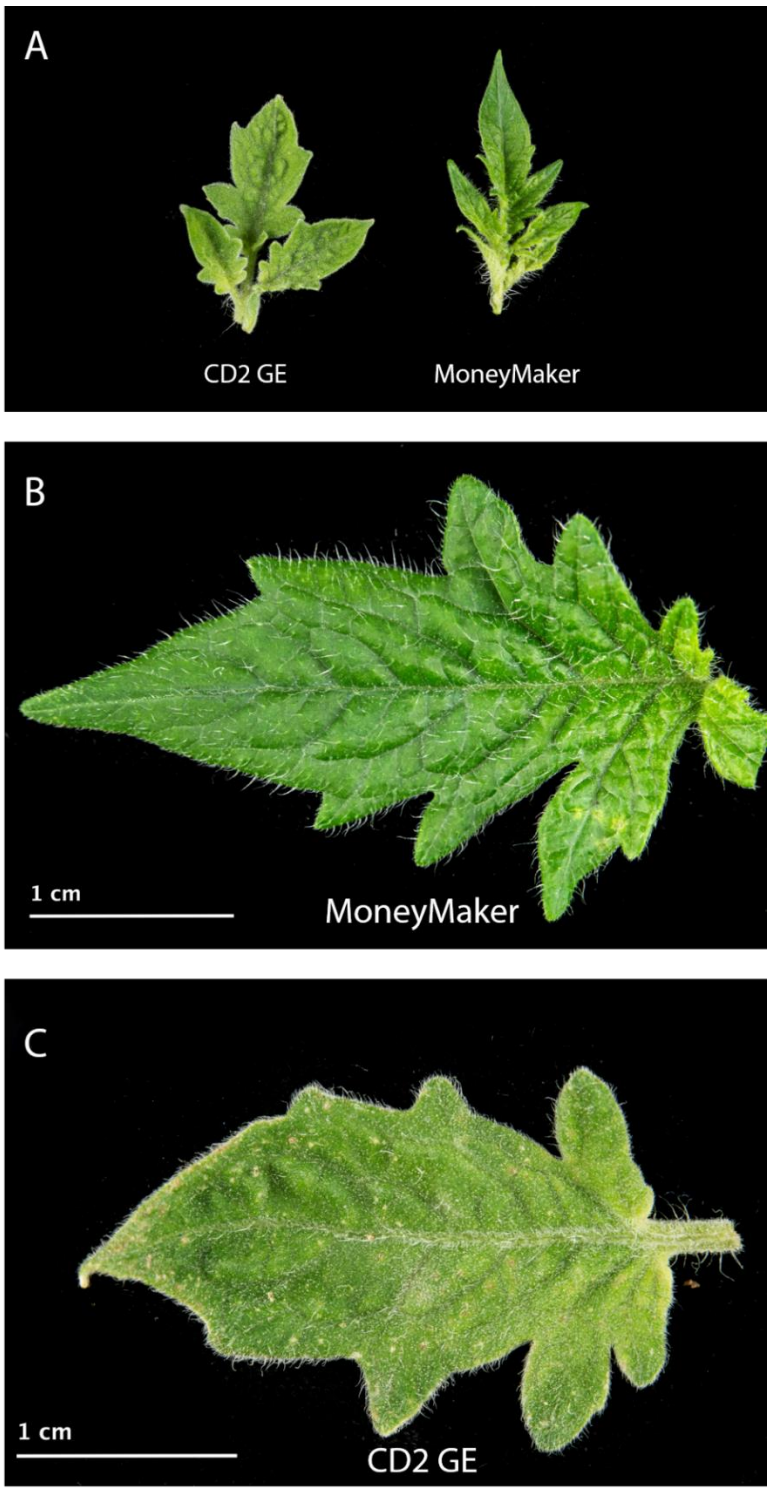

Figure 6.27.-Leaves from *S. lycopersicum* cv. Moneymaker and *CD2* genome-edited line (*CD2/cd2*). A) Young *CD2* GE (left) and MoneyMaker (right) leaves. B) Close up view of a control MoneyMaker leaf. C) Close up view from a *CD2* GE leaf. *CD2* GE leaves had a glossy surface.

was reduced in the heterozygous line, but the total trichome density appeared to be substantially higher than WT controls (Fig. 6.28).

6.5.-Discussion.

6.5.1.-Genome editing of HD-ZIP IV genes affect trichome density and trichome type distribution.

Among the genes known to be involved in trichome development in tomato (Table 6.1), two of them are homeodomain leucine-zipper (HD-ZIP) IV transcription factors: *Woolly* (Yang et al., 2011a) and *CD2* (Nadakuduti et al., 2012). HD-ZIP transcription factors are found only in plants, and their DNA binding domain consists of a homeobox domain followed by a leucine-zipper motif that is used for dimerization with other proteins (Ariel et al., 2007). Four different subfamilies have been described for the HD-ZIP factors, according to the protein domains present in the C-terminal region and their function (Ariel et al., 2007, Elhiti and Stasolla, 2009). Subfamily IV, which includes *Woolly* and *CD2*, has a steroidogenic acute regulatory protein-related lipid transfer (START) domain in the C-terminal region (Elhiti and Stasolla, 2009). No specific lipid ligands have been identified in plants (Schrick et al., 2004), although the need for a ligand for functional activity has been reported by heterologous expression in yeast (Schrick et al., 2014) and correct functioning of HD-ZIP IV genes seem to be related to biosynthesis of fatty acids and sterols (Lung et al., 2018).

The function of described HD-ZIP IV transcription factors is often related to epidermal development. In *Arabidopsis,* 16 HD-ZIP IV genes have been identified (Nakamura et al., 2006). *GLABRA2* (*GL2*) was the first HD-ZIP IV identified as a negative regulator of root hair development (Masucci et al., 1996) and as a positive regulator of trichome expansion (Rerie et al., 1994). Two HD-ZIP IV genes, *PROTODERMAL FACTOR 2* (*PDF2*) and *MERISTEM LAYER 1* (*ATM1*) are necessary for development of the epidermal layer, as evidenced by the lack of epidermis in double mutants in *Arabidopsis* (Abe et al., 2003). *HDG1* is involved in cuticle regulation (Wu et al., 2011). *ANTHOCYANINLESS 2* is another member of this family with a role in anthocyanin biosynthesis in subepidermal layers and in root development (Kubo et al., 1999). *HDG2* is highly expressed in stomatal meristemoids and is essential for stomatal patterning (Peterson et al., 2013). The high number of genes in the subfamily and their relatively specialised functions in the development of epidermis causes a high degree of redundancy in the family, and most single mutants do not develop strong phenotypes (Ariel et al., 2007).

The role of HD-ZIP IV genes in development of multicellular trichomes has been described for several species. For example, in *Artemisia annua,* two HD-ZIP IV genes regulate trichome initiation, *AaHD1* (Yan et al., 2017) and *AaHD8* (Yan et al., 2018). AaHD8 binds AaMIXTA1, a MYB protein from the *MIXTA/MIXTA-like* subfamily, and thus regulates the expression of *AaHD1* (Yan

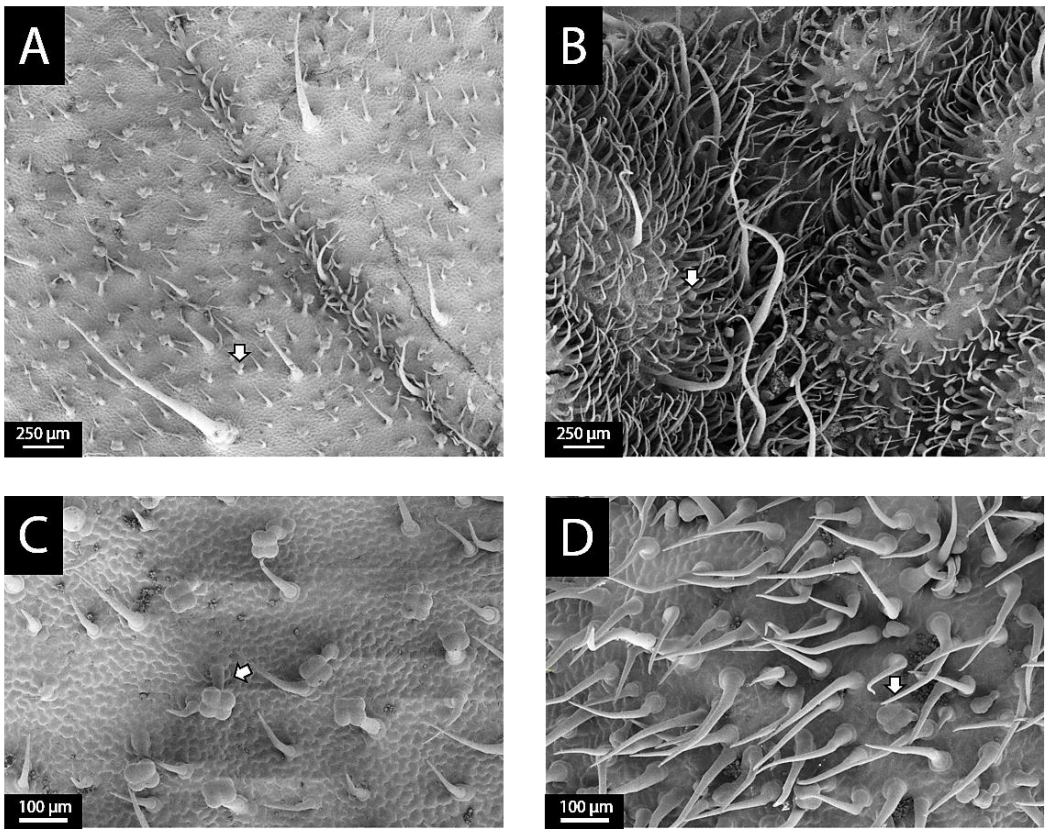

Figure 6.28.-Adaxial leaf surface of control *S. lycopersicum* cv. MoneyMaker and the *CD2* genome-edited line. A and C) Micrograph of the surface of a control MoneyMaker leaf. B and D) Micrograph of the surface of *CD2* GE line. Scale bars are shown in each micrograph. White arrows point type VI glandular trichomes.

et al., 2018). In melon, *CmGL* is a HD-ZIP IV which regulates trichome initiation, and knock-out mutants have completely glabrous aerial organs (Zhu et al., 2018a). In cucumber, *CsGL3* has an equivalent role, and when mutated, causes a glabrous phenotype (Pan et al., 2015). In cotton, *GhHD1* regulates fibre (trichome) initiation in seeds (Walford et al., 2012). With this general knowledge about the function of this gene family, HD-ZIP IV seem to have a conserved function in development of the epidermis, and more specifically trichome development.

In tomato, 15 class IV HD-ZIP genes have been described (Gao et al., 2015). Among these, only two have been functionally characterised to some extent, *Woolly* and *CD2* (Table 6.1). *Woolly* was identified in the a mutant line that had an extremely hairy phenotype (Yang et al., 2011a). A point mutation close to the C-terminus caused an amino acid substitution that affected the function of the gene, promoting trichome growth in the mutant line. The mutation was dominant, and homozygous lines were not viable and were aborted at the embryo stage (Yang et al., 2011a). Lines overexpressing the mutated version of the gene were similarly compromised in normal development. The use of RNAi lines to silence *Woolly* expression showed that the main role of *Woolly* involves the promotion of long type I trichomes in tomato (Yang et al., 2011a). It was suggested that silencing of *Woolly* might reduce slightly the density of all other trichome types, apart from type I, but a proper quantification of this phenomenon was not carried out (Yang et al., 2011a). My analysis of homozygous GE lines in this chapter confirmed these ideas. Type I trichome formation was almost completely abolished in the GE lines (Fig. 6.4) and the total trichome density was greatly reduced in GE leaves (Fig. 6.5 and 6.6A). Whether or not *Woolly* controls specifically the production of type I trichome (which would reduce total trichome density in KO mutants) or has a more general role in trichome initiation is not clear from the data I have gathered so far. A more detailed analysis of mature vegetative tissues will reveal whether other trichome types are also affected. The activity of the *Woolly* promoter (in agreement with the available expression data, Fig. 6.29) in tomato revealed a high expression in young leaves and flower buds which is in accordance with its function in trichome development (Yang et al., 2011a). However, a low level of expression of *Woolly* occurs in roots (Fig. 6.29A), and specifically in lateral root primordia (Yang et al., 2011a). Interestingly, plants overexpressing the mutated *Woolly* allele did not develop lateral roots (Yang et al., 2011a). I observed a dramatic reduction in the root hair numbers and length in the KO *Woolly* GE lines (Fig. 6.7), indicating an important role for Woolly in the development of epidermis in underground tissues too. I did not observe a clear effect of loss of *Woolly* activity on lateral root formation in the GE mutant, but delays in germination and growth of the mutant complicated comparisons between lines. This expression pattern is reminiscent of the one reported for *SlMIXTA-like* (see *Chapter 5*). Moreover, the RNAseq data available from the *S. pennellii* IL leaves (Chitwood et al., 2013)

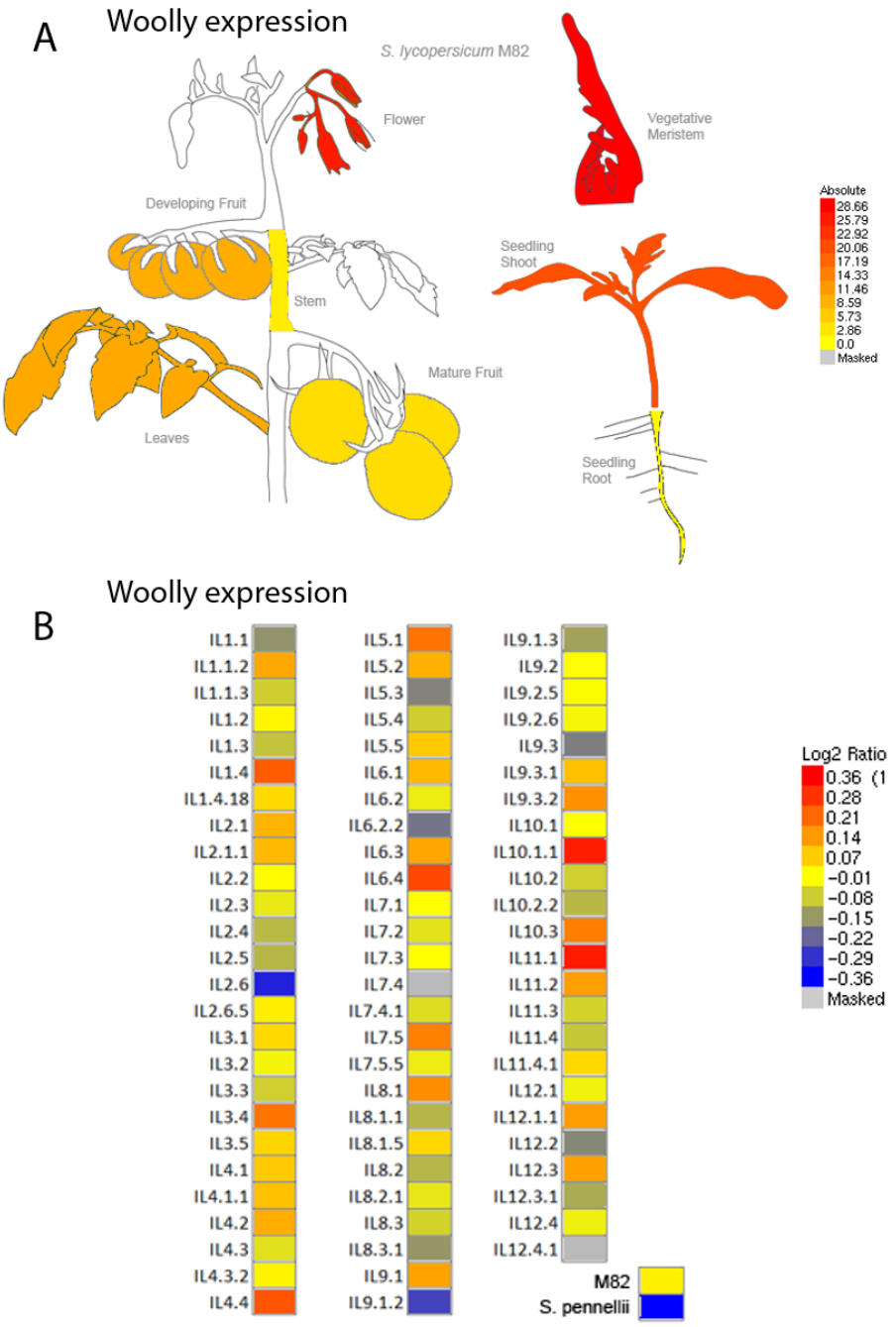

Figure 6.29.-Expression level of Woolly in different tissues and *S. pennellii* ILs. A) Absolute expression level of *Woolly* in *S. lycopersicum* cv. M82 based on RNAseq data generated by (Koenig et al., 2013). B) Relative expression level of *Woolly* in leaves of the *S. pennellii* ILs, from the RNAseq data generated by (Chitwood et al., 2013). The images in A and B were generated using the eFP expression browser (Winter et al., 2007).

indicates that IL 2-6 (which showed low expression of *SlMIXTA-like* in *Chapter 4*) also showed the lowest expression level for *Woolly* among all the ILs (Fig. 6.29B). These overlapping expression patterns and related functions (both in trichome development and lateral root development) suggest that there might be common regulatory elements governing their expression and function. However, the fact that SlMIXTA-like is a negative regulator of trichome initiation (see *chapter 5*) and Woolly is a positive regulator (Fig. 6.6A) of trichome development raises questions about how their function can be related. The analysis of double mutants generated by crossing the *SlMIXTA-like* KO line described in *chapter 5* and the *Woolly* GE mutant described in this chapter will help in understanding this mechanism.

Woolly interacts with the small cyclin SlCycB2 (Yang et al., 2011a, Gao et al., 2017) and with the C2H2 zinc-finger transcription factor HAIR (Chang et al., 2018). SlCycB2 is a B type cyclin, proteins which are responsible for determining the transition to the mitotic phase in the cell cycle (Dewitte and Murray, 2003). This specific cyclin has a role in cell division in multicellular trichomes in tomato, as shown by RNAi and overexpression of the gene in tomato (Gao et al., 2017). Silencing of *SlCycB2* causes an increase in non-glandular trichome density with and a near total absence of type I trichomes as well as the presence of aberrant multibranched trichomes. I also observed this in my VIGS assays (see *Chapter 4*). Overexpression of the cyclin, however, causes a reduction in density of all trichome types. Non-glandular trichomes were specifically affected and were completely absent in these lines (Gao et al., 2017). These results seem to indicate that spatiotemporal regulation of *SlCycB2* expression is essential for trichome development, perhaps because all trichome of tomato are multicellular. Due to its interaction with Woolly, and the role of Woolly in promoting type I trichome growth (and possibly trichome initiation, as shown in Fig. 6.6A), the functionality of Woolly may be SlCycB2-dependent. However, this simple model has some contradictions because knock-out mutations of *Woolly* cause a reduction in trichome density (Fig. 6.6A) while the silencing of *SlCycB2* causes an increase in trichome density (Gao et al., 2017), indicating that the functions of these genes is more complex than proposed hitherto. The development of *SlCycB2* GE lines and the resulting lines from crossing these to *Woolly* GE mutants should help gain new insight in these processes. However, the recent discovery of *HAIR* as the gene underlying the *hairless* phenotype in IL 10-2 (see *Chapters 3 and 4*) has shed new light on the process of development of type I trichomes (Chang et al., 2018). *HAIR* is a C2H2 zinc finger transcription factor closely related to *Arabidopsis* regulators of trichome initiation like *GLABROUS INFLORESCENCE STEMS* (GIS) or *ZINC FINGER PROTEIN* genes (*ZFP5, 6* and *8*) (Zhou et al., 2012, Zhou et al., 2013, Kim et al., 2018b), especially in the context of transition from juvenile to adult traits (Gan et al., 2006). Silencing of *HAIR* by RNAi showed a phenotype very similar to that observed for the silencing (Chang et al., 2018) or

knock-out of *Woolly* (Fig. 6.6), with a reduction in trichome density and complete absence of type I trichomes. The fact that *Arabidopsis* genes related to *HAIR* are mostly functional in tissues developed during the adult phase led me to question whether the function of *Woolly* in trichome development is most relevant in mature tissues and whether the quantitative analyses performed on the first true leaf (Fig. 6.6) were not fully representative of phenotype resulting from knocking out *Woolly*. This is especially relevant as hypocotyls of IL 10-2 (which carry a mutated version of *HAIR*) do not have a *hairless* phenotype and are indistinguishable from M82 seedlings (see *Chapter* 4). A more detailed analysis of mature tissues of Woolly GE lines is currently ongoing and will provide us with new information about the role of *Woolly* and *HAIR* in the transition to the adult phase and the impact of the knock-out of *Woolly* function on different trichome types. In conclusion, *HAIR,* together with *SlCycB2* and *Woolly* seem to have a role in regulation of type I trichomes. However, my data suggest that they might have a more general role in trichome initiation and root hair development.

A different allele of *Woolly*, with an extra amino acid change in the C-terminus, was also investigated by ectopic expression in *Nicotiana tabacum* (Yang et al., 2015). This version of *Woolly* caused a massive increase in trichome density and the formation of aberrant multicellular trichomes. RNAseq analysis of transgenic tobacco plants showed differential expression of homologs of trichome-related genes (as the *NtWoolly* or *NtCycB2* genes). This might suggest that Woolly can regulate its own expression and adds to the evidence that trichome regulatory pathways are shared between different *Solanaceae* species. Moreover, both described *Woolly* alleles are, given the effect of the knock-out and RNAi silencing, gain-of-function mutations in the sense that the function of the gene is enhanced. These mutations are lethal for developing embryos when homozygous (Yang et al., 2011a), but homozygous *Woolly* GE mutants showed no strong developmental deficiencies, suggesting that its function might not be essential for embryo or plant development (Fig. 6.4) or its function can be compensated by other HD-ZIP genes in tomato.

CUTIN DEFICIENT 2 (*CD2*) is another member of the class IV HD-ZIP gene family, and it has been characterised as a regulator of cuticle synthesis and deposition, although its function seems to concern mainly the cuticle of fruit, which has been suggested to be differentially regulated compared to cuticle development in leaves (Nadakuduti et al., 2012). However, changes in the alkanes and cutin monomers were observed in leaves of *cd2* mutants, together with a semi-dwarf phenotype and increased water loss (Nadakuduti et al., 2012). I observed a glossy appearance to the leaves in my *CD2* GE line (Fig. 6.27), suggesting that the mutation also affects vegetative tissues. Interestingly, type IV trichome density was reduced greatly in *cd2* mutants, and stomatal density was also reduced. Total trichome density has not been reported for this

mutant, and it would be useful to determine whether this gene governs trichome initiation in a way similar to *Woolly* (Fig. 6.4 and 6.5) or whether this is a side effect of metabolic changes in the epidermis. A preliminary observation of the T0 line suggested that, although type VI trichome density is reduced, total trichome density is increased (Fig. 6.28). The effect of metabolic changes leading to changes in type VI trichome density has been reported previously, for example in tomato plants where the MEP pathway enzyme *SlDXS2* was silenced (Paetzold et al., 2010) or in mutants of the phenylpropanoid pathway enzyme *SlCHI* (Kang et al., 2014). Moreover, my observations on water-stressed plants showed that water availability influences the development and determination of final density of trichomes and stomata (see *Chapter 7*), and these changes in trichome and stomatal density can be driven by the increase in cuticular water loss caused by the *CD2* mutation (Nadakuduti et al., 2012), which could explain a higher total trichome density (Fig. 6.28) and lower stomatal density (Nadakuduti et al., 2012). Analysis of T1 homozygous GE plants will assist in determining the true trichome phenotype. In any case, a functional relationship between regulators of cuticle synthesis and deposition and trichome development has been reported for several genes in tomato and other species. This is the case for *SlMIXTA-like*, which is a positive regulator of cuticle deposition and conical cell formation (Lashbrooke et al., 2015), and a negative regulator of trichome initiation (see *chapter 5*). Moreover, SlSHN3, an AP2 transcription factor which regulates fruit cuticle formation, seems to act upstream of SlMIXTA-like, indicating that the regulation of both pathways is closely linked. In *Artemisia annua,* AaMIXTA1 regulates both cuticle and trichome formation, and does this through interactions with HD-ZIP factors (Pu et al., 2018, Yan et al., 2018). In fact, the *CD2* homolog in *A. annua,* AaHDG8 (Fig. 6.30), directly regulates cuticle formation and trichome initiation by binding and activating AaMIXTA1. Perhaps the analogous interaction occurs in tomato. This could be tested by combining the mutations of MIXTA/MIXTA-like genes and HD-ZIP genes, by crossing the GE mutants I have generated (including the SlMIXTA-like KO mutant generated for *chapter 5*). Similarly, interaction analysis of the two gene families in yeast or *in planta* might provide information about the conservation level of these interaction-mediated mechanisms in plants. The expression pattern of *CD2* is reminiscent of *Woolly* (Fig. 6.31), although there is a lack of detailed promoter analysis to determine spatiotemporal expression of this gene. Moreover, the expression of CD2 in the ILs (Fig. 6.31) does not correlate with observed changes in type VI trichome density (see *Chapter 3*), indicating that probably the function of this gene is not altered in *S. pennellii.*

I analysed the phylogenetic relationship between tomato HD-ZIP IV genes and the ones functionally characterised in other plant species (Fig. 6.30). The number of genes in this family in tomato is relatively large, and at least four gene duplications have been identified by sequence

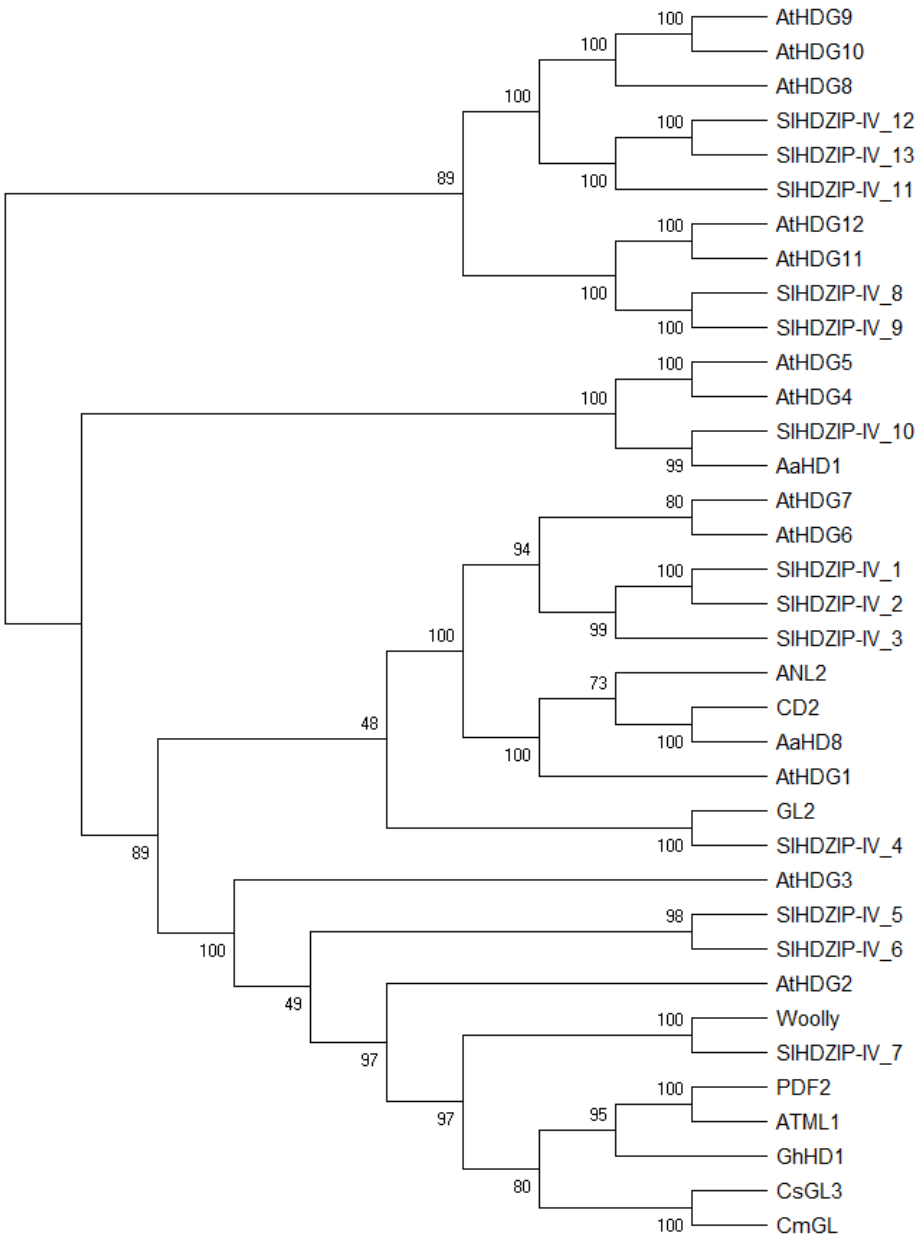

Figure 6.30.- Phylogenetic tree showing relationships between HD-ZIP class IV proteins in tomato and other species. The amino acid sequence of HD-ZIP class IV transcription factors from tomato (15 genes), *Arabidopsis thaliana* (16 genes), *Artemisia annua* (2 genes), cucumber (one gene), melon (one gene) and cotton (one gene) were used to build the phylogenetic tree. Sequences were aligned using ClustalW and the tree was built using the neighbour-joining method, based on the evolutionary distance computed by the JTT matrix-based method. The bootstrap values are shown for each branch (bootstrap replicates=1000).

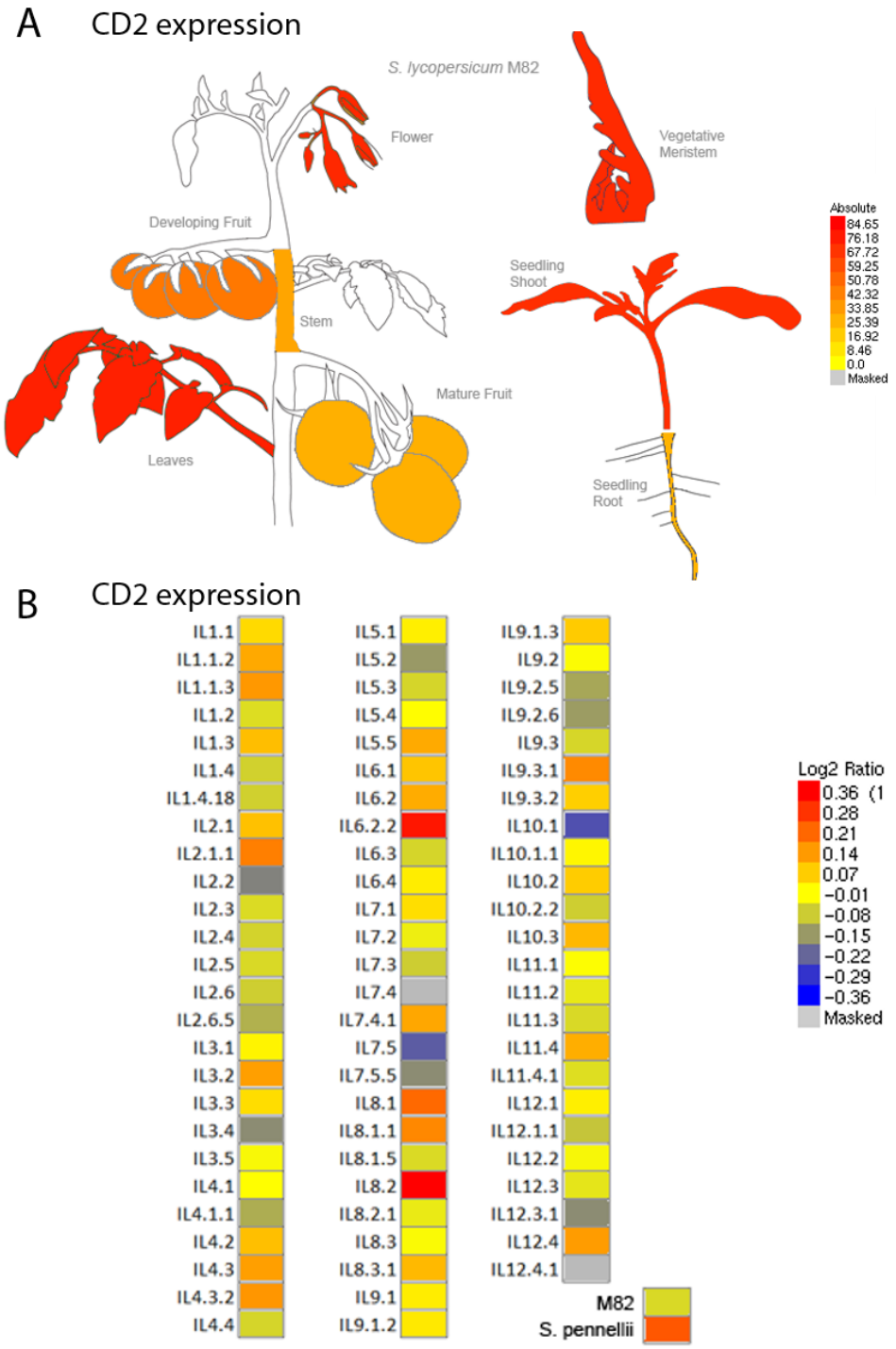

Figure 6.31.-Expression level of *CD2* in different tissues and *S. pennellii* ILs. A) Absolute expression level of *CD2* in *S. lycopersicum* cv. M82 based on RNAseq data generated by (Koenig et al., 2013). B) Relative expression level of *CD2* in leaves of the *S. pennellii* ILs, from the RNAseq data generated by (Chitwood et al., 2013). The images in A and B were generated using the eFP expression browser (Winter et al., 2007).

analysis (Gao et al., 2015). Different members of this gene family in *Arabidopsis* are redundant in function, since most of the single mutants displayed no mutant phenotype (Ariel et al., 2007). In fact, *Woolly* has a paralog in tomato on chromosome 10 (*SlHDZIP-IV 7*) generated by direct duplication (Gao et al., 2015) which is likely to be functional, as it is expressed in most tissues in a similar fashion to *Woolly* or *CD2* (Fig. 6.32) and actually its expression is lower in IL 10-1 (Fig. 6.32), which is a line with consistently low trichome density (see *chapter 3*). Moreover, some of these HD-ZIP genes encode proteins homologues to fully characterised proteins with functions in trichome and cuticle development in other species, like SlHDZIP-IV 10 and AaHD1 (Yan et al., 2018) or SlHDZIP-IV 4 and GL2 (Rerie et al., 1994). This evolutionary relationship (Fig. 6.30) indicates that many of the genes are likely to work redundantly or at least in complementary ways in controlling epidermal development and metabolism and should therefore be considered new targets for research. The generation of CRISPR/Cas9 GE knock-out lines for these genes, combined with crosses to generate lines with multiple mutations will be very helpful in untangling the complex regulatory network controlled by this gene family.

In conclusion, my analysis of the newly generated GE mutants for *Woolly* and *CD2* have helped specify more precisely their roles in determination of trichome density (decrease of total trichome density in *Woolly* GE leaves and apparent increase in trichome density *CD2* GE leaves) and trichome type (reduction of type VI glandular trichome in *CD2* GE leaves that were heterozygous for the KO allele). Moreover, I have characterised new effects of the mutations, as the reduction in root hair density and root hair length in *Woolly* GE KO plants and the glossy surface of *CD2* GE heterozygous leaves. Finally, I have set out new goals for further understanding of their functions and their interaction with other major regulators of epidermal development.

6.5.2.-Genome editing of *Hairless* affects trichome morphology and causes sterility.

Hairless encodes a Specifically Rac1-Associated protein (SRA1) which forms part of the WAVE complex, a multiprotein structure responsible for actin filament formation and branching in Eukaryotes (Chen et al., 2010). Specifically, SRA1 binds to different membrane receptors and scaffold proteins which then stimulates actin nucleation via the Actin-related protein 2/3 complex (Arp2/3), which generates branched actin filaments (Chen et al., 2014). The phenotype of the *hairless* mutant consists of the presence of bent swollen trichomes, although no effect on trichome density or types of trichomes was observed (Reeves, 1977, Kang et al., 2016). This trichome phenotype is similar to that observed in mutants affecting the SRA1 and Nap (another member of the WAVE complex) proteins of *Arabidopsis* (Brembu et al., 2004). However, in the case of *Arabidopsis*, the mutations were associated with additional developmental defects, including leaf epinasty, reduction in chlorophyll levels, reduced seed set and deformed siliques

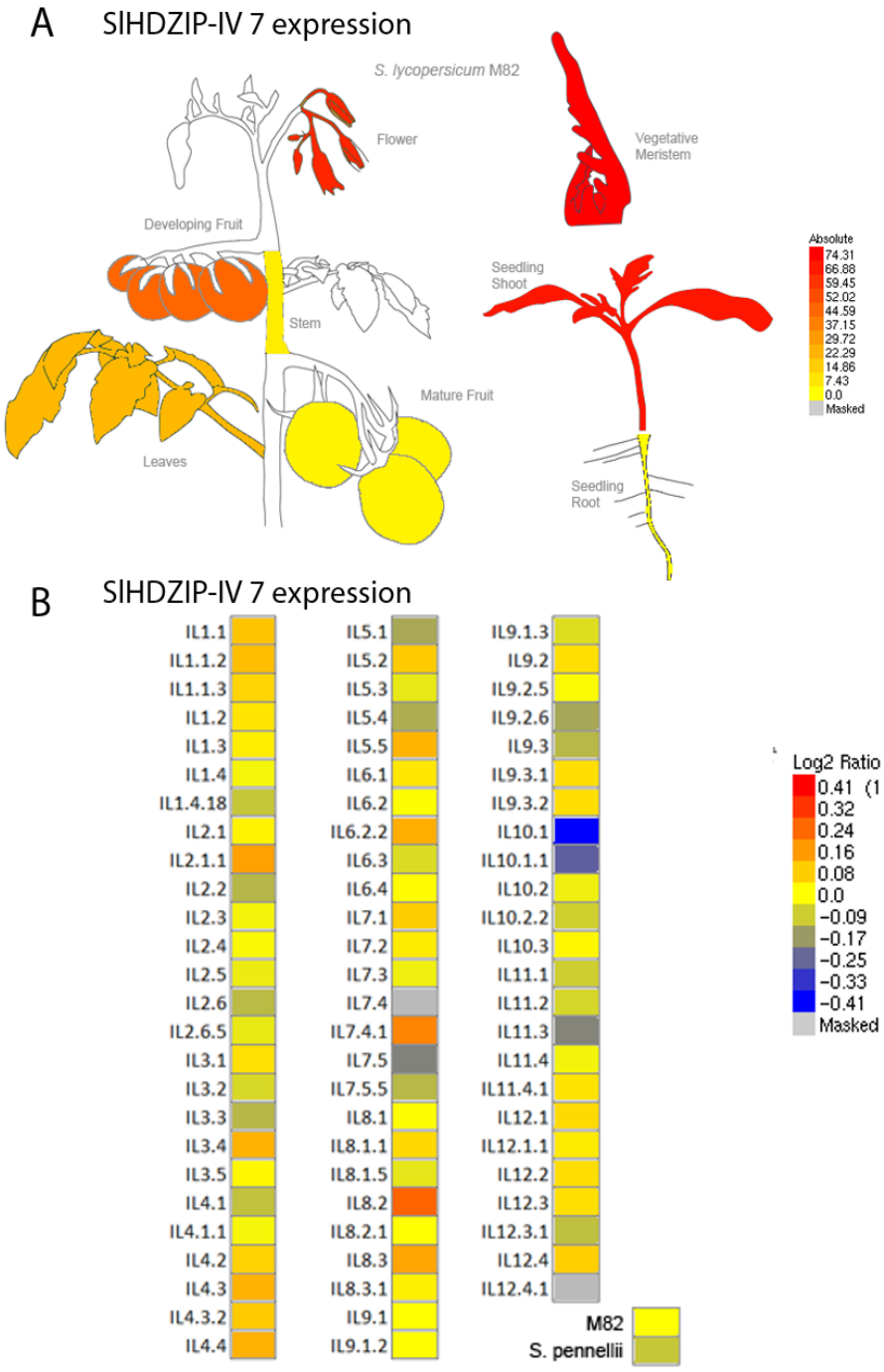

Figure 6.32.-Expression level of *SlHDZIP-IV 7* in different tissues and *S. pennellii* ILs. A) Absolute expression level of *SlHDZIP-IV 7* in *S. lycopersicum* cv. M82 based on RNAseq data generated by (Koenig et al., 2013). B) Relative expression level of *SlHDZIP-IV 7* in leaves of the *S. pennellii* ILs, from the RNAseq data generated by (Chitwood et al., 2013). The images in A and B were generated using the eFP expression browser (Winter et al., 2007).

(Li et al., 2004). In comparison, the *hairless* mutant in tomato does not present the same growth defects and shows only an increased stem fragility (Dempsey and Sherif, 1987, Kang et al., 2016). This was due to the defects in the development of the secondary walls of vascular bundles, indicating that actin dynamics might be essential to regulate the biosynthesis and deposition of cell wall components (Stratmann and Bequette, 2016). Metabolic profiling of trichomes in the *hairless* mutant of tomato showed an absence of sesquiterpenes and flavonoids typically produced by type VI trichomes, while monoterpenes, also produced in type VI trichomes, were still present (Kang et al., 2010a). The main difference between these metabolites is that both sesquiterpenes and flavonoids are produced in the cytosol of type VI trichomes, while monoterpenes are produced in plastids (Kang et al., 2016), which also points towards an important role of actin dynamics in influencing metabolism in the cytosol, perhaps by limiting the ability of the glandular cells of type VI trichomes to differentiate fully. This reduction in type VI-secreted molecules also had an effect on resistance to herbivory (Kang et al., 2010a), with a lower tolerance in *hairless* mutants.

The reason underpinning the different phenotypes observed in *Arabidopsis* and tomato WAVE complex mutants might be due to the nature of the specific mutations. In the case of tomato, the *hairless* mutation is caused by a 3 kb deletion in the last exon of the SRA1 gene. The *SRA1* gene is a long gene (approximately 46 kb) that spans two annotated genes in tomato (Solyc11g013280 and Solyc11g013290, with the first one shown in Fig. 6.8) with a total of 30 exons. Therefore, it might be predicted that the mutation does not completely eliminate the function of the SRA1 protein and maybe affects its binding affinity to specific ligands. Two binding sites for SRA1 to interact with the Rac1 GTPase, activator of the WAVE complex, have been identified (Chen et al., 2017), and both are still present in the predicted sequence of the mutated protein in tomato. This could indicate that the activation of the Arp2/3 complex downstream of the Rac1/SRA1 interaction might still occur while other interactions with membrane proteins are impaired, affecting the specificity of the actin dynamics in response to external or internal stimuli. The amino acid residues identified in the interacting surface between SRA1 and the WAVE complex interacting receptor surface (WIRS) motif (Chen et al., 2014) are present in the mutant protein, but they lie close to the C-terminus and the early STOP codon in the mutant (Kang et al., 2016), makes them more likely to be non-functional or at least affected in their binding properties. In contrast, the analysed *Arabidopsis* mutants had T-DNA insertions in the 5' UTR region and the 6th exon respectively which caused a loss-of-function mutation (Brembu et al., 2004).

I targeted the second exon of the gene in my GE approach (Fig. 6.8) and manage to generate a biallelic plant with two mutant alleles causing early STOP codons and a truncated protein (62 or

63 aa long) lacking all the important interaction motifs discussed above (Fig. 6.8 and 6.9). This line showed the *hairless* phenotype, with a clear visual aberrant surface (Fig. 6.10) and with aberrant trichomes, folded and swollen like the ones observed in the *hairless* mutant (Fig. 6.11). Apart from this, no other clear growth defect was observed in vegetative tissues or flowers. However, the plant did fail to set fruit repeatedly, and showed aborted flowers in four successively developing trusses. Thus, the mutation seems to affect either the development of pollen and/or ovules, or they might have impaired ripening of ovaries in developing fruit. The line is currently being propagated vegetatively and I plan to pollinate MoneyMaker flowers with *Hairless* GE pollen to test whether there is a defect in pollen development or whether the mutations can be maintained as heterozygotes for future studies of the T1 plants. Analysis of the expression of SRA1 in tomato indicates that it is expressed throughout fruit development at stable levels, probably indicating a constitutive function in fruits (Fernandez-Pozo et al., 2017). However, its expression occurs in all tissues at similar levels and no aberrant phenotypes were observed in stems or leaves (roots have not yet been analysed). The expression level of *Hairless* in pollen or ovules is not reported in the main databases (SolGenomics Network, (Fernandez-Pozo et al., 2015a)), but for *Arabidopsis,* the homologous gene (AtSRA1, AT2G35110) has a relatively low expression in pollen grains both during microgametogenesis and pollen germination but is highly expressed in the stigma and ovaries (Fig. 6.33). The stigma in *Arabidopsis* is covered by papillae, which are outgrowths similar to trichomes and their development may be impaired in the *AtSRA1* mutants. In tomato, the stigma is also papillate and it is wet in contrast to the dry stigma in *Arabidopsis* (Heslop-Harrison and Shivanna, 1977, Kadej et al., 1985). The mutation in the *Hairless* GE line might be affecting the development of these papillae or the production of the stigmatic secretion may be altered by the loss of *Hairless* function (in an analogous way to the change in type VI trichome composition (Kang et al., 2010a), which might prevent pollen recognition or germination. This would explain why seed set is reduced in the *Arabidopsis* mutant without causing full sterility. In any case, anatomical analysis of floral organs in the *hairless* KO mutant will be carried out when new flowers are available, and reciprocal crosses between WT and GE plants will help identify the cause of the sterile phenotype.

The absence of fruits and seeds of the *Hairless* GE line has so far prevented the analysis of T1 plants, which would have allowed the analysis of root phenotypes and quantitative epidermal analyses. Despite this, I did manage to generate a full knock-out mutant for the *SRA1* gene in tomato which has allowed the study of the effects of the mutation on trichome development and plant reproduction.

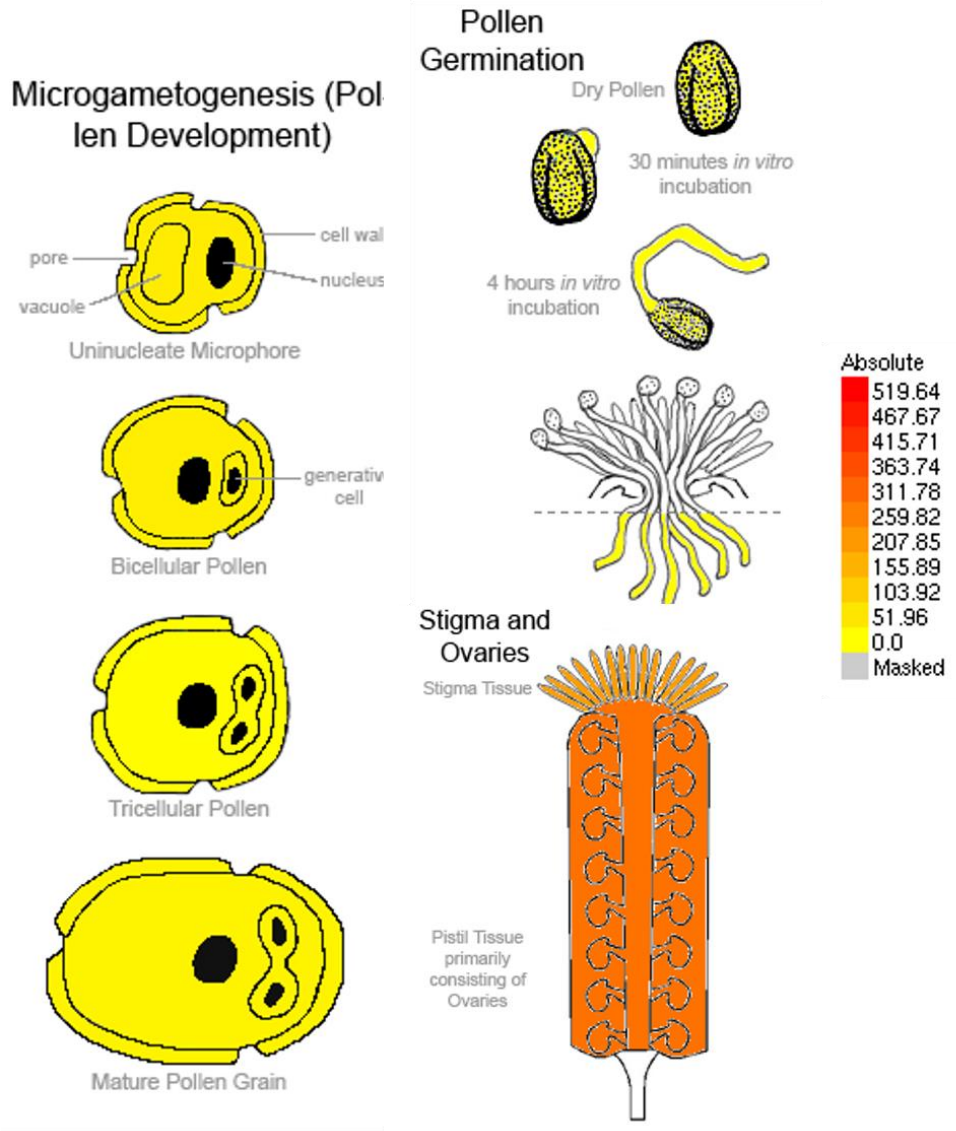

Figure 6.33.-Expression level of *AtSRA1* in pollen grains and female organs. The images were generated using the eFP expression browser (Winter et al., 2007), with data from (Honys and Twell, 2004, Swanson et al., 2005, Qin et al., 2009).

6.5.3.-Genome editing of *DWARF* causes dwarfism, delay in growth and affects pavement cell size.

DWARF encodes the enzyme responsible for the C-6 oxidation of 6-deoxocastasterone to castasterone which is the immediate precursor of brassinolide (Bishop et al., 1999), the most biologically active form of brassinosteroids (BR) (Vriet et al., 2013). Mutations in this gene have been characterised for their effects on many developmental processes. A comprehensive analysis of the physiological and developmental functions of *DWARF* and, therefore, BR was reported by (Li et al., 2016b). Among other effects, BR deficiencies were associated with a decrease in gibberellin accumulation and an increase in ethylene accumulation, a delay in germination and growth, decrease photosynthesis rate and reduced fruit lycopene (Li et al., 2016b). Moreover, *DWARF* is responsible for the semi dwarf phenotype in the widely-used MicroTom cultivar (Martí et al., 2006), which carries a mutation that causes missplicing between the last two exons of the gene (Fig. 6.12). Although there has been no clear study on the effect of BR on trichome development in tomato, a mutant affecting different branch of the BR biosynthetic pathway, *dpy* (Koka et al., 2000), in the MicroTom background showed elevated trichome density (Campos et al., 2009). Other effects of BR on epidermal development in *Arabidopsis* include regulation of pavement cell division and expansion (Zhiponova et al., 2013) and regulation of stomatal development and aperture (Gudesblat et al., 2012, Ha et al., 2016), although no clear effect of BR deficiencies has been reported on trichome development in *Arabidopsis*. The fact that trichome density is affected by BR in tomato (Campos et al., 2009) and *DWARF* is expressed in trichomes (Spyropoulou et al., 2014) led me to analyse the effect of editing of *DWARF* on trichome development in a MoneyMaker background.

I targeted the second exon of the gene (Fig. 6.12) and obtained one plant carrying a KO allele, causing a truncated protein as a result of an early STOP codon in the coding sequence (Fig. 6.12B and C). The T1 homozygous plants showed clear dwarfism (Fig. 6.13) reminiscent of the phenotype of the strong d^x allele (Bishop et al., 1999), which likely produced a knock-out allele. I observed some of the expected developmental effects of loss of *DWARF* function, such as delay in germination and growth, reduced height, reduced number of leaflets per leaf and leaf curling (Fig. 6.13) as described by (Li et al., 2016b). Interestingly, indeterminate growth was not affected (Fig. 6.16) which indicates that only the *Self-pruning* mutation in MicroTom is responsible for its determinate growth (Martí et al., 2006). Flower development was affected, with reduced size of all floral whorls (Fig. 6.14), while fruits showed a delay in ripening but with MoneyMaker-like size (Fig. 6.15). The delay in ripening might be a direct cause of a reduced accumulation of ethylene (Li et al., 2016b), which drives ripening in tomato and other climacteric fruits (Giovannoni et al., 1999). The lack of effect on fruit size (Fig. 6.15) is likely due to the presence of a second cytochrome P-450 (CYP85A3) which is able to catalyse the same reaction in fruit that

DWARF carries out in vegetative tissues (Nomura et al., 2005). This indicates that the small fruit size in MicroTom must be due to mutations of another gene than *DWARF*.

I analysed the leaf surface of *DWARF* GE lines to determine whether there were any differences in trichome development. An overview of the adaxial side of the first leaf showed no apparent difference between the GE line and MoneyMaker leaves in terms of trichome density (Fig. 6.17). All trichome types were found in the *DWARF* GE line (Fig. 6.17), indicating that BR signalling does not affect trichome identity. The extreme curling of the leaves complicated the quantitative analysis and I could not quantify stomatal and trichome density as I had done for other GE mutants. However, there was no clear effect of the mutation on trichome density (Fig. 6.17C and D). That would mean that the increase in trichome density observed in the *dpy* mutant was unlikely to be a direct consequence of the impairment of BR biosynthesis, but maybe an added effect of the double mutation in *DWARF* and *DPY*. A second explanation could be that BR has an effect on trichome density as a result of the reduction in pavement cell size and division, and therefore in leaf area. I measured the size of pavement cells and I observed a significant reduction in cell size in the *DWARF* GE line (Fig. 6.18), which would lead to a lower trichome density when calculated on the basis of area. Many studies on trichomes have been done in MicroTom due to its relatively short lifecycle and the lower resources needed to maintain MicroTom plants (Li et al., 2004, Wada et al., 2014, Zhang et al., 2015, Vendemiatti et al., 2017). My preliminary results indicate that no differences should be expected in trichome density or trichome type determination between MicroTom and other non-dwarf cultivars. A more in-depth study of the *dpy* mutant would be beneficial to determine the pathway through which trichome development is regulated by this gene. However, the effect of BR signalling in stomatal and pavement cell development, as well as the physiological and developmental effects of BR deficiency in tomato (Li et al., 2016b) might probably affect trichome development under different conditions (as observed under stress conditions described in *chapters 7 and 8*), and the use of cultivars without hormonal deficiencies might give more accurate information about how trichomes develop in *Solanum* species.

6.5.4.-Genome editing of *SlMX1* affects trichome density by reducing non-glandular trichome formation.

SlMX1 is a member of the *MIXTA/MIXTA-like* gene family. This gene is closely related to other MIXTA genes in tomato (see *chapter 5*) and to *AmMIXTA*, the first gene of the family identified in snapdragon (Noda et al., 1994). The function of *SlMX1* in tomato has been characterised by means of RNAi silencing and overexpression (Ewas et al., 2016, Ewas et al., 2017), which showed it is a positive regulator of trichome initiation in the tomato epidermis and of carotenoid

accumulation in tomato fruit. However, although effects on trichome density have been reported for RNAi lines (Ewas et al., 2017), a full picture of the role of *SlMX1* in this process is not yet available. Trichome density is expressed as number of trichomes per unit area, without taking into consideration effects on pavement cell number or size by (Ewas et al., 2017). Moreover, although the presence of different trichome types was reported, no quantitative analysis regarding type-specific effects of *SlMX1* silencing were carried out. Finally, stomatal density, tightly related to trichome density (see *chapters 7 and 8*) was not reported. Therefore, I chose *SlMX1* as one of the target genes for the production of CRISPR/Cas9 GE mutants. I targeted the first exon of the *SlMX1* gene with the aim of producing knock-out mutations in the gene (Fig. 6.19A). I obtained two different mutant alleles in the T0, the first one with a 30 bp deletion (the expected mutation delimited by the two sgRNAs) and a second one with a 4 bp deletion in the coding sequence (Fig. 6.19B). The first allele (*SlMX1* GE #1, *slmx1Δ10*) resulted in a protein lacking 10 amino acids in the N-terminal region of the transcription factor, where the DNA-binding domain is located, while the second allele (*SlMX1* GE #2, *slmx1*) led to a translation frame shift and early STOP codon, generating a truncated protein only 34 aa long (Fig. 6.19C). The *SlMX1* GE #1 allele was found to be homozygous in the T1 generation and these plants were used for the analysis carried out for this chapter. The *SlMX1* GE #2 allele was found only in heterozygotes in the T1 generation, and therefore *SlMX1/slmx1* plants were used for analysis. These results indicate that SlMX1 is essential for proper plant development, and at least one functional copy must be present in the genome for viability. Moreover, this observation suggests that *SlMX1* GE #1 is a weak allele and that the protein which it encodes retains some functionality. I did not observe a reduction in germination rate between the line carrying the *SlMX1* GE #2 allele and MoneyMaker, which seems to indicate that the homozygous knock-out mutation is not affecting embryo development but rather plays a role in gametogenesis or seed development. Reciprocal crosses with MoneyMaker and analysis of the offspring will help identify the cause of the problem. Expression of *SlMX1* does not take place in ovules or seeds (Zhang et al., 2016), suggesting that the most likely cause for the absence of homozygous plants is male sterility and analysis of pollen morphology and germination might be of interest. The generation of double haploids via in vitro culture of ovules might possibly be used as a technique to overcome this problem (Zhao et al., 2014).

I observed a visual reduction in trichome density in stems and leaves of *SlMX1/slmx1* plants (Fig. 6.20), similar to the phenotype reported for RNAi lines (Ewas et al., 2016). Moreover, I observed a semi dwarf phenotype in the two GE lines, with reduced height, slight leaf curling, wider stems, reduced number of leaves per leaflet and reduced leaf size (Fig. 6.20 and 6.21). This phenotype suggests that SlMX1 might be either a direct or indirect regulator of BR signalling. This could be

expected given the fact that the key enzyme in BR biosynthesis in tomato is expressed in trichomes (Spyropoulou et al., 2014). Also, the effect on carotenoid content in fruit reported for the RNAi line (Ewas et al., 2016) might be directly linked to the expected reduction of ethylene in BR-deficient plants in combination with a more direct regulation of genes in the pathway (Ewas et al., 2017). Assessment of the phenotype after application of exogenous BR might be of interest in determining the causes for the mild dwarfism observed. It is interesting to note that hypocotyls in the GE *SlMX1/slmx1* heterozygous plants did not show a reduction in trichome density similar to the one observed in vegetative stems (Fig. 6.21), suggesting that trichome development is differentially regulated in embryonic tissue. This phenomenon was also observed in *Woolly* GE KO lines (see *section 6.4.1*) and IL 10-2 (see *chapter 4*), which seems to indicate that *Hair, Woolly* and *SlMX1* do not regulate trichome initiation in hypocotyls. This situation is analogous to the *cpc* mutant in *Arabidopsis,* which has a reduced number of root hairs in mature roots, but which shows WT-like phenotype in the hypocotyl-root junction (Wada et al., 2015). In addition to this, cell fate determination and stomatal development seem to be regulated differentially in hypocotyls and cotyledons or leaves in *Arabidopsis* (Fuentes et al., 2012) with GL2 and CPC playing roles in stomatal development in hypocotyls but not in leaves. The development of mutants for other key players in trichome formation (Table 6.1) and generation of lines harbouring multiple mutations in these genes will be essential to understand the regulation of cell fate determination in different tissues.

A lower trichome density was also observed for both GE lines (*slmx1Δ10/slmx1Δ10* and *SlMX1/slmx1)* under the SEM (Fig. 6.22), where the number of trichomes was clearly reduced. I observed an almost complete absence of non-glandular trichomes (Fig. 6.22B and D). I analysed quantitatively the adaxial surface of MoneyMaker and *SlMX1* GE #1 and #2. I observed a similar reduction in trichome density and trichome-to-stomata ratio in both GE lines compared to MoneyMaker (Fig 6.23 and 6.24). Stomatal density did not change significantly, but we observed a trend to higher values in the GE lines. The phenotype of the homozygous GE #1 line and the heterozygous GE #2 line were comparable, reinforcing the idea that the protein encoded by the GE #1 allele retains some functionality. To determine whether the reduction in total trichome density affected all trichome types or rather was the consequence of a type-specific effect, I compared the number of each trichome type in a given area (Fig. 6.25). I found that only non-glandular trichomes were affected, with a very low non-glandular trichome number in the two GE lines. This phenotype resonates with my observations for silencing of *SlMX2*, another member of the *MIXTA/MIXTA-like* family, which also reduced total trichome density by reduction in the number of non-glandular trichomes (see *chapter 4*). In fact, both genes are very closely related phylogenetically (see *chapter 5*), and it is likely that they perform equivalent

functions and can act redundantly to some extent. However, it is also possible that the reduction in the total trichome density affects mostly non-glandular trichomes given these are the most common type in adult leaves (Fig. 6.25) (Vendemiatti et al., 2017). There might be also a post-initiation mechanism regulating trichome identity which might be controlled directly or indirectly by *SlMX1*. Different trichome types are, in any case, expected to be regulated by different factors due to observation in tobacco mutants affecting only one trichome type (Glover, 2000). Further analysis of the different stages of trichome development, coupled with analysis of double mutants for *SlMX1* and *SlMX2* will contribute to the understanding of the complex regulation of trichomes in tomato.

The expression of *SlMX1* is relatively low in most tissues (Fig. 6.34A), and an absolute null expression of the gene was reported for mature leaves (which might not be necessary after trichome initiation) and in fruit (which would indicate that maybe changes in carotenoid level are not a consequence of direct regulation but rather a side effect of changes in hormone homeostasis) (Fig. 6.34A). Interestingly, *SpMX1* was highly expressed in *S. pennellii* leaves, with a 4-fold higher expression level than *S. lycopersicum* (Fig. 6.34B). This contrasts with the situation for *SlMX2*, another member of *the MIXTA/MIXTA-like* family which has the ability to regulate trichome initiation (see *chapter 4*) and which is not expressed in *S. pennellii*, and it is unlikely that the *S. pennellii* allele encodes a functional protein due to a deletion of the gene. This indicates that both SlMX1 and SlMX2 likely perform similar functions in tomato, both showing relatively low levels of expression in the tissues where they are required, and with the ability to complement each other's activity. In *S. pennellii,* however, this activity is limited to *SpMX1* due to the loss of function of the *SpMX2* allele. Also, the higher trichome density observed in *S. pennellii* leaves (see *chapter 3*) could be explained by this increase in the expression of *SpMX1* in leaves (Fig 6.34B). In addition to this, the expression analysis of the ILs indicates that *SlMX1* expression is reduced in IL 8-1 (Fig. 6.34B), which was one of the lines I characterised for its consistent lower trichome density (see *chapter 3*). The phenotype could therefore be explained for this change in expression. The genomic region covered by IL 8-1 may therefore be a good source for candidate upstream regulators or interaction partners for *SlMX1*, that can regulate its activity to modulate trichome density in leaves. Further research on genes in this interval will contribute to the current understanding of *SlMX1* regulation.

As discussed above, *SlMX1* encodes a protein belonging to a clade which includes the protein products of other the 3 *MIXTA/MIXTA-like* genes which are closely related between them and distinct from the SlMIXTA-like clade (see *chapter 5*). These proteins are SlMX2 and SlMX3A/B, two genes on chromosome 5 (Solyc05g007690 and Solyc05g007710) which share 90% identity between their amino acid sequences and are probably the result of a direct duplication. These

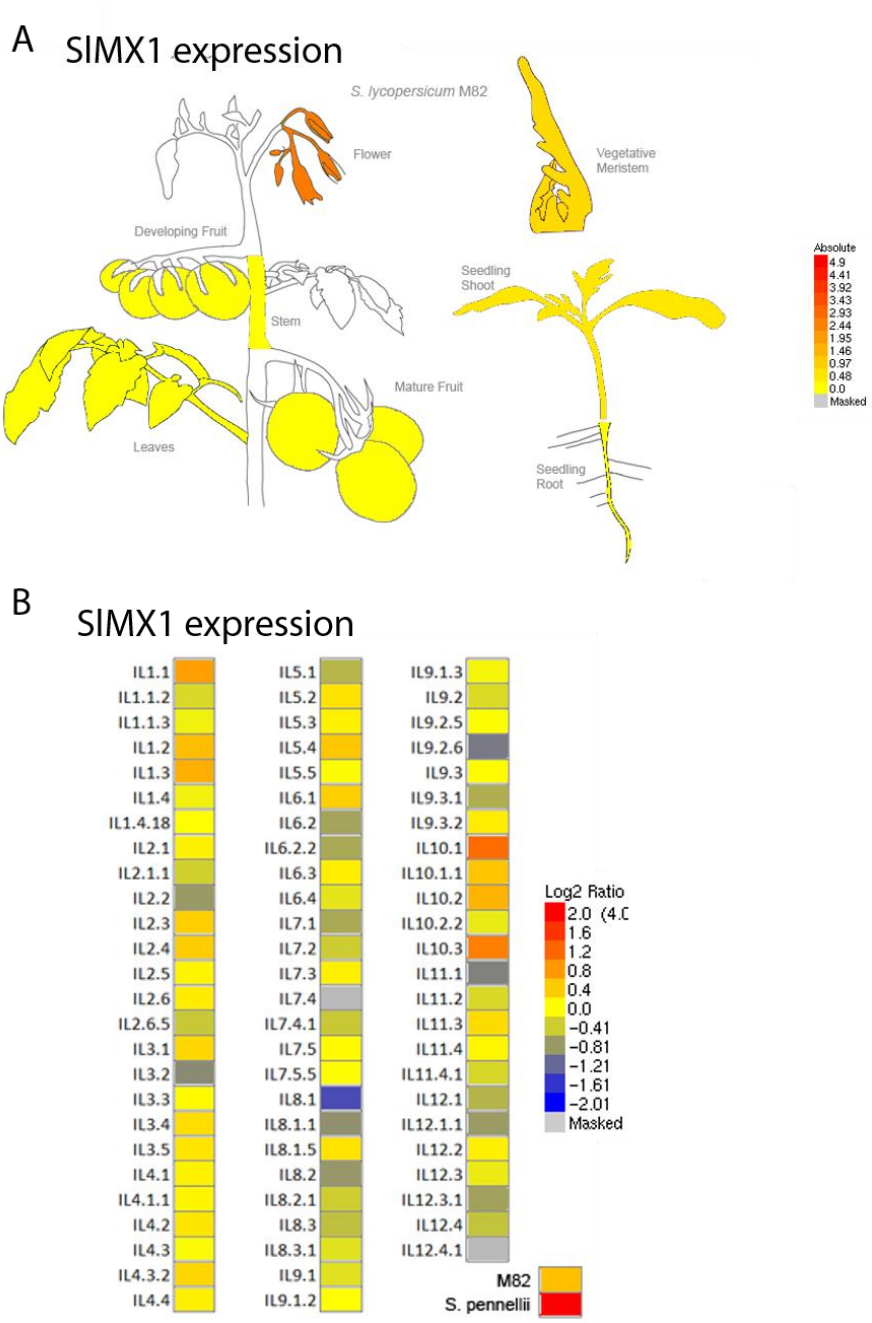

Figure 6.34.-Expression level of *SlMX1* in different tissues and *S. pennellii* ILs. A) Absolute expression level of *SlMX1* in *S. lycopersicum* cv. M82 based on RNAseq data generated by (Koenig et al., 2013). B) Relative expression level of *SlMX1* in leaves of the *S. pennellii* ILs, from the RNAseq data generated by (Chitwood et al., 2013). The images in A and B were generated using the eFP expression browser (Winter et al., 2007).

genes very likely perform redundant or complementary functions in terms of initiating and promoting trichome development.

Both *SlMX3A* and *SlMX3B* have a variable expression in the IL lines, but both of them have a consistently lower expression in ILs 4-1 and 8-1, both of which have a low trichome density (Fig. 6.35 and *chapter 3*). *SlMX3A* is expressed at higher level in M82 than in *S. pennellii* (Fig. 6.35A) while for *SlMX3B*, the expression level is similar in both species (Fig. 6.35B), which might suggest different functions for these genes in both species. The regions contained in ILs 4-1 and 8-1 have already being targeted as probably bearing regulatory loci affecting *MIXTA/MIXTA-like* gene expression following the analysis described in this thesis. Further analysis of the function of these two uncharacterised genes by silencing, GE and overexpression will be essential to achieve a clear picture of the functional overlapping and compartmentalisation of functions in trichome development in this gene family.

In conclusion, SlMX1 is a regulator of trichome initiation in tomato and affects mainly non-glandular type V trichomes. It seems to be essential for seed development and does not affect trichome development in hypocotyls. It may act redundantly with other members of the gene family, and also with HD-ZIP IV transcription factors (see section 6.4.1). Crosses between the GE lines generated and the generation of some of the remaining ones (Table 6.1) are still necessary to determine the exact function of this gene and its relationship with others.

6.5.5.-An updated model for trichome development in tomato.

The data gathered from analysis of GE KO lines as well as other assays described in *chapters 4* and *5* have provided new insights into how thrichome development is regulated in tomato, leading to the generation of an updated model of regulation of trichome initiation and trichome type determination (Fig. 6.36).

6.6.-Conclusion.

In this chapter, I generated new mutants for genes already characterised for playing role in trichome development in tomato using CRISPR/Cas9 as a tool for gene editing. I managed to obtain GE mutant alleles for *Woolly, CD2, SlMX1, Hairless* and *DWARF*, and I was able to revisit the phenotypes caused by these mutations and characterise more precisely the functions of these genes. I determined that Woolly plays a role in root hair formation and that it affects total trichome density. I observed an increase in total trichome density in CD2 GE mutants, which was accompanied by a reduction in the number of type VI trichomes. I determined that Hairless plays a role not only in trichome development but also in fruit set and that DWARF does not seem to affect trichome initiation directly, but it affects the size of pavement cells in leaves. Finally, SlMX1 affects total trichome density through a dramatic reduction in the number of non-

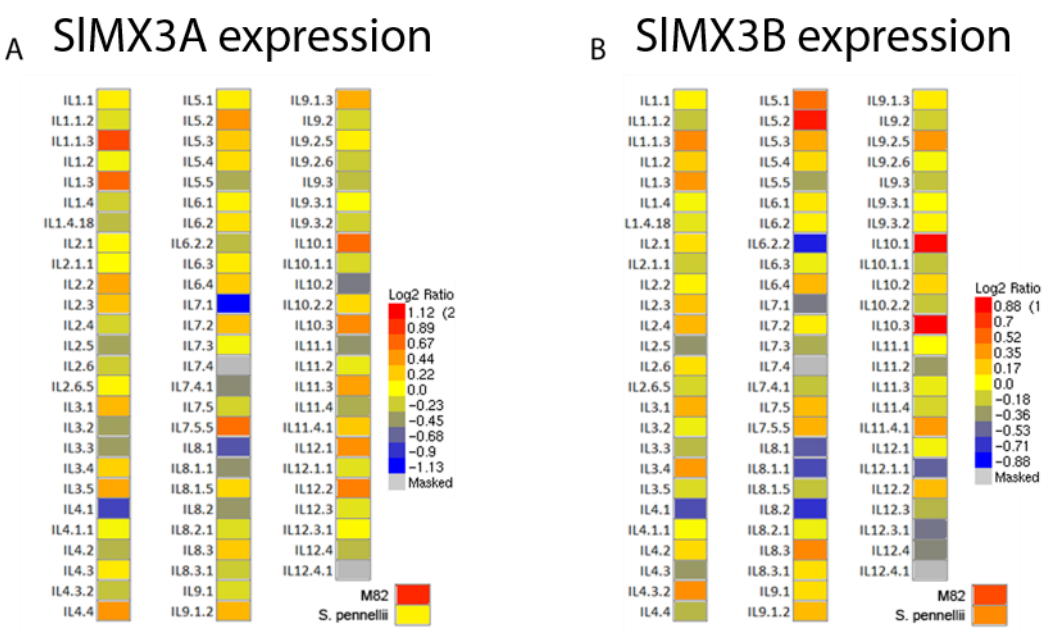

Figure 6.35.-Expression level of *SlMX3A* and *SlMX3B* in the *S. pennellii* ILs. A) Relative expression level of *SlMX3A* in leaves of the *S. pennellii* ILs, from the RNAseq data generated by (Chitwood et al., 2013). B) Relative expression level of *SlMX3B* in leaves of the *S. pennellii* ILs, from the RNAseq data generated by (Chitwood et al., 2013). The images in A and B were generated using the eFP expression browser (Winter et al., 2007).

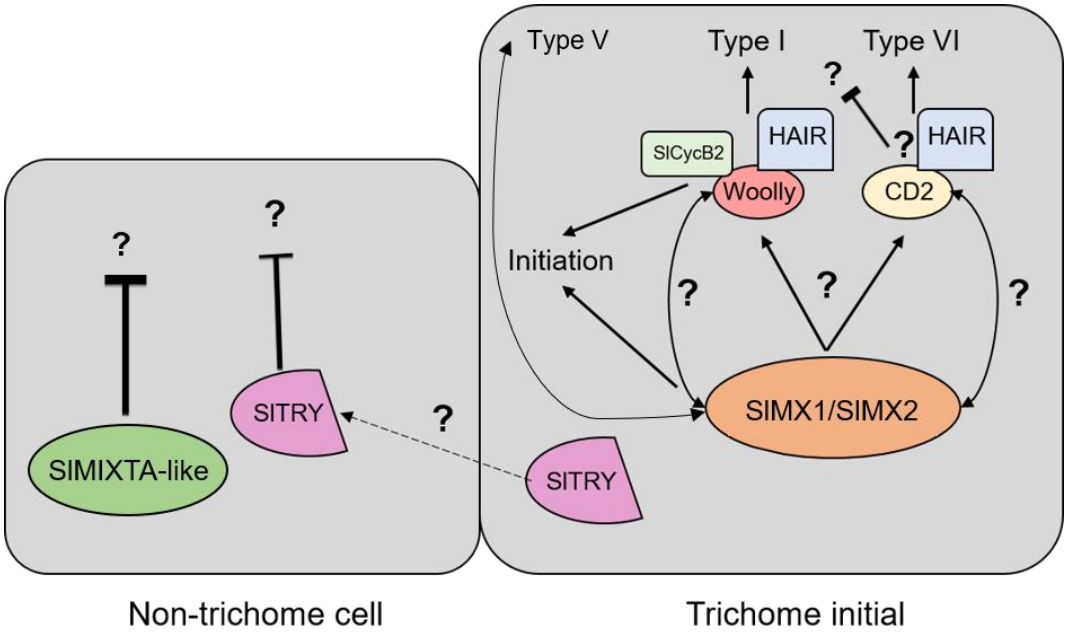

Figure 6.36.-Model for transcriptional regulation of trichome development in tomato. Initiation is activated by SlMX1 or SlMX2 and the Woolly-HAIR-SlCycB2 complex. This complex can also regulate type I trichome morphogenesis. CD2 controls type VI trichome morphogenesis and regulates the density of other trichome types. SlTRY is a negative regulator of trichome initiation and might act as the R3 MYB genes in *Arabidopsis.* SlMIXTA-like negatively regulates trichome initiation and prevents the initiation of trichomes in adjacent cells. SlMX1 and SlMX2 positively regulate non-glandular type V trichomes. Positive interactions are indicated with an arrow line and negative interactions with a T-shaped line. Question marks indicate possible interactions that have not been proved experimentally. Fine-dashed arrow indicate cell-to-cell movement.

glandular type V trichomes. I believe that all these new observations will help to untangle the complicated network governing trichome formation in tomato. My analyses have allowed the addition of new information to the current model for trichome development in tomato. Moreover, the newly created GE lines can be used for future research, especially by generating lines bearing multiple mutations via crossing of the lines described in this chapter.

Chapter 7 – Analysis of the role of trichomes and stomata on the response to drought stress

The content of this chapter is based on the peer-reviewed article "The ratio of trichomes to stomata is associated with water use efficiency in tomato" published in The Plant Journal (DOI 10.1111/tpj.14055). I have obtained written authorisation from the copyright holder, Jon Wiley and Sons, under the licence number 4407691181023 to reuse figures or text from the published article. The work described in this chapter benefitted from the contribution of our collaborators in the University of the Balearic Islands, Spain and particular contributions are indicated throughout the text.

7.1.-Abstract.

In this chapter I described the analysis of the photosynthetic activity, gas exchange and water use efficiency of selected *Solanum pennellii* x *S. lycopersicum* cv. M82 introgression lines, coupled with extensive epidermal phenotyping of leaves, performed in the field under Mediterranean conditions. The ILs were chosen based on the screen described in *chapter 3,* including lines with low trichome density (ILs 4-1 and 10-2) and high trichome density (M82 and IL 11-3). This work showed a strong link between high trichome density (and high trichome-to-stomata ratio) and water use efficiency, indicating that the epidermal structures such as trichomes and stomata can be targeted for the development of drought-tolerant tomato cultivars.

7.2.-Introduction

7.2.1.-Drought stress and its effect on tomato production.

Food production needs to be increased to meet the demand of the World's population, estimated to near 10 billion people by 2050 (United Nations, 2015). This challenge is aggravated by changes in climatic conditions, which are predicted to lead to intense drought periods in already water-limited semi-arid tropical and subtropical regions (IPCC, 2007, Berger et al., 2016), including the Mediterranean basin. Among the different biotic and abiotic stresses that reduce crop productivity, drought stress has been identified as the most limiting factor (Valliyodan and Nguyen, 2006, Mishra et al., 2012). The development of crop varieties with increased drought tolerance and improved water use efficiency (WUE) is essential to meet the challenges that agriculture will face in the near future. Understanding the mechanisms involved in responses to water stress in different commercially important crops has become a priority (Monneveux et al., 2013, Zhang et al., 2014, Todaka et al., 2015, Nakashima and Suenaga, 2017). However, drought tolerance is a complex trait that involves different key processes operating at metabolic, molecular, morphological and developmental levels. Tomato (*Solanum lycopersicum*) is one of the most important commercial crops, grown in virtually all regions of the word and with a

production of more than 150 million tonnes per year (FAO, 2014). Moreover, tomato is a high water-demanding crop (Mekonnen and Hoekstra, 2011).

Our current understanding of the response to drought in tomato is very limited, although the release of new transcriptomic datasets is contributing to generate a clearer picture of the factors involved (Iovieno et al., 2016). For example, the hormone abscisic acid (ABA) is known to drive the drought response, controlling stomatal aperture (Pantin et al., 2013) and regulating cuticle composition (Macková et al., 2013) to prevent water loss from stomatal or cuticular transpiration. Plants can also regulate their osmotic potential by accumulating organic or inorganic solutes in their leaves (Albaladejo et al., 2017). Finally, plant growth is altered under drought conditions, first limiting the growth of aerial organs as a consequence of the reduction in photosynthetic rate associated with stomatal closure and to minimise the surface for transpiration (Gargallo-Garriga et al., 2014), and promoting root growth and changes in root architecture to maximise water uptake (Uga et al., 2013). There has been a number of attempts to increase performance of tomato under water stress, by using traditional varieties (Galmes et al., 2013, Patane et al., 2016, Fullana-Pericàs et al., 2017), transgenic approaches (Hsieh et al., 2002, Zhang et al., 2011, Munoz-Mayor et al., 2012, Rai et al., 2013) and wild tomato species (Gujjar et al., 2014, Tapia et al., 2016) , with mixed results. Among the wild tomato relatives, *Solanum pennellii* has been characterised for having a high degree of drought tolerance (Kahn et al., 1993, Bolger et al., 2014). This tolerance has been associated to an ability of *S. pennellii* leaves to control water loss by reducing stomatal density and aperture, and consequently, water loss trough stomata (Egea et al., 2018), although other epidermal traits have not been analysed in terms of drought response.

The combination of these, together with new approaches, will be necessary to reach the goal of more water-use efficient tomato varieties.

7.2.2.-The role of the epidermis in response to drought stress.

In aerial organs of most terrestrial plants, including tomato (*Solanum lycopersicum*), the epidermis is scattered with stomata and trichomes, which are specialised structures that fulfil a number of physiological functions. Stomata are epidermal pores that regulate gas exchange and contribute directly to maintenance of water status. Trichomes are epidermal outgrowths with diverse roles in defence against biotic and abiotic stresses. For its function in limiting water losses, the epidermis and its specialised structures have become promising targets to improve the drought tolerance and water use efficiency (WUE) of major crops (Antunes et al., 2012, Galmes et al., 2013, Franks et al., 2015).

Stomata consist of two specialised guard cells which modulate their turgor via ABA-signalling pathways to regulate the pore aperture in response to environmental stimuli, such as light intensity or carbon dioxide concentration (Hetherington and Woodward, 2003). Uptake of atmospheric CO_2 and water losses occur through stomatal pores, and therefore, stomatal size and density directly determine photosynthesis activity and stomatal conductance to water, affecting water use efficiency (WUE). The effect of differences in stomatal density and size, and its relationship to drought tolerance, have been widely studied and reports are available for a number of species (Masle et al., 2005, Lawson and Blatt, 2014). For instance, some studies indicated a strong link between low stomatal density and improved performance under water deficit conditions. For example, in *Arabidopsis thaliana*, the *atdtm1* mutant had lower stomatal density and high tolerance to severe water deficit (Zhao et al., 2017). Soybean overexpressing the transcription factor GsWRKY20 displayed lower stomatal density and improved drought tolerance (Ning et al., 2017). A similar effect in stomatal density and fitness under drought conditions was observed in tomato lines overexpressing the enzyme CKX3 (Farber et al., 2016). Regarding stomatal size, smaller stomata have been associated to a faster stomatal response and improved ability to adapt to environmental stress (Drake et al., 2013). In addition, stomatal density changes in plants subjected to water stress (Hamanishi et al., 2012). Reductions in stomatal density in water-stressed plants have been reported in wheat (Li et al., 2017) and umbu tree (Silva et al., 2009). For other species, on the contrary, stomatal density increases under drought conditions, as in common bean (Gan et al., 2010) and *Leymus chinensis* (Xu and Zhou, 2008). Moreover, developmental negative associations between stomatal density and size have been reported (Galmés et al., 2007, Franks and Beerling, 2009, Khazaei et al., 2010, Li et al., 2017). However, for Mediterranean tomato varieties, a positive correlation between these parameters has been observed under stress conditions (Galmes et al., 2013). All these contradictory reports suggest that the effect of water deficit on stomatal density and size differ in different species and cultivars, and the effect of these changes on WUE must be researched further.

A role for trichomes in tolerance and adaptation to limitations in water availability has been proposed and researched in a number of species. In *Arabidopsis lyrata*, trichome production has been linked to improved performance under drought conditions (Sletvold and Ågren, 2012). In tomato, SlMX1-overexpressing plants with high trichome density showed tolerance to water stress compared to unmodified plants (Ewas et al., 2016). In watermelon, wild, drought-tolerant genotypes have increased trichome density compared to domesticated, drought sensitive varieties (Mo et al., 2016). In addition, trichome formation is induced upon drought in several species, such as barley (Liu and Liu, 2016), aubergine (Fu et al., 2013) and olive (Boughalleb and

Hajlaoui, 2011). In addition to this, transcriptomic analysis of drought-stressed *Arabidopsis thaliana* (Bechtold et al., 2016) showed upregulation of genes related to trichome development as TT8 (Baudry et al., 2006) or KAK (Patra et al., 2013), indicating an important role for trichomes in the response to drought. The specific function of trichomes in terms of drought tolerance is, however, unclear. It has been suggested that trichomes limit H_2O losses by transpiration through an increase of the leaf-air boundary layer resistance (Palliotti, 1994, Guerfel et al., 2009, Mo et al., 2016b), although this could also affect CO_2 uptake negatively, reducing the photosynthetic rate and the water use efficiency. Trichomes also protect leaves from UV-related photoinhibition (Savé et al., 2000, Galmés et al., 2007b) and prevent leaf overheating (Ehleringer and Mooney, 1978). In specialised plants, especially *Bromeliads* lacking roots, trichomes are used for direct leaf water uptake from dew or fog (Ohrui et al., 2007, Pina et al., 2016). These findings suggest an important role for trichomes in plant water relations.

Finally, the cuticle covers the epidermal surface, and its thickness as well as wax and cutin composition are determinant factors in limiting water loss through extra-stomatal transpiration (Riederer and Schreiber, 2001). Drought stress has been reported to increase cuticle thickness and cause an increase in the content of alkanes in wheat (Bi et al., 2017). In tomato, ABA regulates the cuticle thickness and cutin composition in leaves and fruits (Martin et al., 2017), indicating an important role under drought conditions. It is interesting to note that genes involved in cuticle formation are also linked to trichome and stomatal development, as AtMYB16 and AtMYB106, both playing roles in cuticle deposition and trichome initiation and branching (Baumann et al., 2007, Gilding and Marks, 2010, Oshima and Mitsuda, 2013). In tomato, this is the case of SlMYB16, a direct regulator of cuticle deposition (Lashbrooke et al., 2015) which regulates trichome initiation and patterning, as well as stomatal development (see *chapter 5*) or CD2, which regulates cutin biosynthesis and affects glandular trichome density (Nadakuduti et al., 2012) and possibly non-glandular trichome density (see *chapter 6*). Whether these epidermal traits are directly regulated by these transcription factors or the observed phenotypes are collateral effects of the regulation of other pathways (ABA-signalling, for example) remains to be determined, and further investigation will be required.

In this chapter, I describe the response to drought of selected lines from the *S. pennellii* x *S. lycopersicum* cv. M82 introgression line (IL) population, based on their different trichome phenotypes, and the potential of these to generate lines with improved water use efficiency. I also describe the effect of drought stress on epidermal development, with an emphasis on changes in trichome and stomatal densities.

7.3.-Methods

7.3.1.-Plant material.

Three ILs from the *S. pennellii* IL population were selected based on the trichome phenotype, as characterised in *chapter 3*: IL 4-1, IL 10-2 and IL 11-3. The phenotype of each lines in indicated in Table 7.1. Plants for these ILs were grown alongside *S. lycopersicum* cv. M82, the cultivated parent of the IL population, as a control line. The trichome density on the adaxial and abaxial epidermis of the first fully-expanded true leaf was analysed to determine whether their values were comparable (Fig. 7.1), and I observed no differences between trichome density on both leaf surfaces and a strong correlation between trichome density values for both surfaces, which led me to use adaxial values for the assays described in this chapter.

7.3.2.-Growth conditions in glasshouse and field experiments.

Seeds from the four lines were germinated and grown for four weeks in greenhouses at the University of the Balearic Islands (UIB, Majorca) with natural light and average maximum temperatures of 25 °C. Twelve plants per line were placed outdoors in the UIB experimental field for acclimation for 2 weeks before being transferred to 50 L pots containing a mixture of bog peat-based horticultural substrate (Prohumin-Potting Soil Klasmann-Deilmann, Projar S.A., Valencia, Spain) and perlite (granulometry A13, Projar S.A., Valencia, Spain) in a 4:1 proportion (v/v). The environmental conditions were as follows: with average daily temperatures (°C) of 22.8 ± 0.3, 25.7 ± 0.3, 25.0 ± 0.2 and 22.7 ± 0.4; average daily minimum temperatures (°C) during the day of 16.5 ± 0.5, 20.3 ± 0.3, 19.5 ± 0.4 and 17.8 ± 0.4, and average daily maximum temperatures (°C) of 31.1 ± 0.4, 35.5 ± 0.4, 33.5 ± 0.3 and 34.7 ± 0.6 respectively for June, July, August and September. Plants were watered to field capacity every other day and fertilized weekly with 50% Hoagland's solution for two months before beginning the drought treatment.

Plants were subjected to two different water regimes: well-watered (WW) and water deficit (WD). Watering regimes and plant water consumption were monitored by weighing and watering the potted plants every two days. For the WW treatment, four plants per line were maintained at field capacity, with a pot water content ranging between 100 % field capacity just after irrigation (corresponding to 9.3 L of water per pot) and 69.3 ± 0.1 % field capacity (on average throughout the treatment period) (Fig. 7.2). For the WD treatment, irrigation of four plants was progressively reduced until halving the pot water content compared to WW plants. Then, WD plants were maintained at a pot water content ranging between 30.3 ± 0.1 % field capacity before irrigation and 46.3 ± 0.1 field capacity after irrigation (Fig. 7.2). The four remaining plants per line were used for biomass-related measurements. The total water supplied and dry biomass of each plant was recorded upon experiment completion (Table 7.2). Three weeks were allowed from treatment application for the development of new leaves under

IL	Phenotype first generation	Phenotype second generation
M82	Standard for trichome density	Standard for trichome density
4-1	Low trichome density, no type VI trichomes	Low trichome density
10-2	Low trichome density, aberrant trichomes	Average trichome density, aberrant trichomes
11-3	Average trichome density	High trichome density

Table 7.1.-Introgression lines (ILs) selected for drought tolerance assays. For each IL, the phenotype observed in the screens of the two generations of the IL populations, as described in *chapter 3*, is included.

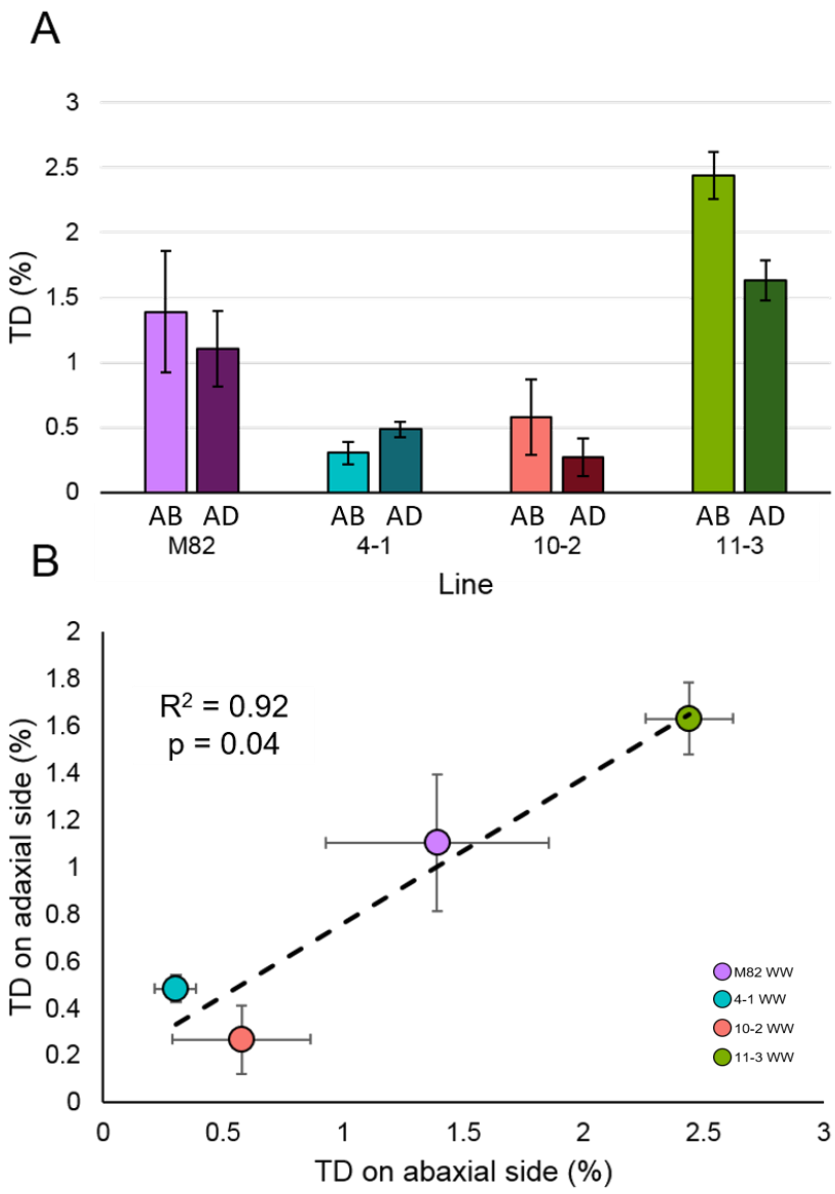

Figure 7.1.-Trichome densities on abaxial and adaxial sides of leaves of M82, IL4-1, IL10-2 and IL11-3 grown under greenhouse conditions. (A) Trichome density for the abaxial (light colours, labelled AB) and adaxial (dark colours, labelled AD) sides of leaves are shown for M82 (purple), IL4-1 (turquoise), IL10-2 (pink) and IL11-3 (green) plants grown under greenhouse conditions (n=3). (B) The correlation between trichome density on the abaxial and adaxial sides is shown, colour-coded as in A. The Pearson correlation index is shown in the graph.

	WW		WD	
	Dry biomass (g)	Total water supplied (kg)	Dry biomass (g)	Total water supplied (kg)
M-82	75.1 ± 6.5^{a}	52.3 ± 1.8^{ab}	80.5 ± 4.4^{ab}	39.4 ± 0.6^{a*}
4-1	78.0 ± 3.2^{a}	56.4 ± 1.0^{a}	65.4 ± 1.1^{b*}	40.7 ± 0.9^{a*}
10-2	92.0 ± 5.5^{a}	54.7 ± 1.8^{ab}	90.1 ± 10.5^{a}	40.7 ± 2.7^{a*}
11-3	79.3 ± 3.3^{a}	49.6 ± 1.2^{b}	85.7 ± 2.0^{ab}	35.8 ± 1.0^{a*}

Table 7.2.-Dry biomass and total water supplied to plants upon experiment completion for lines M82, IL 4-1, IL 10-2 and IL 11-3. Dry biomass and total water supplied are expressed as mean±SE of four plants per line and treatment. Analysis of variance (ANOVA) was used to test for differences between lines. Different letters represent statistically significant differences according to Tukey test (P<0.05) within each treatment. Stars indicate significant differences between treatments for each line.

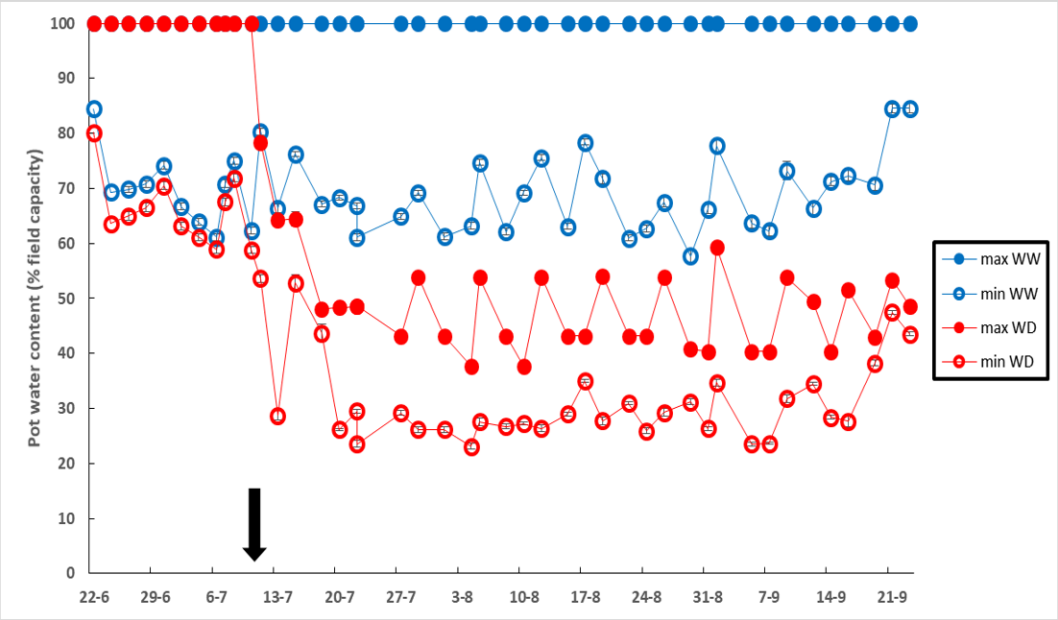

Figure 7.2.-Evolution of the pot water content during the experiment for the WW (blue) and WD (red) plants. Empty dots correspond to the minimum value (i.e., just before irrigation) and solid dots represent the maximum value (i.e., just after irrigation) after treatment establishment. The arrow indicates when the treatment application started (11th July). All values are averages ± S.E. considering all the plants for each treatment.

the new water regime before any measurement was performed. The distinct water regimes were maintained by Pere Antoni Mulet.

7.3.3.-Epidermal characterisation.

I used the data generated in *chapter 3* as glasshouse values of trichome density, stomatal density and trichome to stomata ratio for comparison between the epidermal features of the selected lines in the glasshouse and the field. For field characterisation of the epidermis on plants grown under field condition before drought onset, I used terminal leaflets of fully-expanded leaves at the same position from six plants per line. For characterisation after drought treatment, I sampled three plants per line and treatment. Leaf sections of 0.5 x 0.5 cm were taken as samples. The adaxial surface of these sections was imaged at room temperature, without coating inside a Hitachi 3400N variable pressure SEM (Hitachi High-Tecnhology, Japan). We generated 8-10 micrographs of approximately 0.3 mm^2 per sample and trichomes, stomata and pavement cells were counted manually. Trichome and stomatal density were expressed as percentage of total epidermal cells and in terms of number per unit area. Trichome to stomata ratio was calculated by dividing trichome density by stomatal density. Stomatal size was calculated as pore length, using the Fiji software (Schindelin et al., 2012) for image analysis.

7.3.4.-Plant water status and growth measurements

Plant water status was measured as midday leaf water potential (Ψ_{leaf}) (n=4 per line and treatment) using a Scholander pressure chamber as described by (Turner, 1988).

For calculation of the whole-plant water use efficiency (WUE_b), four plants per line were harvested at the time of drought treatment application. Seventy-four days after treatment application, four plants per line and per treatment (WW and WD) were harvested. Leaves, shoots and roots were oven-dried at 60 °C and weighed (dry weight, DW). The biomass production during the drought treatment was calculated as the difference between the dry weight of the plants harvested at the end of the experiment (DW_{final}) and the dry weight of the plants harvested before treatment application ($DW_{initial}$). Water consumption was monitored every other day by gravitational means and the total water consumption (TWC) of each plant was estimated from these values. WUE_b was calculated as follows:

$$WUE_b = \frac{DW_{final} - DW_{inital}}{TWC}$$

Mateu Fullana-Pericas contributed to collect data for the described assays.

7.3.5.-Leaf morphological determinations.

Leaf thickness (*LT*) was measured using callipers at the terminal leaflet of a young fully-expanded leaf with callipers. Leaf mass area (*LMA*) was calculated from the same terminal leaflets, as the

dry mass to leaf area ratio. Dry mass was measured by weighing after oven-drying leaves at 60 °C for 48 h. The leaf area was digitally measured from pictures of the leaves using Fiji (Schindelin et al., 2012). Both *LT* and *LMA* were measured for one leaf per plant (n=4 per line and treatment).

Mateu Fullana-Pericas contributed to collect data for the described assays.

7.3.6.-Leaf gas exchange measurements.

Measurements were performed with an open infrared gas-exchange analyser equipped with a leaf chamber fluorometer (Li-6400-40, Li-Cor Inc, Lincoln, USA) from 9:00 to 12:00 and 16:00 to 19:00. The conditions in the chamber consisted of leaf temperatures of 31-33 °C, vapour pressure deficit of 2.0-3.0 kPa and an air flow of 500 µmol (air) min^{-1}. For net CO_2 assimilation rate-substomatal CO_2 concentration (A_N-C_i) curves, the ambient concentration of CO_2 in the chamber (C_a) was set at 400, 0, 50, 100, 200, 300, 600, 900, 1500, 2000 and 400 µmol CO_2 mol^{-1} air, at a saturating photosynthetic photon flux density (PPFD) of 1500 µmol m^{-2} s^{-1} (with 10% blue light) allowing 4 min between measurements for the chamber to reach a steady state. Corrections for CO_2 leakage in and out of the leaf chamber of the Li-6400-40 were applied to all gas-exchange data, as described by (Flexas et al., 2007).

Mesophyll conductance to CO_2 (g_m) was estimated according to (Harley et al., 1992) as

$$g_m = \frac{A_N}{C_i} - \frac{\Gamma^*[ETR + 8(A_N + R_L)]}{ETR - 4(A_N + R_L)}$$

where Γ^* is the chloroplast CO_2 compensation point in the absence of day respiration, *ETR* is the electron transport rate, and R_L is the rate of non-photorespiratory CO_2 evolution in the light. *ETR* and R_L were calculated as described by (Galmes et al., 2011). Γ^* was retrieved from *in vitro*-based measurements for *S. lycopersicum* by (Hermida-Carrera et al., 2016), and adjusted for the leaf temperature during measurement.

Total leaf conductance (g_{tot}) was calculated assuming the stomatal conductance (g_s) and mesophyll conductance (g_m) were in series, such that:

$$g_{tot} = \frac{1}{\frac{1}{g_s} + \frac{1}{g_m}}$$

A_N-C_i curves were transformed into A_N-chloroplastic CO_2 concentration (C_c) curves using estimated values of g_m. From A_N-C_C curves, the maximum velocity of Rubisco carboxylation (V_{cmax}) was calculated as described by (Bernacchi et al., 2002), but using specific values of Rubisco kinetics for *S. lycopersicum* adjusted to the measured leaf temperature during measurement (Hermida-Carrera et al., 2016). The intrinsic water use efficiency (WUE_i) was calculated as the ratio between the net photosynthetic rate (A_N) and the stomatal conductance (g_s), A_N/g_s.

We determined the daily carbon fixation rate (*C 24h*) by measuring the net CO_2 exchange rate at 2 h intervals over 24 h. These measurements were performed after drought treatment (n=4 per line and per treatment) using an open infrared gas-exchange analyser equipped with a clear chamber (Li-6400-40, Li-Cor Inc, Lincoln, USA). Three measurements were performed at ambient CO_2 and light and averaged per plant and time point. The daily fixation rate was calculated as the integral value for the curve generated by the point measurements.

Mateu Fullana-Pericas contributed to collect data for the described assays.

7.3.7.-Determination of leaf δ ^{13}C isotope composition

The dried leaves used to calculate LMA were ground to fine dust for determination of carbon isotopic composition. Samples were subjected to combustion in an elemental analyser (Thermo Flash EA 1112 Series, Bremen, Germany) and CO_2 was injected into a continuous-flow isotope ratio mass spectrometer (Thermo-Finnigan Delta XP, Bremen, Germany). Peach leaf standards (NIST 1547) were run every six samples. The standard deviation of the analysis was <0.2%. These measurements were made by Mateu Fullana-Pericas.

7.3.8.-Statistical analysis.

I used univariate analysis of variance (ANOVA) to assess the differences between lines and treatments. I used a Tukey test as a post-hoc test to call significant differences between lines or treatments, setting the p-value cut-off at 0.05. The relationship between variables in each experiment was determined by correlation coefficient (R^2). I used R software and the R package *agricolae* (https://tarwi.lamolina.edu.pe/~fmendiburu/) for all statistical analysis.

7.4.-Results.

7.4.1.-Characterisation of epidermal features of selected lines under glasshouse and field conditions before drought treatment.

I selected three ILs which had differences on their trichome phenotype according to my observations, as described in *chapter* 3 and summarised in Table 7.1.

I characterised the epidermal features of the three selected ILs (4-1, 10-2 and 11-3) and the parental line M82 in plants grown under full field capacity conditions in the field before the onset of water deficit conditions and compared it to the data I generated for glasshouse-grown plants (Fig. 7.3). Under glasshouse conditions, ILs 4-1 and 10-2 showed a low trichome density phenotype while M82 and IL 11-3 showed a higher trichome density phenotype. Although field-grown plants displayed substantially higher TD than greenhouse-grown plants, IL 4-1 had lower trichome density than IL 11-3 and M82, and IL 11-3 had higher trichome density than IL 10-2 and 4-1 (Fig. 7.3A). I also observed differences among lines in their stomatal densities. Under greenhouse conditions, IL 4-1 had higher stomatal density than M82 and IL 10-2, and M82 had

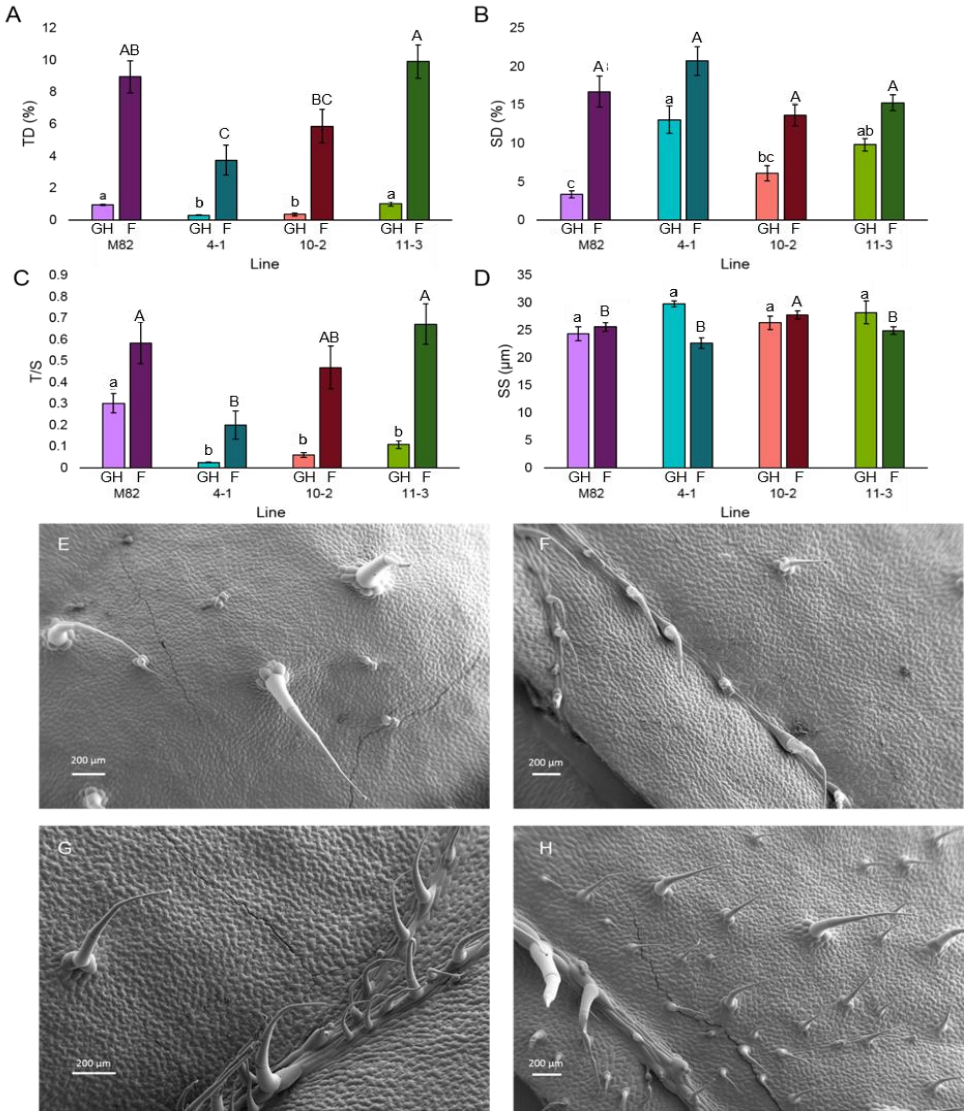

Figure 7.3.-Initial morphological characterisation of lines M82, 4-1, 10-2 and 11-3 grown under greenhouse (GH) and field conditions (F) before the onset of drought treatment. (A) Trichome density (TD), (B) stomatal density (SD), (C) trichome-to-stomata ratio (T/S) and (D) stomatal size (SS) are expressed as mean ± SE of three to six replicates per line and treatment. TD and SD were calculated as percentage of total epidermal cells. SS was calculated as pore length. Different letters denote statistically significant differences by Tukey analysis (P<0.05) within greenhouse-grown plants (lower case) and field-grown plants (upper case). For panels A, B, C and D purple bars represent M82, turquoise represents IL4-1, red represents IL10-2 and green IL11-3, with light and dark colours representing greenhouse (labelled GH) and field (labelled F) conditions, respectively Representative scanning electron micrographs for each line are shown: (E) M82, (F) 4-1, (G) 10-2 and (H) 1

a lower stomatal density than IL 11-3 and 4-1. In field-grown plants, no significant differences were observed between lines for stomatal density (Fig. 7.3B).

I calculated the ratio of trichomes-to-stomata (T/S) as an integrative parameter for epidermal anatomy. I observed a substantially higher T/S in M82 compared to the other lines under greenhouse conditions, whereas in field plants, IL 4-1 showed lower T/S than M82 and IL 11-3 (Fig. 7.3C). Stomatal size showed no significant differences between lines under greenhouse conditions. Under field conditions, however, IL 10-2 had a larger stomatal size than the other lines under study. Unlike the higher values observed for trichome and stomatal density in field-grown plants compared to greenhouse plants, SS values were within a similar range under both growth conditions (Fig. 7.3D). In general, the analysis of epidermal features and the comparison between greenhouse- and field-grown plants indicated stable genetic components in the determining of trichome density.

7.4.2.-Characterisation of photosynthetic parameters of selected ILs under field conditions before drought treatment.

I examined whether there were differences in parameters related to gas exchange, carbon fixation and RubisCO kinetics between the lines under study. We observed no significant differences in net photosynthetic rate (A_N), daily carbon fixation rate (*C24h*), stomatal conductance (g_s), leaf mesophyll conductance (g_m), leaf total conductance (g_{tot}), maximum RubisCO carboxylation rate (V_{cmax}) or intrinsic water use efficiency (WUE_i) (Table 7.3), although we observed a trend to a lower WUE_i in IL 4-1 compared to M82 (p-value < 0.06).

7.4.3.-Characterisation of epidermal phenotype under different water regimes.

In samples collected from lines under water deficit conditions, IL 4-1 showed lower trichome density than the other lines (Fig. 7.4A). Leaves that developed under water-deficit conditions showed a higher trichome density in ILs 4-1 and 11-3 compared to leaves developed under well-watered conditions. There were no significant differences for stomatal density between lines under water-deficit conditions. The ratio of trichome to stomata (T/S) was significantly lower in IL 4-1 compared to IL 11-3 (Fig. 7.4B). Although differences in T/S between well-watered and water-deficit plants were not significant, there was a trend for higher T/S under water-deficit conditions for IL 11-3 (p-value<0.1). In leaves developed under water-deficit conditions, stomatal size showed no significant differences between lines, but IL 4-1 had lower stomatal size in leaves developed under water-deficit conditions compared to well-water values. (Fig. 7.4C). For the rest of the lines, no significant differences were observed when comparing the two water regimes. I observed no relationship between trichome and stomatal density when all data points were considered together but I observed an inverse association between these parameters in water-deficit plants (R^2=0.94 P-value=0.03, Fig. 7.4D).

	A_N	C 24h	g_s	g_m	g_{tot}	V_{cmax}	WUE_i
Acc.	µmol CO_2 $m^{-2}s^{-1}$	mol CO_2 m^{-2} day^{-1}	mol H_2O $m^{-2}s^{-1}$	mol CO_2 $m^{-2}s^{-1}$	mol CO_2 m^{-2} s^{-1}	µmol CO_2 $m^{-2}s^{-1}$	µmol CO_2 mol^{-1} H_2O
M-82	17.1 ± 1.16 [a]	0.45 ± 0.03 [a]	0.29 ± 0.046 [a]	0.10 ± 0.015 [a]	0.075 ± 0.016 [a]	262 ± 4.26 [a]	58.04 ± 3.70 [a]
4-1	19.7 ± 1.35 [a]	0.46 ± 0.07 [a]	0.43 ± 0.027 [a]	0.13 ± 0.004 [a]	0.107 ± 0.013 [a]	240 ± 2.76 [a]	46.34 ± 2.68 [a]
10-2	19.4 ± 1.26 [a]	0.42 ± 0.04 [a]	0.30 ± 0.026 [a]	0.13 ± 0.015 [a]	0.088 ± 0.006 [a]	313 ± 5.29 [a]	66.22 ± 7.09 [a]
11-3	22.1 ± 1.43 [a]	0.49 ± 0.04 [a]	0.35 ± 0.026 [a]	0.14 ± 0.017 [a]	0.102 ± 0.004 [a]	363 ± 6.92 [a]	64.64 ± 4.56 [a]

Table 7.5.-Leaf morphological traits and photosyntetical characterization of the lines M82, 4-1, 10-2 and 11-3 under field conditions before the onset of the drought treatment. Net CO_2 assimilation rate (A_N), daily carbon fixation rate (C 24h) stomatal conductance (g_s), mesophyll conductance (g_m), total carbon conductance (g_{tot}), maximum velocity of Rubisco carboxylation (V_{cmax}) and intrinsic water use efficiency (WUE_i) are expressed as mean±SE of five measurements per line. Analysis of variance (ANOVA) was used to test for differences between lines. Different letters represent statistically significant differences according to Tukey test (P<0.05).

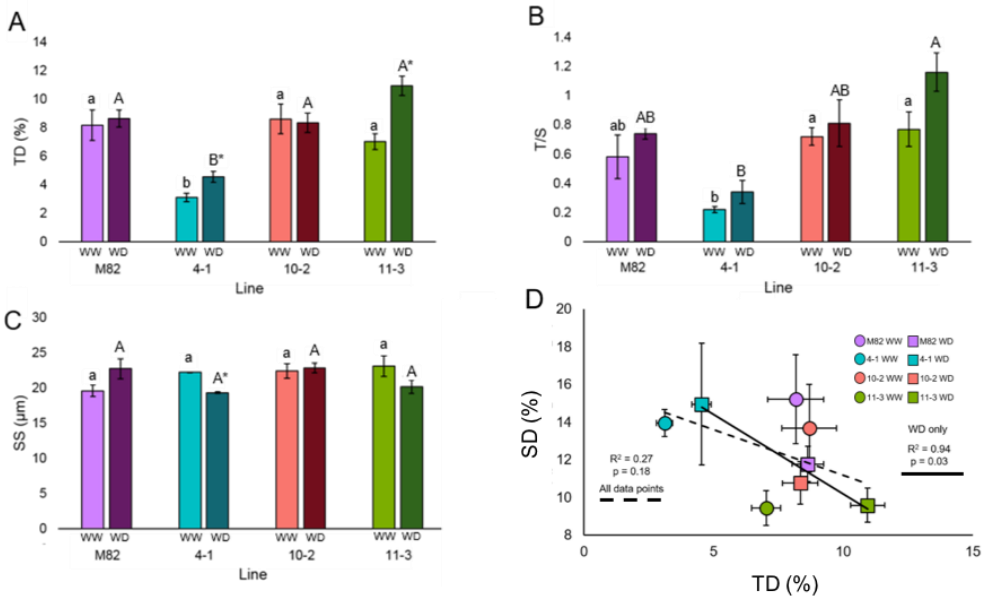

Figure 7.4.-Characterisation of epidermal features in lines M82, 4-1, 10-2 and 11-3 under water deficit (WD) and well-watered (WW) conditions in the field. (A) Trichome density (TD) is expressed as a percentage of the numbers of trichomes per epidermal cell. (B) Trichome-to-stomata ratio (T/S) is expressed as the total number of trichomes divided by total number of stomata in a given area. (C) Stomatal size (SS) is expressed as pore length. Different letters denote statistically significant differences identified by Tukey analysis (P<0.05) within WW plants (lower case) and WD plants (upper case). Asterisks represent significant differences for each line between treatments according to the Tukey test (P<0.05). (D) A correlation between TD and SD was observed only under WD conditions according to Pearson test (P<0.05) with the correlation index shown in the graph. For panels A, B and C, purple bars represent M82, turquoise represents IL 4-1, red represents IL 10-2 and green IL 11-3, with light and dark colours representing WW and WD treatments, respectively. In panel D, squares represent WD values and circles represent WW values, and are colour coded as in panels A, B and C. Dashed line represents the regression line for all data point (P>0.05) and the solid line represents the regression line for WD data points (P=0.03). Values are mean ± SE (n=3).

7.4.4.-Comparative analysis of morphological, photosynthetic and water status parameters under different water regimes.

I evaluated the effects of differences in the densities of trichomes on water status of plants under well-watered and water-deficit conditions in the field. We observed a lower midday leaf water potential (Ψ_{leaf}) in IL 10-2 compared to M82 and IL 11-3 under WW conditions (Table 7.4). Under water-deficit conditions, IL 11-3 had higher Ψ_{leaf} than IL 10-2. All lines showed a lower Ψ_{leaf} under water-deficit conditions except for IL 11-3, where no difference was observed. The leaf mass area (*LMA*) was lower in ILs 4-1 and 11-3 under water-deficit conditions compared to the other lines, but I observed no differences among lines under well-watered conditions or between water regimes (Table 7.4). Leaf thickness (*LT*) was higher in IL 11-3 compared to IL 4-1 under well-watered conditions, but under water-deficit conditions, *LT* in IL 11-3 was significantly lower than in IL 10-2 (Table 7.4). Whole-plant water use efficiency (WUE_b) showed no differences between lines under well-watered conditions (Table 7.4). Under water-deficit conditions, WUE_b was lower in IL 4-1 compared to IL 11-3. In M82 and IL 11-3, WUE_b was higher in water-deficit plants compared to well-watered plants.

A_N, *C 24h*, g_s, g_m, g_{tot}, V_{cmax} and WUE_i showed no significant differences between lines under well-watered conditions in the field (Table 7.5). In contrast, under WD conditions, IL 4-1 had a significantly lower WUE_i than the other lines. IL 11-3 had a significantly higher WUE_i in water-deficit compared to well-watered conditions (Table 7.5). The leaf carbon isotope composition (δ^{13C}) showed no significant differences between lines within each treatment or between treatments for any line. However, leaf δ^{13C} correlated with WUE_i (R^2=0.67, p-value=0.01) (Fig. 7.5A). We also observed a tight positive correlation (R^2=0.66, p-value=0.01) between WUE_i and WUE_b (Fig. 7.5B)

7.4.5.-Relationships between epidermal features and photosynthetic parameters.

I found an inverse correlation between trichome density and g_s (R^2=0.58, p-value=0.03) (Fig. 7.6A), and a positive correlation between stomatal density per area unit and g_s (R^2=0.56, p-value=0.03) (Fig. 7.6B). Therefore, changes in the density of trichomes and stomata had opposite effects on gas exchange. Importantly, trichome density was positively correlated with WUE_i (R^2=0.88, p-value=0.00) (Fig. 7.6C), while stomatal density showed no correlation with WUE_i. As expected from the observed relationship between WUE_i and WUE_b (Fig. 7.5B), trichome density was positively correlated with WUE_b (R^2=0.59, p-value=0.03, Fig. 7.7A). Interestingly, stomatal density was negatively correlated with WUE_b (R^2=0.50, p-value<0.05, Fig. 7.7B). Finally, a strong positive association was found between T/S and WUE_i (R^2=0.86 p-value=0.00) (Fig. 7.8A) and WUE_b (R^2=0.72 p-value=0.01) (Fig. 7.8B).

	WW				WD			
	Ψ_{leaf}	LMA	LT	WUE_b	Ψ_{leaf}	LMA	LT	WUE_b
Acc.	MPa	g m^{-2}	mm	g kg^{-1} H_2O	MPa	g m^{-2}	Mm	g kg^{-1} H_2O
M-82	-0.74 ± 0.04 [a]	79.45 ± 9.56 [a]	0.70 ± 0.05 [ab]	0.76 ± 0.12 [a]	-1.01 ± 0.07 [ab*]	96.01 ± 3.41 [a]	0.76 ± 0.04 [ab]	1.14 ± 0.09 [ab*]
4-1	-0.86 ± 0.06 [ab]	58.12 ± 4.33 [a]	0.63 ± 0.03 [b]	0.74 ± 0.04 [a]	-1.18 ± 0.05 [ab*]	63.83 ± 6.69 [b]	0.66 ± 0.05 [ab]	0.79 ± 0.02 [b]
10-2	-0.99 ± 0.04 [b]	82.37 ± 6.58 [a]	0.69 ± 0.01 [ab]	0.89 ± 0.1 [a]	-1.21 ± 0.07 [b*]	98.65 ± 5.72 [a]	0.81 ± 0.02 [a*]	1.12 ± 0.17 [ab]
11-3	-0.74 ± 0.07 [a]	71.20 ± 9.45 [a]	0.80 ± 0.03 [a]	0.85 ± 0.05 [a]	-0.93 ± 0.08 [a]	64.18 ± 6.35 [b]	0.63 ± 0.03 [b*]	1.36 ± 0.06 [a*]

Table 7.6.-Morphological and water status characterisation of lines M82, 4-1, 10-2 and 11-3 under well-watered (WW) and water deficit (WD) conditions in the field. Midday leaf water potential (Ψ_{leaf}), leaf mass per area (*LMA*), leaf thickness (*LT*) and plant-level water use efficiency (WUE_b) are shown. Values are means ± SE of three to four replicates per line and treatment. Different letters denote statistically significant differences by Tukey analysis ($P<0.05$) within each treatment between lines, and asteriks denote statistically significant differences ($P<0.05$) between treatments for each line.

WW

Acc.	A_N µmol CO_2 $m^{-2}s^{-1}$	C 24h mol m^{-2} day^{-1}	g_s mol H_2O $m^{-2}s^{-1}$	g_m mol CO_2 $m^{-2}s^{-1}$	g_{tot} mol CO2 $m^{-2}s^{-1}$	V_{cmax} µmol CO2 $m^{-2}s^{-1}$	WUE_i µmol CO_2 mol^{-1} H_2O
M-82	13.22 ± 1.16 [a]	0.34 ± 0.03 [a]	0.222 ± 0.046 [a]	0.087 ± 0.015 [a]	0.049 ± 0.006 [a]	304.05 ± 57.19 [a]	66.22 ± 11.52 [a]
4-1	15.31 ± 1.35 [a]	0.34 ± 0.08 [a]	0.272 ± 0.027 [a]	0.088 ± 0.004 [a]	0.058 ± 0.003 [a]	349.38 ± 107.21 [a]	57.09 ± 4.68 [a]
10-2	16.87 ± 1.26 [a]	0.42 ± 0.04 [a]	0.229 ± 0.026 [a]	0.123 ± 0.015 [a]	0.063 ± 0.004 [a]	335.96 ± 49.79 [a]	75.88 ± 7.33 [a]
11-3	15.82 ± 1.43 [a]	0.44 ± 0.05 [a]	0.243 ± 0.026 [a]	0.102 ± 0.017 [a]	0.061 ± 0.010 [a]	336.77 ± 38.46 [a]	65.60 ± 2.11 [a]

WD

Acc.	A_N µmol CO_2 $m^{-2}s^{-1}$	C 24h mol m^{-2} day^{-1}	g_s mol H_2O $m^{-2}s^{-1}$	g_m mol CO_2 $m^{-2}s^{-1}$	g_{tot} mol CO2 $m^{-2}s^{-1}$	V_{cmax} µmol CO2 $m^{-2}s^{-1}$	WUE_i µmol CO_2 mol^{-1} H_2O
M-82	11.52 ± 0.80 [a]	0.31 ± 0.04 [a]	0.165 ± 0.021 [a]	0.084 ± 0.010 [a]	0.046 ± 0.005 [a]	271.97 ± 22.89 [a]	71.44 ± 4.26 [ab]
4-1	12.53 ± 0.80 [a]	0.30 ± 0.03 [a]	0.233 ± 0.009 [a]	0.083 ± 0.016 [a]	0.052 ± 0.006 [a]	217.25 ± 26.34 [a]	53.74 ± 2.76 [b]

Table 7.7.-Photosynthetic characterization of lines M82, 4-1, 10-2 and 11-3 under well-watered (WW) and water deficit (WD) conditions in the field. Net photosynthetic rate (A_N), daily carbon fixation rate (*C24H*), stomatal conductance (g_s), mesophyll conductance (g_m), total leaf conductance (g_{tot}), maximum velocity of Rubisco carboxylation (V_{cmax}) and intrinsic water use efficiency (WUE_i) are shown. Values are means ± standard error of four replicates per line and treatment. Different letters denote statistically significant differences by Tukey analysis (P<0.05) within each treatment between lines, and asteriks denote statistically significant differences (P<0.05) between treatments for each line.

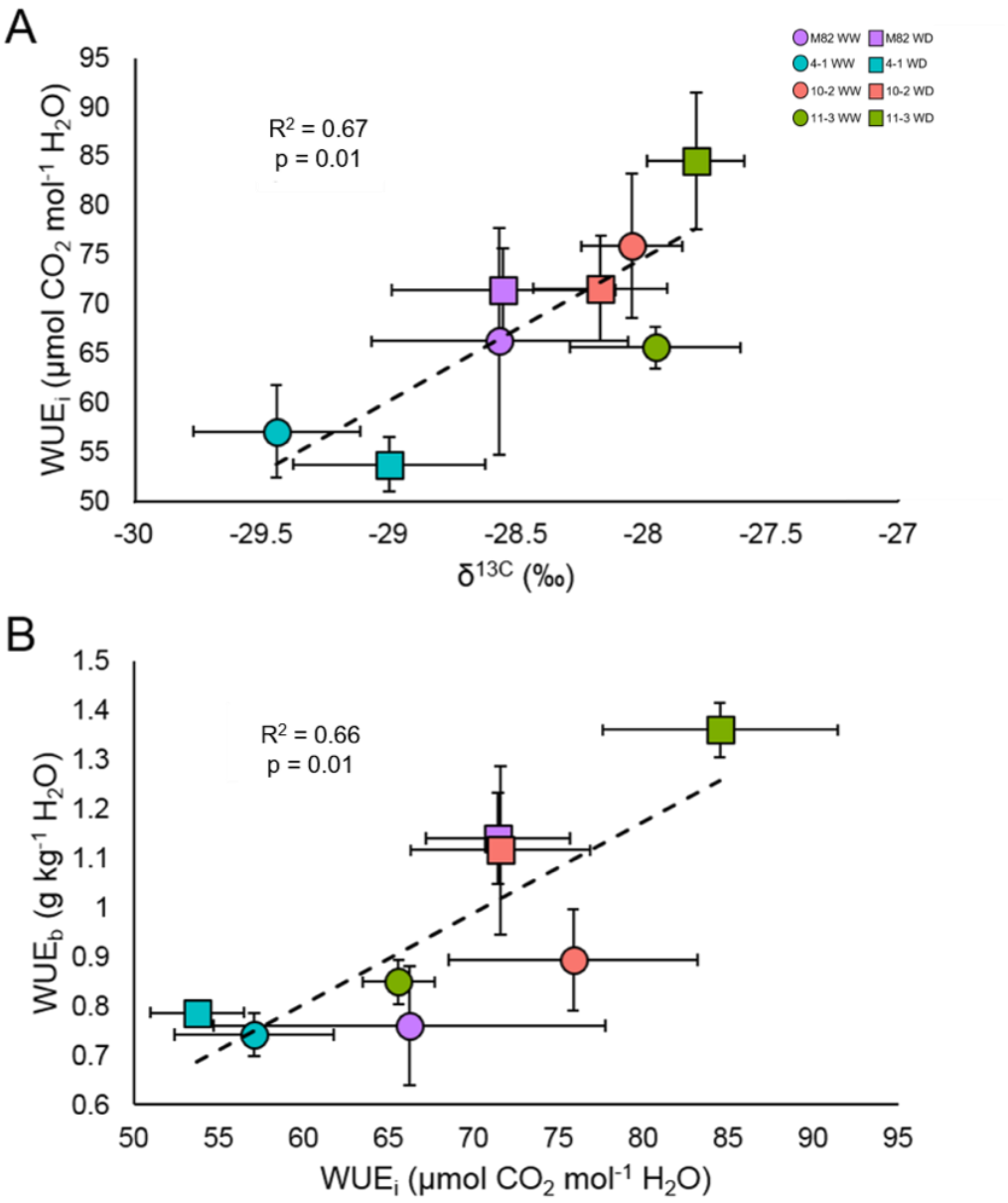

Figure 7.5.-Correlations between carbon isotope composition and intrinsic water use efficiency and between intrinsic water use efficiency and plant-level water use efficiency in lines M82, 4-1, 10-2 and 11-3. (A) The correlation between leaf δ^{13C} and intrinsic water use efficiency (WUE_i) (B) The correlation between the intrinsic WUE_i and the plant-level water use efficiency (WUE_b). Correlation coefficients and p-values by Pearson tests are shown in each graph. Purple markers represent M82, turquoise markers represent IL 4-1, red markers represent IL 10-2 and green markers represent IL 11-3. Circles represent WW values and squares represent WD values of field-grown plants. Values are means ± SE (n=4).

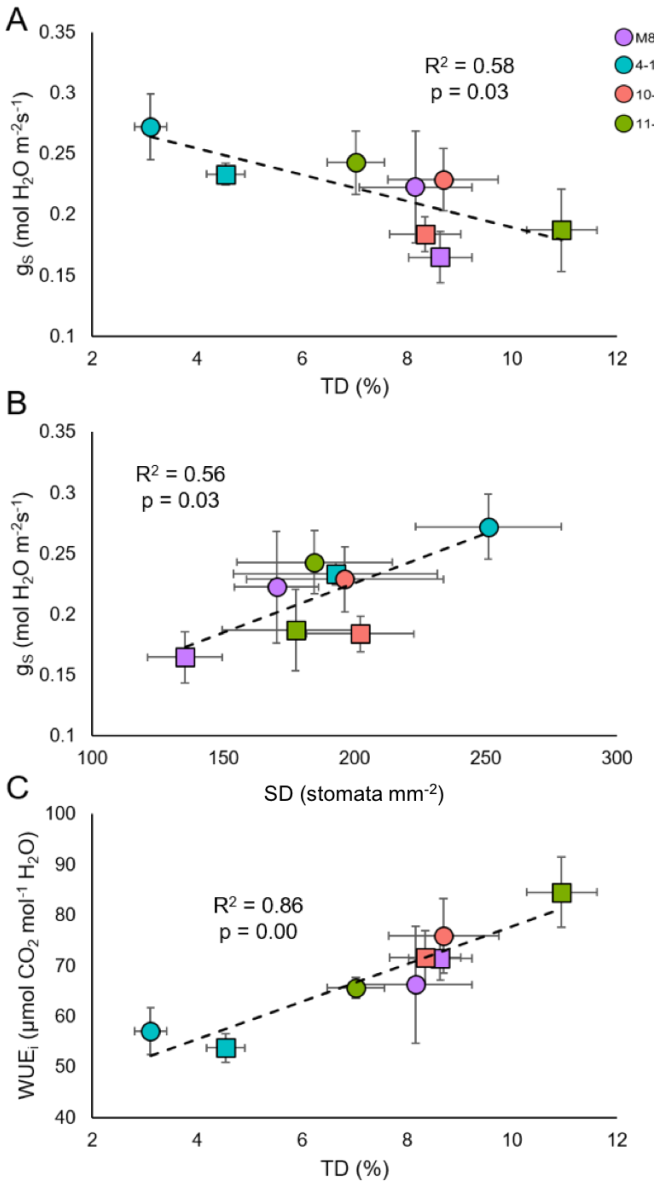

Figure 7.6.-Relationships between trichome and stomatal densities and photosynthetic parameters in lines M82, 4-1, 10-2 and 11-3. (A) The inverse correlation between trichome density and stomatal conductance (g_s), (B) the positive association between stomatal density and stomatal conductance (g_s) and (C) the positive association between trichome density and intrinsic water use efficiency (WUE_i). Correlation coefficients and p-values calculated by Pearson test are displayed in each graph. Purple markers represent M82, turquoise markers represent IL 4-1, red markers represent IL 10-2 and green markers represent IL 11-3. Circles represent values under WW conditions in the field and squares represent values under WD conditions in the field. Values are means ± SE (n=3-4).

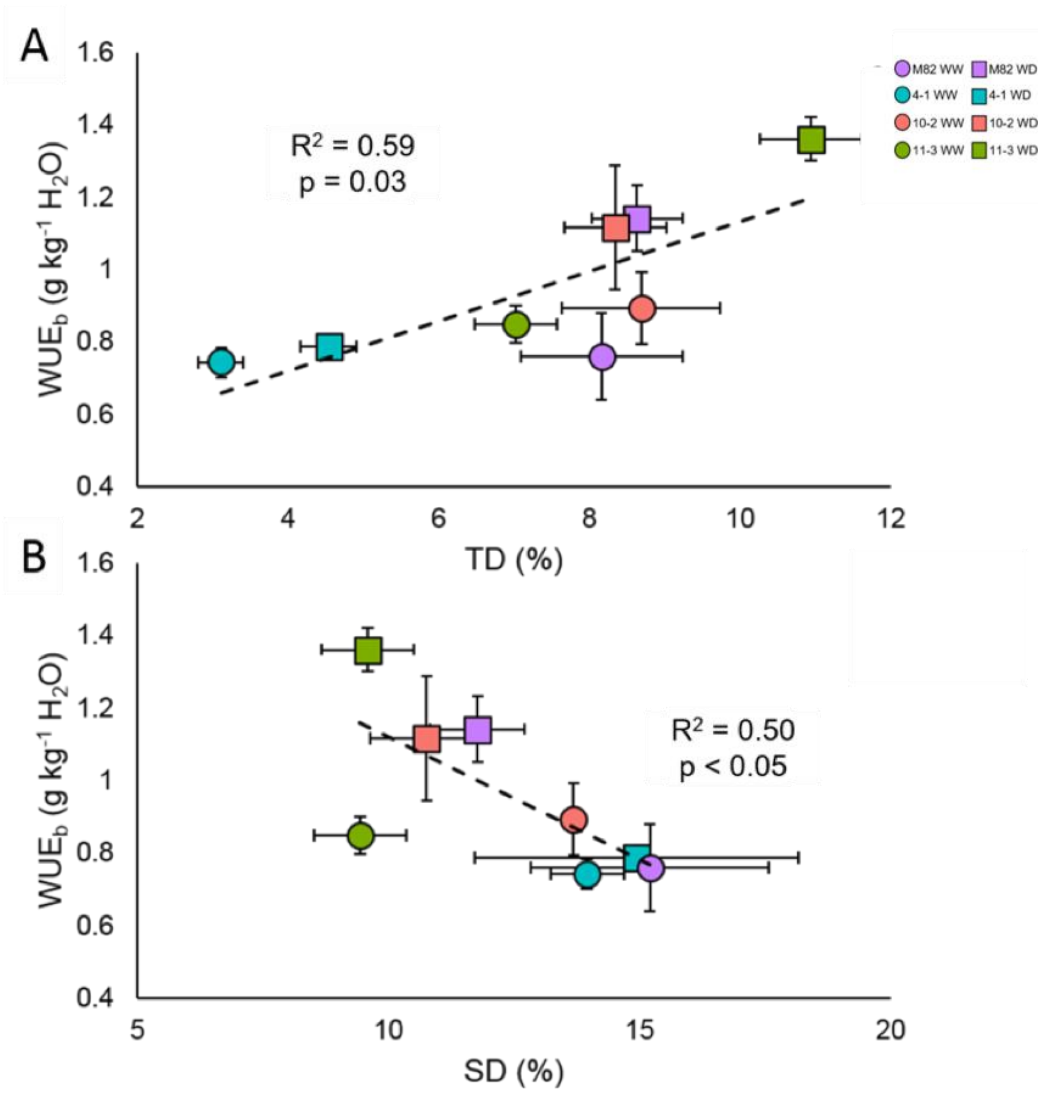

Figure 7.7.-Relationship between epidermal features and plant-level water use efficiency (WUE_b) in plants under well-watered (WW) and water deficit (WD) conditions in the field. (A) The correlation between trichome density and plant-level WUE_b. (B) The correlation between stomatal density and plant-level WUE_b. Correlation coefficients and p-values from Pearson tests are displayed in each graph. Purple markers represent M82, turquoise markers represent IL 4-1, red markers represent IL 10-2 and green markers represent IL 11-3. Circles represent values from WW conditions and squares represent values from WD conditions. Values are mean ± SE (n=3-4).

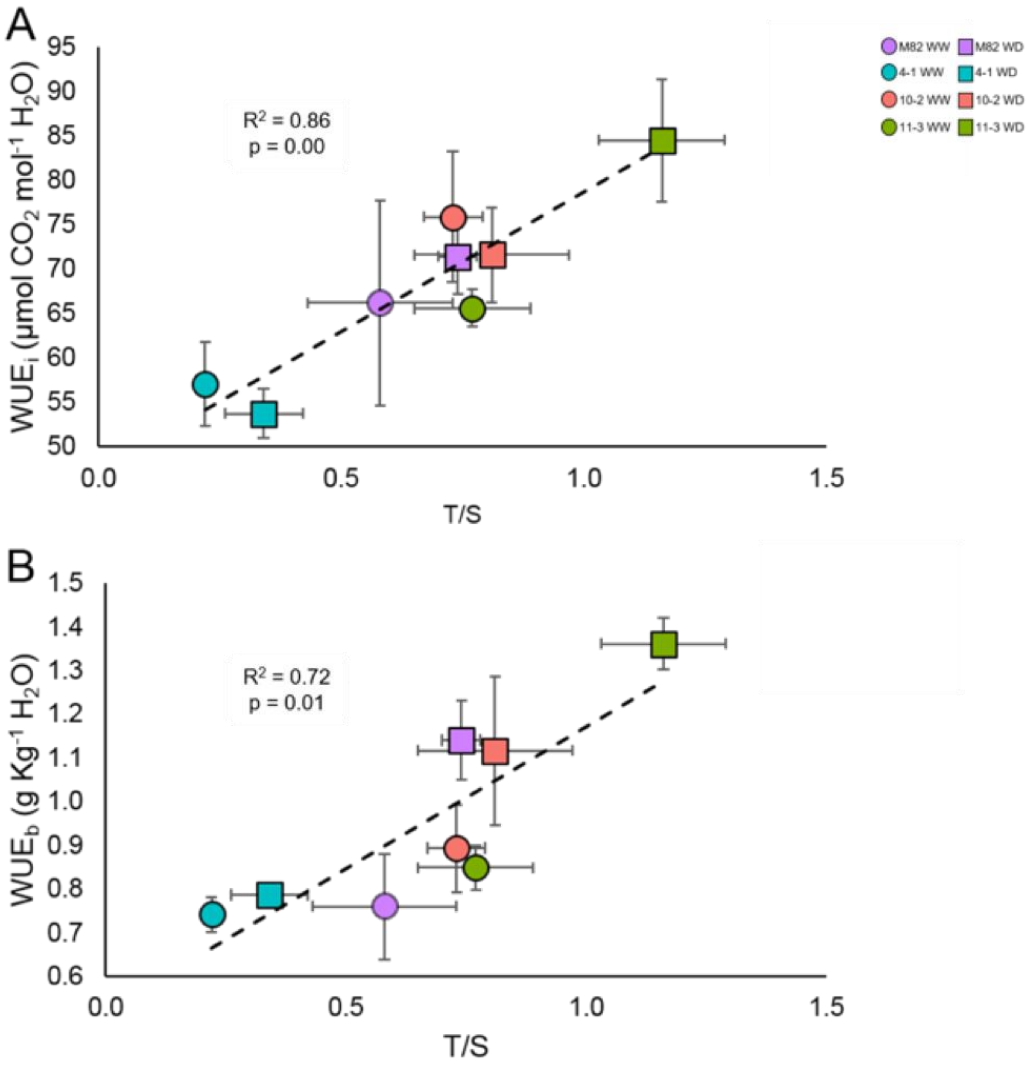

Figure 7.8.-Relationship between trichome/stomata ratios and photosynthetic parameters in lines M82, IL4-1, IL10-2 and IL11-3. (A) The correlation between trichome/stomata ratio (T/S) and intrinsic water use efficiency (WUE_i) and (B) The correlation between trichome/stomata ratio (T/S) and plant-level water use efficiency (WUEb). Correlation coefficients, calculated by Pearson tests (*P*<0.001 for A, *P*<0.01 for B), are shown in each graph. Purple markers represent M82, turquoise markers represent IL 4-1, red markers represent IL 10-2 and green markers represent IL 11-3. Circles represent values from WW conditions in the field and squares represent values from WD conditions in the field. Values are means ± SE (n=3-4).

7.5.-Discussion

7.5.1.-Water availability affects the development of the leaf epidermis.

I observed a 10-to-15-fold higher TD in leaves grown under field conditions compared to glasshouse-grown plants (Fig. 7.3a). These differences were likely due to differences in the age of the plant as well as changes in environmental conditions between the glasshouse and the field. Trichome development is reported to change with the age of the plant, with the first leaves showing a higher density of type IV glandular trichomes than leaves emerging later in the plant development (Vendemiatti et al., 2017) and higher trichome density observed in late leaves of tomato (Gurr and McGrath, 2001). Moreover, environmental factors, such as temperature, photoperiod, light intensity or soil humidity, have direct effects on trichome development in several species. For example, tomato plants grown under short day photoperiod conditions had a lower trichome density than those grown under long day photoperiod conditions (Gianfagna et al., 1992), although the content of sesquiterpenes produced by glandular trichomes was affected in the opposite direction, maybe indicating that the trichome type distribution can be also affected by photoperiod. Because the imaging method used to quantify trichome and stomatal density was relatively destructive, I could not test the effect of different water regimes on trichome types, as most of them were broken to a certain extent. Long day photoperiods have also been linked to an induction in trichome formation in *Arabidopsis* (Chien and Sussex, 1996) and in mint, higher light intensity is associated with higher trichome density (Souza et al., 2016). Despite the dramatic change between environmental conditions in the greenhouse and the field, the relative differences in trichome density were conserved between lines (Fig. 7.3A), indicating strong genetic control of trichome development in the selected ILs. We observed a 1.5-to-5-fold higher SD in field-grown plants (Fig. 7.3B). These differences could also be a function of the age of the plant when leaves were sampled. In poplar, the leaf age and position were the main factor affecting stomatal density in experiments on the effect of changes on CO_2 concentration in leaf development (Ceulemans et al., 1995), indicating that this must be taken in consideration when performing any comparative experiments. Environmental conditions could also have an effect on stomatal density, as observed for trichome density. Some examples of this type of environmental effects have been reported. For instance, in oak trees, leaves developed under higher temperature showed a reduction in stomatal density (Beerling and Chaloner, 1993). In grapevines, higher soil temperatures reduced stomatal density (Rogiers et al., 2011). Unlike the observation for trichomes, relative differences in stomatal density between lines were not conserved in different environments, pointing to differential regulation of both features.

I assessed the changes in leaf anatomy in water-deficit plants compared to well-watered plants. We observed a higher trichome density in ILs 4-1 and 11-3 under WD conditions compared to WW plants (Fig. 7.4A). Increases in trichome density upon herbivore and water stress have been reported previously in several species. Induction of trichome formation by herbivory is discussed extensively in *chapter 8*. Induction of trichome formation in leaves developed after drought stress has been observed in aubergine (Fu et al., 2013) and *Arabidopsis* (Bjorkman et al., 2008) as part of the adaptive stress response. In fact, transcriptomic studies in water-stressed *A. thaliana* plants showed upregulation of genes related to trichome initiation and morphogenesis (TT8, BRICK1, KAK) but not of genes involved in stomatal initiation (Bechtold et al., 2016). Not all the lines in this study showed uniform responses, with IL 4-1 showing bigger changes upon drought treatment (lower stomatal size, higher trichome density) (Fig. 7.4). This could be explained by a greater inability of IL 4-1 to control water loss, as indicated by its lower WUE_b and WUE_i (Tables 7.4 and 7.5) leading to more severe physiological stress in this line and, subsequently, a stronger response to water deficit. In any case, these leaf adaptive changes did not account for an increase in WUE (Tables 7.4 and 7.5) probably due to a lower overall trichome density in IL 4-1.

I observed an inverse association between trichome density and stomatal density only under water-deficit conditions (Fig. 7.4D), in agreement with previous reports in tobacco overexpressing AmMIXTA (Glover et al., 1998) and the *Woolly* mutant in tomato (Glover, 2000), although quantitative data are not shown for this last report. Developmentally, trichomes and stomata originate from protodermal cells (Morohashi and Grotewold, 2009, Pillitteri and Dong, 2013), and the inverse association observed suggests that regulation of their development might be linked. Similar relationships have been found in *Arabidopsis thaliana* trichome mutants (Bean et al., 2002), where altered trichome phenotypes affected stomatal patterning. In aubergine, increases in trichome density have been associated with increases in stomatal (Fu et al., 2013), in contrast to our observations, indicating that there may be different developmental associations even between related *Solanum* species. The fact that the trichome and stomatal densities were not correlated when both well-watered and water-deficit plants were considered (Fig. 7.4D) might be a result of the lack of genetic differences in stomatal density, as only trichome density was clearly different between the assessed lines (Fig. 7.3B). However, the observed association suggests that the developmental response of the leaf to drought stress involves changes in the determination of cell fate in the whole epidermal tissue, affecting simultaneously trichome and stomatal densities, and this might occur through different regulatory mechanisms under different water regimes. In conclusion, we observed an important effect of water availability on leaf anatomy and determination of epidermal features.

7.5.2.-Potential of the natural variability in the *S. pennellii* IL population to develop drought-tolerant varieties.

M82, the cultivated parent of the IL population, is a highly inbred tomato cultivar that has traditionally been used as a check variety in breeding programmes (Grandillo et al., 1999) and as a reference cultivar for scientific research, used in relation to response to water stress as a drought-sensitive cultivar (Iovieno et al., 2016), in contrast to the drought-tolerant *S. pennellii* (Egea et al., 2018). The natural variation within the IL population provides an excellent platform to investigate the role of differences in epidermal features on performance under water stress. The intrinsic water use efficiency (WUE_i) is an important target for crop improvement with respect to drought tolerance, although it needs to be considered carefully as it might not be directly related to improved fruit productivity (Blum, 2005, Blum, 2009), as it is measured in vegetative organs, and it does not consider parameters as fruit set or fruit size. I observed a lower WUE_i for IL 4-1 under water-deficit conditions compared to the other lines under study (Table 7.5), whereas WUE_i in IL 11-3 was higher under water-deficit compared to well-watered conditions (Table 7.5). This increase in WUE_i has been reported in drought tolerant varieties in several crops, including mulberry (Guha et al., 2010), sorghum (Fracasso et al., 2016) and wheat (Liu et al., 2016a), although it might not always have a positive effect on fruit yield. Interestingly, none of the ILs under study were considered before for WUE improvement as they showed no differences in $\delta^{13}C$ compared to M82 in a $\delta^{13}C$ screen of the population (Xu et al., 2008), in agreement with our results, so this epidermis-based analysis provides an alternative path for increased WUE. Therefore, the genomic region introgressed from *S. pennellii* in IL 11-3 could be selected to generate more water-use efficient tomato cultivars.

The accuracy of WUE_i as a measure of drought tolerance has been questioned due to the lack of correlation with whole-plant measurements of WUE (Medrano et al., 2015). In fact, in newer tomato cultivars, a decrease in WUE_i, driven by selection under high-light and well-watered conditions, has been reported to be accompanied by increases in agronomic WUE (yield per water used) (Barrios-Masias and Jackson, 2014). Therefore, biomass-based parameters, specifically plant-level water use efficiency (WUE_b), were also investigated in this study, although specific differences in fruit production or harvest index between ILs, reported by (Caruso et al., 2016), were not considered. WUE_b under water deficit conditions was lower in IL 4-1 than in IL 11-3 (Table 7.4). Moreover, M82 and IL 11-3 plants grown under water-deficit conditions had higher WUE_b values compared to well-watered plants (Table 7.4). The observed correlation WUE_i-WUE_b,(Figure 5b) supports the use of WUE_i as a measure of drought tolerance under the described experimental conditions. In a similar way, leaf $\delta^{13}C$ has been used as a marker of the plant's WUE (Farquhar and Richards, 1984), and in tomato and *S. pennellii* it has been reported

to correlate with WUE_b (Martin and Thorstenson, 1988). In this work, I found a correlation between leaf $\delta^{13}C$ and WUE_i (Fig. 7.5A), suggesting that leaf $\delta^{13}C$ can be used as a tool for selection of high WUE_i lines in tomato. However, I did not observe a significant correlation between leaf $\delta^{13}C$ and WUE_b, which might hinder the applicability of my findings.

7.5.3.-The role of the epidermal structures during drought stress.

Water stress responses involve changes in leaf anatomy, including changes in the leaf thickness affecting CO_2 diffusion (Niinemets et al., 2009, Galmes et al., 2013) and epidermal features, where there has been a focus on stomata because of their direct role in gas exchange and transpiration (Galmés et al., 2007a, Xu and Zhou, 2008). Although I observed differences in leaf thickness in ILs 4-1 and 11-3 when WW and WD plants were compared (Table 7.4), no correlation was found between leaf thickness and any gas exchange parameter. Importantly, I observed a significant, inverse correlation between g_s and stomatal density per area (Fig. 7.6), but not between g_s and stomatal density as a percentage of epidermal cells. This result suggests that SD per area should be used preferentially when assessing gas exchange parameters.

However, my findings also support a major role for trichomes in gas exchange and determination of WUE. The correlation observed between trichome density and WUE_i and WUE_b (Fig. 7.6B and 7.7A) suggests that trichome density has a positive effect in terms of drought tolerance. The lack of differences in trichome types in the lines under study (see *chapter 3*) indicates that the observed effects are due to trichome density rather than other trichome parameters. Several roles have been suggested for trichomes in plant drought tolerance, including protection against photodamage (Galmés et al., 2007b) and effects on the resistance of the air-leaf boundary layer (Boughalleb and Hajlaoui, 2011) On the basis that trichome density is negatively associated with g_s (Fig. 7.6A), my data suggest that trichomes in tomato might play a role in avoiding excessive water loss through stomata by changing the resistance of the boundary layer, as proposed in previous studies in olive tree and watermelon (Guerfel et al., 2009, Mo et al., 2016). Another possible explanation for the correlation between trichome density and WUE involves the mutually exclusive developmental association between trichomes and stomata. Increased trichome initiation as part of the response to drought (a possibility supported by the expression analysis in *Arabidopsis* (Bechtold et al., 2016)), could lead to lower stomatal density which could lead to an improved WUE. Finally, genes involved in ABA signalling, known to play a role in drought response, are expressed in trichomes (Ren et al., 2010, Daszkowska-Golec, 2016), and have a direct role in the systemic regulation of the response to drought. For example, the tomato homolog of the WRKY transcription factor AtABO3 (ABA OVERSENSITIVE3) (Ren et al, 2010) or the bZIP transcription factor AtABF1 (ABRE BINDING FACTOR1) (Yoshida et al, 2015) are both expressed in trichomes in tomato according to available RNAseq data (Spyropoulou et al., 2014).

Changes in trichome density could lead to changes in the transcript abundance of these or other ABA-related factors. In fact, the expression level of SlABO3 (Solyc09g015770) is slightly higher in leaves in IL 11-3 compared to ILs 4-1 and 10-2 according to available RNAseq data (Chitwood et al., 2013), although the overall expression levels are low and stable throughout the population, suggesting that this might be a direct effect of a higher trichome density. SlABF1 (Solyc11g044560) is located in the genomic region introgressed from *S. pennellii* in IL 11-3, indicating a possible role for trichome-expressed ABA-related genes in the observed drought response.

Whole-plant water-use efficiency (WUE_b) was also correlated with stomatal density (Fig. 7.7B), although the impact of stomatal density on WUE was lower than that of trichome density, because there was no correlation between WUE_i and stomatal density at the leaf level, and when correlation coefficients between trichome density-WUE_b and stomatal density-WUE_b were compared, the effect of stomatal density on WUE_b was lower than that of trichome density (Fig. 7.6 and 7.7). The fact that both stomata and trichomes were involved in drought response was not surprising, given the developmental link we observed under water-deficit conditions (Fig. 7.4D) and the direct role of stomata in gas exchange (Fig. 7.6B). In fact, the ratio of trichomes-to-stomata (T/S), which gives information about the relationship between both structures, showed a strong correlation with both WUE_i and WUE_b (Fig. 7.8). In addition to this, T/S is unitless and is not expressed either in terms of leaf area or percentage of epidermal cells, overcoming the differences observed in correlations between developmental and photosynthetic traits. It is interesting to note that T/S becomes a more prominent parameter under water-deficit conditions, when both trichome density and stomatal density change together (Fig. 7.4D), while under well-watered conditions, when there is no correlation between them (Fig. 7.4D) or significant changes between lines, the genotype-specific trichome density is likely to be the main player in the relation between epidermis and WUE. In conclusion, T/S plays an important role in the efficiency by which water is used by tomato, and differences in T/S could be used to develop more drought-tolerant tomato varieties.

7.6.-Conclussion

In this chapter, I analysed the effect of genetically determined epidermal traits on the response to water deficit, using lines selected from the *S. pennellii* IL population that had a distinct trichome phenotype. I observed that lines with a high trichome density and low stomatal density performed better under drought conditions and proposed the use of the trichome to stomata ratio as an integrative parameter of the epidermal architecture which can be used as a measurement of drought tolerance.

I also analysed the effect of drought conditions on the development of new leaves, in comparison with leaves developed under well-watered conditions. I observe a trend towards higher density values for most lines under study. I also observed a tight correlation between trichome and stomatal density in leaves developed under water deficit, suggesting that their development is linked under stress conditions.

My results suggest that the epidermis plays an important role in drought response and that the natural variation present in wild tomato species, specifically *S. pennellii*, can be exploited to develop varieties with increase water use efficiency.

Chapter 8 – Analysis of the role of trichomes in the response to whitefly infestation.

8.1.-Abstract

In this chapter I described the analysis of selected tomato lines, including *Solanum pennellii* x *Solanum lycopersicum* cv.M82 introgression lines (ILs) as well as overexpression and CRISPR/Cas9-generated knock-out mutants, in terms of resistance to the infestation by the whitefly species *Trialeurodes vaporariorum*. The degree of tolerance was assessed in non-choice assays and the number of empty pupae cases on the abaxial leaves of the tomato plants was used as an indicator of the degree of infestation. I observed a strong negative association between trichome density and whitefly reproductive success among the ILs. I also found a line, IL 8-1, with a consistent high degree of tolerance to whitefly infestation. Finally, I observed a reduced number of empty pupae cases in the *DWARF* knock-out mutant, probably due to the smaller leaf area.

8.2.-Introduction

8.2.1.-Whitefly infestation as a threat to tomato production.

Whiteflies are small insects belonging to the family *Aleyrodidae* within the order *Hemiptera* order (Byrne and Bellows, 1991). Whiteflies are sap-feeding and they pierce the leaf to gain access to the phloem of the host plant, secreting excess sugars in form of honeydew (Inbar and Gerlin, 2008). Whitefly feeding affects plant biomass production and crop yield (Lindquist et al., 1972). The life cycle of the whitefly, which has been studied mostly in *Bemisia tabaci* and *Trileurodes vaporariorum*, two species which pose a substantial threat to crops, involves several developmental stages. The length of the life cylce is temperature-dependent, ranging from 2-3 weeks to several months (Inbar and Gerlin, 2008). Reproduction is arrhenotokous in most whitefly species, with unfertilised eggs becoming male individuals and fertilised eggs becoming female individuals (Byrne and Bellows, 1991). The whitefly life cycle (Fig. 8.1) starts with eggs laid by the female individuals normally on the abaxial surface of the youngest leaves (Ohnesorge et al., 1980). Once the eggs hatch, the immature whitefly goes through four distinct instar stages (first to fourth), with the first instar being mobile (also referred to as crawler) and the second to fourth instars being sessile. Some changes in appearance and metabolism take place in the different instar stages, until finally the mature fly is released, leaving the empty case of the fourth instar attached to the leaf. The fourth instar is opaque and it is also known as the pupa (Byrne and Bellows, 1991). Whiteflies are normally ready to mate again within a few hours to several days after pupal eclosion (Byrne and Bellows, 1991).

The most studied members of the family, *B. tabaci* and *T. vaporariorum,* are highly polyphagous and reports of their presence exist worldwide for most crops as well as aromatic and ornamental plants, including tomato, aubergine, potato, sunflower, common bean, roses, dahlias, mint and thyme to name a few (Evans and Hamon, 2002). Apart from the direct effects on yield caused

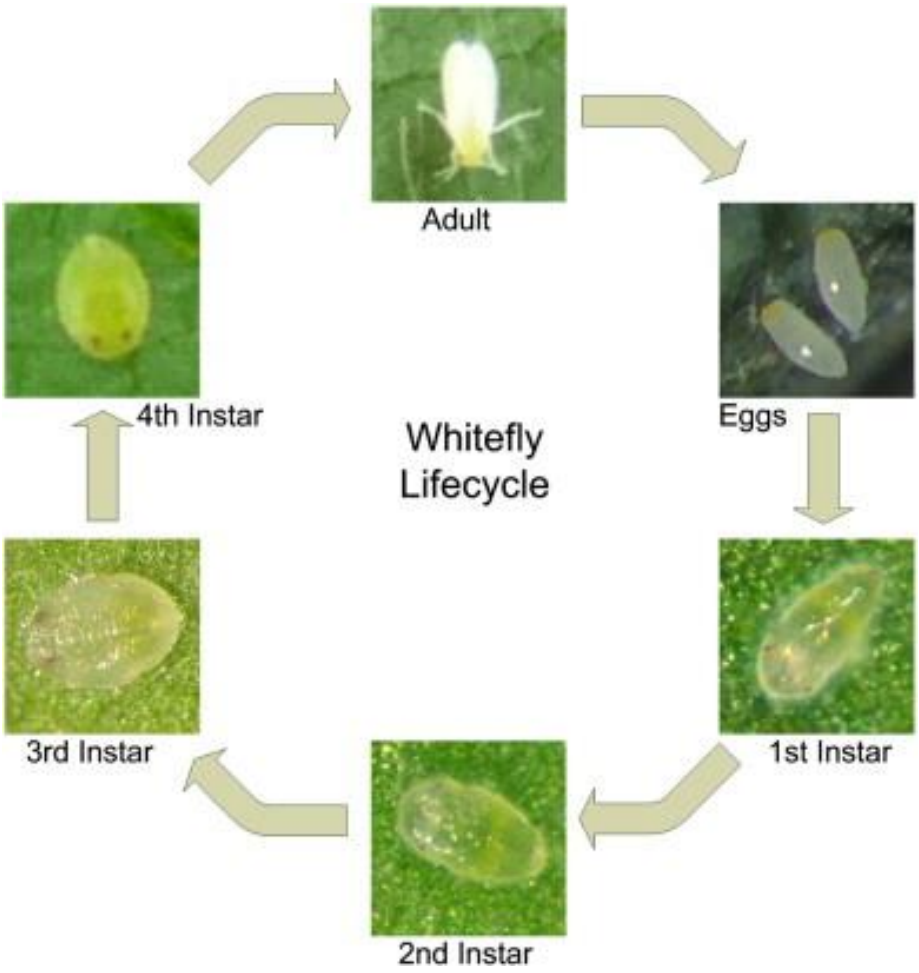

Figure 8.1.-Stages of whitefly life cycle. Six developmental stages are described in the life cycle of whiteflies, starting from eggs to adult fly going through four nymph instar stages. The fourth instar is often considered a pupa, and the empty cases left by mature adult flies are quantified in this chapter as a measure of the reproduction rate. This image is reproduced from (Barbedo, 2014) with written permission from Elsevier, the copyright holder.

by whitefly feeding on host plants, whiteflies act as vectors for serious viral diseases (Jones, 2003) including Tomato Yellow Leaf Curl Virus (Kil et al., 2016) and Tomato Chlorosis Virus (Louro et al., 2000), which affect dramatically the yield in tomato and can infect other hosts (Jones, 2003). *Bemisia tabaci* is able to act as a vector of a large number of viruses (over 300 species according to the latest reports (Navas-Castillo et al., 2011), while the number of viruses transmitted by *T. vaporariorum* is limited and restricted to a few species of the genera *Crinivirus* and *Torradovirus* (Jones, 2003, Navas-Castillo et al., 2011).

Whiteflies have a bigg impact in crops grown in the tropical and subtropical regions of the world, where their reproduction is not hindered by low temperatures during the winter months (Liu et al., 2016). However, whiteflies have posed a threat to glasshouse-grown crops for many years in temperate regions, and they have become adapted to crops grown in open fields (Wintermantel, 2004). Although pest control has been implemented with relative success, as the use of whitefly parasitoids (Liu et al., 2015) and chemical pesticides (Naveen et al., 2017), increasing crop resistance to whitefly infestation through breeding or biotechnology is the most sustainable approach to the problem. In the case of tomato, wild relative species such as *Solanum pennellii* and *Solanum habrochaites* show a high degree of resistance to whiteflies (Heinz and Zalom, 1995), which indicates that the genetic variation within the *Solanum* genus can be exploited to breed for whitefly resistance.

8.2.2.-The role of trichomes in resistance to insect attack.

The epidermis is the first barrier that protects the plant from detrimental environmental conditions, including insect herbivory. All epidermal components play a role in mediating insect-plant interactions. The lipid composition of the cuticle, when altered in *glossy* mutants with impaired wax biosynthesis, affected resistance to insect herbivory in several species (Eigenbrode and Espelie, 1995) and analysis of the three dimensional structure of cuticle waxes indicates that plants might have evolved surfaces on their leaves that hinder insect attachment (Gorb and Gorb, 2017). Oviposition in some insect species, including whiteflies, takes place in the substomatal cavity or in slits in the epidermal cells (Buckner et al., 2002). Whiteflies and other sap-feeding insects need to pierce the leaf surface to reach the phloem bundles. The mechanical properties of the leaf, its surface and the structures present in it are determinants of insect infestation (Peeters et al., 2007).

Trichomes are the most prominent epidermal structure and they can contribute to limiting damage related from insect herbivory. Trichomes, which can be non-glandular or glandular, act first as a physical barrier that can impede insect feeding, oviposition or larval development (Levin, 1973, Riddick and Simmons, 2014). In tomato, trichomes are also believed to act as

mechanoreceptors to elicit a systemic response in plants when trichomes are broken as a consequence of herbivore contact (Peiffer et al., 2009).

However, the main focus of interest in insect-plant interactions has been on glandular trichomes and their exudates. For example, in sunflower, secreted sesquiterpenes and diterpenes associated with glandular trichomes have a positive effect on resistance to the sunflower moth (Prasifka, 2015). In *Datura wrightii*, varieties with glandular trichomes producing sticky exudates showed increased resistance to whitefly attack but, in turn, attracted the insect species *Tupiocoris notatus*, indicating that glandular trichomes provide resistance only to a limited number of small herbivores (van Dam and Hare, 1998). In potato, glandular trichomes from the wild relative *Solanum berthaultii* provided resistance against the Colorado potato beetle (Dimock and Tingey, 1988). Similar observations have been reported for alfalfa and the potato leafhopper (Casteel et al., 2006) or petunia and *Spodoptera littoralis* (Sasse et al., 2016), indicating a widespread role for glandular trichomes in protection against insect herbivory.

Tomato trichomes have been studied extensively in cultivated and wild species, and the morphological and metabolic differences conferred by trichomes have been tested in relation to insect resistance (Simmons and Gurr, 2005). *S. pennellii*, for example, has a high degree of resistance against whitefly (Heinz and Zalom, 1995), thrips (Smeda et al., 2016) and other insect species (Juvik et al., 1982), associated with the high density of type IV glandular trichomes which secrete acyl sugars (Fobes et al., 1985). The composition of the acyl chain and sugar rings of acyl sugars are different between the wild species and cultivated tomato, with glucose rings and four-carbon acyl chains showing stronger activity as insecticides (Leckie et al., 2016). The insect-resistant wild tomato *Solanum habrochaites* also shows a higher type IV trichome density and a different acyl sugar composition (Ghosh et al., 2014). Type VI glandular trichomes produce terpenes and methyl ketones which are also associated with improved insect resistance (Bergau et al., 2015). For example, the *hairless* mutation in tomato causes a reduction in the biosynthesis of sesquiterpenes and polyphenolic compounds in type VI trichomes, and this results in increased susceptibility to *Manduca sexta* (Kang et al., 2010a). In *S. habrochaites,* the sesquiterpene zingiberene, produced in type VI trichomes, increases resistance to whitefly (Freitas et al., 2002). Finally, type VII trichomes are also glandular, but their abundance is very low, and they are not present in resistant species such as *S. pennellii* (Simmons and Gurr, 2005), so their role in insect resistance is relatively understudied. In a study of the interaction between tomato and the aphid *Myzus persicae*, the density of type VII trichomes was associated with a degree of arthropod repellence (Simmons et al., 2003), but further analysis of the metabolic activity of these trichomes is required.

In this chapter, I describe the analysis of selected *S. lycopersicum* x *S. pennellii* introgression lines (ILs), as well as overexpression and genome-edited lines, with different trichome phenotypes of the resistance to the glasshouse whitefly species *Trialeurodes vaporariorum,* and the effect of whitefly infestation on epidermal development.

8.3.-Methods

8.3.1.-Plant material and insects.

Eight introgression lines from the *S. pennellii* x *S. lycopersicum* cv. M82 where selected based on their trichome phenotypes in the analyses performed in *chapter 3*. The number and description of these lines can be found in Table 8.1. These lines were grown along with M82 plants, which were used as controls for all experiments involving the ILs. Three SlMIXTA-like overexpression lines (OE #1, #2 and #3) and three genome-edited lines (SlMIXTA-like KO, Woolly GE #1 and DWARF GE #1) were selected based on their leaf phenotype. The source and description of each line can be found in Table 8.2. MoneyMaker plants were used as controls for these lines and grown together with them.

Whiteflies (*Trialeurodes vaporariorum*) were reared in 52-cm × 52-cm × 50-cm cages on Chinese aster (*Callistephus chinensis)* under controlled-environment conditions with a 14-h-day (90 µmol m^{-2} s^{-1} at 20°C) and a 10-h-night (18°C) photoperiod.

8.3.2.-Non-choice whitefly assays.

Three to four five-week-old plants were bagged in fine-mesh plastic bags to allow gas exchange while keeping whiteflies in close proximity to the plant and avoiding infestation by other insect species. 20 whitefly individuals were deposited on each bagged plant and plants were grown for 5 weeks, adjusting the bag to allow plant growth and monitoring whitefly behaviour to ensure a full life cycle (Fig. 1) was completed. After 5 weeks, four leaves per plant (position 3 to position 6) were excised and the number of empty pupa cases on the abaxial side was counted manually. For DWARF GE plants, six leaves per plant were analysed, given the difference in growth rate.

For the length of the assay, tomato plants were grown under controlled conditions with 14-h-day (90 µmol m^{-2} s^{-1} at 20°C) and a 10-h-night (18°C) photoperiod and maintaining adequate water supply.

8.3.3.-Analysis of epidermis of the ILs before and after insect attack.

Leaf samples were collected from fully expanded leaves before subjecting the plants to insect attack (leaf in position 3) and after the non-choice assay was complete (leaf in position 8 to 10). Leaf samples consisted of square sections of approximately 0.5 x 0.5 cm which were fixed chemically in a glutaraldehyde 2.5%-cacodylate solution and dehydrated through an ethanol

IL	Phenotype first generation	Phenotype second generation
M82	Standard for trichome density	Standard for trichome density
1-4	Average trichome density	Average trichome density
2-2	Low trichome density	Low trichome density
2-6-5	Low trichome density	Average trichome density
4-1	Low trichome density, no type VI trichomes	Low trichome density
8-1	Low trichome density	Low trichome density
8-2-1	Low trichome density	Low trichome density
10-2	Low trichome density, aberrant trichomes	Average trichome density, aberrant trichomes
11-3	Average trichome density	High trichome density

Table 8.1.- Introgression lines (ILs) selected for insect tolerance assays. For each IL, the phenotype observed in the screens of the two generations of the IL populations, as described in *chapter 3*, is included.

Line	Described phenotype	Source
MoneyMaker	Standard for trichome density	Commercially available
***SlMIXTA-like* OE #1**	Low trichome density	Chapter 5
***SlMIXTA-like* OE #2**	Low trichome density	Chapter 5
***SlMIXTA-like* OE #3**	Low trichome density	Chapter 5
***SlMIXTA-like* KO**	High trichome density, trichome clustering	Chapter 5
***DWARF* GE #1**	Dwarfism, leaf curling, BR-deficient	Chapter 6
***Woolly* GE #1**	Low trichome density, no type I trichomes	Chapter 6

Table 8.2.-Overexpression and gene-edited lines selected for insect tolerance assays. For each line, the phenotype observed, and the source of the lines is indicated.

series before imaging by SEM under room temperature (see *chapter 2* for details). Three to four samples per line were analysed and 8-10 micrographs of approximately 0.3 mm^2 were analysed to determine trichome and stomatal densities. Trichomes, stomata and pavement cells were counted manually, and trichome and stomatal density were calculated as percentage of total epidermal cells. The trichome to stomata ratio was calculated by dividing the trichome density by the stomatal density. Trichomes were assigned to the different trichome type groups according to established classification (Luckwill, 1943, Simmons and Gurr, 2005). I classified type I and IV together in the same group and all non-glandular trichomes as type V. Broken and aberrant trichomes were also recorded.

8.3.4.-Statistical analysis.

Differences between the number of pupa cases on the leaves of different lines were called by performing a t-test between each selected line and the M82 control value for IL experiments or MoneyMaker control value for experiments with the other lines. The p-value cut-off was set at 0.05. Differences in trichome density, stomatal density and trichome-to-stomata ratio were assessed by univariate analysis of variance (ANOVA) between lines and time points and significance was determined by a post-hoc Duncan test ($p\text{-value}<0.05$). The relationship between variables was determined by correlation analysis (R^2). All the analyses were performed using the R software and the package *agricolae* (https://tarwi.lamolina.edu.pe/~fmendiburu/).

8.4.-Results

8.4.1.-Whitefly reproductive behaviour on leaves of selected *S. pennellii* ILs.

I selected 8 ILs to test for tolerance to whitefly infestation based on the trichome phenotypes I recorded in *chapter 3* (Table 8.1). This subset of ILs included lines with consistent low trichome density in the two generations which I screened (ILs 2-2, 4-1, 8-1 and 8-2-1), with different phenotypes in both generations (ILs 2-6-5, 10-2 and 11-3) and with consistent trichome density comparable to the control line M82 (IL 1-4). Some of the selected lines had other differences, such as the low to null presence of type VI trichomes in IL 4-1, the presence of aberrant trichomes in IL 10-2. The line M82 was used as a standard for the other lines. Finally, IL 8-1 and IL 11-3 show differences in the composition of acyl sugars in their trichome secretions (Schilmiller et al., 2010).

After a whitefly life cycle in a non-choice experiment, I quantified the number of empty pupa cases on the abaxial side of the infested leaves. For most ILs, whiteflies showed similar reproductive behaviour and offspring numbers (Fig. 8.2). However, I observed a significantly lower number of pupa cases in leaves of ILs 8-1 and 11-3 compared with M82 leaves (Fig. 8.2).

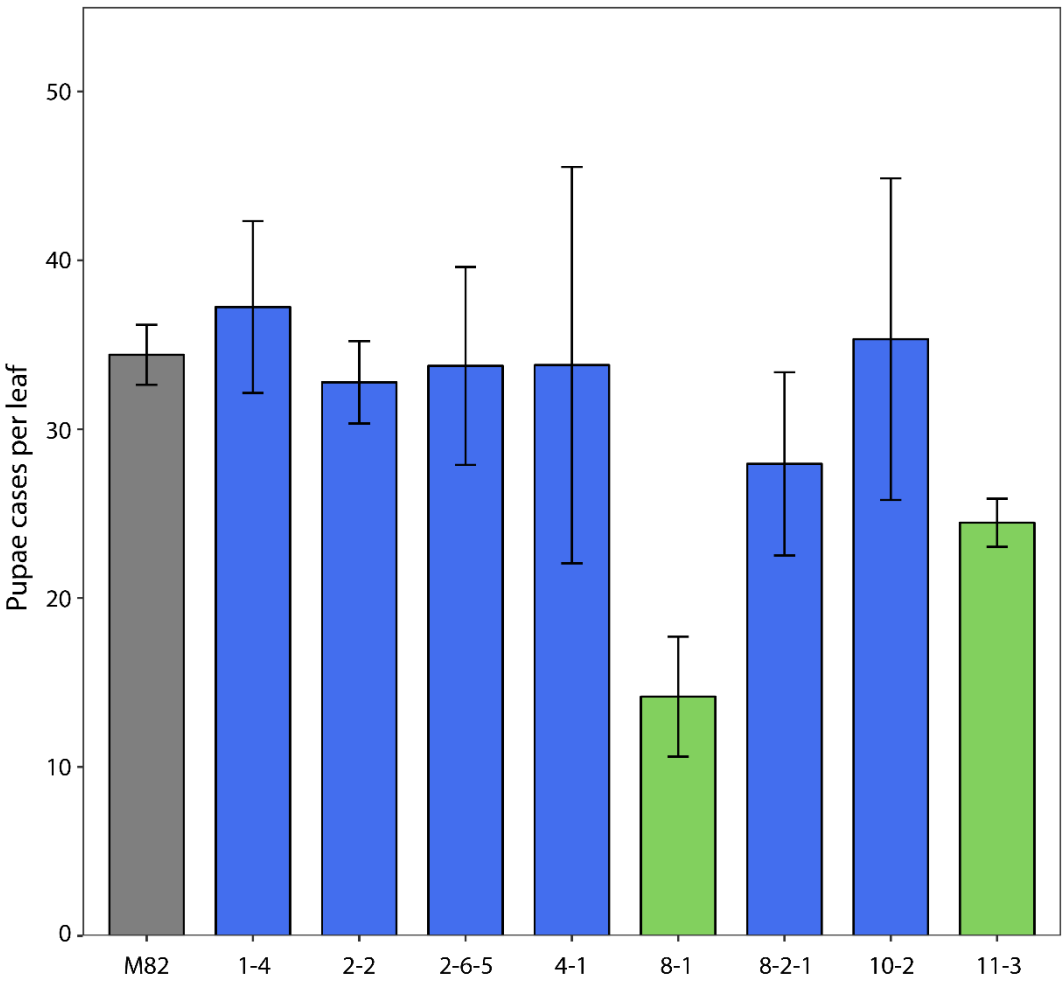

Figure 8.210.-Number of pupae cases per leaf in tomato plants five weeks after infestation. Pupae cases after mature fly release were quantified on the abaxial surface of the first eight leaves of each plant (n=3 per line, except for IL 10-2 where n=2). Values are expressed as mean±SEM. The grey bar indicates values for M82. Blue bars indicate ILs showing values not significantly different from M82, and green bars indicate ILs showing a significant reduction in the number of pupae cases per leaf (p-value<0.05).

8.4.2.-Effect of whitefly infestation on epidermal development.

I analysed the epidermal surface of leaves harvested before and after insect attack from M82 plants and the selected ILs. Before insect attack, IL 11-3 showed the highest average trichome density, being significantly higher than the values recorded for ILs 1-4, 4-1 and 10-2. The rest of the lines under study showed intermediate trichome density (Fig. 8.3A). After insect attack, IL 10-2 showed the highest average trichome density, with a significant higher trichome density than M82 and ILs 1-4, 2-2, 4-1 and 8-1. Interestingly, IL 4-1 had the lowest trichome density, and it was significantly lower compared to all the other lines under study after insect attack (Fig. 8.3A). For most of the lines analysed, trichome density increased dramatically after insect attack, except for M82 and ILs 4-1 and 8-1 (Fig. 8.3A).

Stomatal density showed fewer differences between lines in this assay. Before insect attack, all lines showed a comparable stomatal density with no significant differences observed between lines (Fig. 8.3B). After insect attack, ILs 2-6-5 and 10-2 had a lower stomatal density compared to IL 8-1, while all other lines had an intermediate phenotype (Fig. 8.3B). When values of stomatal density where compared before and after insect attack, most lines showed a trend to lower stomatal density, with ILs 8-2-1 and 10-2 showing a significantly lower stomatal density after insect attack (Fig. 8.3B).

I calculated the trichome to stomata ratio as an integrative parameter of the epidermal structures. Before insect attack, most lines showed a similar trichome to stomata ratio, with only IL 4-1 having a lower value compared to IL 2-2 (Fig. 8.3C). After insect attack, the trichome to stomata ratio was similar for all lines (Fig. 8.3C). Finally, the trichome to stomata ratio tended to be higher for all lines when values before and after insect attack

were considered, and actually for ILs 1-4, 2-6-5, 8-2-1 and 10-2 it was significantly higher (Fig. 8.3C).

I observed a negative correlation between trichome and stomatal density, but only for values after insect attack (R^2=0.63, p-value=0.01) (Fig. 8.4).

I classified the trichomes observed in the leaves of the assessed lines into the different type groups described by (Simmons and Gurr, 2005). For the trichomes developed before insect attack, the most abundant trichome type was type V (non-glandular), with glandular type VI trichomes being absent in the assessed tissue in ILs 1-4, 2-2, 2-6-5, 4-1, 8-2-1 and 11-3 (Fig. 8.5A). After insect attack, the percentage of type V trichomes increased for most lines in detriment of type I and type VII, and type VI became present in all lines and more abundant in most of them compared to the percentages before insect attack, although in IL 10-2 the abundance of type VI trichomes decreased (Fig. 8.5B). Interestingly, the percentage of each trichome type did not

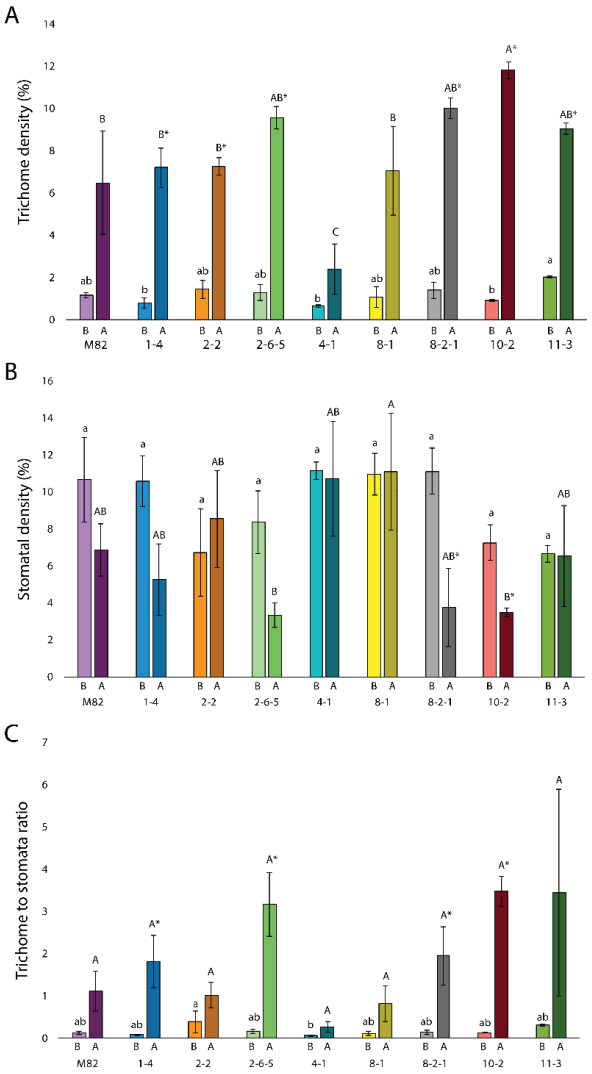

Figure 8.311.-Quantitative analysis of the epidermis of ILs under study before and after insect attack. A) Trichome density, expressed as percentage of total epidermal cells, of the adaxial surface of leaves from each IL. B) Stomatal density, expressed as percentage of total epidermal cells, of the adaxial surface of leaves from each IL. C) Trichome to stomata ratio of the adaxial surface of leaves from each IL. Values are expressed as mean±SEM (n=3 per line and time point, except for 10-2 before insect attack, where n=2). Purple bars represent M82 values; blue bars, IL 1-4; orange, IL 2-2; pale green, IL 2-6-5; turquoise, IL 4-1; yellow, IL 8-1; grey, IL 8-2-1; pink, IL 10-2 and green, IL 11-3. Light colours represent values before insect attack (labelled B) and dark colours represent values after insect attack (labelled A). Different letters indicate significant differences between lines for each time point (lower case for "before" values and upper case for "after" values), according to Duncan test (p-value<0.05). Stars indicate significant differences between time points for each line, according to a t-test (p-value<0.05).

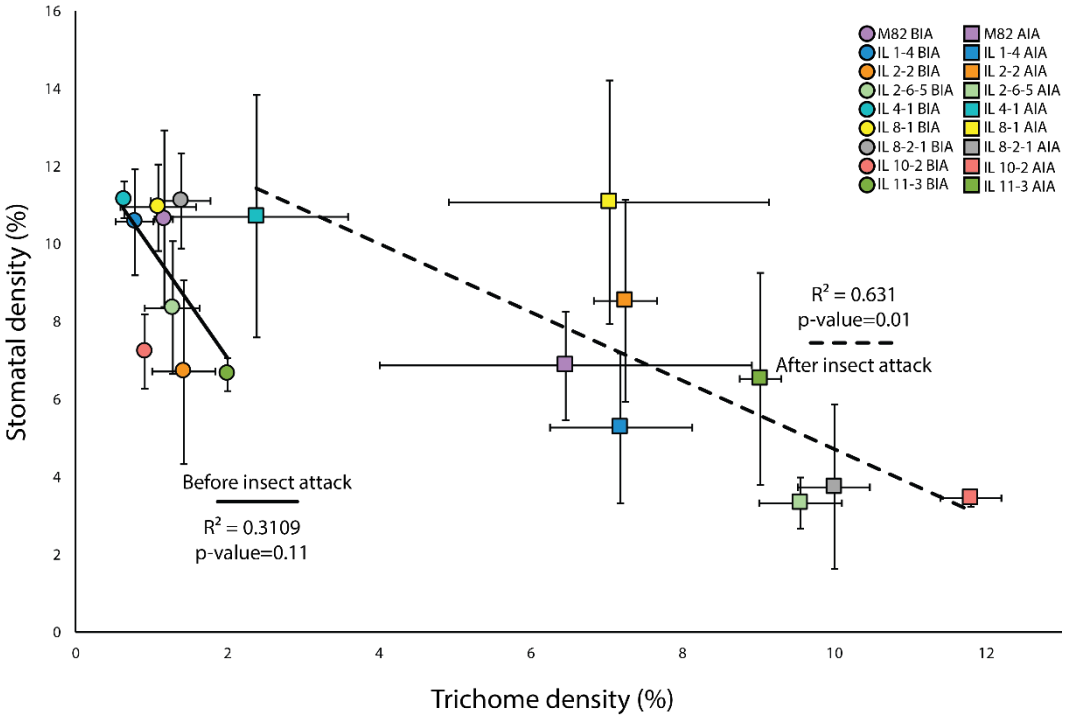

Figure 8.4.-Correlation between trichome and stomatal density for leaves assessed before insect attack (BIA) and after insect attack (AIA). A negative correlation was found between trichome and stomatal density only in plants assessed after insect attack according to Pearson's test (p-value=0.01, dashed line) while this was not observed for values before insect attack (p-value=0.11, solid line). Correlation indexes are shown in the graph. Each data point is expressed as mean ± SEM (n=3, except for IL 10-2 BIA, where n=2). Purple markers represent M82 values; blue, IL 4-1; orange, IL 2-2; pale green, IL 2-6-5; turquoise, IL 4-1; yellow, IL 8-1; grey, IL 8-2-1; pink, IL 10-2 and green, IL 11-3. Circle represent values before insect attack and squares represent values after insect attack.

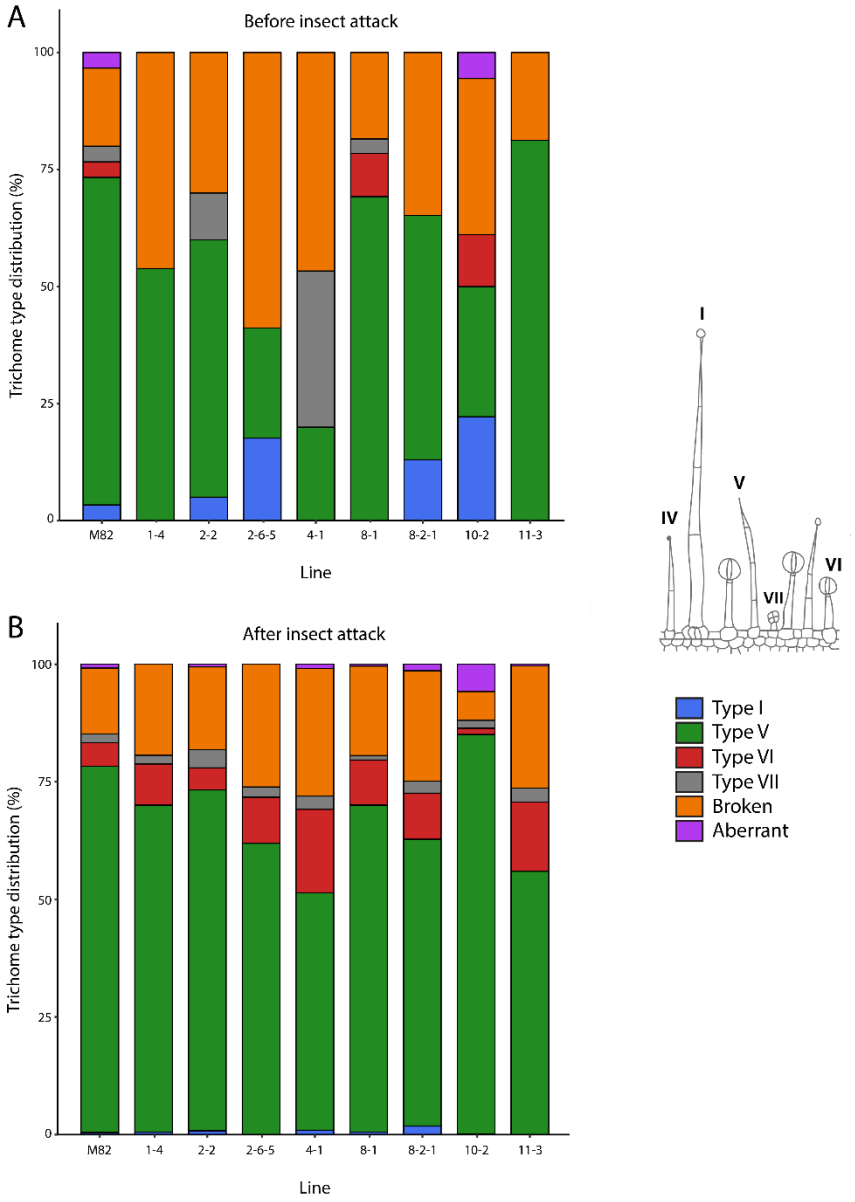

Figure 8.5.- Percentage of each trichome type in leaves of ILs before and after insect attack. A) Trichome type distribution in ILs before insect. B) Trichome type distribution in ILs after insect attack. Percentage is calculated considering the total trichome number for three leaves per line and time point. The blue bar represents type I; the green bar, type V; the red bar, type VI; the grey bar, type VII; the orange bar, broken trichomes and the purple bar, aberrant trichomes. A schematic view of each trichome type is shown in the figure. For this thesis, type I and IV are considered the same type and included under "type I" in the classification.

change substantially in M82 (Fig. 8.5B) It is important to note that the percentage of broken trichomes was high in all samples and might have masked the actual trichome type distribution (Fig. 8.5).

8.4.3.-Effect of trichome density on whitefly reproductive behaviour.

I observed a strong negative correlation between the number of pupa cases per leaf and the trichome density for each line (R^2=0.72, p-value<0.01) (Fig. 8.6), but only when the value for IL 8-1 was not considered, as it laid a long way off the regression line. For all other lines, the relationship between both the trichome density and the number of pupa cases was statistically significant.

8.4.4.-Whitefly reproductive behaviour on leaves of selected overexpression and gene-edited lines.

I selected some of the lines generated in this thesis on the basis of their differences in trichome phenotype (Table 8.2). This set of lines included SlMIXTA-like overexpression lines (OE #1-#3, described in *chapter 5*) which had lower trichome density than the untransformed MoneyMaker line, an SlMIXTA-like knock-out line (described in *chapter 5*), which showed trichome clustering and an increase in trichome density compared with MoneyMaker, a DWARF gene-edited line (DWARF GE #1, described in *chapter 6*) which showed an acute dwarfism due to its inability to synthesis brassinolide, and a Woolly gene-edited line (Woolly GE #1, described in *chapter 6*) which had low trichome density and absence of long, type-I trichomes.

I quantified the number of pupa cases on leaves of MoneyMaker and SlMIXTA-like OE lines in two successive assays (Fig. 8.7). In both cases, I did not observe any significant difference between the OE lines and MoneyMaker (Fig. 8.7). No significant differences were observed either between number of whitefly pupa cases in Woolly GE #1 or SlMIXTA-like GE #1 lines (Fig. 8.8A and B). The number of empty pupa cases was substantially lower in DWARF GE #1 leaves, and significantly different from the values for MoneyMaker (Fig. 8.8C).

8.5.-Discussion

8.5.1.-Natural variation in the trichome phenotype of *S. pennellii* ILs as a source of increased tolerance to whitefly infestation.

Wild relatives of the cultivated tomato have been reported to have an increased resistance to insect attack, including improved tolerance to infestation by whitefly species (Channarayappa et al., 1992, Heinz and Zalom, 1995, Nombela et al., 2000, Simmons and Gurr, 2005, Vosman et al., 2018). *Solanum pennellii* has repeatedly showed a high degree of resistance to whitefly attack (Liedl et al., 1995, van den Oever-van den Elsen et al., 2016, Vosman et al., 2018), and this trait has been associated to the composition and amount of secreted acyl sugars by type IV

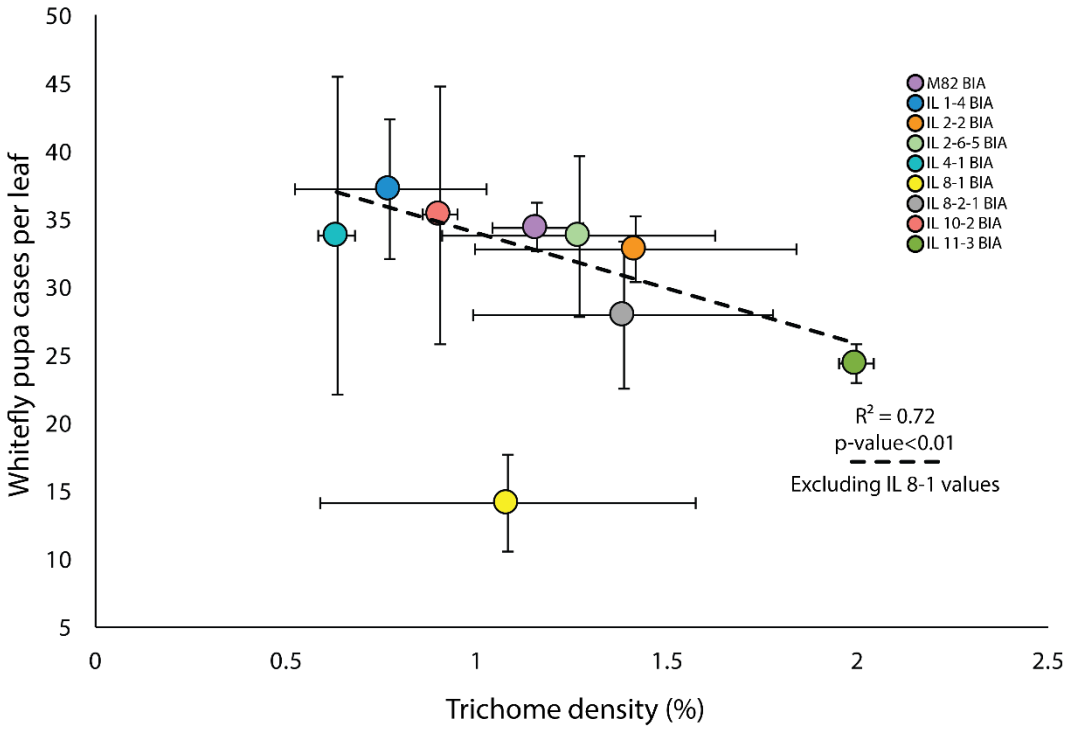

Figure 8.612.- Correlation between trichome density before insect attack (BIA) and whitefly pupa cases per leaf. A negative correlation was found between trichome density and pupa cases per leaf only when IL 8-1 values (highly resistant line) were excluded, according to Pearson's test (p-value<0.01, dashed line). Correlation index is shown in the graph. Each data point is expressed as mean±SEM (n=3, except for IL 10-2 BIA, where n=2). Purple markers represent M82 values; blue, IL 4-1; orange, IL 2-2; pale green, IL 2-6-5; turquoise, IL 4-1; yellow, IL 8-1; grey, IL 8-2-1; pink, IL 10-2 and green, IL 11-3.

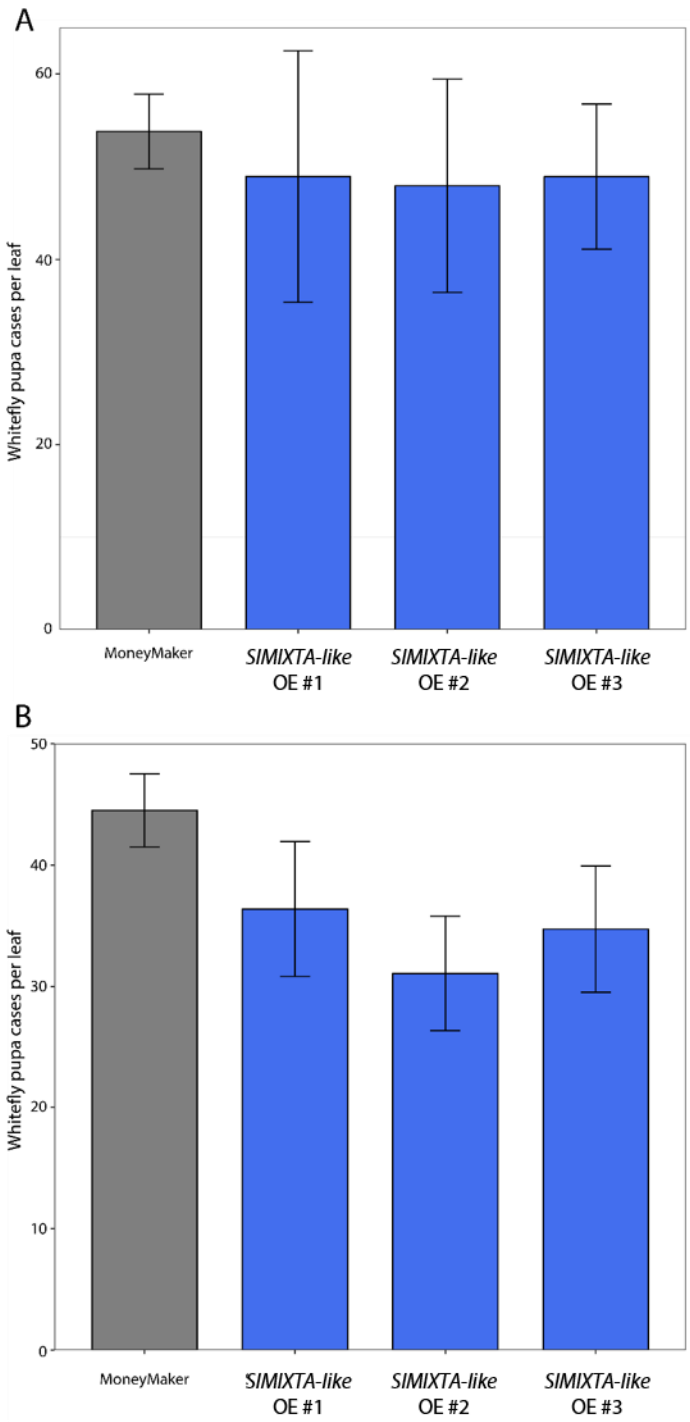

Figure 8.7.-Number of pupae cases per leaf in *SlMIXTA-like* OE and MoneyMaker plants five weeks after infestation. *SlMIXTA-like* OE lines #1, #2 and #3 were tested for their tolerance to insect attack in two successive assays (A and B). Pupae cases after mature fly release were quantified on the abaxial surface of the third to the sixth leaf of each plant (n=4). Values are expressed as mean±SEM. The grey bar indicates values for MoneyMaker control plants. No significant differences were found between lines.

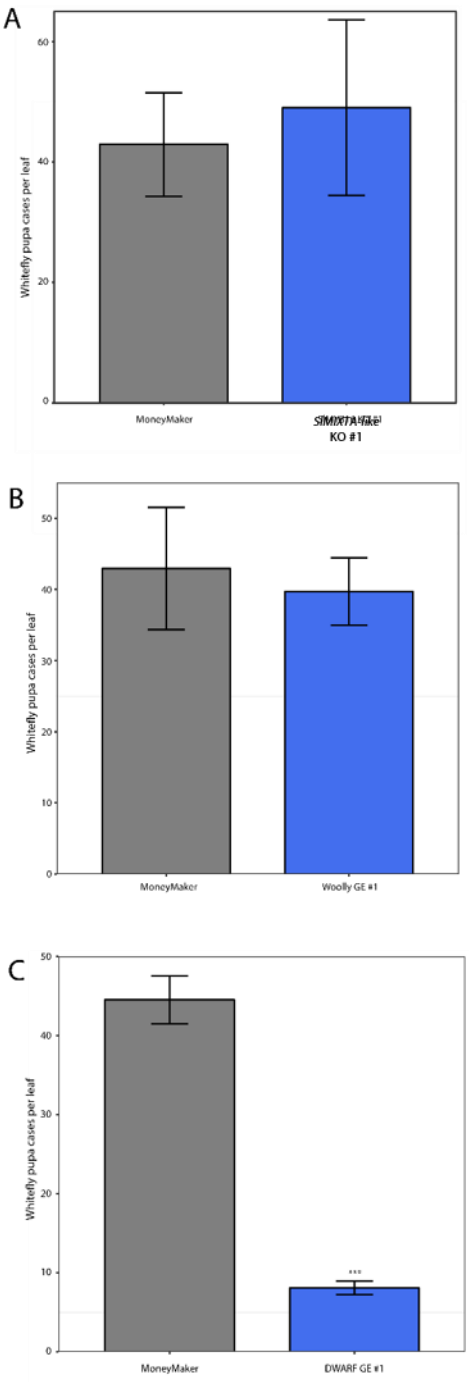

Figure 8.8.-Number of pupa cases per leaf in selected GE plants and MoneyMaker plants five weeks after infestation. A) Pupa cases per leaf in in MoneyMaker (grey bar) and *SlMIXTA-like* GE #1 (blue bar). B) Pupa cases per leaf in in MoneyMaker (grey bar) and *Woolly* GE #1 (blue bar). C) Pupa cases per leaf in in MoneyMaker (grey bar) and *DWARF* GE #1 (blue bar). Pupae cases after mature fly release were quantified on the abaxial surface of the third to the sixth leaf of each plant (n=4-5). Values are expressed as mean±SEM. Three starts indicate significant difference according to a t-test (p-value<0.05).

trichomes (Leckie et al., 2016). For this chapter, I selected a subset of ILs previously analysed in terms of trichome density (see *chapter 3*) to test their tolerance to whitefly (*Trialeurodes vaporariorum*) attack and try to establish any links between trichome density and whitefly performance.

Two of the ILs, 8-1 and 11-3, included in this assay showed an increased resistance to whitefly infestation, as the number of pupa cases per leaf in a non-choice test was significantly lower (Fig. 8.2). IL 8-1 had a significantly lower trichome density in the phenotyping screen I carried out, as described in *chapter 3*, and was also one of the lines showing lower trichome density values in the assessment performed in this chapter, especially after insect attack (Fig. 8.3A). The source of resistance in this line cannot be, therefore, associated to a high trichome density, as described for glandular trichome density in tomato (Silva et al., 2014) and other species such as cotton (Zhu et al., 2018b) or pelargonium (Avery et al., 2015). Apart from its low leaf trichome density, IL 8-1 did not show a large number of type I/IV trichomes (Fig. 8.5), sites of acyl sugar biosynthesis (Fobes et al., 1985, Schilmiller et al., 2012), suggesting that the observed resistance cannot be explained by an increase in the density or composition of trichome types in this

IL. Metabolomic analysis of IL 8-1 showed that the composition of the acyl sugars secreted by type I/IV trichomes in this line differ from those observed in M82, with a major presence of isobutyl (i-C4) acyl chains compared to the more abundant C5 acyl chains in M82 (Schilmiller et al., 2010). In IL 8-1, there is a reduction in total content of sucrose with 3 isopentyl (i-C5) substitutions and an increase in content of sucrose with one to three isobutyl (i-C4) substitutions (Fig. 8.9). Studies using purified acyl sugars from *S. pennellii* (with 75% of their components bearing isobutyl (i-C4) moieties) and *S. lycopersicum* (with 75% of the acyl sugars molecules containing isopentyl (i-C5) moieties) showed that the i-C4 acyl sugars were more effective in reducing whitefly and thrips oviposition (Leckie et al., 2016). The gene responsible for this shift in acyl sugar composition has been identified as a trichome-specific isopropylmalate synthase (Ning et al., 2015), which in *S. pennellii* is mutated and lacks the C-terminal region. These reports suggest strongly that the observed increase in resistance to whitefly is explained by the composition of changes in trichome exudates. In the future, I aim to test whether the level of resistance of IL 8-1 is comparable to that of *S. pennellii*. I will also generate knock-out lines for the isopropylmalate (Ning et al., 2015) using CRISPR/Cas9 to test whether this gene is actually responsible for the observed resistance to whitefly infestation.

In the case of IL 11-3, where fewer empty pupa cases were found on the leaves of whitefly-infested plants (Fig. 8.2), the trichome density was higher than that of M82 in the second generation of the IL population (see *chapter 3*), although it did not show a significantly higher trichome density compared with M82 in the first IL generation, but its average trichome density

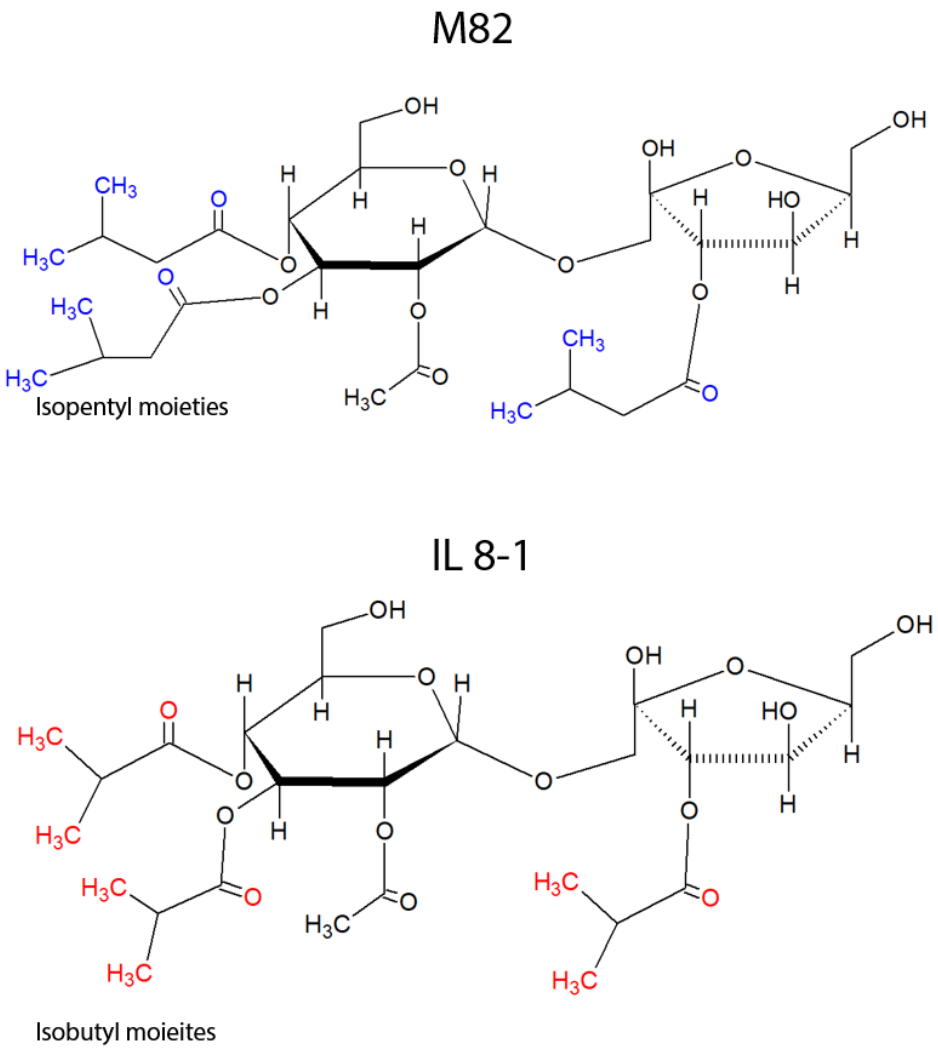

Figure 8.9.-Chemical structure of the most common acyl sugar produced in *S. lycopersicum* cv. M82 and the modified version found in IL 8-1. A sucrose molecule with three isopentyl substitutions (i-C5) – marked in blue- and an acetyl substitution is the most common acyl sugar form in M82. In IL 8-1, this form is less abundant and the isopentyl moieties are often replaced by isobutyl (i-C4) -marked in red- moieties. The i-C4 substitutions provide greater insecticide properties to the molecule.

was the highest of the whole population. This situation is similar to that observed for ILs before insect attack (Fig. 8.3A), where the value for trichome density in IL 11-3 was the highest among all the studied lines. Moreover, analysis of the acyl sugar content and composition in this line (Schilmiller et al., 2010) and other breeding lines derived from crosses with *S. pennellii* (Leckie et al., 2013) has shown that IL 11-3 has a significantly lower acyl sugar content compared to the rest of the IL population. Moreover, the composition of acyl sugars was slightly different in IL 11-3, with no acylation in the furanose ring of the acyl sucrose, the most common acyl sugar molecule in *S. lycopersicum,* due to a defective version of an acyl transferase in *S. pennellii* (Schilmiller et al., 2015). However, this specific acyl sugar has not been associated with insect resistance, suggesting that the acyl sugar content and composition do not play a role in the observed tolerance to whitefly shown in IL 11-3, especially since its low acyl sugar content would be predicted to have a negative effect on herbivore resistance. I also found a higher tolerance to drought stress in IL 11-3 (see *chapter 7*) which was linked to the high trichome to stomata ratio in this line. The high trichome density in IL 11-3 could explain the observed improved resistance to whitefly attack, in agreement with previous studies on total trichome density and whitefly oviposition in different tomato cultivars (Sanchez-Pena et al., 2006). In contrast, there are some reports in tomato where choice assays done with *B. tabaci* and tomato showed an oviposition preference for lines with high non-glandular trichome density (Heinz and Zalom, 1995, Oriani and Vendramim, 2010). The absence of large differences in the composition of the different trichome types in the assessed lines (Fig. 8.5), the non-choice nature of my experiments or differences in measuring oviposition or mature pupa cases might explain the differences between my observations and those of (Heinz and Zalom, 1995, Oriani and Vendramim, 2010).

Interestingly, I did not observe any of the selected ILs with a lower whitefly resistance than M82, even when most of the ILs were selected for having low trichome density (Table 8.1), with some consistently showing low trichome density under the conditions of the assay (IL 4-1, for example in Fig. 8.3). This suggests that the contribution of total trichome density to herbivory resistance may be limited to a certain extent and other factors, such as chemical composition of trichomes exudates (although the amounts of trichome exudates may be influenced by trichome density), may play more prominent roles as the first defence against pests.

In conclusion, the natural variation in trichome phenotypes (both at the developmental and metabolic levels) found in the *S. pennellii* IL population could be exploited to increase the tolerance of tomato plants to whitefly attack, as observed for ILs 8-1 and 11-3, with the latter contributing a traditionally overlooked source of resistance based on total trichome density rather than type I/IV density or acyl sugar composition.

8.5.2.-Epidermal dynamics upon insect infestation in tomato.

Plants are often subjected to herbivory and have developed different ways of responding to insect-related stress, including a first barrier to prevent insect feeding and reproduction (trichomes, cuticle, leaf thickness and constitutively produced defence metabolites) and a second barrier that involves transcriptome reprogramming, normally driven by the defence hormone jasmonate (JA) (Koo and Howe, 2009), either to alter development to minimise insect damage or increase the resources devoted to the production of defence structures and metabolites (Gatehouse, 2002, Kerchev et al., 2012). The leaf epidermis is the first barrier encountered by herbivores, and its morphology and mechanical properties play a major role in reducing the effect of insect damage (Fürstenberg-Hägg et al., 2013). Trichomes are one of the most specialised structures of the leaf epidermis and their role in defence against insects, especially glandular trichomes, has been reported frequently (Levin, 1973, Valverde et al., 2001, Tian et al., 2012).

I observed that changes in the epidermis of the selected ILs (Table 8.1) of leaves developed after insect attack. Trichome density increased substantially in leaves assessed after insect attack for most lines (Fig. 8.3A), suggesting that whitefly infestation elicits the subsequent development of leaves with higher trichome density. Increases in trichome density as part of the JA-mediated induced response to herbivory and wounding have been reported in several species, including willow (Bjorkman et al., 2008), tomato (Li et al., 2004, Escobar-Bravo et al., 2017) and *A. thaliana* (Qi et al., 2011). Transcriptomic analysis of cotton cultivars with different degrees of resistance to whitefly (*Bemisia tabaci*) showed differential expression of genes involved in trichome development such as a close homolog of AtGL3, GhDEL61 (Shangguan et al., 2016) or α-expansins (Li et al., 2016a), indicating that the response to whitefly attack likely involves upregulation of regulators of trichome formation. Moreover, I observed that trichome density and the number of pupa cases on leaves were negatively correlated in the lines under study, once IL 8-1 was excluded from the analysis (Fig. 8.6). These results suggest that trichome density is tightly linked to the reproductive success of whiteflies, but that other factors, such as the composition of the acyl sugar secretion (which can more effectively reduce whitefly oviposition (Leckie et al., 2016)) play a more prominent role, likely masking any effects associated to trichome density in IL 8-1.

Stomatal density did not change clearly following insect attack, although for many lines there was a trend towards lower stomatal density after attack (Fig. 8.3B). There was no clear connection between this reduction in stomatal density and increased resistance to whitefly attack. Some whitefly species insert their eggs into the stomatal cavity, but in the case of *T. vaporariorum*, used in this study, eggs are laid in slits made by the ovipositor on the leaf surface

(Buckner et al., 2002). A reduction in stomatal density might be a broad-spectrum response against insect herbivory, particularly for species that insert their eggs in the stomatal cavity, contributing to a reduction in the number of oviposition foci available on the leaf. Insect feeding and reproduction also affect the water status of the leaf as water losses occur through insect-mediated wounds (Aldea et al., 2005), and a decrease in stomatal density could contribute to maintaining favourable water status. Herbivory is known to affect primary metabolism, and this generally involves a decrease in the photosynthetic rate as part of the plant's response to stress, in this case biotic challenge. (Schwachtje and Baldwin, 2008, Bolton, 2009). The adaptive consequences of reducing photosynthesis in response to stress is unclear, but limitation of carbon fixation may increase the amount of reactive oxygen species (ROS) produced by the electron transport chain in the chloroplast, which might have a defensive role (Kerchev et al., 2012). A reduction in stomatal density could affect positively infested plants, both by maintaining its water status and by producing ROS as a defence mechanism. However, I did not observe any correlations between stomatal density and whitefly reproductive behaviour, suggesting that changes in stomatal density are unlikely to have a direct impact on whiteflies.

As expected from the opposite directions of changes in trichome and stomatal densities, the trichome-to-stomata ratio, an integrative parameter of the leaf epidermis which has been associated with drought tolerance (see *chapter 7*), increased after insect attack in most lines. However, I found no correlation between the trichome to stomata ratio and whitefly reproductive behaviour, suggesting that in the case of herbivory response, this parameter is unlikely to be as useful for selection of tolerant lines as it proved to be for water stress tolerance (Galdon-Armero et al., 2018). The lack of a clear role for changes in stomatal density, the absence of correlation between stomatal density (or trichome to stomata ratio) and whitefly pupa cases on leaves and the fact that trichome and stomatal density are strongly correlated in leaves developed after insect attack (Fig. 8.4) support the idea that the changes in stomatal density are a side effect of the increases in trichome density, perhaps affecting negatively the number of protodermal cells available to undergo differentiation into stomata, after a larger proportion of this pool commit to trichome development. This mutually exclusive relationship between trichome and stomatal development has been discussed in *chapter 7* as an explanation correlation observed between trichome and stomatal density. This supports my observations in tomato cultivars M82 and MoneyMaker (see *chapters 3 and 4*). Similar observations have been made in tobacco ectopically expressing *AmMIXTA* (Glover et al., 1998).

Whitefly attack had an effect on the type of trichomes present in leaves developed after infestation (Fig. 8.5). Although changes were relatively small in M82 controls, the most evident changes involved an increase in the percentage of type VI glandular trichomes and an increase

in the percentage of non-glandular type V trichomes in detriment of type I/IV trichomes in the ILs(Fig. 8.5). The trend to a higher number of type VI trichomes had been reported previously as a consequence of herbivory and jasmonate application (Oney and Bingham, 2014). The ketones and sesquiterpenes produced by type VI trichomes have insecticide effects on *Lepidotera* species (Lin et al., 1987) and an early mapping of QTLs affecting type VI trichome density and whitefly oviposition suggested a possible link between these two traits (Maliepaard et al., 1995). Therefore, an increase in type VI trichome density after insect attack might be a beneficial part of the response to herbivory in tomato. It is interesting to note that IL 4-1, which consistently showed a low to null presence of type VI trichomes (Fig. 8.5A and *chapter 3*) showed a large percentage of this trichome type after insect attack (Fig. 8.5B), suggesting that the absence of type VI trichomes in the assessed tissue was a consequence of the low total trichome density in this IL – and probably the consequence of the defective allele of *SlMX2* in this line (see *chapter 4*)- rather than a type-specific effect or an impairment of trichome type determination. The increase in the percentage of type V trichomes following insect attack and the concomitant reduction in type IV/I trichomes is most likely a consequence of the difference in leaf age. The presence of type IV/I trichomes is high in juvenile leaves and progressively reduced in newly developed leaves until they are almost absent in mature leaves, while non-glandular type V trichomes show exactly the opposite trend, with a progressive increase associated with plant age (Vendemiatti et al., 2017). Therefore, the observations before and after insect attack affecting these trichome types reflects the normal development of the plant. The presence of glandular type IV/I trichomes could be more beneficial given the proven insecticidal effects of their acyl sugar secretions (Leckie et al., 2016). However, a high density of non-glandular trichomes has been associated with improved resistance against some insect species such as the Colorado potato beetle (Tian et al., 2012), so a potential beneficial effect of increased non-glandular trichome density cannot be excluded. In all my observations, the number of broken trichomes in the assessed samples was relatively large and many of these observations could be skewed as a consequence.

8.5.3.-Whitefly reproductive behaviour on selected overexpression and genome-edited lines.

I selected some of the lines developed in *chapters 5* and *6* that showed differences in trichome density or other clear phenotypes, such as the dwarfism of the DWARF GE line (Table 8.2). The three SlMIXTA-like OE lines that had been analysed in detail in *chapter 5* showed a clear reduction of trichome density and an increase in stomatal density. However, when I quantified the number of empty pupa cases on the leaves of these lines, I did not observe any significant differences in comparison to the MoneyMaker control plants (Fig. 8.7). Although I found an association between trichome density and whitefly resistance in my analysis of the ILs (Fig. 8.6),

I did not observe an increase in the number of empty pupa cases in any of the lines with low trichome density (IL 4-1, for example). This suggests that the whitefly reproductive behaviour is not governed by trichome density in those lines and either the maximal reproductive performance is reached in the control MoneyMaker plants or that other factors that limit insect growth and reproduction (ROS formation, for example) might play more important roles, masking any effects of the reduction of trichome density. I also tested a SlMIXTA-like KO line for whitefly resistance (Fig. 8.8A). This line showed an increase in trichome density, which in this case was accompanied by an increase in stomatal density (see *chapter 5*). This line did not show any difference to MoneyMaker in terms of whitefly resistance, although the highest values for pupa cases were recorded in SlMIXTA-like KO lines (Fig. 8.8A). As discussed for OE lines, the gene might be involved in regulating other pathways related to defence. In fact, a conserved MYC2 binding motif is found in the SlMIXTA-like promoter, and MYC2 is a regulator of the jasmonate signalling pathway (Dombrecht et al., 2007), and therefore part of the systemic response to herbivory. Also, the high stomatal density in this line might be detrimental for the plant, as plants tended to reduce their stomatal density after insect attack (Fig. 8.3) and might also limit any potential advantage of a high trichome density. Finally, SlMIXTA-like regulates cutin biosynthesis and deposition (Lashbrooke et al., 2015), and it might affect insect attachment to the leaf (Gorb and Gorb, 2017) or its ability to pierce the surface to feed or lay eggs. The possible role of SlMIXTA-like in plant-insect interactions need to be studied further, including metabolic analysis of trichome secretions and effects of the overexpression and knock-out of the jasmonate pathway.

The Woolly GE lines showed a reduction in trichome density, and long type I trichomes were practically absent (see *chapter 6*). These lines behaved similarly to the MoneyMaker control in terms of whitefly resistance (Fig. 8.8B), suggesting once more that trichome density can only contribute within limits to defence against insect attack. The *Woolly* mutant, which shows a hyperproduction of non-glandular trichomes (Yang et al., 2011a), also showed a reduced production of monoterpenes and sesquiterpenes with insecticidal action and a reduction in the expression of PIN2 (Tian et al., 2012), a protease inhibitor which has been associated to herbivore resistance (Ryan, 1990). This indicates that other defence pathways might be controlled directly or indirectly by *Woolly* and therefore the effect of trichome density might be masked or relatively small.

In the case of the DWARF GE line, the plants showed an extreme dwarfism, with curled leaves, reduced number of leaflets and limited height (see *chapter 6*). However, no evident effect on trichome density was observed, and the suggested increase in pubescence reported for the BR-deficient *pdy* mutant in tomato (Campos et al., 2009) is probably due to the reduction in leaf

area and cell size (see *chapter 6*). The number of pupa cases on the leaves of the DWARF GE line was reduced dramatically compared to the MoneyMaker control (Fig. 8.8A). Brassinosteroids are phytohormones involved in a broad range of physiological processes. A role for brassinosteroids in regulating the response to herbivory in tomato has been reported in an antagonistic way to the jasmonate signalling pathway (Campos et al., 2009). The BR-deficient *dpy* mutant showed an increase in herbivore-related beneficial traits (increase in pubescence, production of the insecticide compound zingiberene and expression of protease inhibitors) while the JA-deficient *jai1-1* showed the opposite phenotype. Through study of the double mutant, it was concluded that BR acts upstream of JA, and therefore BR directly regulates JA-related responses and, ultimately, the degree of the response to herbivory (Campos et al., 2009). Moreover, *Nicotiana attenuata* plants where BAK1, a BR coreceptor essential for BR signalling in plants (Li et al., 2002), was silenced showed a reduction in JA content and alterations of the JA-mediated response to herbivory (Yang et al., 2011b). Therefore, the deficiency in BR biosynthesis in the DWARF GE line may be affecting the JA response and explain the observed effect on whitefly reproduction. Another possible explanation might be related to the area of the leaf available for oviposition. The leaf area in the DWARF GE line is greatly reduced compared to MoneyMaker leaves (see *chapter 6*), and some insect species adjust oviposition to the available leaf surface, as in the case of the leaf-miner (De Sibio and Rossi, 2012) or the European corn borer (Spangler and Calvin, 2000). BR-deficiency might be linked to improved tolerance to whitefly attack and the molecular and physiological basis of this phenomenon need to be explored further.

8.6.-Conclusion

In this chapter I analysed the effect of differences in trichome density, due both to natural variation present in the IL population and due to overexpression or knock-out of trichome regulators, on the reproductive behaviour of the glasshouse whitefly *Trialeurodes vaporariorum*. I also investigated the developmental effect of whitefly infestation on the trichome phenotype of newly developed leaves. I conclude that trichomes play an important role in controlling whitefly reproductive behaviour in two different ways. First, some trichome-secreted metabolites have a more effective insecticidal effect, as observed for IL 8-1. Second, trichome density is highly correlated to the number of whitefly offspring and the high-trichome density of IL 11-3 led to an increased resistance to whitefly reproduction. I also showed that insect attack elicits a developmental response which involves rearrangements in epidermal cell development, with an increase in trichome density and a concomitant decrease in stomatal density, which may offer tolerance to whitefly.

I also investigated the role of BR in herbivore response using the DWARF GE line developed for this thesis. BR-deficiency led to a very resistant phenotype, although whether this is due to a more intense JA-mediated response or to anatomical differences between lines remains to be determined.

The work presented in this chapter supports the use of trichomes as a tool for improved insect tolerance and as a target for breeding programs in tomato.

Acknowledgement to contributors

This chapter benefitted of the contribution of the Nuffield student Cara Moss, who worked under my supervision four weeks in 2018. She helped in the analysis of SEM images and counting of epidermal cells.

Chapter 9 – General discussion and future prospects

9.1.-General discussion.

The work described in this thesis aimed to deepen the current understanding of the development of multicellular trichomes in *Solanum lycopersicum* (tomato) by exploiting the natural genetic variation in the wild relative *Solanum pennellii* and the power of the CRISPR/Cas9 system to generate precise knock-out mutants of genes of interest. In addition to this, I explored the implications of changes in trichome features (with a focus on trichome density) on the fitness of the plant under drought and herbivory stresses. The data generated in this study have helped identify new regulators of trichome development and have contributed to a clearer model for trichome initiation and morphogenesis in tomato and related species.

9.1.1.-Natural genetic variation in *S. pennellii* led to the identification of new regulators of trichome development.

In *chapter 3*, I described the screen of the epidermal structures on leaves of the *S. pennellii* x *S. lycopersicum* cv. M82 ILs, which led to the identification of ILs with consistent differences to the wild type M82 over two generations in terms of trichome density (Fig. 3.3 and 3.4) and trichome patterning (Fig. 3.8). With the aid of the precise mapping of the introgressed genomic regions of *S. pennellii* in each IL (Chitwood et al., 2013), the availability of well annotated genomes of *S. lycopersicum* and *S. pennellii* (The Tomato Genome, 2012, Bolger et al., 2014) and the transcriptomic information available for trichome-specific genes (Spyropoulou et al., 2014) and leaves of the ILs (Chitwood et al., 2013), I selected a number of candidate genes that were likely to be involved in either trichome initiation or trichome morphogenesis, depending on the phenotype with which they were associated. The function of these genes (Tables 4.1-4.4) was tested by virus-induced gene silencing (VIGS), as described in *chapter 4*. These assays led to the identification of three genes with a likely role in trichome development: *SlMIXTA-like* (Solyc02g088190), *SlMX2* (Solyc04g005600) and *SlCycB2* (Solyc10g083140).

SlMIXTA-like was selected as a candidate gene involved in the aberrant trichome patterning phenotype observed in ILs 2-5/2-6, which had clusters of two to three trichomes on the leaf surface (Fig. 3.8). When *SlMIXTA-like* was silenced by VIGS, I observed similar trichome clusters on leaves (Fig. 4.4). *SlMIXTA-like* had been characterised before for its role in conical cell development in fruit and in cutin synthesis and deposition (Lashbrooke et al., 2015), and a closely related gene in petunia (*PhMYB1*), a likely homolog based on its phylogenetic relationship with *SlMIXTA-like* (Fig. 4.24), which had been characterised for its role in conical cell development in petals (Baumann et al., 2007). However, no evidence of a role for SlMIXTA-like in trichome development were reported. I characterised SlMIXTA-like functionally by a combination of approaches as described in *chapter 5*. Lines overexpressing *SlMIXTA-like* showed a decrease in trichome density in their leaves (Fig. 5.3 and 5.4), while *SlMIXTA-like* knock-out

plants showed an increase of trichome density as well as clustered trichomes on their leaves (Fig. 5.9 and 5.11). I also confirmed the role of SlMIXTA-like in controlling conical cell development in petals (Fig. 5.19) and fruits (Fig. 5.20). My data indicate that SlMIXTA-like is a negative regulator of trichome initiation and a key factor regulating the developmental pattern of trichomes of the epidermis of tomato leaves.

SlMX2 is a *MIXTA* gene, closely related structurally to known regulators of trichome development such as *MIXTA* in *Antirrhinum majus* (Noda et al., 1994) and *SlMX1* in tomato (Ewas et al., 2016). *SlMX2* was selected as a candidate gene responsible for the low trichome density observed in IL 4-1 (Fig. 3.3 and 3.4). When SlMX2 was silenced by VIGS, I observed a significant reduction of trichome density, which affected primarily non-glandular type V trichomes (Fig 4.9). My data suggest that this gene is responsible for the development of type V trichomes, which would explain the total absence of non-glandular trichomes in *S. pennellii*, where *SpMX2* is not expressed (Fig. 4.25) and lacks the sequence encoding the DNA-binding domain (Fig. 4.8). Moreover, the close relationship between SlMX2 and other MIXTA proteins in tomato (SlMX1 and SlMX3A and B) (Fig. 4.24) indicates likely functional redundancy.

SlCycB2 is a well-characterised type-B cyclin which regulates trichome development in tomato via interaction with the HD-ZIP class IV transcription factor Woolly (Yang et al., 2011a). This gene was selected as a candidate for the trichome phenotype of IL 10-2, which had aberrant branched trichomes as well as a *hairless*-like phenotype (Fig. 4.12 and 4.13). When SlCycB2 was silenced, I observed aberrant branched trichomes on the surface of leaves and stems (Fig. 4.17) in agreement with previous analyses of overexpression and RNAi lines (Gao et al., 2017). However, the gene responsible for the *hairless*-like phenotype was not any of my candidate genes (Table 4.3). A C2H2 zinc finger transcription factor, HAIR, was recently identified as encoded by the gene responsible for this trichome phenotype. HAIR regulates long type I trichome development via interaction with Woolly (Chang et al., 2018). However, this gene showed no expression in the RNAseq data from leaves for all the ILs as well as the parental line M82 (Chitwood et al., 2013), and therefore was never considered as a candidate gene contributing to the phenotype of IL 10-2.

In conclusion, the work described in *chapters 3, 4* and *5* helped identify new regulators of trichome development in tomato by analysing the phenotypic variation in the *S. pennellii* x *S. lycopersicum* cv. M82 IL population, and contributed to creating a clearer model for the regulation of trichome development in tomato(Fig. 6.36).

9.1.2.-CRISPR/Cas9-mediated gene editing of regulators of trichome development reveal their precise functions.

In *chapter 6*, I aimed to generate knock-out (KO) lines for structural and regulatory genes with a reported role in trichome development in tomato (Table 6.1) using the CRISPR/Cas9 gene editing system. I managed to produce mutant lines for Woolly, CD2, SlMX1, DWARF and Hairless. The analysis of the epidermis of the leaves in these lines provided insights about the precise function of these proteins in trichome development.

Woolly and CD2 are HD-ZIP class IV transcription factors. This gene family includes known regulators of trichome development in other species, such as GL2 in *Arabidopsis thaliana*, which regulates trichome morphogenesis (Rerie et al., 1994) and AaHD1 and AaHD8 in *Artemisia annua* (Yan et al., 2017, Yan et al., 2018). Woolly controls type I trichome development in tomato, with RNAi lines showing an almost complete absence of this trichome type (Yang et al., 2011a). However, whether Woolly regulates trichome initiation or only type I trichome morphogenesis was not clear from the analyses performed previously (Yang et al., 2011a, Yang et al., 2015). My *Woolly* gene-edited (GE) KO lines showed a drastic reduction of trichome density (Fig. 6.5 and 6.6), therefore suggesting its function is essential for trichome initiation. CD2 is a known regulator of cuticle biosynthesis and *cd2* mutants showed a reduction in type VI trichomes (Nadakuduti et al., 2012), which indicates that CD2 might play a role specifically in morphogenesis of this trichome type. My analysis of a heterozygous CD2 GE KO line confirmed this, with a reduction in density of type VI trichomes (Fig. 6.28), but this was accompanied by a substantial increase in total trichome density (Fig. 6.28), suggesting that CD2 also plays a role in trichome initiation as well as differentiation of type VI trichomes.

SlMX1 is a MIXTA transcription factor controlling trichome initiation in tomato (Ewas et al., 2016). However, whether SlMX1 controls the initiation of specific trichome types or not was not clear from the published reports (Ewas et al., 2016, Ewas et al., 2017). I could not obtain a homozygous SlMX1 GE KO line probably due to male sterility of the KO pollen (see *chapter 6*), but I analysed a heterozygous line (*SlMX1/slmx1*) and a homozygous line with a 10-amino acid deletion in the DNA-binding domain (*slmx1Δ10/slmx1Δ10*) (Fig. 6.19). Both SlMX1 GE lines showed reductions in trichome density (Fig. 6.23 and 6.24), and more interestingly, this reduction primarily affected non-glandular type V trichomes (Fig. 6.25), indicating that SlMX1 regulates the initiation of non-glandular trichomes. This phenotype is similar to the one observed for VIGS of SlMX2 (Fig. 4.9), suggesting functional overlap between closely related MIXTA transcription factors in tomato.

I generated a dwarf line by gene-editing of DWARF, a key enzyme in the synthesis of brassinolide. Although brassinosteroids had been reported to play a role in regulation of trichome density in

tomato (Campos et al., 2009), I did not observe a clear difference in DWARF GE lines compared to control lines in terms of trichome phenotypes (Fig. 6.17). Given the smaller size of pavement cells in the DWARF GE line (Fig. 6.18), an apparent higher trichome density could be the result of a reduction in the total leaf area, rather than an effect on the total trichome number.

Finally, *Hairless* encodes the SRA1 component of the WAVE complex in tomato, which is involved in the organisation of the actin cytoskeleton required for polar growth in trichomes (Kang et al., 2016). The *hairless* mutant shows distorted swollen trichomes that do not stand erect (Kang et al., 2010a), and this phenotype was also observed in the Hairless GE KO line I generated (Fig. 6.11) and the distortion affected all trichome types.

The data I gathered from the GE lines, together with the results from *chapters 4* and *5*, contributed to establish a better model for trichome initiation and morphogenesis in tomato (Fig. 6.36).

9.1.3.-The role of trichomes in tolerance to biotic and abiotic stresses.

I selected ILs with different trichome phenotypes from my screen of the population in *chapter 3* to test whether traits related to trichome formation were involved in determining the fitness of tomato plants under stress conditions, specifically drought (*chapter 7*) and herbivory (*chapter 8*).

Trichomes have been reported to provide resistance to drought conditions (Sletvold and Ågren, 2012). I selected a line with low trichome density, IL 4-1, a line with aberrant trichomes, IL 10-2, and a line with relatively high trichome density, IL 11-3 (Table 7.1) for drought resistance experiments. Comparative analysis of the intrinsic water use efficiency of these lines, together with the parental line of the ILs, M82, under well-watered and water-deficit conditions revealed that IL 11-3 had an increased tolerance to water scarcity (Table 7.5). Moreover, a strong correlation was observed between trichome density and water use efficiency (Fig. 7.6) and also between trichome-to-stomata ratio and water use efficiency (Fig. 7.8) under droughted conditions. My results suggest that trichomes can provide increased tolerance to drought conditions, in agreement with previous reports (Ewas et al., 2016), although the precise mechanism by which trichomes affect the water status of the plant remains elusive.

Trichomes are considered the first defence barrier against small herbivores (Levin, 1973), and glandular trichomes in tomato are known to produce metabolites with insecticidal or repellent properties (Liedl et al., 1995, Bleeker et al., 2012). I tested the level of resistance of selected ILs to glasshouse whitefly (*Trialeurodes vaporariorum*) infestation. I selected a set of ILs (Table 8.1) which showed different trichome phenotypes in *chapter 3*, and some of them showed differences in the composition of their trichome exudates. Specifically, IL 8-1 showed a shift in

the composition of the acyl substitutions in acyl sugars and IL 11-3 showed a reduction of the total content of acyl sugars (Schilmiller et al., 2010). I observed increased resistance to whitefly in these two lines, IL 8-1 and IL 11-3 (Fig. 8.2). However, IL 8-1 showed a low trichome density, while IL 11-3 showed a high trichome density (Fig. 3.3 and 3.4). This indicates that the chemical resistance provided by the modified acyl sugars in IL 8-1 (Leckie et al., 2016) likely plays a more important role than the resistance associated with elevated trichome density. However, overall, the reproductive behaviour of the whiteflies was tightly associated to trichome density (Fig. 8.6), suggesting that this trait might also be important in tolerance to whitefly in the absence of an effective chemical barrier.

In conclusion, my results highlight the important physiological roles that trichomes plays in *S. lycopersicum* and provide a new source of variation for agronomical improvement of tomato cultivars.

9.2.-Future prospects.

The data I collected and analysed for this thesis have contributed to answering some questions regarding the regulation of multicellular trichomes in tomato as well as their role in stress responses. However, it has also led to new biological questions that remain unanswered. In this section, I discuss briefly some prospects for this project.

9.2.1.-Can we find more regulators of trichome development using the IL population?

The pipeline designed to screen the ILs by SEM coupled with transcriptomic analysis and transient silencing by VIGS of candidate genes has proven to be quite effective to identify key regulators of trichome development. However, due to time constraints, some genomic regions with potential have remained unexplored in this thesis. For example, IL 11-3, which reproducibly showed high trichome density (Fig. 3.4, 7.3 and 8.3) as well as an increased resistance to drought (Table 7.5) and herbivory (Fig. 8.2) is especially interesting, and the analysis of this introgressed region from *S. pennellii* will probably lead to the identification of new genes involved in trichome development.

9.2.2.-Are other MIXTA and HD-ZIP class IV transcription factors involved in trichome development?

Most of the regulators of trichome development identified in this thesis or in previous studies belong to the MIXTA or the HD-ZIP class IV families. It would be interesting to determine whether other genes, which remain uncharacterised, play similar or complementary roles in this developmental process. For example, SlMX1 and SlMX2 have been shown to play very similar roles in trichome initiation in tomato (Fig. 4.9 and 6.23), and they are closely related structurally to SlMX3A and SlMX3B (Fig. 4.24). Woolly and CD2, two HD-ZIP class IV proteins, play different

roles in trichome development in tomato (Fig. 6.5 and 6.28). It would be interesting to study the role of other genes of this family, such as SlHDZIP-IV 7, a direct duplication of Woolly, or SlHDZIP-IV 4, the closest member of the family to GL2 in *A. thaliana* (Fig. 6.30). Testing the function of these genes by gene-editing or overexpression would contribute to gaining a better understanding of the different roles of MIXTA and HD-ZIP transcription factors in tomato

9.2.3.-Does the development of root hairs and trichomes share common regulators?

In *Arabidopsis thaliana*, many of the regulators involved in trichome development are also important in determining root hair development, although they often act in opposite ways (Ishida et al., 2008). For example, GL2 promotes trichome development but inhibits root hair formation in *Arabidopsis* (Rerie et al., 1994, Masucci et al., 1996). I have observed a link between the regulation of trichomes and root hairs in Woolly GE KO plants, where the suppression of the gene led to a massive reduction of trichomes on the leaf epidermis (Fig. 6.6) as well as a reduction in the number of root hairs (Fig. 6.7). I plan to analyse the root epidermis of other GE lines (including the ones generated in *chapter 6* as well as others still under production) by optical and scanning electron microscopy to determine the extent of the shared regulation between developmental of both types of cell outgrowths.

9.2.4.-How do trichomes increase the tolerance to drought?

My results in *chapter 7* clearly indicate that trichome density (as well as stomatal density) plays a major role in determining the water use efficiency of a specific tomato cultivar, and therefore its ultimate tolerance to drought. However, whether this effect is due to a more efficient dissipation of the excess energy from UV radiation, to an increase of the resistance of the leaf-air boundary layer, to changes in ABA content or to the concomitant changes in stomatal density remains unclear. The measurement of water use efficiency in leaves where trichomes have been removed mechanically would provide some insights in the mechanism behind our observations.

9.2.5.-Can we generate whitefly-resistant plants using CRISPR/Cas9 gene editing?

The most resistant line to whitefly infestation among those that I studied in *chapter 8* was IL 8-1, which had a different acylation pattern in the acyl sugar secretions of type I and type IV trichomes. This shift in the acyl sugar composition has been attributed to a defective isopropylmalate synthase, which in *S. pennellii* lacks the C-terminus and is not functional (Ning et al., 2015). In the near future, I aim to test whether editing of the gene encoding this enzyme in commercial cultivars can increase the resistance to whitefly infestation. If this trait can be generated easily by CRISPR/Cas9-mediated gene editing, whitefly resistance could be introduced into any tomato cultivar in a straight-forward way.

References

Abe, M., Katsumata, H., Komeda, Y. and Takahashi, T. (2003) Regulation of shoot epidermal cell differentiation by a pair of homeodomain proteins in *Arabidopsis*. *Development*, **130**, 635-643.

Adams, W.W. and Martin, C.E. (1986) Morphological changes accompanying the transition from juvenile (atmospheric) to adult (tank) forms in the Mexican epiphyte *Tillandsia deppeana (Bromeliaceae*). *American Journal of Botany*, **73**, 1207-1214.

Ajello, L. (1941) Cytology and cellular interrelations of cystolith formation in *Ficus elastica*. *American Journal of Botany*, **28**, 589-594.

Albaladejo, I., Meco, V., Plasencia, F., Flores, F.B., Bolarin, M.C. and Egea, I. (2017) Unravelling the strategies used by the wild tomato species Solanum pennellii to confront salt stress: From leaf anatomical adaptations to molecular responses. *Environmental and Experimental Botany*, **135**, 1-12.

Aldea, M., Hamilton, J.G., Resti, J.P., Zangerl, A.R., Berenbaum, M.R. and De Lucia, E.H. (2005) Indirect effects of insect herbivory on leaf gas exchange in soybean. *Plant, Cell & Environment*, **28**, 402-411.

Alseekh, S., Ofner, I., Pleban, T., Tripodi, P., Di Dato, F., Cammareri, M., Mohammad, A., Grandillo, S., Fernie, A.R. and Zamir, D. (2013) Resolution by recombination: breaking up *Solanum pennellii* introgressions. *Trends in Plant Science*, **18**, 536-538.

An, C. and Mou, Z. (2011) Salicylic acid and its function in plant immunity. *Journal of integrative plant biology*, **53**, 412-428.

An, L., Zhou, Z., Yan, A. and Gan, Y. (2011) Progress on trichome development regulated by phytohormone signaling. *Plant signaling & behavior*, **6**, 1959-1962.

Antunes, W.C., Provart, N.J., Williams, T.C.R. and Loureiro, M.E. (2012) Changes in stomatal function and water use efficiency in potato plants with altered sucrolytic activity. *Plant, Cell & Environment*, **35**, 747-759.

Aoki, K., Ogata, Y., Igarashi, K., Yano, K., Nagasaki, H., Kaminuma, E. and Toyoda, A. (2013) Functional genomics of tomato in a post-genome-sequencing phase. *Breeding Science*, **63**, 14-20.

Appelhagen, I., Thiedig, K., Nordholt, N., Schmidt, N., Huep, G., Sagasser, M. and Weisshaar, B. (2014) Update on transparent testa mutants from Arabidopsis thaliana: characterisation of new alleles from an isogenic collection. *Planta*, **240**, 955-970.

Arce-Rodríguez, M.L. and Ochoa-Alejo, N. (2017) An R2R3-MYB Transcription Factor in Capsaicinoid Biosynthesis. *Plant Physiol.*

Archer, K.J. and Cole, A.L.J. (1986) Cuticle, cell wall ultrastucture and disease resistance in maidenhair fern. *New Phytologist*, **103**, 341-348.

Ariel, F.D., Manavella, P.A., Dezar, C.A. and Chan, R.L. (2007) The true story of the HD-Zip family. *Trends in Plant Science*, **12**, 419-426.

Arpat, A.B., Waugh, M., Sullivan, J.P., Gonzales, M., Frisch, D., Main, D., Wood, T., Leslie, A., Wing, R.A. and Wilkins, T.A. (2004) Functional genomics of cell elongation in developing cotton fibers. *Plant Mol.Biol.*, **54**, 911-929.

Avery, P.B., Kumar, V., Simmonds, M.S.J. and Faull, J. (2015) Influence of leaf trichome type and density on the host plant selection by the greenhouse whitefly, *Trialeurodes vaporariorum* (Hemiptera: Aleyrodidae). *Appl. Entomol. Zoolog.*, **50**, 79-87.

Azoulay-Shemer, T., Palomares, A., Bagheri, A., Israelsson-Nordstrom, M., Engineer, C.B., Bargmann, B.O.R., Stephan, A.B. and Schroeder, J.I. (2015) Guard cell photosynthesis is critical for stomatal turgor production, yet does not directly mediate CO_2- and ABA-induced stomatal closing. *Plant J*, **83**, 567-581.

Balcke, G.U., Bennewitz, S., Bergau, N., Athmer, B., Henning, A., Majovsky, P., Jiménez-Gómez, J.M., Hoehenwarter, W. and Tissier, A. (2017) Multi-Omics of tomato glandular trichomes reveals distinct features of central carbon metabolism supporting high productivity of specialized metabolites. *The Plant Cell*, **29**, 960-983.

Ballester, A.R., Molthoff, J., de Vos, R., Hekkert, B., Orzaez, D., Fernandez-Moreno, J.P., Tripodi, P., Grandillo, S., Martin, C., Heldens, J., Ykema, M., Granell, A. and Bovy, A.

(2010) Biochemical and molecular analysis of pink tomatoes: deregulated expression of the gene encoding transcription factor SlMYB12 leads to pink tomato fruit color. *Plant Physiol*, **152**, 71-84.

Bar, M. and Ori, N. (2014) Leaf development and morphogenesis. *Development (Cambridge, England)*, **141**, 4219-4230.

Barbedo, J.G.A. (2014) Using digital image processing for counting whiteflies on soybean leaves. *Journal of Asia-Pacific Entomology*, **17**, 685-694.

Bargel, H., Koch, K., Cerman, Z. and Neinhuis, C. (2006) Evans Review No. 3: Structure-function relationships of the plant cuticle and cuticular waxes a smart material? *Functional Plant Biology*, **33**, 893-910.

Barrantes, W., Fernandez-del-Carmen, A., Lopez-Casado, G., Gonzalez-Sanchez, M.A., Fernandez-Munoz, R., Granell, A. and Monforte, A.J. (2014) Highly efficient genomics-assisted development of a library of introgression lines of *Solanum pimpinellifolium*. *Molecular Breeding*, **34**, 1817-1831.

Basu, D., El-Assal Sel, D., Le, J., Mallery, E.L. and Szymanski, D.B. (2004) Interchangeable functions of Arabidopsis PIROGI and the human WAVE complex subunit SRA1 during leaf epidermal development. *Development (Cambridge, England)*, **131**, 4345-4355.

Baudry, A., Caboche, M. and Lepiniec, L. (2006) TT8 controls its own expression in a feedback regulation involving TTG1 and homologous MYB and bHLH factors, allowing a strong and cell-specific accumulation of flavonoids in *Arabidopsis thaliana*. *The Plant Journal*, **46**, 768-779.

Bauer, P., Elbaum, R. and Weiss, I.M. (2011) Calcium and silicon mineralization in land plants: Transport, structure and function. *Plant Science*, **180**, 746-756.

Baulcombe, D. (2004) RNA silencing in plants. *Nature*, **431**, 356.

Baumann, K., Perez-Rodriguez, M., Bradley, D., Venail, J., Bailey, P., Jin, H., Koes, R., Roberts, K. and Martin, C. (2007) Control of cell and petal morphogenesis by R2R3 MYB transcription factors. *Development*, **134**, 1691-1701.

Bean, G.J., Marks, M.D., Hülskamp, M., Clayton, M. and Croxdale, J.L. (2002) Tissue patterning of *Arabidopsis* cotyledons. *New Phytologist*, **153**, 461-467.

Bechtold, U., Penfold, C.A., Jenkins, D.J., Legaie, R., Moore, J.D., Lawson, T., Matthews, J.S., Vialet-Chabrand, S.R., Baxter, L., Subramaniam, S., Hickman, R., Florance, H., Sambles, C., Salmon, D.L., Feil, R., Bowden, L., Hill, C., Baker, N.R., Lunn, J.E., Finkenstadt, B., Mead, A., Buchanan-Wollaston, V., Beynon, J., Rand, D.A., Wild, D.L., Denby, K.J., Ott, S., Smirnoff, N. and Mullineaux, P.M. (2016) Time-Series Transcriptomics Reveals That AGAMOUS-LIKE22 Affects Primary Metabolism and Developmental Processes in Drought-Stressed Arabidopsis. *Plant Cell*, **28**, 345-366.

Becker, A. and Lange, M. (2010) VIGS – genomics goes functional. *Trends in Plant Science*, **15**, 1-4.

Bedi, S., Sengupta, S., Ray, A. and Nag Chaudhuri, R. (2016) ABI3 mediates dehydration stress recovery response in Arabidopsis thaliana by regulating expression of downstream genes. *Plant science : an international journal of experimental plant biology*, **250**, 125-140.

Beerling, D.J. and Chaloner, W.G. (1993) The impact of atmospheric CO_2 and temperature changes on stomatal density: observation from *Quercus robur Lammas* leaves. *Annals of Botany*, **71**, 231-235.

Bergau, N., Bennewitz, S., Syrowatka, F., Hause, G. and Tissier, A. (2015) The development of type VI glandular trichomes in the cultivated tomato *Solanum lycopersicum* and a related wild species *S. habrochaites*. *Bmc Plant Biology*, **15**, 15.

Berger, J., Palta, J. and Vadez, V. (2016) Review: An integrated framework for crop adaptation to dry environments: Responses to transient and terminal drought. *Plant Science*, **253**, 58-67.

Bergmann, D.C., Lukowitz, W. and Somerville, C.R. (2004) Stomatal Development and Pattern Controlled by a MAPKK Kinase. *Science*, **304**, 1494-1497.

Bergmann, D.C. and Sack, F.D. (2007) Stomatal development. *Annu Rev Plant Biol*, **58**, 163-181.

Berry, J.A., Beerling, D.J. and Franks, P.J. (2010) Stomata: key players in the earth system, past and present. *Curr Opin Plant Biol*, **13**, 233-240.

Bi, H., Kovalchuk, N., Langridge, P., Tricker, P.J., Lopato, S. and Borisjuk, N. (2017) The impact of drought on wheat leaf cuticle properties. *BMC Plant Biology*, **17**, 85.

Bickford, C. (2016) *Ecophysiology of leaf trichomes*.

Bishop, G.J., Nomura, T., Yokota, T., Harrison, K., Noguchi, T., Fujioka, S., Takatsuto, S., Jones, J.D. and Kamiya, Y. (1999) The tomato DWARF enzyme catalyses C-6 oxidation in brassinosteroid biosynthesis. *Proc Natl Acad Sci U S A*, **96**, 1761-1766.

Bjorkman, C., Dalin, P. and Ahrne, K. (2008) Leaf trichome responses to herbivory in willows: induction, relaxation and costs. *New Phytologist*, **179**, 176-184.

Bleeker, P.M., Mirabella, R., Diergaarde, P.J., VanDoorn, A., Tissier, A., Kant, M.R., Prins, M., de Vos, M., Haring, M.A. and Schuurink, R.C. (2012) Improved herbivore resistance in cultivated tomato with the sesquiterpene biosynthetic pathway from a wild relative. *Proceedings of the National Academy of Sciences of the United States of America*, **109**, 20124-20129.

Bolger, A., Scossa, F., Bolger, M.E., Lanz, C., Maumus, F., Tohge, T., Quesneville, H., Alseekh, S., Sorensen, I., Lichtenstein, G., Fich, E.A., Conte, M., Keller, H., Schneeberger, K., Schwacke, R., Ofner, I., Vrebalov, J., Xu, Y.M., Osorio, S., Aflitos, S.A., Schijlen, E., Jimenez-Gomez, J.M., Ryngajllo, M., Kimura, S., Kumar, R., Koenig, D., Headland, L.R., Maloof, J.N., Sinha, N., van Ham, R., Lankhorst, R.K., Mao, L.Y., Vogel, A., Arsova, B., Panstruga, R., Fei, Z.J., Rose, J.K.C., Zamir, D., Carrari, F., Giovannoni, J.J., Weigel, D., Usadel, B. and Fernie, A.R. (2014) The genome of the stress-tolerant wild tomato species *Solanum pennellii*. *Nature Genet.*, **46**, 1034-+.

Bolotin, A., Quinquis, B., Sorokin, A. and Ehrlich, S.D. (2005) Clustered regularly interspaced short palindrome repeats (CRISPRs) have spacers of extrachromosomal origin. *Microbiology (Reading, England)*, **151**, 2551-2561.

Bolton, M.D. (2009) Primary metabolism and plant defense—fuel for the fire. *Molecular Plant-Microbe Interactions*, **22**, 487-497.

Boom, A., Sinninge Damsté, J.S. and de Leeuw, J.W. (2005) Cutan, a common aliphatic biopolymer in cuticles of drought-adapted plants. *Organic Geochemistry*, **36**, 595-601.

Boughalleb, F. and Hajlaoui, H. (2011) Physiological and anatomical changes induced by drought in two olive cultivars (cv Zalmati and Chemlali). *Acta Physiol. Plant.*, **33**, 53-65.

Boughton, A.J., Hoover, K. and Felton, G.W. (2005) Methyl jasmonate application induces increased densities of glandular trichomes on tomato, *Lycopersicon esculentum*. *Journal of chemical ecology*, **31**, 2211-2216.

Boutros, M. and Ahringer, J. (2008) The art and design of genetic screens: RNA interference. *Nature Reviews Genetics*, **9**, 554.

Brembu, T., Winge, P., Seem, M. and Bones, A.M. (2004) NAPP and PIRP encode subunits of a putative wave regulatory protein complex involved in plant cell morphogenesis. *Plant Cell*, **16**, 2335-2349.

Breuninger, H., Rikirsch, E., Hermann, M., Ueda, M. and Laux, T. (2008) Differential expression of WOX genes mediates apical-basal axis formation in the *Arabidopsis* embryo. *Developmental Cell*, **14**, 867-876.

Brocard-Gifford, I., Lynch, T.J., Garcia, M.E., Malhotra, B. and Finkelstein, R.R. (2004) The Arabidopsis thaliana ABSCISIC ACID-INSENSITIVE8 locus encodes a novel protein mediating abscisic acid and sugar responses essential for growth. *Plant Cell*, **16**, 406-421.

Brockington, S.F., Alvarez-Fernandez, R., Landis, J.B., Alcorn, K., Walker, R.H., Thomas, M.M., Hileman, L.C. and Glover, B.J. (2013) Evolutionary analysis of the MIXTA gene family highlights potential targets for the study of cellular differentiation. *Molecular biology and evolution*, **30**, 526-540.

Buckner, J.S., Freeman, T.P., Ruud, R.L., Chu, C.-c. and Henneberry, T.J. (2002) Characterization and functions of the whitefly egg pedicel. *Archives of Insect Biochemistry and Physiology*, **49**, 22-33.

Bucksch, A., Atta-Boateng, A., Azihou, A.F., Battogtokh, D., Baumgartner, A., Binder, B.M., Braybrook, S.A., Chang, C., Coneva, V., DeWitt, T.J., Fletcher, A.G., Gehan, M.A., Diaz-Martinez, D.H., Hong, L.L., Iyer-Pascuzzi, A.S., Klein, L.L., Leiboff, S., Li, M., Lynch, J.P., Maizel, A., Maloof, J.N., Markelz, R.J.C., Martinez, C.C., Miller, L.A., Mio, W., Palubicki, W., Poorter, H., Pradal, C., Price, C.A., Puttonen, E., Reese, J.B., Rellan-Alvarez, R., Spalding, E.P., Sparks, E.E., Topp, C.N., Williams, J.H. and Chitwood, D.H. (2017) Morphological plant modeling: unleashing geometric and topological potential within the Plant Sciences. *Front. Plant Sci.*, **8**, 16.

Budke, J.M., Goffinet, B. and Jones, C.S. (2012) The cuticle on the gametophyte calyptra matures before the sporophyte cuticle in the moss *Funaria hygrometrica* (Funariaceae). *Am J Bot*, **99**, 14-22.

Burt, S. (2004) Essential oils: their antibacterial properties and potential applications in foods—a review. *International Journal of Food Microbiology*, **94**, 223-253.

Byrne, D.N. and Bellows, T.S. (1991) Whitefly biology. *Annual Review of Entomology*, **36**, 431-457.

Calafiore, R., Ruggieri, V., Raiola, A., Rigano, M.M., Sacco, A., Hassan, M.I., Frusciante, L. and Barone, A. (2016) Exploiting genomics resources to identify candidate genes underlying antioxidants content in tomato fruit. *Front. Plant Sci.*, **7**, 14.

Calo, L., Garcia, I., Gotor, C. and Romero, L.C. (2006) Leaf hairs influence phytopathogenic fungus infection and confer an increased resistance when expressing a Trichoderma alpha-1,3-glucanase. *J Exp Bot*, **57**, 3911-3920.

Campos, M.L., de Almeida, M., Rossi, M.L., Martinelli, A.P., Litholdo Junior, C.G., Figueira, A., Rampelotti-Ferreira, F.T., Vendramim, J.D., Benedito, V.A. and Pereira Peres, L.E. (2009) Brassinosteroids interact negatively with jasmonates in the formation of anti-herbivory traits in tomato. *Journal of Experimental Botany*, **60**, 4347-4361.

Canady, M.A., Meglic, V. and Chetelat, R.T. (2005) A library of *Solanum lycopersicoides* introgression lines in cultivated tomato. *Genome*, **48**, 685-697.

Casteel, C.L., Ranger, C.M., Backus, E.A., Ellersieck, M.R. and Johnson, D.W. (2006) Influence of plant ontogeny and abiotic factors on resistance of glandular-haired alfalfa to potato leafhopper *(Hemiptera : Cicadellidae)*. *Journal of Economic Entomology*, **99**, 537-543.

Causse, M., Desplat, N., Pascual, L., Le Paslier, M.C., Sauvage, C., Bauchet, G., Berard, A., Bounon, R., Tchoumakov, M., Brunel, D. and Bouchet, J.P. (2013) Whole genome resequencing in tomato reveals variation associated with introgression and breeding events. *BMC Genomics*, **14**, 14.

Ceulemans, R., Van Praet, L. and Jiang, X.N. (1995) Effects of CO_2 enrichment, leaf position and clone on stomatal index and epidermal cell density in *poplar* (Populus). *New Phytologist*, **131**, 99-107.

Chang, J., Yu, T., Gao, S., Xiong, C., Xie, Q., Li, H., Ye, Z. and Yang, C. (2016) Fine mapping of the *dialytic* gene that controls multicellular trichome formation and stamen development in tomato. *TAG. Theoretical and applied genetics. Theoretische und angewandte Genetik*, **129**, 1531-1539.

Chang, J., Yu, T., Yang, Q., Li, C., Xiong, C., Gao, S., Xie, Q., Zheng, F., Li, H., Tian, Z., Yang, C. and Ye, Z. (2018) Hair, encoding a single C2H2 zinc-finger protein, regulates multicellular trichome formation in tomato. *The Plant Journal*, **0**.

Channarayappa, C., Shivashankar, G., Muniyappa, V. and Frist, R.H. (1992) Resistance of *Lycopersicon* species to *Bemisia tabaci*, a tomato leaf curl virus vector. *Canadian Journal of Botany*, **70**, 2184-2192.

Chapman, J.R., Taylor, Martin R.G. and Boulton, Simon J. (2012) Playing the end game: DNA double-strand break repair pathway choice. *Molecular Cell*, **47**, 497-510.

Chater, C.C.C., Caine, R.S., Fleming, A.J. and Gray, J.E. (2017) Origins and evolution of stomatal development. *Plant Physiol*, **174**, 624-638.

Chen, B., Brinkmann, K., Chen, Z., Pak, Chi W., Liao, Y., Shi, S., Henry, L., Grishin, Nick V., Bogdan, S. and Rosen, Michael K. (2014) The WAVE regulatory complex links diverse receptors to the actin cytoskeleton. *Cell*, **156**, 195-207.

Chen, B.Y., Chou, H.T., Brautigam, C.A., Xing, W.M., Yang, S., Henry, L., Doolittle, L.K., Walz, T. and Rosen, M.K. (2017) Rac1 GTPase activates the WAVE regulatory complex through two distinct binding sites. *eLife*, **6**, 22.

Chen, Y.-A., Wen, Y.-C. and Chang, W.-C. (2012) AtPAN: an integrated system for reconstructing transcriptional regulatory networks in Arabidopsis thaliana. *BMC Genomics*, **13**, 85.

Chen, Z., Borek, D., Padrick, S.B., Gomez, T.S., Metlagel, Z., Ismail, A.M., Umetani, J., Billadeau, D.D., Otwinowski, Z. and Rosen, M.K. (2010) Structure and control of the actin regulatory WAVE complex. *Nature*, **468**, 533.

Chien, J.C. and Sussex, I.M. (1996) Differential regulation of trichome formation on the adaxial and abaxial leaf surfaces by Gibberellins and photoperiod in Arabidopsis thaliana (L) Heynh. *Plant Physiol.*, **111**, 1321-1328.

Chitwood, D.H., Kumar, R., Headland, L.R., Ranjan, A., Covington, M.F., Ichihashi, Y., Fulop, D., Jimenez-Gomez, J.M., Peng, J., Maloof, J.N. and Sinha, N.R. (2013) A quantitative genetic basis for leaf morphology in a set of precisely defined tomato introgression lines. *Plant Cell*, **25**, 2465-2481.

Cho, H.T. and Cosgrove, D.J. (2002) Regulation of root hair initiation and expansin gene expression in Arabidopsis. *Plant Cell*, **14**, 3237-3253.

Choi, Y.E., Harada, E., Wada, M., Tsuboi, H., Morita, Y., Kusano, T. and Sano, H. (2001) Detoxification of cadmium in tobacco plants: formation and active excretion of crystals containing cadmium and calcium through trichomes. *Planta*, **213**, 45-50.

Cominelli, E., Sala, T., Calvi, D., Gusmaroli, G. and Tonelli, C. (2008) Over-expression of the *Arabidopsis* AtMYB41 gene alters cell expansion and leaf surface permeability. *Plant J*, **53**, 53-64.

Coneva, V., Frank, M.H., Balaguer, M.A.D., Li, M., Sozzani, R. and Chitwood, D.H. (2017) Genetic Architecture and Molecular Networks Underlying Leaf Thickness in Desert-Adapted Tomato Solanum pennellii. *Plant Physiol.*, **175**, 376-391.

Cosgrove, D. (2000) *Loosening of plant cell walls by expansins*.

Cosgrove, D.J. (1998) Cell wall loosening by expansins. *Plant Physiol.*, **118**, 333-339.

Cosgrove, D.J. (2015) Plant expansins: diversity and interactions with plant cell walls. *Curr Opin Plant Biol*, **25**, 162-172.

Cosgrove, D.J. (2016) Plant cell wall extensibility: connecting plant cell growth with cell wall structure, mechanics, and the action of wall-modifying enzymes. *Journal of Experimental Botany*, **67**, 463-476.

Curvers, K., Seifi, H., Mouille, G., de Rycke, R., Asselbergh, B., Van Hecke, A., Vanderschaeghe, D., Höfte, H., Callewaert, N., Van Breusegem, F. and Höfte, M. (2010) Abscisic Acid Deficiency Causes Changes in Cuticle Permeability and Pectin Composition That Influence Tomato Resistance to Botrytis cinerea. *Plant Physiol.*, **154**, 847-860.

Dai, Q., Geng, L., Lu, M., Jin, W., Nan, X., He, P.-a. and Yao, Y. (2017) Comparative transcriptome analysis of the different tissues between the cultivated and wild tomato. *PLOS ONE*, **12**, e0172411.

Dalin, P., Ågren, J., Björkman, C., Huttunen, P. and Kärkkäinen, K. (2008) *Leaf Trichome Formation and Plant Resistance to Herbivory*.

Das, A. (2015) Anticancer effect of antimalarial artemisinin compounds. *Annals of Medical and Health Sciences Research*, **5**, 93-102.

De Sibio, P.R. and Rossi, M.N. (2012) Oviposition of a leaf-miner on *Erythroxylum tortuosum* (Erythroxylaceae) leaves: hierarchical variation of physical leaf traits. *Aust. J. Bot.*, **60**, 136-142.

Dempsey, W.H. and Sherif, T.H.I. (1987) Brittleness in the stem of the seven 'hairless' mutants. *Report of the Tomato Genetics Cooperative*, **37**, 4.

Deng, W., Yang, Y., Ren, Z., Audran-Delalande, C., Mila, I., Wang, X., Song, H., Hu, Y., Bouzayen, M. and Li, Z. (2012) The tomato SlIAA15 is involved in trichome formation and axillary shoot development. *New Phytologist*, **194**, 379-390.

Desvoyes, B., Ramirez-Parra, E., Xie, Q., Chua, N.-H. and Gutierrez, C. (2006) Cell type-specific role of the retinoblastoma/E2F pathway during Arabidopsis leaf development. *Plant Physiol.*, **140**, 67-80.

Dewitte, W. and Murray, J.A.H. (2003) The plant cell cycle. *Annual Review of Plant Biology*, **54**, 235-264.

Di Stilio, V.S., Martin, C., Schulfer, A.F. and Connelly, C.F. (2009) An ortholog of MIXTA-like2 controls epidermal cell shape in flowers of *Thalictrum*. *New Phytologist*, **183**, 718-728.

Dimock, M.B. and Tingey, W.M. (1988) Host acceptance behaviour of Colorado potato beetle larvae influenced by potato glandular trichomes. *Physiological Entomology*, **13**, 399-406.

Dombrecht, B., Xue, G.P., Sprague, S.J., Kirkegaard, J.A., Ross, J.J., Reid, J.B., Fitt, G.P., Sewelam, N., Schenk, P.M., Manners, J.M. and Kazan, K. (2007) MYC2 differentially modulates diverse jasmonate-dependent functions in *Arabidopsis*. *Plant Cell*, **19**, 2225-2245.

Dong, J., MacAlister, C.A. and Bergmann, D.C. (2009) BASL controls asymmetric cell division in Arabidopsis. *Cell*, **137**, 1320-1330.

Dong, Y., Burch-Smith, T.M., Liu, Y., Mamillapalli, P. and Dinesh-Kumar, S.P. (2007) A ligation-independent cloning tobacco rattle virus vector for high-throughput virus-induced gene silencing identifies roles for NbMADS4-1 and -2 in floral development. *Plant Physiol*, **145**, 1161-1170.

Dow, G.J., Berry, J.A. and Bergmann, D.C. (2014) The physiological importance of developmental mechanisms that enforce proper stomatal spacing in *Arabidopsis thaliana*. *New Phytologist*, **201**, 1205-1217.

Drake, P.L., Froend, R.H. and Franks, P.J. (2013) Smaller, faster stomata: scaling of stomatal size, rate of response, and stomatal conductance. *J Exp Bot*, **64**, 495-505.

Du, M., Zhao, J., Tzeng, D.T.W., Liu, Y., Deng, L., Yang, T., Zhai, Q., Wu, F., Huang, Z., Zhou, M., Wang, Q., Chen, Q., Zhong, S., Li, C.-B. and Li, C. (2017) MYC2 orchestrates a hierarchical transcriptional cascade that regulates jasmonate-mediated plant immunity in tomato. *The Plant Cell*.

Du, Y. and Scheres, B. (2017) PLETHORA transcription factors orchestrate de novo organ patterning during *Arabidopsis* lateral root outgrowth. *Proceedings of the National Academy of Sciences*, **114**, 11709-11714.

Edwards, D. (1993) Cells and tissues in the vegetative sporophytes of early land plants. *New Phytologist*, **125**, 225-247.

Egea, I., Albaladejo, I., Meco, V., Morales, B., Sevilla, A., Bolarin, M.C. and Flores, F.B. (2018) The drought-tolerant Solanum pennellii regulates leaf water loss and induces genes involved in amino acid and ethylene/jasmonate metabolism under dehydration. *Scientific Reports*, **8**, 2791.

Ehleringer, J.R. (1988) Comparative ecophysiology of *Encelia farinosa* and *Encelia frutescens* : I. energy balance considerations. *Oecologia*, **76**, 553-561.

Ehleringer, J.R. and Mooney, H.A. (1978) Leaf hairs: effects on physiological activity and adaptive value to a desert shrub. *Oecologia*, **37**, 183-200.

Eigenbrode, S.D. and Espelie, K.E. (1995) Effects of plant epicuticular lipids on insect herbivores. *Annual Review of Entomology*, **40**, 171-194.

Elhiti, M. and Stasolla, C. (2009) Structure and function of homodomain-leucine zipper (HD-Zip) proteins. *Plant Signaling & Behavior*, **4**, 86-88.

Escobar-Bravo, R., Klinkhamer, P.G.L. and Leiss, K.A. (2017) Induction of jasmonic acid-associated defenses by thrips alters host suitability for conspecifics and correlates with increased trichome densities in tomato. *Plant and Cell Physiology*, **58**, 622-634.

Eshed, Y. and Zamir, D. (1995) An introgression line population of *Lycopersicon pennellii* in the cultivated tomato enables the identification and fine mapping of yield-associated QTL. *Genetics*, **141**, 1147-1162.

Estornell, L.H., Orzaez, D., Lopez-Pena, L., Pineda, B., Anton, M.T., Moreno, V. and Granell, A. (2009) A multisite gateway-based toolkit for targeted gene expression and hairpin RNA silencing in tomato fruits. *Plant Biotechnol J*, **7**, 298-309.

Evans, G.A. and Hamon, A.B. (2002) Whitefly taxonomic and ecological website: an on-line interactive catalog of the whiteflies *(Hemiptera: Aleyrodidae)* of the World and their parasites and predators.

Ewas, M., Gao, Y., Ali, F., Nishawy, E.M., Shahzad, R., Subthain, H., Amar, M., Martin, C. and Luo, J. (2017) RNA-seq reveals mechanisms of SlMX1 for enhanced carotenoids and terpenoids accumulation along with stress resistance in tomato. *Sci. Bull.*, **62**, 476-485.

Ewas, M., Gao, Y., Wang, S., Liu, X., Zhang, H., Nishawy, E.M.E., Ali, F., Shahzad, R., Ziaf, K., Subthain, H., Martin, C. and Luo, J. (2016) Manipulation of SlMXl for enhanced carotenoids accumulation and drought resistance in tomato. *Science Bulletin*, **61**, 1413-1418.

Exposito-Rodriguez, M., Borges, A.A., Borges-Perez, A. and Perez, J.A. (2008) Selection of internal control genes for quantitative real-time RT-PCR studies during tomato development process. *BMC Plant Biol*, **8**, 131.

Fahlgren, N., Montgomery, T.A., Howell, M.D., Allen, E., Dvorak, S.K., Alexander, A.L. and Carrington, J.C. (2006) Regulation of AUXIN RESPONSE FACTOR3 by TAS3 ta-siRNA Affects Developmental Timing and Patterning in Arabidopsis. *Current Biology*, **16**, 939-944.

Fahn, A. (1988) Secretory tissues in vascular plants. *New Phytologist*, **108**, 229-257.

Fahn, A. (2000) Structure and function of secretory cells. In *Advances in Botanical Research*: Academic Press, pp. 37-75.

Farber, M., Attia, Z. and Weiss, D. (2016) Cytokinin activity increases stomatal density and transpiration rate in tomato. *Journal of Experimental Botany*, **67**, 6351-6362.

Fauset, S., Freitas, H.C., Galbraith, D.R., Sullivan, M.J.P., Aidar, M.P.M., Joly, C.A., Phillips, O.L., Vieira, S.A. and Gloor, M.U. (2018) Differences in leaf thermoregulation and water use strategies between three co-occurring Atlantic forest tree species. *Plant, Cell & Environment*, **41**, 1618-1631.

Fei, Z., Joung, J.G., Tang, X., Zheng, Y., Huang, M., Lee, J.M., McQuinn, R., Tieman, D.M., Alba, R., Klee, H.J. and Giovannoni, J.J. (2011) Tomato Functional Genomics Database: a comprehensive resource and analysis package for tomato functional genomics. *Nucleic Acids Res*, **39**, D1156-1163.

Fernandez-Moreno, J.-P., Levy-Samoha, D., Malitsky, S., Monforte, A.J., Orzaez, D., Aharoni, A. and Granell, A. (2017) Uncovering tomato quantitative trait loci and candidate genes for fruit cuticular lipid composition using the *Solanum pennellii* introgression line population. *Journal of Experimental Botany*, **68**, 2703-2716.

Fernandez-Pozo, N., Menda, N., Edwards, J.D., Saha, S., Tecle, I.Y., Strickler, S.R., Bombarely, A., Fisher-York, T., Pujar, A., Foerster, H., Yan, A.M. and Mueller, L.A. (2015a) The Sol Genomics Network (SGN)-from genotype to phenotype to breeding. *Nucleic Acids Res.*, **43**, D1036-D1041.

Fernandez-Pozo, N., Rosli, Hernan G., Martin, Gregory B. and Mueller, Lukas A. (2015b) The SGN VIGS Tool: User-Friendly Software to Design Virus-Induced Gene Silencing (VIGS) Constructs for Functional Genomics. *Molecular Plant*, **8**, 486-488.

Fernandez-Pozo, N., Zheng, Y., Snyder, S.I., Nicolas, P., Shinozaki, Y., Fei, Z., Catala, C., Giovannoni, J.J., Rose, J.K.C. and Mueller, L.A. (2017) The Tomato Expression Atlas. *Bioinformatics*, **33**, 2397-2398.

Fernandez, V., Khayet, M., Montero-Prado, P., Heredia-Guerrero, J.A., Liakopoulos, G., Karabourniotis, G., Del Rio, V., Dominguez, E., Tacchini, I., Nerin, C., Val, J. and Heredia, A. (2011) New insights into the properties of pubescent surfaces: peach fruit as a model. *Plant Physiol*, **156**, 2098-2108.

Fernández, V., Sancho-Knapik, D., Guzmán, P., Peguero-Pina, J.J., Gil, L., Karabourniotis, G., Khayet, M., Fasseas, C., Heredia-Guerrero, J.A., Heredia, A. and Gil-Pelegrín, E. (2014) Wettability, polarity, and water absorption of Holm Oak leaves: effect of leaf side and age. *Plant Physiol.*, **166**, 168-180.

Fernie, A.R., Tadmor, Y. and Zamir, D. (2006) Natural genetic variation for improving crop quality. *Current Opinion in Plant Biology*, **9**, 196-202.

Finkers, R., van Heusden, A.W., Meijer-Dekens, F., van Kan, J.A.L., Maris, P. and Lindhout, P. (2007) The construction of a *Solanum habrochaites* LYC4 introgression line population and the identification of QTLs for resistance to *Botrytis cinerea*. *Theor. Appl. Genet.*, **114**, 1071-1080.

Fleming, A.J., McQueen-Mason, S., Mandel, T. and Kuhlemeier, C. (1997) Induction of leaf primordia by the cell wall protein expansin. *Science*, **276**, 1415-1418.

Flowers, T., Flowers, S., Hajibagheri, M. and Yeo, A. (1990) Salt tolerance in the halophytic wild rice, *Porteresia coarctata* Tateoka. *New Phytologist*, **114**, 675-684.

Fobes, J.F., Mudd, J.B. and Marsden, M.P. (1985) Epicuticular lipid accumulation on the leaves of *Lycopersicon pennellii* (Corr.) D'Arcy and L*ycopersicon esculentum* Mill. *Plant Physiol*, **77**, 567-570.

Fracasso, A., Trindade, L.M. and Amaducci, S. (2016) Drought stress tolerance strategies revealed by RNA-Seq in two sorghum genotypes with contrasting WUE. *BMC Plant Biol*, **16**, 115.

Frank, M.J., Cartwright, H.N. and Smith, L.G. (2003) Three Brick genes have distinct functions in a common pathway promoting polarized cell division and cell morphogenesis in the maize leaf epidermis. *Development*, **130**, 753-762.

Franks, P.J. and Beerling, D.J. (2009) Maximum leaf conductance driven by CO2 effects on stomatal size and density over geologic time. *Proc Natl Acad Sci U S A*, **106**, 10343-10347.

Franks, P.J., W. Doheny-Adams, T., Britton-Harper, Z.J. and Gray, J.E. (2015) Increasing water-use efficiency directly through genetic manipulation of stomatal density. *New Phytologist*, **207**, 188-195.

Frary, A., Göl, D., Keleş, D., Ökmen, B., Pınar, H., Şığva, H.Ö., Yemenicioğlu, A. and Doğanlar, S. (2010) Salt tolerance in *Solanum pennellii:* antioxidant response and related QTL. *BMC Plant Biology*, **10**, 58.

Freitas, J.A., Maluf, W.R., Cardoso, M.D., Gomes, L.A.A. and Bearzotti, E. (2002) Inheritance of foliar zingiberene contents and their relationship to trichome densities and whitefly resistance in tomatoes. *Euphytica*, **127**, 275-287.

Frerigmann, H., Böttcher, C., Baatout, D. and Gigolashvili, T. (2012) Glucosinolates are produced in trichomes of Arabidopsis thaliana. *Front. Plant Sci.*, **3**, 242.

Fu, D.-Q., Zhu, B.-Z., Zhu, H.-L., Jiang, W.-B. and Luo, Y.-B. (2005) Virus-induced gene silencing in tomato fruit. *The Plant Journal*, **43**, 299-308.

Fu, Q.S., Yang, R.C., Wang, H.S., Zhao, B., Zhou, C.L., Ren, S.X. and Guo, Y.-D. (2013) Leaf morphological and ultrastructural performance of eggplant (*Solanum melongena* L.) in response to water stress. *Photosynthetica*, **51**, 109-114.

Fuentes, S., Canamero, R.C. and Serna, L. (2012) Relationship between brassinosteroids and genes controlling stomatal production in the Arabidopsis hypocotyl. *Int. J. Dev. Biol.*, **56**, 675-680.

Fulcher, N. and Riha, K. (2015) Using Centromere Mediated Genome Elimination to Elucidate the Functional Redundancy of Candidate Telomere Binding Proteins in Arabidopsis thaliana. *Frontiers in Genetics*, **6**, 349.

Fullana-Pericàs, M., Conesa, M.À., Soler, S., Ribas-Carbó, M., Granell, A. and Galmés, J. (2017) Variations of leaf morphology, photosynthetic traits and water-use efficiency in Western-Mediterranean tomato landraces. *Photosynthetica*, **55**, 121-133.

Fürstenberg-Hägg, J., Zagrobelny, M. and Bak, S. (2013) Plant defense against insect herbivores. *Int J Mol Sci*, **14**, 10242-10297.

Galdon-Armero, J., Fullana-Pericas, M., Mulet, P.A., Conesa, M.A., Martin, C. and Galmes, J. (2018) The ratio of trichomes to stomata is associated with water use efficiency in tomato. *The Plant Journal*, **0**.

Galmés, J., Flexas, J., Savé, R. and Medrano, H. (2007a) Water relations and stomatal characteristics of Mediterranean plants with different growth forms and leaf habits: responses to water stress and recovery. *Plant and Soil*, **290**, 139-155.

Galmés, J., Medrano, H. and Flexas, J. (2007b) Photosynthesis and photoinhibition in response to drought in a pubescent (var. minor) and a glabrous (var. palaui) variety of *Digitalis minor*. *Environmental and Experimental Botany*, **60**, 105-111.

Galmes, J., Ochogavia, J.M., Gago, J., Roldan, E.J., Cifre, J. and Conesa, M.A. (2013) Leaf responses to drought stress in Mediterranean accessions of Solanum lycopersicum: anatomical adaptations in relation to gas exchange parameters. *Plant, Cell & Environment*, **36**, 920-935.

Gan, Y., Kumimoto, R., Liu, C., Ratcliffe, O., Yu, H. and Broun, P. (2006) *GLABROUS INFLORESCENCE STEMS* modulates the regulation by gibberellins of epidermal differentiation and shoot maturation in *Arabidopsis*. *The Plant Cell*, **18**, 1383-1395.

Gan, Y., Liu, C., Yu, H. and Broun, P. (2007) Integration of cytokinin and gibberellin signalling by Arabidopsis transcription factors GIS, ZFP8 and GIS2 in the regulation of epidermal cell fate. *Development (Cambridge, England)*, **134**, 2073-2081.

Gan, Y., Zhou, L., Shen, Z.-J., Shen, Z.-X., Zhang, Y.-Q. and Wang, G.-X. (2010) Stomatal clustering, a new marker for environmental perception and adaptation in terrestrial plants. *Botanical Studies*, **51**.

Gangappa, S.N., Prasad, V.B.R. and Chattopadhyay, S. (2010) Functional interconnection of MYC2 and SPA1 in the photomorphogenic seedling development of *Arabidopsis*. *Plant Physiol*, **154**, 1210-1219.

Gao, S., Gao, Y., Xiong, C., Yu, G., Chang, J., Yang, Q., Yang, C. and Ye, Z. (2017) The tomato B-type cyclin gene, SlCycB2, plays key roles in reproductive organ development, trichome initiation, terpenoids biosynthesis and *Prodenia litura* defense. *Plant Science*, **262**, 103-114.

Gao, X., Wheeler, T., Li, Z., Kenerley, C.M., He, P. and Shan, L. (2011) Silencing GhNDR1 and GhMKK2 compromises cotton resistance to Verticillium wilt. *Plant J*, **66**, 293-305.

Gao, Y., Gao, S., Xiong, C., Yu, G., Chang, J., Ye, Z. and Yang, C. (2015) Comprehensive analysis and expression profile of the homeodomain leucine zipper IV transcription factor family in tomato. *Plant Physiology and Biochemistry*, **96**, 141-153.

Gargallo-Garriga, A., Sardans, J., Perez-Trujillo, M., Rivas-Ubach, A., Oravec, M., Vecerova, K., Urban, O., Jentsch, A., Kreyling, J., Beierkuhnlein, C., Parella, T. and Penuelas, J. (2014) Opposite metabolic responses of shoots and roots to drought. *Scientific Reports*, **4**, 7.

Gatehouse, J.A. (2002) Plant resistance towards insect herbivores: a dynamic interaction. *New Phytologist*, **156**, 145-169.

Geisler, M., Nadeau, J. and Sack, F.D. (2000) Oriented asymmetric divisions that generate the stomatal spacing pattern in Arabidopsis are disrupted by the too many mouths mutation. *The Plant Cell*, **12**, 2075-2086.

George, G.M., van der Merwe, M.J., Nunes-Nesi, A., Bauer, R., Fernie, A.R., Kossmann, J. and Lloyd, J.R. (2010) Virus-induced gene silencing of plastidial soluble inorganic

pyrophosphatase impairs essential leaf anabolic pathways and reduces drought stress tolerance in Nicotiana benthamiana. *Plant Physiol*, **154**, 55-66.

Ghosh, B., Westbrook, T.C. and Jones, A.D. (2014) Comparative structural profiling of trichome specialized metabolites in tomato (*Solanum lycopersicum*) and *S. habrochaites*: acylsugar profiles revealed by UHPLC/MS and NMR. *Metabolomics*, **10**, 496-507.

Gianfagna, T.J., Carter, C.D. and Sacalis, J.N. (1992) Temperature and photoperiod influence trichome density and sesquiterpene content of *Lycopersicon hirsutum f. hirsutum*. *Plant Physiol.*, **100**, 1403-1405.

Gibbs, D.J., Voß, U., Harding, S.A., Fannon, J., Moody, L.A., Yamada, E., Swarup, K., Nibau, C., Bassel, G.W., Choudhary, A., Lavenus, J., Bradshaw, S.J., Stekel, D.J., Bennett, M.J. and Coates, J.C. (2014) AtMYB93 is a novel negative regulator of lateral root development in *Arabidopsis*. *The New phytologist*, **203**, 1194-1207.

Gilding, E.K. and Marks, M.D. (2010) Analysis of purified *glabra3-shapeshifter* trichomes reveals a role for NOECK in regulating early trichome morphogenic events. *Plant J*, **64**, 304-317.

Giovannoni, J., Yen, H., Shelton, B., Miller, S., Vrebalov, J., Kannan, P., Tieman, D., Hackett, R., Grierson, D. and Klee, H. (1999) Genetic mapping of ripening and ethylene-related loci in tomato. *Theor. Appl. Genet.*, **98**, 1005-1013.

Glas, J.J., Schimmel, B.C.J., Alba, J.M., Escobar-Bravo, R., Schuurink, R.C. and Kant, M.R. (2012) Plant glandular trichomes as targets for breeding or engineering of resistance to herbivores. *International Journal of Molecular Sciences*, **13**, 17077-17103.

Glauser, G., Grata, E., Dubugnon, L., Rudaz, S., Farmer, E.E. and Wolfender, J.L. (2008) Spatial and temporal dynamics of jasmonate synthesis and accumulation in Arabidopsis in response to wounding. *The Journal of biological chemistry*, **283**, 16400-16407.

Glover, B.J. (2000) Differentiation in plant epidermal cells. *Journal of Experimental Botany*, **51**, 497-505.

Glover, B.J., Airoldi, C.A. and Moyroud, E. (2016) Epidermis: outer cell layer of the plant. In *eLS*.

Glover, B.J., Bunnewell, S. and Martin, C. (2004) Convergent evolution within the genus Solanum: the specialised anther cone develops through alternative pathways. *Gene*, **331**, 1-7.

Glover, B.J. and Martin, C. (2000) Specification of epidermal cell morphology. In *Advances in Botanical Research*: Academic Press, pp. 193-217.

Glover, B.J., Perez-Rodriguez, M. and Martin, C. (1998) Development of several epidermal cell types can be specified by the same MYB-related plant transcription factor. *Development*, **125**, 3497-3508.

Goldberg, R.B., de Paiva, G. and Yadegari, R. (1994) Plant embryogenesis: zygote to seed. *Science*, **266**, 605-614.

Goley, E.D. and Welch, M.D. (2006) The ARP2/3 complex: an actin nucleator comes of age. *Nature Reviews Molecular Cell Biology*, **7**, 713.

Gorb, E.V. and Gorb, S.N. (2017) Anti-adhesive effects of plant wax coverage on insect attachment. *J Exp Bot*, **68**, 5323-5337.

Gramazio, P., Prohens, J., Plazas, M., Mangino, G., Herraiz, F.J. and Vilanova, S. (2017) Development and genetic characterization of advanced backcross materials and an introgression line population of *Solanum incanum* in a *S. melongena* background. *Front. Plant Sci.*, **8**, 15.

Grandillo, S., Zamir, D. and Tanksley, S.D. (1999) Genetic improvement of processing tomatoes: A 20 years perspective. *Euphytica*, **110**, 85-97.

Gray, W.M. (2004) Hormonal Regulation of Plant Growth and Development. *PLoS Biology*, **2**, e311.

Greenboim-Wainberg, Y., Maymon, I., Borochov, R., Alvarez, J., Olszewski, N., Ori, N., Eshed, Y. and Weiss, D. (2005) Cross talk between gibberellin and cytokinin: the Arabidopsis

GA response inhibitor SPINDLY plays a positive role in cytokinin signaling. *Plant Cell*, **17**, 92-102.

Grefen, C., Stadele, K., Ruzicka, K., Obrdlik, P., Harter, K. and Horak, J. (2008) Subcellular localization and in vivo interactions of the Arabidopsis thaliana ethylene receptor family members. *Molecular plant*, **1**, 308-320.

Grissa, I., Vergnaud, G. and Pourcel, C. (2007) CRISPRFinder: a web tool to identify clustered regularly interspaced short palindromic repeats. *Nucleic Acids Res.*, **35**, W52-W57.

Gudesblat, G.E., Betti, C. and Russinova, E. (2012) Brassinosteroids tailor stomatal production to different environments. *Trends in Plant Science*, **17**, 685-687.

Guerfel, M., Baccouri, O., Boujnah, D., Chaïbi, W. and Zarrouk, M. (2009) Impacts of water stress on gas exchange, water relations, chlorophyll content and leaf structure in the two main Tunisian olive (Olea europaea L.) cultivars. *Scientia Horticulturae*, **119**, 257-263.

Guha, A., Sengupta, D., Kumar Rasineni, G. and Ramachandra Reddy, A. (2010) An integrated diagnostic approach to understand drought tolerance in mulberry (Morus indica L.). *Flora - Morphology, Distribution, Functional Ecology of Plants*, **205**, 144-151.

Gujjar, R.S., Akhtar, M., Rai, A. and Singh, M. (2014) Expression analysis of drought-induced genes in wild tomato line (Solanum habrochaites). *Curr. Sci.*, **107**, 496-502.

Gurr, G.M. and McGrath, D. (2001) Effect of plant variety, plant age and photoperiod on glandular pubescence and host-plant resistance to potato moth (*Phthorimaea operculella*) in *Lycopersicon spp*. *Ann. Appl. Biol.*, **138**, 221-230.

Ha, Y., Shang, Y. and Nam, K.H. (2016) Brassinosteroids modulate ABA-induced stomatal closure in Arabidopsis. *J Exp Bot*, **67**, 6297-6308.

Haecker, A., Groß-Hardt, R., Geiges, B., Sarkar, A., Breuninger, H., Herrmann, M. and Laux, T. (2004) Expression dynamics of WOX genes mark cell fate decisions during early embryonic patterning in *Arabidopsis thaliana*. *Development*, **131**, 657-668.

Hajjar, R. and Hodgkin, T. (2007) The use of wild relatives in crop improvement: a survey of developments over the last 20 years. *Euphytica*, **156**, 1-13.

Hamanishi, E.T., Thomas, B.R. and Campbell, M.M. (2012) Drought induces alterations in the stomatal development program in Populus. *Journal of Experimental Botany*, **63**, 4959-4971.

Han, X., Hu, Y., Zhang, G., Jiang, Y., Chen, X. and Yu, D. (2018) Jasmonate negatively regulates stomatal development in *Arabidopsis* cotyledons. *Plant Physiol.*, **176**, 2871-2885.

Handley, R., Ekbom, B. and Ågren, J. (2005) Variation in trichome density and resistance against a specialist insect herbivore in natural populations of Arabidopsis thaliana. *Ecological Entomology*, **30**, 284-292.

Hanley, M.E., Lamont, B.B., Fairbanks, M.M. and Rafferty, C.M. (2007) Plant structural traits and their role in anti-herbivore defence. *Perspectives in Plant Ecology, Evolution and Systematics*, **8**, 157-178.

Hara, K., Kajita, R., Torii, K.U., Bergmann, D.C. and Kakimoto, T. (2007) The secretory peptide gene EPF1 enforces the stomatal one-cell-spacing rule. *Genes & development*, **21**, 1720-1725.

Hara, K., Yokoo, T., Kajita, R., Onishi, T., Yahata, S., Peterson, K.M., Torii, K.U. and Kakimoto, T. (2009) Epidermal Cell Density is Autoregulated via a Secretory Peptide, EPIDERMAL PATTERNING FACTOR 2 in Arabidopsis Leaves. *Plant and Cell Physiology*, **50**, 1019-1031.

Hassan, H., Scheres, B. and Blilou, I. (2010) JACKDAW controls epidermal patterning in the *Arabidopsis* root meristem through a non-cell-autonomous mechanism. *Development (Cambridge, England)*, **137**, 1523-1529.

Hauser, M.-T. (2014) Molecular basis of natural variation and environmental control of trichome patterning. *Front. Plant Sci.*, **5**, 320.

Heichel, G.H. and Anagnostakis, S.L. (1978) Stomatal response to light of *Solanum pennellii, Lycopersicon esculentum*, and a graft-induced chimera. *Plant Physiol.*, **62**, 387-390.

Heinz, K.M. and Zalom, F.G. (1995) Variation in trichome-based resistance to *Bemisia argentifolii (Homoptera: Aleyrodidae*) oviposition on tomato. *Journal of Economic Entomology*, **88**, 1494-1502.

Hepworth, C., Caine, R.S., Harrison, E.L., Sloan, J. and Gray, J.E. (2018) Stomatal development: focusing on the grasses. *Current Opinion in Plant Biology*, **41**, 1-7.

Heslop-Harrison, Y. and Shivanna, K.R. (1977) The receptive surface of the angiosperm stigma. *Annals of Botany*, **41**, 1233-1258.

Hetherington, A.M. and Woodward, F.I. (2003) The role of stomata in sensing and driving environmental change. *Nature*, **424**, 901-908.

Hirt, H. (1996) In and out of the plant cell cycle. *Plant Mol.Biol.*, **31**, 459-464.

Holloway, P.J. and Baker, E.A. (1974) The aerial surfaces of higher plants. *Principles and Techniques of Scanning Electron Microscopy*, 181-205.

Honys, D. and Twell, D. (2004) Transcriptome analysis of haploid male gametophyte development in Arabidopsis. *Genome biology*, **5**, R85.

Hossain, Z., Amyot, L., McGarvey, B., Gruber, M., Jung, J. and Hannoufa, A. (2012) The translation elongation factor eEF-1Bβ1 is involved in cell wall biosynthesis and plant development in *Arabidopsis thaliana*. *PLOS ONE*, **7**, e30425.

Hsieh, T.H., Lee, J.T., Charng, Y.Y. and Chan, M.T. (2002) Tomato plants ectopically expressing Arabidopsis CBF1 show enhanced resistance to water deficit stress. *Plant Physiol.*, **130**, 618-626.

Huchelmann, A., Boutry, M. and Hachez, C. (2017) Plant glandular trichomes: natural cell factories of high biotechnological interest. *Plant Physiol.*, **175**, 6-22.

Hülskamp, M. (2004) Plant trichomes: a model for cell differentiation. *Nature Reviews Molecular Cell Biology*, **5**, 471.

Hunt, L. and Gray, J.E. (2009) The signaling peptide EPF2 controls asymmetric cell divisions during stomatal development. *Current biology : CB*, **19**, 864-869.

Igarashi, A., Yamagata, K., Sugai, T., Takahashi, Y., Sugawara, E., Tamura, A., Yaegashi, H., Yamagishi, N., Takahashi, T., Isogai, M., Takahashi, H. and Yoshikawa, N. (2009) Apple latent spherical virus vectors for reliable and effective virus-induced gene silencing among a broad range of plants including tobacco, tomato, Arabidopsis thaliana, cucurbits, and legumes. *Virology*, **386**, 407-416.

Inbar, M. and Gerlin, D. (2008) Plant-mediated interactions between whiteflies, herbivores, and natural enemies. *Annual Review of Entomology*, **53**, 431-448.

Ingram, G.C., Magnard, J.-L., Vergne, P., Dumas, C. and Rogowsky, P.M. (1999) ZmOCL1, an HDGL2 family homeobox gene, is expressed in the outer cell layer throughout maize development. *Plant Mol.Biol.*, **40**, 343-354.

Iovieno, P., Punzo, P., Guida, G., Mistretta, C., Van Oosten, M.J., Nurcato, R., Bostan, H., Colantuono, C., Costa, A., Bagnaresi, P., Chiusano, M.L., Albrizio, R., Giorio, P., Batelli, G. and Grillo, S. (2016) Transcriptomic Changes Drive Physiological Responses to Progressive Drought Stress and Rehydration in Tomato. *Front. Plant Sci.*, **7**.

IPCC (2007) Climate Change 2007: Synthesis Report. Contributionof Working Groups I, Ii and Iii to the Fourth Assessment Report of the Intergovernmental Panel on Climate Change.

Ishida, T., Kurata, T., Okada, K. and Wada, T. (2008) A genetic regulatory network in the development of trichomes and root hairs. *Annual Review of Plant Biology*, **59**, 365-386.

Ishino, Y., Shinagawa, H., Makino, K., Amemura, M. and Nakata, A. (1987) Nucleotide sequence of the iap gene, responsible for alkaline phosphatase isozyme conversion in Escherichia coli, and identification of the gene product. *Journal of Bacteriology*, **169**, 5429-5433.

Ito, Y., Nishizawa-Yokoi, A., Endo, M., Mikami, M. and Toki, S. (2015) CRISPR/Cas9-mediated mutagenesis of the RIN locus that regulates tomato fruit ripening. *Biochemical and Biophysical Research Communications*, **467**, 76-82.

Jacobsen, S.E. and Olszewski, N.E. (1993) Mutations at the SPINDLY locus of Arabidopsis alter gibberellin signal transduction. *Plant Cell*, **5**, 887-896.

Jacques, E., Verbelen, J.-P. and Vissenberg, K. (2014) *Review on shape formation in epidermal pavement cells of the Arabidopsis leaf*.

Jaffé, F.W., Tattersall, A. and Glover, B.J. (2007) A truncated MYB transcription factor from *Antirrhinum majus* regulates epidermal cell outgrowth. *Journal of Experimental Botany*, **58**, 1515-1524.

Javelle, M., Vernoud, V., Rogowsky, P.M. and Ingram, G.C. (2011) Epidermis: the formation and functions of a fundamental plant tissue. *The New phytologist*, **189**, 17-39.

Jeffree, C.E. (2006) The fine structure of the plant cuticle. *Biology of the plant cuticle*, **23**, 11-125.

Jeong, N.-R., Kim, H., Hwang, I.-T., Howe, G.A. and Kang, J.-H. (2017) Genetic analysis of the tomato inquieta mutant links the ARP2/3 complex to trichome development. *Journal of Plant Biology*, **60**, 582-592.

Jetter, R., Kunst, L. and Samuels, A.L. (2008) Composition of plant cuticular waxes. *Biology of the plant cuticle*, **23**, 145-181.

Jinek, M., Chylinski, K., Fonfara, I., Hauer, M., Doudna, J.A. and Charpentier, E. (2012) A programmable dual-RNA–Guided DNA endonuclease in adaptive bacterial immunity. *Science*, **337**, 816-821.

Johnson, C.S., Kolevski, B. and Smyth, D.R. (2002) TRANSPARENT TESTA GLABRA2, a Trichome and Seed Coat Development Gene of Arabidopsis, Encodes a WRKY Transcription Factor. *Plant Cell*, **14**, 1359-1375.

Jones, D.R. (2003) Plant viruses transmitted by whiteflies. *European Journal of Plant Pathology*, **109**, 195-219.

Jung, Y.J., Nou, I.S., Cho, Y.G., Kim, M.K., Kim, H.T. and Kang, K.K. (2016) Identification of an SNP variation of elite tomato (Solanum lycopersicum L.) lines using genome resequencing analysis. *Hortic. Environ. Biotechnol.*, **57**, 173-181.

Juvik, J.A., Berlinger, M.J., Ben-David, T. and Rudich, J. (1982) Resistance among accessions of the genera *Lycopersicon* and *Solanum* to four of the main insect pests of tomato in Israel. *Phytoparasitica*, **10**, 145-156.

Kadej, A.J., Wilms, H.J. and Willemse, M.T.M. (1985) Stigma and stigmatoid tissue of *Lycopersicon esculentum* Mill. *Acta Botanica Neerlandica*, **34**, 95-103.

Kahn, T.L., Fender, S.E., Bray, E.A. and O'Connell, M.A. (1993) Characterization of expression of drought- and abscisic acid-regulated tomato genes in the drought-resistant species *Lycopersicon pennellii*. *Plant Physiol.*, **103**, 597-605.

Kanaoka, M.M., Pillitteri, L.J., Fujii, H., Yoshida, Y., Bogenschutz, N.L., Takabayashi, J., Zhu, J.-K. and Torii, K.U. (2008) SCREAM/ICE1 and SCREAM2 specify three cell-state transitional steps leading to *Arabidopsis* stomatal differentiation. *The Plant Cell*, **20**, 1775-1785.

Kang, J.-H., Shi, F., Jones, A.D., Marks, M.D. and Howe, G.A. (2010a) Distortion of trichome morphology by the *hairless* mutation of tomato affects leaf surface chemistry. *Journal of Experimental Botany*, **61**, 1053-1064.

Kang, J.H., Campos, M.L., Zemelis-Durfee, S., Al-Haddad, J.M., Jones, A.D., Telewski, F.W., Brandizzi, F. and Howe, G.A. (2016) Molecular cloning of the tomato Hairless gene implicates actin dynamics in trichome-mediated defense and mechanical properties of stem tissue. *J Exp Bot*, **67**, 5313-5324.

Kang, J.H., Liu, G., Shi, F., Jones, A.D., Beaudry, R.M. and Howe, G.A. (2010b) The tomato *odorless-2* mutant is defective in trichome-based production of diverse specialized metabolites and broad-spectrum resistance to insect herbivores. *Plant Physiol*, **154**, 262-272.

Kang, J.H., McRoberts, J., Shi, F., Moreno, J.E., Jones, A.D. and Howe, G.A. (2014) The flavonoid biosynthetic enzyme chalcone isomerase modulates terpenoid production in glandular trichomes of tomato. *Plant Physiol*, **164**, 1161-1174.

Karimi, M., Inze, D. and Depicker, A. (2002) GATEWAY vectors for *Agrobacterium*-mediated plant transformation. *Trends Plant Sci*, **7**, 193-195.

Karlova, R., van Haarst, J.C., Maliepaard, C., van de Geest, H., Bovy, A.G., Lammers, M., Angenent, G.C. and de Maagd, R.A. (2013) Identification of microRNA targets in tomato fruit development using high-throughput sequencing and degradome analysis. *Journal of Experimental Botany*, **64**, 1863-1878.

Kasili, R., Huang, C.-C., Walker, J.D., Simmons, L.A., Zhou, J., Faulk, C., Hülskamp, M. and Larkin, J.C. (2011) BRANCHLESS TRICHOMES links cell shape and cell cycle control in Arabidopsis trichomes. *Development (Cambridge, England)*, **138**, 2379-2388.

Kaur, P., Samuel, D.V.K. and Bansal, K.C. (2010) Fruit-specific over-expression of *LeEXP1* gene in tomato alters fruit texture. *Journal of Plant Biochemistry and Biotechnology*, **19**, 177-183.

Kay, Q.O.N., Daoud, H.S. and Stirton, C.H. (1981) Pigment distribution, light reflection and cell structure in petals. *Botanical Journal of the Linnean Society*, **83**, 57-83.

Kazama, H., Dan, H., Imaseki, H. and Wasteneys, G.O. (2004) Transient exposure to ethylene stimulates cell division and alters the fate and polarity of hypocotyl epidermal cells. *Plant Physiol*, **134**, 1614-1623.

Kerchev, P.I., Fenton, B., Foyer, C.H. and Hancock, R.D. (2012) Plant responses to insect herbivory: interactions between photosynthesis, reactive oxygen species and hormonal signalling pathways. *Plant, Cell & Environment*, **35**, 441-453.

Kevan, P.G. and Lane, M.A. (1985) Flower petal microtexture is a tactile cue for bees. *Proceedings of the National Academy of Sciences*, **82**, 4750-4752.

Khazaei, H., Monneveux, P., Hongbo, S. and Mohammady, S. (2010) Variation for stomatal characteristics and water use efficiency among diploid, tetraploid and hexaploid Iranian wheat landraces. *Genet Resour Crop Evol*, **57**, 307-314.

Khosla, A., Paper, J.M., Boehler, A.P., Bradley, A.M., Neumann, T.R. and Schrick, K. (2014) HD-Zip Proteins GL2 and HDG11 Have Redundant Functions in Arabidopsis Trichomes, and GL2 Activates a Positive Feedback Loop via MYB23. *Plant Cell*, **26**, 2184-2200.

Kil, E.-J., Kim, S., Lee, Y.-J., Byun, H.-S., Park, J., Seo, H., Kim, C.-S., Shim, J.-K., Lee, J.-H., Kim, J.-K., Lee, K.-Y., Choi, H.-S. and Lee, S. (2016) Tomato yellow leaf curl virus (TYLCV-IL): a seed-transmissible geminivirus in tomatoes. *Scientific Reports*, **6**, 19013.

Kim, J.-S., Yamaguchi-Shinozaki, K. and Shinozaki, K. (2018a) ER-Anchored Transcription Factors bZIP17 and bZIP28 Regulate Root Elongation. *Plant Physiol.*

Kim, J., Lee, H.W., Kang, N.Y., Pandey, S., Cho, C. and Lee, S.H. (2017) Dimerization in LBD16 and LBD18 transcription factors is critical for lateral root formation. *Plant Physiol.*

Kim, J.E., Oh, S.K., Lee, J.H., Lee, B.M. and Jo, S.H. (2014) Genome-Wide SNP calling using next generation sequencing data in tomato. *Mol. Cells*, **37**, 36-42.

Kim, S.Y., Hyoung, S., So, W.M. and Shin, J.S. (2018b) The novel transcription factor TRP interacts with ZFP5, a trichome initiation-related transcription factor, and negatively regulates trichome initiation through gibberellic acid signaling. *Plant Mol.Biol.*, **96**, 315-326.

Kirik, V., Lee, M.M., Wester, K., Herrmann, U., Zheng, Z., Oppenheimer, D., Schiefelbein, J. and Hulskamp, M. (2005) Functional diversification of MYB23 and GL1 genes in trichome morphogenesis and initiation. *Development (Cambridge, England)*, **132**, 1477-1485.

Kirik, V., Simon, M., Huelskamp, M. and Schiefelbein, J. (2004a) The ENHANCER OF TRY AND CPC1 gene acts redundantly with TRIPTYCHON and CAPRICE in trichome and root hair cell patterning in Arabidopsis. *Developmental biology*, **268**, 506-513.

Kirik, V., Simon, M., Wester, K., Schiefelbein, J. and Hulskamp, M. (2004b) ENHANCER of TRY and CPC 2 (ETC2) reveals redundancy in the region-specific control of trichome development of Arabidopsis. *Plant molecular biology*, **55**, 389-398.

Kirik, V., Simon, M., Wester, K., Schiefelbein, J. and Hulskamp, M. (2004c) ENHANCER of TRY and CPC 2 (ETC2) reveals redundancy in the region-specific control of trichome development of Arabidopsis. *Plant Mol.Biol.*, **55**, 389-398.

Klepikova, A.V., Kasianov, A.S., Gerasimov, E.S., Logacheva, M.D. and Penin, A.A. (2016) A high resolution map of the Arabidopsis thaliana developmental transcriptome based on RNA-seq profiling. *The Plant Journal*, **88**, 1058-1070.

Koenig, D., Jiménez-Gómez, J.M., Kimura, S., Fulop, D., Chitwood, D.H., Headland, L.R., Kumar, R., Covington, M.F., Devisetty, U.K., Tat, A.V., Tohge, T., Bolger, A., Schneeberger, K., Ossowski, S., Lanz, C., Xiong, G., Taylor-Teeples, M., Brady, S.M., Pauly, M., Weigel, D., Usadel, B., Fernie, A.R., Peng, J., Sinha, N.R. and Maloof, J.N. (2013) Comparative transcriptomics reveals patterns of selection in domesticated and wild tomato. *Proceedings of the National Academy of Sciences*, **110**, E2655-E2662.

Koka, C.V., Cerny, R.E., Gardner, R.G., Noguchi, T., Fujioka, S., Takatsuto, S., Yoshida, S. and Clouse, S.D. (2000) A putative role for the tomato genes DUMPY and CURL-3 in brassinosteroid biosynthesis and response. *Plant Physiol*, **122**, 85-98.

Kolattukudy, P.E. (2001) Polyesters in higher plants. In *Biopolyesters* (Babel, W. and Steinbüchel, A. eds). Berlin, Heidelberg: Springer Berlin Heidelberg, pp. 1-49.

Kong, D., Karve, R., Willet, A., Chen, M.-K., Oden, J. and Shpak, E.D. (2012) Regulation of plasmodesmatal permeability and stomatal patterning by the glycosyltransferase-like protein KOBITO1. *Plant Physiol.*, **159**, 156-168.

Koo, A.J. and Howe, G.A. (2009) The wound hormone jasmonate. *Phytochemistry*, **70**, 1571-1580.

Koornneef, M., Jorna, M.L., Brinkhorst-van der Swan, D.L.C. and Karssen, C.M. (1982) The isolation of abscisic acid (ABA) deficient mutants by selection of induced revertants in non-germinating gibberellin sensitive lines of Arabidopsis thaliana (L.) heynh. *Theor. Appl. Genet.*, **61**, 385-393.

Kranz, H.D., Denekamp, M., Greco, R., Jin, H., Leyva, A., Meissner, R.C., Petroni, K., Urzainqui, A., Bevan, M., Martin, C., Smeekens, S., Tonelli, C., Paz-Ares, J. and Weisshaar, B. (1998) Towards functional characterisation of the members of the R2R3-MYB gene family from Arabidopsis thaliana. *The Plant Journal*, **16**, 263-276.

Krauss, P., Markstadter, C. and Riederer, M. (1997) Attenuation of UV radiation by plant cuticles from woody species. *Plant, Cell & Environment*, **20**, 1079-1085.

Kriton, K., Tobias, S.H., Tasos, A. and Maria, H.J. (2008) RNA silencing movement in plants. *Biology of the Cell*, **100**, 13-26.

Kubo, H., Peeters, A.J.M., Aarts, M.G.M., Pereira, A. and Koornneef, M. (1999) ANTHOCYANINLESS2, a homeobox gene affecting anthocyanin distribution and root development in *Arabidopsis*. *The Plant Cell*, **11**, 1217-1226.

Kung, S.H., Lund, S., Murarka, A., McPhee, D. and Paddon, C.J. (2018) Approaches and recent developments for the commercial production of semi-synthetic artemisinin. *Front Plant Sci*, **9**.

Kupper, H., Lombi, E., Zhao, F.J. and McGrath, S.P. (2000) Cellular compartmentation of cadmium and zinc in relation to other elements in the hyperaccumulator *Arabidopsis halleri*. *Planta*, **212**, 75-84.

Kwak, S.-H., Shen, R. and Schiefelbein, J. (2005) Positional Signaling Mediated by a Receptor-like Kinase in Arabidopsis. *Science*, **307**, 1111-1113.

Kwak, S.-H., Woo, S., Lee, M.M. and Schiefelbein, J. (2014) Distinct signaling mechanisms in multiple developmental pathways by the SCRAMBLED receptor of *Arabidopsis*. *Plant Physiol.*, **166**, 976-987.

Lacomme, C. and Chapman, S. (2008) Use of potato virus X (PVX)-based vectors for gene expression and virus-induced gene silencing (VIGS). *Current protocols in microbiology*, **Chapter 16**, Unit 16I.11.

Lai, L.B., Nadeau, J.A., Lucas, J., Lee, E.K., Nakagawa, T., Zhao, L., Geisler, M. and Sack, F.D. (2005) The Arabidopsis R2R3 MYB proteins FOUR LIPS and MYB88 restrict divisions late in the stomatal cell lineage. *Plant Cell*, **17**, 2754-2767.

Lampard, G.R., MacAlister, C.A. and Bergmann, D.C. (2008) *Arabidopsis* stomatal initiation is controlled by MAPK-mediated regulation of the bHLH SPEECHLESS. *Science*, **322**, 1113-1116.

Lampard, G.R., Wengier, D.L. and Bergmann, D.C. (2014) Manipulation of mitogen-activated protein kinase kinase signaling in the Arabidopsis stomatal lineage reveals motifs that contribute to protein localization and signaling specificity. *The Plant Cell*, tpc. 114.127415.

Landy, A. (1989) Dynamic, structural, and regulatory aspects of lambda site-specific recombination. *Annual Review of Biochemistry*, **58**, 913-941.

Larkin, J.C., Brown, M.L. and Schiefelbein, J. (2003) How do cells know what they want to be when they grow up? Lessons from epidermal patterning in *Arabidopsis*. *Annual Review of Plant Biology*, **54**, 403-430.

Larkin, J.C., Marks, M.D., Nadeau, J. and Sack, F. (1997) Epidermal cell fate and patterning in leaves. *The Plant Cell*, **9**, 1109-1120.

Larkin, J.C., Oppenheimer, D.G., Lloyd, A.M., Paparozzi, E.T. and Marks, M.D. (1994) Roles of the GLABROUS1 and TRANSPARENT TESTA GLABRA genes in *Arabidopsis* trichome development. *Plant Cell*, **6**, 1065-1076.

Larkin, J.C., Young, N., Prigge, M. and Marks, M.D. (1996) The control of trichome spacing and number in Arabidopsis. *Development (Cambridge, England)*, **122**, 997-1005.

Lashbrooke, J., Adato, A., Lotan, O., Alkan, N., Tsimbalist, T., Rechav, K., Fernandez-Moreno, J.-P., Widemann, E., Grausem, B., Pinot, F., Granell, A., Costa, F. and Aharoni, A. (2015) The tomato MIXTA-like transcription factor coordinates fruit epidermis, conical cell development and cuticular lipid biosynthesis and assembly. *Plant Physiol.*, **169**, 2553-2571.

Lawson, T. and Blatt, M.R. (2014) Stomatal size, speed, and responsiveness impact on photosynthesis and water use efficiency. *Plant Physiol.*, **164**, 1556-1570.

Laxmi, A., Paul, L.K., Peters, J.L. and Khurana, J.P. (2004) Arabidopsis constitutive photomorphogenic mutant, bls1, displays altered brassinosteroid response and sugar sensitivity. *Plant molecular biology*, **56**, 185-201.

Leckie, B.M., D'Ambrosio, D.A., Chappell, T.M., Halitschke, R., De Jong, D.M., Kessler, A., Kennedy, G.G. and Mutschler, M.A. (2016) Differential and synergistic functionality of acylsugars in suppressing oviposition by insect herbivores. *Plos One*, **11**, 19.

Leckie, B.M., De Jong, D.M. and Mutschler, M.A. (2013) Quantitative trait loci regulating sugar moiety of acylsugars in tomato. *Molecular Breeding*, **31**, 957-970.

Lee, J.S., Hnilova, M., Maes, M., Lin, Y.-C.L., Putarjunan, A., Han, S.-K., Avila, J. and Torii, K.U. (2015) Competitive binding of antagonistic peptides fine-tunes stomatal patterning. *Nature*, **522**, 439.

Lee, J.S., Kuroha, T., Hnilova, M., Khatayevich, D., Kanaoka, M.M., McAbee, J.M., Sarikaya, M., Tamerler, C. and Torii, K.U. (2012) Direct interaction of ligand–receptor pairs specifying stomatal patterning. *Genes & Development*, **26**, 126-136.

Lee, M.M. and Schiefelbein, J. (1999) WEREWOLF, a MYB-related protein in Arabidopsis, is a position-dependent regulator of epidermal cell patterning. *Cell*, **99**, 473-483.

Lee, S.B. and Suh, M.C. (2015) Advances in the understanding of cuticular waxes in *Arabidopsis thaliana* and crop species. *Plant Cell Rep*, **34**, 557-572.

Leveau Johan, H.J. (2006) *Microbial communities in the phyllosphere*.

Levin, D.A. (1973) The Role of Trichomes in Plant Defense. *The Quarterly Review of Biology*, **48**, 3-15.

Levinson, H.Z. (1976) The defensive role of alkaloids in insects and plants. *Experientia*, **32**, 408-411.

Li, C., Ng, C.K.Y. and Fan, L.-M. (2015) MYB transcription factors, active players in abiotic stress signaling. *Environmental and Experimental Botany*, **114**, 80-91.

Li, J., Wen, J., Lease, K.A., Doke, J.T., Tax, F.E. and Walker, J.C. (2002) BAK1, an *Arabidopsis* LRR receptor-like protein kinase, interacts with BRI1 and modulates brassinosteroid signaling. *Cell*, **110**, 213-222.

Li, J., Zhu, L., Hull, J.J., Liang, S., Daniell, H., Jin, S. and Zhang, X. (2016a) Transcriptome analysis reveals a comprehensive insect resistance response mechanism in cotton to infestation by the phloem feeding insect *Bemisia tabaci* (whitefly). *Plant Biotechnol J*, **14**, 1956-1975.

Li, L., Zhao, Y., McCaig, B.C., Wingerd, B.A., Wang, J., Whalon, M.E., Pichersky, E. and Howe, G.A. (2004) The tomato homolog of CORONATINE-INSENSITIVE1 is required for the maternal control of seed maturation, jasmonate-signaled defense responses, and glandular trichome development. *The Plant Cell*, **16**, 126-143.

Li, X.-J., Chen, X.-J., Guo, X., Yin, L.-L., Ahammed, G.J., Xu, C.-J., Chen, K.-S., Liu, C.-C., Xia, X.-J., Shi, K., Zhou, J., Zhou, Y.-H. and Yu, J.-Q. (2016b) DWARF overexpression induces alteration in phytohormone homeostasis, development, architecture and carotenoid accumulation in tomato. *Plant Biotechnology Journal*, **14**, 1021-1033.

Li, Y., Li, H., Li, Y. and Zhang, S. (2017) Improving water-use efficiency by decreasing stomatal conductance and transpiration rate to maintain higher ear photosynthetic rate in drought-resistant wheat. *The Crop Journal*, **5**, 231-239.

Li, Y., Sorefan, K., Hemmann, G. and Bevan, M.W. (2004c) *Arabidopsis* NAP and PIR regulate actin-based cell morphogenesis and multiple developmental processes. *Plant Physiol.*, **136**, 3616-3627.

Liang, G., He, H., Li, Y., Ai, Q. and Yu, D. (2014) MYB82 functions in regulation of trichome development in Arabidopsis. *Journal of Experimental Botany*, **65**, 3215-3223.

Liedl, B.E., Lawson, D.M., White, K.K., Shapiro, J.A., Cohen, D.E., Carson, W.G., Trumble, J.T. and Mutschler, M.A. (1995) Acylsugars of wild tomato *Lycopersicon pennellii* alters settling and reduces oviposition of *Bemisia argentifolii (Homoptera: Aleyrodidae*). *Journal of Economic Entomology*, **88**, 742-748.

Lim, C.W., Baek, W., Jung, J., Kim, J.-H. and Lee, S.C. (2015) Function of ABA in Stomatal Defense against Biotic and Drought Stresses. *International Journal of Molecular Sciences*, **16**, 15251-15270.

Lin, G., Zhang, L., Han, Z., Yang, X., Liu, W., Li, E., Chang, J., Qi, Y., Shpak, E.D. and Chai, J. (2017) A receptor-like protein acts as a specificity switch for the regulation of stomatal development. *Genes & development*, **31**, 927-938.

Lin, S.Y.H., Trumble, J.T. and Kumamoto, J. (1987) Activity of volatile compounds in glandular trichomes of *Lycopersicon* species against two insect herbivores. *Journal of chemical ecology*, **13**, 837-850.

Lin, T., Zhu, G.T., Zhang, J.H., Xu, X.Y., Yu, Q.H., Zheng, Z., Zhang, Z.H., Lun, Y.Y., Li, S., Wang, X.X., Huang, Z.J., Li, J.M., Zhang, C.Z., Wang, T.T., Zhang, Y.Y., Wang, A.X., Zhang, Y.C., Lin, K., Li, C.Y., Xiong, G.S., Xue, Y.B., Mazzucato, A., Causse, M., Fei, Z.J., Giovannoni, J.J., Chetelat, R.T., Zamir, D., Stadler, T., Li, J.F., Ye, Z.B., Du, Y.C. and Huang, S.W. (2014) Genomic analyses provide insights into the history of tomato breeding. *Nature Genet.*, **46**, 1220-1226.

Lindquist, R.K., Bauerle, W.L. and Spadafora, R.R. (1972) Effect of the greenhouse whitefly on yields of greenhouse tomatoes. *Journal of Economic Entomology*, **65**, 1406-1408.

Liscum, E. and Reed, J.W. (2002) Genetics of Aux/IAA and ARF action in plant growth and development. *Plant molecular biology*, **49**, 387-400.

Liu, E.K., Mei, X.R., Yan, C.R., Gong, D.Z. and Zhang, Y.Q. (2016a) Effects of water stress on photosynthetic characteristics, dry matter translocation and WUE in two winter wheat genotypes. *Agricultural Water Management*, **167**, 75-85.

Liu, S.B., Zhou, R.G., Dong, Y.C., Li, P. and Jia, J.Z. (2006) Development, utilization of introgression lines using a synthetic wheat as donor. *Theor. Appl. Genet.*, **112**, 1360-1373.

Liu, T.-X., Stansly, P.A. and Gerling, D. (2015) Whitefly parasitoids: distribution, life history, bionomics, and utilization. *Annual Review of Entomology*, **60**, 273-292.

Liu, X. and Liu, C. (2016) Effects of drought-stress on *Fusarium* crown rot development in barley. *PLOS ONE*, **11**, e0167304.

Liu, X., Wu, S., Xu, J., Sui, C. and Wei, J. (2017) Application of CRISPR/Cas9 in plant biology. *Acta Pharmaceutica Sinica B*, **7**, 292-302.

Liu, X., Zhang, Y., Xie, W., Wu, Q. and Wang, S. (2016b) The suitability of biotypes Q and B of *Bemisia tabaci (*Gennadius) (Hemiptera: Aleyrodidae) at different nymphal instars as hosts for *Encarsia formosa* Gahan (Hymenoptera: Aphelinidae). *PeerJ*, **4**, e1863.

Liu, Y., Schiff, M. and Dinesh-Kumar, S.P. (2002) Virus-induced gene silencing in tomato. *The Plant Journal*, **31**, 777-786.

Louro, D., Accotto, G.P. and Vaira, A.M. (2000) Occurrence and diagnosis of Tomato Chlorosis Virus in Portugal. *European Journal of Plant Pathology*, **106**, 589-592.

Luckwill, L. (1943) The genus *Lycopersicon*; an historical, biological, and taxonomic survey of the wild and cultivated tomatoes. *Aberdeen, The University Press*.

Lung, S.C., Liao, P., Yeung, E.C., Hsiao, A.S., Xue, Y. and Chye, M.L. (2018) Arabidopsis ACYL-COA-BINDING PROTEIN1 interacts with STEROL C4-METHYL OXIDASE1-2 to modulate gene expression of homeodomain-leucine zipper IV transcription factors. *New Phytologist*, **218**, 183-200.

MacAlister, C.A., Ohashi-Ito, K. and Bergmann, D.C. (2007) Transcription factor control of asymmetric cell divisions that establish the stomatal lineage. *Nature*, **445**, 537-540.

Machado, A., Wu, Y., Yang, Y., Llewellyn, D.J. and Dennis, E.S. (2009) The MYB transcription factor GhMYB25 regulates early fibre and trichome development. *Plant J*, **59**, 52-62.

Macková, J., Vašková, M., Macek, P., Hronková, M., Schreiber, L. and Šantrůček, J. (2013) Plant response to drought stress simulated by ABA application: Changes in chemical composition of cuticular waxes. *Environmental and Experimental Botany*, **86**, 70-75.

Maes, L. and Goossens, A. (2010) Hormone-mediated promotion of trichome initiation in plants is conserved but utilizes species- and trichome-specific regulatory mechanisms. *Plant Signal Behav*, **5**, 205-207.

Maes, L., Inze, D. and Goossens, A. (2008) Functional specialization of the TRANSPARENT TESTA GLABRA1 network allows differential hormonal control of laminal and marginal trichome initiation in *Arabidopsis* rosette leaves. *Plant Physiol*, **148**, 1453-1464.

Magnum, O.S.F., Gabriel, L., Saleh, A., Laise, R.S., Mariana, C., Fuentes, S.V., Silvestre, L.B., Dimitrios, F., Björn, U., Lopes, B.L., M., D.F., Ronan, S., L., A.W., Magdalena, R., Nathalia, S., R., F.A., Fernando, C. and Adriano, N.N. (2018) The genetic architecture of photosynthesis and plant growth-related traits in tomato. *Plant, Cell & Environment*, **41**, 327-341.

Maliepaard, C., Bas, N., van Heusden, S., Kos, J., Pet, G., Verkerk, R., Vrieunk, R., Zabel, P. and Lindhout, P. (1995) Mapping of QTLs for glandular trichome densities and *Trialeurodes vaporariorum* (greenhouse whitefly) resistance in an F2 from *Lycopersicon esculentum × Lycopersicon hirsutum f. glabratum*. *Heredity*, **75**, 425.

Manning, K., Tor, M., Poole, M., Hong, Y., Thompson, A.J., King, G.J., Giovannoni, J.J. and Seymour, G.B. (2006) A naturally occurring epigenetic mutation in a gene encoding an SBP-box transcription factor inhibits tomato fruit ripening. *Nat Genet*, **38**, 948-952.

Marcos, A., Triviño, M., Fenoll, C. and Mena, M. (2016) Too many faces for TOO MANY MOUTHS? *New Phytologist*, **210**, 779-785.

Marcotrigiano, M. and Bernatzky, R. (1995) Arrangement of cell layers in the shoot apical meristems of periclinal chimeras influences cell fate. *The Plant Journal*, **7**, 193-202.

Marks, M.D., Wenger, J.P., Gilding, E., Jilk, R. and Dixon, R.A. (2009) Transcriptome analysis of Arabidopsis wild-type and gl3-sst sim trichomes identifies four additional genes required for trichome development. *Molecular plant*, **2**, 803-822.

Marowa, P., Ding, A. and Kong, Y. (2016) Expansins: roles in plant growth and potential applications in crop improvement. *Plant Cell Reports*, **35**, 949-965.

Martí, E., Gisbert, C., Bishop, G.J., Dixon, M.S. and García-Martínez, J.L. (2006) Genetic and physiological characterization of tomato cv. Micro-Tom. *Journal of Experimental Botany*, **57**, 2037-2047.

Martin, C., Bhatt, K., Baumann, K., Jin, H., Zachgo, S., Roberts, K., Schwarz-Sommer, Z., Glover, B. and Perez-Rodrigues, M. (2002) The mechanics of cell fate determination in petals. *Philosophical Transactions of the Royal Society B: Biological Sciences*, **357**, 809-813.

Martin, C., Zhang, Y., Tomlinson, L., Kallam, K., Luo, J., Jones, J.D., Granell, A., Orzaez, D. and Butelli, E. (2012) Colouring up Plant Biotechnology. In *Recent Advances in Polyphenol Research*.

Martin, C.E. (1994) Physiological ecology of the *Bromeliaceae*. *The Botanical Review*, **60**, 1-82.

Martin, L.B.B., Romero, P., Fich, E.A., Domozych, D.S. and Rose, J.K.C. (2017) Cuticle biosynthesis in tomato leaves is developmentally regulated by abscisic acid. *Plant Physiol.*, **174**, 1384-1398.

Masle, J., Gilmore, S.R. and Farquhar, G.D. (2005) The ERECTA gene regulates plant transpiration efficiency in *Arabidopsis*. *Nature*, **436**, 866-870.

Masucci, J.D., Rerie, W.G., Foreman, D.R., Zhang, M., Galway, M.E., Marks, M.D. and Schiefelbein, J.W. (1996) The homeobox gene GLABRA2 is required for position-dependent cell differentiation in the root epidermis of Arabidopsis thaliana. *Development*, **122**, 1253-1260.

Mathur, J. (2004) Cell shape development in plants. *Trends Plant Sci*, **9**, 583-590.

Mathur, J. and Chua, N.H. (2000) Microtubule stabilization leads to growth reorientation in Arabidopsis trichomes. *Plant Cell*, **12**, 465-477.

Mathur, J., Spielhofer, P., Kost, B. and Chua, N. (1999) The actin cytoskeleton is required to elaborate and maintain spatial patterning during trichome cell morphogenesis in Arabidopsis thaliana. *Development (Cambridge, England)*, **126**, 5559-5568.

Mauricio, R. (1998) Costs of Resistance to Natural Enemies in Field Populations of the Annual Plant Arabidopsis thaliana. *The American Naturalist*, **151**, 20-28.

McDowell, E.T., Kapteyn, J., Schmidt, A., Li, C., Kang, J.H., Descour, A., Shi, F., Larson, M., Schilmiller, A., An, L.L., Jones, A.D., Pichersky, E., Soderlund, C.A. and Gang, D.R. (2011) Comparative functional genomic analysis of *Solanum* glandular trichome types. *Plant Physiol.*, **155**, 524-539.

McQueen-Mason, S., Durachko, D.M. and Cosgrove, D.J. (1992) Two endogenous proteins that induce cell wall extension in plants. *Plant Cell*, **4**, 1425-1433.

McQueen-Mason, S.J. and Cosgrove, D.J. (1995) Expansin mode of action on cell walls. Analysis of wall hydrolysis, stress relaxation, and binding. *Plant Physiol*, **107**, 87-100.

Mei, H.W., Xu, J.L., Li, Z.K., Yu, X.Q., Guo, L.B., Wang, Y.P., Ying, C.S. and Luo, L.J. (2006) QTLs influencing panicle size detected in two reciprocal introgressive line (IL) populations in rice (*Oryza sativa* L.). *Theor. Appl. Genet.*, **112**, 648-656.

Mekonnen, M.M. and Hoekstra, A.Y. (2011) The green, blue and grey water footprint of crops and derived crop products. *Hydrol. Earth Syst. Sci.*, **15**, 1577-1600.

Melaragno, J.E., Mehrotra, B. and Coleman, A.W. (1993) Relationship between Endopolyploidy and Cell Size in Epidermal Tissue of Arabidopsis. *Plant Cell*, **5**, 1661-1668.

Mellon, J.E., Zelaya, C.A., Dowd, M.K., Beltz, S.B. and Klich, M.A. (2012) Inhibitory effects of gossypol, gossypolone, and apogossypolone on a collection of economically important filamentous fungi. *Journal of agricultural and food chemistry*, **60**, 2740-2745.

Meng, X., Chen, X., Mang, H., Liu, C., Yu, X., Gao, X., Torii, K.U., He, P. and Shan, L. (2015) Differential Function of Arabidopsis SERK Family Receptor-like Kinases in Stomatal Patterning. *Current biology : CB*, **25**, 2361-2372.

Merlot, S., Gosti, F., Guerrier, D., Vavasseur, A. and Giraudat, J. (2001) The ABI1 and ABI2 protein phosphatases 2C act in a negative feedback regulatory loop of the abscisic acid signalling pathway. *Plant J.*, **25**, 295-303.

Mishra, K.B., Iannacone, R., Petrozza, A., Mishra, A., Armentano, N., La Vecchia, G., Trtílek, M., Cellini, F. and Nedbal, L. (2012) Engineered drought tolerance in tomato plants is reflected in chlorophyll fluorescence emission. *Plant Science*, **182**, 79-86.

Mo, Y., Yang, R., Liu, L., Gu, X., Yang, X., Wang, Y., Zhang, X. and Li, H. (2016) Growth, photosynthesis and adaptive responses of wild and domesticated watermelon genotypes to drought stress and subsequent re-watering. *Plant Growth Regulation*, **79**, 229-241.

Mojica, F.J.M., Díez-Villaseñor, C.s., García-Martínez, J. and Soria, E. (2005) Intervening sequences of regularly spaced prokaryotic repeats derive from foreign genetic elements. *Journal of Molecular Evolution*, **60**, 174-182.

Monneveux, P., Ramirez, D.A. and Pino, M.T. (2013) Drought tolerance in potato (S. tuberosum L.) Can we learn from drought tolerance research in cereals? *Plant Science*, **205**, 76-86.

Morales-Navarro, S., Pérez-Díaz, R., Ortega, A., de Marcos, A., Mena, M., Fenoll, C., González-Villanueva, E. and Ruiz-Lara, S. (2018) Overexpression of a SDD1-like gene from wild tomato decreases stomatal density and enhances dehydration avoidance in *Arabidopsis* and cultivated tomato. *Front. Plant Sci.*, **9**.

Morohashi, K. and Grotewold, E. (2009) A Systems Approach Reveals Regulatory Circuitry for Arabidopsis Trichome Initiation by the GL3 and GL1 Selectors. *PLOS Genetics*, **5**, e1000396.

Mucciarelli, M., Camusso, W., Bertea, C.M., Bossi, S. and Maffei, M. (2001) Effect of (+)-pulegone and other oil components of *Mentha×piperita* on cucumber respiration. *Phytochemistry*, **57**, 91-98.

Munoz-Mayor, A., Pineda, B., Garcia-Abellan, J.O., Anton, T., Garcia-Sogo, B., Sanchez-Bel, P., Flores, F.B., Atares, A., Angosto, T., Pintor-Toro, J.A., Moreno, V. and Bolarin, M.C. (2012) Overexpression. of dehydrin tas14 gene improves the osmotic stress imposed by drought and salinity in tomato. *J. Plant Physiol.*, **169**, 459-468.

Nabity, P.D., Zavala, J.A. and DeLucia, E.H. (2013) Herbivore induction of jasmonic acid and chemical defences reduce photosynthesis in Nicotiana attenuata. *Journal of Experimental Botany*, **64**, 685-694.

Nadakuduti, S.S., Pollard, M., Kosma, D.K., Allen, C., Ohlrogge, J.B. and Barry, C.S. (2012) Pleiotropic phenotypes of the *sticky peel* mutant provide new insight into the role of CUTIN DEFICIENT2 in epidermal cell function in tomato. *Plant Physiol.*, **159**, 945-960.

Nadakuduti, S.S., Uebler, J.B., Liu, X., Jones, A.D. and Barry, C.S. (2017) Characterization of trichome-expressed BAHD acyltransferases in *Petunia axillaris* reveals distinct acylsugar assembly mechanisms within the *Solanaceae*. *Plant Physiol.*, **175**, 36-50.

Naito, Y., Hino, K., Bono, H. and Ui-Tei, K. (2015) CRISPRdirect: software for designing CRISPR/Cas guide RNA with reduced off-target sites. *Bioinformatics*, **31**, 1120-1123.

Nakamura, M., Katsumata, H., Abe, M., Yabe, N., Komeda, Y., Yamamoto, K.T. and Takahashi, T. (2006) Characterization of the Class IV Homeodomain-Leucine Zipper Gene Family in Arabidopsis. *Plant Physiol.*, **141**, 1363-1375.

Nakashima, K. and Suenaga, K. (2017) Toward the Genetic Improvement of Drought Tolerance in Crops. *Jarq - Jpn. Agric. Res. Q.*, **51**, 1-10.

Nardi, C., Escudero, C., Villarreal, N., Martinez, G. and Civello, P.M. (2013) The carbohydrate-binding module of Fragaria x ananassa expansin 2 (CBM-FaExp2) binds to cell wall polysaccharides and decreases cell wall enzyme activities "in vitro". *Journal of plant research*, **126**, 151-159.

Navas-Castillo, J., Fiallo-Olivé, E. and Sánchez-Campos, S. (2011) Emerging virus diseases transmitted by whiteflies. *Annual Review of Phytopathology*, **49**, 219-248.

Naveen, N.C., Chaubey, R., Kumar, D., Rebijith, K.B., Rajagopal, R., Subrahmanyam, B. and Subramanian, S. (2017) Insecticide resistance status in the whitefly, *Bemisia tabaci* genetic groups Asia-I, Asia-II-1 and Asia-II-7 on the Indian subcontinent. *Scientific Reports*, **7**, 40634.

Ning, J., Moghe, G.D., Leong, B., Kim, J., Ofner, I., Wang, Z., Adams, C., Jones, A.D., Zamir, D. and Last, R.L. (2015) A feedback-insensitive isopropylmalate synthase affects acylsugar composition in cultivated and wild tomato. *Plant Physiol.*, **169**, 1821-1835.

Ning, W.F., Zhai, H., Yu, J.Q., Liang, S., Yang, X., Xing, X.Y., Huo, J.L., Pang, T., Yang, Y.L. and Bai, X. (2017) Overexpression of Glycine soja WRKY20 enhances drought tolerance and improves plant yields under drought stress in transgenic soybean. *Molecular Breeding*, **37**, 10.

Nobel, P.S. (2009) Chapter 8 - Leaves and Fluxes. In *Physicochemical and Environmental Plant Physiology (Fourth Edition)* (Nobel, P.S. ed. San Diego: Academic Press, pp. 364-437.

Noda, K., Glover, B.J., Linstead, P. and Martin, C. (1994) Flower colour intensity depends on specialized cell shape controlled by a Myb-related transcription factor. *Nature*, **369**, 661-664.

Nodine, M.D., Yadegari, R. and Tax, F.E. (2007) RPK1 and TOAD2 are two receptor-like kinases redundantly required for arabidopsis embryonic pattern formation. *Dev Cell*, **12**, 943-956.

Nombela, G., Beitia, F. and Muniz, M. (2000) Variation in tomato host response to *Bemisia tabaci (Hemiptera: Aleyrodidae)* in relation to acyl sugar content and presence of the nematode and potato aphid resistance gene Mi. *Bulletin of entomological research*, **90**, 161-167.

Nomura, T., Kushiro, T., Yokota, T., Kamiya, Y., Bishop, G.J. and Yamaguchi, S. (2005) The last reaction producing brassinolide is catalyzed by cytochrome P-450s, CYP85A3 in tomato and CYP85A2 in Arabidopsis. *The Journal of biological chemistry*, **280**, 17873-17879.

Oda, Y. (2015) Cortical microtubule rearrangements and cell wall patterning. *Front Plant Sci*, **6**.

Ofner, I., Lashbrooke, J., Pleban, T., Aharoni, A. and Zamir, D. (2016) *Solanum pennellii* backcross inbred lines (BILs) link small genomic bins with tomato traits. *Plant J*, **87**, 151-160.

Ohashi-Ito, K. and Bergmann, D.C. (2007) Regulation of the *Arabidopsis* root vascular initial population by LONESOME HIGHWAY. *Development*, **134**, 2959-2968.

Ohnesorge, B., Sharaf, N. and Allawi, T. (1980) Population studies on the tobacco whitefly *Bemisia tabaci Genn. (Homoptera; Aleyrodidae*) during the winter season. *Zeitschrift für Angewandte Entomologie*, **90**, 226-232.

Ohrui, T., Nobira, H., Sakata, Y., Taji, T., Yamamoto, C., Nishida, K., Yamakawa, T., Sasuga, Y., Yaguchi, Y., Takenaga, H. and Tanaka, S. (2007) Foliar trichome- and aquaporin-aided water uptake in a drought-resistant epiphyte *Tillandsia ionantha* Planchon. *Planta*, **227**, 47-56.

Oka, A., Aoyama, T., Honma, T. and Sakai, H. (2002) The trascription factor-type response regulator ARR1 is involved in an early step of cytokinin signal transduction. *Plant and Cell Physiology*, **43**, S20-S20.

Oney, M.A. and Bingham, R.A. (2014) Effects of simulated and natural herbivory on tomato (*Solanum lycopersicum var. esculentum*) leaf trichomes. *BIOS*, **85**, 192-198.

Oppenheimer, D.G., Herman, P.L., Sivakumaran, S., Esch, J. and Marks, M.D. (1991) A MYB gene required for leaf trichome differentiation in Arabidopsis is expressed in stipules. *Cell*, **67**, 483-493.

Oriani, M.A.d.G. and Vendramim, J.D. (2010) Influence of trichomes on attractiveness and ovipositional preference of *Bemisia tabaci* (Genn.) B biotype (*Hemiptera: Aleyrodidae)* on tomato genotypes. *Neotropical Entomology*, **39**, 1002-1007.

Orzaez, D., Medina, A., Torre, S., Fernández-Moreno, J.P., Rambla, J.L., Fernández-del-Carmen, A., Butelli, E., Martin, C. and Granell, A. (2009) A visual reporter system for virus-induced gene silencing in tomato fruit based on anthocyanin accumulation. *Plant Physiol.*, **150**, 1122-1134.

Oshima, Y. and Mitsuda, N. (2013) The MIXTA-like transcription factor MYB16 is a major regulator of cuticle formation in vegetative organs. *Plant Signaling & Behavior*, **8**, e26826.

Oshima, Y., Shikata, M., Koyama, T., Ohtsubo, N., Mitsuda, N. and Ohme-Takagi, M. (2013) MIXTA-like transcription factors and WAX INDUCER1/SHINE1 coordinately regulate cuticle development in *Arabidopsis* and *Torenia fournieri*. *The Plant Cell*, **25**, 1609-1624.

Otles, S. and Yalcin, B. (2012) Phenolic Compounds Analysis of Root, Stalk, and Leaves of Nettle. *The Scientific World Journal*, **2012**, 564367.

Paetzold, H., Garms, S., Bartram, S., Wieczorek, J., Urós-Gracia, E.-M., Rodríguez-Concepción, M., Boland, W., Strack, D., Hause, B. and Walter, M.H. (2010) The Isogene 1-Deoxy-D-Xylulose 5-Phosphate Synthase 2 Controls Isoprenoid Profiles, Precursor Pathway Allocation, and Density of Tomato Trichomes. *Molecular Plant*, **3**, 904-916.

Palliotti, A.B.G.R.P. (1994) Peltate trichomes effects on photosynthetic gas exchange of Olea Europea L. leaves. *Life Science Advances*.

Pan, Y.P., Bo, K.L., Cheng, Z.H. and Weng, Y.Q. (2015) The loss-of-function GLABROUS 3 mutation in cucumber is due to LTR-retrotransposon insertion in a class IV HD-ZIP transcription factor gene CsGL3 that is epistatic over CsGL1. *Bmc Plant Biology*, **15**, 15.

Pantin, F., Monnet, F., Jannaud, D., Costa, J.M., Renaud, J., Muller, B., Simonneau, T. and Genty, B. (2013) The dual effect of abscisic acid on stomata. *The New phytologist*, **197**, 65-72.

Park, Y.B. and Cosgrove, D.J. (2011) Changes in cell wall biomechanical properties in the xyloglucan-deficient xxt1/xxt2 mutant of Arabidopsis. *Plant Physiol.*

Park, Y.B. and Cosgrove, D.J. (2012) A revised architecture of primary cell walls based on biomechanical changes induced by substrate-specific endoglucanases. *Plant Physiol.*

Pastore, J.J., Limpuangthip, A., Yamaguchi, N., Wu, M.F., Sang, Y., Han, S.K., Malaspina, L., Chavdaroff, N., Yamaguchi, A. and Wagner, D. (2011) LATE MERISTEM IDENTITY2 acts together with LEAFY to activate APETALA1. *Development*, **138**, 3189-3198.

Patane, C., Scordia, D., Testa, G. and Cosentino, S.L. (2016) Physiological screening for drought tolerance in Mediterranean long-storage tomato. *Plant Science*, **249**, 25-34.

Pathan, A.K., Bond, J. and Gaskin, R.E. (2008) Sample preparation for scanning electron microscopy of plant surfaces—Horses for courses. *Micron*, **39**, 1049-1061.

Patra, B., Pattanaik, S. and Yuan, L. (2013) Ubiquitin protein ligase 3 mediates the proteasomal degradation of GLABROUS 3 and ENHANCER OF GLABROUS 3, regulators of trichome development and flavonoid biosynthesis in Arabidopsis. *The Plant Journal*, **74**, 435-447.

Pattanaik, S., Patra, B., Singh, S.K. and Yuan, L. (2014) An overview of the gene regulatory network controlling trichome development in the model plant, Arabidopsis. *Front. Plant Sci.*, **5**.

Payne, C.T., Zhang, F. and Lloyd, A.M. (2000) GL3 encodes a bHLH protein that regulates trichome development in arabidopsis through interaction with GL1 and TTG1. *Genetics*, **156**, 1349-1362.

Payne, T., Clement, J., Arnold, D. and Lloyd, A. (1999) Heterologous myb genes distinct from GL1 enhance trichome production when overexpressed in Nicotiana tabacum. *Development (Cambridge, England)*, **126**, 671-682.

Payne, W.W. (1978) A glossary of plant hair terminology. *Brittonia*, **30**, 239-255.

Peeters, P.J., Sanson, G. and Read, J. (2007) Leaf biomechanical properties and the densities of herbivorous insect guilds. *Functional Ecology*, **21**, 246-255.

Peiffer, M., Tooker, J.F., Luthe, D.S. and Felton, G.W. (2009) Plants on early alert: glandular trichomes as sensors for insect herbivores. *The New phytologist*, **184**, 644-656.

Peng, Z., He, S., Sun, J., Pan, Z., Gong, W., Lu, Y. and Du, X. (2016) Na^+ compartmentalization related to salinity stress tolerance in upland cotton (*Gossypium hirsutum*) seedlings. *Scientific Reports*, **6**, 34548.

Peralta, I.E., Spooner, D.M., Knapp, S. (2008) Taxonomy of wild tomatoes and their relatives (*Solanum* sect. *Lycopersicoides*, sect. *Juglandifolia*, sect. *Lycopersicon; Solanaceae*). . *Syst. Bot. Monographs* **84**.

Perazza, D., Vachon, G. and Herzog, M. (1998) Gibberellins promote trichome formation by Up-regulating GLABROUS1 in arabidopsis. *Plant Physiol*, **117**, 375-383.

Péret, B., Larrieu, A. and Bennett, M.J. (2009) Lateral root emergence: a difficult birth. *Journal of Experimental Botany*, **60**, 3637-3643.

Perez-Rodriguez, M., Jaffe, F.W., Butelli, E., Glover, B.J. and Martin, C. (2005) Development of three different cell types is associated with the activity of a specific MYB transcription factor in the ventral petal of *Antirrhinum majus* flowers. *Development*, **132**, 359-370.

Perpina, G., Esteras, C., Gibon, Y., Monforte, A.J. and Pico, B. (2016) A new genomic library of melon introgression lines in a cantaloupe genetic background for dissecting desirable agronomical traits. *Bmc Plant Biology*, **16**, 21.

Pesch, M., Dartan, B., Birkenbihl, R., Somssich, I.E. and Hulskamp, M. (2014) Arabidopsis TTG2 regulates TRY expression through enhancement of activator complex-triggered activation. *Plant Cell*, **26**, 4067-4083.

Peterson, K.M., Shyu, C., Burr, C.A., Horst, R.J., Kanaoka, M.M., Omae, M., Sato, Y. and Torii, K.U. (2013) Arabidopsis homeodomain-leucine zipper IV proteins promote stomatal development and ectopically induce stomata beyond the epidermis. *Development*, **140**, 1924-1935.

Pillitteri, L.J., Bogenschutz, N.L. and Torii, K.U. (2008) The bHLH protein, MUTE, controls differentiation of stomata and the hydathode pore in *Arabidopsis*. *Plant and Cell Physiology*, **49**, 934-943.

Pillitteri, L.J. and Dong, J. (2013) Stomatal development in *Arabidopsis*. *The Arabidopsis Book* **11**, e0162.

Pillitteri, L.J., Sloan, D.B., Bogenschutz, N.L. and Torii, K.U. (2007) Termination of asymmetric cell division and differentiation of stomata. *Nature*, **445**, 501-505.

Pina, A., Zandavalli, R.B., Oliveira, R.S., Martins, F.R. and Soares, A.A. (2016) Dew absorption by the leaf trichomes of Combretum leprosum in the Brazilian semiarid region. *Funct. Plant Biol.*, **43**, 851-861.

Plett, J.M., Mathur, J. and Regan, S. (2009) Ethylene receptor ETR2 controls trichome branching by regulating microtubule assembly in Arabidopsis thaliana. *Journal of Experimental Botany*, **60**, 3923-3933.

Plett, J.M., Wilkins, O., Campbell, M.M., Ralph, S.G. and Regan, S. (2010) Endogenous overexpression of *Populus* MYB186 increases trichome density, improves insect pest resistance, and impacts plant growth. *Plant J*, **64**, 419-432.

Pollard, M., Beisson, F., Li, Y. and Ohlrogge, J.B. (2008) Building lipid barriers: biosynthesis of cutin and suberin. *Trends in Plant Science*, **13**, 236-246.

Pozo, M.J., Lopez-Raez, J.A., Azcon-Aguilar, C. and Garcia-Garrido, J.M. (2015) Phytohormones as integrators of environmental signals in the regulation of mycorrhizal symbioses. *The New phytologist*, **205**, 1431-1436.

Prasifka, J.R. (2015) Variation in the number of capitate glandular trichomes in wild and cultivated sunflower germplasm and its potential for use in host plant resistance. *Plant Genet. Resour.-Charact. Util.*, **13**, 68-74.

Prescott-Allen, C. and Prescott-Allen, R. (1986) *The first resource* New Haven: Yale University Press.

Pu, S., Xueqing, F., Qian, S., Meng, L., Qifang, P., Yueli, T., Weimin, J., Zongyou, L., Tingxiang, Y., Yanan, M., Minghui, C., Xiaolong, H., Pin, L., Ling, L., Xiaofen, S. and Kexuan, T. (2018) The roles of AaMIXTA1 in regulating the initiation of glandular trichomes and cuticle biosynthesis in *Artemisia annua*. *New Phytologist*, **217**, 261-276.

Qi, T.C., Song, S.S., Ren, Q.C., Wu, D.W., Huang, H., Chen, Y., Fan, M., Peng, W., Ren, C.M. and Xie, D.X. (2011) The Jasmonate-ZIM-Domain proteins interact with the WD-Repeat/bHLH/MYB complexes to regulate jasmonate-mediated anthocyanin accumulation and trichome initiation in *Arabidopsis thaliana*. *Plant Cell*, **23**, 1795-1814.

Qi, X., Han, S.-K., Dang, J.H., Garrick, J.M., Ito, M., Hofstetter, A.K. and Torii, K.U. (2017) Autocrine regulation of stomatal differentiation potential by EPF1 and ERECTA-LIKE1 ligand-receptor signaling. *eLife*, **6**, e24102.

Qin, F., Kodaira, K.-S., Maruyama, K., Mizoi, J., Tran, L.-S.P., Fujita, Y., Morimoto, K., Shinozaki, K. and Yamaguchi-Shinozaki, K. (2011) SPINDLY, a Negative Regulator of Gibberellic Acid Signaling, Is Involved in the Plant Abiotic Stress Response. *Plant Physiol.*, **157**, 1900-1913.

Qin, Y.-M., Hu, C.-Y., Pang, Y., Kastaniotis, A.J., Hiltunen, J.K. and Zhu, Y.-X. (2007) Saturated Very-Long-Chain Fatty Acids Promote Cotton Fiber and Arabidopsis Cell Elongation by Activating Ethylene Biosynthesis. *The Plant Cell*, **19**, 3692-3704.

Qin, Y., Leydon, A.R., Manziello, A., Pandey, R., Mount, D., Denic, S., Vasic, B., Johnson, M.A. and Palanivelu, R. (2009) Penetration of the stigma and style elicits a novel transcriptome in pollen tubes, pointing to genes critical for growth in a pistil. *PLOS Genetics*, **5**, e1000621.

Quadrana, L., Rodriguez, M.C., Lopez, M., Bermudez, L., Nunes-Nesi, A., Fernie, A.R., Descalzo, A., Asis, R., Rossi, M., Asurmendi, S. and Carrari, F. (2011) Coupling virus-induced gene silencing to exogenous green fluorescence protein expression provides a highly efficient system for functional genomics in Arabidopsis and across all stages of tomato fruit development. *Plant Physiol*, **156**, 1278-1291.

QulRing, D.T., Timmins, P.R. and Park, S.J. (1992) Effect of Variations in Hooked Trichome Densities of Phaseolus vulgaris on Longevity of Liriomyza trifolii (Diptera: Agromyzidae) Adults. *Environmental Entomology*, **21**, 1357-1361.

Rai, A.C., Singh, M. and Shah, K. (2013) Engineering drought tolerant tomato plants over-expressing BcZAT12 gene encoding a C2H2 zinc finger transcription factor. *Phytochemistry*, **85**, 44-50.

Ramadan, T. and Flowers, T.J. (2004) Effects of salinity and benzyl adenine on development and function of microhairs of Zea mays L. *Planta*, **219**, 639-648.

Rath, D., Amlinger, L., Rath, A. and Lundgren, M. (2015) The CRISPR-Cas immune system: Biology, mechanisms and applications. *Biochimie*, **117**, 119-128.

Read, N.D. and Jeffree, C.E. (1991) Low-temperature scanning electron microscopy in biology. *Journal of Microscopy*, **161**, 59-72.

Reeves, A.F. (1977) Tomato trichomes and mutations affecting their development. *American Journal of Botany*, **64**, 186-189.

Rerie, W.G., Feldmann, K.A. and Marks, M.D. (1994) The GLABRA2 gene encodes a homeo domain protein required for normal trichome development in *Arabidopsis*. *Genes & Development*, **8**, 1388-1399.

Rick, C.M. (1973) Potential genetic resources in tomato species: clues from observations in native habitats. In *Genes, Enzymes, and Populations* (Srb, A.M. ed. Boston, MA: Springer US, pp. 255-269.

Rick, C.M. and Chetelat, R.T. (1995) Utilization of related wild species for tomato improvement: International Society for Horticultural Science (ISHS), Leuven, Belgium, pp. 21-38.

Riddick, E.W. and Simmons, A.M. (2014) Do plant trichomes cause more harm than good to predatory insects? *Pest management science*, **70**, 1655-1665.

Riederer, M. and Schreiber, L. (2001) Protecting against water loss: analysis of the barrier properties of plant cuticles. *Journal of Experimental Botany*, **52**, 2023-2032.

Rigano, M.M., Arena, C., Di Matteo, A., Sereno, S., Frusciante, L. and Barone, A. (2014) *Eco-physiological response to water stress of drought-tolerant and drought-sensitive tomato genotypes*.

Roda, A., Nyrop, J. and English-Loeb, G. (2003) Leaf pubescence mediates the abundance of non-prey food and the density of the predatory mite Typhlodromus pyri. *Experimental & applied acarology*, **29**, 193-211.

Rogiers, S.Y., Hardie, W.J. and Smith, J.P. (2011) Stomatal density of grapevine leaves (*Vitis vinifera* L.) responds to soil temperature and atmospheric carbon dioxide. *Aust. J. Grape Wine Res.*, **17**, 147-152.

Rojas, E.R., Hotton, S. and Dumais, J. (2011) Chemically mediated mechanical expansion of the pollen tube cell wall. *Biophysical journal*, **101**, 1844-1853.

Ron, M., Dorrity, M.W., de Lucas, M., Toal, T., Hernandez, R.I., Little, S.A., Maloof, J.N., Kliebenstein, D.J. and Brady, S.M. (2013) Identification of novel loci regulating interspecific variation in root morphology and cellular development in tomato. *Plant Physiol.*, **162**, 755-768.

Ron, M., Kajala, K., Pauluzzi, G., Wang, D., Reynoso, M.A., Zumstein, K., Garcha, J., Winte, S., Masson, H., Inagaki, S., Federici, F., Sinha, N., Deal, R.B., Bailey-Serres, J. and Brady, S.M. (2014) Hairy root transformation using *Agrobacterium rhizogenes* as a tool for exploring cell type-specific gene expression and function using tomato as a model. *Plant Physiol*, **166**, 455-469.

Rose, J.K.C., Cosgrove, D.J., Albersheim, P., Darvill, A.G. and Bennett, A.B. (2000) Detection of expansin proteins and activity during tomato fruit ontogeny. *Plant Physiol.*, **123**, 1583-1592.

Ryan, C.A. (1990) Protease inhibitors in plants: genes for improving defenses against insects and pathogens. *Annual Review of Phytopathology*, **28**, 425-449.

Sahu, P.P., Puranik, S., Khan, M. and Prasad, M. (2012) Recent advances in tomato functional genomics: utilization of VIGS. *Protoplasma*, **249**, 1017-1027.

Saibo, N.J., Vriezen, W.H., Beemster, G.T. and Van Der Straeten, D. (2003) Growth and stomata development of Arabidopsis hypocotyls are controlled by gibberellins and modulated by ethylene and auxins. *The Plant journal : for cell and molecular biology*, **33**, 989-1000.

Salazar-Henao, J.E., Vélez-Bermúdez, I.C. and Schmidt, W. (2016) The regulation and plasticity of root hair patterning and morphogenesis. *Development (Cambridge, England)*, **143**, 1848-1858.

San-Bento, R., Farcot, E., Galletti, R., Creff, A. and Ingram, G. (2014) Epidermal identity is maintained by cell–cell communication via a universally active feedback loop in *Arabidopsis thaliana*. *The Plant Journal*, **77**, 46-58.

San, Z. and Ke_Fu, Z. (2003) Discussion on the problem of salt gland of Glycine soja. *植物学报(英文版)*, **5**, 010.

Sanchez-Pena, P., Oyama, K., Nunez-Farfan, J., Fornoni, J., Hernandez-Verdugo, S., Marquez-Guzman, J. and Garzon-Tiznado, J.A. (2006) Sources of resistance to whitefly (*Bemisia spp.*) in wild populations of *Solanum lycopersicum* var. Cerasiforme (Dunal) spooner GJ Anderson et RK Jansen in Northwestern Mexico. *Genet Resour Crop Evol*, **53**, 711-719.

Sarret, G., Harada, E., Choi, Y.-E., Isaure, M.-P., Geoffroy, N., Fakra, S., Marcus, M.A., Birschwilks, M., Clemens, S. and Manceau, A. (2006) Trichomes of tobacco excrete zinc as zinc-substituted calcium carbonate and other zinc-containing compounds. *Plant Physiol.*, **141**, 1021-1034.

Sasse, J., Schlegel, M., Borghi, L., Ullrich, F., Lee, M., Liu, G.W., Giner, J.L., Kayser, O., Bigler, L., Martinoia, E. and Kretzschmar, T. (2016) *Petunia hybrida* PDR2 is involved in herbivore defense by controlling steroidal contents in trichomes. *Plant Cell Environ.*, **39**, 2725-2739.

Savage, N.S., Walker, T., Wieckowski, Y., Schiefelbein, J., Dolan, L. and Monk, N.A. (2008) A mutual support mechanism through intercellular movement of CAPRICE and GLABRA3 can pattern the Arabidopsis root epidermis. *PLoS Biol*, **6**, e235.

Savaldi-Goldstein, S. and Chory, J. (2008) Growth coordination and the shoot epidermis. *Current opinion in plant biology*, **11**, 42-48.

Savé, R., Biel, C. and de Herralde, F. (2000) Leaf pubescence, water relations and chlorophyll fluorescence in two subspecies of *Lotus Creticus* L. *Biologia Plantarum*, **43**, 239-244.

Schaller, G.E. (2012) Ethylene and the regulation of plant development. *BMC Biology*, **10**, 9.

Schellmann, S., Schnittger, A., Kirik, V., Wada, T., Okada, K., Beermann, A., Thumfahrt, J., Jurgens, G. and Hulskamp, M. (2002) TRIPTYCHON and CAPRICE mediate lateral inhibition during trichome and root hair patterning in *Arabidopsis*. *Embo J.*, **21**, 5036-5046.

Schiefelbein, J., Zheng, X. and Huang, L. (2014) Regulation of epidermal cell fate in Arabidopsis roots: the importance of multiple feedback loops. *Front. Plant Sci.*, **5**, 47.

Schilmiller, A., Shi, F., Kim, J., Charbonneau, A.L., Holmes, D., Daniel, J.A. and Last, R.L. (2010) Mass spectrometry screening reveals widespread diversity in trichome specialized metabolites of tomato chromosomal substitution lines. *The Plant Journal*, **62**, 391-403.

Schilmiller, A.L., Charbonneau, A.L. and Last, R.L. (2012) Identification of a BAHD acetyltransferase that produces protective acyl sugars in tomato trichomes. *Proc Natl Acad Sci U S A*, **109**, 16377-16382.

Schilmiller, A.L., Last, R.L. and Pichersky, E. (2008) Harnessing plant trichome biochemistry for the production of useful compounds. *Plant J*, **54**, 702-711.

Schilmiller, A.L., Moghe, G.D., Fan, P., Ghosh, B., Ning, J., Jones, A.D. and Last, R.L. (2015) Functionally divergent alleles and duplicated loci encoding an acyltransferase contribute to acylsugar metabolite diversity in *Solanum* trichomes. *Plant Cell*, **27**, 1002-1017.

Schindelin, J., Arganda-Carreras, I., Frise, E., Kaynig, V., Longair, M., Pietzsch, T., Preibisch, S., Rueden, C., Saalfeld, S., Schmid, B., Tinevez, J.-Y., White, D.J., Hartenstein, V., Eliceiri, K., Tomancak, P. and Cardona, A. (2012) Fiji: an open-source platform for biological-image analysis. *Nature Methods*, **9**, 676.

Schmalenbach, I., March, T.J., Bringezu, T., Waugh, R. and Pillen, K. (2011) High-resolution genotyping of wild barley introgression lines and fine-mapping of the threshability locus *thresh-1* using the Illumina GoldenGate assay. *G3: Genes|Genomes|Genetics*, **1**, 187-196.

Schmidt, R., Schippers, J.H., Mieulet, D., Obata, T., Fernie, A.R., Guiderdoni, E. and Mueller-Roeber, B. (2013) MULTIPASS, a rice R2R3-type MYB transcription factor, regulates adaptive growth by integrating multiple hormonal pathways. *Plant J*, **76**, 258-273.

Schnittger, A., Folkers, U., Schwab, B., Jurgens, G. and Hulskamp, M. (1999) Generation of a spacing pattern: the role of triptychon in trichome patterning in Arabidopsis. *Plant Cell*, **11**, 1105-1116.

Schnittger, A., Jurgens, G. and Hulskamp, M. (1998) Tissue layer and organ specificity of trichome formation are regulated by GLABRA1 and TRIPTYCHON in Arabidopsis. *Development*, **125**, 2283-2289.

Schnittger, A., Schöbinger, U., Bouyer, D., Weinl, C., Stierhof, Y.D. and Hülskamp, M. (2002) Ectopic D-type cyclin expression induces not only DNA replication but also cell division in Arabidopsis trichomes. *Proceedings of the National Academy of Sciences of the United States of America*, **99**, 6410-6415.

Schrick, K., Bruno, M., Khosla, A., Cox, P.N., Marlatt, S.A., Roque, R.A., Nguyen, H.C., He, C.W., Snyder, M.P., Singh, D. and Yadav, G. (2014) Shared functions of plant and mammalian StAR-related lipid transfer (START) domains in modulating transcription factor activity. *BMC Biol.*, **12**, 20.

Schrick, K., Nguyen, D., Karlowski, W.M. and Mayer, K.F. (2004) START lipid/sterol-binding domains are amplified in plants and are predominantly associated with homeodomain transcription factors. *Genome biology*, **5**, R41.

Schwab, B., Folkers, U., Ilgenfritz, H. and Hülskamp, M. (2000) Trichome morphogenesis in *Arabidopsis*. *Philosophical transactions of the Royal Society of London. Series B, Biological sciences*, **355**, 879-883.

Schwachtje, J. and Baldwin, I.T. (2008) Why does herbivore attack reconfigure primary metabolism? *Plant Physiol.*, **146**, 845-851.

Scoville, A.G., Barnett, L.L., Bodbyl-Roels, S., Kelly, J.K. and Hileman, L.C. (2011) Differential regulation of a MYB transcription factor is correlated with transgenerational epigenetic

inheritance of trichome density in *Mimulus guttatus*. *The New phytologist*, **191**, 251-263.

Senthil-Kumar, M., Hema, R., Anand, A., Kang, L., Udayakumar, M. and Mysore, K.S. (2007) A systematic study to determine the extent of gene silencing in Nicotiana benthamiana and other Solanaceae species when heterologous gene sequences are used for virus-induced gene silencing. *The New phytologist*, **176**, 782-791.

Senthil-Kumar, M. and Mysore, K.S. (2011) New dimensions for VIGS in plant functional genomics. *Trends in Plant Science*, **16**, 656-665.

Seo, P.J., Lee, S.B., Suh, M.C., Park, M.-J., Go, Y.S. and Park, C.-M. (2011) The MYB96 transcription factor regulates cuticular wax biosynthesis under drought conditions in *Arabidopsis*. *The Plant Cell*, **23**, 1138-1152.

Serna, L. and Martin, C. (2006) Trichomes: different regulatory networks lead to convergent structures. *Trends in Plant Science*, **11**, 274-280.

Shangguan, X.-X., Yang, C.-Q., Zhang, X.-F. and Wang, L.-J. (2016) Functional characterization of a basic helix-loop-helix (bHLH) transcription factor GhDEL65 from cotton (Gossypium hirsutum). *Physiologia Plantarum*, **158**, 200-212.

Sharlach, M., Dahlbeck, D., Liu, L., Chiu, J., Jimenez-Gomez, J.M., Kimura, S., Koenig, D., Maloof, J.N., Sinha, N., Minsavage, G.V., Jones, J.B., Stall, R.E. and Staskawicz, B.J. (2013) Fine genetic mapping of RXopJ4, a bacterial spot disease resistance locus from *Solanum pennellii* LA716. *TAG. Theoretical and applied genetics. Theoretische und angewandte Genetik*, **126**, 601-609.

Shin, R., Burch, A.Y., Huppert, K.A., Tiwari, S.B., Murphy, A.S., Guilfoyle, T.J. and Schachtman, D.P. (2007) The *Arabidopsis* transcription factor MYB77 modulates auxin signal transduction. *Plant Cell*, **19**, 2440-2453.

Shinozaki, Y., Nicolas, P., Fernandez-Pozo, N., Ma, Q., Evanich, D.J., Shi, Y., Xu, Y., Zheng, Y., Snyder, S.I., Martin, L.B.B., Ruiz-May, E., Thannhauser, T.W., Chen, K., Domozych, D.S., Catalá, C., Fei, Z., Mueller, L.A., Giovannoni, J.J. and Rose, J.K.C. (2018) High-resolution spatiotemporal transcriptome mapping of tomato fruit development and ripening. *Nature Communications*, **9**, 364.

Shpak, E.D., McAbee, J.M., Pillitteri, L.J. and Torii, K.U. (2005) Stomatal patterning and differentiation by synergistic interactions of receptor kinases. *Science*, **309**, 290-293.

Silva, E.C., Nogueira, R.J.M.C., Vale, F.H.A., Araújo, F.P.d. and Pimenta, M.A. (2009) Stomatal changes induced by intermittent drought in four umbu tree genotypes. *Brazilian Journal of Plant Physiology*, **21**, 33-42.

Silva, K.F.A.S., Michereff-Filho, M., Fonseca, M.E.N., Silva-Filho, J.G., Texeira, A.C.A., Moita, A.W., Torres, J.B., Fernández-Muñoz, R. and Boiteux, L.S. (2014) Resistance to *Bemisia tabaci* biotype B of *Solanum pimpinellifolium* is associated with higher densities of type IV glandular trichomes and acylsugar accumulation. *Entomol. Exp. Appl.*, **151**, 218-230.

Simmons, A.T. and Gurr, G.M. (2005) Trichomes of *Lycopersicon* species and their hybrids: effects on pests and natural enemies. *Agricultural and Forest Entomology*, **7**, 265-276.

Simmons, A.T., Gurr, G.M., McGrath, D., Nicol, H.I. and Martin, P.M. (2003) Trichomes of *Lycopersicon spp*. and their effect on *Myzus persicae (Sulzer) (Hemiptera: Aphididae*). *Australian Journal of Entomology*, **42**, 373-378.

Simpson, M.G. (2010) Front matter. In *Plant Systematics (Second Edition)*. San Diego: Academic Press, pp. i-iii.

Singh, S. (2014) Chapter Three - Guttation: New Insights into Agricultural Implications. In *Advances in Agronomy* (Sparks, D.L. ed: Academic Press, pp. 97-135.

Skaltsa, H., Verykokidou, E., Harvala, C., Karabourniotis, G. and Manetasi, Y. (1994) UV-B protective potential and flavonoid content of leaf hairs of *Quercus ilex*. *Phytochemistry*, **37**, 987-990.

Sletvold, N. and Ågren, J. (2012) Variation in tolerance to drought among Scandinavian populations of *Arabidopsis lyrata*. *Evolutionary Ecology*, **26**, 559-577.

Sletvold, N., Huttunen, P., Handley, R., Kärkkäinen, K. and Ågren, J. (2010) Cost of trichome production and resistance to a specialist insect herbivore in Arabidopsis lyrata. *Evolutionary Ecology*, **24**, 1307-1319.

Smart, C.D., Tanksley, S.D., Mayton, H. and Fry, W.E. (2007) Resistance to *Phytophthora infestans* in *Lycopersicon pennellii*. *Plant Dis.*, **91**, 1045-1049.

Smeda, J.R., Schilmiller, A.L., Last, R.L. and Mutschler, M.A. (2016) Introgression of acylsugar chemistry QTL modifies the composition and structure of acylsugars produced by high-accumulating tomato lines. *Molecular Breeding*, **36**, 160.

Smith, D.L. and Watt, W.M. (1986) Distribution of lithocysts, trichomes, hydathodes and stomata in leaves of *Pilea cadierei* Gagnep. & Guill. (Urticaceae). *Annals of Botany*, **58**, 155-166.

Smith, L.G. and Oppenheimer, D.G. (2005) Spatial control of cell expansion by the plant cytoskeleton. *Annual review of cell and developmental biology*, **21**, 271-295.

Snyder, J.C. and Hyatt, J.P. (1984) Influence of daylenght on trichome densities and leaf volatiles of *Lycopersicon* species. *Plant Science Letters*, **37**, 177-181.

Souza, M.A.A.d., Santos, L.A.d., Brito, D.M.C.d., Rocha, J.F., Castro, R.N., Fernandes, M.S. and Souza, S.R.d. (2016) Influence of light intensity on glandular trichome density, gene expression and essential oil of menthol mint (Mentha arvensis L.). *Journal of Essential Oil Research*, **28**, 138-145.

Spangler, S.M. and Calvin, D.D. (2000) Influence of sweet corn growth stages on European corn borer (*Lepidoptera : Crambidae*) oviposition. *Environmental Entomology*, **29**, 1226-1235.

Spyropoulou, E., Haring, M. and Schuurink, R. (2014) RNA sequencing on Solanum lycopersicum trichomes identifies transcription factors that activate terpene synthase promoters. *BMC Genomics*, **15**, 402.

Steinmuller, D. and Tevini, M. (1985) Action of ultraviolet radiation (UV-B) upon cuticular waxes in some crop plants. *Planta*, **164**, 557-564.

Steve, H., Paul, B., Cynthia, G. and P., P.G. (2002) Barley stripe mosaic virus-induced gene silencing in a monocot plant. *The Plant Journal*, **30**, 315-327.

Stratmann, J.W. and Bequette, C.J. (2016) Hairless but no longer clueless: understanding glandular trichome development. *Journal of Experimental Botany*, **67**, 5285-5287.

Sugano, S.S., Shimada, T., Imai, Y., Okawa, K., Tamai, A., Mori, M. and Hara-Nishimura, I. (2010) Stomagen positively regulates stomatal density in Arabidopsis. *Nature*, **463**, 241-244.

Sun, L., Zhang, A., Zhou, Z., Zhao, Y., Yan, A., Bao, S., Yu, H. and Gan, Y. (2015) GLABROUS INFLORESCENCE STEMS3 (GIS3) regulates trichome initiation and development in Arabidopsis. *New Phytologist*, **206**, 220-230.

Swanson, R., Clark, T. and Preuss, D. (2005) Expression profiling of Arabidopsis stigma tissue identifies stigma-specific genes. *Sexual Plant Reproduction*, **18**, 163-171.

Szalma, S.J., Hostert, B.M., LeDeaux, J.R., Stuber, C.W. and Holland, J.B. (2007) QTL mapping with near-isogenic lines in maize. *Theor. Appl. Genet.*, **114**, 1211-1228.

Szymanski, D.B. (2005) Breaking the WAVE complex: the point of Arabidopsis trichomes. *Current Opinion in Plant Biology*, **8**, 103-112.

Szymanski, D.B., Jilk, R.A., Pollock, S.M. and Marks, M.D. (1998) Control of GL2 expression in Arabidopsis leaves and trichomes. *Development (Cambridge, England)*, **125**, 1161-1171.

Tan, J., Walford, S.-A., Dennis, E.S. and Llewellyn, D. (2016) Trichomes control flower bud shape by linking together young petals. *Nature Plants*, **2**, 16093.

Tanksley, S.D. and McCouch, S.R. (1997) Seed banks and molecular maps: unlocking genetic potential from the wild. *Science*, **277**, 1063-1066.

Tapia, G., Mendez, J. and Inostroza, L. (2016) Different combinations of morpho-physiological traits are responsible for tolerance to drought in wild tomatoes Solanum chilense and Solanum peruvianum. *Plant Biol.*, **18**, 406-416.

Tardieu, F. and Davies, W.J. (1992) Stomatal response to abscisic acid is a function of current plant water status. *Plant Physiol.*, **98**, 540-545.

ten Hove, C.A., Bochdanovits, Z., Jansweijer, V.M., Koning, F.G., Berke, L., Sanchez-Perez, G.F., Scheres, B. and Heidstra, R. (2011) Probing the roles of LRR RLK genes in Arabidopsis thaliana roots using a custom T-DNA insertion set. *Plant molecular biology*, **76**, 69-83.

ten Hove, C.A., Lu, K.-J. and Weijers, D. (2015) Building a plant: cell fate specification in the early *Arabidopsis* embryo. *Development*, **142**, 420-430.

Tester, M. and Davenport, R. (2003) Na+ tolerance and Na+ transport in higher plants. *Ann Bot*, **91**, 503-527.

The Tomato Genome, C. (2012) The tomato genome sequence provides insights into fleshy fruit evolution. *Nature*, **485**, 635.

Thines, B., Katsir, L., Melotto, M., Niu, Y., Mandaokar, A., Liu, G., Nomura, K., He, S.Y., Howe, G.A. and Browse, J. (2007) JAZ repressor proteins are targets of the SCF(COI1) complex during jasmonate signalling. *Nature*, **448**, 661-665.

Tian, D., Peiffer, M., De Moraes, C.M. and Felton, G.W. (2014) Roles of ethylene and jasmonic acid in systemic induced defense in tomato (Solanum lycopersicum) against Helicoverpa zea. *Planta*, **239**, 577-589.

Tian, D., Tooker, J., Peiffer, M., Chung, S. and Felton, G. (2012) Role of trichomes in defense against herbivores: comparison of herbivore response to *woolly* and *hairless* trichome mutants in tomato (*Solanum lycopersicum*). *Planta*, **236**, 1053-1066.

Tian, J., Han, L., Feng, Z., Wang, G., Liu, W., Ma, Y., Yu, Y. and Kong, Z. (2015) Orchestration of microtubules and the actin cytoskeleton in trichome cell shape determination by a plant-unique kinesin. *eLife*, **4**.

Tian, N., Liu, F., Wang, P., Zhang, X., Li, X. and Wu, G. (2017) The molecular basis of glandular trichome development and secondary metabolism in plants. *Plant Gene*, **12**, 1-12.

Todaka, D., Shinozaki, K. and Yamaguchi-Shinozaki, K. (2015) Recent advances in the dissection of drought-stress regulatory networks and strategies for development of drought-tolerant transgenic rice plants. *Front. Plant Sci.*, **6**, 20.

Tominaga-Wada, R., Nukumizu, Y., Sato, S. and Wada, T. (2013) Control of plant trichome and root-hair development by a tomato (*Solanum lycopersicum*) R3 MYB transcription factor. *PLoS ONE*, **8**, e54019.

Tominaga-Wada, R. and Wada, T. (2018) Effect of amino acid substitution of CAPRICE on cell-to-cell movement ability in Arabidopsis root epidermis. *Developmental Biology*, **435**, 1-5.

Torii, K.U., Kanaoka, M.M., Pillitteri, L.J. and Bogenschutz, N.L. (2007) Stomatal development: three steps for cell-type differentiation. *Plant signaling & behavior*, **2**, 311-313.

Traw, M.B. and Bergelson, J. (2003) Interactive effects of jasmonic acid, salicylic acid, and gibberellin on induction of trichomes in *Arabidopsis*. *Plant Physiol.*, **133**, 1367-1375.

Ueta, R., Abe, C., Watanabe, T., Sugano, S.S., Ishihara, R., Ezura, H., Osakabe, Y. and Osakabe, K. (2017) Rapid breeding of parthenocarpic tomato plants using CRISPR/Cas9. *Scientific Reports*, **7**, 8.

Uga, Y., Sugimoto, K., Ogawa, S., Rane, J., Ishitani, M., Hara, N., Kitomi, Y., Inukai, Y., Ono, K., Kanno, N., Inoue, H., Takehisa, H., Motoyama, R., Nagamura, Y., Wu, J.Z., Matsumoto, T., Takai, T., Okuno, K. and Yano, M. (2013) Control of root system architecture by DEEPER ROOTING 1 increases rice yield under drought conditions. *Nature Genet.*, **45**, 1097-+.

United Nations, D.o.E.a.S.A., Population Division (2015) World Population Prospects: The 2015 Revision.

Uzelac, B., Janošević, D., Stojičić, D. and Budimir, S. (2015) In vitro morphogenesis and secretion of secondary metabolites of Nicotiana tabacum tall glandular trichomes. *Botanica Serbica*, **39**.

Valliyodan, B. and Nguyen, H.T. (2006) Understanding regulatory networks and engineering for enhanced drought tolerance in plants. *Current Opinion in Plant Biology*, **9**, 189-195.

Valverde, P.L., Fornoni, J. and NÚÑez-Farfán, J. (2001) Defensive role of leaf trichomes in resistance to herbivorous insects in *Datura stramonium*. *Journal of Evolutionary Biology*, **14**, 424-432.

van Dam, N.M. and Hare, J.D. (1998) Differences in distribution and performance of two sap-sucking herbivores on glandular and non-glandular *Datura wrightii*. *Ecol. Entomol.*, **23**, 22-32.

van den Oever-van den Elsen, F., Lucatti, A.F., van Heusden, S., Broekgaarden, C., Mumm, R., Dicke, M. and Vosman, B. (2016) Quantitative resistance against *Bemisia tabaci* in *Solanum pennellii*: Genetics and metabolomics. *Journal of Integrative Plant Biology*, **58**, 397-412.

Van Leene, J., Hollunder, J., Eeckhout, D., Persiau, G., Van De Slijke, E., Stals, H., Van Isterdael, G., Verkest, A., Neirynck, S., Buffel, Y., De Bodt, S., Maere, S., Laukens, K., Pharazyn, A., Ferreira, P.C.G., Eloy, N., Renne, C., Meyer, C., Faure, J.D., Steinbrenner, J., Beynon, J., Larkin, J.C., Van de Peer, Y., Hilson, P., Kuiper, M., De Veylder, L., Van Onckelen, H., Inzé, D., Witters, E. and De Jaeger, G. (2010) Targeted interactomics reveals a complex core cell cycle machinery in Arabidopsis thaliana. *Molecular Systems Biology*, **6**.

Van Schie, C.C.N., Ament, K., Schmidt, A., Lange, T., Haring, M.A. and Schuurink, R.C. (2007) Geranyl diphosphate synthase is required for biosynthesis of gibberellins. *The Plant Journal*, **52**, 752-762.

Varaud, E., Brioudes, F., Szécsi, J., Leroux, J., Brown, S., Perrot-Rechenmann, C. and Bendahmane, M. (2011) AUXIN RESPONSE FACTOR8 regulates *Arabidopsis* petal growth by interacting with the bHLH transcription factor BIGPETALp. *The Plant Cell*, **23**, 973-983.

Vendemiatti, E., Zsögön, A., Silva, G.F.F.e., de Jesus, F.A., Cutri, L., Figueiredo, C.R.F., Tanaka, F.A.O., Nogueira, F.T.S. and Peres, L.E.P. (2017) Loss of type-IV glandular trichomes is a heterochronic trait in tomato and can be reverted by promoting juvenility. *Plant Science*, **259**, 35-47.

Veytsman, B.A. and Cosgrove, D.J. (1998) A Model of Cell Wall Expansion Based on Thermodynamics of Polymer Networks. *Biophysical journal*, **75**, 2240-2250.

Villagarcia, H., Morin, A.C., Shpak, E.D. and Khodakovskaya, M.V. (2012) Modification of tomato growth by expression of truncated ERECTA protein from *Arabidopsis thaliana*. *Journal of Experimental Botany*, **63**, 6493-6504.

Vofely, R.V., Gallagher, J., Pisano, G.D., Bartlett, M. and Braybrook, S.A. (2018) Of puzzles and pavements: a quantitative exploration of leaf epidermal cell shape. *bioRxiv*.

von Groll, U., Berger, D. and Altmann, T. (2002) The subtilisin-like serine protease SDD1 mediates cell-to-cell signaling during *Arabidopsis* stomatal development. *The Plant Cell*, **14**, 1527-1539.

Vosman, B., van't Westende, W.P.C., Henken, B., van Eekelen, H., de Vos, R.C.H. and Voorrips, R.E. (2018) Broad spectrum insect resistance and metabolites in close relatives of the cultivated tomato. *Euphytica*, **214**, 14.

Vriet, C., Russinova, E. and Reuzeau, C. (2013) From squalene to brassinolide: the steroid metabolic and signaling pathways across the plant kingdom. *Molecular Plant*, **6**, 1738-1757.

Wada, T., Hayashi, N. and Tominaga-Wada, R. (2015) Root hair formation at the root-hypocotyl junction in CPC-LIKE MYB double and triple mutants of Arabidopsis. *Plant Signaling & Behavior*, **10**, 4.

Wada, T., Kunihiro, A. and Tominaga-Wada, R. (2014) Arabidopsis CAPRICE (MYB) and GLABRA3 (bHLH) Control Tomato (Solanum lycopersicum) Anthocyanin Biosynthesis. *Plos One*, **9**, 9.

Wada, T., Tachibana, T., Shimura, Y. and Okada, K. (1997) Epidermal cell differentiation in *Arabidopsis* determined by a Myb homolog, CPC. *Science*, **277**, 1113-1116.

Wagner, G.J., Wang, E. and Shepherd, R.W. (2004) New approaches for studying and exploiting an old protuberance, the plant trichome. *Ann Bot*, **93**, 3-11.

Walford, S.A., Wu, Y., Llewellyn, D.J. and Dennis, E.S. (2011) GhMYB25-like: a key factor in early cotton fibre development. *Plant J*, **65**, 785-797.

Walford, S.A., Wu, Y.R., Llewellyn, D.J. and Dennis, E.S. (2012) Epidermal cell differentiation in cotton mediated by the homeodomain leucine zipper gene, GhHD-1. *Plant J.*, **71**, 464-478.

Walker, A.R., Davison, P.A., Bolognesi-Winfield, A.C., James, C.M., Srinivasan, N., Blundell, T.L., Esch, J.J., Marks, M.D. and Gray, J.C. (1999) The TRANSPARENT TESTA GLABRA1 locus, which regulates trichome differentiation and anthocyanin biosynthesis in Arabidopsis, encodes a WD40 repeat protein. *Plant Cell*, **11**, 1337-1350.

Walker, J.D., Oppenheimer, D.G., Concienne, J. and Larkin, J.C. (2000) SIAMESE, a gene controlling the endoreduplication cell cycle in *Arabidopsis thaliana* trichomes. *Development*, **127**, 3931-3940.

Wan, Q., Zhang, H., Ye, W., Wu, H. and Zhang, T. (2014) Genome-wide transcriptome profiling revealed cotton fuzz fiber development having a similar molecular model as *Arabidopsis* trichome. *PLOS ONE*, **9**, e97313.

Wang, L., Einig, E., Almeida-Trapp, M., Albert, M., Fliegmann, J., Mithöfer, A., Kalbacher, H. and Felix, G. (2018) The systemin receptor SYR1 enhances resistance of tomato against herbivorous insects. *Nature Plants*, **4**, 152-156.

Wang, M., Zhao, P., Cheng, H., Han, L., Wu, X., Gao, P., Wang, H., Yang, C., Zhong, N., Zuo, J. and Xia, G. (2013) The cotton transcription factor GhTCP14 functions in auxin-mediated epidermal cell differentiation and elongation. *Plant Physiol.*

Wang, S. and Chen, J.-G. (2014) Regulation of cell fate determination by single-repeat R3 MYB transcription factors in Arabidopsis. *Front. Plant Sci.*, **5**, 133.

Wang, T., Li, R., Wen, L., Fu, D., Zhu, B., Luo, Y. and Zhu, H. (2015a) Functional analysis and RNA sequencing indicate the regulatory role of Argonaute1 in tomato compound leaf development. *PLOS ONE*, **10**, e0140756.

Wang, X., Jing, Y.J., Zhang, B.C., Zhou, Y.H. and Lin, R.C. (2015b) Glycosyltransferase-like protein ABI8/ELD1/KOB1 promotes Arabidopsis hypocotyl elongation through regulating cellulose biosynthesis. *Plant Cell Environ.*, **38**, 411-422.

Wang, X.Q., Wu, W.H. and Assmann, S.M. (1998) Differential responses of abaxial and adaxial guard cells. **118**, 1421-1429.

War, A.R., Paulraj, M.G., Ahmad, T., Buhroo, A.A., Hussain, B., Ignacimuthu, S. and Sharma, H.C. (2012) Mechanisms of plant defense against insect herbivores. *Plant signaling & behavior*, **7**, 1306-1320.

Waterhouse, P.M. and Fusaro, A.F. (2006) Viruses face a double defense by plant small RNAs. *Science*, **313**, 54-55.

Wentworth, M., Murchie, E.H., Gray, J.E., Villegas, D., Pastenes, C., Pinto, M. and Horton, P. (2006) Differential adaptation of two varieties of common bean to abiotic stress: II. Acclimation of photosynthesis. *J Exp Bot*, **57**, 699-709.

Werker, E. (2000) Trichome diversity and development. In *Advances in Botanical Research*: Academic Press, pp. 1-35.

Wester, K., Digiuni, S., Geier, F., Timmer, J., Fleck, C. and Hulskamp, M. (2009) Functional diversity of R3 single-repeat genes in trichome development. *Development (Cambridge, England)*, **136**, 1487-1496.

Whitney, H.M., Bennett, K.M.V., Dorling, M., Sandbach, L., Prince, D., Chittka, L. and Glover, B.J. (2011) Why do so many petals have conical epidermal cells? *Annals of Botany*, **108**, 609-616.

Whitney, H.M., Chittka, L., Bruce, T.J.A. and Glover, B.J. (2009a) Conical epidermal cells allow bees to grip flowers and increase foraging efficiency. *Current Biology*, **19**, 948-953.

Whitney, H.M., Kolle, M., Andrew, P., Chittka, L., Steiner, U. and Glover, B.J. (2009b) Floral iridescence, produced by diffractive optics, acts as a cue for animal pollinators. *Science*, **323**, 130-133.

Wilkens, R.T., Shea, G.O., Halbreich, S. and Stamp, N.E. (1996) Resource availability and the trichome defenses of tomato plants. *Oecologia*, **106**, 181-191.

Williams, W.G., Kennedy, G.G., Yamamoto, R.T., Thacker, J.D. and Bordner, J. (1980) 2-Tridecanone: A Naturally Occurring Insecticide from the Wild Tomato Lycopersicon hirsutum f.glabratum. *Science*, **207**, 888-889.

Willmer, C. and Fricker, M. (1996) *Stomata*: Springer Netherlands.

Winter, D., Vinegar, B., Nahal, H., Ammar, R., Wilson, G.V. and Provart, N.J. (2007) An "Electronic Fluorescent Pictograph" browser for exploring and analyzing large-scale biological data sets. *PLOS ONE*, **2**, e718.

Wintermantel, W.M. (2004) Emergence of greenhouse whitefly (*Trialeurodes vaporariorum*) transmitted criniviruses as threats to vegetable and fruit production in North America. *APSnet Features*.

Wu, R., Li, S., He, S., Waßmann, F., Yu, C., Qin, G., Schreiber, L., Qu, L.J. and Gu, H. (2011) CFL1, a WW Domain Protein, regulates cuticle development by modulating the function of HDG1, a Class IV Homeodomain transcription factor, in rice and *Arabidopsis*. *Plant Cell*, **23**, 3392-3411.

Wu, Y., Machado, A.C., White, R.G., Llewellyn, D.J. and Dennis, E.S. (2006) Expression profiling identifies genes expressed early during lint fibre initiation in cotton. *Plant & cell physiology*, **47**, 107-127.

Xu, Z. and Zhou, G. (2008) Responses of leaf stomatal density to water status and its relationship with photosynthesis in a grass. *J Exp Bot*, **59**, 3317-3325.

Xue, D., Zhang, X., Lu, X., Chen, G. and Chen, Z.-H. (2017) Molecular and evolutionary mechanisms of cuticular wax for plant drought tolerance. *Front. Plant Sci.*, **8**, 621.

Yan, A., Pan, J.B., An, L.Z., Gan, Y.B. and Feng, H.Y. (2012) The responses of trichome mutants to enhanced ultraviolet-B radiation in *Arabidopsis thaliana*. *J. Photochem. Photobiol. B-Biol.*, **113**, 29-35.

Yan, T., Chen, M., Shen, Q., Li, L., Fu, X., Pan, Q., Tang, Y., Shi, P., Lv, Z., Jiang, W., Ma, Y.-n., Hao, X., Sun, X. and Tang, K. (2017) HOMEODOMAIN PROTEIN 1 is required for jasmonate-mediated glandular trichome initiation in Artemisia annua. *New Phytologist*, **213**, 1145-1155.

Yan, T., Li, L., Xie, L., Chen, M., Shen, Q., Pan, Q., Fu, X., Shi, P., Tang, Y., Huang, H., Huang, Y., Huang, Y. and Tang, K. (2018) A novel HD-ZIP IV/MIXTA complex promotes glandular trichome initiation and cuticle development in *Artemisia annua*. *The New phytologist*, **218**, 567-578.

Yanagisawa, M., Desyatova, A.S., Belteton, S.A., Mallery, E.L., Turner, J.A. and Szymanski, D.B. (2015) Patterning mechanisms of cytoskeletal and cell wall systems during leaf trichome morphogenesis. *Nature Plants*, **1**, 15014.

Yang, C., Gao, Y., Gao, S., Yu, G., Xiong, C., Chang, J., Li, H. and Ye, Z. (2015) Transcriptome profile analysis of cell proliferation molecular processes during multicellular trichome formation induced by tomato Wov gene in tobacco. *BMC Genomics*, **16**, 868.

Yang, C., Li, H., Zhang, J., Luo, Z., Gong, P., Zhang, C., Li, J., Wang, T., Zhang, Y., Lu, Y.e. and Ye, Z. (2011a) A regulatory gene induces trichome formation and embryo lethality in tomato. *Proceedings of the National Academy of Sciences*, **108**, 11836-11841.

Yang, D.H., Hettenhausen, C., Baldwin, I.T. and Wu, J. (2011b) BAK1 regulates the accumulation of jasmonic acid and the levels of trypsin proteinase inhibitors in *Nicotiana attenuata*'s responses to herbivory. *J Exp Bot*, **62**, 641-652.

Yang, M. and Sack, F.D. (1995) The too many mouths and four lips mutations affect stomatal production in *Arabidopsis*. *The Plant Cell*, **7**, 2227-2239.

Yang, S., Cai, Y., Liu, X., Dong, M., Zhang, Y., Chen, S., Zhang, W., Li, Y., Tang, M., Zhai, X., Weng, Y. and Ren, H. (2018) A CsMYB6-CsTRY module regulates fruit trichome initiation in cucumber. *Journal of Experimental Botany*, **69**, 1887-1902.

Yang, S.B., Yu, Q.H., Wang, B.K., Yang, T., Li, N., Tang, Y.P., Aisimutuola, P., Wang, Q., Xu, J. and Gao, J. (2016) Identification of QTLs for red fruit firmness using the wild tomato species *Solanum pennellii* LA716 introgression lines. *Plant Breed.*, **135**, 728-734.

Yeats, T.H. and Rose, J.K.C. (2013) The formation and function of plant cuticles. *Plant Physiol.*, **163**, 5-20.

Yokoyama, R., Shinohara, N., Asaoka, R., Narukawa, H. and Nishitani, K. (2014) The biosynthesis and function of polysaccharide components of the plant cell wall. *Plant Cell Wall Patterning and Cell Shape; Fukuda, H., Ed*, 3-34.

Yoshida, Y., Sano, R., Wada, T., Takabayashi, J. and Okada, K. (2009) Jasmonic acid control of GLABRA3 links inducible defense and trichome patterning in Arabidopsis. *Development (Cambridge, England)*, **136**, 1039-1048.

Young, A.M., Schaller, M. and Strand, M. (1984) Floral nectaries and trichomes in relation to pollination in some species of *Theobroma* and *Herrania* (Sterculiaceae). *American Journal of Botany*, **71**, 466-480.

Yuan, C., Li, C., Yan, L., Jackson, A.O., Liu, Z., Han, C., Yu, J. and Li, D. (2011) A high throughput barley stripe mosaic virus vector for virus induced gene silencing in monocots and dicots. *PLoS One*, **6**, e26468.

Zeiger, E. (1983) The biology of stomatal guard cells. *Annual Review of Plant Physiology*, **34**, 441-474.

Zhang, F., Gonzalez, A., Zhao, M., Payne, C.T. and Lloyd, A. (2003) A network of redundant bHLH proteins functions in all TTG1-dependent pathways of Arabidopsis. *Development (Cambridge, England)*, **130**, 4859-4869.

Zhang, S., Xu, M., Qiu, Z., Wang, K., Du, Y., Gu, L. and Cui, X. (2016a) Spatiotemporal transcriptome provides insights into early fruit development of tomato (Solanum lycopersicum). *Scientific Reports*, **6**, 23173.

Zhang, X., Yan, F., Tang, Y., Yuan, Y., Deng, W. and Li, Z. (2015) Auxin Response Gene *SlARF3* plays multiple roles in tomato development and is involved in the formation of epidermal cells and trichomes. *Plant and Cell Physiology*, **56**, 2110-2124.

Zhang, X.H., Zou, Z., Gong, P.J., Zhang, J.H., Ziaf, K., Li, H.X., Xiao, F.M. and Ye, Z.B. (2011) Over-expression of microRNA169 confers enhanced drought tolerance to tomato. *Biotechnol. Lett.*, **33**, 403-409.

Zhang, X.K., Lu, G.Y., Long, W.H., Zou, X.L., Li, F. and Nishio, T. (2014) Recent progress in drought and salt tolerance studies in Brassica crops. *Breed. Sci.*, **64**, 60-73.

Zhang, Y., Guo, X. and Dong, J. (2016b) Phosphorylation of the polarity protein BASL differentiates asymmetric cell fate through MAPKs and SPCH. *Current Biology*, **26**, 2957-2965.

Zhao, H., Wang, X., Zhu, D., Cui, S., Li, X., Cao, Y. and Ma, L. (2012) A single amino acid substitution in IIIf subfamily of basic helix-loop-helix transcription factor AtMYC1 leads to trichome and root hair patterning defects by abolishing its interaction with partner proteins in Arabidopsis. *The Journal of biological chemistry*, **287**, 14109-14121.

Zhao, H., Wang, X.X., Du, Y.C., Zhu, D.W., Guo, Y.M., Gao, J.C., Li, F. and Snyder, J.C. (2014) Haploid induction via *in vitro g*ynogenesis in tomato *(Solanum lycopersicum* L.). *J. Integr. Agric.*, **13**, 2122-2131.

Zhao, L., Li, Y., Xie, Q. and Wu, Y. (2017) Loss of CDKC;2 increases both cell division and drought tolerance in *Arabidopsis thaliana*. *The Plant journal : for cell and molecular biology*.

Zhao, L. and Sack, F.D. (1999) Ultrastructure of stomatal development in *Arabidopsis* (Brassicaceae) leaves. *American Journal of Botany*, **86**, 929-939.

Zhao, M., Morohashi, K., Hatlestad, G., Grotewold, E. and Lloyd, A. (2008) The TTG1-bHLH-MYB complex controls trichome cell fate and patterning through direct targeting of regulatory loci. *Development*, **135**, 1991-1999.

Zhiponova, M.K., Vanhoutte, I., Boudolf, V., Betti, C., Dhondt, S., Coppens, F., Mylle, E., Maes, S., González-García, M.-P., Caño-Delgado, A.I., Inzé, D., Beemster, G.T.S., Veylder, L. and Russinova, E. (2013) Brassinosteroid production and signaling differentially control cell division and expansion in the leaf. *New Phytologist*, **197**, 490-502.

Zhou, Z., An, L., Sun, L. and Gan, Y. (2012) ZFP5 encodes a functionally equivalent GIS protein to control trichome initiation. *Plant Signal Behav*, **7**, 28-30.

Zhou, Z., An, L., Sun, L., Zhu, S., Xi, W., Broun, P., Yu, H. and Gan, Y. (2011) Zinc finger protein5 is required for the control of trichome initiation by acting upstream of zinc finger protein8 in Arabidopsis. *Plant Physiol*, **157**, 673-682.

Zhou, Z., Sun, L., Zhao, Y., An, L., Yan, A., Meng, X. and Gan, Y. (2013) Zinc Finger Protein 6 (ZFP6) regulates trichome initiation by integrating gibberellin and cytokinin signaling in Arabidopsis thaliana. *New Phytologist*, **198**, 699-708.

Zhu, H., Sun, X., Zhang, Q., Song, P., Hu, Q., Zhang, X., Li, X., Hu, J., Pan, J., Sun, S., Weng, Y. and Yang, L. (2018a) GLABROUS (CmGL) encodes a HD-ZIP IV transcription factor playing roles in multicellular trichome initiation in melon. *TAG. Theoretical and applied genetics. Theoretische und angewandte Genetik*, **131**, 569-579.

Zhu, J.-K. (2016) Abiotic stress signaling and responses in plants. *Cell*, **167**, 313-324.

Zhu, J.-Y., Sae-Seaw, J. and Wang, Z.-Y. (2013) Brassinosteroid signalling. *Development (Cambridge, England)*, **140**, 1615-1620.

Zhu, L.Z., Li, J.Y., Xu, Z.P., Manghwar, H., Liang, S.J., Li, S.L., Alariqi, M., Jin, S.X. and Zhang, X.L. (2018b) Identification and selection of resistance to *Bemisia tabaci* among 550 cotton genotypes in the field and greenhouse experiments. *Front. Agric. Sci. Eng.*, **5**, 236-252.

Zhu, M.K., Meng, X.Q., Cai, J., Li, G., Dong, T.T. and Li, Z.Y. (2018c) Basic leucine zipper transcription factor SIbZIP1 mediates salt and drought stress tolerance in tomato. *Bmc Plant Biology*, **18**, 14.

Zoulias, N., Harrison, E.L., Casson, S.A. and Gray, J.E. (2018) Molecular control of stomatal development. *Biochemical Journal*, **475**, 441-454.

Appendix 1 – List of primers

Appendix 1.- List of primers. The name, sequence and use of the primer is shown for each entry. For qPCR primers, the primer efficiency estimate is shown in the "Use" column, calculated as described in chapter 2.

Primer	Sequence	Use
SlMIXTA-like-VIGS F	GGGGACAAGTTTGTACAAAAAAGCAGGCTTATTAGCTTATATCGAAGAA	VIGS cloning
SlMIXTA-like-VIGS R	GGGGACCACTTTGTACAAGAAAGCTGGGTAGGTCACTGGGTCGATCCC	VIGS cloning
SlEXP15-VIGS F	GGGGACAAGTTTGTACAAAAAAGCAGGCTTAATGGCTCTTTTAGCTATCCTT	VIGS cloning
SlEXP15-VIGS R	GGGGACCACTTTGTACAAGAAAGCTGGGTAGAAATTGGTGGCTGTTAC	VIGS cloning
SlMX2-VIGS F	GGGGACAAGTTTGTACAAAAAAGCAGGCTTACTTTATCGTCGTCCTCAT	VIGS cloning
SlMX2-VIGS R	GGGGACCACTTTGTACAAGAAAGCTGGGTACTGGAAAAAGCTCATCTAA	VIGS cloning
sMYB102-VIGS F	GGGGACAAGTTTGTACAAAAAAGCAGGCTTAATGCATGCGGAGGTCACG	VIGS cloning
sMYB102-VIGS R	GGGGACCACTTTGTACAAGAAAGCTGGGTATTATGTTTCTTTCTCGTCTGCTTT	VIGS cloning
bZIP17-VIGS F	GGGGACAAGTTTGTACAAAAAAGCAGGCTTAATGAGCGATATTTCTGGT	VIGS cloning
bZIP17-VIGS R	GGGGACCACTTTGTACAAGAAAGCTGGGTAATAATTCAGCCCTCCGCAATTG	VIGS cloning
SlABI8-VIGS F	GGGGACAAGTTTGTACAAAAAAGCAGGCTTAATGGCGGGTCTTTTCGCT	VIGS cloning
SlABI8-VIGS R	GGGGACCACTTTGTACAAGAAAGCTGGGTAATCCCTGAAATACGGGAA	VIGS cloning
SlCycB2-VIGS F	GGGGACAAGTTTGTACAAAAAAGCAGGCTTAATGTCCCCGACGAATTCA	VIGS cloning
SlCycB2-VIGS R	GGGGACCACTTTGTACAAGAAAGCTGGGTATTATTTTTTCTCATAGATAA	VIGS cloning
MYB102-VIGS F	GGGGACAAGTTTGTACAAAAAAGCAGGCTTAAGGTCTTTCTAACAGTGG	VIGS cloning
MYB102-VIGS R	GGGGACCACTTTGTACAAGAAAGCTGGGTATGCTGCTGTGATTGCCTA	VIGS cloning
SlLHW-VIGS F	GGGGACAAGTTTGTACAAAAAAGCAGGCTTAATGGGGTATTTGCTGAAA	VIGS cloning
SlLHW-VIGS R	GGGGACCACTTTGTACAAGAAAGCTGGGTAGATTTGACTTTCCATCATCATT	VIGS cloning
SlEIF1-VIGS F	GGGGACAAGTTTGTACAAAAAAGCAGGCTTACGATATGAAAAAACTTGAAGAAG	VIGS cloning
SlEIF1-VIGS R	GGGGACCACTTTGTACAAGAAAGCTGGGTAGCAAAACAGATGGCATAA	VIGS cloning

SlMIXTA-like qPCR F	GTCGGCCATAGCCACTCATT	qPCR 108%
SlMIXTA-like qPCR R	CACTGGGTCGATCCCCATTT	qPCR 108%
SlMX2 qPCR F	GGTTTGAAGAAAGGGCCATGG	qPCR 104%
SlMX2 qPCR R	ACAACTCCTTCCACATCTCTGA	qPCR 104%
SlActin qPCR F	GGGGGCTATGAATGCACGGT	qPCR 102%
SlActin qPCR R	GGCAATGCATCAGGCACCTC	qPCR 102%
SlGAPDH qPCR F	GGCTGCAATCAAGGAGGAA	qPCR 91%
SlGAPDH qPCR R	ATGCTTGACCTGCTGTCACC	qPCR 91%
SlMIXTA-like F	GGGGACAAGTTTGTACAAAAAAGCAGGCTTAATGGGTCGATCTCCGTGT	CDS cloning
SlMIXTA-like R	GGGGACCACTTTGTACAAGAAAGCTGGGTATTAGAACATAGATGAATC	CDS cloning
SpMIXTA-like F	GGGGACAAGTTTGTACAAAAAAGCAGGCTTAATGGGTCGATCTCCGTGT	CDS cloning
SpMIXTA-like R	GGGGACCACTTTGTACAAGAAAGCTGGGTATTAGAACATAGATGAATC	CDS cloning
SlMIXTA-like sgRNA 1 F	ATTGAAGAAGAGCAAGATGAGAT	CRISPR cloning
SlMIXTA-like sgRNA 1 R	AAACATCTCATCTTGCTCTTCTT	CRISPR cloning
SlMIXTA-like sgRNA 2 F	GTGATTGTAATTTGCAGTTTCTGTCCCGTT	CRISPR cloning
SlMIXTA-like sgRNA 2 R	CTAAAACGGGACAGAAACTGCAAATTACAA	CRISPR cloning
proMIXTA-like F	GGGGACCACTTTGTACAAGAAAGCTGGGTACGACGAAATGGCGACTAT	Promoter cloning
proMIXTA-like R	GGGGACAAGTTTGTACAAAAAAGCAGGCTTAATAGAGTCGAAAAAACGT	Promoter cloning
35S F	CTATCCTTCGCAAGACCCTTC	Genotyping
SlMIXTA-like R2	CACTGGGTCGATCCCCATTT	Genotyping
proMIXTA-like F2	TCCAAAGCAGTTACCGGAGT	Genotyping
GFP R	TCAGCTTGCCGTAGGTGGCATC	Genotyping
SlMIXTA-like KO F	TTGAAGCACCATCAATTTTCTTT	Genotyping
SlMIXTA-like KO R	TGAATCGCATACCAGCTTTG	Genotyping
SlMIXTA-like qPCR F	GTCGGCCATAGCCACTCATT	qPCR 108%
SlMIXTA-like qPCR R	CACTGGGTCGATCCCCATTT	qPCR 108%

Woolly sgRNA 1 F	ATTGTATGTTGGTAAATCAGCCCT	CRISPR cloning
Woolly sgRNA 1 R	AAACAGGGCTGATTTACCAACATA	CRISPR cloning
Woolly sgRNA 2 F	GTGATTGTTCCTCAGCCCGAAGCTCCTGTT	CRISPR cloning
Woolly sgRNA 2 R	CTAAAACAGGAGCTTCGGGCTGAGGAACAA	CRISPR cloning
Hairless sgRNA 1 F	ATTGCTAAAATCAATTGACGGTG	CRISPR cloning
Hairless sgRNA 1 R	AAACCACCGTCAATTGATTTTAG	CRISPR cloning
Hairless sgRNA 2 F	GTGATTGCAGATGGACTGCACGAGTTGTT	CRISPR cloning
Hairless sgRNA 2 R	CTAAAACAACTCGTGCAGTCCATCTGCAA	CRISPR cloning
DWARF sgRNA 1 F	ATTGATCATAGACTGTGGGTATCC	CRISPR cloning
DWARF sgRNA 1 R	AAACGGATACCCACAGTCTATGAT	CRISPR cloning
DWARF sgRNA 2 F	GTGATTGTTGGTCTCTGATCATTGTAGTT	CRISPR cloning
DWARF sgRNA 2 R	CTAAAACTACAATGATCAGAGACCAACAA	CRISPR cloning
CD2 sgRNA 1 F	ATTGCCATGAGAATTCGATACTA	CRISPR cloning
CD2 sgRNA 1 R	AAACTAGTATCGAATTCTCATGG	CRISPR cloning
CD2 sgRNA 2 F	GTGATTGCCAATTTGTACTAATTGTGGGTT	CRISPR cloning
CD2 sgRNA 2 R	CTAAAACCCACAATTAGTACAAATTGGCAA	CRISPR cloning
SlMX1 sgRNA 1 F	ATTGAAAAAAATGGATGTGGTAGT	CRISPR cloning
SlMX1 sgRNA 1 R	AAACACTACCACATCCATTTTTTT	CRISPR cloning
SlMX1 sgRNA 2 F	GTGATTGTCAGTATATATTAACGTACGTT	CRISPR cloning
SlMX1 sgRNA 2 R	CTAAAACGTACGTTAATATATACTGACAA	CRISPR cloning
Woolly F	TCACATGAAATGGCATTCAAA	Genotyping
Woolly R	CAGCAGCGTACATTTCTCCA	Genotyping
Hairless F	CTCGACTTCCTTTGCAGCTT	Genotyping
Hairless R	AGGCATGTCATGTGACTCCA	Genotyping
DWARF F	GAAAAACCAAAGAGCCAGGT	Genotyping
DWARF R	AAATCCGCGATGATAGTTGG	Genotyping
CD2 F	TGTGGGTTTCTGCTTCTGAA	Genotyping
CD2 R	TCAGCCTAGCATTTTCAATCCT	Genotyping
SlMX1 F	GGACCATGGACTCCTGAAGA	Genotyping
SlMX1 R	GGGCTGATTAAAACCTGAAAA	Genotyping

pDONR207/TOPO F	GTAAAACGACGGCCAG	Sequencing
pDONR207/TOPO R	CAGGAAACAGCTATGAC	Sequencing
pTRV2 F	CTCAAGGAAGCACGATGAG	Sequencing
RB R	CCCGCCAATATATCCTGTC	Sequencing

Appendix 2 – List of plasmids

Plasmid	Description	Resistance	Source
pDONR207	Entry vector for Gateway cloning	Gentamycin Chloramphenicol	Invitrogen, UK
pDONR207-SlMIXTA-like VIGS	Entry vector for Gateway cloning bearing SlMIXTA-LIKE VIGS fragment.	Gentamycin	This thesis
pDONR207-EXP15 VIGS	Entry vector for Gateway cloning bearing SlEXP15 VIGS fragment.	Gentamycin	This thesis
pDONR207-SlMX2 VIGS	Entry vector for Gateway cloning bearing SlMX2 VIGS fragment.	Gentamycin	This thesis
pDONR207-sMYB10-2 VIGS	Entry vector for Gateway cloning bearing sMYB10-2 VIGS fragment.	Gentamycin	This thesis
pDONR207-SlbZIP17 VIGS	Entry vector for Gateway cloning bearing SlbZIP17 VIGS fragment.	Gentamycin	This thesis
pDONR207-SlABI8 VIGS	Entry vector for Gateway cloning bearing SlABI8 VIGS fragment.	Gentamycin	This thesis
pDONR207-SlCycB2 VIGS	Entry vector for Gateway cloning bearing SlCycB2 VIGS fragment.	Gentamycin	This thesis
pDONR207-MYB10-2 VIGS	Entry vector for Gateway cloning bearing MYB10-2 VIGS fragment.	Gentamycin	This thesis
pDONR207-SlLHW VIGS	Entry vector for Gateway cloning bearing SlLHW VIGS fragment.	Gentamycin	This thesis
pDONR207-SlELF1 VIGS	Entry vector for Gateway cloning bearing SlElF1 VIGS fragment.	Gentamycin	This thesis
pTRV2-D/R-GW	Binary vector for VIGS with Gateway™ cassette and Del/Ros1 silencing fragment	Kanamycin Chloramphenicol	Orzaez et al., 2009
pTRV1	Binary vector for VIGS (required for silencing together with pTRV2)	Kanamycin	
pTRV2-D/R-SlMIXTA-like	Binary vector for VIGS bearing SlMIXTA-like VIGS fragment.	Kanamycin	This thesis
pTRV2-D/R-SlEXP15	Binary vector for VIGS bearing SlEXP15 VIGS fragment	Kanamycin	This thesis
pTRV2-D/R-SlMX2	Binary vector for VIGS bearing SlMX2 VIGS fragment.	Kanamycin	This thesis
pTRV2-D/R-sMYB10-2	Binary vector for VIGS bearing sMYB10-2 VIGS fragment.	Kanamycin	This thesis

Plasmid	Description	Resistance	Source
pTRV2-D/R-SlbZIP17	Binary vector for VIGS bearing SlbZIP17 VIGS fragment.	Kanamycin	This thesis
pTRV2-D/R-SlABI8	Binary vector for VIGS bearing SlABI8 VIGS fragment.	Kanamycin	This thesis
pTRV2-D/R-SlCycB2	Binary vector for VIGS bearing SlCycB2 VIGS fragment.	Kanamycin	This thesis
pTRV2-D/R-MYB10-2	Binary vector for VIGS bearing MYB10-2 VIGS fragment.	Kanamycin	This thesis
pTRV2-D/R-SlLHW	Binary vector for VIGS bearing SlLHW VIGS fragment.	Kanamycin	This thesis
pTRV2-D/R-SlEIF1	Binary vector for VIGS bearing SlEIF1 VIGS fragment.	Kanamycin	This thesis
pDONR207-SlMIXTA-like	Entry vector for Gateway cloning bearing SlMIXTA-LIKE CDS.	Gentamycin	This thesis
pDONR207-SpMIXTA-like	Entry vector for Gateway cloning bearing SpMIXTA-LIKE CDS.	Gentamycin	This thesis
pDONR207-proMIXTA-LIKE	Entry vector for Gateway cloning bearing SlMIXTA-LIKE promoter.	Gentamycin	This thesis
pBIN19-35S-GW	Binary vector for overexpression in plants with Gateway casette.	Kanamycin Chloramphenicol	Martin group
pBIN19-35S-SlMIXTA-LIKE	Binary vector for overexpression of SlMIXTA-LIKE in tomato.	Kanamycin	This thesis
pBIN19-35S-SpMIXTA-LIKE	Binary vector for overexpression of SpMIXTA-LIKE in tomato.	Kanamycin	This thesis
pICSL002218A	Level 2 Golden Gate completely functional for CRISPR/Cas9	Kanamycin	TSL SynBio (Mark Youles)
pICSL002218A SlMIXTA-like	Level 2 Golden Gate completely functional for CRISPR/Cas9 bearing SlMIXTA-LIKE sgRNA 1 and 2	Kanamycin	This thesis
pKGWFS7	Binary vector for promoter activity analysis with a Gateway cassette followed by a GFP:GUS fusion.	Kanamycin	Karimi et al., 2002
pICSL002218A	Level 2 Golden Gate completely functional for CRISPR/Cas9	Kanamycin	TSL SynBio (Mark Youles)
pICSL002218A SlMIXTA-like	Level 2 Golden Gate completely functional for CRISPR/Cas9 bearing SlMIXTA-LIKE sgRNA 1 and 2	Kanamycin	This thesis

Plasmid	Description	Resistance	Source
pKGWFS7 proMIXTA-LIKE	Binary vector bearing a proMIXTA-LIKE:GFP:GUS cassette.	Kanamycin	This thesis
pICSL002218A Woolly	Level 2 Golden Gate completely functional for CRISPR/Cas9 bearing Woolly sgRNA 1 and 2	Kanamycin	This thesis
pICSL002218A Hairless	Level 2 Golden Gate completely functional for CRISPR/Cas9 bearing Hairless sgRNA 1 and 2	Kanamycin	This thesis
pICSL002218A DWARF	Level 2 Golden Gate completely functional for CRISPR/Cas9 bearing DWARF sgRNA 1 and 2	Kanamycin	This thesis
pICSL002218A CD2	Level 2 Golden Gate completely functional for CRISPR/Cas9 bearing CD2 sgRNA 1 and 2	Kanamycin	This thesis
pICSL002218A SlMX1	Level 2 Golden Gate completely functional for CRISPR/Cas9 bearing SlMX1 sgRNA 1 and 2	Kanamycin	This thesis

Appendix 3 – Media and stock solutions

Appendix 3.-Media recipes and stock solutions.

Media recipes

LB (Luria-Bertani)

Tryptone	10 g/L
Yeast extract	5 g/L
Sodium chloride	10 g/L
Formedium agar	11 g/L (for solid plates)

SOC (Super Optimal broth with Catabolite repression)

Tryptone	20 g/L
Yeast extract	5 g/L
Sodium chloride	0.58 g/L
Potassium chloride	0.186 g/L
Magnesium chloride	2.03 g/L
Magnesium sulphate	2.46 g/L
Glucose	3.6 g/L

TY (Tryptone-Yeast extract)

Tryptone	5 g/L
Yeast extract	3 g/L
Calcium chloride hexahydrate	1.32g/L
Formedium agar	10 g/L (for solid plates)

MS (Murashige-Skoog) + 3% sucrose

MS media with vitamins	4.41 g/L
Ammonium nitrate	1650.00 mg/L
Calcium chloride	332.20 mg/L
Magnesium sulphate	180.69 mg/L
Potassium nitrate	1900.00 mg/L
Potassium phosphate	170.00 mg/L
Boric acid	6.20 mg/L
Cobalt chloride	0.025 mg/L
Copper sulphate	0.025 mg/L
EDTA disodium salt	37.30 mg/L
Ferrous sulphate	27.80 mg/L
Manganese sulphate	16.90 mg/L
Molybdic acid	0.213 mg/L
Glycine	2.00 mg/L
Myo-inositol	100.00 mg/L
Nicotinic acid	0.50 mg/L
Pyridoxine HCl	0.50 mg/L
Thiamine HCl	0.10 mg/L

Sucrose	30 g/L

Germination media

MS media with vitamins	4.4 g/L
Agarose	6 g/L
pH 5.8 (KOH)	

Cell suspension media

MS media with vitamins	4.4 g/L
Sucrose	10 g/L
Agarose	6 g/L
2,4-D	0.5 mg/L
pH 5.7 (KOH)	

Regeneration media

MS media with Nitch's vitamins	4.4 g/L
Biotin	0.05 mg/L
Folic acid	0.5 mg/L
Sucrose	20 g/L
Agargel	4 g/L
Zeatin riboside	2 mg/L
Kanamycin	100 mg/L
Cefotaxime	250 mg/L
pH 6.0 (KOH)	

Rooting media

MS media with vitamins	2.2 g/L
Sucrose	5 g/L
Gelrite	2.25 g/L
IBA	2 mg/L
Kanamycin	100 mg/L
Cefotaxime	250 mg/L
pH 6.0 (KOH)	

Stock antibiotic, hormone and other solutions

Antibiotic	Concentration	Working dilution	Solvent
Gentamycin	100 mg/mL	1:5000	Water
Kanamycin	100 mg/mL	1:1000	Water
Chloramphenicol	37 mg/mL	1:1000	Ethanol
X-gal	20 mg/mL	1:1000	DMSO
IPTG	0.1 mM	1:1000	Water

Ampicillin	100 mg/mL	1:1000	Water
Spectomycin	100 mg/mL	1:1000	Water
Rifampicin	50 mg/mL	1:1000	Methanol
Cefotaxime	250 mg/mL	1:1000	Water
2,4-D	0.5 mg/mL	1:1000	Ethanol
Zeatin riboside	2 mg/mL	1:1000	Water
IBA	4 mg/mL	1:2000	Water

Appendix 4 – Publication

the plant journal

SEB Society for Experimental Biology

The Plant Journal (2018) **96,** 607–619 doi: 10.1111/tpj.14055

The ratio of trichomes to stomata is associated with water use efficiency in *Solanum lycopersicum* (tomato)

Javier Galdon-Armero[1], Mateu Fullana-Pericas[2], Pere A. Mulet[2], Miquel A. Conesa[2], Cathie Martin[1] and Jeroni Galmes[2,*]

[1]*Department of Metabolic Biology, John Innes Centre, Colney Lane, Norwich NR4 7UH, UK, and*

[2]*Research Group on Plant Biology under Mediterranean Conditions – INAGEA, Universitat de les Illes Balears, Carretera de Valldemossa km 7.5, 07122 Palma, Spain*

Received 8 January 2018; revised 3 July 2018; accepted 10 July 2018; published online 1 August 2018.

*For correspondence (e-mail jeroni.galmes@uib.cat).

[The copyright line for this article was changed on 21 December 2018 after original online publication].

SUMMARY

Trichomes are specialised structures that originate from the aerial epidermis of plants, and play key roles in the interaction between the plant and the environment. In this study we investigated the trichome phenotypes of four lines selected from the *Solanum lycopersicum* × *Solanum pennellii* introgression line (IL) population for differences in trichome density, and their impact on plant performance under water-deficit conditions. We performed comparative analyses at morphological and photosynthetic levels of plants grown under well-watered (WW) and also under water-deficit (WD) conditions in the field. Under WD conditions, we observed higher trichome density in ILs 11-3 and 4-1, and lower stomatal size in IL 4-1 compared with plants grown under WW conditions. The intrinsic water use efficiency (WUE_i) was higher under WD conditions in IL 11-3, and the plant-level water use efficiency (WUE_b) was also higher in IL 11-3 and in M82 for WD plants. The ratio of trichomes to stomata (*T*/*S*) was positively correlated with WUE_i and WUE_b, indicating an important role for both trichomes and stomata in drought tolerance in tomato, and offering a promising way to select for improved water use efficiency of major crops.

Keywords: trichomes, stomata, water use efficiency, tomato, introgression lines, drought tolerance.

INTRODUCTION

The epidermis is the outermost tissue of all plant organs and acts as a first contact point with their surroundings. It plays a key role in all plant–environment interactions, and is essential for the maintenance of physiologically favourable conditions (Glover *et al.*, 2016). In the aerial organs of most terrestrial plants, including *Solanum lycopersicum* (tomato), the epidermis is patterned with trichomes, which are epidermal outgrowths with diverse roles in the defence against biotic and abiotic stresses. The epidermis also contains stomata, which are epidermal pores that regulate gas exchange and contribute directly to the control of water status. The cuticle that covers the surface of the epidermis is a hydrophobic layer, consisting of cutin and waxes, that prevents uncontrolled water loss (Riederer and Schreiber, 2001). As a result of their function in limiting water losses, specialised structures in the epidermis are promising targets to improve the drought tolerance and water use efficiency (WUE) of major crops (Antunes *et al.*, 2012; Galmes *et al.*, 2013; Franks *et al.*, 2015).

Trichomes in *Solanum* are multicellular and have been classified into eight different types according to the presence or absence of glandular cells, and the shape and number of cells (Luckwill, 1943; McDowell *et al.*, 2011). Research on trichomes has traditionally focused on understanding the specialised metabolic pathways operating in glandular trichomes (Schilmiller *et al.*, 2008; Kang *et al.*, 2014; Spyropoulou *et al.*, 2014); however, trichomes also play a series of important physiological roles, including tolerance to biotic and abiotic stresses, especially in terms of tolerance to insect attack (Bleeker *et al.*, 2012; Tian *et al.*, 2012) and drought (Hauser, 2014).

A role for trichomes in tolerance and adaptation to water stress has been reported for several species. In *Arabidopsis lyrata*, trichome production has been linked to improved performance under drought conditions (Sletvold and Ågren, 2012). In tomato, SlMX1-overexpressing plants with high trichome density showed a higher tolerance to water stress compared with unmodified plants (Ewas *et al.*, 2016). In *Citrullus lanatus* (watermelon), wild, drought-tolerant genotypes have increased trichome density compared with domesticated, drought-sensitive varieties (Mo *et al.*, 2016). In addition, trichome formation is increased in

plants grown under water stress, such as *Hordeum vulgare* (barley; Liu and Liu, 2016), *Solanum melongena* (aubergine; Fu *et al.*, 2013) and *Olea europaea* (olive; Boughalleb and Hajlaoui, 2011). Trichomes may limit water loss by transpiration through an increase of the leaf–air boundary layer resistance (Palliotti *et al.*, 1994; Guerfel *et al.*, 2009; Mo *et al.*, 2016). Trichomes also protect leaves from UV-related photoinhibition (Savé *et al.*, 2000; Galmés *et al.*, 2007a), either by reflection of UV radiation or absorption by pigmented molecules (Holmes and Keiller, 2002), and prevent leaf overheating (Ehleringer and Mooney, 1978). These findings indicate an important role for trichomes in plant–water relations.

Stomata consist of two specialised guard cells, which modulate their turgor to regulate the pore aperture in response to environmental stimuli, such as light intensity or CO_2 concentration (Hetherington and Woodward, 2003). The effect of stomatal density and size on drought tolerance has been widely studied for many species (Masle *et al.*, 2005; Wentworth *et al.*, 2006; Lawson and Blatt, 2014). Recent studies have shown a link between low stomatal density and improved performance under water-deficit conditions (Farber *et al.*, 2016; Zhao *et al.*, 2017). In addition, evidence exists that plants adjust their stomatal density under water-stress conditions (Galmés *et al.*, 2007b; Hamanishi *et al.*, 2012). Reductions in stomatal density in water-stressed plants have been reported in *Triticum aestivum* (wheat; Li *et al.*, 2017) and *Spondias tuberosa* (the umbu tree; Silva *et al.*, 2009). In contrast, for other species, stomatal density increases under drought conditions, as in *Phaseolus vulgaris* (the common bean; Gan *et al.*, 2010) and *Leymus chinensis* (Xu and Zhou, 2008). These contradictory observations suggest that the effect of water deficit on stomatal density differs between species, and it should be investigated on a case-by-case basis.

Solanum pennellii is a drought-tolerant wild tomato species that originates from the Peruvian deserts (Rick, 1973; Kahn *et al.*, 1993; Peralta *et al.*, 2008), with important differences at the physiological, morphological and molecular levels to the cultivated tomato, *S. lycopersicum*, including increased trichome density (Simmons and Gurr, 2005; Moyle, 2008). The *S. lycopersicum* × *S. pennellii* introgression line (IL) population (Eshed and Zamir, 1995; Zamir, 2001) consists of near-isogenic lines with relatively small fragments of the *S. pennellii* genome in the genetic background of the cultivated tomato, M82. This population has been used successfully before to characterise various aspects of the response of tomato to water stress (Barrios-Masias *et al.*, 2014; Rigano *et al.*, 2016). Therefore, the *S. lycopersicum* × *S. pennellii* IL population provides an excellent platform to investigate the role of differences in epidermal features on performance under water stress.

In this study, we have investigated the effect of differences in trichome density on the response to water stress using several lines from the IL population. We hypothesised that changes in trichome density, introgressed from drought-tolerant *S. pennellii*, would lead to changes in WUE, adding to the current understanding of the relationship between water stress and epidermal features, and building a foundation for improvement of tomato under drought stress. We determined that higher trichome densities result in improved WUE, especially under water-deficit conditions. We also determined the impact of water stress on the phenotype of newly developed tissues to characterise the epidermal responses to drought stress in tomato.

RESULTS

Phenotypic characterisation of tomato lines under glasshouse and field conditions before drought treatment

After a preliminary visual inspection of the 76 lines of the IL population, we chose three ILs (IL 4-1, 10-2 and 11-3) and the parental line M82, for their distinct trichome phenotypes, for further analysis.

We characterised the epidermal features of the three selected ILs (4-1, 10-2 and 11-3) and the parental line M82 in plants grown under full field capacity conditions both in the glasshouse and in the field before the onset of water-deficit conditions (Figure 1). Under glasshouse conditions, ILs 4-1 and 10-2 showed a low trichome density (TD) phenotype, whereas M82 and IL 11-3 showed a high-TD phenotype. Although field-grown plants displayed substantially higher TD than glasshouse-grown plants, IL 4-1 had a lower TD than IL 11-3 and M82, and IL 11-3 had a higher TD than ILs 10-2 and 4-1 (Figure 1a). We also observed differences among lines in their stomatal densities (SD). Under glasshouse conditions, IL 4-1 had a higher SD than M82 and IL 10-2, and M82 had a lower SD than ILs 11-3 and 4-1. In field-grown plants, no significant differences were observed between lines for SD (Figure 1b). Similar to the observations for TD, SD values were generally higher under field conditions. When TD and SD were calculated in terms of area units, we observed identical differences between lines for glasshouse-grown plants, and similar relative values for field-grown plants (Figure S1). We calculated the ratio of trichomes to stomata (*T*/*S*) as an integrative parameter for epidermal anatomy. We observed a substantially higher *T*/*S* in M82 compared with the other lines under glasshouse conditions, whereas in field plants, IL 4-1 showed a lower *T*/*S* than M82 and IL 11-3 (Figure 1c). Stomatal size (SS) showed no significant differences between lines under glasshouse conditions. Under field conditions, however, IL 10-2 had a higher SS than the other lines under study. Unlike the higher values observed for TD and SD in field-grown plants compared with

glasshouse plants, the SS values were within a similar range under both growth conditions (Figure 1d).

We categorised trichomes into different types according to the established classification (Luckwill, 1943; McDowell *et al*., 2011) and measured the length of type-I trichomes in glasshouse-grown plants to determine whether there were differences in other trichome parameters between the ILs (Figure S2). We observed no significant differences in the percentage of different trichome types or trichome length. In general, the analysis of epidermal features and the comparison between glasshouse- and field-grown plants indicated stable genetic components in the determination of trichome density.

Characterisation of photosynthetic parameters under field conditions before drought treatment

We examined whether there were differences in parameters related to gas exchange, carbon fixation and RubisCO kinetics between the lines under study. We observed no significant differences in the net photosynthetic rate (A_N), daily carbon fixation rate (C_{24h}), stomatal conductance (g_s), leaf mesophyll conductance (g_m), leaf total conductance (g_{tot}), maximum RubisCO carboxylation rate (V_{cmax}) or intrinsic water use efficiency (WUE_i) (Table S1), although we observed a trend to lower WUE_i values in IL 4-1 compared with M82 ($P < 0.06$).

Comparative characterization of epidermal features under well-watered (WW) and water-deficit (WD) conditions in the field

In samples collected from lines under WD conditions, IL 4-1 showed a lower TD than the other lines (Figure 2a). Leaves that developed under WD conditions showed a higher TD in ILs 4-1 and 11-3, compared with leaves developed under WW conditions. There were no significant differences for SD between lines under WD conditions (Figure S3). When TD and SD were measured in terms of area unit, we observed a consistently low TD in IL 4-1 compared with ILs 10-2 and 11-3, and there were no differences for SD between lines or treatments (Figure S4). The *T*/*S* ratio was significantly lower in IL 4-1 compared with IL 11-3 (Figure 2b). Although differences in *T*/*S* between WW and WD plants were not significant, there was a trend for higher *T*/*S* under WD for IL 11-3 ($P < 0.1$). In leaves developed under WD conditions, SS showed no significant differences between lines, but IL 4-1 had lower SS in leaves developed under WD conditions compared with leaves developed under WW conditions (Figure 2c). For the rest of the lines, no significant differences were observed when comparing WW and WD conditions. We observed no relationship between TD and SD when all data points were considered together, but we observed an inverse association between TD and SD in WD plants ($R^2 = 0.94$; $P = 0.03$; Figure 2d).

Comparative analysis of morphological parameters and water status under WW and WD conditions in the field

We evaluated the effects of differences in the densities of trichomes on water status of plants under WW and WD conditions in the field. We observed a lower midday leaf water potential (Ψ_{leaf}) in IL 10-2 compared with M82 and IL 11-3 under WW conditions (Table 1). Under WD conditions, IL 11-3 had higher Ψ_{leaf} than IL 10-2. All lines showed a lower Ψ_{leaf} under WD conditions except for IL 11-3, where no difference was observed.

The leaf mass area (LMA) was lower in ILs 4-1 and 11-3 under WD conditions compared with the other lines, but no differences amongst lines under WW conditions or between WW and WD treatments were observed (Table 1). Leaf thickness (LT) was higher in IL 11-3 compared with IL 4-1 under WW conditions, but under WD conditions LT in IL 11-3 was significantly lower than in IL 10-2 (Table 1).

Whole-plant water use efficiency (WUE_b) showed no differences between lines under WW conditions (Table 1). Under WD conditions, WUE_b was lower in IL 4-1 compared with IL 11-3. In M82 and IL 11-3, WUE_b was higher in WD plants compared with WW plants.

Comparative analysis of photosynthetic parameters under WW and WD conditions in the field

The parameters A_N, C_{24h}, g_s, g_m, g_{tot}, V_{cmax} and WUE_i showed no significant differences between lines under WW conditions in the field (Table 2). In contrast, under WD conditions, IL 4-1 had a significantly lower WUE_i than the other lines. IL 11-3 had a significantly higher WUE_i in WD compared with WW conditions (Table 2).

The leaf carbon isotope composition ($\delta^{13}C$) showed no significant differences between lines within each treatment or between treatments for any line; however, leaf $\delta^{13}C$ was correlated with WUE_i ($R^2 = 0.67$, $P = 0.01$; Figure S5a). We also observed a tight positive correlation ($R^2 = 0.66$, $P = 0.01$) between WUE_i and WUE_b (Figure S5b).

Relationships between epidermal features and photosynthetic parameters

We found an inverse correlation between TD and g_s ($R^2 = 0.58$, $P = 0.03$; Figure 3a), and we also observed a positive correlation between SD per unit area and g_s ($R^2 = 0.56$, $P = 0.03$; Figure 3b). Therefore, changes in the density of trichomes and stomata had opposite effects at the gas-exchange level. Importantly, TD was positively correlated with WUE_i ($R^2 = 0.88$, $P = 0.00$; Figure 3c). SD showed no correlation with WUE_i. As expected from the observed relationship between WUE_i and WUE_b (Figure S5b), TD was positively correlated with WUE_b ($R^2 = 0.59$, $P = 0.03$; Figure S6a). Interestingly, SD was negatively correlated with WUE_b ($R^2 = 0.50$, $P < 0.05$; Figure S6b). The correlation between TD and WUE_i and WUE_b

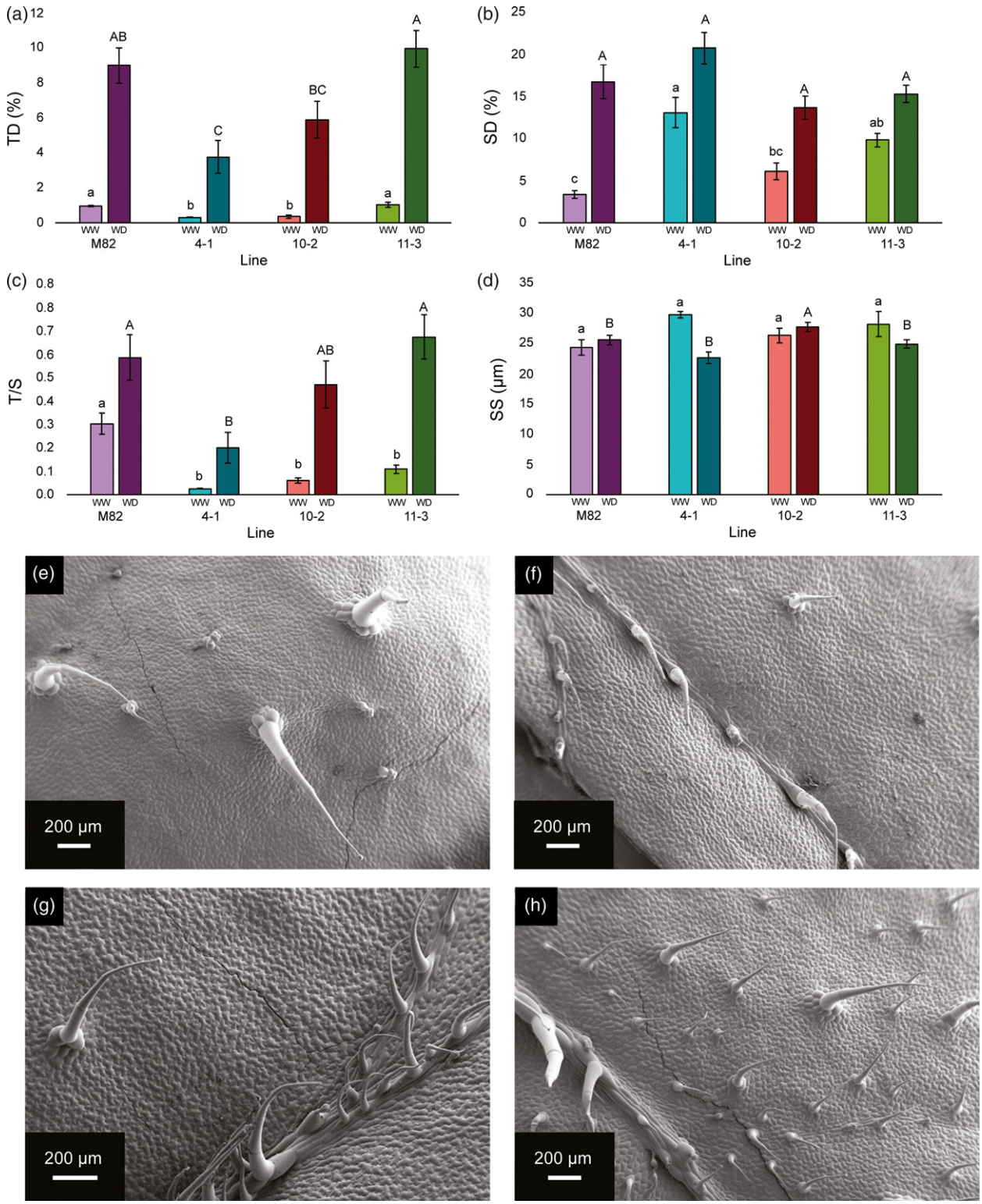

Figure 1. Initial morphological characterization of lines M82, 4-1, 10-2 and 11-3 grown under glasshouse (GH) and field (F) conditions before the onset of drought treatment. (a) Trichome density (TD), (b) stomatal density (SD), (c) trichome-to-stomata ratio (*T*/*S*) and (d) stomatal size (*SS*) are expressed as mean ± SE of between three and six replicates per line and treatment. TD and SD were calculated as a percentage of the total number of epidermal cells. *SS* was calculated as pore length. Different letters denote statistically significant differences by Tukey's analysis ($P < 0.05$) within glasshouse-grown plants (lower case) and field-grown plants (upper case). For panels (a)–(d), purple bars represent M82, turquoise represents 4-1, red represents 10-2 and green represents 11-3, with lighter and darker shades representing GH and F conditions, respectively. Representative scanning electron micrographs for each line: (e) M82, (f) 4-1, (g) 10-2 and (h) 11-3.

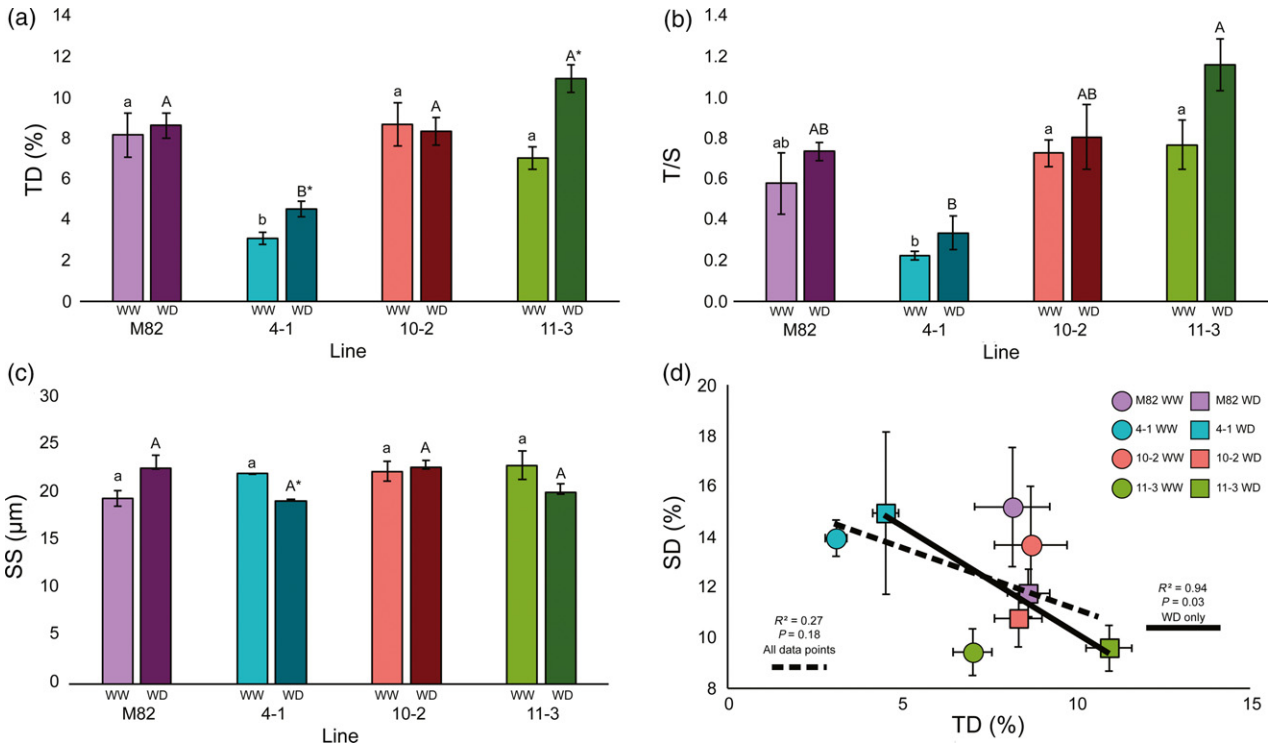

Figure 2. Characterization of epidermal features in lines M82, 4-1, 10-2 and 11-3 under water-deficit (WD) and well-watered (WW) conditions in the field. (a) Trichome density (TD) is expressed as a percentage of the number of trichomes per epidermal cell. (b) Trichome-to-stomata ratio (*T*/*S*) is expressed as the total number of trichomes divided by the total number of stomata in a given area. (c) Stomatal size (*SS*) is expressed as pore length. Different letters denote statistically significant differences identified by Tukey's analysis ($P < 0.05$) within WW plants (lower case) and WD plants (upper case). Asterisks represent significant differences for each line between treatments according to the Tukey's test ($P < 0.05$). (d) A correlation between TD and SD was observed only under WD conditions, according to Pearson's test ($P < 0.05$), with the correlation index shown in the graph. For panels (a)–(c), purple bars represent M82, turquoise represents 4-1, red represents 10-2 and green represents 11-3, with light and dark colours representing WW and WD treatments, respectively. In panel (d), squares represent WD values and circles represent WW values, and are colour coded as in panels (a)–(c). The dashed line represents the regression line for all data points ($P > 0.05$) and the solid line represents the regression line for WD data points ($P = 0.03$). Values are means ± SEs ($n = 3$).

was maintained when TD was expressed per unit area (Figure S7), but this was not the case for the correlation between SD and WUE_b, which was only observed when SD was expressed as a percentage of epidermal cells. Finally, a strong positive association was found between *T*/*S* and WUE_i ($R^2 = 0.86$, $P = 0.00$; Figure 4a) and WUE_b ($R^2 = 0.72$, $P = 0.01$; Figure 4b).

DISCUSSION

The development of leaf trichomes is influenced by water availability

We observed a 10- to 15-fold higher TD in leaves grown under field conditions compared with glasshouse-grown plants (Figures 1a and S1). These differences were likely to have resulted from differences in the age of the plant as well as changes in environmental conditions between the glasshouse and the field. Trichome development is reported to change with the age of the plant (Telfer *et al.*, 1997; Vendemiatti *et al.*, 2017), with higher TD observed in the late leaves of tomato (Gurr and McGrath, 2001). Moreover, environmental factors, such as temperature, photoperiod, light intensity or soil humidity have direct effects on trichome development in several species, including tomato (Wellso and Hoxie, 1982; Gianfagna *et al.*, 1992; Chien and Sussex, 1996; Souza *et al.*, 2016). Despite the dramatic change between environmental conditions in the glasshouse and the field, the relative differences in TD were conserved between lines (Figure 1a), indicating strong genetic control of trichome development in the selected ILs. We observed a 1.5- to 5.0-fold higher SD in field-grown plants (Figure 1b). These differences could also be a function of the age of the plant when leaves were sampled (Ceulemans *et al.*, 1995) as well as the environmental conditions (Beerling and Chaloner, 1993; Rogiers *et al.*, 2011). Unlike the observation for TD, relative differences in SD between lines were not conserved in different environments, pointing to the differential regulation of TD and SD.

We assessed the changes in leaf anatomy in WD plants compared with WW plants. We observed a higher TD in ILs 4-1 and 11-3 under WD conditions compared with WW

Table 1 Morphological and water status characterisation of lines M82, 4-1, 10-2 and 11-3 under well-watered (WW) and water deficit (WD) conditions in the field. Midday leaf water potential (Ψ_{leaf}), leaf mass per area (LMA), leaf thickness (LT) and plant-level water use efficiency (WUE_b) are shown. Values are means ± SE of three to four replicates per line and treatment. Different letters denote statistically significant differences by Tukey analysis ($P < 0.05$) within each treatment between lines, and asteriks denote statistically significant differences ($P < 0.05$) between treatments for each line

	WW				WD			
Acc.	Ψ_{leaf} MPa	LMA g m^{-2}	LT mm	WUE_b g kg^{-1} H_2O	Ψ_{leaf} MPa	LMA g m^{-2}	LT mm	WUE_b g kg^{-1} H_2O
M-82	-0.74 ± 0.04^{a}	79.45 ± 9.56^{a}	0.70 ± 0.05^{ab}	0.76 ± 0.12^{a}	$-1.01 \pm 0.07^{ab*}$	96.01 ± 3.41^{a}	0.76 ± 0.04^{ab}	$1.14 \pm 0.09^{ab*}$
4-1	-0.86 ± 0.06^{ab}	58.12 ± 4.33^{a}	0.63 ± 0.03^{b}	0.74 ± 0.04^{a}	$-1.18 \pm 0.05^{ab*}$	63.83 ± 6.69^{b}	0.66 ± 0.05^{ab}	0.79 ± 0.02^{b}
10-2	-0.99 ± 0.04^{b}	82.37 ± 6.58^{a}	0.69 ± 0.01^{ab}	0.89 ± 0.1^{a}	$-1.21 \pm 0.07^{b*}$	98.65 ± 5.72^{a}	$0.81 \pm 0.02^{a*}$	1.12 ± 0.17^{ab}
11-3	-0.74 ± 0.07^{a}	71.20 ± 9.45^{a}	0.80 ± 0.03^{a}	0.85 ± 0.05^{a}	-0.93 ± 0.08^{a}	64.18 ± 6.35^{b}	$0.63 \pm 0.03^{b*}$	$1.36 \pm 0.06^{a*}$

Table 2 Photosynthetic characterization of lines M82, 4-1, 10-2 and 11-3 under well-watered (WW) and water deficit (WD) conditions in the field. Net photosynthetic rate (A_N), daily carbon fixation rate (C_{24h}), stomatal conductance (g_s), mesophyll conductance (g_m), total leaf conductannce (g_{tot}), maximum velocity of Rubisco carboxylation (V_{cmax}) and intrinsic water use efficiency (WUE_i) are shown. Values are means ± standard error of four replicates per line and treatment. Different letters denote statistically significant differences by Tukey analysis ($P < 0.05$) within each treatment between lines, and asteriks denote statistically significant differences ($P < 0.05$) between treatments for each line

Acc.	A_N μmol CO_2 m^{-2} sec^{-1}	C_{24h} mol m^{-2} day^{-1}	g_s mol H_2O m^{-2} sec^{-1}	g_m mol CO_2 m^{-2} sec^{-1}	g_{tot} mol CO2 m^{-2} sec^{-1}	V_{cmax} μmol CO2 m^{-2} sec^{-1}	WUE_i μmol CO_2 mol^{-1} H_2O
WW							
M-82	13.22 ± 1.16^{a}	0.34 ± 0.03^{a}	0.222 ± 0.046^{a}	0.087 ± 0.015^{a}	0.049 ± 0.006^{a}	304.05 ± 57.19^{a}	66.22 ± 11.52^{a}
4-1	15.31 ± 1.35^{a}	0.34 ± 0.08^{a}	0.272 ± 0.027^{a}	0.088 ± 0.004^{a}	0.058 ± 0.003^{a}	349.38 ± 107.21^{a}	57.09 ± 4.68^{a}
10-2	16.87 ± 1.26^{a}	0.42 ± 0.04^{a}	0.229 ± 0.026^{a}	0.123 ± 0.015^{a}	0.063 ± 0.004^{a}	335.96 ± 49.79^{a}	75.88 ± 7.33^{a}
11-3	15.82 ± 1.43^{a}	0.44 ± 0.05^{a}	0.243 ± 0.026^{a}	0.102 ± 0.017^{a}	0.061 ± 0.010^{a}	336.77 ± 38.46^{a}	65.60 ± 2.11^{a}
WD							
M-82	11.52 ± 0.80^{a}	0.31 ± 0.04^{a}	0.165 ± 0.021^{a}	0.084 ± 0.010^{a}	0.046 ± 0.005^{a}	271.97 ± 22.89^{a}	71.44 ± 4.26^{ab}
4-1	12.53 ± 0.80^{a}	0.30 ± 0.03^{a}	0.233 ± 0.009^{a}	0.083 ± 0.016^{a}	0.052 ± 0.006^{a}	217.25 ± 26.34^{a}	53.74 ± 2.76^{b}
10-2	13.20 ± 1.59^{a}	0.38 ± 0.03^{a}	0.184 ± 0.014^{a}	0.101 ± 0.018^{a}	0.052 ± 0.006^{a}	253.63 ± 49.58^{a}	71.60 ± 5.29^{ab}
11-3	15.57 ± 2.38^{a}	0.39 ± 0.03^{a}	0.187 ± 0.034^{a}	0.143 ± 0.044^{a}	0.061 ± 0.013^{a}	321.88 ± 52.84^{a}	$84.52 \pm 6.92^{a*}$

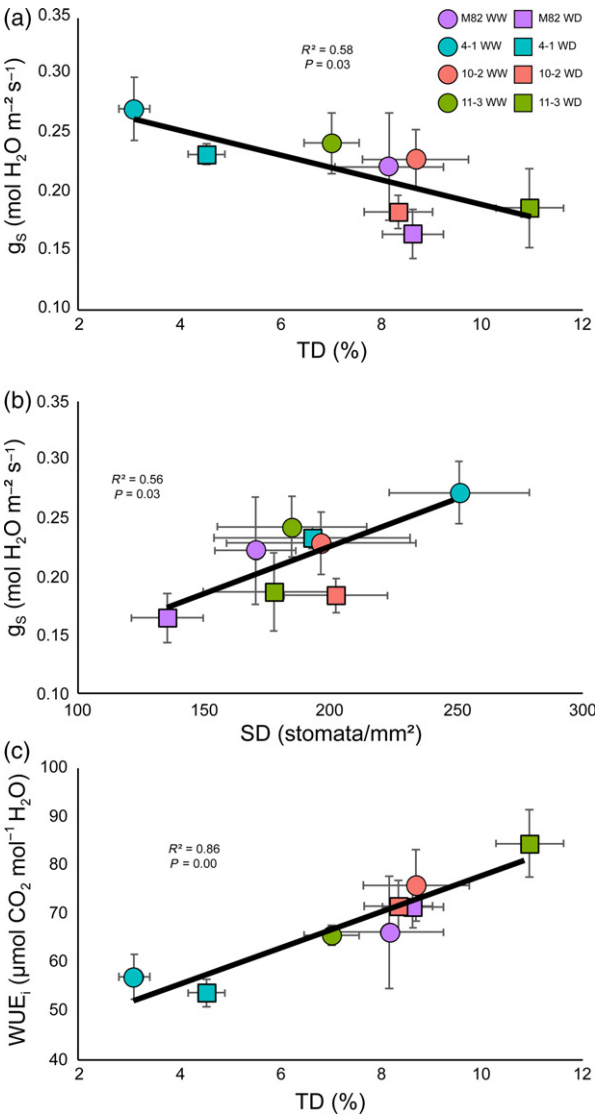

Figure 3. Relationships between trichome and stomatal densities and photosynthetic parameters in lines M82, 4-1, 10-2 and 11-3: (a) inverse correlation between trichome density and stomatal conductance (g_s); (b) positive association between stomatal density and stomatal conductance (g_s); and (c) positive association between trichome density and intrinsic water use efficiency (WUE_i). Correlation coefficients and *P* values calculated by Pearson's test are displayed in each graph. Purple markers represent M82, turquoise markers represent 4-1, red markers represent 10-2 and green markers represent 11-3. Circles represent values under well-watered (WW) conditions in the field and squares represent values under water-deficit (WD) conditions in the field. Values are means ± SEs (n = 3–4).

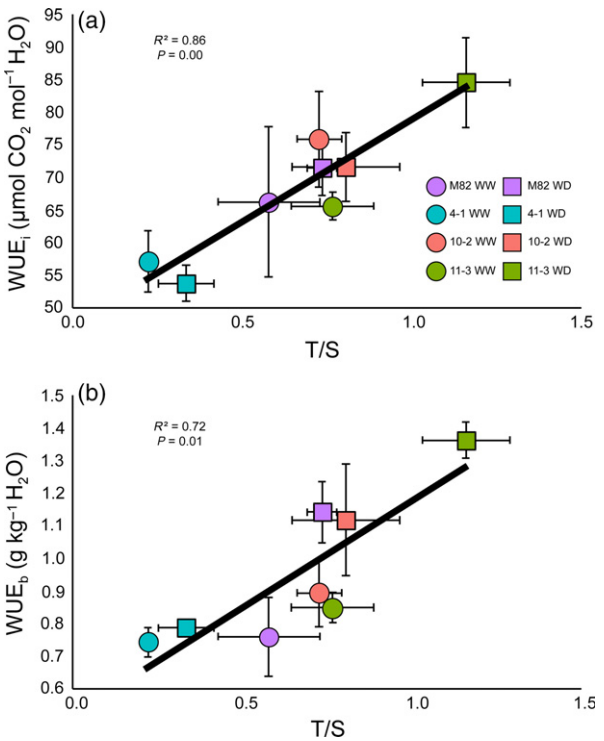

Figure 4. Relationship between trichome/stomata ratios and photosynthetic parameters in lines M82, 4-1, 10-2, and 11-3: (a) correlation between trichome/stomata ratio (*T*/*S*) and intrinsic water use efficiency (WUE_i); and (b) correlation between *T*/*S* and plant-level water use efficiency (WUE_b). Correlation coefficients, calculated by Pearson's test ($P < 0.001$ for a; $P < 0.01$ for b), are shown in each graph. Purple markers represent M82, turquoise markers represent 4-1, red markers represent 10-2 and green markers represent 11-3. Circles represent values from well-watered (WW) conditions in the field and squares represent values from water-deficit (WD) conditions in the field. Values are means ± SEs (n = 3–4).

conditions (Figure 2a). Increases in TD with herbivore and water stress have been reported previously in several species (Traw and Bergelson, 2003; Bjorkman *et al.*, 2008; Fu *et al.*, 2013), as part of the adaptive stress response. In fact, transcriptomic studies in water-stressed *Arabidopsis thaliana* plants showed an upregulation of genes related to trichome initiation and morphogenesis (TT8, BRICK1, KAK), but not of genes involved in stomatal initiation (Bechtold *et al.*, 2016). Not all the lines in this study showed uniform responses, with IL 4-1 showing bigger changes upon WD treatment (lower SS, higher TD) (Figure 2). This could be explained by a greater inability of IL 4-1 to control water loss, as indicated by its lower WUE_b and WUE_i (Tables 1 and 2), leading to more severe physiological stress in this line and, subsequently, a stronger response to WD. In any case, these leaf adaptive changes did not account for an increase in WUE (Tables 1 and 2), probably because of a lower overall TD in IL 4-1.

We observed an inverse association between trichome density (TD) and stomatal density (SD) only under WD conditions (Figure 2d), in agreement with previous reports in *Nicotiana tabacum* (tobacco) and tomato (Glover *et al.*, 1998; Glover, 2000). Developmentally, trichomes and stomata originate from protodermal cells (Morohashi and Grotewold, 2009; Pillitteri and Dong, 2013), and the inverse association observed suggests that the regulation of their development might be linked. Similar relationships have been found in trichome mutants of *A. thaliana* (Bean *et al.*, 2002), where altered trichome phenotypes affected

stomatal patterning. In aubergine, increases in TD have been associated with increases in SD (Fu *et al.*, 2013), in contrast to our observations, indicating that there may be different developmental associations even between related *Solanum* species. The correlation was not observed when TD and SD per area were used, suggesting that TD and SD as percentage of epidermal cells might give a better representation of the developmental changes in the epidermis. The fact that TD and SD were not correlated when both WW and WD plants were considered (Figure 2d) might be a result of the lack of genetic differences in SD, as only TD was clearly different between the assessed lines (Figures 1b and S1b). However, the observed TD–SD association suggests that the developmental response of the leaf to drought stress involves changes in the determination of cell fate in the whole epidermal tissue, simultaneously affecting TD and SD, and this might occur through different regulatory mechanisms under different water regimes. In conclusion, we observed an important effect of water availability on leaf anatomy and the determination of epidermal features.

Variation amongst the ILs and the potential for developing drought-tolerant varieties

The highly inbred tomato cultivar M82 has traditionally been used as a check variety in breeding programmes (Grandillo *et al.*, 1999) and as a reference cultivar for scientific research, used in relation to the response to water stress as a drought-sensitive cultivar (Iovieno *et al.*, 2016), in contrast with the drought-tolerant *S. pennellii* (Egea *et al.*, 2018). The IL population has been used extensively for functional and physiological studies (Steinhauser *et al.*, 2011; Chitwood *et al.*, 2013; de Oliveira Silva *et al.*, 2018), and the natural variation within the IL population provides an excellent platform to investigate the role of differences in epidermal features on performance under water stress.

The intrinsic water use efficiency (WUE_i) is an important target for crop improvement with respect to drought tolerance, although it needs to be considered carefully as it might not be directly related to improved fruit productivity (Blum, 2005, 2009). We observed a lower WUE_i for IL 4-1 under WD conditions compared with the other lines under study (Table 2), whereas WUE_i in IL 11-3 was higher under WD compared with WW conditions (Table 2). This increase in WUE_i has been reported in drought-tolerant varieties in several crops (Guha *et al.*, 2010; Fracasso *et al.*, 2016; Liu *et al.*, 2016), although it might not always have a positive effect on fruit yield. Interestingly, none of the ILs under study were considered before for WUE improvement as they showed no differences in $\delta^{13}C$ compared with M82 (Xu *et al.*, 2008), in agreement with our results, so this epidermis-based analysis provides an alternative path for increased WUE. Therefore, the genomic region introgressed from *S. pennellii* in IL 11-3 could be selected to generate more water use efficient tomato cultivars.

The accuracy of WUE_i as a measure of drought tolerance has been questioned because of the lack of correlation with whole-plant measurements of WUE (Medrano *et al.*, 2015). In fact, in newer tomato cultivars, a decrease in WUE_i, driven by selection under high light levels and well-watered conditions, has been reported to be accompanied by increases in agronomic WUE (yield per water used; Barrios-Masias and Jackson, 2014). Therefore, biomass-based parameters, specifically plant-level water use efficiency (WUE_b), were also investigated in this study, although specific differences in fruit production or harvest index between ILs were not considered (Caruso *et al.*, 2016). WUE_b under WD was lower in IL 4-1 than in IL 11-3 (Table 1). Moreover, M82 and IL 11-3 plants grown under WD conditions had higher WUE_b values compared with WW plants (Table 1). The observed WUE_i–WUE_b correlation (Figure S5b) supports the use of WUE_i as a measure of drought tolerance under our experimental conditions. In a similar way, leaf $\delta^{13}C$ has been used as a marker of the WUE of a plant (Farquhar and Richards, 1984), and in tomato and *S. pennellii* it has been reported to correlate with WUE_b (Martin and Thorstenson, 1988). In this work, we found a correlation between leaf $\delta^{13}C$ and WUE_i (Figure S5a), suggesting that leaf $\delta^{13}C$ can be used as a tool for selection of high-WUE_i lines in tomato. We did not observe a significant correlation between leaf $\delta^{13}C$ and WUE_b, however, which might hinder the applicability of our findings.

The role of epidermal features during WD

Water-stress responses involve changes in leaf anatomy, including changes in the leaf thickness affecting CO_2 diffusion (Niinemets *et al.*, 2009; Galmes *et al.*, 2013) and epidermal features, where there has been a focus on the stomata because of their direct role in gas exchange and transpiration (Galmés *et al.*, 2007a; Xu and Zhou, 2008). Although we observed differences in LT in ILs 4-1 and 11-3 when WW and WD plants were compared (Table 1), no correlation was found between LT and any gas exchange parameter. Importantly, we observed a significant, inverse correlation between g_s and SD per area (Figure 3), but not between g_s and SD as a percentage of epidermal cells. This result suggests that SD per area should be used preferentially when assessing gas exchange parameters.

Our findings also support a major role for trichomes in gas exchange and the determination of WUE, however. The correlation observed between TD and WUE_i and WUE_b (Figures 3b, S6a and S7) suggests that TD has a positive effect in terms of drought tolerance. The lack of differences in trichome types or trichome length in the lines under study (Figure S2) indicates that the observed effects are linked to TD rather than to other trichome parameters. Several roles

have been suggested for trichomes in plant drought tolerance (Galmés *et al.*, 2007a; Boughalleb and Hajlaoui, 2011). On the basis that TD is negatively associated with g_s (Figure 3a), our data suggest that trichomes in tomato might play a role in avoiding excessive water loss by changing the resistance of the boundary layer, as proposed in previous studies (Guerfel *et al.*, 2009; Mo *et al.*, 2016). Another possible explanation for the correlation between TD and WUE involves the mutually exclusive developmental association between trichomes and stomata. Increased trichome initiation as part of the response to drought (a possibility supported by expression analysis in Arabidopsis; Bechtold *et al.*, 2016), could lead to lower SD that could lead to an improved WUE. Genes involved in ABA signalling, known to play a role in the drought response, are expressed in trichomes (Ren *et al.*, 2010; Daszkowska-Golec, 2016). For example, the tomato homologue of the WRKY transcription factor ABA OVERSENSITIVE 3 (AtABO3) (Ren *et al.*, 2010) or the bZIP transcription factor ABRE BINDING FACTOR 1 (AtABF1) (Yoshida *et al.*, 2015) are both expressed in trichomes in tomato according to the available RNAseq data (Spyropoulou *et al.*, 2014). Changes in TD could lead to changes in the transcript abundance of these or other ABA-related factors. In fact, the expression level of SlABO3 is slightly higher in leaves of IL 11-3 compared with leaves of ILs 4-1 and 10-2 according to the available RNAseq data (Chitwood *et al.*, 2013), and SlABF1 is located in the genomic region introgressed from *S. pennellii* in IL 11-3, indicating a possible role for trichome-expressed ABA-related genes in the observed drought response.

Whole-plant water use efficiency (WUE_b) was also correlated with SD (Figure S6b), although the impact of SD on WUE was lower than that of TD, because there was no correlation between WUE_i and SD at the leaf level, and when correlation coefficients for TD–WUE_b and SD–WUE_b were compared, the effect of SD on WUE_b was lower than that of TD (Figures 3 and S6). The fact that both stomata and trichomes were involved in the drought response was not surprising, given the developmental link that we observed under WD conditions (Figure 2d) and the direct role of stomata in gas exchange (Figure 3b). In fact, the ratio of trichomes to stomata (*T*/*S*), which gives information about the relationship between both structures, showed a strong correlation with both WUE_i and WUE_b (Figure 4). In addition to this, *T*/*S* is unitless and is not expressed either in terms of leaf area or percentage of epidermal cells, thereby overcoming the differences observed in correlations between developmental and photosynthetic traits. It is interesting to note that *T*/*S* becomes a more prominent parameter under WD conditions, when both TD and SD change together (Figure 2d), whereas under WW conditions, when there is no correlation between them (Figure 2d) or significant changes between lines (Figure S4), the genotype-specific TD is likely to be the main player in the relation between epidermis and WUE. In conclusion, *T*/*S* plays an important role in the efficiency by which water is used by tomato, and differences in *T*/*S* could be used to develop more drought-tolerant tomato varieties.

EXPERIMENTAL PROCEDURES

Preliminary characterization of epidermal cells

From a visual inspection of 76 *S. lycopersicum* cv. M82 × *S. pennellii* ac. LA716 ILs (Eshed and Zamir, 1995), grown under glasshouse conditions, we selected four lines (ILs 4-1, 10-2 and 11-3, and M82) displaying a clear visual trichome phenotype. IL 4-1 (LA4048) had an apparent lower trichome density (TD) than the parental line M82, IL 10-2 (LA4089) had a hairless-like phenotype, and IL 11-3 (LA4092) had an apparently higher TD compared with the parental line M82 (LA3475). We characterised the trichome densities of the adaxial and abaxial sides of leaves from the four lines under study. This analysis indicated similar values for TD on both sides of the leaf in all four lines and a strong correlation ($R^2 = 0.92$, $P = 0.04$) between the values on both sides of the leaf (Figure S8), which allowed us to work with values on the adaxial surface in all future investigations.

The epidermal features of these four lines were characterised further using scanning electron microscopy (SEM) of plants grown both under glasshouse and field conditions. For glasshouse assays, three or four plants per line were grown under water field capacity at the John Innes Centre (https://www.jic.ac.uk), using natural light with an average temperature of between 20 and 22°C. The terminal leaflet of the first leaf of 4-week-old plants was excised, and inter-vein sections of approximately 0.5 × 0.5 cm were taken as samples. These sections were vacuum-fixed in a glutaraldehyde 2.5% cacodylate solution and dehydrated through an ethanol series. Samples were dried in a Leica CPD300 critical-point dryer (Leica Microsystems, http://www.leica.com), to avoid the collapse of trichomes, and were gold-coated before imaging in a Zeiss Supra 55 VP SEM (Zeiss, https://www.zeiss.com) at 20°C and under high-vacuum conditions, generating between eight and 15 micrographs of approximately 0.3 mm^2 per sample of the adaxial surface.

Characterisation under field conditions was carried out in the experimental plot at the University of the Balearic Islands (UIB, http://www.uib.eu). The environmental conditions during plant growth are detailed in the next section. Six plants were sampled for each line under study. Terminal leaflets of fully expanded leaves at the same position were excised and sections of 0.5 × 0.5 cm were taken as samples. The adaxial surface of these sections was imaged at 20°C, without coating, inside a Hitachi 3400N variable pressure SEM (Hitachi High-Tecnhology, https://www.hitachi-hightech.com). We generated between eight and 10 micrographs of approximately 0.3 mm^2 per sample, and trichomes, stomata and pavement cells were counted manually. In both analyses, trichome and stomatal densities were expressed both as a percentage of epidermal cells and as density per area. Trichomes were classified in types and had their length measured. For trichome density, all types of trichome were considered together. The ratio of trichomes to stomata was calculated as trichome density divided by stomatal density.

Field growth conditions and drought treatment

Seeds from the four lines were germinated and grown for 4 weeks in glasshouses at the University of the Balearic Islands (UIB) with natural light and average maximum temperatures of 25°C in

March–April 2016. Twelve plants per line were placed outdoors in the UIB experimental field for acclimation for 2 weeks before being transferred to 50-L pots containing a mixture of bog peat-based horticultural substrate (Prohumin-Potting Soil Klasmann-Deilmann; Projar, https://www.projar.es) and perlite (granulometry A13; Projar) in a 4 : 1 proportion (v/v). The environmental conditions from June to September 2016 were those typical for a Mediterranean summer: with average daily temperatures of 22.8 ± 0.3, 25.7 ± 0.3, 25.0 ± 0.2 and 22.7 ± 0.4°C; average daily minimum temperatures of 16.5 ± 0.5, 20.3 ± 0.3, 19.5 ± 0.4 and 17.8 ± 0.4°C; and average daily maximum temperatures of 31.1 ± 0.4, 35.5 ± 0.4, 33.5 ± 0.3 and 34.7 ± 0.6°C, respectively, for June, July, August and September. Plants were watered to field capacity every other day and fertilised weekly with 50% Hoagland's solution for 2 months before beginning the drought treatment.

From 11 July, plants were subjected to two different water regimes: WW and WD. Watering regimes and plant water consumption were monitored by weighing and watering the potted plants every 2 days. For the WW treatment, four plants per line were maintained at field capacity, with a pot water content ranging between 100% field capacity just after irrigation (corresponding to 9.3 L of water per pot) and 69.3 ± 0.1% field capacity (on average throughout the treatment period) (Figure S9). For the WD treatment, the irrigation of four plants was progressively reduced until halving the pot water content compared with the WW plants. Then, WD plants were maintained at a pot water content ranging between 30.3 ± 0.1% field capacity before irrigation and 46.3 ± 0.1% field capacity after irrigation (Figure S9). The four remaining plants per line were used for biomass-related measurements. The total water supplied and dry biomass of each plant was recorded upon experiment completion (Table S2). Three weeks were allowed from treatment application for the development of new leaves under the new water regime before any measurement was performed.

All leaf-based measurements and samples were taken from the terminal leaflets of the youngest fully expanded leaves generated after application of the treatment. Epidermal features (trichome and stomatal densities, stomatal size and ratio of trichomes to stomata) were evaluated as described for glasshouse-grown plants in the 'Preliminary characterization of plant material' section.

Plant water status and growth-related measurements

Plant water status was measured as midday leaf water potential (Ψ_{leaf}) (n = 4 per line and treatment) using a Scholander pressure chamber (Soilmoisture Equipment Corp., https://www.soilmoisture.com), as described by Turner (1988).

For the calculation of WUE_b, four plants per line were harvested at the time of drought treatment. Seventy-four days after treatment application, four plants per line and per treatment (WW and WD) were harvested. Leaves, shoots and roots were oven-dried separately at 60°C and weighed (dry weight, DW). Biomass production during the drought treatment was calculated as the difference between the DW of the plants harvested at the end of the experiment (DW_{final}) and the *DW* of the plants harvested before the treatment ($DW_{initial}$). Water consumption was monitored every other day by weighing the pots containing the plants, and the total water consumption (TWC) of each plant was estimated from these values. WUE_b was calculated as follows: $WUE_b = (DW_{final} - DW_{initial})/TWC$.

Leaf morphological determinations

Leaf thickness (LT) was determined for the middle part of the terminal leaflet of a young fully-expanded leaf with callipers, avoiding regions of the leaf with major veins. Leaf mass area (LMA) was calculated from the same terminal leaflets, as the dry mass to leaf area ratio. Dry mass was measured by weighing after oven-drying leaves at 60°C for 48 h. The leaf area was digitally measured from pictures of the leaves using IMAGEJ 1.49 (National Institutes of Health, https://imagej.nih.gov/ij/) before drying. Both LT and LMA were measured for one leaf per plant (n = 4 per line and treatment).

Leaf gas exchange and chlorophyll *a* fluorescence

Measurements were performed with an open infrared gas-exchange analyser equipped with a leaf chamber fluorometer (Li-6400-40; LI-COR, https://www.licor.com) from 09:00 to 12:00 h and from 16:00 to 19:00 h in the first 2 weeks of August 2016. Preliminary tests confirmed non-significant differences between morning and afternoon measurements. The conditions in the chamber consisted of leaf temperatures of 31–33°C, a vapour pressure deficit of 2.0–3.0 kPa and an air flow of 500 μmol (air) min^{-1}. For net CO_2 assimilation rate–substomatal CO_2 concentration (A_N–C_i) curves, the ambient concentration of CO_2 in the chamber (C_a) was set at 400, 0, 50, 100, 200, 300, 600, 900, 1500, 2000 and 400 μmol CO_2 mol^{-1} air, at a saturating photosynthetic photon flux density (PPFD) of 1500 μmol m^{-2} sec^{-1} (with 10% blue light), allowing 4 min between measurements for the chamber to reach a steady state. Corrections for CO_2 leakage in and out of the leaf chamber of the Li-6400-40 were applied to all gas-exchange data, as described by Flexas *et al.* (2007).

Mesophyll conductance to CO_2 (g_m) was estimated according to (Harley *et al.*, 1992) as:

$$g_m = A_N/C_i - (\Gamma^*[\mathrm{ETR} + 8(A_N + R_L)]/[\mathrm{ETR} - 4(A_N + R_L)]),$$

where Γ^* is the chloroplast CO_2 compensation point in the absence of day respiration, ETR is the electron transport rate and R_L is the rate of non-photorespiratory CO_2 evolution under light. ETR and R_L were calculated as described by Galmes *et al.* (2011). Γ^* was retrieved from *in vitro*-based measurements for *S. lycopersicum* by Hermida-Carrera *et al.* (2016), but adjusted for the leaf temperature during the measurement.

Total leaf conductance (g_{tot}) was calculated assuming the stomatal conductance (g_s) and mesophyll conductance (g_m) were in series, such that: $g_{tot} = 1/(1/g_s + 1/g_m)$.

A_N–C_i curves were transformed into A_N-chloroplastic CO_2 concentration (C_c) curves using estimated values of g_m. From A_N–C_C curves, the maximum velocity of Rubisco carboxylation (V_{cmax}) was calculated as described by (Bernacchi *et al.*, 2002), but using specific values of Rubisco kinetics for *S. lycopersicum* adjusted to the leaf temperature during the measurement (Hermida-Carrera *et al.*, 2016). The intrinsic water use efficiency (WUE_i) was calculated as the ratio between the net photosynthetic rate (A_N) and the stomatal conductance (g_s), A_N/g_s.

We determined the daily carbon fixation rate (C_{24h}) by measuring the net CO_2 exchange rate at 2-h intervals over 24 h. These measurements were performed after drought treatment (n = 4 per line and per treatment) using an open infrared gas-exchange analyser equipped with a clear chamber (Li-6400-40; LI-COR). Three measurements were performed under ambient CO_2 and light levels, averaged per plant and per time point. The daily fixation rate was calculated as the integral value for the curve generated by the point measurements.

Leaf $\delta^{13}C$ isotope composition

The dried leaves used to calculate *LMA* were ground to fine dust for the determination of carbon isotopic composition. Samples

were subjected to combustion in an elemental analyser (Thermo Flash EA 1112 Series; ThermoFisher Scientific, http://www.thermofisher.com) and CO_2 was injected into a continuous-flow isotope ratio mass spectrometer (Thermo-Finnigan Delta XP; ThermoFisher Scientific). Peach leaf standards (NIST 1547) were run every six samples. The standard deviation of the analysis was <0.2%.

Statistical analysis

The differences between lines, treatments and interactions were assessed by univariate analysis of variance (ANOVA). Significant differences between means were determined by a post-hoc Tukey's test ($P < 0.05$). The relationship between variables in each experiment was determined by correlation coefficient (R^2). The analyses were performed using R 3.2.2 (R Core Team, https://www.r-project.org).

ACKNOWLEDGEMENTS

We thank Kim Findlay, Elaine Barclay and Ferran Hierro for the technical support in SEM image acquisition. We are grateful to Cyril Douthe for LI-COR technical assistance. This article benefitted from insightful discussions with Prof. James Brown (JIC). We appreciate the financial support of the Rotation Studentship from the John Innes Foundation, the Institute Strategic Program Understanding and Exploiting Plant and Microbial Secondary Metabolism (BB/J004596/1) from the UK Biotechnology and Biological Sciences Research Council (BBSRC) to JIC, as well as the project AGL2013–42364R (Plan Nacional, Spain) awarded to Dr Galmés and the European funded COST ACTION FA1106 QualityFruit. We are grateful to Mr Miquel Truyols and collaborators of the UIB Experimental Field and Glasshouses (UIB Grant 15/2015) for their support of our experiments.

CONFLICT OF INTEREST

The authors declare no conflicts of interest.

SUPPORTING INFORMATION

Additional Supporting Information may be found online in the Supporting Information section at the end of the article.

Figure S1. Initial morphological characterization of lines M82, 4-1, 10-2 and 11-3 grown under glasshouse (GH) and field conditions (F) before the onset of drought treatment.

Figure S2. Percentage of trichome types and trichome length in plants grown under glasshouse conditions.

Figure S3. Stomatal density in lines M82, 4-1, 10-2 and 11-3 under water-deficit (WD) and well-watered (WW) conditions in the field.

Figure S4. Trichome and stomatal densities in lines M82, 4-1, 10-2 and 11-3 under water-deficit (WD) and well-watered (WW) conditions in the field, expressed in terms of area.

Figure S5. Correlations between carbon isotope composition and intrinsic water use efficiency, and between intrinsic water use efficiency and plant-level water use efficiency, in lines M82, 4-1, 10-2 and 11-3.

Figure S6. Relationship between epidermal features and plant-level water use efficiency (WUE_b) in plants under well-watered (WW) and water-deficit (WD) conditions in the field.

Figure S7. Correlations between trichome density expressed per unit area and water use in lines M82, 4-1, 10-2 and 11-3 under WW and WD conditions.

Figure S8. Trichome densities on abaxial and adaxial sides of leaves of lines M82, 4-1, 10-2 and 11-3 grown under glasshouse conditions.

Figure S9. Evolution of the pot water content during the experiment for the well-watered (WW, blue) and water-deficit (WD, red) plants.

Table S1. Leaf morphological traits and photosynthetic characterization of the lines M82, 4-1, 10-2 and 11-3 under field conditions before the onset of the drought treatment.

Table S2. Dry biomass and total water supplied to plants upon completion of the experiment for lines M82, 4-1, 10-2 and 11-3.

REFERENCES

Antunes, W.C., Provart, N.J., Williams, T.C.R. and Loureiro, M.E. (2012) Changes in stomatal function and water use efficiency in potato plants with altered sucrolytic activity. *Plant Cell Environ.* **35**, 747–759.

Barrios-Masias, F.H. and Jackson, L.E. (2014) California processing tomatoes: morphological, physiological and phenological traits associated with crop improvement during the last 80 years. *Eur. J. Agron.* **53**, 45–55.

Barrios-Masias, F.H., Chetelat, R.T., Grulke, N.E. and Jackson, L.E. (2014) Use of introgression lines to determine the ecophysiological basis for changes in water use efficiency and yield in California fprocessing tomatoes. *Funct. Plant Biol.* **41**, 119–132.

Bean, G.J., Marks, M.D., Hülskamp, M., Clayton, M. and Croxdale, J.L. (2002) Tissue patterning of *Arabidopsis* cotyledons. *New Phytol.* **153**, 461–467.

Bechtold, U., Penfold, C.A., Jenkins, D.J., *et al.* (2016) Time-series transcriptomics reveals that AGAMOUS-LIKE22 affects primary metabolism and developmental processes in drought-stressed *Arabidopsis*. *Plant Cell*, **28**, 345–366.

Beerling, D.J. and Chaloner, W.G. (1993) The impact of atmospheric CO_2 and temperature changes on stomatal density: observation from *Quercus robur* lammas leaves. *Ann. Bot.* **71**, 231–235.

Bernacchi, C.J., Portis, A.R., Nakano, H., von Caemmerer, S. and Long, S.P. (2002) Temperature response of mesophyll conductance. Implications for the determination of rubisco enzyme kinetics and for limitations to photosynthesis *in vivo*. *Plant Physiol.* **130**, 1992–1998.

Bjorkman, C., Dalin, P. and Ahrne, K. (2008) Leaf trichome responses to herbivory in willows: induction, relaxation and costs. *New Phytol.* **179**, 176–184.

Bleeker, P.M., Mirabella, R., Diergaarde, P.J., VanDoorn, A., Tissier, A., Kant, M.R., Prins, M., de Vos, M., Haring, M.A. and Schuurink, R.C. (2012) Improved herbivore resistance in cultivated tomato with the sesquiterpene biosynthetic pathway from a wild relative. *Proc. Natl Acad. Sci. USA*, **109**, 20124–20129.

Blum, A. (2005) Drought resistance, water-use efficiency, and yield potential - are they compatible, dissonant, or mutually exclusive? *Aust. J. Agric. Res.* **56**, 1159–1168.

Blum, A. (2009) Effective use of water (EUW) and not water-use efficiency (WUE) is the target of crop yield improvement under drought stress. *Field. Crop. Res.* **112**, 119–123.

Boughalleb, F. and Hajlaoui, H. (2011) Physiological and anatomical changes induced by drought in two olive cultivars (*cv Zalmati and Chemlali*). *Acta Physiol. Plant.* **33**, 53–65.

Caruso, G., Gomez, L.D., Ferriello, F., *et al.* (2016) Exploring tomato *Solanum pennellii* introgression lines for residual biomass and enzymatic digestibility traits. *BMC Genet.* **17**, 56.

Ceulemans, R., Van Praet, L. and Jiang, X.N. (1995) Effects of CO_2 enrichment, leaf position and clone on stomatal index and epidermal cell density in poplar (*Populus*). *New Phytol.* **131**, 99–107.

Chien, J.C. and Sussex, I.M. (1996) Differential regulation of trichome formation on the adaxial and abaxial leaf surfaces by Gibberellins and photoperiod in *Arabidopsis thaliana (L) Heynh*. *Plant Physiol.* **111**, 1321–1328.

Chitwood, D.H., Kumar, R., Headland, L.R., *et al.* (2013) A quantitative genetic basis for leaf morphology in a set of precisely defined tomato introgression lines. *Plant Cell*, **25**, 2465–2481.

Daszkowska-Golec, A. (2016) The role of abscisic acid in drought stress: how ABA helps plants to cope with drought stress. In: *Drought Stress Tolerance in Plants, Vol 2: Molecular and Genetic Perspectives* (Hossain, M.A., Wani, S.H., Bhattacharjee, S., Burritt, D.J. and Tran, L.-S.P., eds). Cham: Springer International Publishing, pp. 123–151.

Egea, I., Albaladejo, I., Meco, V., Morales, B., Sevilla, A., Bolarin, M.C. and Flores, F.B. (2018) The drought-tolerant *Solanum pennellii* regulates leaf

water loss and induces genes involved in amino acid and ethylene/jasmonate metabolism under dehydration. *Sci. Rep.* **8**, 2791.

Ehleringer, J.R. and Mooney, H.A. (1978) Leaf hairs: effects on physiological activity and adaptive value to a desert shrub. *Oecologia*, **37**, 183–200.

Eshed, Y. and Zamir, D. (1995) An introgression line population of *Lycopersicon pennellii* in the cultivated tomato enables the identification and fine mapping of yield-associated QTL. *Genetics*, **141**, 1147–1162.

Ewas, M., Gao, Y.Q., Wang, S.C., *et al.* (2016) Manipulation of SIMXI for enhanced carotenoids accumulation and drought resistance in tomato. *Sci. Bull.* **61**, 1413–1418.

Farber, M., Attia, Z. and Weiss, D. (2016) Cytokinin activity increases stomatal density and transpiration rate in tomato. *J. Exp. Bot.* **67**, 6351–6362.

Farquhar, G. and Richards, P. (1984) Isotopic composition of plant carbon correlates with water-use efficiency of wheat genotypes. *Funct. Plant Biol.* **11**, 539–552.

Flexas, J., Diaz-Espejo, A., Berry, J.A., Cifre, J., Galmes, J., Kaldenhoff, R., Medrano, H. and Ribas-Carbo, M. (2007) Analysis of leakage in IRGA's leaf chambers of open gas exchange systems: quantification and its effects in photosynthesis parameterization. *J. Exp. Bot.* **58**, 1533–1543.

Fracasso, A., Trindade, L.M. and Amaducci, S. (2016) Drought stress tolerance strategies revealed by RNA-Seq in two sorghum genotypes with contrasting WUE. *BMC Plant Biol.* **16**, 115.

Franks, P.J., Doheny-Adams T, W., Britton-Harper, Z.J. and Gray, J.E. (2015) Increasing water-use efficiency directly through genetic manipulation of stomatal density. *New Phytol.* **207**, 188–195.

Fu, Q.S., Yang, R.C., Wang, H.S., Zhao, B., Zhou, C.L., Ren, S.X. and Guo, Y.-D. (2013) Leaf morphological and ultrastructural performance of eggplant (*Solanum melongena L.*) in response to water stress. *Photosynthetica*, **51**, 109–114.

Galmes, J., Conesa, M.A., Ochogavia, J.M., Perdomo, J.A., Francis, D.M., Ribas-Carbo, M., Save, R., Flexas, J., Medrano, H. and Cifre, J. (2011) Physiological and morphological adaptations in relation to water use efficiency in Mediterranean accessions of *Solanum lycopersicum*. *Plant Cell Environ.* **34**, 245–260.

Galmes, J., Ochogavia, J.M., Gago, J., Roldan, E.J., Cifre, J. and Conesa, M.A. (2013) Leaf responses to drought stress in Mediterranean accessions of *Solanum lycopersicum*: anatomical adaptations in relation to gas exchange parameters. *Plant Cell Environ.* **36**, 920–935.

Galmés, J., Medrano, H. and Flexas, J. (2007a) Photosynthesis and photoinhibition in response to drought in a pubescent (*var. minor*) and a glabrous (*var. palaui*) variety of *Digitalis minor*. *Environ. Exp. Bot.* **60**, 105–111.

Galmés, J., Flexas, J., Savé, R. and Medrano, H. (2007b) Water relations and stomatal characteristics of Mediterranean plants with different growth forms and leaf habits: responses to water stress and recovery. *Plant Soil*, **290**, 139–155.

Gan, Y., Zhou, L., Shen, Z.-J., Shen, Z.-X., Zhang, Y.-Q. and Wang, G.-X. (2010) Stomatal clustering, a new marker for environmental perception and adaptation in terrestrial plants. *Bot. Stud.* **51**, 325–336.

Gianfagna, T.J., Carter, C.D. and Sacalis, J.N. (1992) Temperature and photoperiod influence trichome density and sesquiterpene content of *Lycopersicon- hirsutum F. hirsutum*. *Plant Physiol.* **100**, 1403–1405.

Glover, B.J. (2000) Differentiation in plant epidermal cells. *J. Exp. Bot.* **51**, 497–505.

Glover, B.J., Perez-Rodriguez, M. and Martin, C. (1998) Development of several epidermal cell types can be specified by the same MYB-related plant transcription factor. *Development*, **125**, 3497–3508.

Glover, B.J., Airoldi, C.A. and Moyroud, E. (2016). Epidermis: outer cell layer of the plant. In eLS. Chichester, UK: John Wiley & Sons, Ltd. https://doi.org/10.1002/9780470015902.a0002072.pub3

Grandillo, S., Zamir, D. and Tanksley, S.D. (1999) Genetic improvement of processing tomatoes: a 20 years perspective. *Euphytica*, **110**, 85–97.

Guerfel, M., Baccouri, O., Boujnah, D., Chaïbi, W. and Zarrouk, M. (2009) Impacts of water stress on gas exchange, water relations, chlorophyll content and leaf structure in the two main Tunisian olive (*Olea europaea L.*) cultivars. *Sci. Hortic.* **119**, 257–263.

Guha, A., Sengupta, D., Kumar Rasineni, G. and Ramachandra Reddy, A. (2010) An integrated diagnostic approach to understand drought tolerance in mulberry (*Morus indica L.*). *Flora – Morphol Distrib Funct Ecol Plants*, **205**, 144–151.

Gurr, G.M. and McGrath, D. (2001) Effect of plant variety, plant age and photoperiod on glandular pubescence and host-plant resistance to potato moth (*Phthorimaea operculella*) in *Lycopersicon* spp. *Ann. Appl. Biol.* **138**, 221–230.

Hamanishi, E.T., Thomas, B.R. and Campbell, M.M. (2012) Drought induces alterations in the stomatal development program in *Populus*. *J. Exp. Bot.* **63**, 4959–4971.

Harley, P.C., Loreto, F., Di Marco, G. and Sharkey, T.D. (1992) Theoretical considerations when estimating the mesophyll conductance to co2 flux by analysis of the response of photosynthesis to CO2. *Plant Physiol.* **98** (4), 1429–1436.

Hauser, M.-T. (2014) Molecular basis of natural variation and environmental control of trichome patterning. *Front. Plant Sci.* **5**, 320.

Hermida-Carrera, C., Kapralov, M.V. and Galmés, J. (2016) Rubisco catalytic properties and temperature response in crops. *Plant Physiol.* **171**(4), 2549–2561. https://doi.org/10.1104/pp.16.01846

Hetherington, A.M. and Woodward, F.I. (2003) The role of stomata in sensing and driving environmental change. *Nature*, **424**, 901–908.

Holmes, M.G. and Keiller, D.R. (2002) Effects of pubescence and waxes on the reflectance of leaves in the ultraviolet and photosynthetic wavebands: a comparison of a range of species. *Plant Cell Environ.* **25**, 85–93.

Iovieno, P., Punzo, P., Guida, G., *et al.* (2016) Transcriptomic changes drive physiological responses to progressive drought stress and rehydration in tomato. *Front. Plant Sci.* **7**, 371.

Kahn, T.L., Fender, S.E., Bray, E.A. and O'Connell, M.A. (1993) Characterization of expression of drought- and abscisic acid-regulated tomato genes in the drought-resistant species *Lycopersicon pennellii*. *Plant Physiol.* **103**, 597–605.

Kang, J.H., McRoberts, J., Shi, F., Moreno, J.E., Jones, A.D. and Howe, G.A. (2014) The flavonoid biosynthetic enzyme chalcone isomerase modulates terpenoid production in glandular trichomes of tomato. *Plant Physiol.* **164**, 1161–1174.

Lawson, T. and Blatt, M.R. (2014) Stomatal size, speed, and responsiveness impact on photosynthesis and water use efficiency. *Plant Physiol.* **164**, 1556–1570.

Li, Y., Li, H., Li, Y. and Zhang, S. (2017) Improving water-use efficiency by decreasing stomatal conductance and transpiration rate to maintain higher ear photosynthetic rate in drought-resistant wheat. *Crop J.* **5**, 231–239.

Liu, X. and Liu, C. (2016) Effects of Drought-Stress on Fusarium Crown Rot Development in Barley. *PLoS ONE*, **11**, e0167304.

Liu, E.K., Mei, X.R., Yan, C.R., Gong, D.Z. and Zhang, Y.Q. (2016) Effects of water stress on photosynthetic characteristics, dry matter translocation and WUE in two winter wheat genotypes. *Agric. Water Manag.* **167**, 75–85.

Luckwill, L. (1943) *The genus Lycopersicon: a historical, biological, and taxonomic survey of the wild and cultivated tomatoes*. Aberdeen: The University Press.

Martin, B. and Thorstenson, Y.R. (1988) Stable carbon isotope composition ($\delta^{13}C$), water use efficiency, and biomass productivity of *Lycopersicon esculentum*, *Lycopersicon pennellii*, and the F(1) hybrid. *Plant Physiol.* **88**, 213–217.

Masle, J., Gilmore, S.R. and Farquhar, G.D. (2005) The ERECTA gene regulates plant transpiration efficiency in *Arabidopsis*. *Nature*, **436**, 866–870.

McDowell, E.T., Kapteyn, J., Schmidt, A., *et al.* (2011) Comparative functional genomic analysis of *Solanum* glandular trichome types. *Plant Physiol.* **155**, 524–539.

Medrano, H., Tomás, M., Martorell, S., Flexas, J., Hernández, E., Rosselló, J., Pou, A., Escalona, J.-M. and Bota, J. (2015) From leaf to whole-plant water use efficiency (WUE) in complex canopies: limitations of leaf WUE as a selection target. *Crop J.* **3**, 220–228.

Mo, Y., Yang, R., Liu, L., Gu, X., Yang, X., Wang, Y., Zhang, X. and Li, H. (2016) Growth, photosynthesis and adaptive responses of wild and domesticated watermelon genotypes to drought stress and subsequent re-watering. *Plant Growth Regul.* **79**, 229–241.

Morohashi, K. and Grotewold, E. (2009) A systems approach reveals regulatory circuitry for *Arabidopsis* trichome initiation by the GL3 and GL1 selectors. *PLoS Genet.* **5**, e1000396.

Moyle, L.C. (2008) Ecological and evolutionary genomics in the wild tomatoes (*Solanum sect. Lycopersicon*). *Evolution*, **62**, 2995–3013.

Niinemets, U., Diaz-Espejo, A., Flexas, J., Galmes, J. and Warren, C.R. (2009) Role of mesophyll diffusion conductance in constraining potential photosynthetic productivity in the field. *J. Exp. Bot.* **60**, 2249–2270.

de Oliveira Silva, F.M., Lichtenstein, G., Alseekh, S., *et al.* (2018) The genetic architecture of photosynthesis and plant growth-related traits in tomato. *Plant Cell Environ.* **41**, 327–341.

Palliotti, A., Bongi, G. and Rocchi, P. (1994) Peltate trichomes effects on photosynthetic gas exchange of *Olea Europea L.* leaves. *Life Sci. Adv. Plant Physiol.* **13**, 35–44.

Peralta, I.E., Spooner, D.M. and Knapp, S. (2008) Taxonomy of wild tomatoes and their relatives (S*olanum sect Lycopersicoides, sect,* Juglandifolia, sect. Lycopersicon; Solanaceae). *Syst. Bot. Monographs*, **84**, 186.

Pillitteri, L.J. and Dong, J. (2013) Stomatal development in Arabidopsis. *Arabidopsis Book*, **11**, e0162.

Ren, X., Chen, Z., Liu, Y., Zhang, H., Zhang, M., Liu, Q., Hong, X., Zhu, J.K. and Gong, Z. (2010) ABO3, a WRKY transcription factor, mediates plant responses to abscisic acid and drought tolerance in *Arabidopsis*. *Plant J.* **63**, 417–429.

Rick, C.M. (1973) Potential genetic resources in tomato species: clues from observations in native habitats. In *Genes, Enzymes, and Populations* (Srb, A.M. ed.). Boston, MA: Springer US, pp. 255–269.

Riederer, M. and Schreiber, L. (2001) Protecting against water loss: analysis of the barrier properties of plant cuticles. *J. Exp. Bot.* **52**, 2023–2032.

Rigano, M.M., Arena, C., Di Matteo, A., Sellitto, S., Frusciante, L. and Barone, A. (2016) Eco-physiological response to water stress of drought-tolerant and drought-sensitive tomato genotypes. *Plant Biosystems*, **150**, 682–691.

Rogiers, S.Y., Hardie, W.J. and Smith, J.P. (2011) Stomatal density of grapevine leaves (*Vitis vinifera L.*) responds to soil temperature and atmospheric carbon dioxide. *Aust. J. Grape Wine Res.* **17**, 147–152.

Savé, R., Biel, C. and de Herralde, F. (2000) Leaf Pubescence, Water Relations and Chlorophyll Fluorescence in Two Subspecies of Lotus Creticus L. *Biol. Plant.* **43**, 239–244.

Schilmiller, A.L., Last, R.L. and Pichersky, E. (2008) Harnessing plant trichome biochemistry for the production of useful compounds. *Plant J.* **54**, 702–711.

Silva, E.C., Nogueira, R.J.M.C., Vale, F.H.A., Araújo, F.P.D. and Pimenta, M.A. (2009) Stomatal changes induced by intermittent drought in four umbu tree genotypes. *Braz. J. Plant. Physiol.* **21**, 33–42.

Simmons, A.T. and Gurr, G.M. (2005) Trichomes of *Lycopersicon* species and their hybrids: effects on pests and natural enemies. *Agric. For. Entomol.* **7**, 265–276.

Sletvold, N. and Ågren, J. (2012) Variation in tolerance to drought amongst Scandinavian populations of *Arabidopsis lyrata*. *Evol. Ecol.* **26**, 559–577.

Souza, M.A.A.D., Santos, L.A.D., Brito, D.M.C.D., Rocha, J.F., Castro, R.N., Fernandes, M.S. and Souza, S.R.D. (2016) Influence of light intensity on glandular trichome density, gene expression and essential oil of menthol mint (*Mentha arvensis L.*). *J. Essent. Oil Res.* **28**, 138–145.

Spyropoulou, E., Haring, M. and Schuurink, R. (2014) RNA sequencing on S*olanum lycopersicum* trichomes identifies transcription factors that activate terpene synthase promoters. *BMC Genom.* **15**, 402.

Steinhauser, M.C., Steinhauser, D., Gibon, Y., Bolger, M., Arrivault, S., Usadel, B., Zamir, D., Fernie, A.R. and Stitt, M. (2011) Identification of enzyme activity Quantitative Trait Loci in a *Solanum lycopersicum* X *Solanum pennellii* Introgression Line population. *Plant Physiol.* **157**, 998–1014.

Telfer, A., Bollman, K.M. and Poethig, R.S. (1997) Phase change and the regulation of trichome distribution in *Arabidopsis thaliana*. *Development*, **124**, 645–654.

Tian, D., Tooker, J., Peiffer, M., Chung, S. and Felton, G. (2012) Role of trichomes in defense against herbivores: comparison of herbivore response to *woolly* and *hairless* trichome mutants in tomato (*Solanum lycopersicum*). *Planta*, **236**, 1053–1066.

Traw, M.B. and Bergelson, J. (2003) Interactive effects of jasmonic acid, salicylic acid, and gibberellin on induction of trichomes in *Arabidopsis*. *Plant Physiol.* **133**, 1367–1375.

Turner, N.C. (1988) Measurement of plant water status by the pressure chamber technique. *Irrig. Sci.* **9**, 289–308.

Vendemiatti, E., Zsögön, A., Silva, G.F.F.E., de Jesus, F.A., Cutri, L., Figueiredo, C.R.F., Tanaka, F.A.O., Nogueira, F.T.S. and Peres, L.E.P. (2017) Loss of type-IV glandular trichomes is a heterochronic trait in tomato and can be reverted by promoting juvenility. *Plant Sci.* **259**, 35–47.

Wellso, S.G. and Hoxie, R.P. (1982) The Influence of environment on the expression of trichomes in wheat. *Crop Sci.* **22**, 879–886.

Wentworth, M., Murchie, E.H., Gray, J.E., Villegas, D., Pastenes, C., Pinto, M. and Horton, P. (2006) Differential adaptation of two varieties of common bean to abiotic stress: acclimation of photosynthesis. *J. Exp. Bot.* **57**, 699–709.

Xu, Z. and Zhou, G. (2008) Responses of leaf stomatal density to water status and its relationship with photosynthesis in a grass. *J. Exp. Bot.* **59**, 3317–3325.

Xu, X., Martin, B., Comstock, J.P., Vision, T.J., Tauer, C.G., Zhao, B., Pausch, R.C. and Knapp, S. (2008) Fine mapping a QTL for carbon isotope composition in tomato. *Theor. Appl. Genet.* **117**, 221.

Yoshida, T., Fujita, Y., Maruyama, K., Mogami, J., Todaka, D., Shinozaki, K. and Yamaguchi-Shinozaki, K. (2015) Four *Arabidopsis* AREB/ABF transcription factors function predominantly in gene expression downstream of SnRK2 kinases in abscisic acid signalling in response to osmotic stress. *Plant Cell Environ.* **38**, 35–49.

Zamir, D. (2001) Improving plant breeding with exotic genetic libraries. *Nat. Rev. Genet.* **2**, 983–989.

Zhao, L., Li, Y., Xie, Q. and Wu, Y. (2017) Loss of *CDKC;2* increases both cell division and drought tolerance in *Arabidopsis thaliana*. *Plant J.* **91**, 816–828.